Section 10(i)

Future Directions & New Concepts

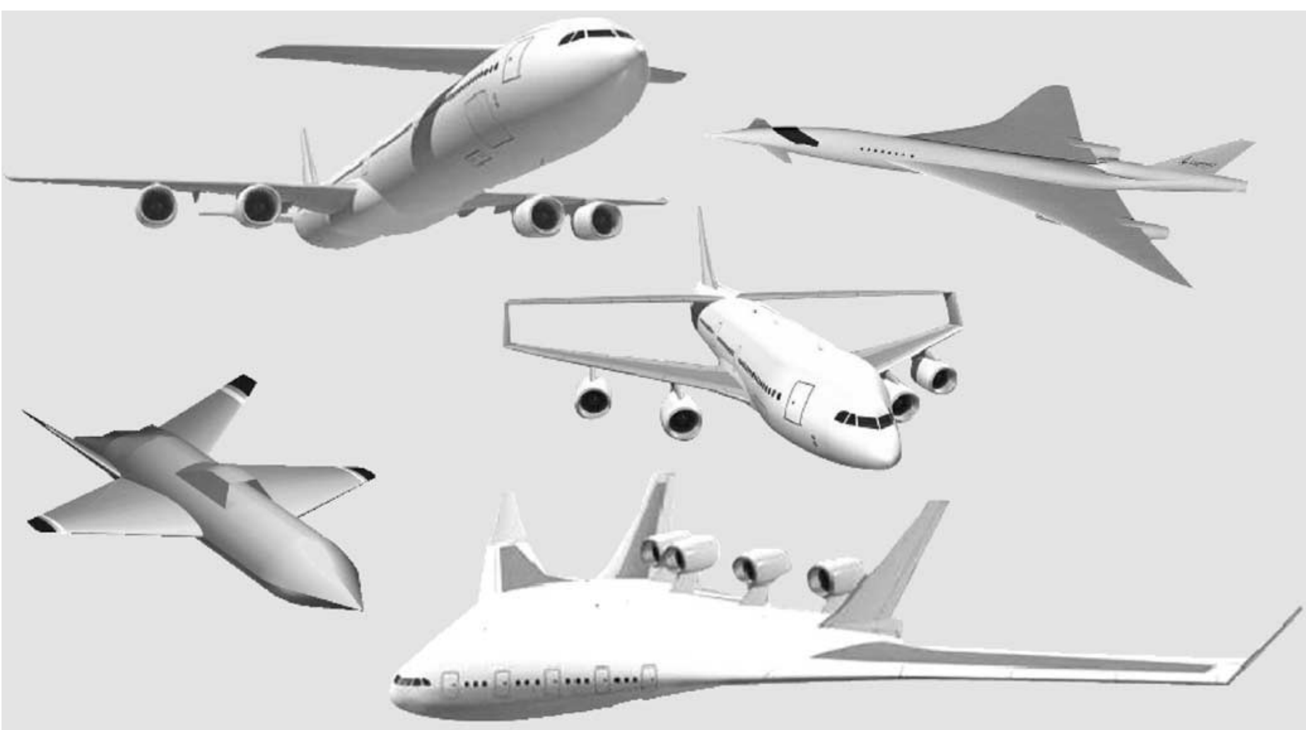

Ref: Paper 38 (2002), Progress in Aerospace Sciences
Navier-Stokes Solvers in European Aircraft Design
Vos, Rizzi, Darracq and Hirschel, 2002

Alternative Configurations

- Conventional Design
  - A cylindrical fuselage with a low mounted, high aspect ratio wing, a horizontal tail and a vertical fin for stability and control, and engines mounted either under the wing or directly to the fuselage for thrust
  - This design layout has lasted for almost 60 years
  - Traditional approach is incremental technological progression
  - It is believed that this design morphology and paradigm has or is soon to reach its limits of further development potential
- Future requirements call for
  - Further improvement in vehicular and operational efficiency
  - Reduction in the environmental impact both from a benign ecological influence perspective, and, due to many airports incorporating a comprehensive noise and emissions based fees structure
  - Ever increasing operational autonomy and safety
- Advanced concepts are borne from the motivation to achieve a somewhat greater magnitude improvement
  - A spectacular leap forward in design efficacy is only accomplished through concurrent optimisation of aerodynamics, propulsion, structures and system disciplines, i.e. holistic design
  - Typically, such configurations achieve greater than 20% reduction in fuel burn and greater than 10% reduction in design weights
  - By virtue of combining these improvements into a common platform, the result generally produces a configuration that radically departs from the conventional, in many instances appearing quite unusual
- Among the many possibilities being investigated by manufacturers
  - Three-surface
  - Blended Wing Body
  - Strut/Truss Braced wings
  - Dual wings and biplanes
  - Oblique Wing
  - Joined Wings
  - C-wing

Alternative Configurations (cont.)

Various morphology concepts expounded by NASA

- Design offices cannot rely very much on existing databases or empirical laws, nor on experience accumulated by engineers
  - Owing to such minimal practical experience with advanced configurations, the technical risk is considered to be very high
  - Best approach to estimating various functional relationships is via quasi-analytical algorithms

Alternative Configurations (cont.)

- Three-surface aircraft
  - The three-surface aircraft is based on ideas developed on fighter aircraft
    - It has an additional pair of Canard wings in front of the wing, generates both positive lift and pitching moment while giving opportunity to minimize drag in a variety of flight conditions
    - May improve flight control characteristics
    - Improved qualities during cruise and high lift conditions are also expected
  - There are two types of three-surface configurations
    - <u>Lifting Canards</u> – typically fixed surface serving only as a lift-balancing surface
    - <u>Control Canards</u> – all movable surface with double hinged flaps, scheduled in accordance with elevator deflection
  - This particular aircraft concept is generally configured to be naturally unstable and flight control computers are used for stabilising the aircraft
  - Three-surface layouts can be configured to have positive static longitudinal stability
    - Can assist in reducing significant levels of wave drag for high-speed transports with large trim drag qualities
    - Alternatively, the horizontal stabiliser can be configured to generate positive lift together with the wing and the third [Canard] surface used to achieve balance (trimming)
  - Drawbacks include weight penalty, maintenance cost, ramp safety, and, increased design, development and manufacturing cost

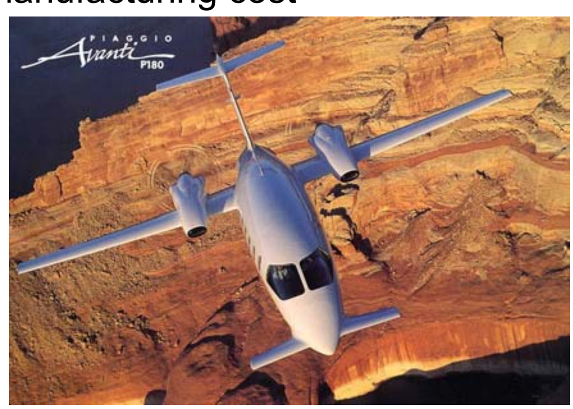

Various three-surface transport designs

Alternative Configurations (cont.)

- Blended Wing Body
  - Also known as the "flying wing" or "span-loaders" is an old concept developed during World War II
  - The idea is to produce an aircraft with a physical wing thickness large enough to permit seating of passengers/payload within the wing itself
    - By dispensing with the usual cylindrical pressure-vessel fuselage, the wetted area can be dramatically reduced
    - Additionally, can fashion a wing design that is tailored to promote close approximation to an elliptical lift distribution
    - Aerodynamic lift coincides with vehicle inertial loads
    - Shape lends itself to desirable area distribution – improved high-speed drag
    - It is argued that the configuration can generate a significant relative double-digit increase in operating lift-to-drag ratio
  - It is therefore no surprise that it is currently being investigated by industry and by research centres
    - The main interest in this concept is the large reduction in fuel consumption compared to conventional designs, combined with a large transport capacity (up to 1000 passengers)
    - It is expected that the next generation (at least 20-30 years from now) of large civil transport aircraft will be based on the flying wing concept
  - Disadvantages
    - Integration of pressurised passenger cabins, cargo compartments, fuel tanks and landing gear
    - Emergency egress – arrangement of exits and risks during ditching
    - Lack of window cut-outs for passengers
    - Passenger comfort during vehicle in-flight manouevres
    - Configuration not practical for aircraft smaller than large narrow-bodies

Boeing (left) and Airbus (right) BWB design studies

Alternative Configurations (cont.)

- Truss/Strut-Braced Wings
  - Pfenninger has long advocated strut bracing to improve the performance of conventional transports
  - Structural benefits
    - The vertical force of the strut produces a shear force discontinuity along the span
    - This shear force discontinuity creates a break in the bending moment slope, which reduces the bending moment inboard of the strut
    - The strut vertical offset provides a favourable moment that creates a spanwise bending moment curve discontinuity; this discontinuity further reduces the bending moment inboard of the strut
    - A decrease in bending moment means that the weight of the material required to counter that moment will be reduced, thus, the strut provides bending load alleviation to the wing
  - Allows for reduced wing thickness and sweep, resulting in an enhanced extent of low drag laminar flow, as well as increased span
  - Pfenninger's designs for such aircraft yielded L/D values in the 40s, over twice current levels of ultra-long haul equipment
  - The concept was not adopted primarily because there was debate whether a transonic strut braced wing could be designed with acceptable shock drag
    - This can possibly be mitigated in light of future CFD capabilities

Pfenninger Strut-Braced Wing concept (NASA Photo)

Alternative Configurations (cont.)

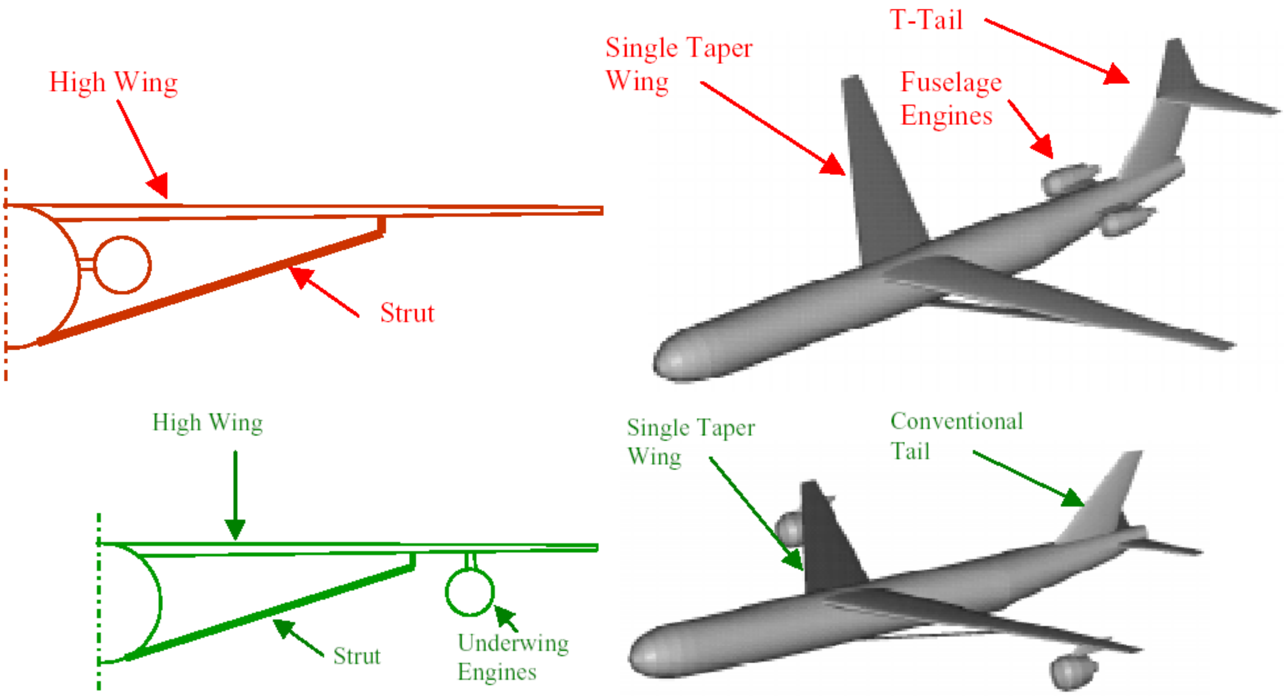

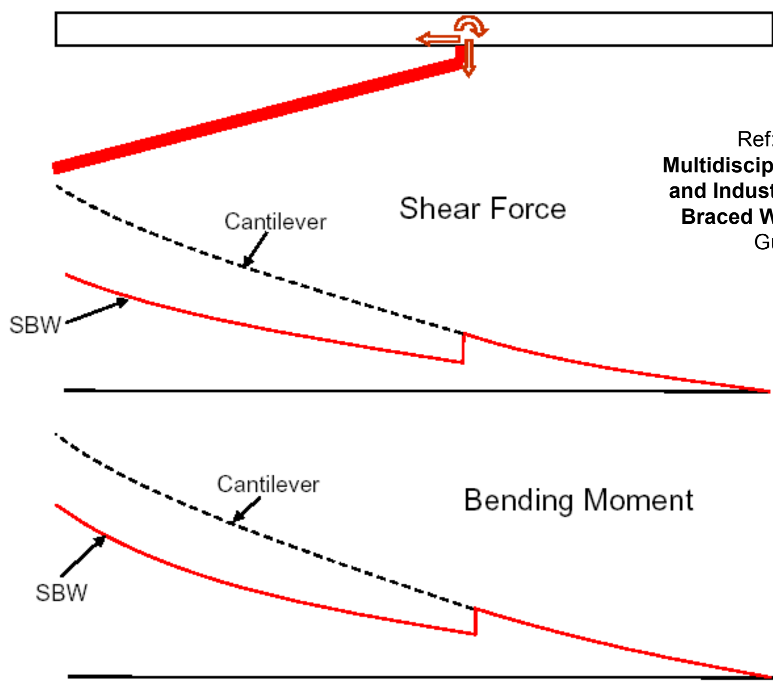

Ref: Virginia Polytechnic
Multidisciplinary Design Optimization and Industry Review of a 2010 Strut-Braced Wing Transonic Transport
Gundlach et al, 1999

Strut-Braced Wing with alternative engine installations, and, shear force and bending moment Diagrams

Alternative Configurations (cont.)

- Design studies of the 2010 SBW transonic transport completed by Virginia Polytechnic have shown a potential to shave up to 10% of MTOW defined by design mission requirements
- One approach for major drag-due-to-lift reduction is wingtip engine placement
  - Whitcomb and others have shown that up to 50% drag-due-to-lift reductions are obtainable
  - Detrimental to field performance during OEI conditions, e.g. minimum control speeds
  - Probably requires a third engine in the empennage region and utilisation of thrust vectoring on all engines to handle the OEI problem

The "Green" aircraft SBW proposal by Airbus as part of the 2020 Vision project

Alternative Configurations (cont.)

- Closely Coupled Dual-wings
  - Result of experimentation done by Olson, Selberg and Rhodes
    - Showed that both closely coupled dual-wing and swept forward swept rearward (connected at the wingtip) systems exhibit aerodynamic advantages over single wing configurations
  - Adaptive Tandem Wing
    - The wing structure involves a tandem arrangement, joined at the tip
    - Under low-speed conditions a structure is deployed across the inter wing gap, on both the upper and lower surface, to provide a large single flying surface
      - The optimisation of the deployed inter-wing cover provides the low speed performance of the wing
    - At high-speed conditions the structure is withdrawn to expose the tandem wing arrangement
      - As the tandem wing is only exposed under high-speed conditions it need only be optimised for high speed performance only
      - The image inserts show the configuration in High speed mode
    - Purported to be simpler, cheaper, lighter and more easily maintained due to deployment mechanisms and structures

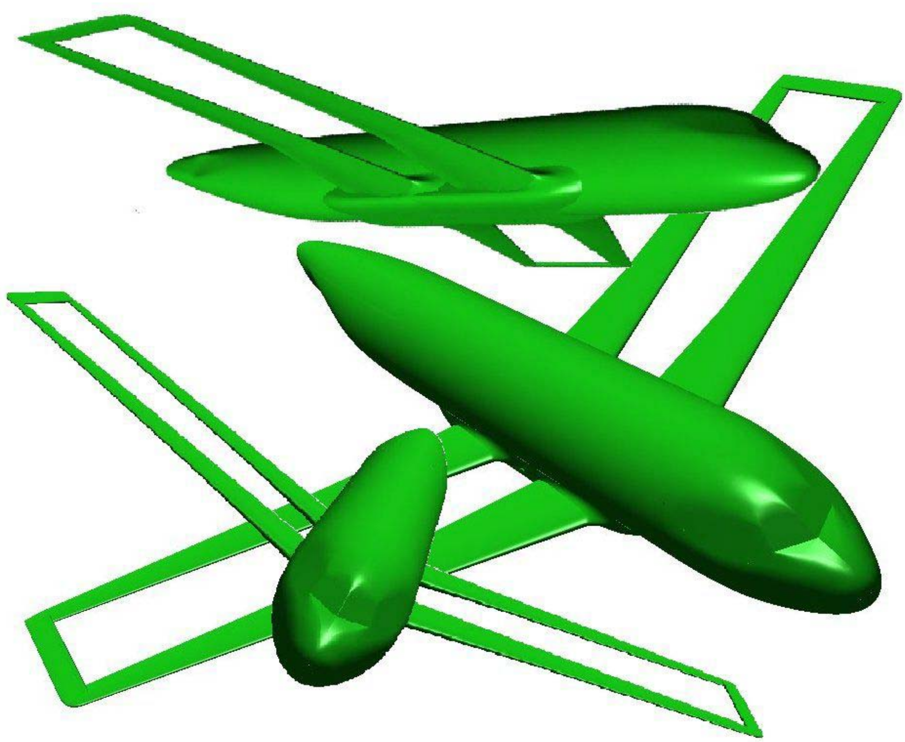

Adaptive Tandem Wing concept (BAE Systems research)

Alternative Configurations (cont.)

- Bi-planes
  - Known to decrease vortex-induced drag at the same operating lift as a monoplane; based on work done by Prandtl, Munk and Kroo
  - Investigations show this configuration could be used for transonic and low-supersonic speeds
    - Tendency to lower the wave drag due to lift and/or volume
    - Still valid for supersonic flight if Mach cones do not intersect
  - One example is the Twin-Oblique Lifting Surface (TOLS)
    - A hybrid concept which comprises two independent, fixed, skewed wings linked by a wing-pylon-engine bracing structural system (WPEBS)

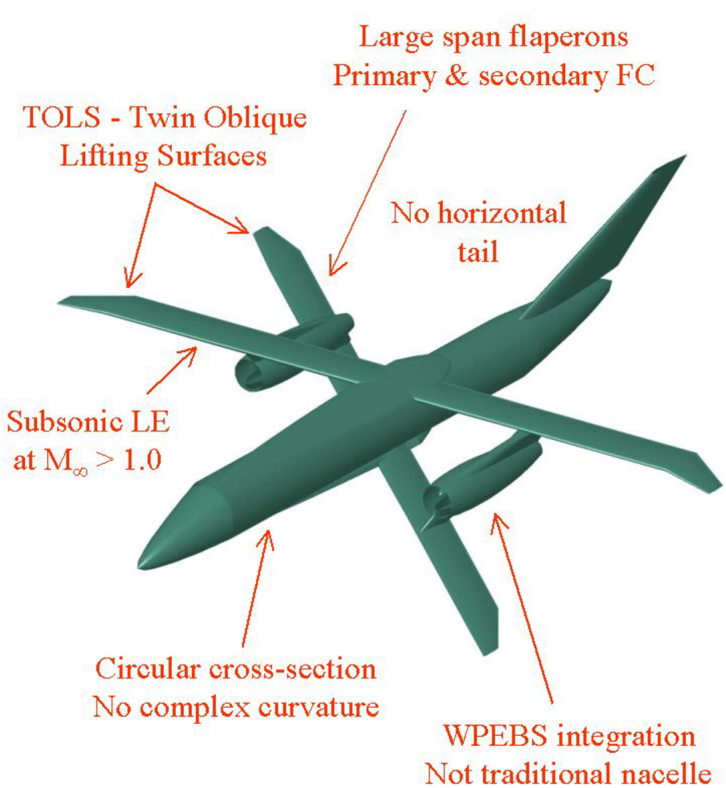

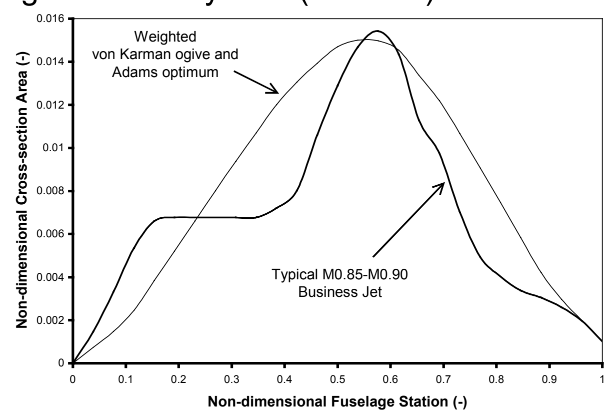

High-speed business jet

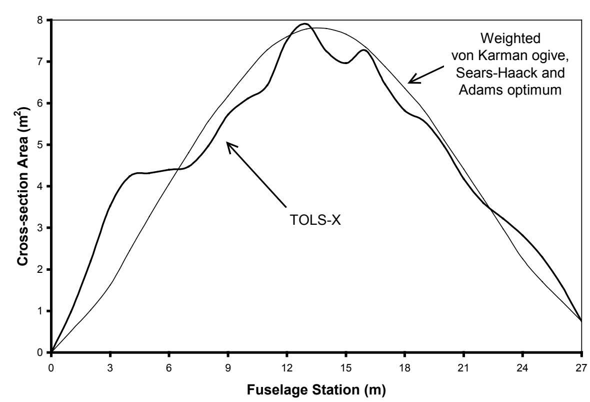

TOLS-X

The Twin Oblique Lifting Surfaces (TOLS) configuration

- TOLS draws upon the following concepts
  - Oblique Wing
  - Closely coupled dual-wings
  - Strut-Braced Wing

Alternative Configurations (cont.)

- Oblique Wing
  - Vogt first put forth a variable sweep oblique wing aircraft design proposal in the 1940s
    - It was an unconventional asymmetric aircraft design, it was one of the first concerted attempts to reconcile conflicting conditions of wing sweep optimality for low and high speed performance
  - Campbell, Drake and Jones found interest in such a configuration because analysis and wind tunnel testing indicated that elliptical oblique wings would provide minimum wave drag in supersonic flow

Dryden Flight Research Center ECN 15846 Photographed 1980
AD-1

Example of an operational oblique wing prototype

  - Disadvantages
    - Problems with low-speed aero-elastic divergence associated with a high aspect ratio, forward swept semi-wing
    - Adequate handling of longitudinal and lateral motion coupling produced by the interaction of highly non-linear aerodynamic and inertial moments
    - Lack of rigid body and wing structural mode coupling
    - Requires a wing pivot mechanism

Alternative Configurations (cont.)

- Joined-Wing
  - This layout is based on an idea by Prof. Prandtl published in 1924
  - Postulated to have a very high aerodynamic efficiency both in terms of drag and maximum lift
    - Significant reduction in vortex-induced drag
    - Purportedly triangulation generated by having forward wings low and aft wing high can be aligned with the net force vector (lift plus drag)
  - Good stability and control
  - Should give an opportunity for a significant reduction in the gross weight of the aircraft via a reduction in fuel useful load (improved specific air range)
  - The aerodynamics of this configuration is very complex due to the interference between the two wings
  - Disadvantages
    - Empty weight reduction is minimal or comparable
    - Increased level of interference drag
    - Rotation of the aft wing's lift vector
    - Inability to attain a very high lift coefficient for the aft wing
    - Ramp safety
    - More complicated further product development from baseline

Lockheed proposal (left) and released by University of Pisa (right)

Loughborough University/Virginia Polytechnic "Ikelos"

Alternative Configurations (cont.)

- C-Wing
  - Proposed by Kroo and McMasters is essentially adding a pair of horizontal winglets to a pair of winglets
  - Some of the passengers are seated inside the pressurized inner wing
  - This configuration limits wing span while affording good vortex-induced drag efficiency
  - When configured properly and attached to a highly swept wing, the horizontal winglets act as T-tail type horizontal stabilizers
    - The winglets also functional for directional stability and control

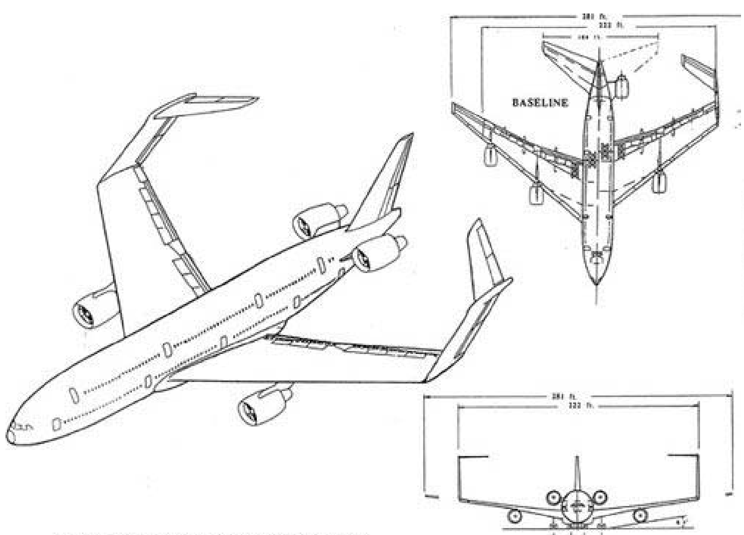

ALTERNATIVE C-WING CONFIGURATION FOR A VERY LARGE SUBSONIC TRANSPORT AIRPLANE

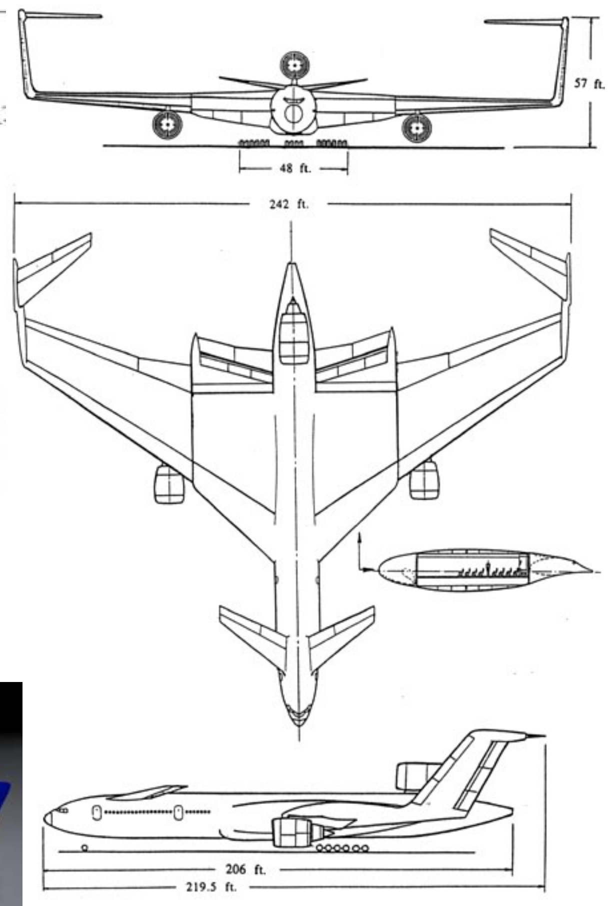

Final Preliminary C-Wing Transport - Model 2020A.

Large C-wing transport proposals: Stanford University (top left and right) and NASA (bottom left)

Alternative Configurations (cont.)

- Other Choices
  - From: Bushnell, D.M., “Advanced Civilian Aeronautical Concepts”, Discussion paper, NASA-Langley Research Centre, 1996
  - Parasol Wing
    - This is an old approach wherein reflections of the fuselage nose shock provides favourable interference lift and subsequent aft body region thrust
    - Estimated L/D improvements are in the range of 25-30%
    - Required advanced technologies include flow separation control for the shock-boundary layer interaction regions and fluidic or variable physical geometry to work the “off-design” issues
  - Strut-Braced “Extreme Arrow”
    - Pfenninger has also advocated an externally strut-braced HSCT with truly revolutionary cruise performance – an L/D of order 20, over twice that of the best of the current approaches
    - The strut bracing allows use of an extreme arrow wing planform with minimal wave drag-due-to-lift and extensive laminar flow (“controlled”)
    - Mid-wing fuel canisters are used to provide favourable wave interference and load alleviation with extensive “natural” laminar flow on both the fuel canisters and the fuselage
  - Alternative HSCT Approaches
    - Northrup studied a “reverse delta” configuration for purposes of obtaining extensive regions of “natural” laminar flow on the wing
    - Some “novel” general concepts with application across the configuration spectrum include use of flow separation control at cruise to allow full exploitation of inviscid design precepts
      - Benefits include enhanced wing leading edge thrust, increased upper surface lift, increased fuselage lift/camber (reduced wave DDL) and enhanced performance of favourable wave interference (via shock-boundary layer separation control)

Asset supersonic laminar flow business jet concepts

Additional Reading

- Schmitt, D., Strohmayer, A., "Does the Air Transport Market Need "Unconventional Aircraft Configurations?", Paper 151, ICAS 2002 Congress, September 2002
- Jarry, P., "Market Drivers and Innovation Behind the Airbus Products", Invited Presentation, ICAS 2002
- Liebeck, R.H., "Design of the Blended-Wing-Body Subsonic Transport", 2002 Wright Brothers Lecture, AIAA-2002-0002, 2002
- Gundlach IV, J.F, Naghshineh-Pour, A., Gern, F., Tetrault P-A., Ko, A., Schetz, J.A., Mason, W.H., Kapania, R.K., Grossman, B., Haftka (University of Florida), R.T., "Multidisciplinary Design Optimisation and Industry Review of a 2010 Strut-Braced Wing Transonic Transport", MAD 99-06-03, Multidisciplinary Analysis and Design Center for Advanced Vehicles, Department of Aerospace and Ocean Engineering Virginia Polytechnic Institute and State University, June 1999
- Rhodes, M.D., Selberg, B.P., "Benefits of Dual Wings over Single Wings for High-Performance Business Airplanes", AIAA Journal of Aircraft, Vol. 21 No. 2, 1983
- Isikveren, A.T., "High-Performance Executive Transport Design Employing Twin Oblique Lifting Surfaces", SAE Paper 2001-01-3031, World Aviation Congress and Exposition, September 2001
- Jones, R.T., Nisbet J.W., "Transonic Transport Wings – Oblique or Swept?", Astronautics and Aeronautics, January 1974
- van der Velden, A.J.M, Torenbeek, E., "Design of a Small Oblique-Wing Transport Aircraft", Journal of Aircraft, Vol. 26, No. 3, March 1989
- Wolkovitch, J., "The Joined Wing: An Overview", AIAA Journal of Aircraft, 1985
- McMasters, J.H., Kroo, I.M., "Advanced Configurations for Very Large Transport Airplanes", Aircraft Design 1 (1998) 217-242, Aircraft Design Journal, pp. 217-242

Additional Reading

- Burley, C.L., Huebner, L.D., Lamar, J.E., McKinley, Jr., R.E., Sexstone, M.G., Torres, A.O., Scott, R.C., Small, W.J., Yaros, S.F., “Synergistic Airframe-Propulsion Interactions and Integrations”, NASA/TM-1998-207644, March 1998

DOES THE AIR TRANSPORT MARKET NEED "UNCONVENTIONAL AIRCRAFT CONFIGURATIONS"?

D. Schmitt, A. Strohmayer
Chair of Aeronautical Engineering
Technische Universität München
85747 Garching

Keywords:
(air transport, market requirements; aircraft design; unconventional configurations; scenario process; robust strategy; new technologies)

Abstract

In the past the engineering spirit and imagination was the driver for new aircraft developments, combined with new technologies, which have led to new aircraft programmes, each new programme showing at least a 10% economical benefit to its competing flying aircraft. During the last two decades technological progress seems to have decelerated or – in other words - the aircraft industry has achieved a high technical standard and has become a mature industry.

There are however a lot of new technical concepts like Flying Wing, Tandem Wing, Three Surface Aircraft Concepts etc. where the inventors claim enormous advantages compared to today's conventional airliners. But does the market need these new vehicles?

The Institute of Aeronautical Engineering at the Technische Universität München has initiated a scenario process with students and experts from industry to establish and analyse a series of air transport scenarios for the year 2030 out of which the market possibilities for future civil transport aircraft have been identified.

In all scenarios, most of the market requirements could be fulfilled by conventional configurations, but sometimes with some stringent requirements like for example noise requirements. Some of the requirements however lead to configurations in unconventional layout.

In a next step these unconventional configurations have been further analysed with respect to additional needs in new technologies, development methods and tools and operational requirements. Based on these additional demands from all scenarios, a fairly robust technology strategy can be developed.

The paper will shortly describe the scenario process, will develop the methodology to define the robust technology strategy and will use a typical, possible scenario to demonstrate and validate the proposed method.

1 Introduction

In the past the engineering spirit and imagination was the driver for new aircraft developments, combined with the introduction of new technologies, which had led to new aircraft programmes showing at least a 10% economical benefit to its competing aircraft flying already. During the last two decades technological progress seems to have decelerated. But it could also be argued, that the commercial aircraft industry has achieved a high and efficient technical standard and has become a technically mature industry. A typical sign of a mature industry is the fact that market forces are dominant to technological progress and innovation. Another fact which supports the thesis of a mature industry can be the fact, that most of the aircraft flying today are looking more or less the same. The payload is transported in a circular cross fuselage, the necessary aerodynamic lift is generated by a pair of wings which are fixed in the middle of the lower part of the fuselage, the wings are moderately swept, aircraft control is assured by the empennage and their control surfaces at the end of the fuselage, the main undercarriage is fixed to the wing and can be retracted into the fuselage, the engines are installed symmetrically under the wings. There are only few exceptions to this configuration, which has proven to be successful. If we compare the latest designs from Airbus and Boeing, i.e. the A330 versus the B777, or the A321 vs. the B757, it is difficult even for specialists, to differentiate which type of aircraft it might be. It can be concluded that today's aircraft look all very similar and even the new concept for a 500-seater from Airbus, the A380, has selected this configuration concept. This configuration is called the "Conventional Configuration" (CC), which has evolved over the past decades as the optimal design for an efficient economical passenger transport aircraft.

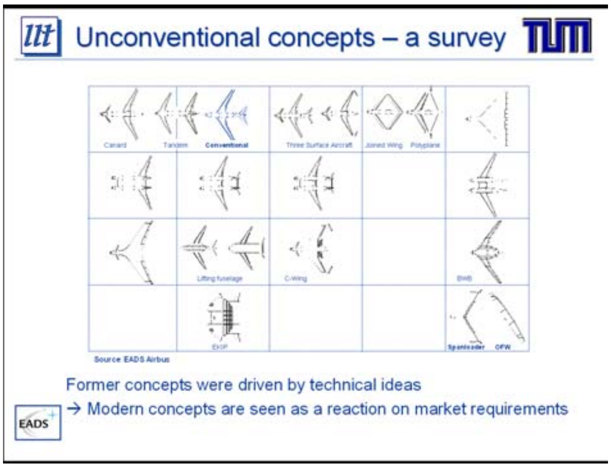

Figure 1

Nevertheless there are a lot of good ideas for new aircraft configurations (see fig.1 and [1]), which look fairly unconventional compared to the flying aircraft today. The so called "Unconventional configurations" are designed and promoted by various highly qualified engineers, who all claim, that their configurations have a lot of specific advantages compared to the conventional designs.

There is however no consistent view, which of these "Unconventional Configurations (UcC) may be viable for a certain task and/or market segment and which not. There are normally two camps. The engineers from the aeronautical industry, who all have a lot of good arguments, why these UcC can not work and a lot of "killer arguments" against the UcC are provided such as: emergency evacuation will never be possible; airport infrastructure will not fit; the aerodynamic interference from a moveable foreplane will be counterproductive to the main wing etc., etc. The engineers from the scientific community have a lot of positive arguments in favour for the UcC, such as: a better aerodynamic L/D; better structural concept with a weight saving potential; less trim drag and the strong argument, that the industry is becoming far too conservative and new ideas are no longer investigated.

Figure 2

The Institute of Aeronautical Engineering in Munich follows and has accepted a change in paradigm and proposes a new system approach, where the operating environment and the market will define the aircraft need and hence the necessary technology level (see fig 2) instead of the technical and technological driven approach.

Being conscious, that market forces will decide in the future, the need to start from a market perspective becomes obvious. The time focus for the market scenario should be rather long (30 years) in order to take into account the long large development cycles in the aeronautical industry. Therefore a market scenario for the year 2030 and later (called 2030+) was chosen and the best methods to be used were investigated.

The use of the scenario methodology has the big advantage that very different views and pictures of the future will be developed, but always a clear path is outlined, how to get from today into this particular scenario. In addition the participants in such a process learn a lot about the more and less important parameters in a scenario process, they get a better understanding, which parameters can be influenced by an actor in the complex market and which are driven by market dynamics and can not be influenced directly.

2. Scenario technique and process in air transport

The use of scenarios to look into the future and develop several different views of the future is a well established tool and methodology for better understanding future market requirements. Several references are describing the scenario methodology [2] – [5] (see fig. 3).

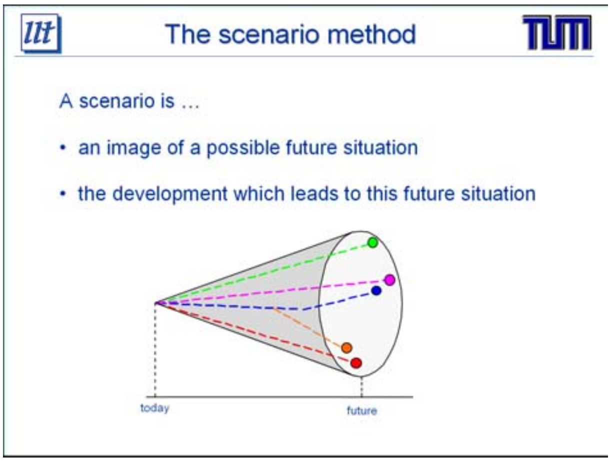

Figure 3

It should however be mentioned, that the best understanding about the methodology and the usefulness of scenarios is in participating directly in a scenario process and discuss and elaborate together with other specialists the future market environment. As part of the educational training programme in Aeronautics, the Institute of Aeronautical Engineering is offering each year a specific course in Scenario technique to their students. Each year the subject is changing and normally, the subjects are selected together with an industry partner who provides the thematic and timely focus and supports the course with some specialists from industry. 5 different scenario workshops have been conducted up to now with a high appreciation from industry about the good contribution and motivation of the students and the good quality of the results [6],[7],[8].

The use of scenarios in the conceptual aircraft design focuses in three different aspects [9]. The results of the scenario process are used to develop from the future market environment a technical product idea and determine from them design requirements. Another possibility is the identification of mandatory and/ or useful technologies which are mandatory or supportive for the new configurational concept. The third aspect is related to the development of evaluation criteria. These aspects are outlined in ref. [8],[9] and [10]. The five basic steps of the scenario method are outlined in fig. 4.

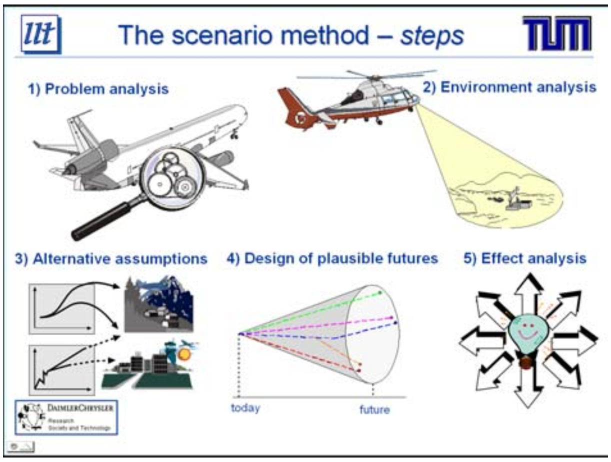

Figure 4

Figure 5

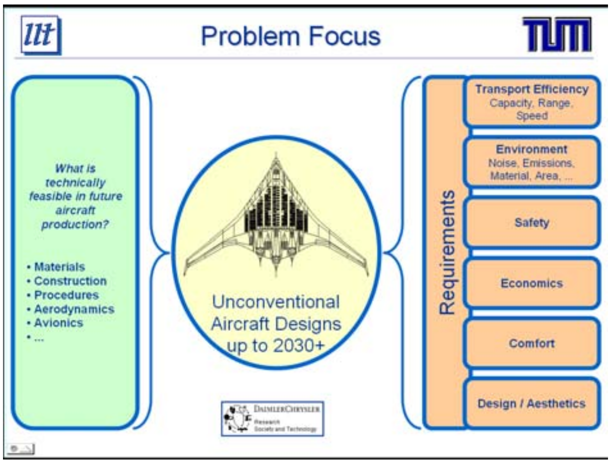

Figure 6

3 The scenario process " Unconventional Aircraft Configurations 2030+"

For this project, a time horizon of 30 years has been chosen. If we bare in mind, that the configuration concept of the future A330/A340 programme from Airbus has been developed already in 1976 and certification has started in 1992, this indicates that new concepts have to be developed fairly early before any chance of realisation will occur. On the other hand, a time horizon of 30 years is fairly long for a scenario process and all results are coupled with a very large uncertainty and risk. Therefore the framework had to be defined before. The following key questions had to be answered before the process (see fig. 5).

From which conditions and requirements in the global air transport business up to the year 2030 will it depend that a future aircraft concept will be of a conventional or can be of an unconventional type (see fig.6)?

How could the spectrum of requirements develop in alternative scenarios?

First of all, the air transport system of today had to be carefully analysed to better understand the interrelationship of all participating partners. On the aircraft industry side factors like ability and willingness to invest, time of development, development cost, accessibility to basic technologies and airline structure had to be investigated. These factors had to be analysed and structured and the most important had been defined.

For these factors a careful description and reasonable assumptions for the probable future development had to be defined. An analysis of the dependency between the different assumptions builds the frame for the different scenarios. Out of these multiple scenarios, some (in the a.m. scenario process only three) typical and different scenarios had to be selected.

All three scenarios have been outlined in detail in [8], but are described with their main features in fig. 7. In this paper we will only show the principle procedure in the context of one scenario, which was called "A Flying World" and shows a fairly positive environment for the aeronautical industry.

Fig. 8 indicates in a cartoon, how the students have characterised the scenario of a "Flying World".

Fig. 9 gives more details about this scenario. In terms of society, economy and politics, the scenario A is described by high mobility, ecological sensibility and increasing depletion of oil resources, leading to high fuel prices and the search for alternative energies. In the airline world, main aspects are strong airline competition, growing airspace capacity with more point to point connections and a sound airline economical basis, where small airlines prove to be more flexible than big alliances. With regard to aircraft manufacturers and their products, many new aircrafts with new technologies will appear on the market, rising development costs and time can be partly compensated with modern tools and methods, and smaller manufacturers can overcome the existing duopoly from Airbus and Boeing.

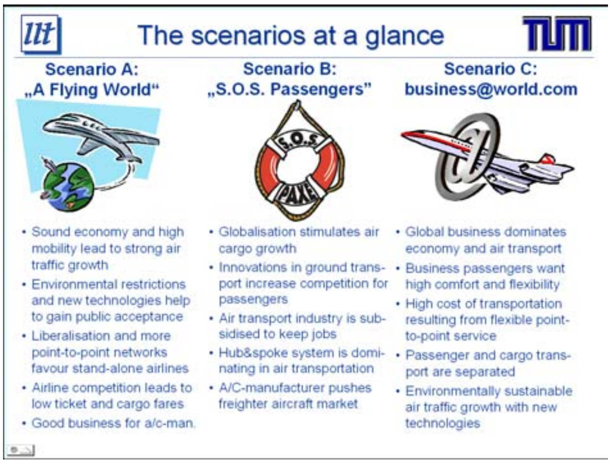

Figure 7

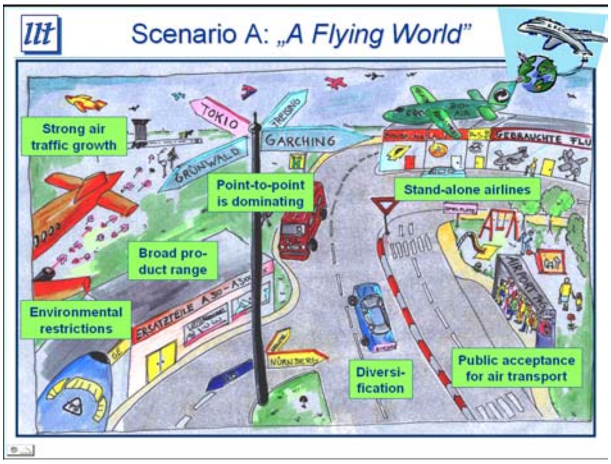

Figure 8

Figure 9

For each of these scenarios a set of requirements for aircraft configurations has been developed. These “Standard and requirement” documents are per se neutral with respect to a configuration. But in these documents, unconventional demands are included which will influence and have impact on today’s configuration and also those requirements which only can be met by new and unconventional designs.

The deduced configurations are in so far not pushed by their technical concept but pulled by market needs and requirements.
These requirements are derived by different actors in the air transport scene as airlines , passengers, airports, air traffic control, from the regulating bodies and political demands and conditions and finally from the aeronautical industry with respect to economy and product strategy.

For each scenario a list of criteria had been formulated with regard to passenger and cargo transport like

- transport performance, range, capacity, speed;
- economy for the airline
- safety for passengers and cargo
- environmental aspects like noise, emissions, recyclable materials, etc.
- requirements to turnaround, development potential and image

A specific payload range diagram had been generated for each scenario showing all interesting areas for intra- and intercontinental ranges (fig. 10). After these general considerations a requirement document has been generated for each aircraft category, deduced strictly from market needs (Fig. 11). Later on configuration proposals have been developed for each requirements document. First it was investigated, whether the requirements could be reasonably met by conventional configurations. If this was not possible unconventional solutions and appropriate configurations have been considered and discussed. Most of the requirement profiles could be fulfilled by conventional configurations, which is fairly obvious. However some requirements could only be met by unconventional configurations.

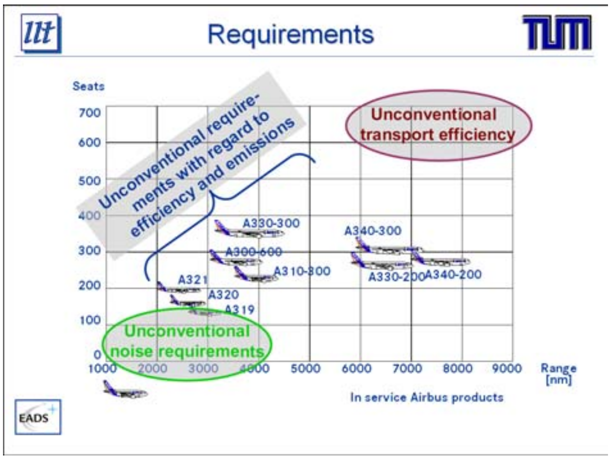

Figure 10

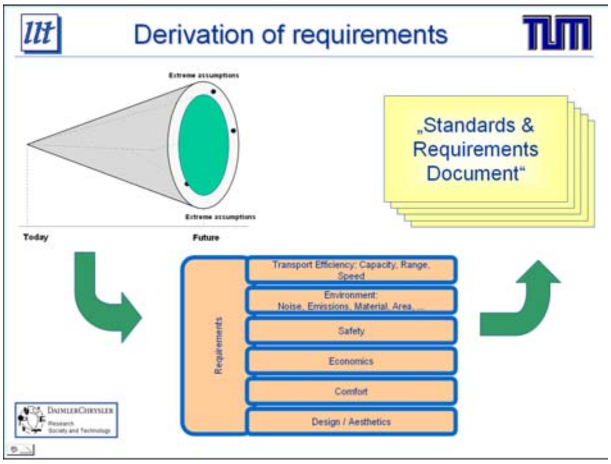

Figure 11

4 Definition of a robust strategy

The next step in the process is the selection of different "unconventional configurations" out of the different scenarios. For each configuration, the standard and requirement documentation exists and has to be properly described.

Figure 12 gives a general overview of this step. In the above mentioned scenario process, six possible new configurations have been identified, where unconventional features could be important for the success of the concept. Fig. 13 shows a typical example of the market applications for scenario A . It should be mentioned, that the requirements for the new freighter aircraft in scenario A will not automatically lead to a "Blended-Wing-Body" configuration. But at least the need for a fast Turnaround time leads to a new concept with nose- or rear-loading door possibilities [15].

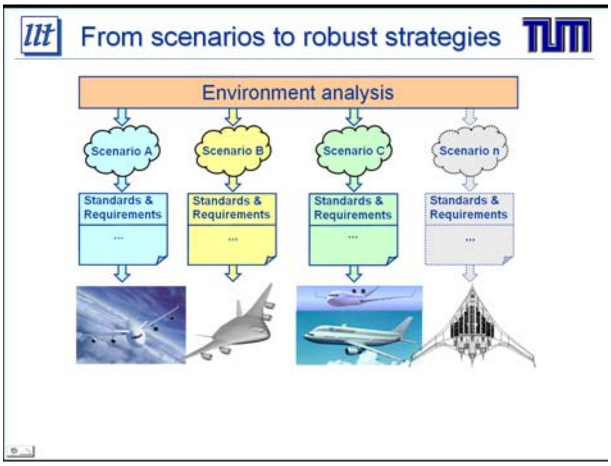

Figure 12

In Scenario A the need for two new concepts has been identified i.e. the "Green SR People Mover" and the "BWB Freighter family". Under the so called "green aircraft" two different aspects are combined, i.e. the "low noise aircraft" and the "alternative fuel aircraft".

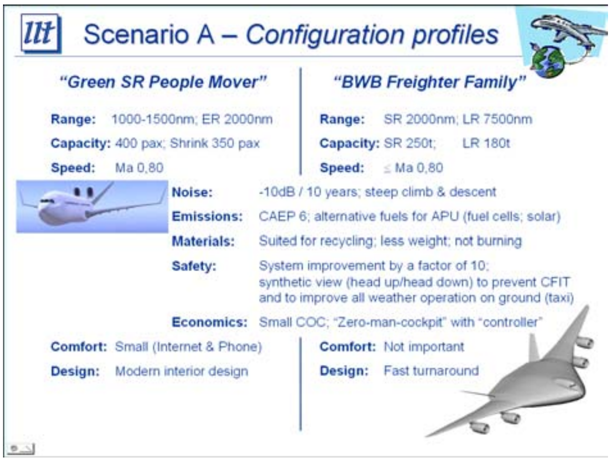

Figure 13

These requirements or configuration profiles are answers to different possible future developments. But as it is unclear which scenario will happen or is more likely to happen, a common set of requirements out of different scenarios has to be derived. The goal for a robust strategy is achieved when out of a variety of scenarios common requirements can be obtained which lead then to configurations which are not optimal for individual scenarios, but fairly robust and the best compromise to meet the needs for a broad range of scenarios.

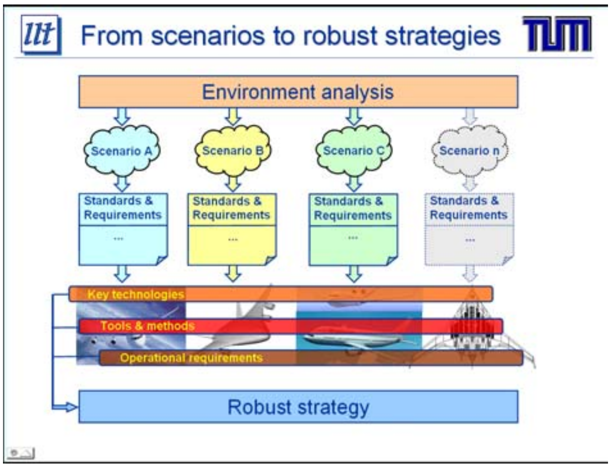

Figure 14

Fig 14 shows the principle procedure for the development of a robust strategy.

However , the goal of a scenario process for students is less the development of a robust product strategy but more the demonstration of the process and the definition of a set of different possible new concepts, which fulfil the future market needs or at least may be of interest for specific market niches. Six principle new concepts (see fig. 15) are the result of the scenario process and are of interest for further investigations. Each concept is based on a set of requirements, which was typical for a specific scenario.

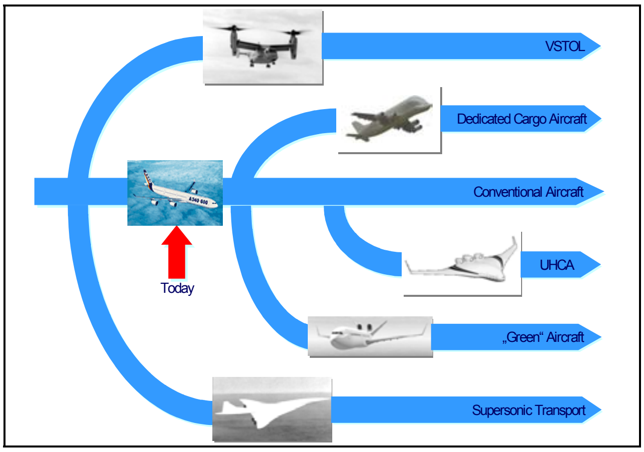

Figure 15

As a general result from the scenario process, it can be stated, that some of the different scenarios lead to requirements, which can not simply be met by conventional configurations. There is room for new concepts in specific market niches.

One of the objective of a scenario process may be the definition of a robust product strategy for the next 30 years. But normally it will be more appropriate to define a robust technology strategy. The development of new technologies and especially the development of those technologies, which fit to several project needs and are most efficient and applicable in different scenarios is an obvious target for scenario processes [9],[11],[12]. Technologies need a much longer time for their development and their readiness for application. It is very important to have the most efficient and most cost effective technologies available, when the market will need and require new products [14].

6 Summary

Assuming a time horizon of thirty years and more, as it is assumed for the development of completely new aircraft concepts, there are a lot of uncertainties and deficiencies about the development of market, customer needs and requirements and necessary technologies. The paper outlines, in which way scenario processes could be used to reduce these uncertainties in a systematic and methodological way. Different outputs can be obtained from scenarios, i.e. requirements, evaluation criteria and technologies.

With the proposed process, the future strategy will be based upon detailed market analysis and a global analysis of market related factors. This procedure will not replace the classical marketing tools like market forecast etc. but will be helpful to reduce the risk of uncertainties in a systematic and methodological way, which is always connected to long term forecast. Another important fact is the participation and discussion during a scenario process, as the complex environment will be carefully structured and the useful discussion between different experts improves the understanding for the global market. This will help considerably to increase the confidence level of a robust product strategy.

References

[1] Eichelbaum F.,
Studien unkonventioneller Konzepte,
Presentation from Airbus at TU München,
Nov. 2000

[2] Becker A. and List S.,
Die Zukunft gestalten mit Szenarien.
In: *Unternehmensplanung – Erfahrungsberichte aus der Praxis.*
Zerres M (editor), FAZ, 1997

[3] Fahey R. and Randall R. (editors),
Learning from the future – competitive foresight scenarios.
1st edition, John Wiley & Sons, 1998.

[4] Strohmayer A.,
Improving aircraft design robustness with scenario methods
2nd International Conference on Advanced Engineering Design, Glasgow, 2001

[5] Gausemeier J., Fink A., Schlake O.,
Planen und Führen mit Szenarien;
München; Hanser Verlag 1995

[6] Strohmayer A. and Jost P.,
Air transport scenario "Flight Unlimited 2015" – how to avoid operational limitations for large civil jet aircraft.
LT-TB-99/4, TU Muenchen, 1999

[7] Strohmayer A.,
Improving aircraft design robustness with scenario methods,
2nd International Conference on Advanced Engineering Design, Glasgow, 2001

[8] Strohmayer A., Becker A.,
Unkonventionelle Flugzeugkonfigurationen 2030+: Welche Marktfaktoren bestimmen die Konfiguration zukünftiger ziviler Transportflugzeuge,
LT-TB01/04, Lehrstuhl für Luftfahrttechnik,
TU München, 2001

[9] A. Strohmayer,
Szenariomethoden im Vorentwurf ziviler Transportflugzeuge,
Doctoral Thesis, Lehrstuhl für Luftfahrttechnik,
TU München, 2001

[10] Meller F., Jost P.,
Key buying factors and added value – a new approach to aircraft evaluation.
In: *DGLR-workshop 'Aircraft evaluation',*
TU Muenchen / DGLR, 1998.

[11] Strohmayer A., Schmitt D.,
Scenario based aircraft design evaluation
Harrogate, ICAS 2000

[12] ECATA Multinational Team Project,
A strategy towards future transport aircraft in unconventional configuration,
Madrid, 2001

[13] Chen G., Yingming H., Nuesser H-G, Wilken D.,
A method of evaluating civil aircraft market adequacy.
DLR, 1997

[14] Szodruch J.,
Increasing aircraft efficiency
In: Nouvelle Revue d'Aéronautique et d'Astronautique, No. 2, 1998, pp. 34-35

[15] Schmitt D.,
Challenges for unconventional transport aircraft configurations,
In: Air&Space Europe, No. 3/4, Vol. 3,
May-August 2001, pp. 67-72

ICAS 2002

Toronto , September 12th 2002

Market Drivers and Innovation behind the Airbus Products

Presented by
Philippe Jarry
Vice President
Aircraft Evaluation

Toronto , September 12th 2002

Market Drivers and Innovation behind the Airbus Products

Contents

At any one time when we are to set the course for the future, we should first check that the objective is clear: not using whatever is available, but using it because it serves the objective. In the field of technology integration in airliners, we think the we should first ask the market to tell us what the main drivers are, then ask the Engineering Community about the technical opportunities that are at hand.

But, prior to make a decision, we should be animated by a vision: our aim, our responsibility, our contribution to the needs people have to move around the planet.

Dream and vision

Source Lilienthal-Museum Anklam

O. Lilienthal,
letter to Moritz von Egidy,
January 1894

"I have often listened to you with enthusiasm, when you refer to the borders not as separating the countries but rather as connecting them. I, too, have made it a lifelong task of mine to add a cultural element to my work, which should result in uniting countries and reconciling their people.
Our experience of today's civilisation suffers from the fact that it only happens on the surface of the earth. We have invented barricades between our countries, custom regulations and constraints and complicated traffic laws and these are only possible because we are not in control of the 'kingdom of the air', and not as 'free as a bird'.

Dreams are authorized to build-up the vision. Some people have contributed to make dreams come true, and in the field of aviation, Herr Otto Lilienthal is certainly one person we should remember. Like others, he has not spared efforts, putting his engineering skills in the adventure, spending all his money, and at the end, giving his life.

What people thought in year 1970

Many thought year 2000 would see

- VTOL aircraft dominate Short and Medium Range
- Supersonic & Hypersonic For Long Range
- Size go beyond 1000 seats and 150 tons of freight
- Propulsion to be either Hydrogen or Nuclear

…

Airbus vision was different

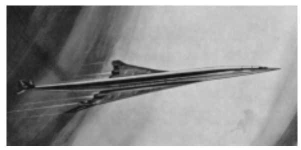

Family would be a keyword
And Technology that brings benefits
And Market Watch : what is needed ? and when ?

Dreams can remain dreams. When looking at what the "experts" believed in 1970 the air Transport industry would look like in year 2000, they were pretty definite!

Look at what happened in fact. Sometimes, the chains of the past are too heavy to allow us to imagine the ruptures that could happen. Sometimes, the rupture scenario is pushed in such a way that it would pre-suppose that all the environment also is subject to a rupture. In the pictures shown, there was absolutely no vision of the environmentalist pressure around the world that makes the air transport vehicle an "unfriendly" neighbor.

So, we need to enlarge our horizons.

Contents

An Air Transport vision

Our Market drivers

Using the new technologies

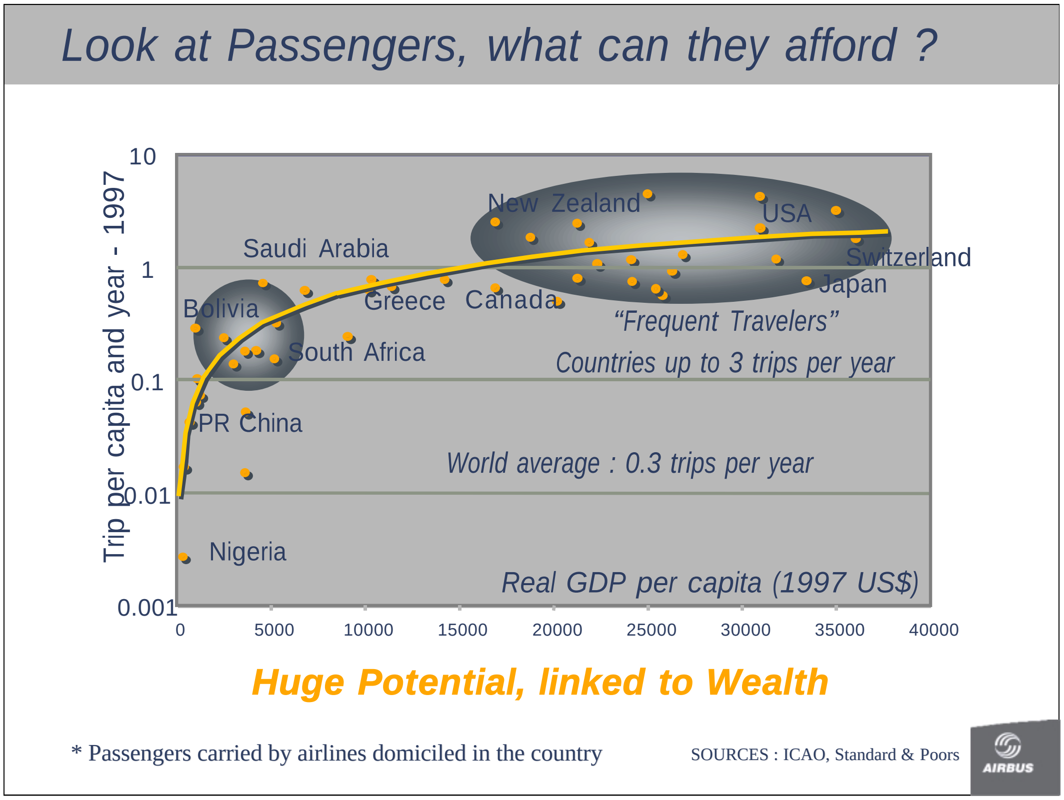

We all believe that air transport has become part of mankind way of life. Untrue!

Only a small portion of the world population "enjoys" the aircraft as a mean of transportation. There is room for improvement in our domain, before we will see the aircraft take part in everyone's life.

Growth, expansion is a buzz word in our industry. We will have to pay attention to the way we allow that growth to happen, and the consequences of such growth. Please note that as the economic development is determining the access to the airplane, the airplane operating cost is the prime issue here.

And people, they are so diverse! Different reasons for travel, meaning different expectations, different ways to enjoy the journey, different ways to look at the airplane. We believe that, in spite of the concurrent development of telecon supports, people will want to continue going around the planet.

To those who put the telecon and the air journey in a competitive situation, I might simply note that we are now asked to develop telecon means…aboard the airliners: the more you travel….the more you communicate…the more you communicate…the more you travel.

Another aspect that we have to consider when imagining the next vehicles and their interiors, access…is the population structure: the age distribution is changing, as is the size of the people.

But aircraft don’t carry only passengers …

- Aircraft carry only 1% of world-wide freight in volume …
- … but 38% in value
- Freight grows more rapidly than Passenger Market
- It’s extremely diversified : flowers,racing cars, live animals, “Beaujolais Nouveau”, computers …

AIRBUS

There is also the “silent” passenger, I mean the freight. A significant contributor to our industry, that is diversifying, and participate to the globalisation of the economy. Air transport of goods contributes to accelerate it. Speed and cost efficiency are the keywords here.

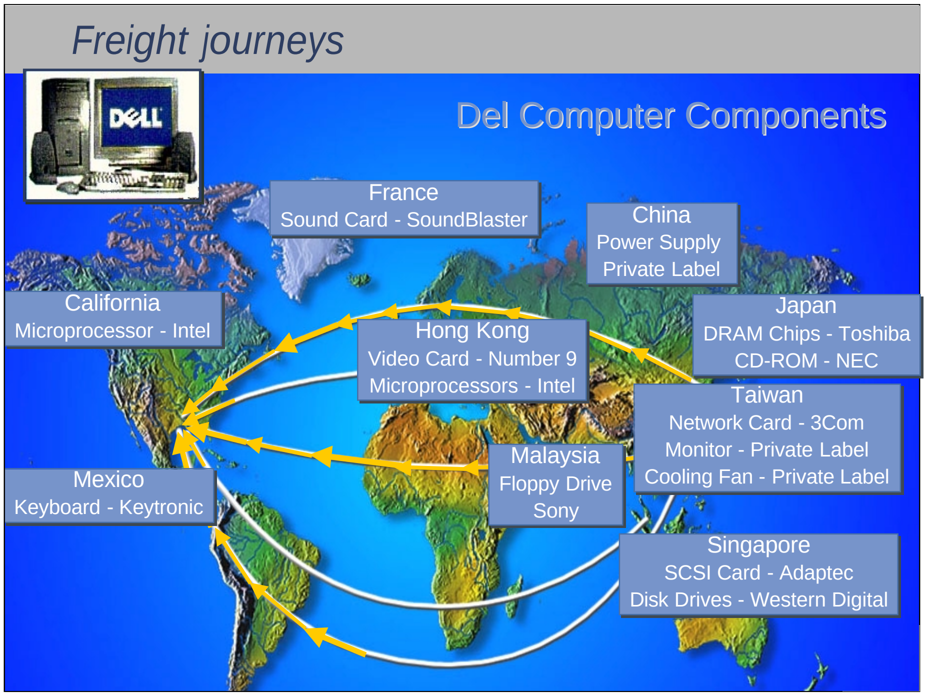

Just as an example, the pc on which I am working for this presentation comes from all over our planet. Flying one way, sometimes flying back and forth, just to make that little piece of equipment : it would be inconcievable to have the elements shipped from harbour to harbour, wasting time and increasing cost and risk.

A major Airlines' driver

A few quotes, read in Airline Business May 2002

"The business people are on the plane but *business fares* have declined"
G. Bethune, Continental

"We need to find an industry answer to the huge increase in war-risk *costs*"
L. Mullin, Delta

" The vicious circle of continuous operating *cash-flow* losses and spiralling debt to replace the aircraft fleet is unsustainable" A. Light, Salomon Smith Barney

Opening one magazine and retaining the keywords that some leaders of the airline industry are using when asked about their business: money, costs, revenues… I t is all there. The economic efficiency of whichever airplane we deliver to them will determine success or failure in a very competitive market. We believe that our airplanes will be evaluated around their economic efficiency, that is their overall life cycle cost and their earning power capabilities.

The Airline revenue nightmare

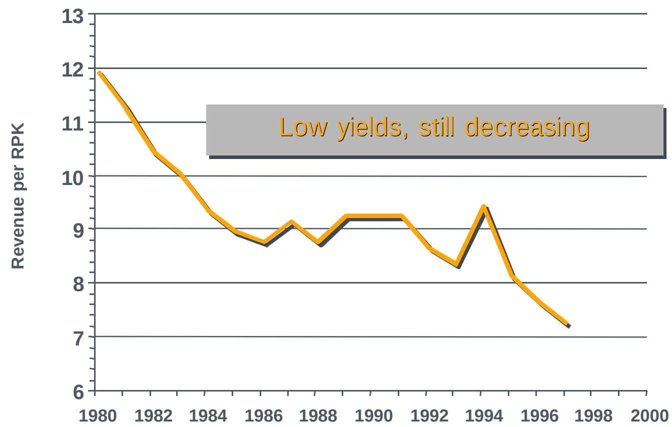

Source: ICAO Civil Aviation Statistics of the World

We said earlier that more people wanted to travel, and that the market is always more competitive. The airlines see, and they contribute to it, a down trend in their unit revenue. They put tremendous efforts in the parallel reduction of their unit costs. Some operators are nowadays referred to as “low-cost”.

The airplanes we will deliver over the coming years and decades will have to integrate the picture of the cost-revenue equation.As we do not believe that a significant portion of the passenger community will accept to see the ticket prices to go up.

The neighbours pressure

High Speed Train 300 km/h, 100 m away	*92 dB(A)*
Express Train 100 km/h, 100 m away	*88 dB(A)*
Bus in town, 8 m away	*82 dB(A)*
A320 during take-off, 700 m away	70 dB(A)

Flying is certainly exciting, but not for everybody… Airport neighbors don't seem to enjoy it. And they are more and more numerous.

Besides the airport neighborhood context, there is the growing concern that we share about the respect of the Environment and the aim of protecting a greener planet.

Air transport has a high degree of visibility, sometimes out of proportion with it real contribution in noise and emissions. It is a fact, and our airliners will need to be exemplary with their environment signature.

Answering the demand with the right tools

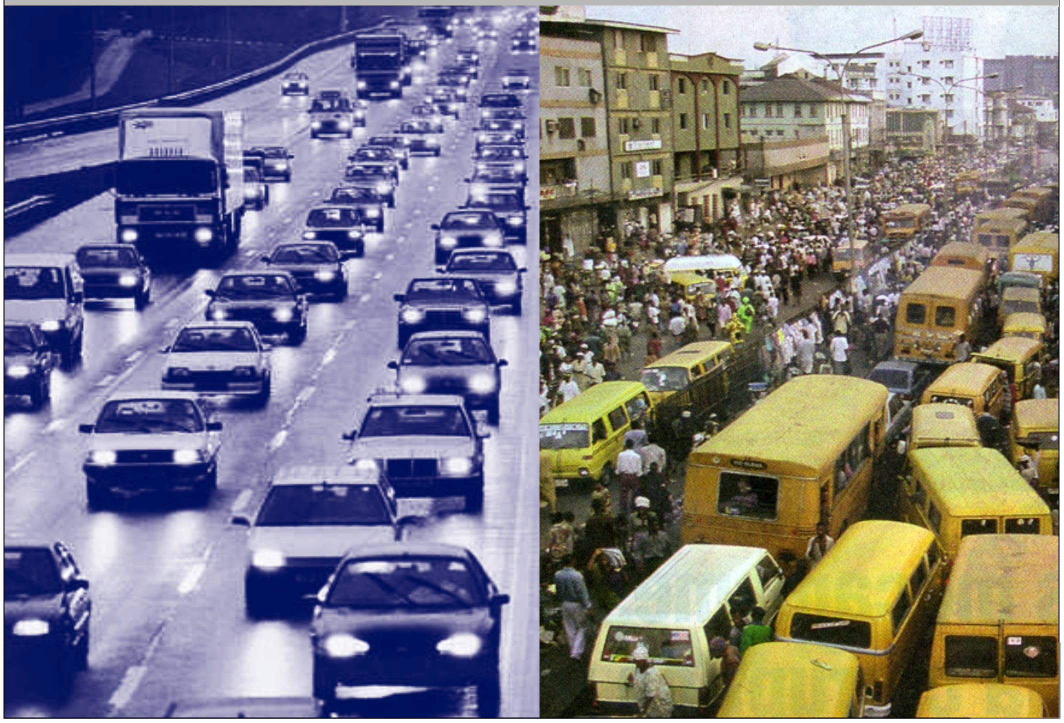

Life would be simple if one solution would fit everyone. This is not the case: diversity in demand, in geographic conditions, in markets require us to propose, at any given moment, a set of airplanes each responding to one set of requirements.

Contents

Meeting the Challenges

Drag Reduction

Weight Reduction

SFC

Priorities for R&T Action

Emissions

Safety & Security

Comfort & Convenience

Cost Reduction

Noise

In facing the challenge of diversity and the need to address the cost/revenue elements, the environment and the passenger service issues, we will have to integrate simultaneously aerodynamics, structure weights, noise reduction, manufacturing cost reduction, while offering a better space for the end customer.

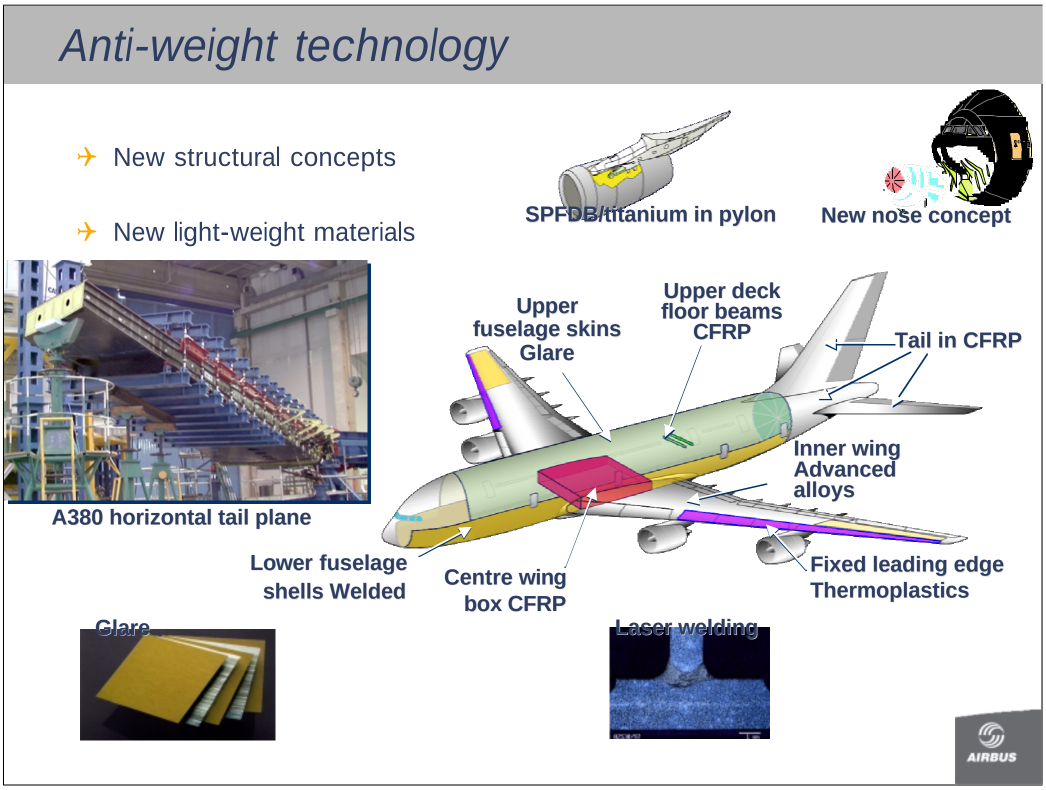

Starting with the aircraft weight, weight being one enemy of the aircraft performance, new materials and new structural concepts contribute to reach our targets. Significant testing is needed to validate the new materials before the decision is made to apply them.

GLARE Technology

- GLARE is a hybrid material, build-up from alternating layers of aluminum foils and unidirectional glass fibers, impregnated with an epoxy based adhesive.

- The "splicing concept" arranges two aluminum foils adjacent to each other (or with a slight overlap), resulting in one of the aluminum layers.
  Such splices are staggered with respect to each other, while the fiber adhesive layers are continuous.

Overlap splice using the "Self Forming Technique"

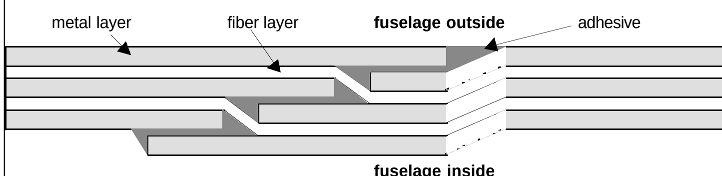

This is the case with Glare, a hybrid material that is selected for some of the fuselage panels of the A380

GLARE: Excellent Crack Growth Behavior

- A340 Large Panel Damage Tolerance Tests
  - crack above broken frame

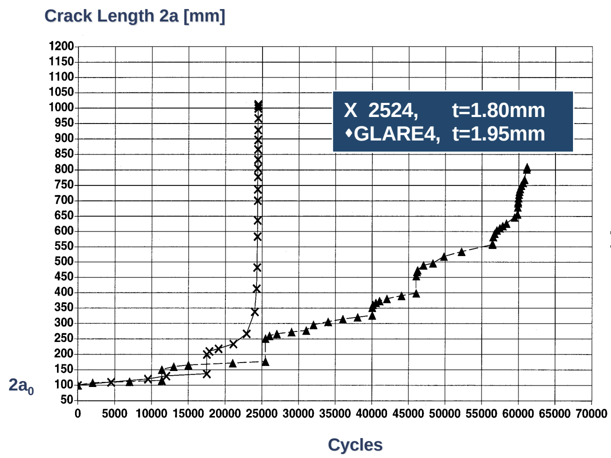

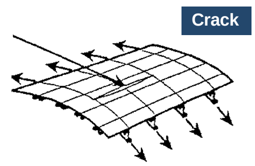

Crack extension by sawcut necessary, since crack stopped propagation.

Major Monolithic CFRP and Thermoplastics Applications

Future Perspectives- Structures

Vision of Composites / Hybrid Materials Application 2020

Immediate Future

25% Weight Share in A380 (2004)

- Section 19 and 19.1
- HTP / VTP
- Movables
- Beams
- Center Wing Box
- Wing Ribs
- Cowlings, Fairings
- Fuselage partly GLARE®

30% Weight Share in A400M (2006)

- Wings

Future (2020)

> 65% Composite Weight Share

- Composite / Hybrid Fuselage
- Objectives:
  30% Fuselage Weight Reduction,
  40% Cost Reduction

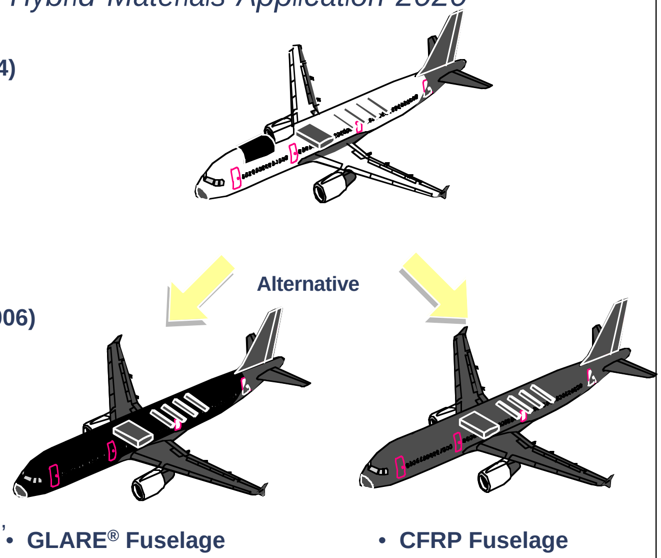

It has been an Airbus tradition to introduce new technologies step by step, as new airplane programs or new variants were under study.

Future Perspectives - Structures

CFRP Wing – Full Scale Test

Welding Technology for lower Fuselage Panels

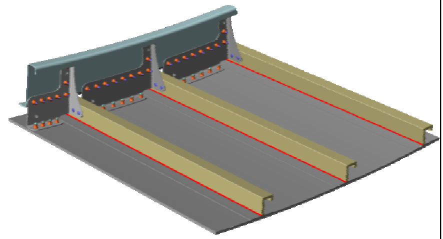

- Near term material candidates:
  Al 6xxx-series Alloys: Al 6013, Al 6056
- Advanced alloys under development:
  AlMgSc & AlMgLiSc & AlCuLiSc
- Initial application: Stringer-to-skin LBW
  for lower fuselage skins.
- Technology readiness for fuselage panels:
  - LBW of single & double curved panels confirmed.
  - More than 50 panels manufactured and successfully tested.
  - Initial application: A318
- Examples for potential further applications.
  - Fuselage panel/clip and clip/frame.
  - Panel/frame in cockpit area.
  - Center fuselage pressure bulk heads.

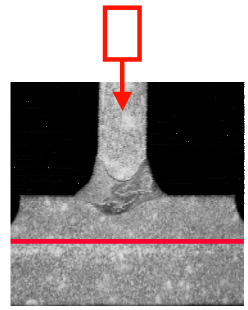

We estimate that welding techniques could lead to about 10% in weight reduction while delivering a 20% reduction in production costs. As an example, the panel riveting speed goes from typically .15 or .25 meter per minute up to 8 to 10 meters per minute.

Full-Scale demonstrator: Resin Film Infusion (RFI)

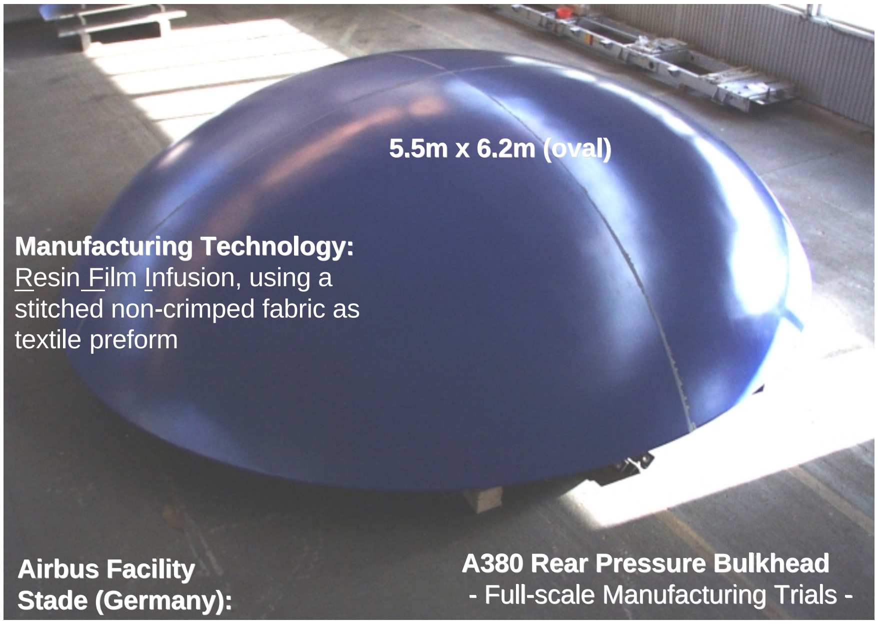

A380 rear pressure bulkhead produced with resin film infusion technology using a non-crimped fabric as textile preform. A340-500/600 bulkhead is manufactured with prepreg tapes. The advantage of CFRP design is a weight reduction of 27% compared to Al-design.

Another composites manufacturing technology is resin transfer moulding. One of the difficulties with "conventional" composites manufacturing , using pre-impregnated material - "prepreg", is that because the component is cured in an autoclave on a tool, all tolerances are thrown to the other surface.

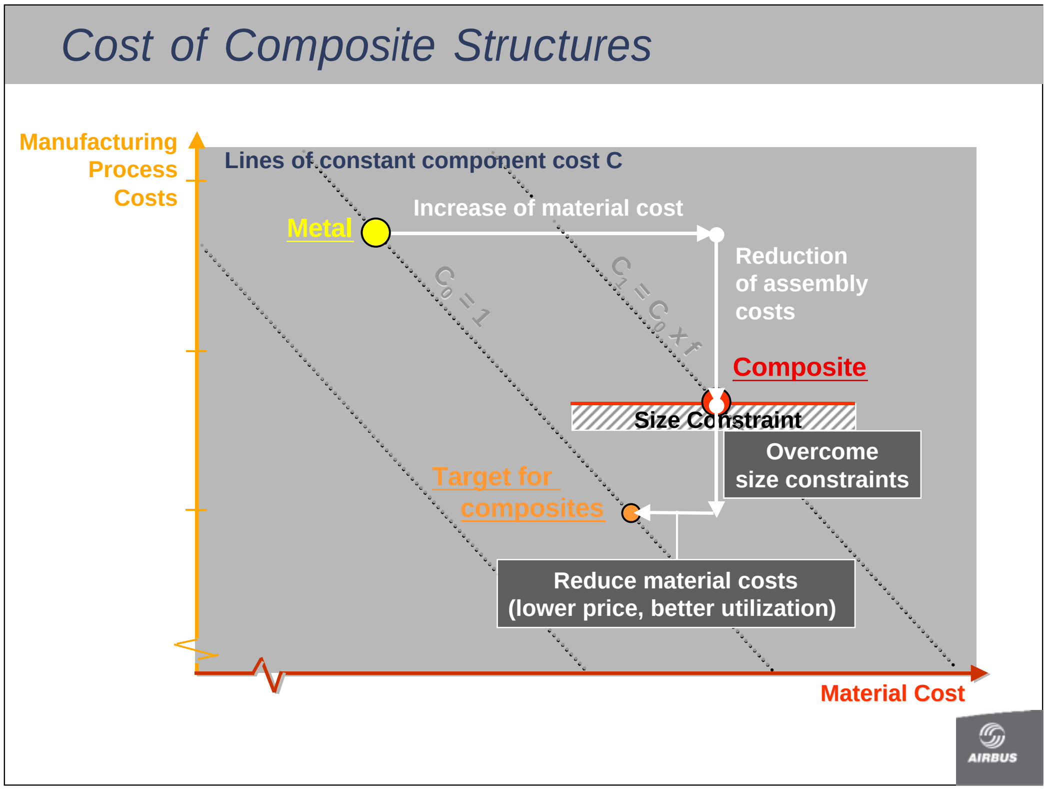

A careful cost/advantage analysis has to be conducted before the application of composites is made.

Here we see 2 Airbus facilities for the welding of both stringers to skins, and frame sections to skins.

Quality control is ensured through rigorous in-process monitoring

The tooling is also very simple and flexible, a holding fixture is all that is required.

Lasers are not only used to cut and weld parts, but increasingly for measurement.

Flexibility in tooling is a key objective within AIRBUS, especially for the A380 programme, and the use of laser measurement helps to make major strides towards this goal even in major assembly stages.

Automated Tape Laying (ATL)

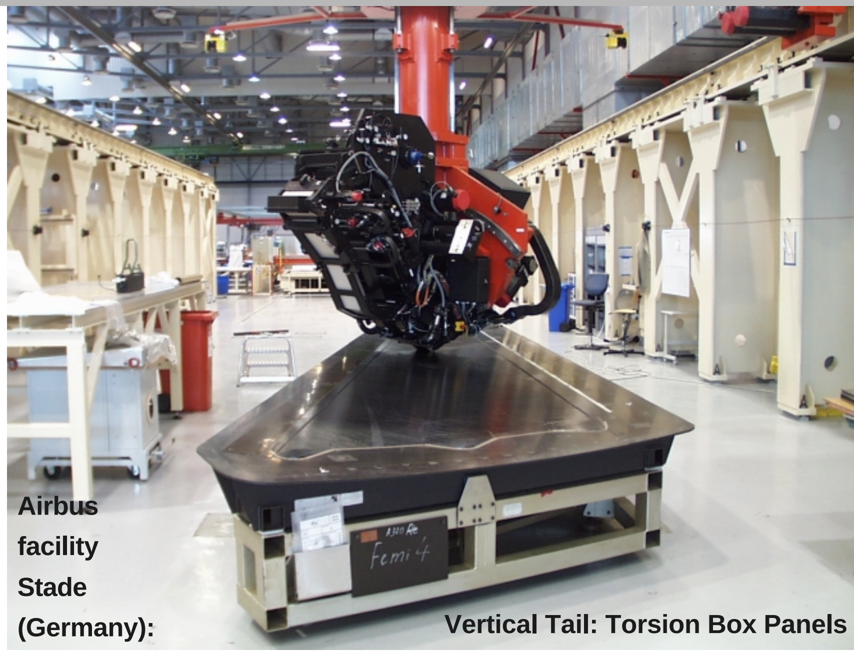

Wing production

Courtesy Air & Cosmos
24 mai 2002

Going to a moving line concept on a sub-assembly like the A320 wings allows for a reduction of production costs and delays by more than 10%. This concept, we feel, is very appropriate for an airplane part that is insensitive to customer customization.

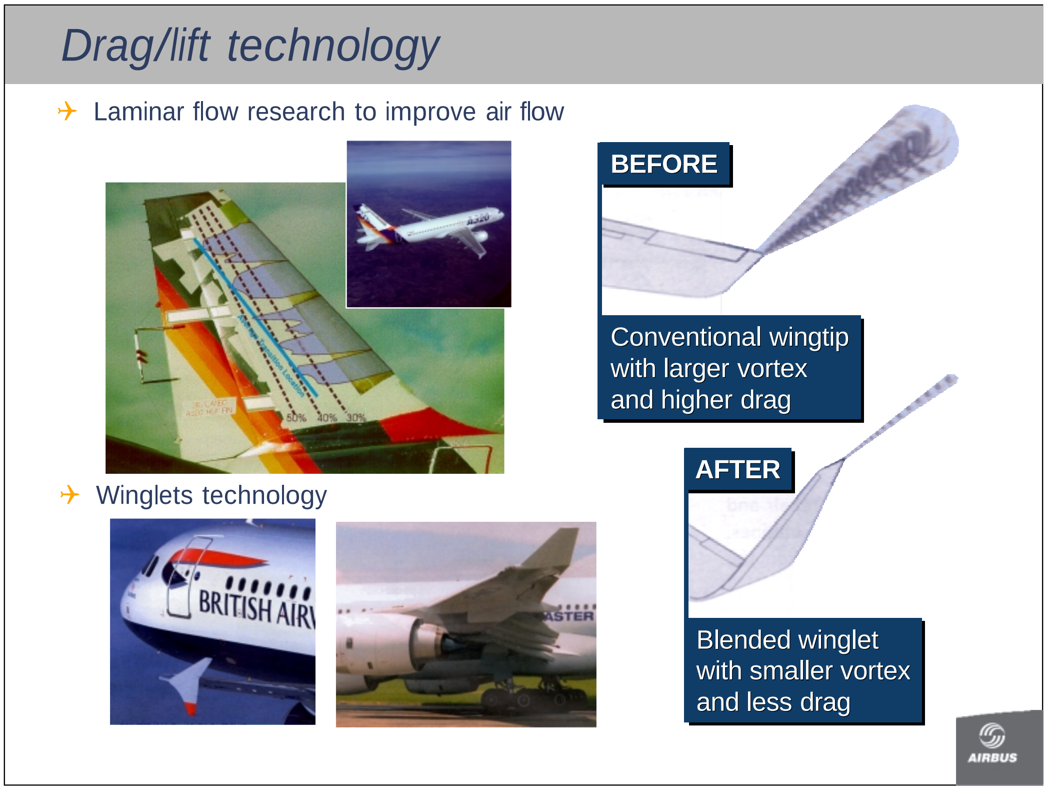

Operating costs reduction and added airplane productivity is obtained through a refinement of the aerolines . Improving the airflow on the surface is one area for research, here above shown in actual flight testing on an A320. The way the wing works evolves with the addition of wing tip devices, whether wing fences, or winglets. Each wing design must be tested with different shapes to determine which gives the best result overall.

Airbus has now launched a technology programme entitled Aircraft Wing with Advanced Technology OpeRation (AWIATOR). It is contributing 60% of the 80 million Euro budget. A large variety of technologies will be investigated, developed and flight-tested on Airbus' flying testbed A340, MSN001. AWIATOR aim is to achieve a five to seven per cent reduction in drag, a two per cent reduction in fuel burn in long-range operation, and a noise reduction of 2 EPNdb. The programme will look at new devices to reduce the aircraft wake, new airbrakes, very large wing tip devices, new devices for flow control..

Alongside Airbus engineering teams in Europe, more than twenty industrial partners in Europe and Israel as well as European research institutes will jointly work to develop and validate the sophisticated technologies. They will be supported by a number of European universities and test centers.

Matrix of wind tunnel test options

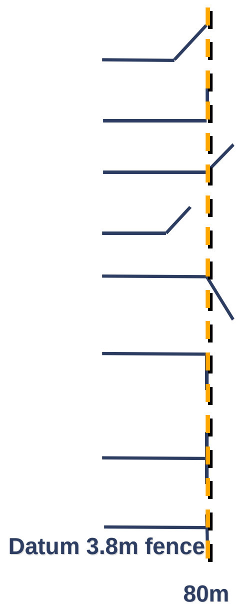

- Many different options tested
- 23 options tested at low speed (initially)
- 8 options tested at high speed (initially)
- Range of sizes from 3.8m to 6m
- Variations of cant angles & toe angles included
- 3.8m fence included (+ toe effect) at both low speed & high speed for correlation with datum

Drag / lift technology

- « Three surface aircraft » concept:
  - Lift distribution
  - Operational consequences
  - On Board noise

This is an example of research being conducted on lift surfaces .

Innovation in systems

High pressure hydraulic test bench

Water test bench

Variable frequency test bench

All systems can be the target for innovation. New technologies in electrical supply and distribution, in hydraulic supply, in water and waste that matters so much (weight, comfort, aircraft dispatch reliability). Full scale testing must be in place years before the airplane is put in service.

A380 innovation in cockpit & navigation

- Cockpit improvements are driven by *Flight safety enhancements*, *Lessons learnt from airlines* and *product added values:*

- camera/video, taxiing aids
- larger & interactive displays,
- FMS interface,
- enhanced ECAM,
- navigation on airports,
- take-off acceleration monitoring,
- on-board Information System
- thrust indication
- vertical situation awareness, collision avoidance
- enhanced crew rest

The "Airbus Cockpit Philosophy", results of customers feed-back, experience, and research on new technology

The Airbus approach in the domain of cockpît innovation is to retain the much airline praised inter-operability (Crew cross qualification between families of airliners) while introducing on the last generation the new technologies that enhance the safety, the crew procedures, the crew awareness, its comfort, etc.

AFIS - global scope

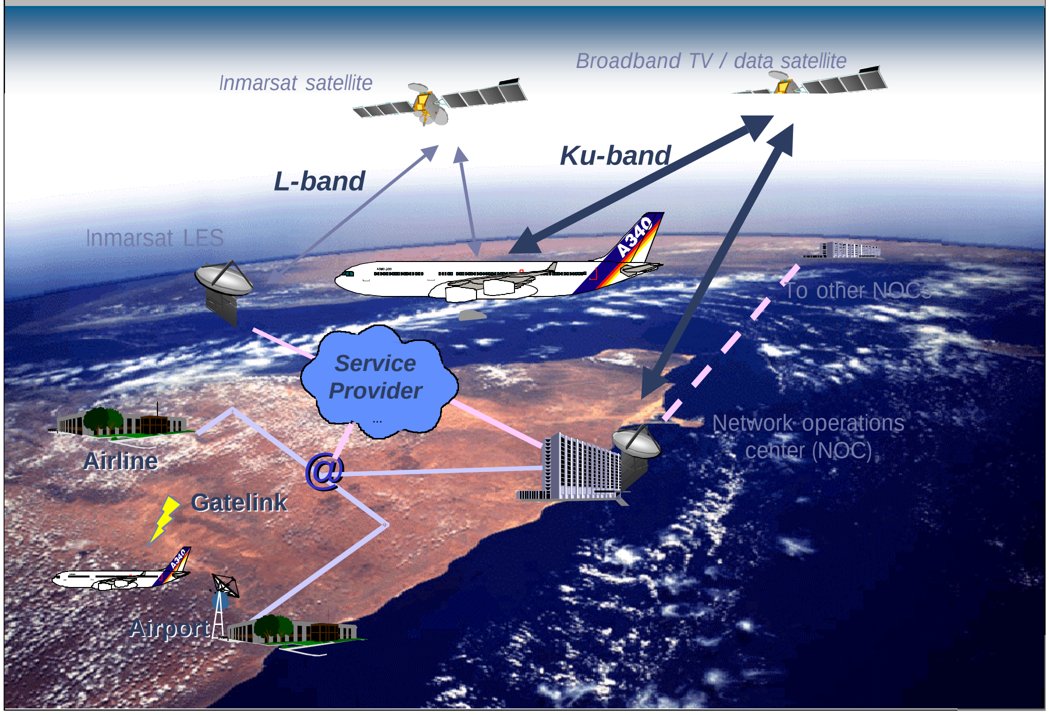

• Access for several users of various applications and services:

Flight crew

Cabin crew

Passengers

• Communication media

Existing ones: VHF/HF/ Satcom

New ones: Gatelink

High Speed Data communication through satellites

• Ground network Airport / Airline / Ground operation center

• End to end service provider: from the airline to the aircraft including content:

- weather maps

-e-mail and internet connections for passengers

<u>Conclusion:</u> Wide scope

Many potential users

Many players

Addressing the noise sources

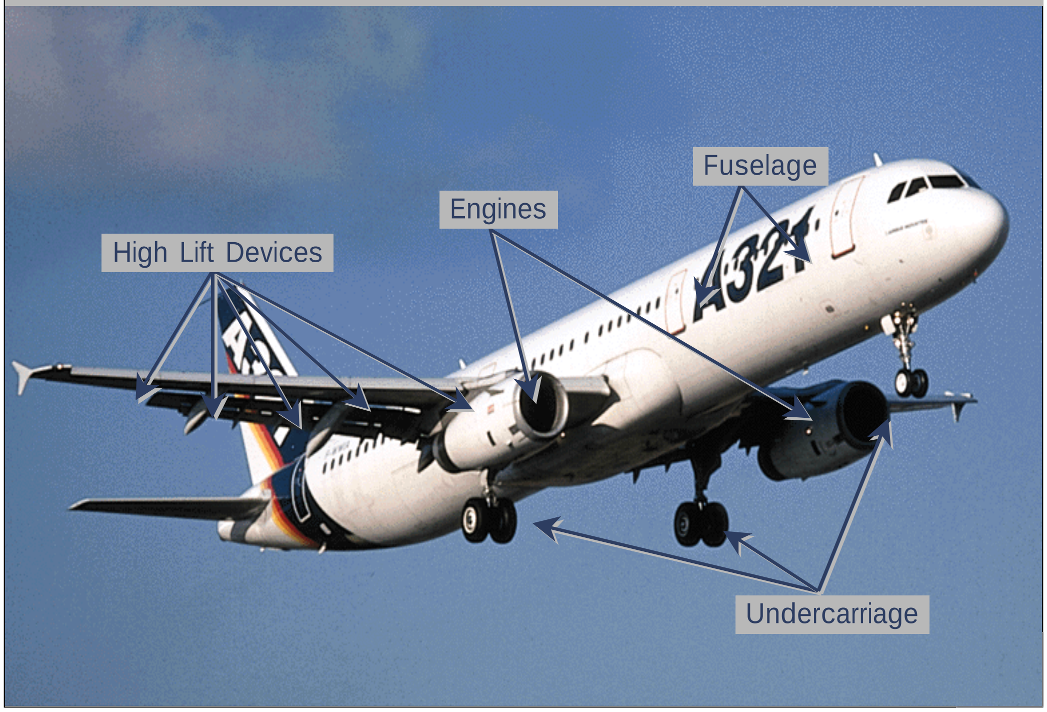

The aircraft external noise is an area that receives close attention and benefits from extensive research. Although the engines are the principal source of noise at take-off, the airframe contributes significantly during approach, a phase that concern significant populations around airports.

Outlined above are the main sources on which we are working: landing gears and high lift devices.

Reducing the noise generation (1)

- Moving from QC4 to QC2 on the A380
- Improved aircraft trajectory
- Actions taken :
  - Powerplant
    - Engines (116” fan,…)
    - Nacelle
  - Aerodynamic
  - Flutter
  - Aircraft configuration
    - Slides
    - Rotor burst
    - Wing/nacelle/pylon changes

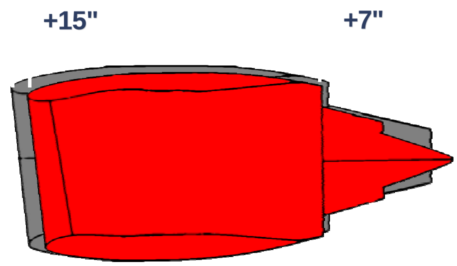

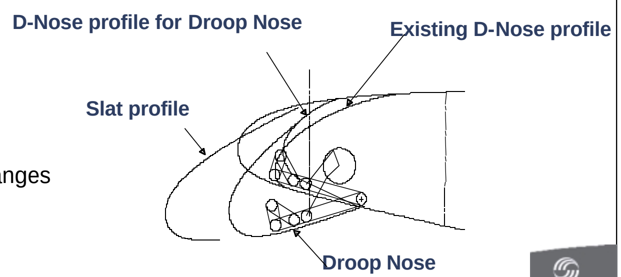

When it became apparent that the market expected that an airplane like the A380 due to enter service in 2006 had to pass the stringent noise requirement of London Heathrow airport (QC2 at take-off), a significant redesign of some areas of the airplane/engine combination was initiated. There was a cost in weight and performance, however the noise performance level was considered as having the n°1 priority.

Fairings for Noise Reduction

Theoretic Optimum

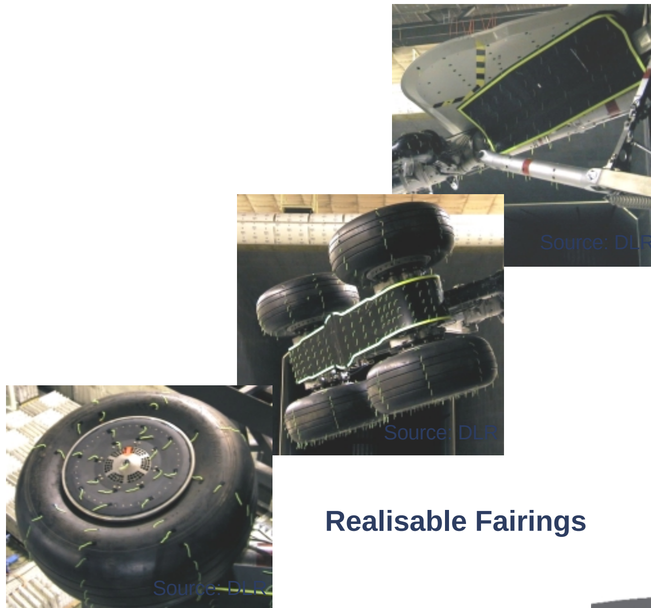

Realisable Fairings

Aerodynamic Noise – High Lift Devices

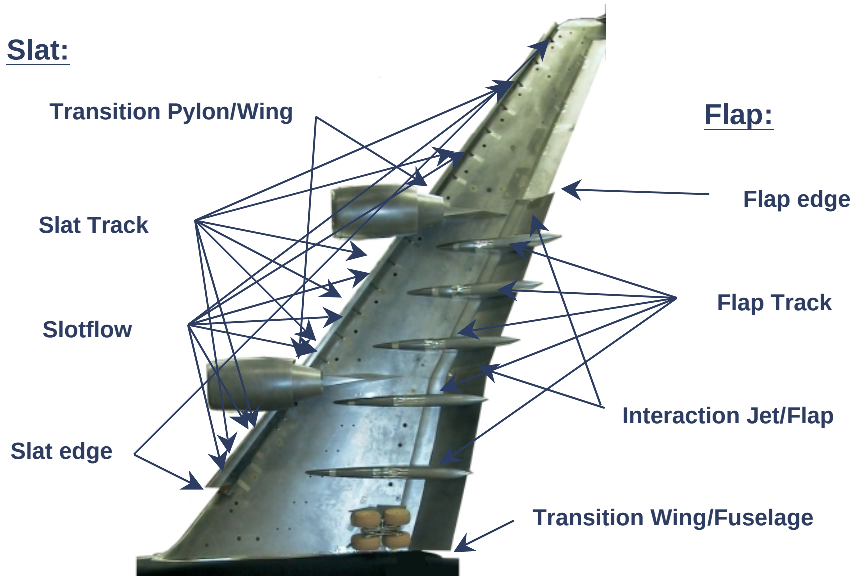

Noise Reduction – Aircraft Configuration

- Rear fuselage-mounted engines with appropriate empennage (V tail…)
- Shielded noise sources:
  - Upstream: Fan noise
  - Downstream: Fan, Combustion, Turbine noise
  - Limited shielding for jet noise;
- 5-9 dB improvement before source modifications

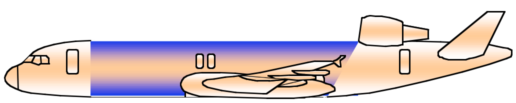

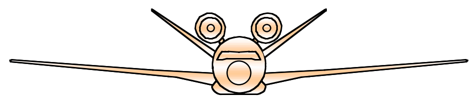

One could think of using the fuselage and the tail to shield the engine noise from reaching the ground. This is one configuration that the Airbus Future projects organization works on when looking for the lowest possible noise signature.

The ever-changing passenger

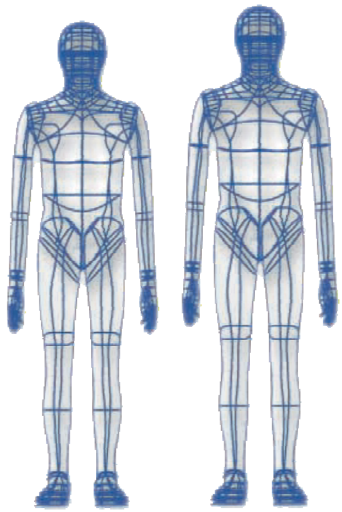

1960 *1990*

- On-board baggage

1960 *1990*

- More leisure
- Less Business
- More demanding

Don't forget the passenger who, by the way, is paying for the trip. He keeps changing, getting bigger, heavier (in most cases), more demanding, and wants to carry more stuff along… We will need to accommodate his numerous requirements.

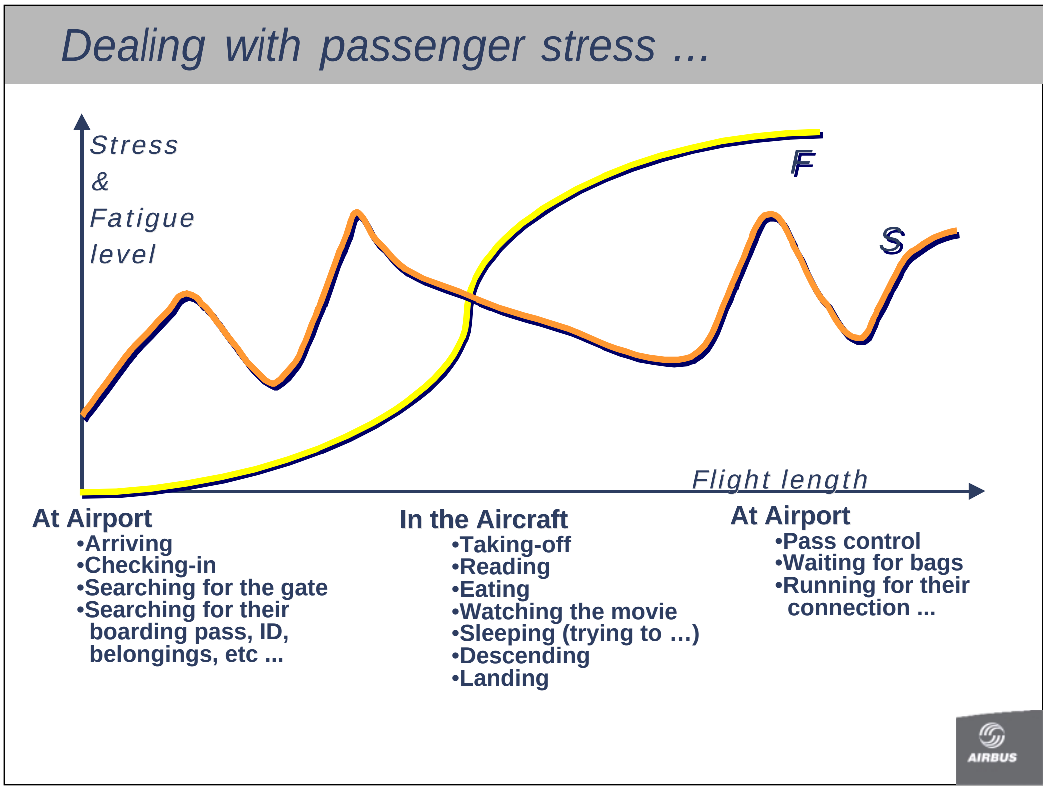

The air journey is not a complete pleasure: the body suffers, the brain and the heart, because of the stress. What can we bring to the passenger to relieve the tension, guarantee his health (air quality, enough volume, some freedom of movement, etc).

Passengers Access to Services

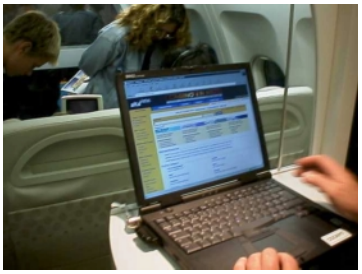

- Via personal laptop
  - E-Mail
  - On-board Internet
  - News, Sports, Business, Weather
  - Live Internet (under study)
  - Connectivity via
    - low speed modem
    - high speed USB or Ethernet
    - wireless LAN

- Via interactive seat-display
  - E-Mail (message service)
  - On-board Internet
  - News, Sports, Business, Weather

The passenger does not want to be disconnected. The air journey is not a journey on a cloud. He/she has left a place, certain people, he/she is going to meet with other people in another place. He/she is leaving, or he/she comes back, leading to a different set of feelings.

Whether in materials, in connections, or in cabin volume uses, new technologies allow for less weight, better flexibility//convertibility, or new opportunities.

And beyond in time ? Product Line of 2020 ?

SMALLER ?

FARTHER ?

FASTER ?

CHEAPER ?

BIGGER ?

GREENER ?

Where do we go from now? We will keep the eyes and ears open to make sure the market drivers are well understood and not overlooked. As far as we can see, we are convinced that the Air Transport industry shall be governed by economic efficiency and environmental concern.


AIRBUS
Setting the Standards

2002 Wright Brothers Lecture

DESIGN OF THE BLENDED-WING-BODY SUBSONIC TRANSPORT

R.H. Liebeck*
The Boeing Company
Long Beach, California

I. Background

It is appropriate to begin with a reference to the Wright Flyer itself, designed and first flown in 1903.

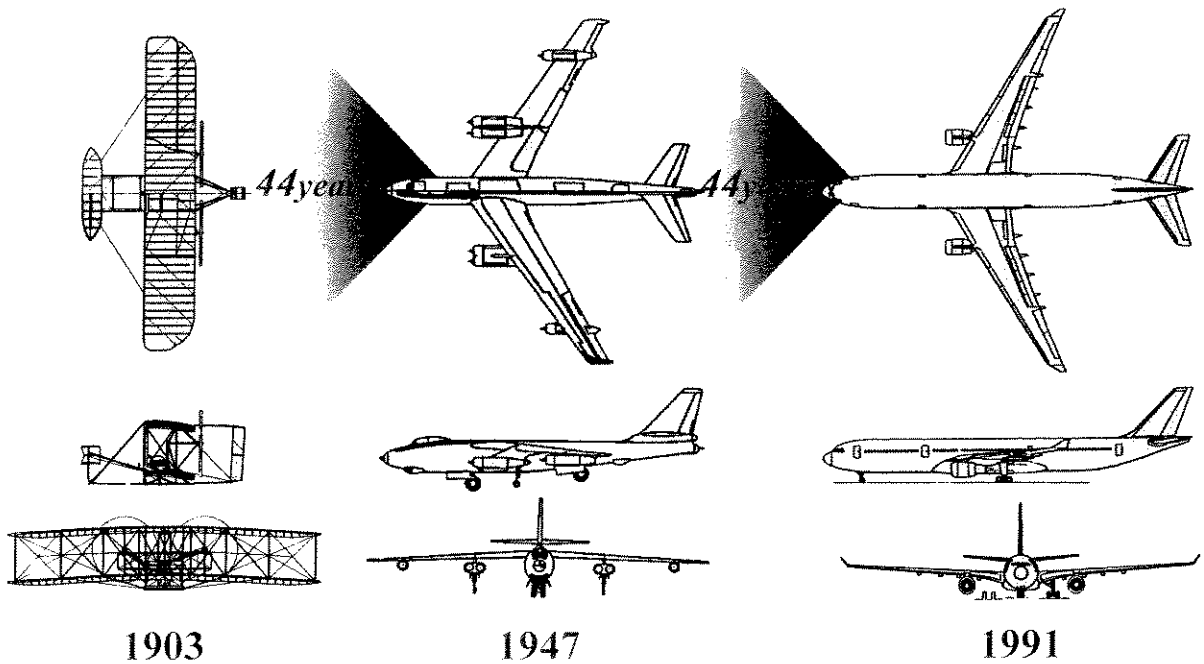

Figure 1 Aircraft Design Evolution: the first and second 44 years

A short 44 years later, the swept-wing Boeing B-47 took flight. Comparing these two airplanes shows a remarkable engineering accomplishment within a period of slightly more than four decades. Embodied in the B-47 are most of the fundamental design features of a modern subsonic jet transport: swept wing and empennage and podded engines hung on pylons beneath and forward of the wing. The Airbus A330, designed 44 years after the B-47, appears to be essentially equivalent, as shown in Figure 1.

Thus, in 1988, when NASA Langley's Dennis Bushnell asked the question: "Is there a renaissance for the long-haul transport?" there was cause for reflection. In response, a brief preliminary design study was conducted at McDonnell Douglas to create and evaluate alternate configurations. A preliminary configuration concept, shown in Figure 2, was the result. Here, the pressurized passenger compartment consisted of adjacent parallel tubes – a lateral

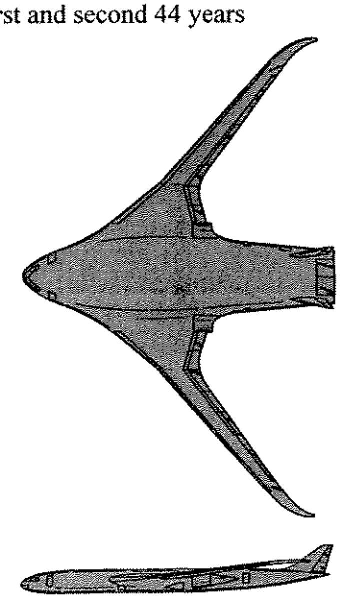

Figure 2 Early blended configuration concept

* Boeing Senior Technical Fellow, AIAA Fellow

extension of the double-bubble concept. Comparison with a conventional configuration airplane sized for the same design mission indicated that the blended configuration was significantly lighter, had a higher lift to drag ratio and a substantially lower fuel burn.

This paper is intended to chronicle the technical development of the Blended-Wing-Body (BWB) concept. Development is broken into three somewhat distinct phases: formulation, initial development and feasibility, and finally a description of the current Boeing BWB baseline airplane. NASA Langley Research Center funded the first two phases.

II. Formulation of the BWB Concept

The performance potential implied by the blended configuration provided the incentive for NASA Langley to fund a small study at McDonnell Douglas to develop and compare advanced technology subsonic transports for the design mission of 800 passengers and a 7000 nautical mile range at a Mach number of 0.85. Composite structure and advanced technology turbofans were utilized.

Defining the pressurized passenger cabin for a very large airplane offers two challenges. First, the square-cube law shows that the cabin surface area per passenger available for emergency egress decreases with increasing passenger count. Second, cabin pressure loads are most efficiently taken in hoop tension. Thus the early study began with an attempt to use circular cylinders for the fuselage pressure vessel as shown in Figure 3, along with the corresponding first-cut at the airplane geometry. The engines are buried in the wing root, and it was intended that passengers could egress from the sides of both the upper and lower levels. Clearly, the concept was headed back to a conventional tube and wing configuration. Therefore, it was decided to

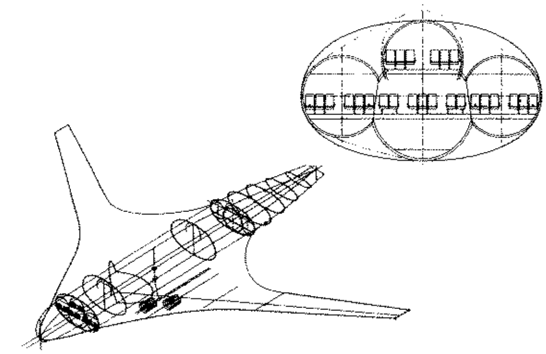

Figure 3 Early configuration with cylindrical pressure vessel and engines buried in the wing root.

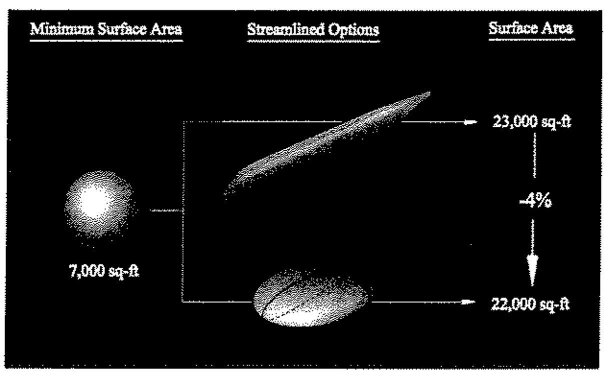

a. Effect of Body Geometry on Surface Area

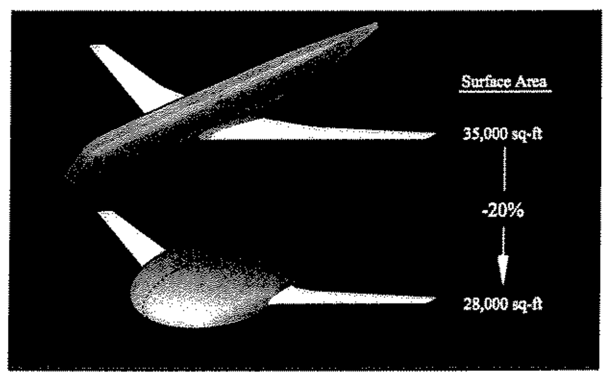

b. Effect of Wing-Body Integration on Surface Area

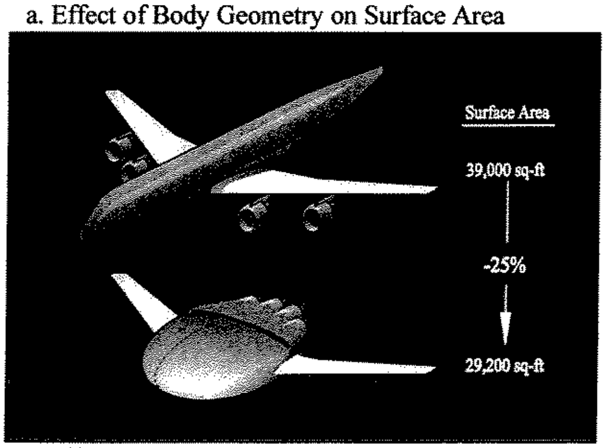

c. Effect of Engine Integration Surface Area

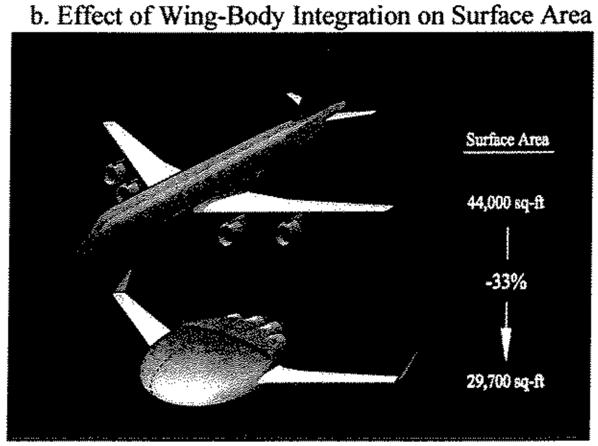

d. Effect of Complete Integration on Surface Area

Figure 4 Genesis of the BWB concept.

abandon the requirement for taking pressure loads in hoop tension, and assume that an alternate efficient structural concept could be developed. Removal of this constraint became pivotal for the development of the BWB.

Passenger cabin definition became the origin of the design, with the hoop tension structural requirement deleted. Three canonical forms shown in Figure 4a, each sized to hold 800 passengers, were considered. The sphere has minimum surface area, however, it is not streamlined. Two canonical streamlined options include the conventional cylinder and a disk, both of which have nearly equivalent surface area. Next, each of these fuselages is placed on a wing that has a total surface area of 15,000 ft^2. Now the effective masking of the wing by the disk fuselage results in a reduction of total aerodynamic wetted area of 7000 ft^2 compared to the cylindrical fuselage plus wing geometry, as shown in Figure 4b. Next, adding engines (Figure 4c) provides a difference in total wetted area of 10,200 ft^2. (Weight and balance require that the engines be located aft on the disk configuration.) Finally, adding the required control surfaces to each configuration as shown in Figure 4d results in a total wetted area difference of 14,300 ft^2, or a reduction of 33%. Since the cruise lift to drag ratio is related to the wetted area aspect ratio, b^2/S_{wet}, the BWB configuration implied a substantial improvement in aerodynamic efficiency.

The disk fuselage configuration sketched in Figure 4d has been used to describe the germination of the BWB concept. Synergy of the basic disciplines is strong. The fuselage is also a wing, an inlet for the engines and a pitch control surface. Verticals provide directional stability, control, and act as winglets to increase the effective aspect ratio. Blending and smoothing the disk fuselage into the wing achieved transformation of the sketch into a realistic airplane configuration. In addition, a nose bullet was added to offer cockpit visibility. This also provides additional effective wing chord at the centerline to offset compressibility drag due to the unsweeping of the isobars at the plane of symmetry.

Modern supercritical airfoils with aft camber and divergent trailing edges were assumed for the outer wing while the centerbody was to be based on a reflexed airfoil for pitch trim. A proper spanload implies a relatively low lift coefficient due to the very large centerbody chords. Therefore airfoil LW102A was designed for $c_l = 0.25$ and $c_{mc/4} = +0.03$ at $M = 0.7$ using the method of Reference 1. The resulting airfoil section is shown in Figure 5, along with a planform indicating how pitch trim is accomplished via centerbody reflex while the outboard wing carries a proper spanload all the way to the wingtip. Blending of this centerbody airfoil with the outboard supercritical sections yielded an aerodynamic configuration with a nearly elliptic spanload. At this early stage of BWB development, the structurally rigid centerbody was regarded as offering "free wingspan." Outer wing geometry was essentially taken from a conventional transport and "bolted" to the side of the centerbody. The result was a wingspan of 349 feet, a trapezoidal aspect ratio of 12, and a longitudinal static margin of – 15%, implying a requirement for a fly-by-wire control system.

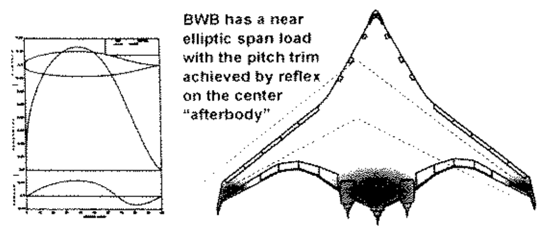

Figure 5 Original centerbody airfoil LW109A and planform showing pitch trim effector.

The aft engine location, dictated by balance requirements, offered the opportunity for swallowing the boundary layer from that portion of the centerbody upstream of the inlet, a somewhat unique advantage of the BWB configuration. In principle, boundary layer swallowing can provide improved propulsive efficiency by reducing the ram drag, and this was the motivation for the wide "mail-slot" inlet sketched in Figure 6. However, this assumed that such an inlet could be designed to provide uniform flow and efficient pressure recovery at the fan face of the engine(s).

Two structural concepts, sketched in Figure 7, were considered for the centerbody pressure vessel. Both required that the cabin be composed of longitudinal compartments to provide for wing ribs 150 inches apart to carry the pressure load. The first concept used a thin, arched pressure vessel above and below each cabin, where the pressure vessel skin takes the load in tension and is independent of the wing skin. A thick sandwich structure for both the upper and lower wing surfaces was the basis for the second concept. In this case, both cabin pressure loads and wing bending loads are taken by the sandwich structure. A potential safety issue exists with the separate arched pressure vessel concept. If a rupture were to occur in the thin arched skin, the cabin pressure would have to be borne by the wing skin, which must in turn be sized to carry the pressure load. Thus, once the wing skin is sized by this condition, in principle there is no need for the inner pressure vessel. Consequently, the thick sandwich concept was chosen for the centerbody structure.

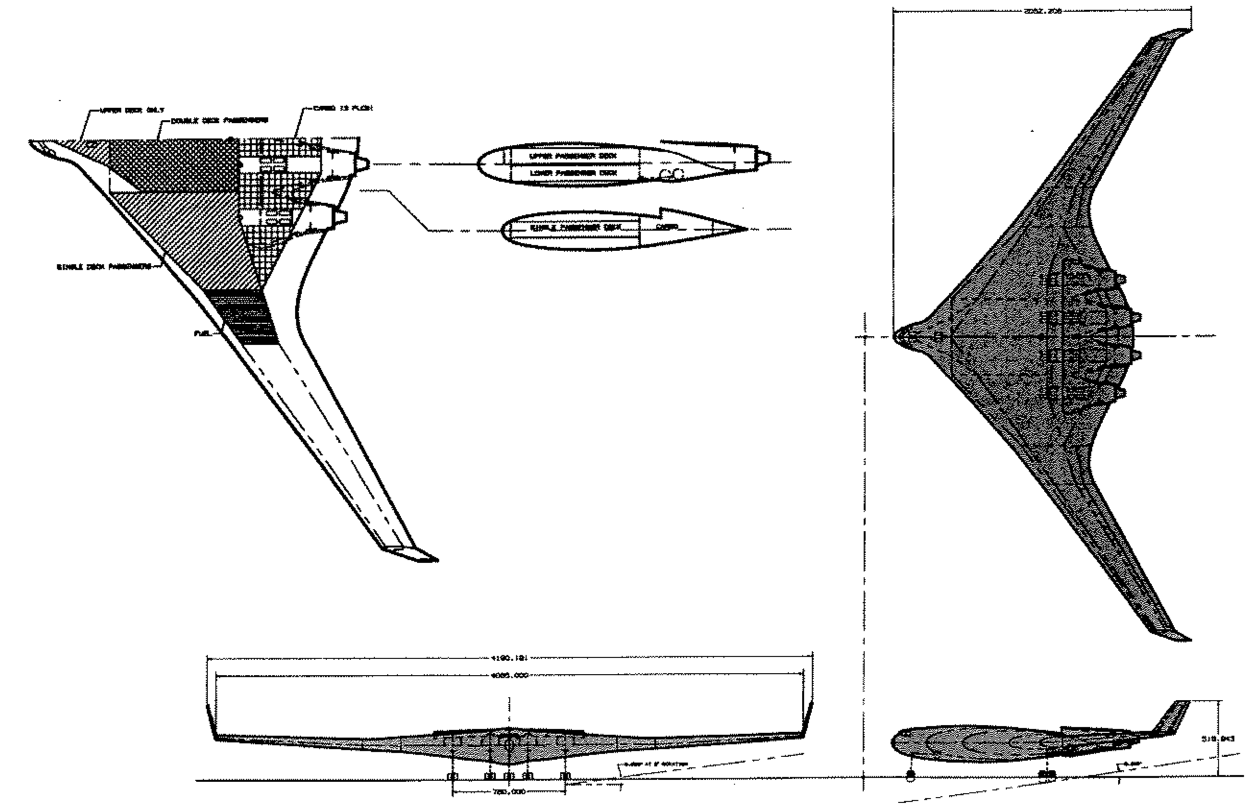

Figure 6 First Generation Blended-Wing-Body

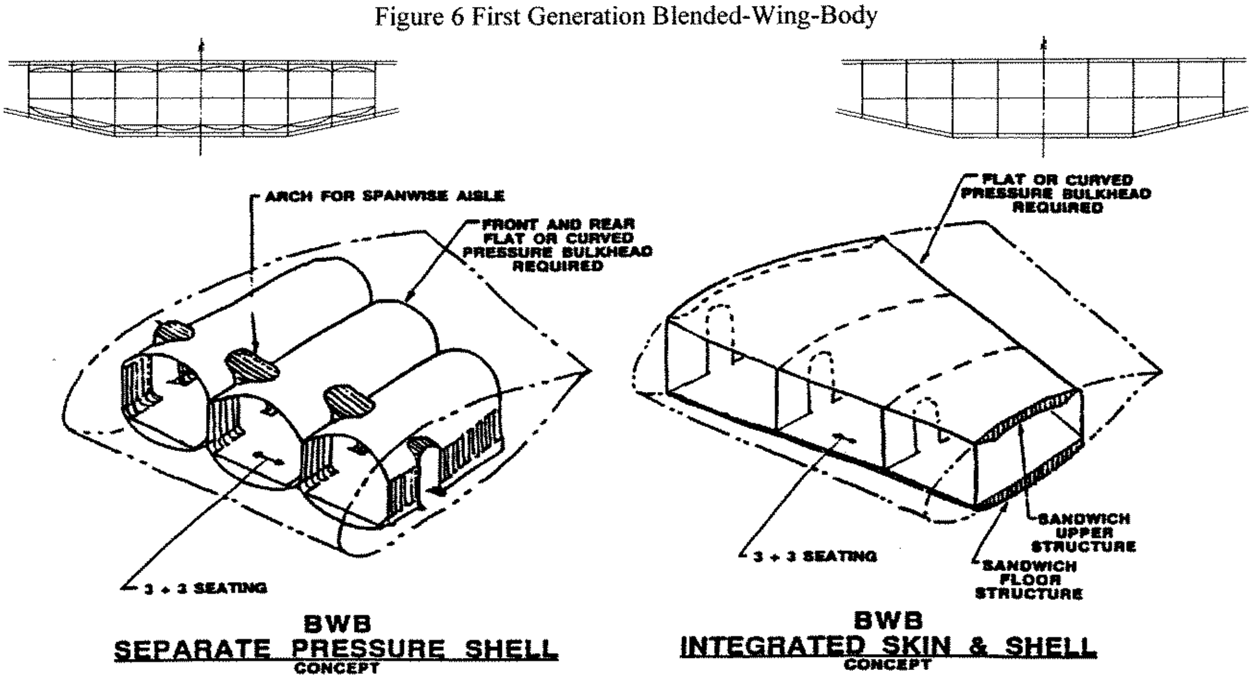

Figure 7 Centerbody pressure vessel structural concepts.

A 3-view of the original BWB is given in Figure 6, and a description of the packaging of the interior is also shown there. Passengers are carried in both single and double deck cabins, and the cargo is carried aft of the passenger cabin. As a tailless configuration, the BWB is a challenge for flight mechanics, and the early control system architecture is shown in the isometric view in Figure 8. A complete description of original BWB study is given in Reference 2. Future generations of BWB designs would begin to address constraints not observed by this initial concept, but the basic character of the aircraft persists to this day.

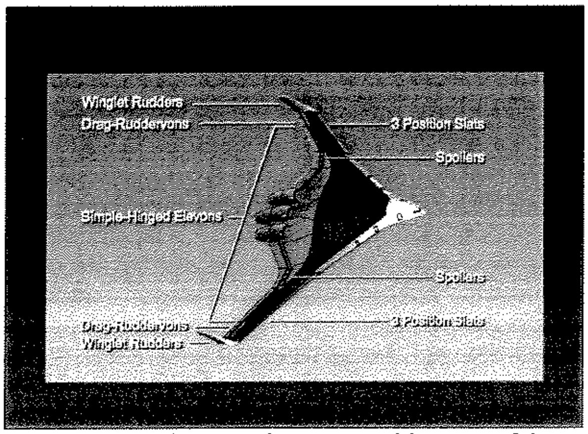

Figure 8 Flight control system architecture of the first-generation BWB

III. BWB Design Constraints

As an integrated airplane configuration, the BWB must satisfy a unique set of design requirements. Included are the following:

Volume
Passengers, cargo and systems must be packaged within the wing itself. This leads to a requirement for the maximum thickness-to-chord ratio on the order of 17%; a value that is much higher than is typically associated with transonic airfoils.

Cruise Deck Angle
Since the passenger cabin is packaged within the centerbody, the centerbody airfoils must be designed to generate the necessary lift at an angle of attack consistent with cabin deck angle requirements (typically less than 3 degrees). Taken by itself, this requirement suggests the use of positive aft camber on the centerbody airfoils.

Trim
A BWB configuration is considered trimmed (at the nominal cruise condition) when the aerodynamic center-of-pressure is coincident with the center-of-gravity, and all of the trailing edge control surfaces are faired. Positive static stability requires that the nose-down pitching moment be minimized. This limits the use of positive aft camber and conflicts with the deck angle requirement above.

Landing Approach Speed and Attitude
BWB trailing edge control surfaces cannot be used as flaps since the airplane has no tail to trim the resulting pitching moments. Trailing edge surface deflection is set by trim requirements, rather than maximum lift. Therefore, the maximum lift coefficient of a BWB will be lower than that of a conventional configuration, and hence the wing loading of a BWB will be lower. Also, since there are no flaps, the BWB's maximum lift coefficient will occur at a relatively large angle-of-attack, and the flight attitude during approach is correspondingly high.

Buffet and Stall
The BWB planform causes the outboard wing to be highly loaded. This puts pressure on the wing designer to increase both the outboard wing chord and washout, which degrades cruise performance. A leading-edge slat is required outboard for low speed stall protection. These issues apply to a conventional configuration, but they are exacerbated by the BWB planform.

Power for Control Surface Actuation
Tailless configurations have short moment arms for pitch and directional control, and therefore multiple, large, rapidly moving control surfaces are required. Trailing-edge devices and winglet rudders are called upon to perform a host of duties including basic trim, control, pitch stability augmentation and wing load alleviation. Since some of the control surfaces can perform multiple functions (e.g. the outboard elevon/drag rudder offers pitch, roll and yaw authority), control surface allocation becomes a critical issue. The mere size of the inboard control surfaces implies a constraint on the airfoil design to minimize hinge moments. Hinge moments are related to the scale of the control surface as follows: The area increases as the square of the scale, and in turn the moment increases with the cube of the scale. Once the hydraulic system is sized to meet the maximum hinge moment, the power requirement becomes a function of rate at which a control surface is moved.

If the BWB is designed with a negative static margin (unstable), it will require active flight control with a high bandwidth, and the control system power required may be prohibitive. Alternatively, designing the airplane to be stable at cruise requires front-loaded airfoils, washout and limited (if any) aft camber. This implies a higher angle-of-attack which in turn threatens the deck angle constraint.

Manufacturing
The aerodynamic solution to the design constraints just listed can readily result in a complex three-dimensional shape that would be difficult and expensive to produce. Therefore, the aerodynamicist must strive for smooth, simply curved surfaces that at the same time satisfy the challenging set of constraints described above.

IV. Initial Development and Feasibility

A NASA/industry/university team was formed in 1994 to conduct a three-year NASA-sponsored study to demonstrate the technical and commercial feasibility of the BWB concept. McDonnell Douglas was the program manager, and the team members included NASA Langley, NASA Lewis, Stanford University, the University of Southern California, the University of Florida and Clark-Atlanta University. The original 800-passenger 7000 nautical mile design mission was retained. This work is summarized in Reference 3.

Configuration definition and sizing
This study began with a refined sizing of the initial BWB configuration of Figure 7 where minimum takeoff gross weight (TOGW) was set as the figure-of-merit. Primary constraints included an 11,000-foot takeoff field length, 150-knot approach speed, low-speed trimmed C_{Lmax} of 1.7, and a cruise Mach number of 0.85. Initial cruise altitude (ICA) was allowed to vary to obtain minimum TOGW, but with the requirement that the ICA be at least 35,000 feet. This yielded a trapezoidal wing of aspect ratio of 10 with a corresponding span of 280 feet and an area of 7840 ft^2. The resulting trapezoidal wing loading was on the order of 100 lb/ft^2 – substantially lower than the 150 lb/ft^2 typical of modern subsonic transports. An explanation offered was that a significant portion of the trapezoidal wing is in effect hidden by the centerbody, and therefore the cost of trapezoidal wing area on airplane drag is reduced. This in turn allowed the airplane to optimize with a larger trapezoidal area to increase span with a relatively low

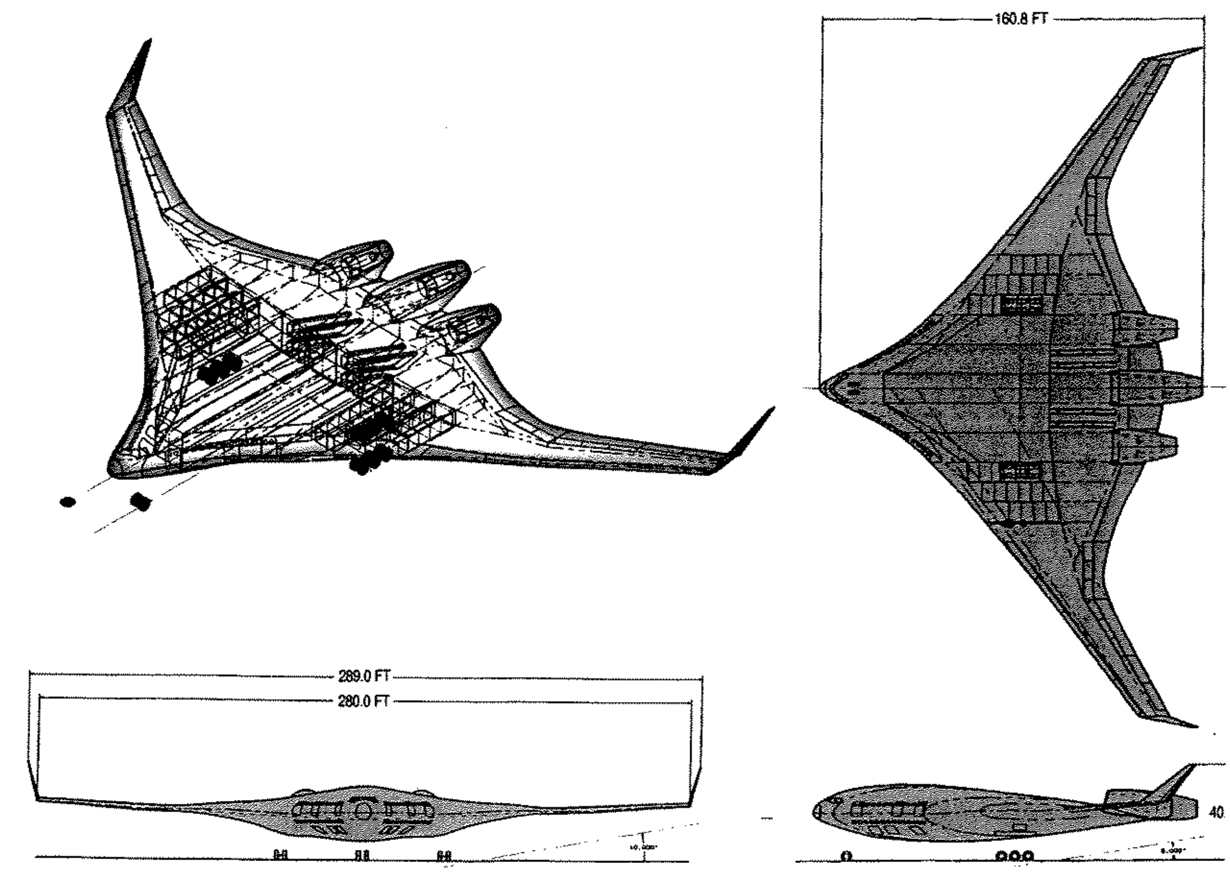

Figure 9 Second-generation Blended-Wing-Body.

cost on weight. A 3-view and isometric of the resulting second-generation BWB is given ih Figure 9.

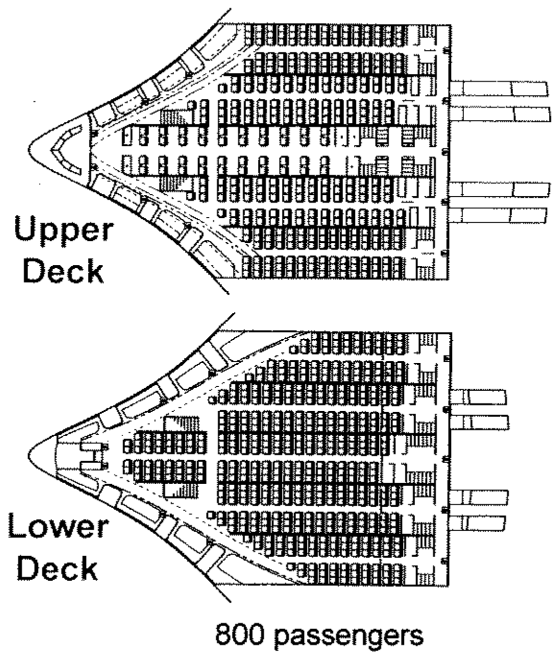

Figure 10 Interior arrangement of passenger cabin.

The double-deck BWB interior was configured with ten 150-inch wide passenger cabin bays as shown in Figure 10, with cargo compartments located outboard Figure 10 Interior arrangement of passenger cabin of the passenger bays and fuel in the wing, outboard of the cargo. Considerations and constraints included weight and balance, maximum offset of the passengers from the vehicle centerline (ride quality) and the external area of the cabin. Since this is the surface area of the pressure vessel, the extent of this area has a significant effect on the structural weight of the centerbody. The cabin partitions are in fact wing ribs that are primary structure. Windows were located in the leading edge on both decks, and the galleys and lavatories were located aft to help provide the passengers with an unobstructed forward view. Egress was via the main cabin doors in the leading edge, and through aft doors in the rear spar.

Aerodynamics

Some insight of the aerodynamic design of the BWB is provided in Figure 11, where the trade between wing chord, thickness and lift coefficient is shown. The outboard wing is moderately loaded, similar to a conventional configuration, where drag is minimized with a balance between wetted area and shock strength. Moving inboard, the centerbody with its very large chord calls for correspondingly lower section lift coefficients to maintain an elliptic spanload. The low section lift requirement allows the very thick airfoils for packaging the passenger compartment and trailing edge reflex for pitch trim.

Navier Stokes computational fluid dynamics (CFD) methodology in both the inverse design and direct solution modes was employed to define the final BWB geometry. A solution showing the pressure

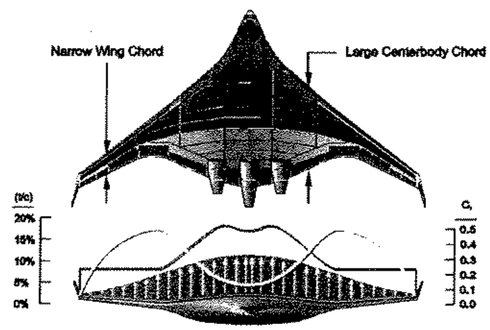

Figure 11 Section lift coefficient and thickness-to-chord ratio variation with span.

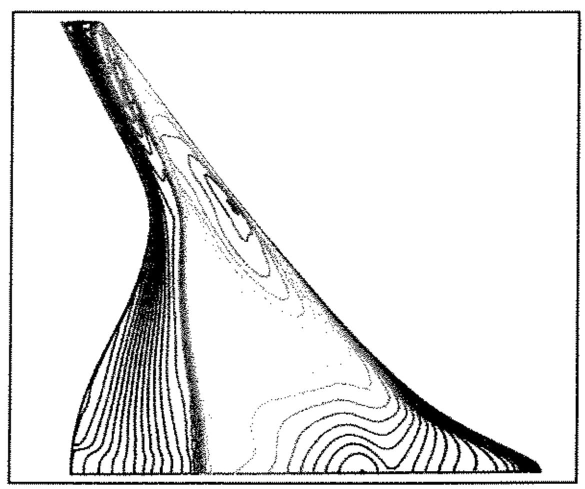

Figure 12 Navier Stokes computed upper surface pressure distributions.

distribution at the mid-cruise condition is shown in Figure 12. The typical shock on the outboard wing is smeared into a compression wave on the centerbody. The flow pattern on the centerbody remained essentially invariant with angle of attack, and flow separation is initiated in the kink region between the outboard wing and the centerbody. Outer wing flow remains attached, providing lateral control into the stall regime. Similarly, the flow over the centerbody remains attached and provides a nearly constant flow environment for the engine inlets. This flow behavior is a consequence of significant lateral flow on the centerbody that provides a three-dimensional relief of compressibility effects. However, the relief on the centerbody is traded for a transonically stressed flow environment in the kink region. This is the ideal spanwise location for the stall to begin, from a flight mechanics point of view: the ailerons remain effective, and pitch-up is avoided.

Wind Tunnel Tests

Transonic and low-speed wind tunnel tests of the BWB configuration of Figure 9 were conducted at NASA LaRC in the National Transonic Facility (NTF), and this represented an invaluable opportunity to test at close to the full-scale Reynolds number. Figure 13 shows the BWB model mounted in the

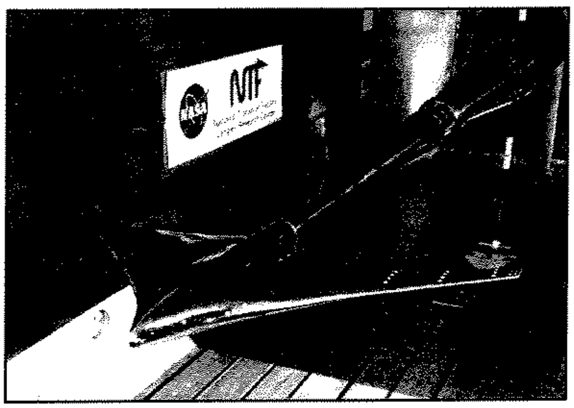

Figure 13 BWB in the NASA LaRC National Transonic Facility (NTF)

tunnel, and NTF results are compared with CFD predictions in Figure 14. Excellent agreement for lift, drag and pitching moment as well as wing

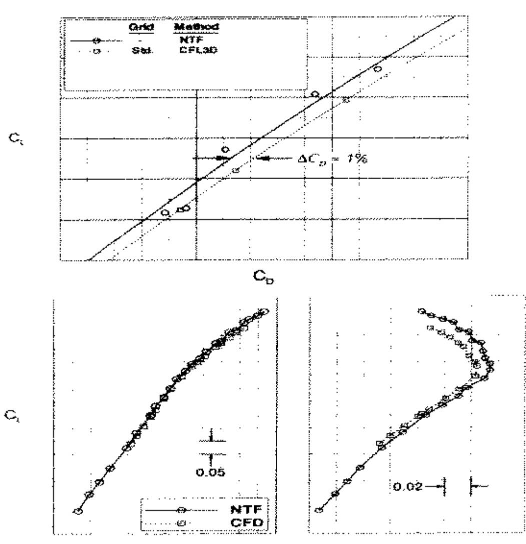

Figure 14 Comparison of CFD predictions with NTF wind tunnel results.

pressure distributions is shown, including up to and beyond buffet onset. A primary objective of the test was to establish the effectiveness of the current state-of-the-art CFD methods for predicting the aerodynamic characteristics of a BWB airplane. The remarkable agreement indicated that CFD could be reliably utilized for the aerodynamic design and analysis.

A low-speed test of a powered 4% scale BWB was conducted in the NASA LaRC 14x22 foot wind tunnel (Figure 15). Results verified trimmed C_{Lmax} estimates, showed favorable stall characteristics and excellent control power through stall. Power effects were found to be much smaller than expected.

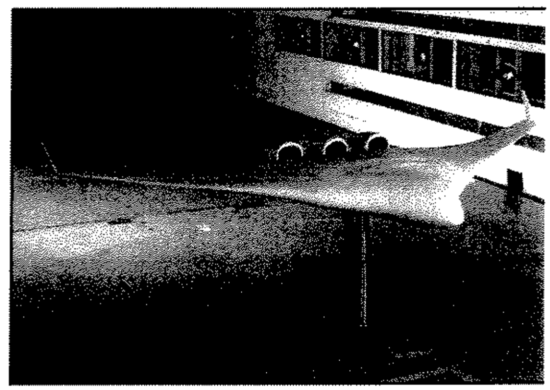

Figure 15 Powered BWB model in the NASA LaRC 14x22 foot tunnel for low-speed test.

Stability and Control

During development of the second-generation BWB it was assumed and accepted that the airplane would be statically unstable in order to achieve high cruise efficiency (L/D). Balance of the airplane was achieved by sliding the wing fore and aft on the centerbody, much like the procedure for a conventional configuration. However, this was clearly a more complex process due to the integrated nature of the BWB. The low effective wing loading meant that a trailing edge flaps would not be required, but a leading-edge slat on the outboard wing is required for the same reason as a conventional airplane, and the simple-hinged trailing-edge control surfaces function as elevons. Flight-critical stability augmentation and envelope protection was considered a requirement.

The outboard elevons are the primary pitch and roll controls, since they have the largest lever arm about the center-of-gravity. Figure 16 shows the pitch authority of the individual elevons, as well as the locus of their effective centers of pressure. It can be seen that they yield relatively short lever arms about the center-of-gravity, and even shorter lever arms about the landing gear for takeoff rotation. However, total control power is substantial due to the full span of elevons. The winglets with rudders provide primary directional stability and control. For the low-speed engine-out condition, the outboard elevons become split drag rudders similar to those on the B-2, as shown in Figure 17.

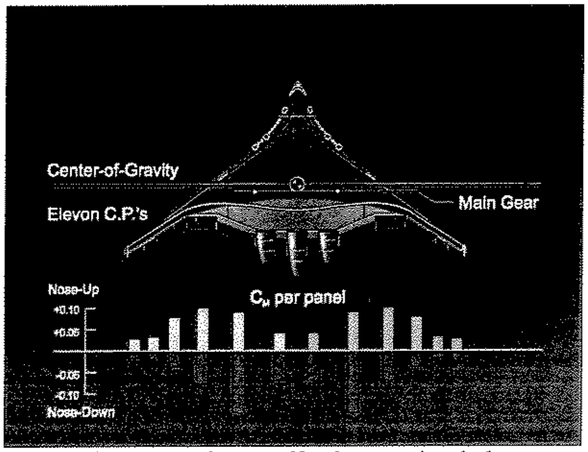

Figure 16 Elevon effectiveness in pitch.

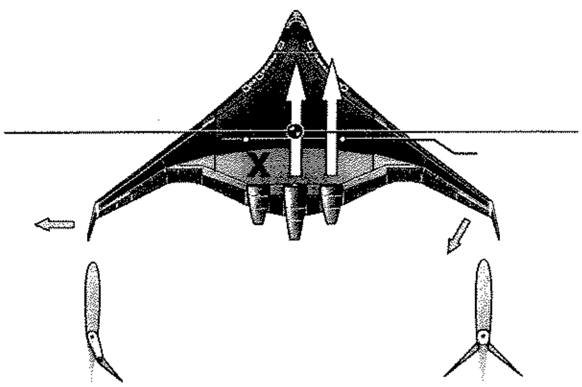

Figure 17 Yaw control

Flight Demonstrator
Low speed flight mechanics were explored with a 6% scale Flight Control Testbed (Figure 18), built at Stanford University under NASA sponsorship. Called the BWB-17, the airplane had a 17-foot wingspan, weighed 120 lbs and was powered by two 35cc two-stroke engines with propellers. The model was dynamically scaled to match the flight characteristics of the full scale BWB. Stability augmentation was provided by an on-board computer, which also recorded flight test parameters. The first flight of the BWB-17 took place on July 29, 1997 at El Mirage Dry Lake in California. Excellent handling qualities were demonstrated within the normal flight envelope.

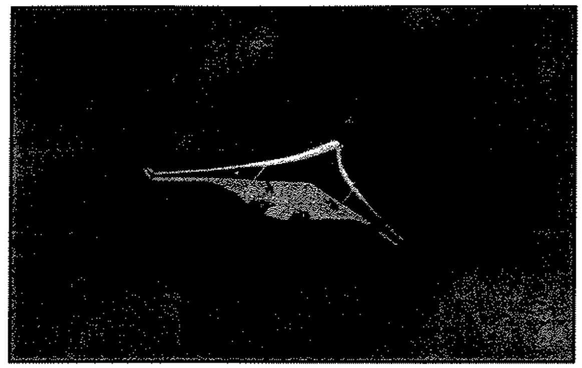
Figure 18 Flight Control Testbed built by Stanford University

Propulsion
The aft engine location on the BWB offers the opportunity for ingestion of the boundary layer generated on the centerbody forward of the inlets. In principle, boundary layer ingestion (BLI) can improve the propulsive efficiency by reducing ram drag. This assumes that an inlet can be designed that provides proper pressure recovery and uniform flow at the fan face of the engine. Alternatively, the boundary can be diverted around the sides of the inlets, but this implies dumping low energy air into an already transonically stressed pressure recovery region. Simply mounting the engines on pylons is another option, but increased wetted area and weight plus nose down thrust moment are detractors from this installation.

NASA-sponsored studies of the BLI concept were conducted at the University of Southern California and at Stanford University. At USC, a wind tunnel simulation was created with an upstream flat plate to generate the boundary layer and various duct geometries leading to a station representing the fan face of the engine where the flow quality was evaluated. Results indicated that proper configurations of vortex generators could provide a reasonably uniform flow at the fan face with acceptable pressure recovery. These results were utilized at Stanford to help guide a theoretical multidisciplinary optimization study of the BWB engine inlet concept. Navier Stokes based CFD was used to represent the centerbody and inlet flow field, and engine performance was modeled as a function of the flow quality at the fan face. The optimizer indicated that minimum fuel burn was obtained with the engine swallowing the boundary layer as opposed to diverting the boundary layer around the inlet. These studies yielded doctoral dissertations at USC (Reference 4) and Stanford (Reference 5).

The aft engine location of the BWB allows for several installation options, however, integration

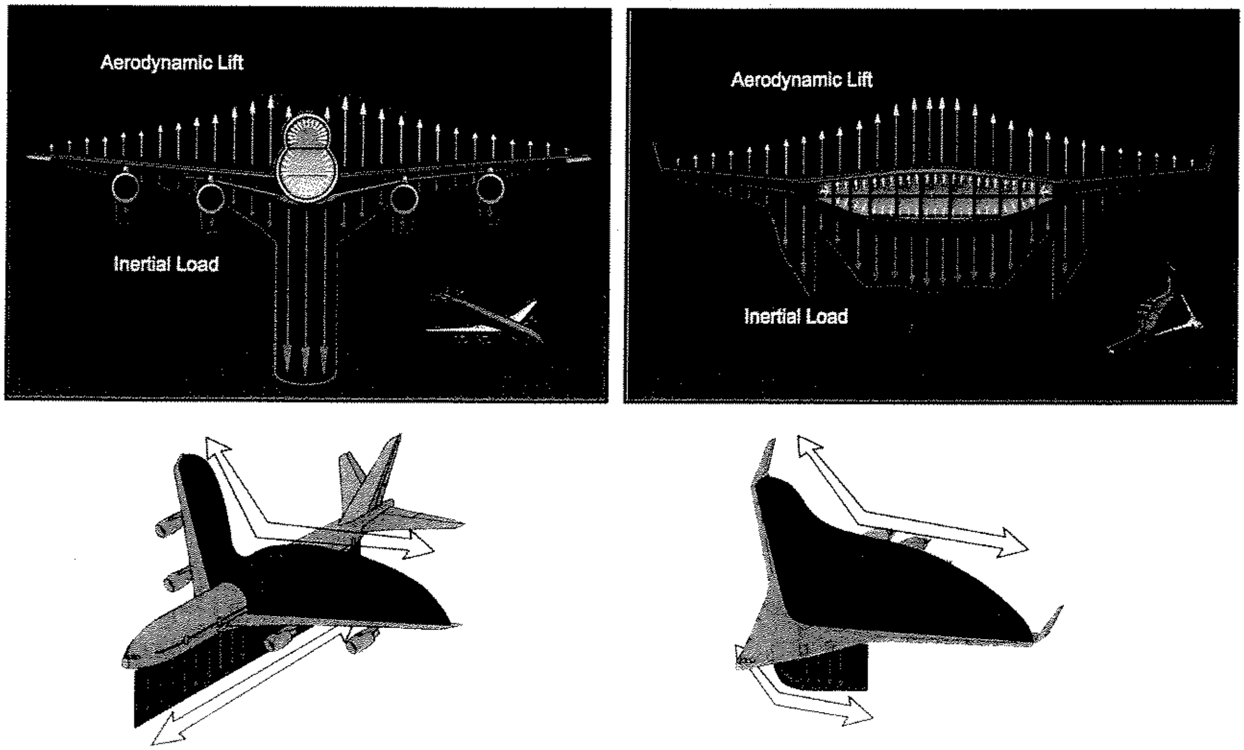

Figure 19 Comparison of aerodynamic, inertial and cabin pressure loads.

affects all of the basic disciplines. Uniquely for a BWB, there is no explicit penalty for the centerline engine of a 3-engine installation. Candidate installation concepts include podded with pylon, upper or lower surface inlet with S-duct, BLI or diverter, and finally the engine count itself. Airplanes were sized for 12 different combinations with appropriate gains and losses for inlet recovery and distortion, wetted area drag (including the adjustment for BLI), weight, and thrust moment. The figure-of-merit was the TOGW. Additional considerations included ditching, emergency egress foreign object damage (FOD), noise, reverse thrust and maintainability. Lower surface inlets were discarded on the basis of FOD and ditching. A 3-engine configuration with upper surface BLI inlets and s-ducts to the engines was selected. If BLI did not prove practical, boundary layer diverters were assumed to be the default.

Structure

The unique element of the BWB structure is the centerbody. As the passenger cabin it must carry the pressure load in bending, and as a wing it must carry the wing bending load. A comparison of the structural loading of a BWB with that of a conventional configuration is given in Figure 19. Peak wing bending moment and shear for the BWB is on the order of one half that of the conventional configuration. The primary challenge was to develop a centerbody structural concept to absorb the cabin pressure load. Unlike a wing, which rarely experiences its design load (typically via a 2.5g gust), the passenger cabin sees its design pressure load on every flight. Thus, on the basis of fatigue alone, the centerbody should be built from composites due to their comparative immunity to fatigue.

The overall structural concept selected for this NASA sponsored study is shown in Figure 20. Outboard wing structure is essentially conventional, and was assumed to be composite. The centerbody structural shell was based on two candidate concepts: a 5-inch thick sandwich, or a skin plus 5-inch deep hat-section stringers. A global finite-element model was analyzed for the combined pressure and wing bending loads on the centerbody. Cabin skin deflection due to a 2x pressure load is shown in Figure 21.

Safety and Environmental

The BWB offers several inherent safety features that are unique to the configuration. An uncontained engine failure cannot impact the pressure vessel, fuel tanks or systems. The pressure vessel itself is unusually robust since its structure has been sized to

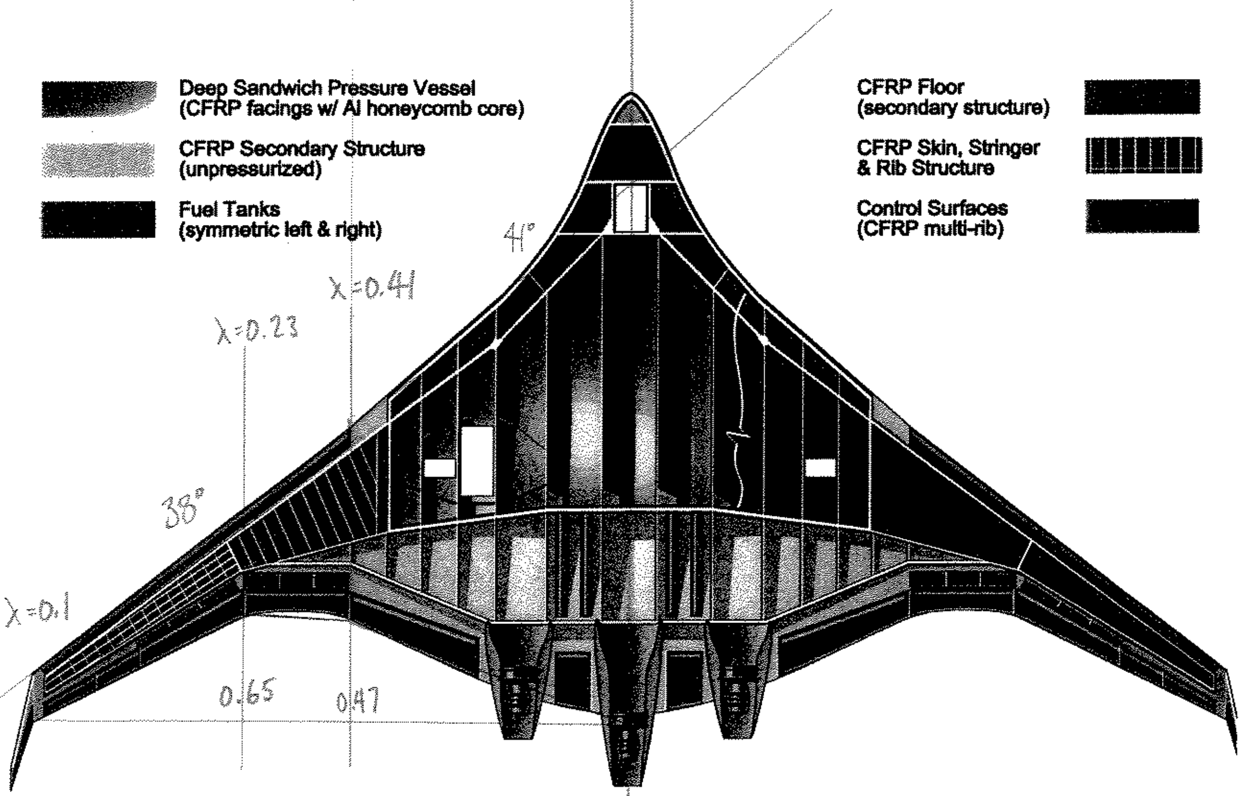

Figure 20 Structural layout of second-generation BWB.

carry both the pressure loads and wing bending loads, and consequently its crashworthiness should be substantial.

Environmentally, the BWB naturally offers a low acoustic signature – before any specific acoustic treatment. The centerbody shields forward radiated fan nose, and engine exhaust noise is not reflected from the lower surface of the wing. Airframe noise is reduced by the absence of a slotted flap trailing edge high-lift system. Engine emissions are reduced in direct proportion to the reduced fuel burn per seat mile described below.

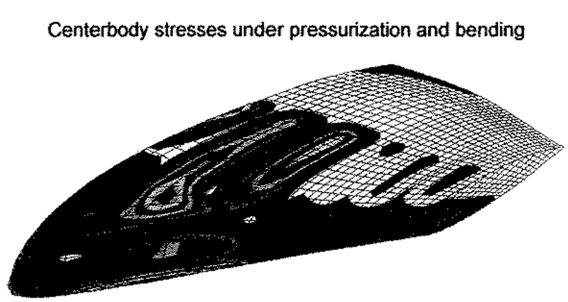

Figure 21 FEM solution showing exaggerated cabin skin deflection at 2x pressure.

Performance
A proper evaluation of the BWB concept required that a conventional subsonic transport be sized to the

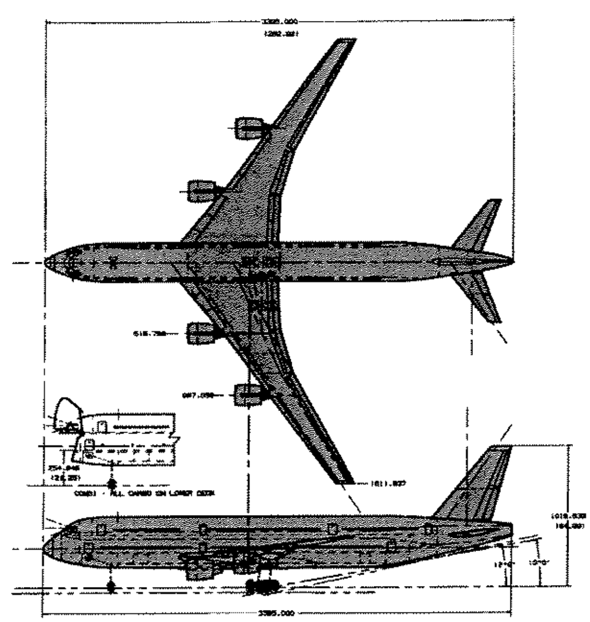

Figure 22 Conventional baseline configuration.

same design mission employing the same composite structure technology and the same class of advanced technology engines. A 2-view of the conventional baseline is shown in Figure 22, and Table 1 compares the performance of the BWB with the baseline. In addition to the significant reduction in weight, the BWB requires one less 60,000 lb-class engine, and its fuel burn per seat mile is 27 percent lower. Given that the configuration was the only technical difference in these two airplanes, the potential for the BWB concept was regarded as remarkable.

Model	BWB	Conventional
Passengers	800	800
Range (n.mi)	7,000	7,000
MTOGW (lb)	823,000	970,000
OEW (lb)	412,000	470,000
Fuel Burned (lb)	213,000	294,000
L/D @ Cruise	23	19
Thrust (total lb)	3x61,600	4x63,600

Table 1 Performance comparison of the second-generation BWB with the conventional baseline airplane.

V. The Boeing BWB-450 Baseline Airplane

The 3-year NASA sponsored study described above demonstrated the feasibility and performance potential of the BWB. Based on these results and predictions, it was decided to initiate a Boeing preliminary design study of a BWB transport. The 800 passenger 7000 nautical mile design mission of the feasibility studies was deemed inappropriate for the in-house evaluation of the BWB. Comparisons with existing airplanes and airplanes of other preliminary design studies would not be possible, and a payload of 800 passengers was simply beyond market forecast data.

Design Requirements and Objectives

The design mission selected for the baseline BWB is given in Table 2. While distinct from existing airplanes, this specification offered the opportunity for some comparison of the resulting BWB with the B747, A340 and the then-pending A3XX. Initial specification of 450 passengers (hence the designation BWB-450) was considered nominal, and the final passenger count would be established as the airplane was configured and sized. Also, while

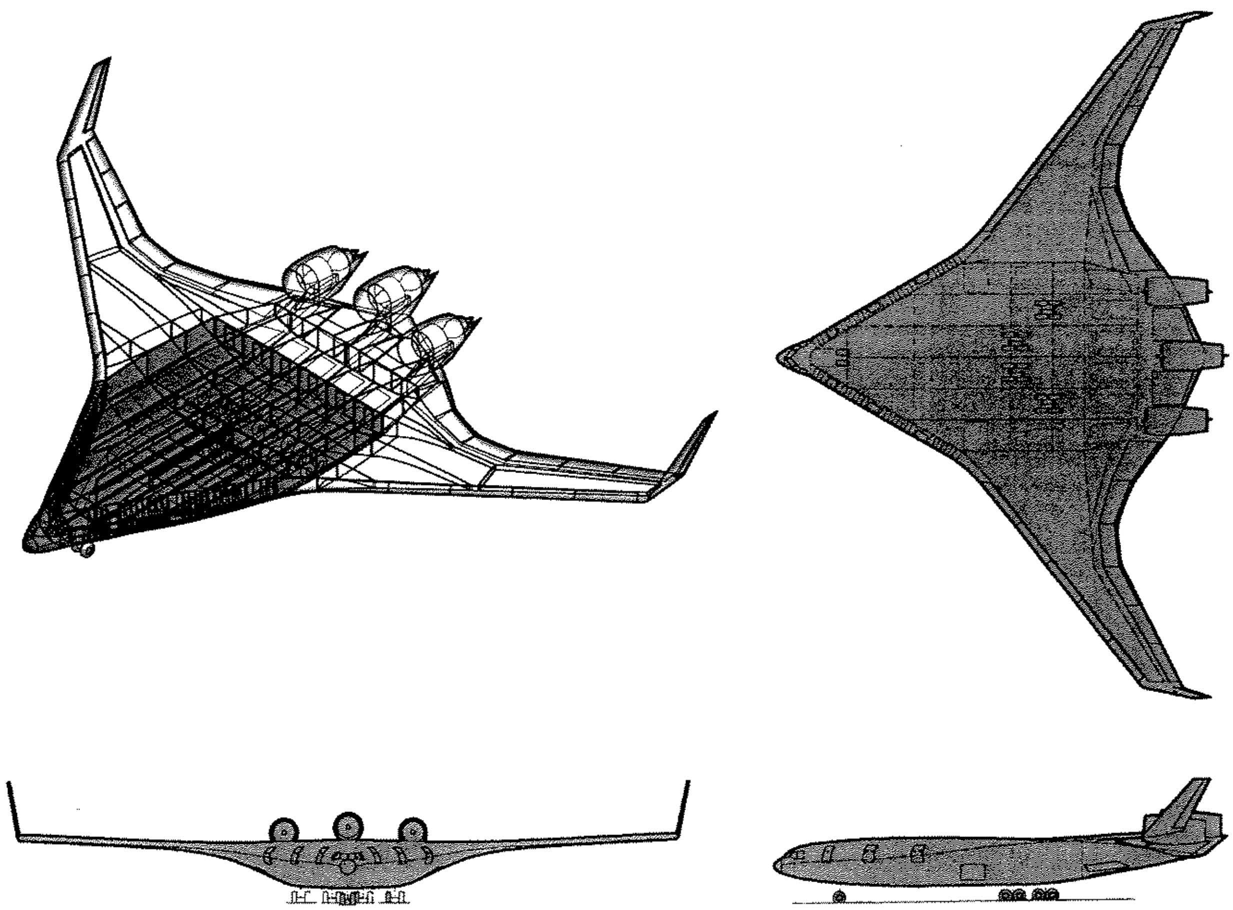

Figure 23 Boeing BWB-450 baseline.

somewhat ignored in the earlier studies, airport compatibility requirements were enforced for the baseline BWB – in particular, the wingspan limit of 260 feet (80 meters).

Mission Description	
Payload:	468 Passengers + Baggage, Three Class Arrangement
Design Range:	7,750 nmi
Crew:	Standard 2 man crew
Reserves:	International Reserve Fuel
	- Fuel equal to 5 percent of Block Fuel
	- 200 nmi Diversion to Alternate Airport
	- Half Hour Hold at 1,500 feet at Holding Speed
Constraints:	11,000 ft Field Length
	140 kts Approach Speed
	2.7 Second Segment Climb Gradient
	300 ft/min excess power at top of climb

Table 2 Design requirements and objectives for the Boeing BWB-450 Baseline.

Configuration of the Boeing BWB-450 Baseline
Per the requirements listed above and the optimization procedure described below, the baseline BWB shown in Figure 23 was created. Minimum TOGW was the objective function. Trapezoidal aspect ratio is 7.55, down substantially from the earlier BWB's, and the wingspan of 249-feet fits easily within the 80-meter box for Class VI airports. Passenger count is 478, based on 3-class international rules. Figure 24 shows the interior arrangement, and Figure 25 Shows representative cross sections of the centerbody. The entire passenger cabin is on the upper deck and cargo is carried on the lower deck, similar to conventional transports. All of the payload is located ahead of the rear spar. Crashworthiness contributed to this arrangement.

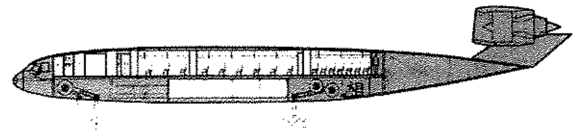

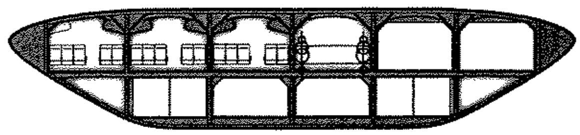

Figure 25 Centerbody interior cross-sections.

Multidisciplinary Design Optimization
As described, the BWB is an integrated configuration where the interaction of the basic disciplines is unusually strong. Conventional design intuition and approach are challenged, if not overwhelmed, when faced with sizing and optimizing the BWB airplane. Enter the method of Reference 6, a pragmatic and functional multidisciplinary airplane design optimization code. This work was originated as Wakayama's doctoral thesis at Stanford and has evolved into a Boeing proprietary code called WingMOD. In the case of the BWB, the airplane is defined by an initial planform and a stack of airfoils whose section characteristics, e.g. moment coefficient (c_{mac}), drag coefficient (c_d), are known as a function of thickness-to-chord ratio (t/c), section lift coefficient (c_l) and Mach number. WingMOD then models the airplane with a vortex-lattice code and monocoque beam analysis, coupled to give static aeroelastic loads. The model is trimmed at several flight conditions to obtain load and induced drag

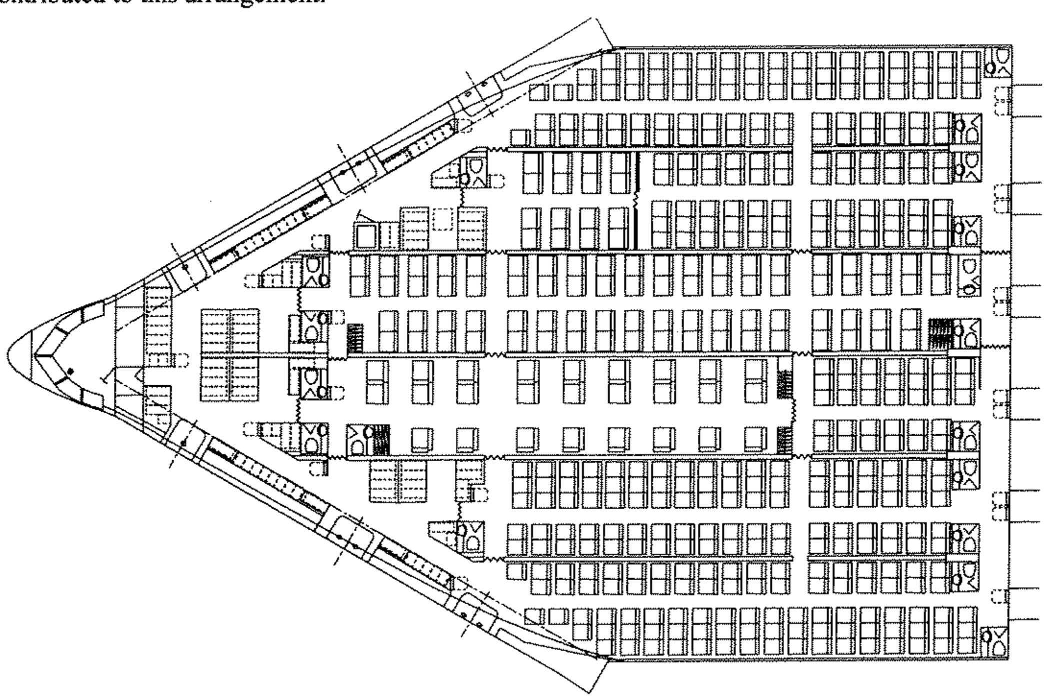

Figure 24 Three-class interior arrangement.

data. Profile and compressibility drag are then evaluated at stations across the span based on the airfoil section properties and the vortex lattice solution. Structural weight is calculated from the maximum elastic loads encountered through a range of flight conditions, including maneuver and vertical and lateral gusts. The structure is sized based on bending strength and buckling stability considerations. Maximum lift is evaluated using a critical section method that declares the wing to be at its maximum useable lift when any spanwise airfoil section reaches its maximum lift coefficient.

Figure 26 shows a small portion of an example WingMOD solution for the baseline BWB-450. The procedure begins with the manual definition of a baseline design (not to be confused with the term "baseline BWB"). Subject to the mission definition and constraints (e.g. range, takeoff field length, approach speed, interior volume, etc), WingMOD provides the definition of the minimum takeoff weight (TOGW) configuration that meets the mission while satisfying all constraints. Put another way, the optimized airplane design is closed and meets all design mission requirements with minimum TOGW.

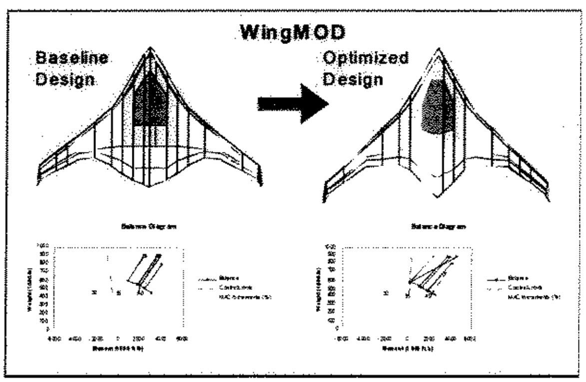

Figure 26 Example WingMOD solution for the BWB baseline.

Aerodynamics
Aerodynamic design of the BWB-450 was coupled with WingMOD to obtain the final aerodynamic definition (outer mold line). Definition of the airfoil stack was a key element to this approach. A new class of transonic airfoils for the centerbody was designed based on constraints of cross-sectional area required to properly hold passengers, baggage and cargo. The new airfoils tightly package the payload without a drag penalty. More significantly, the new airfoils smoothed and flattened the geometry to simplify manufacture. Figure 27 shows a comparison of the centerbody profile of the second-generation BWB with the Boeing BWB-450.

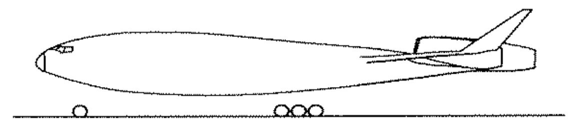

Figure 27 Comparison of centerbody profiles of the second-generation BWB with the Boeing baseline BWB.

The planform also underwent significant change from the second-generation BWB as shown in Figure 28, which also gives the comparison where both planforms are scaled to the same wingspan. Airfoil

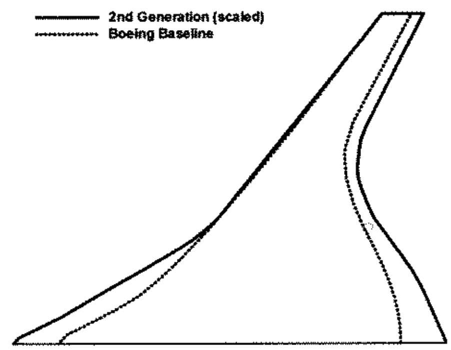

Figure 28 Planform comparisons of the second-generation BWB with the Boeing baseline BWB

chords have been increased on both the outer wing and the centerbody. Buffet onset level and characteristics primarily drove outboard chord increase. Figure 29 compares the lift curves (C_L vs α) and lift versus pitching moment curves (C_L vs C_M) for the BWB-450 and the second-generation BWB. Assuming that buffet C_L is defined at the break in the C_L vs C_M curve, the improvement of the new planform is apparent. Compared to the earlier design, there is almost twice the margin between mid-cruise C_L, 1.3g to buffet and buffet itself. Centerbody chords were increased to reduce their thickness-to-chord and afterbody closure angles. While this increased wetted area, the increased friction drag was more than offset by a reduction in pressure drag. Inboard elevon effectiveness was also improved. Aerodynamic design of the BWB is discussed in more detail in Reference 7.

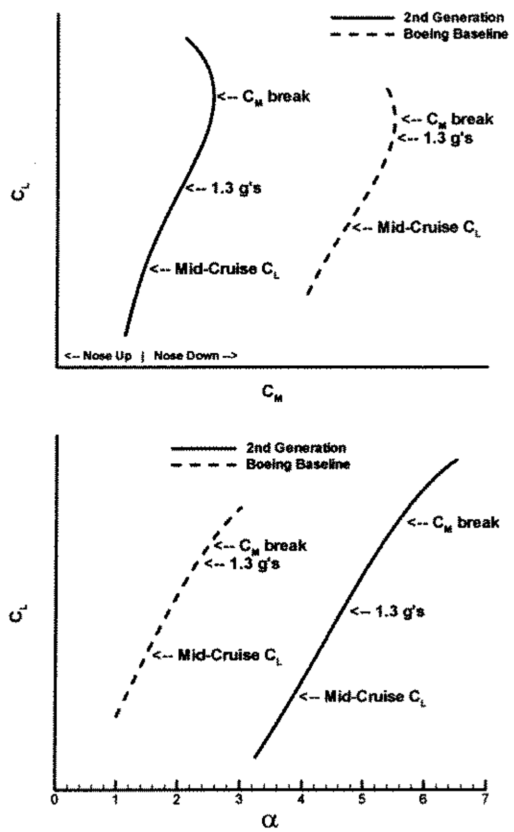

Figure 29 Comparison of lift and moment curves of the second-generation BWB with the Boeing baseline BWB.

Stability and Control

The planform, airfoil stack and twist distribution of the BWB-450 resolves the longitudinal trim problem with more efficiency than most flying-wing airplanes. Historically, flying wings have been trimmed by sweeping the wing and downloading the wingtips. While this approach allows the wingtips to functionally serve as a horizontal tail, it imposes a significant induced drag penalty. The effective aerodynamic wingspan is less than the physical span, and this penalty is a primary reason that flying-wing airplanes have failed to live up to their performance potential. As described earlier, the first- and second-generation BWB were allowed to have significantly negative static margins in order to preserve a near elliptic spanload. The BWB-450 has been trimmed by a careful distribution of spanload coupled with a judicious application of wing washout. The result is a flying-wing airplane that is trimmed at a stable center-of-gravity with all control surfaces faired, and with no induced drag penalty. Setting this design condition at the mid-cruise point results in a trim drag of one count at start-of-cruise (high C_L), and a half count of trim drag at end-of-cruise (lower C_L).

Propulsion

The second-generation BWB assumed boundary-layer ingestion for both the engine installation and the performance estimate. For the BWB-450 it was decided to reduce the technology risk by examining the performance of both boundary-layer diverters and simple podded engines on pylons. Navier-Stokes based CFD was used to evaluate these options. To the extent they were studied, the diverters showed an unacceptable drag increase due to the low energy of the diverted boundary layer plus its interaction with the pressure recovery region of the aft centerbody. Alternatively, the initial modeling of the podded engines on pylons indicated the increase in wetted area was only 4-percent compared to the diverted configuration. The thrust moment, although undesirable, was deemed acceptable. A thorough CFD-based design and analysis study showed that an interference-free podded engine and pylon installation could be achieved, and the net drag penalty was simply due to the wetted area increase. Therefore podded engines on pylons became the selected installation for the baseline BWB.

Structure

The BWB structure is divided into two main components: the centerbody, and the outer wings. Structure of the outer wings is similar to that of a conventional transport. The centerbody is subdivided into the forward pressure vessel and the unpressurized afterbody. Development of the structure for the centerbody and its pressure vessel was approached by defining and comparing several concepts. Weight and cost were the primary figures of merit. One of the most viable concepts was based on a skin/stringer outer surface structure where the stringers are on the order of 5 to 6 inches deep. The internal ribs have Y-braces where they meet the skin to reduce the bending moment on the skin created by the internal pressure. (This could be regarded as a structural analog to the earlier concept of an arched pressure membrane.) As shown in Figure 30, the complete centerbody pressure vessel is composed of the upper and lower surface panels, the rounded leading edge (which also functions as the front spar), the rear main spar, the outer ribs (which must also carry the cabin pressure load in bending) and the internal ribs (which carry the cabin pressure load in tension). The cabin floor simply supports the payload and does not carry wing bending loads. Finite element analyses have been used to develop and verify this structural concept and its weight. The

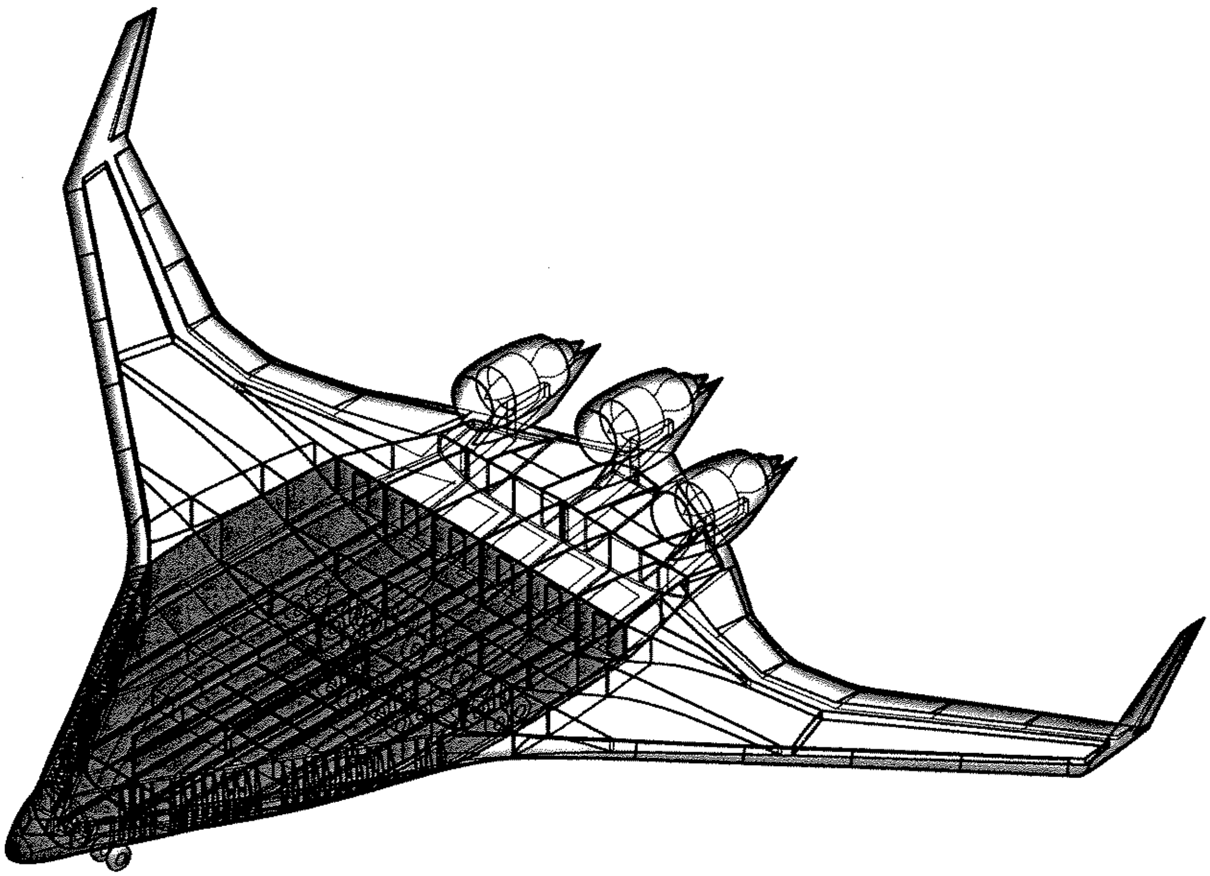

Figure 30 Centerbody structural concept.

final result is an unusually rugged passenger cabin that weighs little more than a conventional fuselage.

Studies to date have assumed composite material for the majority of the BWB primary structure. The outer wings could readily be fabricated from aluminum with the typical 20-percent weight penalty. However, as mentioned earlier, the weight penalty for using aluminum for the centerbody structure would be larger. The design cabin pressure load is experienced on every flight, and thus fatigue becomes the design condition. Since cabin pressure loads are taken in bending, the margin required for aluminum could be prohibitive, while composites are essentially immune to fatigue and hence would suffer no penalty.

Figure 31 shows a comparison of the structural weight fractions of a BWB and a conventional configuration; both sized for the same mission, and both assuming the same composite structure technology. Yes, the centerbody structure of the BWB is heavier than that of a conventional fuselage, but the weight (OEW) of the complete configuration of the BWB is markedly lighter.

Performance

A performance comparison of the Boeing BWB-450 with the Airbus A380-700 is given in Figure 32. Both airplanes are compared for a payload of approximately 480 passengers and a range of 8700 nautical miles. (A380 data is from an Airbus brochure.) Probably the most striking result is the BWB's 32 percent lower fuel burn per seat. Both airplanes are using equivalent technology engines of similar thrust levels, however, A380-700 requires four, while the BWB-450 requires three. Primary structure of the A380-700 is aluminum with the exception of the outer wing panels, which are understood to be composite. The BWB-450 primary structure is essentially all composite. A comparison of the BWB-450 cabin volume with that of the A380-700 is shown in Figure 33.

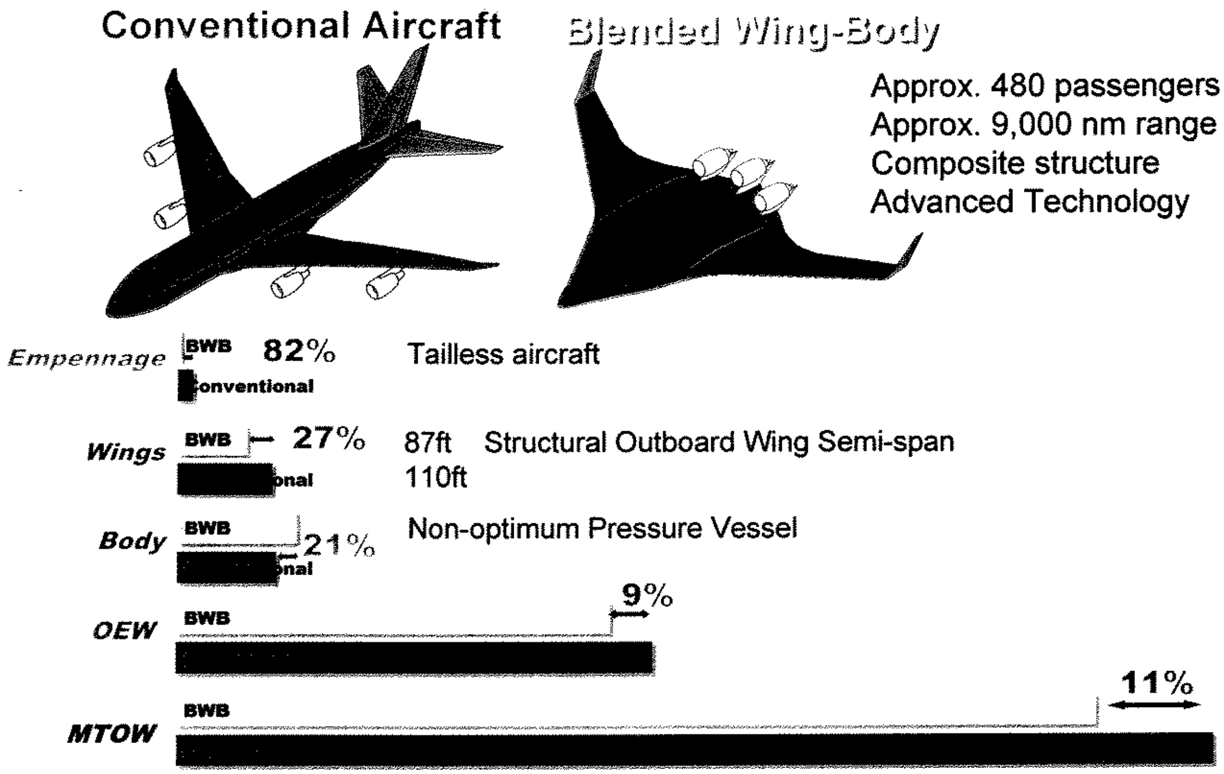

Figure 31 Comparison of structural weight fractions for a BWB and a conventional configuration.

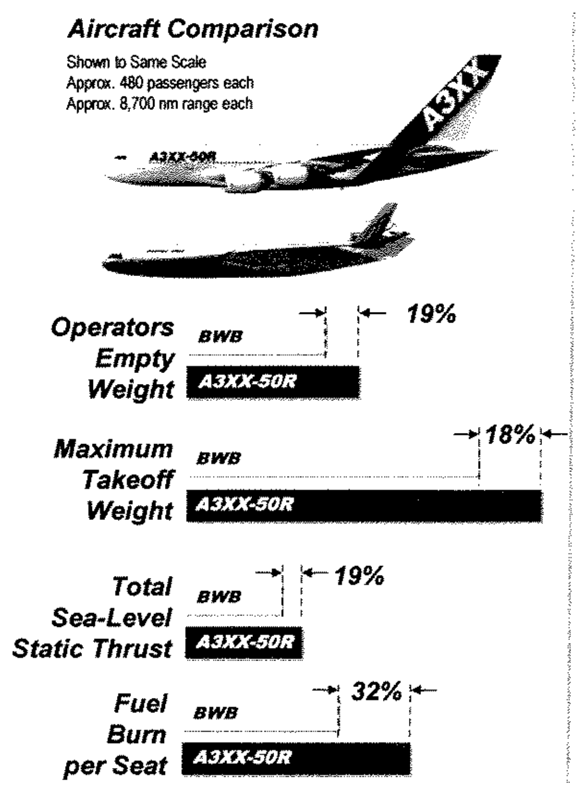

Figure 32 Performance comparison of the BWB-450 with the A380-700.

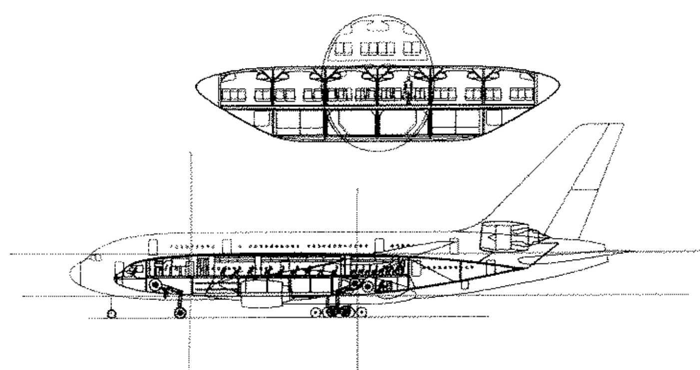

Figure 33 Interior volume comparison of the BWB-450 with the A380-700.

Environment
The Boeing BWB-450 offers the potential for a significant reduction in environmental emissions and noise. Lower total installed thrust and lower fuel burn imply an equivalent reduction in engine emissions, assuming the same engine technology. As discussed earlier, the forward-radiated fan noise is shielded by the vast centerbody, and engine exhaust noise is not reflected by the lower surface of the wing. And, the lower thrust loading itself implies lower noise. There are no slotted trailing-edge flaps, so a major source of airframe noise is eliminated.

Thus, before any specific acoustic treatment, the BWB offers a significant reduction in noise.

VI. Unique Opportunities and Challenges of the BWB Configuration

Creation of the original BWB was motivated by a search for an airplane configuration that could offer improved efficiency over the classic tube and wing. Takeoff weight and fuel burn were the primary figures of merit, and the BWB concept has shown substantial reductions in these two performance parameters, as described above. However, the BWB configuration offers some unique opportunities that were neither envisioned nor planned during its original creation in 1993. Three of these are described below.

Manufacturing Part Count

The BWB is simply a big wing with an integrated fuselage and no empennage, save the winglets/verticals. There are no complex wing-fuselage and fuselage-empennage joints of highly loaded structures at 90 degrees to one another, and there are no fillets. All trailing-edge control surfaces are simple-hinged with no track motion, and there are no spoilers. This manifests a substantial reduction (on the order of 30-percent) in the number of parts when compared to a conventional configuration. A similar reduction in manufacturing recurring cost is implied.

Family and Growth

Reference 2, which describes the early development of the BWB, contains the remark; "Any change such as wing area or cabin volume implies a complete reconfiguration. Stretching is not in the vocabulary." Or so it was thought at the time. As development progressed, it was discovered that the BWB concept could be ideal for a family of airplanes with the potential for substantial commonality among its members. Here "stretching" takes place laterally (spanwise), as opposed to longitudinally. Passenger capacity can be increased by adding a central bay to the centerbody, and vice versa. Wing area and span automatically increase or decrease appropriately with passenger capacity, a quality not offered by the longitudinal stretching of a conventional airplane.

In order to achieve this growth capability, the aerodynamic outer mold lines of all of the family members must remain smooth and provide proper aerodynamic performance. In addition, all of the airplanes must be trimmed and balanced. Geometrically, this has been achieved by essentially defining the centerbody as a ruled surface in the spanwise direction. In turn, this allows the definition of several airplanes ranging, for example, from 250 to 550 passengers as shown in Figure 34. Centerbody cabins are composed of combinations of two or more distinct cabins (shown in green, yellow and orange). The outer wing panels and nose sections (shown in blue) are of identical geometry for all family members. Distinct to each airplane are the transition section aft of the nose, the aft centerbody and engines (shown in gray). Nose gear and outer main gear could be common for all family members, with a center main gear of varying capacity added where required.

A representative set of the airplane family has been examined in depth to establish the potential for commonality. A common part number for the entire outer wing was the goal. Fuel volume of the outer wing is adequate for all members of the family. Navier-Stokes analyses of several of the members of this example family demonstrated proper aerodynamic performance. The airplanes are trimmed and balanced. Finite-element modeling was used to quantify the effect of commonality on the structure. The proposed commonality was feasible, but at cost of increased OEW for the smaller airplanes. If the common part number requirement is relaxed to permit a skin gage change, the OEW penalty is substantially reduced.

Commonality extends naturally to the interior, once the commitment to the centerbody growth concept is made. In principle, the cabin cross section is the same for all of the airplanes, as shown in Figure 35. This implies common galleys, lavatories, bag racks and seats. Substantial maintenance and life-cycle costs are implied for the airline customer.

Put simply, commonality is a constraint, and almost any constraint imposed on an airplane is manifested by an increase in weight. However, the BWB concept appears to offer the opportunity for an unusual level of commonality while maintaining aerodynamic efficiency via the natural variation of wing area and span with weight. This implies significant reductions in part count and learning curve penalties in manufacturing. Enhanced responsiveness to fleet-mix requirements is also implied. It remains to thoroughly evaluate the trade between airplane cost and performance offered by the BWB family concept.

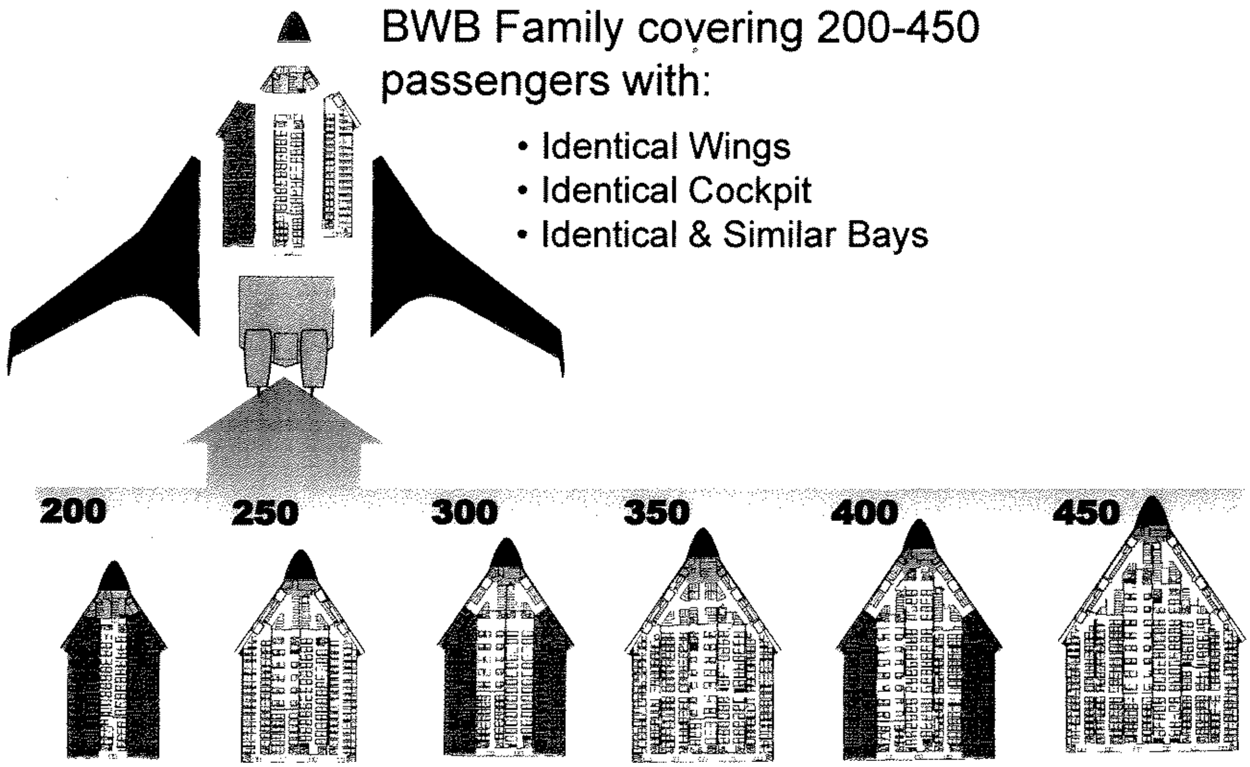

Figure 34 Commonality of a BWB Family.

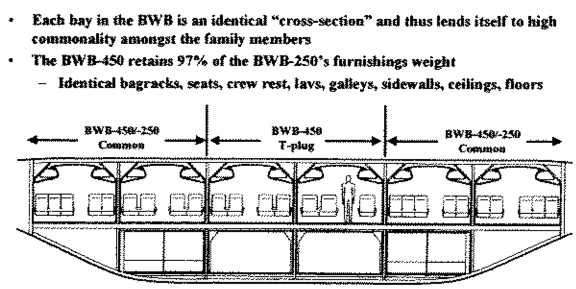

Figure 35 Cabin cross-section growth from 250 to 450 passengers.

Speed

Figure 36 shows a comparison of the BWB-450 cross-sectional area variation S(x) with that of the classical minimum wave drag due to volume Sears-Haak body. Also shown is the variation for an MD-11. It can be observed that the BWB is naturally area-ruled, and hence a higher cruise Mach number should be achievable without a change in the basic configuration geometry. Figure 37 gives the results of a WingMOD-based study for the effect of the design cruise Mach number on BWB performance and weight. All of the designs are closed, trimmed and balanced for the same design mission. Variation between planforms appears slight; however, a comparison between the M = 0.85 and 0.95 shows a significant distinction. Increased Mach number is accommodated by an increase in sweep and chord, which results in a corresponding increase in weight. Some of this weight increase is due to the increase of installed engine SFC with Mach number. The classic aerodynamic parameter ML/D is plotted as a function of the cruise Mach number in Figure 37. A more meaningful plot is given by the variation of the parameter MP/D (P is the design payload weight), also shown in Figure 37. MP/D includes the effect of airplane weight itself, since MP/D = (ML/D) x (P/W).

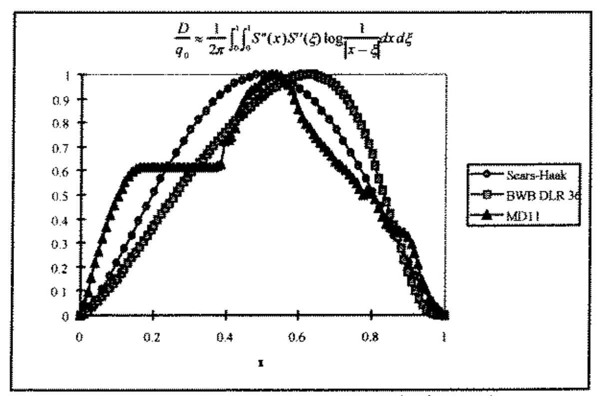

Figure 36 Cross-sectional area variations: $S_{(x)}$ vs x

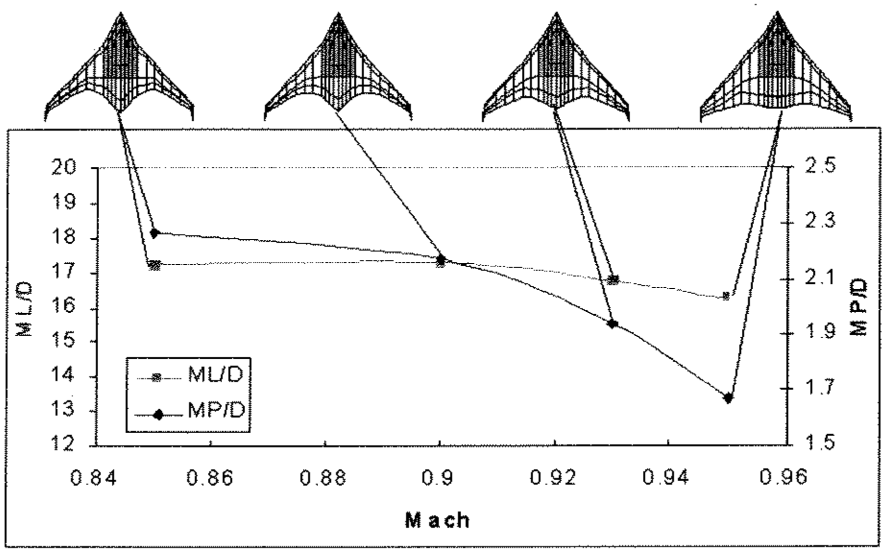

Figure 37 BWB planform, ML/D & MP/D variation with Mach number

These preliminary results suggest that 0.90 could be the "best" cruise Mach number. However, the economic value of speed must be established before selecting a design cruise Mach number. For example, airplane utilization varies directly with speed, and for some longer-range missions, a slight increase in speed could eliminate the requirement for a second crew. The question then becomes "How much of an increase in TOGW and fuel burn can be offset by such issues?" Resolution remains.

Passenger Acceptance, Ride Quality and Emergency Egress

The unique interior configuration of the BWB offers both opportunities and challenges. Vertical walls of the passenger cabins provide a more spacious environment similar to a railroad car rather than the curved walls of a conventional airplane. At the same time, the low capacity of each cabin (approximately 100 passengers) provides an intimacy not available in wide-body conventional transports. However, while there is a window in each main cabin door, there are no windows in the cabin walls. As a surrogate for windows, a flat screen display connected to an array of digital video cameras will make every seat a window seat. Some example interior renderings are shown in Figure 38.

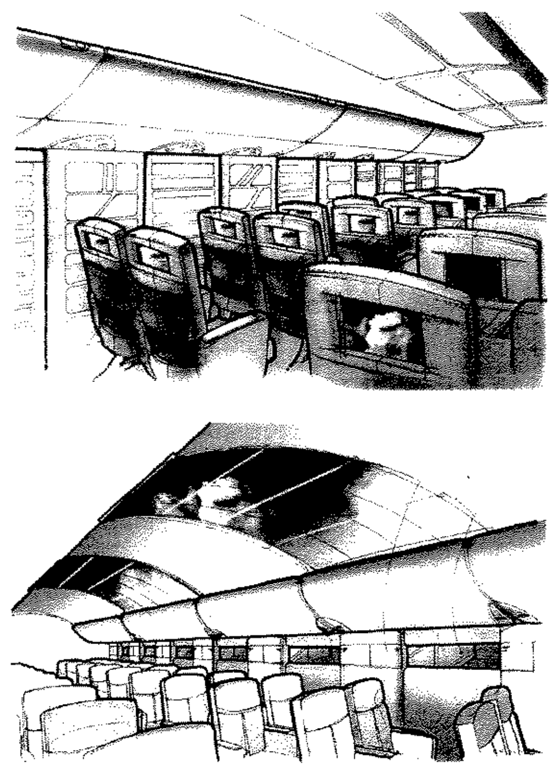

Figure 38 Interior concepts for the BWB.

Ride quality has been a concern due to the lateral offset of the passengers from the center-of-gravity. This has been addressed by comparing the results from piloted flight simulator tests of the BWB-450 and a B747-400 using the same pilots and flight profile. One of the more severe cases studied was a takeoff, go-around and landing in moderate turbulence with a 35-knot crosswind. Lateral and vertical RMS g-levels were comparable for the "worst" seats in both airplanes; however, the frequency content tended to be lower for the BWB. Gust load alleviation was not used on either airplane.

Emergency egress becomes a significant challenge when passenger capacity exceeds 400. This is simply a consequence of the square-cube law: capacity increases with the cube of the length scale while surface area for egress increases with the square of the length scale. The BWB configuration lends itself particularly well to resolving this problem. There is a main cabin door directly in the front of each aisle, and an emergency exit through the aft pressure bulkhead at the back of each aisle. In addition, there are four cross aisles, as shown in Figure 39.

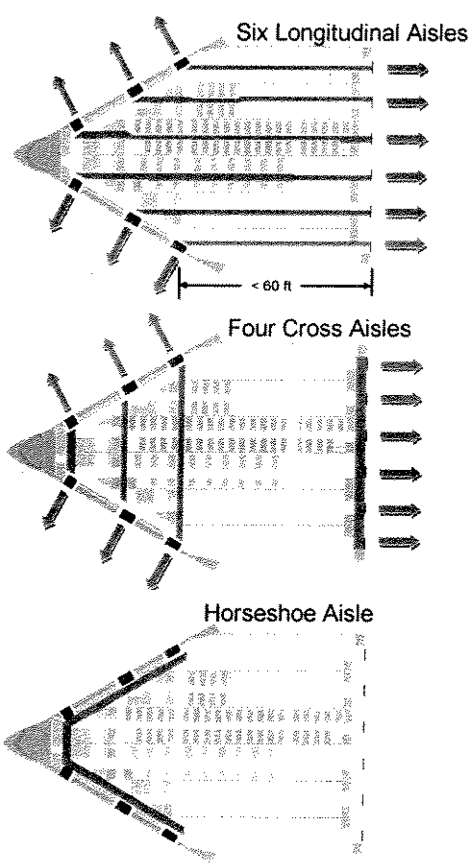

Figure 39 Cabin egress flow patterns.

Thus, from virtually any location in the cabin, a passenger will have a direct view of one or more exits. Unlike a conventional transport, a 90-degree turn will not be required to reach a door from the aisle. Since there is no upper deck, the problems with long slides, slide interference and over-wing exits do not exist. Ultimately, this new class of interior configuration will require a new set of emergency evacuation criteria coordinated with the Federal Aviation Administration.

VII. Summary and Conclusions

Development of the Blended-Wing-Body has progressed steadily over the past seven years. Once-apparent "show-stoppers" have been reduced to technical challenges, or in most cases proper solutions. From a distance, the Boeing BWB-450 baseline airplane shows little distinction from the first-generation BWB developed under NASA sponsorship in 1993. The intent of this paper has been to chronicle the engineering work that has brought the airplane to the state it is in today. Table 3 presents a list of issues and areas of risk. They could readily apply to the BWB. However, they are in fact extracted from Douglas Aircraft Company memoranda written in the 1950's regarding the challenge of moving from the DC-7 to the DC-8. Hopefully our industry will press on, just as Douglas and Boeing did fifty years ago.

- Complex flight control architecture & allocation, with sever hydraulic requirements
- Large auxiliary power requirements
- New class of engine installation
- Flight behavior beyond stall
- High floor angle on take of & approach to landing
- Acceptance by the flying public
- Performance at long range
- Experience & data base for new class of configuration limited to military aircraft

Table 3 Issues and areas of risk. (from Douglas Aircraft Co., circa 1955)

Multidisciplinary Design Optimization and Industry Review of a 2010 Strut-Braced Wing Transonic Transport

By

J. F. Gundlach IV, A. Naghshineh-Pour, F. Gern, P.-A. Tetrault,

A. Ko, J. A. Schetz, W. H. Mason, R. K. Kapania, B. Grossman,

R. T. Haftka (University of Florida)

MAD 99-06-03

June 1999

Multidisciplinary Analysis and Design Center for Advanced Vehicles

Department of Aerospace and Ocean Engineering

Virginia Polytechnic Institute and State University

Blacksburg, VA 24061-0203

Multidisciplinary Design Optimization and Industry Review of a 2010 Strut-Braced Wing Transonic Transport

John F. Gundlach IV

(ABSTRACT)

Recent transonic airliner designs have generally converged upon a common cantilever low-wing configuration. It is unlikely that further large strides in performance are possible without a significant departure from the present design paradigm. One such alternative configuration is the strut-braced wing, which uses a strut for wing bending load alleviation, allowing increased aspect ratio and reduced wing thickness to increase the lift to drag ratio. The thinner wing has less transonic wave drag, permitting the wing to unsweep for increased areas of natural laminar flow and further structural weight savings. High aerodynamic efficiency translates into reduced fuel consumption and smaller, quieter, less expensive engines with lower noise pollution. A Multidisciplinary Design Optimization (MDO) approach is essential to understand the full potential of this synergistic configuration due to the strong interdependency of structures, aerodynamics and propulsion. NASA defined a need for a 325-passenger transport capable of flying 7500 nautical miles at Mach 0.85 for a 2010 date of entry into service. Lockheed Martin Aeronautical systems (LMAS), our industry partner, placed great emphasis on realistic constraints, projected technology levels, manufacturing and certification issues. Numerous design challenges specific to the strut-braced wing became apparent through the interactions with LMAS, and modifications had to be made to the Virginia Tech code to reflect these concerns, thus contributing realism to the MDO results. The SBW configuration is 9.2-17.4% lighter, burns 16.2-19.3% less fuel, requires 21.5-31.6% smaller engines and costs 3.8-7.2% less than equivalent cantilever wing aircraft.

Acknowledgements

This research would not be possible without support, advice, data and other contributions from a number of people and organizations. NASA deserves much credit for having the vision to pursue bold yet promising technologies with the hope of revolutionizing air transportation. Lockheed Martin Aeronautical Systems provided valuable contributions in data, design methods and advice borne from hard-won experience. The SBW team faculty advisors and members of the MAD center have guided the research and offered direction throughout the duration. I would especially like to thank faculty members Dr. Joseph Schetz, Dr. William Mason, Dr. Bernard Grossman, Dr. Rafael Haftka, Dr. Rakesh Kapania, and Dr. Frank Gern for providing guidance in my efforts. My predecessor, Joel Grasmeyer, provided an excellent code, which was thoughtfully documented and free of clutter. I learned a great deal about programming from studying his work. Other members of the SBW team, Amir Naghshineh-Pour, Phillipe-Andre Tetrault, Andy Ko, Mike Libeau and Erwin Sulaeman, have made large contributions to the research and have been very cooperative and generous with their time. I appreciate the friendly work environment and productive atmosphere made possible by the SBW team student members and advisors. Last, but definitely not least, I wish to thank my wife and best friend, Katie Gundlach, for unselfishly giving her loving support.

Contents

List of Figures

List of Tables

Nomenclature

$Angle_{Scrape}$	Angle of Attack for Tail Scrape, deg
AR_{HT}	Horizontal Tail Aspect Ratio
AR_{VT}	Vertical Tail Aspect Ratio
AR_{W}	Wing Aspect Ratio
AR_{Weff}	Effective Wing Aspect Ratio in Ground Effect
BFL	Balanced Field Length, ft
b_{HT}	Horizontal Tail Span, ft
BPR	Bypass Ratio
b_{rudder}	Rudder Span, ft
b_{VT}	Vertical Tail Span, ft
b_{w}	Wing Span, ft
c bar	Average Wing Chord, ft
C_{Df}	Flat Plate Friction Drag Coefficient
$C_{DGround}$	Ground Roll Drag Coefficient
C_{Dm}	Minimum Drag Coefficient
$C_{DmFactor}$	Minimum Drag Coefficient Factor
$C_{DoApproach}$	Landing Approach Zero-Lift Drag Coefficient
C_{Dp}	Profile Drag Coefficient
C_{dwave}	Wave Drag Coefficient of Strip
C_{HTroot}	Horizontal Tail Root Chord, ft
C_{HTtip}	Horizontal Tail Tip Chord, ft
C_{l}	2-D Section Lift Coefficient
C_{L}	Total Lift Coefficient
C_{Lbreak}	Lift Dependent Profile Drag Constant
$Clearance$	Average Ground Clearance, ft
$C_{LGround}$	Lift Coefficient in Ground Effect
C_{Lm}	Lift Coefficient of Minimum Drag Coefficient
$C_{LScrape}$	Scrape Angle Lift Coefficient
$C_{L\alpha}$	Lift Curve Slope
$C_{L\alpha Ground}$	Lift Curve Slope in Ground Effect
C_{L2}	Second Segment Climb Lift Coefficient
$C_{n\ req}$	Required Yawing Moment Coefficient
C_{rudder}	Rudder Average Chord, ft
C_{VTroot}	Vertical Tail Root Chord, ft
C_{VTtip}	Vertical Tail Tip Chord, ft
C_{Wbreak}	Wing Break Chord, ft
C_{Wroot}	Wing Root Chord, ft
C_{Wtip}	Wing Tip Chord, ft
D	Drag, lbs
D_{E}	Drag of Inoperable Engine, lbs
D_{Engine}	Engine Diameter, ft
$D_{Fuselage}$	Fuselage Diameter, ft
dx_htail	Distance from CG to AC of Horizontal Tail, ft
dx_vtail	Distance from CG to AC of Vertical Tail, ft
f	Wingtip Engine Induced Drag Factor
$f_{Approach}$	Landing Approach Drag Factor
f_{Break}	Lift Dependent Profile Drag Constant

FF	Form Factor
$F_{Initial}$	Initial Braking Force, lbs
F_m	Mean Braking Force, lbs
F_{static}	Static Braking Force, lbs
f_6	Wingtip Engine Induced Drag Factor, $AR_W = 6$
f_{12}	Wingtip Engine Induced Drag Factor, $AR_W = 12$
g	Acceleration of Gravity (32.2 ft/sec^2)
h_f	Landing Obstacle Height, ft
h_{Pylon}	Pylon Height, ft
h_{TO}	Height of Object to Clear at Take-Off, ft
k	Lift Dependent Drag Factor
K_{Brake}	Braking Factor
k_{Break}	Lift Dependent Drag Factor
L/D	Lift to Drag Ratio
$L_{WLE,HTLE}$	Streamwise Distance from Wing LE to Horizontal Tail LE, ft
$L_{WLE,VTLE}$	Streamwise Distance from Wing LE to Vertical Tail LE, ft
m	Chordwise Distance from LE of Wing Root to LE of Segment MAC, ft
M	Mach Number
MAC	Mean Aerodynamic Chord, ft
MAC_{HT}	Horizontal Tail Mean Aerodynamic Chord, ft
MAC_{VT}	Vertical Tail Mean Aerodynamic Chord, ft
MAC_W	Wing Mean Aerodynamic Chord, ft
$Margin_{Scrape}$	Tail Scrape Angle Safety Margin, deg
M_{crit}	Critical Mach Number
M_{dd}	Drag Divergent Mach Number
$M_{Landing}$	Landing Mach Number
n	Number of g's
$Offset$	Wing/Strut Aerodynamic Offset, ft
q	Dynamic Pressure, lb/ft^2
R/C	Rate of Climb, ft/sec
$R/C_{CruiseInitial}$	Rate of Climb at Initial Cruise Altitude, ft/sec
$Reserve$	Reserve Range, nmi
s	Chordwise Distance from LE of Segment Root to LE of Segment Tip, ft
S	Wetted Area of Component
S_A	Landing Air Distance, ft
S_B	Landing Braking Distance, ft
S_{FR}	Landing Free Roll Distance, ft
S_{HT}	Horizontal Tail Area, ft^2
S_{ref}	Reference Area (Usually S_w), ft^2
S_{strip}	Planform Area of Strip, ft^2
S_{VT}	Vertical Tail Area, ft^2
S_w	Wing Planform Area, ft^2
S_{wet}	Aircraft Wetted Area, ft^2
sfc	Specific Fuel Consumption at Altitude
sfc_{Static}	Static Fuel Consumption
t/c	Thickness to Chord Ratio
T	Thrust at Given Altitude and Mach number,lbs
$T\ bar$	Mean Thrust of Take-Off Run, lbs
$t/c_{Average}$	Average Thickness to Chord Ratio
t/c_{Break}	Breakpoint Thickness to Chord Ratio

t/c_{Root}	Root Chord Thickness to Chord Ratio
t/c_{Tip}	Tip Chord Thickness to Chord Ratio
T_E	Thrust of Good Engine at Engine-Out Condition, lbs
$Temp$	Temperature at Altitude
$Temp_{SL}$	Temperature at Sea Level
t_{FR}	Time of Landing Free Roll, sec
$T_{SL,static}$	Sea Level Static Thrust, lbs
TVC_{HT}	Horizontal Tail Volume Coefficient
TVC_{vT}	Vertical Tail Volume Coefficient
T/W	Aircraft Thrust to Weight Ratio
V_{TD}	Touch-Down Velocity, ft/sec or kts
W	Aircraft Weight, lbs
$W_{BodyMax}$	Maximum Body and Contents Weight, lbs
$W_{BodyMax,in}$	Input Maximum Body and Contents Weight, lbs
$W_{EconCruise}$	Economic Mission Average Cruise Weight, lbs
$W_{FuelEcon}$	Economic Mission Fuel Weight, lbs
W_{Fuse}	Fuselage Weight, lbs
W_i	Initial Cruise Weight, lbs
$W_{Landing}$	Landing Weight, lbs
W_o	Final Cruise Weight, lbs
W_{TO}	Take-Off Weight, lbs
W_{Wing}	Wing Weight, lbs
$W_{Wing,in}$	Input Wing Weight, lbs
W_{ZF}	Zero Fuel Weight, lbs
$W_{ZF,in}$	Input Zero Fuel Weight, lbs
$X_{Nose,WLE}$	Streamwise Distance from Nose the Wing Root LE, ft
Y_{Eng}	Spanwise Distance to Engine, ft
$\Delta C_{D,CL}$	Additional Profile Drag Due to Lift
ΔS_{TO}	Take-Off Inertia Distance, ft
$\Delta W_{ZF,Econ}$	Change in Zero-Fuel Weight for Econ. Mission, lbs
$\Delta\gamma_2$	Second Segment Climb Gradient Above Minimum
κ_a	Airfoil Technology Factor
γ	Landing Glide Slope
γ_2	Second Segment Climb Gradient
η_{break}	Percentage Semispan of Wing Breakpoint
μ_{Brake}	Braking Coefficient
λ_{HT}	Horizontal Tail Taper Ratio
λ_{VT}	Vertical Tail Taper Ratio
Λ	Sweep Angle
$\Lambda_{HT,LE}$	Horizontal Tail Leading Edge Sweep Angle
$\Lambda_{VT,LE}$	Vertical Tail Leading Edge Sweep Angle
$\Lambda_{W,c/2}$	Wing Half-Chord Sweep Angle
$\Lambda_{W,LE}$	Wing Leading Edge Sweep Angle
ρ	Air Density at Altitude
ρ_{SL}	Air Density at Sea Level
σ'	Ground Effect Drag Factor
$\%b_{\mathrm{rudder}}$	Percentage Vertical Tail Span of Rudder Span
$\%C_{\mathrm{rudder}}$	Percentage Average Vertical Tail Chord of Rudder Chord

Chapter 1

Introduction

Over the last half-century, transonic transport aircraft have converged upon what appears to be two common solutions. Very few aircraft divert from a low cantilever wing with either underwing or fuselage-mounted engines. Within the cantilever wing with underwing engines arrangement (Figure 1.1), a highly trained eye is required to discern an Airbus from a Boeing airliner, or the various models from within a single airframe manufacturer. While subtle differences such as high lift device and control system alternatives distinguish the various aircraft, it is unlikely that large strides in performance will be possible without a significant change of vehicle configuration.

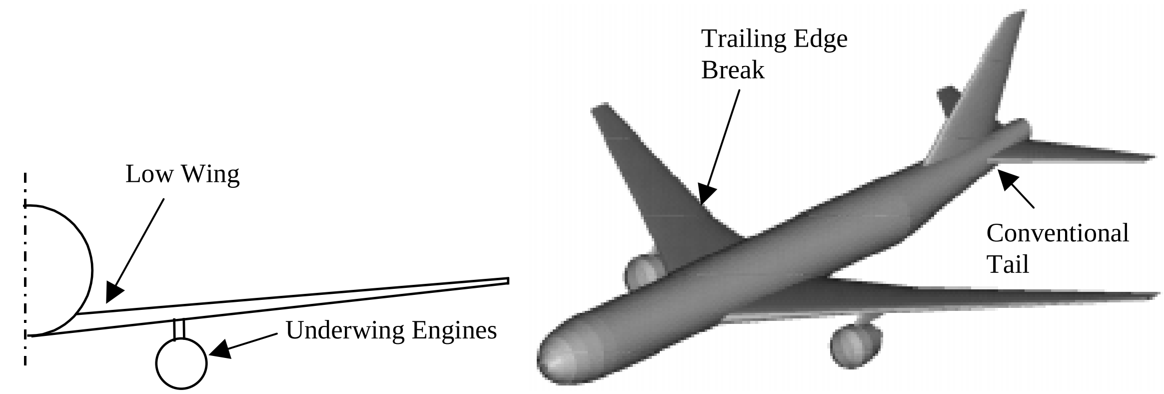

Figure 1.1. Conventional Cantilever Configuration.

Numerous alternative configuration concepts have been introduced over the years to challenge the cantilever wing design paradigm. These include the joined wing [Wolkovitch (1985)], blended wing body [Liebeck et. al. (1998)], twin fuselage [Spearman (1997)], C-wing [Mcmasters et. al. (1999)] and the strut-braced wing, to name a few. This study compares the strut-braced wing (SBW) to the cantilever wing. No attempt has been made to directly compare the strut-braced wing to other alternative configurations. Rather, the cantilever wing configuration is used for reference

The SBW configurations (Figures 1.2-1.4) have the potential for higher aerodynamic efficiency and lower weight than a cantilever wing as a result of favorable interactions between structures, aerodynamics and propulsion. Figure 1.5 shows schematic shear force and bending moment diagrams for a strut-braced wing. The vertical force of the strut produces a shear force discontinuity along the span. This shear force discontinuity creates a break in the bending moment slope, which reduces the bending moment inboard of the strut. Also, the strut vertical offset provides a favorable moment that creates a spanwise bending moment curve discontinuity. This discontinuity further reduces the bending moment inboard of the strut. A decrease in bending moment means that the weight of the material required to counter that moment will be reduced. The strut provides bending load alleviation to the wing, allowing a thickness to chord ratio (*t/c*) decrease, a span increase, and usually a wing weight reduction. Reduced wing thickness decreases the transonic wave drag and parasite drag, which in turn increases the aerodynamic efficiency. These favorable drag effects allow the wing to unsweep for increased regions of natural laminar flow and further wing structural weight savings. Decreased weight, along with increased aerodynamic efficiency permits engine size to be reduced. The strong synergism offers potential for significant increases in performance over the cantilever wing. A Multidisciplinary Design Optimization (MDO) approach is necessary to fully exploit the interdependencies of various design disciplines. Overall, several facets of the analysis favorably interact to produce a highly synergistic design.

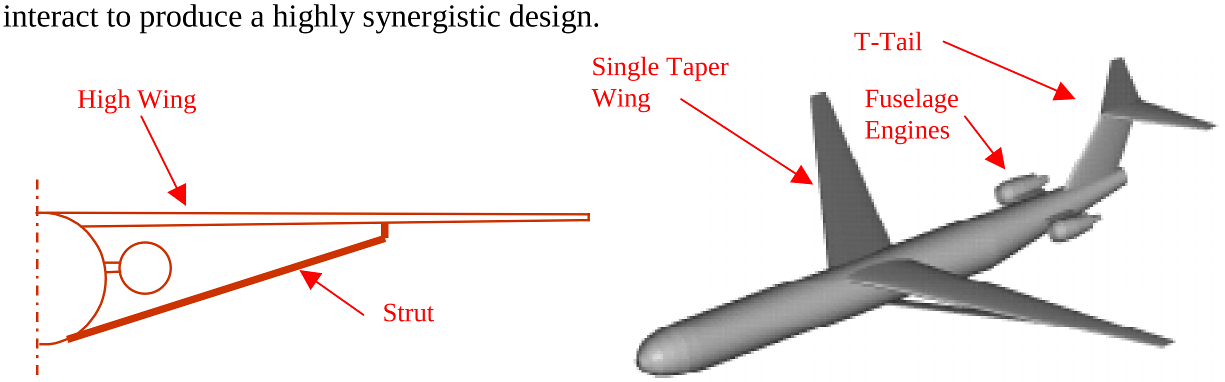

Figure 1.2. Strut-Braced Wing with Fuselage-Mounted Engines.

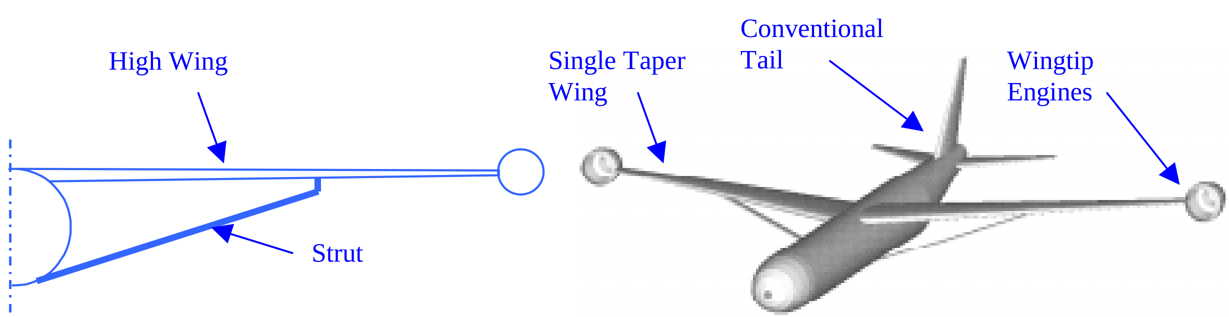

Figure 1.3. Strut-Braced Wing with Tip-Mounted Engines.

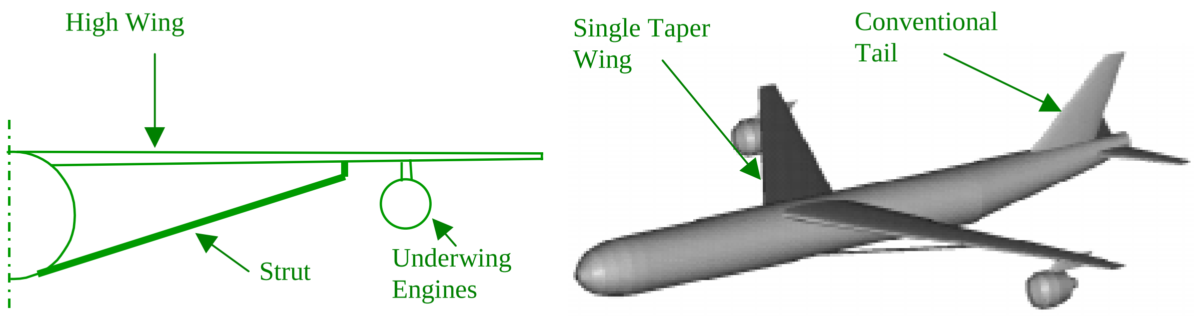

Figure 1.4. Strut-Braced Wing with Underwing Engines.

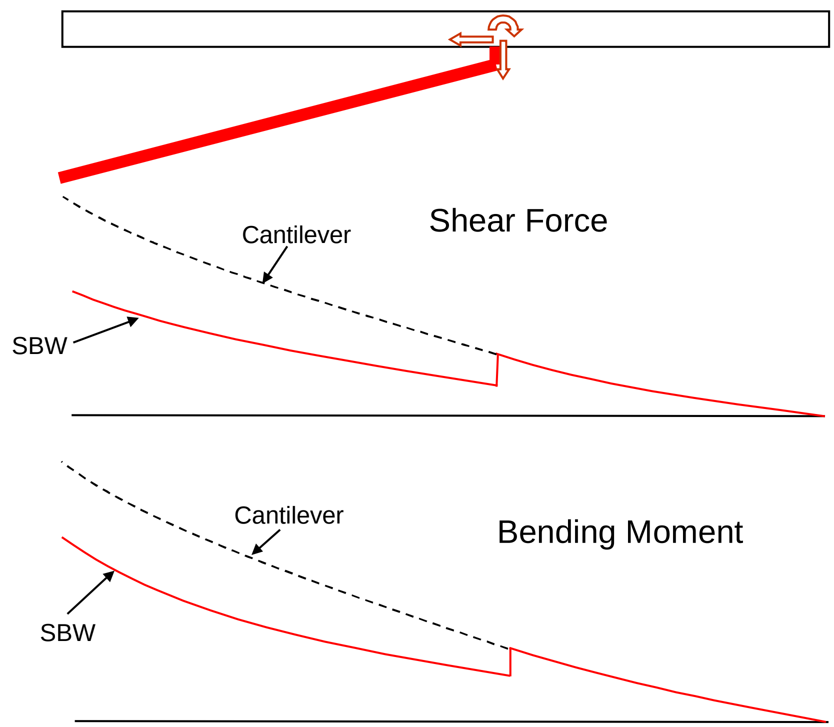

Figure 1.5. Strut-Braced Wing Shear Force and Bending Moment Diagrams.

Werner Pfenninger (1954) originated the idea of using a Truss-Braced Wing (TBW) configuration for a transonic transport at Northrop in the early 1950s (Figure 1.5). The SBW can be considered a subset of the TBW configuration. Pfenninger remained an avid proponent of the concept until his recent retirement from NASA. Several SBW design studies have been performed in the past [Pfenninger (1954), Park (1978), Kulfan et. al. (1978), Jobe et. al. (1978), Turriziani et. al. (1980), Smith et. al. (1981)], though not with a full MDO approach until quite recently [Grasmeyer (1998A,B), Martin et. al. (1998)]. Dennis Bushnell, the Chief Scientist as NASA Langley, tasked the Virginia Tech Multidisciplinary Analysis and Design (MAD) Center to perform MDO analysis of the SBW concept [Grasmeyer (1998A,B)]. Table 1.1 summarizes the major strut braced wing design studies prior to the Virginia Tech work.

Figure 1.5. Werner Pfenninger SBW Concept (NASA Photo).

Table 1.1. Summary of Past Truss-Braced Wing Studies.

Authors/Sponsor Organization	Study Year	Type of Aircraft	Improvements	Comments
Pfenninger, W./ Northrop	1954	Long-Range, Transonic Tranport		
Dollyhigh et. al./ NASA	1977	Mach 0.60-2.86 Fighter	28% Reduction in Zero-Lift Wave Drag	Several Strut Arrangements, Allowed t/c Reduction
Park	1978	Short Haul Transport	Little Improvement	Aerolasticity Effects Considered
Kulfan et. al. and Jobe et. al./ Boeing	1978	Long Range, Large Military Transport,	Higher TOGW than Equivalent Cantilver	Wingspan = 440 ft., Laminar Flow Control
Turriziani et. al./ NASA	1980	Subsonic Business Jet	20% Fuel Savings over Cantilever	Aspect Ratio = 25
Smith et. al./ NASA	1981	High-Altitude Manned Research Aircraft	5% Increase in Range over Cantilever	

This study was funded by NASA with Lockheed Martin Aeronautical Systems (LMAS) as an industry partner. The primary role of the interactions with LMAS was to add practical industry experience to the vehicle study. This was achieved by calibrating the Virginia Tech MDO code to the LMAS MDO code for baseline 1995 and 2010 technology level cantilever wing transports. The details of the baseline cantilever aircraft were provided by LMAS. LMAS also reviewed aspects of the Virginia Tech design methods specific to the strut-braced wing [Martin et. al. (1998)]. The author worked on location at LMAS to upgrade, calibrate and validate the Virginia Tech MDO code before proceeding with optimizations of conventional cantilever and strut-braced wing aircraft.

Performance may be determined from numerous perspectives. Certainly range and passenger load are important. Life cycle cost, take-off gross weight (TOGW), overall size, noise pollution, and fuel consumption are all candidate figures of merit. Other factors such as passenger and aircrew acceptance and certifiability are less easy to quantify but may determine the fate of a potential configuration.

A technology impact study is used to further understand the differences between 1995 and 2010 technology level aircraft, and to see how the SBW and cantilever configurations exploit these technologies. If the SBW can better harness technologies groups, then greater emphasis must be placed on these. Also, synergy in technology interactions will become apparent if the overall difference in 1995 and 2010 design TOGW is greater than the sum of the TOGW differences for the individual technology groups.

The SBW may have wingtip engines, under-wing engines inboard and outboard of the strut, or fuselage-mounted engines with a T-tail. Underwing and wingtip engines use blowing on the vertical tail from the APU to counteract the engine-out yawing moment. Landing gear is on the fuselage in partially protruding pods for SBW cases. The strut intersects the pods at the landing gear bulkhead and wing at the strut offset.

The baseline cantilever aircraft (Figure 1.1) has the engines mounted under a low wing and has a conventional tail. The landing gear is stowed in the wing between the wing box and kick spar. This study uses cantilever configuration optima, rather than a fixed cantilever wing geometry, so direct comparisons with the SBW configurations can be made. The differences in T-tail fuselage-mounted engine and underwing engine cantilever designs is small, so detailed results for only the underwing engine cantilever aircraft are presented here.

Chapter 2

Problem Statement

The primary mission of interest is a 325-passenger, 7500 nautical mile range, Mach 0.85 transport (See Figure 2.1). Reserve fuel sufficient for an extra 500 nautical miles of flight is included, and fixed fuel mass fractions are used for all non-cruise flight segments. An economic mission aircraft that has reduced passenger load and a 4000 nautical mile range, while still capable of fulfilling the full mission, is also considered. Range effects on TOGW and fuel consumption are investigated. Additional goals are to determine the relative benefits of the strut-braced wing configurations over the cantilever configuration at various ranges and to find the sensitivity of all configurations to various technology groups. The selected objective functions are minimum-TOGW, minimum-fuel weight, and maximum range. The technology impact study and range investigations use minimum-TOGW as the objective function.

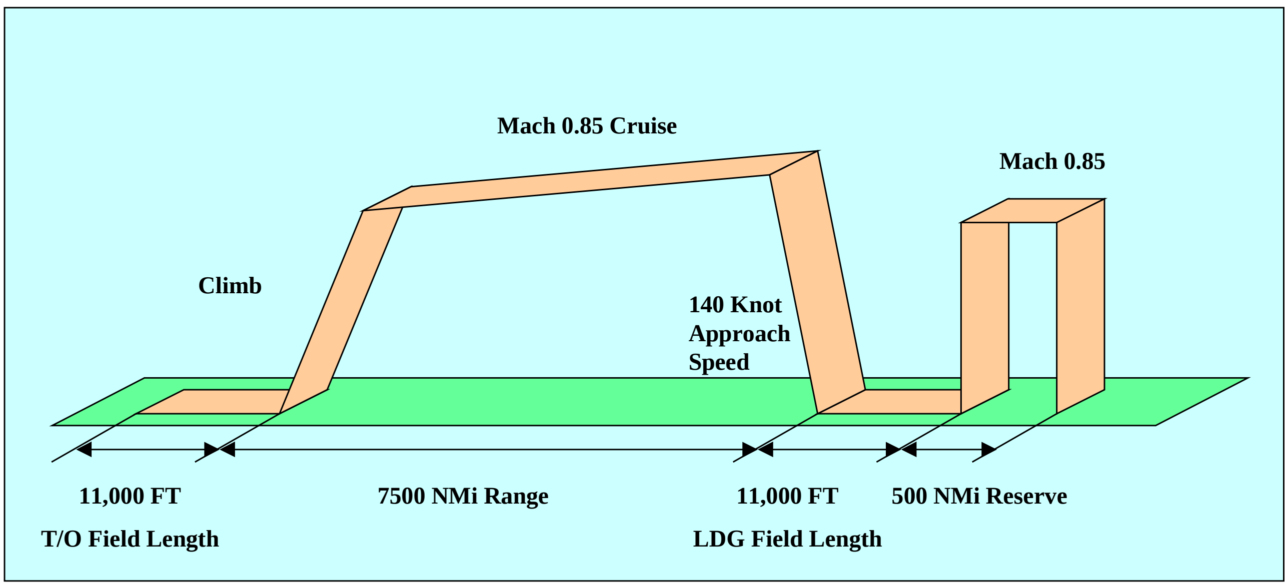

Figure 2.1. Baseline Mission Profile.

Chapter 3

Methodology

3.1 General

The Virginia Tech Truss Braced Wing (TBW) optimization code models aerodynamics, structures/weights, performance, and stability and control of both cantilever and strut-braced wing configurations. Design Optimization Tools (DOT) software by Vanderplatts R&D (1995) optimizes the vehicles with the method of feasible directions. Between 15 and 26 user selected design variables are used in a typical optimization. These include several geometric variables such as wing span, chords, thickness to chord ratios, strut geometry and engine location, plus several additional variables including engine maximum thrust and average cruising altitude (Table 3.1). As many as 17 inequality constraints may be used, including constraints for range, fuel volume, weights convergence, engine-out yawing moment, cruise section C_l limit, balanced field length, second segment climb gradient and approach velocity (Table 3.2). There are also two side constraints to bound each design variable, and each design variable is scaled between 0 and 1 at the lower and upper limits, respectively. Take-off gross-weight, economic mission take-off gross weight, fuel weight and maximum range are important examples among the many possible objective functions that can be minimized.

Some new design variables and constraints presented here were not used by Grasmeyer (1998A,B). New design variables include the wing/strut vertical aerodynamic offset, required thrust, economic mission fuel weight and economic mission average cruise altitude. The wing/strut aerodynamic offset is a surface protruding vertically downwards as shown in Figure 3.1. The required engine thrust is the thrust needed to meet a number of constraints. The engine thrust constraints will be described in more detail later in the text. The economic mission fuel weight is the fuel needed to fly the 4000 nautical mile economic mission, and the economic cruise altitude is the average cruising altitude for the economic mission.

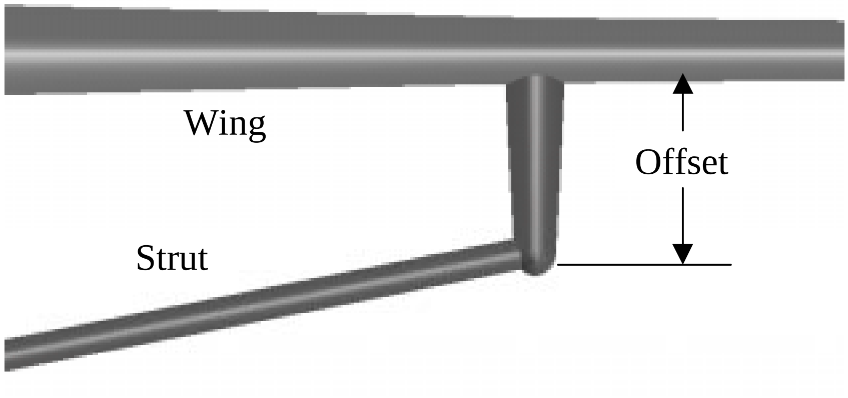

Figure 3.1. Wing/Strut Aerodynamic Offset. (LMAS Figure)

Table 3.1. Design Variables.

1.	Semi-Span of Wing/Strut Intersection
2.	Wing Span
3.	Wing Inboard ¼ Chord Sweep
4.	Wing Outboard ¼ Chord Sweep
5.	Wing Dihedral
6.	Strut ¼ Chord Sweep
7.	Strut Chordwise Offset
8.	*Strut Vertical Aerodynamic Offset
9.	Wing Centerline Chord
10.	Wing Break Chord
11.	Wing Tip Chord
12.	Strut Chord
13.	Wing Thickness to Chord Ratio at Centerline
14.	*Wing Thickness to Chord Ratio at Break
15.	Wing Thickness to Chord Ratio at Tip
16.	Strut Thickness to Chord ratio
17.	Wing Skin Thickness at Centerline
18.	Strut Tension Force
19.	Vertical Tail Scaling Factor
20.	Fuel Weight
21.	Zero Fuel Weight
22.	*Required Thrust
23.	Semispan Location of Engine
24.	Average Cruise Altitude
25.	*Econ. Mission Fuel Weight
26.	*Econ. Mission Average Cruise Altitude

*New Design Variable

Table 3.2 shows that the number of constraints has more than doubled after the research performed by Grasmeyer (1998A,B). New constraints include the climb rate available at the initial cruise altitude, wing weight convergence, maximum body and contents weight convergence, balanced field length, second segment climb, missed approach climb gradient, landing distance, economic mission range, maximum economic mission section lift coefficient and thrust at altitude. The maximum body and contents weight convergence and wing weight convergence constraints are usually turned off when the lagging variable method is used to calculate the corresponding weights. Further details on the weights convergence constraints and the lagging variable method will be given in the structures and weights section. Grasmeyer (1998A,B) calculated the required thrust of the engine by setting the engine thrust equal to the drag at the average cruise condition. In the present code the field performance and rate of climb at initial cruise altitude frequently dictate the required thrust so the thrust at altitude must be met as a constraint.

Table 3.2. Constraints.

1.	Zero Fuel Weight Convergence
2.	Range Calculated >7500 nmi
3.	*Initial Cruise Rate of Climb > 500 ft/min
4.	Cruise Section C_l Limit< 0.7
5.	Fuel Weight < Fuel Capacity
6.	C_n Available > C_n Engine-Out Condition
7.	Wing Tip Deflection < Max Wing Tip Deflection at Taxi Bump Conditions (25 feet)
8.	*Wing Weight Convergence
9.	*Max. Body and Contents Weight Convergence
10.	*Second Segment Climb Gradient > 2.4%
11.	*Balanced Field Length < 11,000 ft
12.	Approach Velocity < 140 kts.
13.	*Missed Approach Climb Gradient > 2.1%
14.	*Landing Distance < 11,000 ft
15.	*Econ. Mission Range Calculated > 4000 nmi
16.	*Econ. Mission Section C_l Limit< 0.7
17.	*Thrust at Altitude > Drag at Altitude

*New Constraint

Each constraint now has a constraint flag in the input file that turns the constraint on if the flag is set to 1 or off if the flag is set to 0. The user now has the option of selectively turning off any constraints by setting the corresponding constraint flag equal to zero, without the need to recompile the code.

Active and violated constraints are now printed during run time. Constraints that are not active or violated are not printed. This feature is very useful, because the code user can observe aspects of the optimization path and determine why the initial guess may not be a feasible design. By witnessing the violated constraints, the user can terminate the current run, modify the input file, attempt a new optimization and find a feasible design from the new inputs.

The MDO code architecture is configured in a modular fashion such that the analysis consists of subroutines representing various design disciplines. The primary analysis modules include: aerodynamics, wing bending material weight, total aircraft weight, stability and control, propulsion, flight performance and field performance. Figure 3.2 is a flow diagram of the MDO code. Initial design variables and parameters are read from an input file. The MDO code manipulates the geometry based on these inputs and passes the information on to the structural optimization and aerodynamics subroutines. The drag is calculated by induced drag, friction and form drag, wave drag, and interference drag subroutines. Additionally, the induced drag subroutine calculates the wing loads. The wing loads are passed to the structural optimization subroutines, which then calculate the aircraft structural weight. The wing bending material weight is calculated in WING.F. Other components of the aircraft structural weights are calculated in FLIPS.F, the weight estimation subroutine modified from FLOPS [McCullers] with LMAS equations. The propulsion analysis calculates the specific fuel consumption at the cruise condition. The specific fuel consumption, L/D, and aircraft weight are passed to the performance module, which calculates the range of the aircraft. The stability and control subroutine determines the engine-out yawing moment and the available yawing moment. The field performance subroutine, FIELD.F, calculates the take-off and landing performance. All constraints and the objective function are evaluated and passed to the optimizer. The optimizer manipulates the design variables until the objective function is optimized and all the constraints are not violated. Details of the analysis will be discussed in further depth in the following sections.

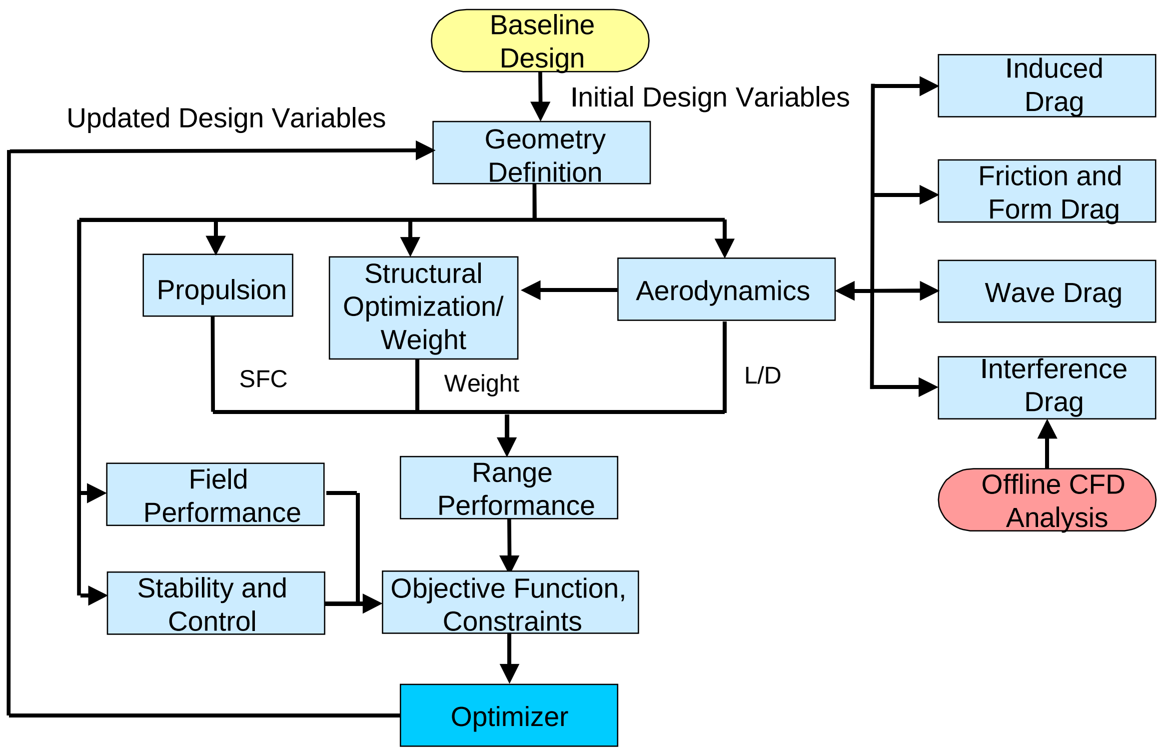

Figure 3.2. MDO Code Architecture.

Differences between the analysis and parameters of cantilever and SBW configurations are present in the design code, as is necessary for such dissimilar vehicles. The primary difference is in the analysis of the wing bending material weight, as discussed in the structures and weights section. The strut has parasite drag and interference drag at the intersections with the fuselage and wing. Also, some geometry differences are justified, such as setting the minimum root chord for the cantilever wing to 52 feet to make room for wing-mounted landing gear and kick spar. The SBW, devoid of any need for a double taper, has the chord linearly interpolated from root to tip. The SBW has a high wing and fuselage mounted gear. It is important to note that, even though the external geometry of the fuselage is identical for all cases, the fuselage weights will generally be different. This is because the fuselage weight is a function of the overall aircraft weight, tail weights, and engine and landing gear placement, all of which vary within a given configuration and from one configuration to another.

3.2 Objective Functions

The baseline mission requires that the aircraft carry 325-passengers for 7500 nautical miles at Mach 0.85. An economic mission of 4000 nautical miles with a reduced passenger load is also of interest, because commercial aircraft seldom operate at their design mission. The economic mission take-off gross weight is minimized for a minimum-economic mission TOGW case, and sometimes evaluated for the minimum-TOGW case. Range effects on take-off gross weight are investigated. A minimum-fuel objective function is also considered.

The economic mission is a 4000 nautical mile range, reduced passenger load flight profile for an aircraft also capable of flying the full 7500 nautical mile, full passenger load mission. The economic mission may be evaluated in two ways. In the first case, the objective function is minimum economic mission TOGW, and the full mission weights must converge and meet all constraints. In the second case, the economic mission TOGW is evaluated for the full mission minimum-TOGW aircraft. The economic fuel weight and economic cruise altitude are selected by the optimizer such that the economic take-off gross weight is minimized, while meeting all of the appropriate constraints.

In the first case, the aircraft geometry, weights, altitude and other variables are allowed to vary as with any other optimization. In addition to these variables, the economic fuel weight and economic cruise altitude are also design variables. Economic range and economic maximum section lift coefficient at cruise constraints are added to the usual constraints.

In the second case, all design variables are now fixed at the minimum-TOGW optimum values. All constraints except for the economic range and economic cruise altitude are turned off. Now the only two design variables are economic cruise altitude and economic fuel weight, and the two constraints are economic range and economic maximum section lift coefficient at cruise.

The economic cruise section C_l limit is the same value as the full mission maximum section C_l. However, it is important to have two separate constraints, because the two mission profiles tend to have different average cruise altitudes. The maximum allowable economic section lift coefficient typically limits the economic average cruise altitude.

The economic flight profile is analyzed at economic cruise weight, which is given by:

$$W_{EconCruise} = W_{ZF} - \Delta W_{ZF,Econ} + \frac{1}{2} \cdot W_{FuelEcon}$$

and at the economic average cruise altitude. The change in economic zero-fuel weight due to reduced passenger and baggage load, $\Delta W_{ZF,Econ}$, was provided by LMAS. The aerodynamics subroutine is called to find the *L/D*, and other terms such as the specific fuel consumption at this condition are determined. Then the Breguet range equation is used to find the calculated range.

The technology impact study investigates the relative benefits of several technology groups when applied to baseline 1995 technology level aircraft. A 1995 aircraft represents the current technology level similar to that of the Boeing 777. Each case is optimized for minimum-TOGW. A technology factor of 1 is associated with a metallic 1995 aircraft benchmark. LMAS prepared several factors to be applied to various vehicle component weights, tail volume coefficients, specific fuel consumption, induced drag, and constants for wave drag and laminar flow. Groupings were made in the following categories: natural laminar flow, other aerodynamics, systems, structural weights and propulsion.

The natural laminar flow group allows laminar flow on the wing, strut, tails, fuselage and nacelles.

Table 3.3. Natural Laminar Flow Technology Group.

1995	2010
No Laminar Flow	Transition *x/c* Calculated on Wings, Strut, and Tails as a Function of Sweep and Mach Number. Transition Reynolds Number on Fuselage and Engine Nacelles Set to 2.5×10^6. Laminar Tech Factor Applied

The other aerodynamics group includes the effects of riblets on the fuselage and nacelles, active load management for induced drag reduction, all moving control surfaces and supercritical airfoils.

Table 3.4. Other Aerodynamics Technology Group.

1995	2010
Low Airfoil Tech Factor Applied (For Wave Drag Korn Equation) Other Aerodynamic Tech Factors = 1.	High Airfoil Tech Factor Applied Induced Drag Tech Factor Applied Fuselage Turbulent Drag Tech Factor Applied

Systems technologies include integrated modular flight controls, fly-by-light and power-by-light, simple high-lift devices, and advanced flight management systems.

Table 3.5. Systems Technology Group.

1995	2010
1995 Horizontal Tail Volume Coefficient All Systems Tech Factors = 1.	Horizontal Tail Volume Coefficient Reduction Controls Weight Tech Factor Applied Hydraulics Weight Tech Factor Applied Avionics Weight Tech Factor Applied Furnishings and Equipment Weight Tech Factor Applied

Airframe technologies reflect composite wing and tails and integrally stiffened fuselage skins.

Table 3.6. Structures Technology Group.

1995	2010
Weights Tech Factors = 1.	Wing Weight Tech Factor Applied Horizontal Tail Weight Tech Factor Applied Vertical Tail Weight Tech Factor Applied Body Weight Tech Factor Applied

The propulsion technology is reflected in reduced specific fuel consumption.

Table 3.7. Propulsion Technology Group.

1995	2010
Specific Fuel Consumption Tech Factor = 1.	Specific Fuel Tech Factor Applied

3.3 Geometry Changes

Previous work by Grasmeyer (1998A,B) used a constant wing thickness to chord ratio, *t/c*, on the outboard panel and an average *t/c* for the inboard section. Calibrations with LMAS baseline designs proved troublesome with this formulation, so the actual *t/c* values at the root, breakpoint and tip are now separately defined to be more consistent.

Changing the formulation introduced some complications. Although WING.F, the wing bending material weight subroutine, requires *t/c* inputs for these three locations, it assumes that the tip *t/c* and break *t/c* are identical. WING.F was modified to correct this. Andy Ko modified the *t/c* interpolation such that the thickness and chord are interpolated linearly rather than linearly interpolating the *t/c*. This ensures that the wing contours remain conic sections, and the new formulation better reflects reality. Figure 3.3 shows the new and old t/c formulations.

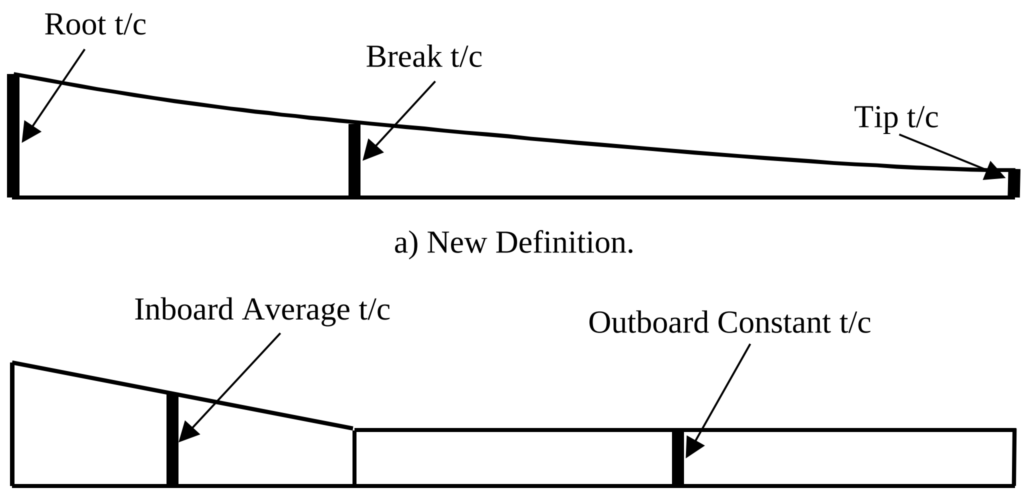

b) Old Definition.

Figure 3.3. *t/c* Definitions.

For a strut-braced wing configuration, the wing has a single taper and the strut has no taper. There is a series of if-then statements in subroutine CONVERT that will automatically interpolate the wing breakpoint chord and set the strut tip chord equal to the strut root chord. The wing breakpoint chord is calculated in this way so that the wing outboard panel is not permitted to have excessive taper (taper ratio > 1). The strut chord is held constant, because the wing/strut intersection interference drag is no longer a function of strut tip chord. Compounding the problem, the strut-offset thickness is increased when the strut tip chord is increased. An increase in strut offset thickness is lighter for a given bending load, because the moment of inertia is higher. These effects combine to produce taper ratios well in excess of 1.0 if the taper ratio is not constrained.

FLIPS.F and FLOPS [McCullers] use different average wing thickness conventions. The original FLOPS uses:

$$t/c_{Average} = \frac{4 \cdot t/c_{Root} + 5 \cdot t/c_{Break} + t/c_{Tip}}{10}$$

and FLIPS.F uses the convention:

$$t/c_{Average} = \frac{4 \cdot t/c_{Root} + t/c_{Tip}}{5}$$

The SBW code originally did not account for the engine moment arm for fuselage mounted engines. The lateral distance from the aircraft centerline to the center of a fuselage-mounted engine is now calculated as:

$$Y_{Engine} = \frac{1}{2} \cdot D_{fuselage} + \frac{1}{2} \cdot D_{Engine} + h_{Pylon}$$

and this value is substituted for the wing-mounted engine Y_{Engine} value normally used for the required yawing moment coefficient calculation.

3.4 Aerodynamics

Numerous iterations of both the Virginia Tech TBW code and Lockheed's version of FLOPS [McCullers] were made so that drag polars produced by each code are consistent at reference design conditions. The drag components considered in the Virginia Tech MDO tool are parasite, induced, interference and wave drag. Unless specified otherwise, the drag model is identical to previous Virginia Tech SBW studies [Grasmeyer (1998A,B)]

To calculate the parasite drag, form factors are applied to the equivalent flat plate skin friction drag of all exposed surfaces on the aircraft. The amounts of laminar flow on the wing and tails are estimated by interpolating Reynolds number vs. sweep data for F-14 and 757 glove experiments [Braslow et. al. (1990)]. Transition locations of the horizontal and vertical tails now follow the same procedures as for the wing and strut, whereas they were considered fully turbulent in previous studies [Grasmeyer (1998A,B)]. The fuselage, nacelle, and pylon transition locations are estimated by an input transition Reynolds number of 2.5 million. Laminar and turbulent flat-plate skin friction form factors are calculated by a hybrid formulation using Lockheed's Modular Drag (MODRAG) formulas and the FRICTION algorithm [Mason] in the Virginia Tech TBW code. The wing, tail surfaces, nacelle and fuselage wetted areas and form factors for friction drag calculations now use the LMAS formulation. The wing thickness distribution for the form/friction drag is found from the new thickness calculation procedure. The engine equivalent length/diameter ratio used for the form drag is modified. The old formulation has identical form factor formulas for both the nacelle and fuselage, but the LMAS procedure has two distinct formulas. Previously, the pylon drag was greater for the wing-mounted engines than for fuselage-mounted engines, but now the drags are equal. The form drag multiplying factor is now the same for both underwing and fuselage-mounted engines. The parasite drag of a component is found by:

$$C_{D_p} = C_{D_f} \cdot FF \cdot \frac{S}{S_{ref}}$$

The induced drag module [Grasmeyer (1997)] uses a discreet vortex method to calculate the induced drag in the Trefftz plane. Given an arbitrary, non-coplanar wing/truss configuration, it provides the optimum load distribution corresponding to the minimum induced drag. This load distribution is then passed to the wing structural design subroutine, WING.F. Induced drag reductions are employed on the wingtip-mounted engine case [Grasmeyer (1998A,B), Patterson et. al. (1987), Miranda et. al. (1986)], with the relative benefits wingtip engines decreasing as the aspect ratio increases (Figure 3.4). The field performance section gives more detail on the wingtip-mounted engine drag reduction.

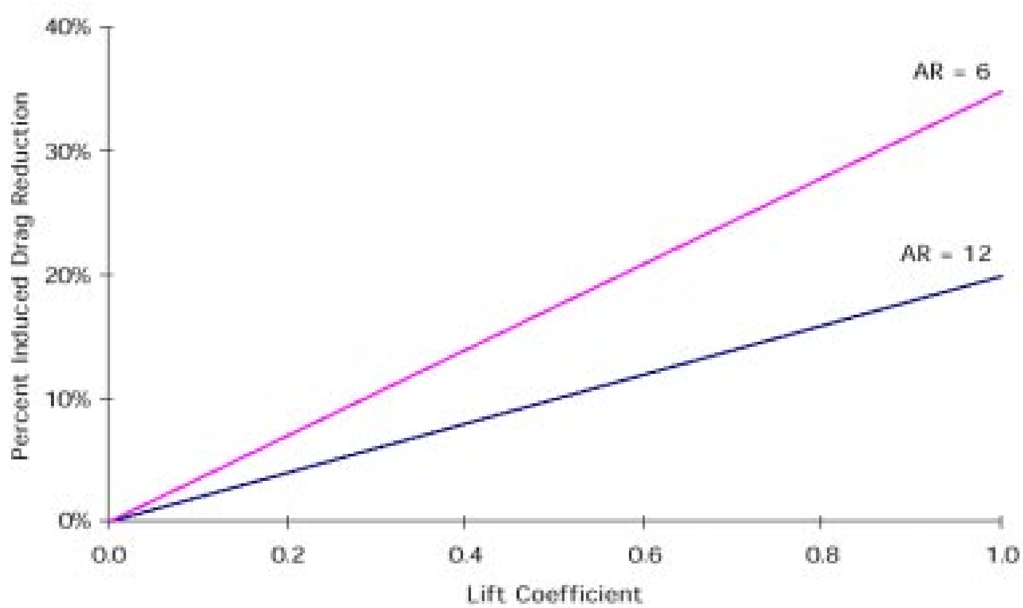

Figure 3.4. Wingtip-Mounted Engine Induced Drag Reduction. [Grasmeyer (1998A,B)]

An additional profile drag due to lift term was added to help correlate the LMAS and VPI drag polars at off-design conditions. The equation is:

$$\Delta C_{D,CL} = \left(\frac{1}{f_{break}} - 1 \right) \cdot \frac{\left(C_L - C_{Lbreak} \right)^2}{\pi \cdot AR_W}$$

where f_{break} and C_{Lbreak} are constant inputs determined from correlation with LMAS drag polars. The overall effect of this drag component at design conditions is small, because C_L is close to C_{Lbreak}.

The interference drag between the wing-fuselage and strut-fuselage intersections are estimated using Hoerner (1965) equations based on subsonic wind tunnel tests. The wing-strut interference drag is based on Virginia Tech CFD results [Tetrault (1998)], and is found to be:

$$C_D = \frac{18}{Offset} \quad \text{(Counts)}$$

Tetrault (1998) used the USM3D CFD code with VGRIDns unstructured grid generator for this analysis. Figure 3.5 shows the correlation between the CFD results and the interference drag equation. A hyperbola is used to fit the data because the interference drag is expected to greatly increase with decreasing arch radii.

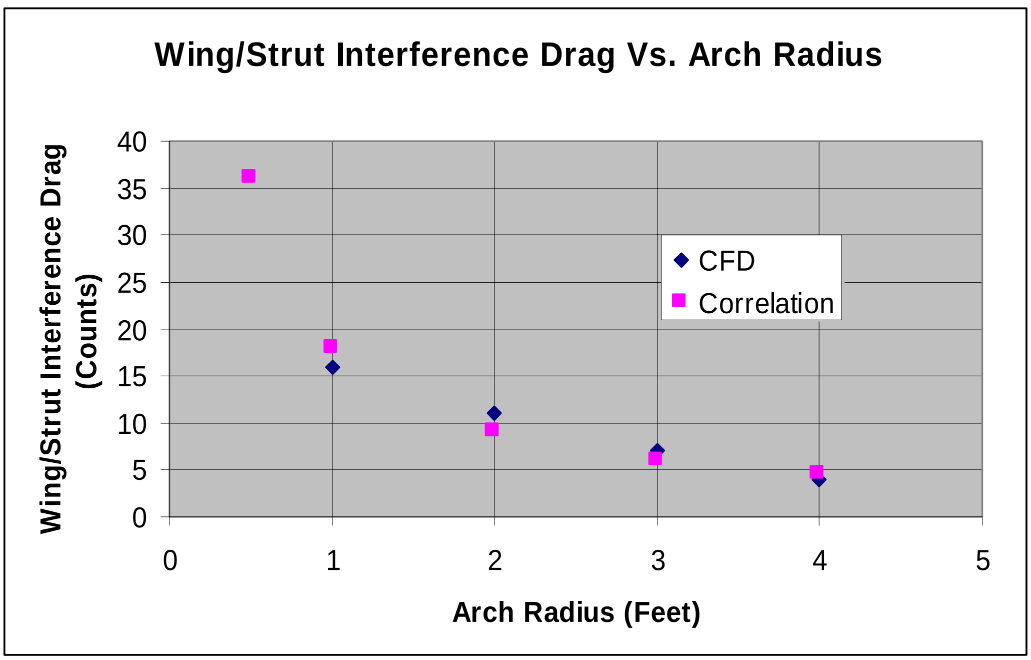

Figure 3.5. Wing/Strut Interference Drag vs. Arch Radius Correlation [Tetrault (1998)].

The wave drag is approximated with the Korn equation, modified to include sweep using simple sweep theory [Grasmeyer (1998A,B), Malone et. al. (1995), Mason (1990)]. This model estimates the drag divergence Mach number as a function of airfoil technology factor, the thickness to chord ratio, the section lift coefficient, and the sweep angle by:

$$M_{dd} = \frac{\kappa_a}{\cos\Lambda} - \frac{t/c}{\cos^2\Lambda} - \frac{c_l}{10\cdot\cos^3\Lambda}$$

The airfoil technology factor, κ_a, was selected by Lockheed to agree with their original formulation. The wing thickness now uses the new thickness calculation procedure. The critical mach number is:

$$M_{crit} = M_{dd} - \left(\frac{0.1}{80}\right)^{1/3}$$

Finally, the wave drag coefficient of a wing strip is calculated with Lock's formula [Hilton (1952)] as:

$$c_{d_{wave}} = 20(M - M_{crit})^4 \frac{S_{strip}}{S_{ref}}$$

The total wave drag is found by integrating the wave drag of the strips along the wing.

The drag polars output from the Virginia Tech MDO tool and Lockheed's modified FLOPS agree within 1% on average for cantilever wing designs. Figure 3.6 Shows a comparison between Virginia Tech and LMAS drag polars for a 1995 technology level cantilever wing aircraft. Note that LMAS does not have a SBW design for direct comparisons, so all correlations were done with cantilever aircraft. The laminar technology factor, airfoil technology factor and all other aerodynamic constants are the same for all configurations, but the former two vary between 1995 and 2010 technology levels.

Technology factors for the technology analysis may be applied to the induced drag term and the turbulent friction drag of the fuselage and nacelles. The induced drag technology factor is applied to the induced drag directly in AERO.F. The turbulent friction drag technology factor is passed from AERO.F to FDRAG.F, where it is multiplied by the turbulent skin friction term.

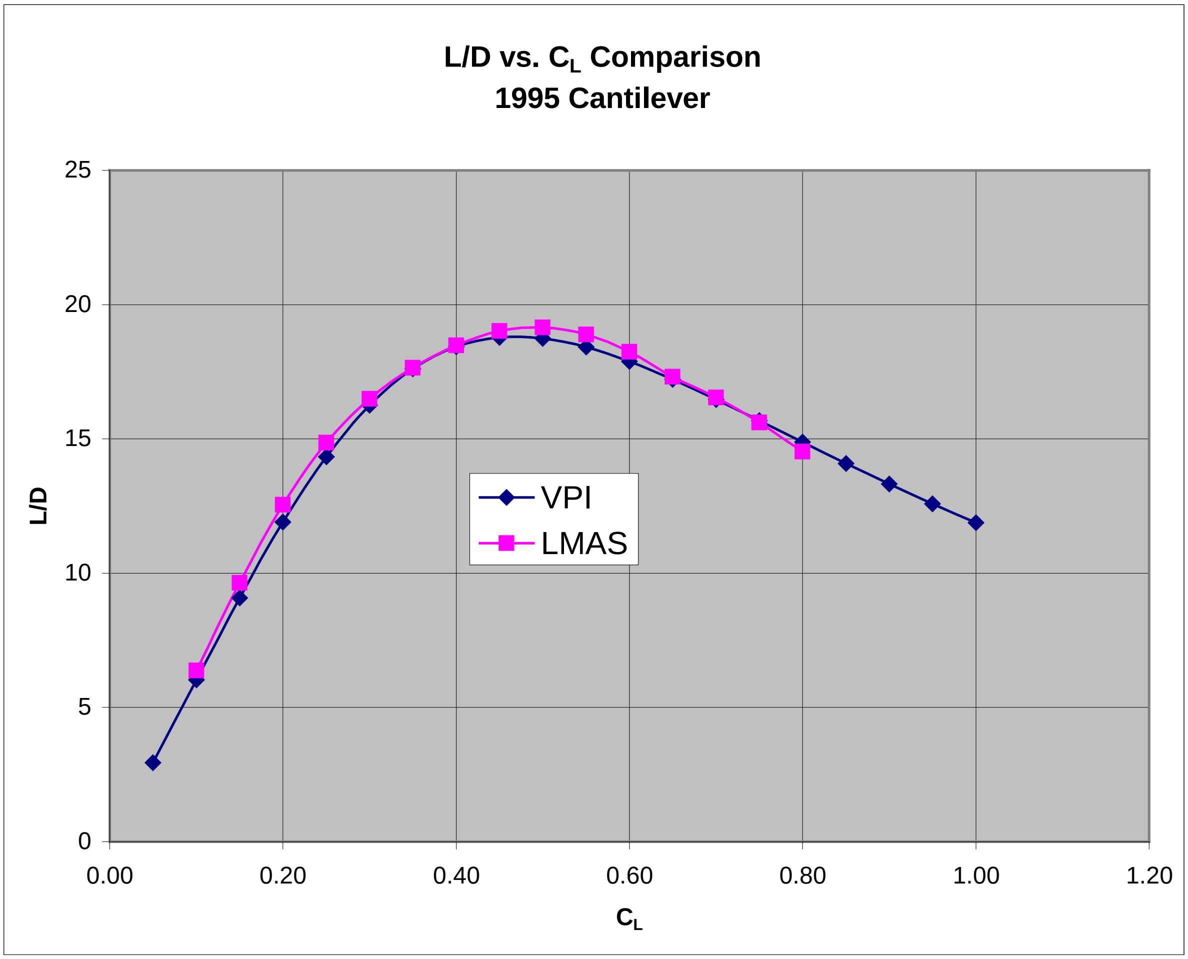

Figure 3.6. Virginia Tech and LMAS Drag Polar Comparison.

3.5 Structures and Weights

The aircraft weight is calculated with several different methods. The majority of the weights equations come from NASA Langley's Flight Optimization System (FLOPS) [McCullers]. Many of the FLOPS equations were replaced with those suggested by LMAS in FLIPS.F. The FLIPS.F and original FLOPS methods do not have the option to analyze the strut-braced wing with the desired fidelity, so a piecewise linear beam model was developed at Virginia Tech to estimate the bending material weight [Naghshineh-Pour et. al. (1998)].

The piecewise linear beam model represents the wing bending material as an idealized double plate model of the upper and lower wing box covers. The vertical offset member discussed in the aerodynamics section was added to the wing/strut intersection to help reduce the interference drag at this intersection. The structural offset length is assumed to be the length of the aerodynamic offset plus some internal distance within the wing. This offset must take both bending and tension loading. Vertical offset weight increases rapidly with increasing length, but the interference drag decreases. The offset length is now a design variable, and the optimizer selects its optimum value. Fortunately, the vertical offset imposes bending moment relief on the wing at the intersection, and the resulting overall influence on the TOGW is negligible. A 10% weight penalty is applied to the piecewise linear beam model to account for non-optimum loading and manufacturing considerations. An additional 1% bending material weight increase is added to the SBW to address the discontinuity in bending moment at the wing/vertical offset intersection. Figure 3.7 shows the wing weight calculation procedure.

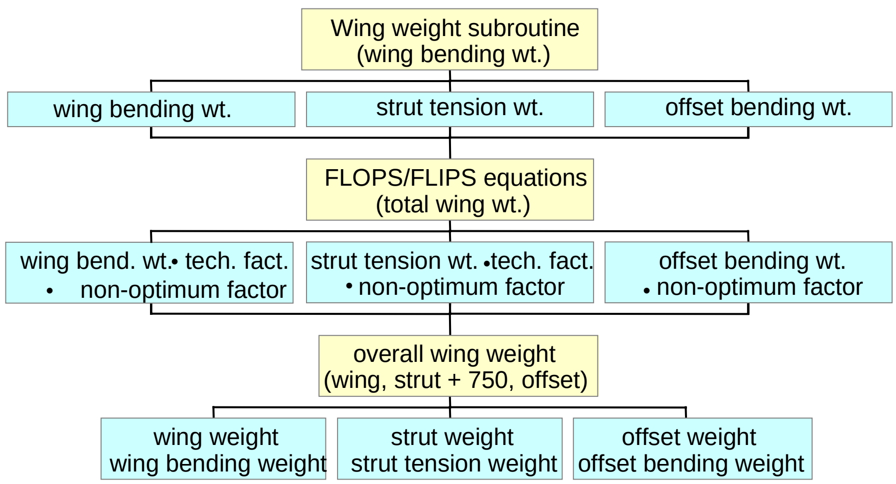

Figure 3.7. Wing Weight Calculation Procedure.

Several modifications have been made to WING.F for the current study. The number of spanwise steps between vortices is decreased from 300 to 30. The taxi load factor was increased from 1.67 to 2.0. A fuel weight distribution error was corrected. A modification was made to the cosine component of the structural wing chord interpolation. The engine load factor of 2.5 was multiplied by 1.5 to account for the safety factor, so the current value is now 3.75. The wing-box chord to wing chord ratio was decreased from 0.5 to 0.45. The minimum gauge thickness was changed from 0.004 to a value specified by LMAS. Aluminum wing allowable stress went from 51,800 psi, the value found in Torenbeek, to a value specified by LMAS. The wing/strut vertical structural offset is now included. The new wing thickness distribution procedure is also now included in WING.F.

Earlier Virginia Tech studies [Grasmeyer (1998A,B), Naghshineh-Pour et. al. (1998)] have shown that the critical structural design case for the single-strut is strut buckling at -1 g loading. To alleviate this stringent requirement, a telescoping sleeve mechanism arrangement is employed such that the strut will engage under positive a load factor, and the wing will essentially act as a cantilever wing under negative loading. LMAS provided a 750-pound weight estimate for the telescoping sleeve mechanism based on landing gear component data. Also, the SBW must contend with the –2 g taxi bump case, where the strut is also inactive.

The wingtip deflection at the taxi bump condition constraint for underwing engines previously only considered the wingtip deflection and not the engine ground strike. Now the sum of the engine diameter, pylon height and downward wing deflection at the engine location give the overall wingtip deflection. The wingtip deflection constraint will be violated if either the wingtip deflection or engine deflection exceed the maximum allowable wingtip deflection value.

Weights calculated in the Virginia Tech TBW code are identical to FLOPS with the exception of nacelle, thrust reverser, landing gear, passenger service, wing, fuselage and tail weights. The above weights are now calculated from proprietary LMAS formulas. Weight technology factors are applied to major structural components and systems to reflect advances in technology levels from composite materials and advanced electronics.

Subroutine FLIPS.F uses a combination of FLOPS weights equations and LMAS equations. The equations themselves are not presented here, but some highlights are described. To account for manufacturing considerations, the cantilever wing bending material weight from WING.F is multiplied by a factor of 1.1. Similarly, SBW wing bending material, strut bending material and strut offset bending material weights from WING.F are multiplied by 1.11 to account for the discontinuous bending moment along the wing at the wing/strut intersection. Systems, landing gear and tail surface weights are calculated first. Then the wing weight, fuselage and zero fuel weights are calculated.

Traditionally, some aircraft weights are implicit functions, and internal iteration loops are required for convergence. However, utilizing the optimizer for zero fuel weight convergence is more efficient and provides smoother gradients. DOT also selects the fuel weight so that the range constraint is not violated. The wing and maximum body and contents weights are also implicit functions. The fuselage, wing, and zero fuel weight equations have the following functional dependencies.

$$W_{Fuse}(W_{BodyMax,in}, W_{ZF,in}, W_{Fuel})$$
$$W_{Wing}(W_{Wing,in}, W_{ZF,in}, W_{Fuel})$$
$$W_{ZF,Calc}(W_{Wing}, W_{Fuse})$$
$$W_{BodyMax}(W_{Fuse}, W_{ZF,Calc})$$

Earlier versions of FLIPS.F let the maximum body and contents weight and the wing weight be design variables that had to converge with their calculated values. Now a lagging variable method is employed. With this procedure the input wing and maximum body and contents weight inputs are set to their respective output values from the previous iteration. The input values for the first iteration are input from the input file. Convergence of wing and maximum body and contents weights are rapid with the lagging variable method and leads to better conditioning of the optimization problem than if these two variables converge as design variables. The original FLOPS weight subroutine does not rely on such convergence methods for any fuselage or wing weight terms and thus has better problem formulation conditioning.

To find the landing gear weight, the landing gear length is calculated by methods differing from both FLOPS and LMAS weights equations. All SBW landing gear lengths are set to 7 feet to allow for ground clearance at landing and for service vehicles, as specified by LMAS. The main landing gear length for the cantilever wing case has a 4-foot ground clearance, plus the nacelle diameter and pylon height. The four-foot nacelle ground clearance was selected arbitrarily. The nose gear is 70% of the main gear length.

The GE-90 engine reference weight is now lower than previous studies, because this quantity no longer includes the inlet and thrust reverser weights. These are now calculated by proprietary LMAS formulas. The reference engine weight is calculated by an engine scaling factor equal to the ratio of required thrust to reference thrust. The wing bending material weight depends on the weight hanging from the engine pylon. This engine pod weight was modified to allow for the new engine weight accounting system.

3.6 Cost Analysis

The FLOPS cost module is used to calculate the acquisition cost, direct operating cost and indirect operating cost in a similar manner as previous studies by Grasmeyer (1998A,B). The total cost for this formulation is found by:

Total Cost = Acquisition Cost + Direct Operating Cost + Indirect Operating Cost

Originally, the FLOPS cost module used the weights produced by the FLOPS weight module for calculations. Now a subroutine COST passes an array of FLIPS.F weight data to FLOPS, overwrites the FLOPS weights, and then calculates cost based on the new FLIPS.F weights. FLOPS is called in a similar method to what was previously done to retrieve the weights data. Now only the cost information and not the FLOPS weights are returned to the main code from COST.

3.7 Stability and Control Analysis

The horizontal and vertical tail areas are first calculated with a tail volume coefficient sizing method. The user specified tail volume coefficients are now based on LMAS statistical data. Grasmeyer (1998A-C) had the tail geometry fixed to that of the Boeing 777. Tail geometric parameters such as taper ratio, aspect ratio and quarter chord sweep are held constant regardless of tail area, but the parameters vary between T-tail and conventional tails. An option exists to input the tail area rather than calculate it from the tail volume coefficient method, but this was not utilized for this study. The tail moment arm is held constant for a given case. The variable used for the tail moment arm, or the distance from the center of gravity to the aerodynamic center of a tail surface, was previously used to define the distance from the leading edge of the wing to the leading edge of the tail surface. Now the distance between the leading edges is calculated from the tail moment arm and wing and tail geometry. Details of the tail geometry formulation are found in Appendix 1.

A vertical tail sizing routine was developed to account for the one engine inoperative condition [Grasmeyer (1998A-C)]. The engine-out constraint is met by constraining the maximum available yawing moment coefficient to be greater than the yawing moment coefficient required to handle the engine-out requirement. The aircraft must be capable of maintaining straight flight at 1.2 times the stall speed, as specified by FAR requirements. The operable engine is at its maximum available thrust. Vertical tail circulation control is permitted only on the underwing and wingtip-mounted engine cases, resulting in vertical tail lift coefficient augmentation and greater available yawing moment. The change in vertical tail lift coefficient for the wingtip-mounted engine and underwing engine outboard of the strut SBW cases is set to 1.0.

The engine-out yawing moment coefficient required to maintain straight flight is given by:

$$C_{n_{req}} = \frac{(T_E + D_E) \cdot Y_{Eng}}{q \cdot S_w \cdot b_w}$$

where T_E is the thrust of the good engine, D_E is the drag on the inoperable engine, and Y_E is the lateral distance to the engine. The lateral force of the vertical tail provides most of the yawing moment required to maintain straight flight after an engine failure.

The maximum available yawing moment coefficient is obtained at an equilibrium flight condition with a given bank angle and a given maximum rudder deflection. FAR 25.149 limits the maximum bank angle to 5^o, and some sideslip angle is allowed. The stability and control derivatives are calculated using empirical methods based on DATCOM as modified by Grasmeyer (1998A-C) to account for vertical tail circulation control.

To allow a 5^o aileron deflection margin for maneuvering, the calculated deflection must be less than 20^o-25^o. The calculated available yawing moment coefficient is constrained in the optimization problem to be greater than the required yawing moment coefficient. If the yawing moment constraint is violated, a vertical tail area multiplying factor is applied by the optimizer.

3.8 Propulsion

A GE-90 class high-bypass ratio turbofan engine is used for this design study. An engine deck was obtained from LMAS, and appropriate curves for specific fuel consumption and maximum thrust as a function of altitude and Mach number were found through regression analysis. The general forms of the equations are identical to those found in Mattingly (1987) for high-bypass ratio turbofan engines, but the coefficients and exponents are modified. Figure 3.8 shows the correlation between the specific fuel consumption and thrust at altitude models and a GE-90-like engine deck. The steps in the specific fuel consumption found in Figure 3.8 are caused by sudden increases in Mach number at the beginning of each climb segment for the LMAS flight profile. The engine size is determined by the thrust required to meet the most demanding of several constraints. These constraints are thrust at average cruise altitude, rate of climb at initial cruise altitude, balanced field length, second segment climb gradient, and missed approach climb gradient. The engine weight is assumed to be linearly proportional to the engine thrust. The engine dimensions vary as the square root of their weight, as is typically done in dynamic scaling of aircraft components. The modified engine dimensions are passed to the aerodynamics and structures routines (neglected in previous Virginia Tech SBW studies). Some concerns have arisen regarding the range through which a GE 90-like engine may be scaled, however no other suitable model is available. The specific fuel consumption model is independent of engine scale. A specific fuel consumption technology factor is applied to reflect advances in engine technology. The formulas for the thrust and specific fuel consumption at altitude are:

$$\frac{T}{T_{SL,Static}} = \left(\left(0.6069 + .5344 \cdot (0.9001 - M)^{2.7981}\right) \cdot \left(\frac{\rho}{\rho_{SL}}\right)^{0.8852} \right)$$

$$sfc = \left(\frac{Temp}{Temp_{SL}}\right)^{0.4704} \left(sfc_{Static} + 0.4021 \cdot M\right)$$

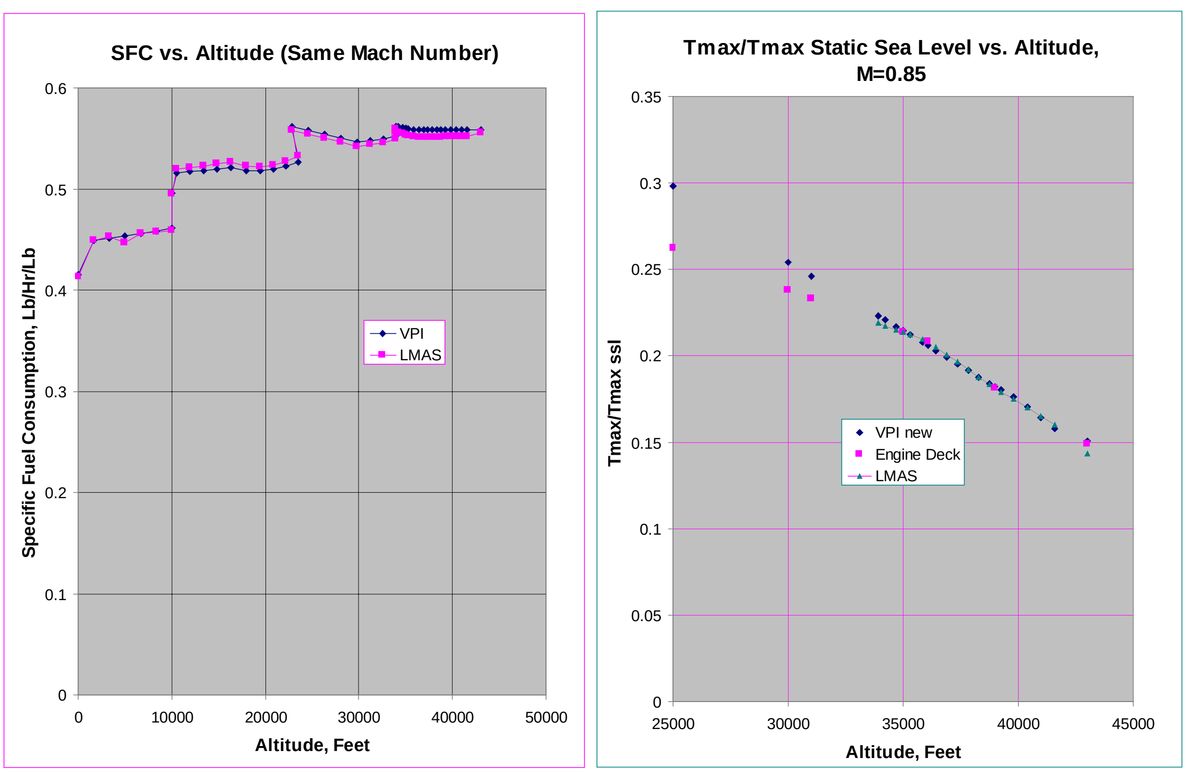

Figure 3.8. Engine Model and Engine Deck Comparison.

3.9 Flight Performance

The calculated range is determined from the Breguet range equation.

$$Range = \frac{(L/D)\cdot V}{sfc} ln\left(\frac{W_i}{W_0}\right) - Reserve$$

The *L/D*, flight velocity and specific fuel consumption are found for the average cruising altitude and fixed Mach number. W_i/W_o is the ratio of initial cruise weight to the zero-fuel weight. The initial cruise weight is 95.6% of the take-off gross weight to account for fuel burned during climb to the initial cruise altitude. A reserve range of 500 nautical miles is used as an approximation to the FAR requirement [Loftin (1980)].

The available rate of climb at the initial cruise altitude is required be greater than 500 feet/second. The average cruise altitude is generally a design variable and is thus known for every iteration. The initial cruise altitude is not known and the following procedure is used to find its value. Mach number and lift coefficient must be constant throughout cruise, and in order for this to be true:

$$\rho \cdot a^2 = \frac{W}{\frac{1}{2} \cdot M^2 \cdot C_L \cdot S_{ref}}$$

where W is the weight at the flight condition and M and C_L are specified. The weight is the initial cruise weight, M is set at 0.85 and C_L is the value from the average cruise condition. The initial altitude is the altitude at which this equation is satisfied for the above conditions. A secant method is employed to solve for the initial cruise altitude by finding the density and sound speed from the STDATM subroutine. If the initial cruise altitude and average cruise altitude are both in the stratosphere, then the temperature is constant and the formula simplifies to:

$$\rho = \frac{W}{\frac{1}{2} \cdot V^2 \cdot C_L \cdot S_{ref}}$$

The initial cruise rate of climb is:

$$R/C_{CruiseInitial} = \left(\frac{T}{W} - \frac{1}{L/D}\right) \cdot M \cdot a$$

with the thrust and weight equal to their values at the initial cruise condition, and the appropriate unit conversions are used. The *L/D* is assumed to be equal to the average cruise *L/D*. The maximum observed *L/D* difference is 2.6%.

3.10 Field Performance

Take-off and landing performance utilizes methods found in Roskam and Lan (1997). The field performance subroutine calculates the second segment climb gradient, the balanced field length, the missed approach climb gradient, and the landing distance. LMAS reviewed the field performance subroutine and decided that it produced results acceptably close to those obtained by their own methods for the 1995 and 2010 technology level cantilever baseline aircraft.

Reference drag polars for the aircraft at take-off and landing were provided by LMAS. Trends are assumed to be the same for both the SBW and cantilever configurations. The actual drag polars utilize corrections based on total aircraft wetted area and wing aspect ratio. The total aircraft wetted area is calculated in AERO.F. It was assumed that, with the level of fidelity of this systems study, the high lift characteristics of the vehicles may be tailored in many ways such that the corrected drag polars can be attained.

A correction factor to the lift dependent drag terms, f, is used for the take-off and landing drag polars of wingtip-mounted engine SBW aircraft. The correction factor is found by an interpolation procedure first developed by Grasmeyer (1998A,B) for cruise induced drag. Note that for all cases other than wingtip-mounted engines, $f = 1$. The factor depends strongly on C_L and varies from one flight condition to another. The factor f can be found by the following procedure:

$$f_6 = 1 - 0.35 \cdot C_L$$

$$f_{12} = 1 - 0.20 \cdot C_L$$

$$f = f_6 + \left(f_{12} - f_6\right) \cdot \frac{\left(AR_W - 6\right)}{\left(12 - 6\right)}$$

All calculations are done for hot day conditions, as specified by LMAS, at sea level. LMAS specified that the temperature of the airport be 83 ^{o}F. Density and sound speed corrections were made to the outputs of the standard atmosphere model.

The balanced field length equation found from Roskam is given below.

$$BFL = \frac{0.863}{1 + 2.3 * \Delta\gamma_2}\left(\frac{W_{TO}/S}{\rho \cdot g \cdot C_{L2}} + h_{TO}\right)\left(\frac{1}{\overline{T}/W_{TO} - \mu'} + 2.7\right) + \frac{\Delta S_{TO}}{\sqrt{\rho/\rho_{SL}}}$$

Some of the parameters are:

$$\Delta\gamma_2 = \gamma_2 - \gamma_{2Min}$$

$$h_{TO} = 35\,ft$$

$$\mu' = 0.010 \cdot C_{L\max TO} + 0.02$$

$$\Delta S_{TO} = 655\,ft$$

The second segment climb gradient is the ratio of rate of climb to the forward velocity at full throttle while one engine is inoperative and the gear is retracted. The second segment climb gradient, γ_2, is found by:

$$\gamma_2 = \frac{R/C}{V} = \frac{T-D}{W} = \frac{T}{W} - \frac{1}{(L/D)}$$

The minimum second segment climb gradients for aircraft having 2-4 engines are presented in Table 3.3. The engine thrust at second segment climb is a function of density and Mach number according to a modified version of Mattingly's equation presented in the propulsion section. The mean thrust for the take-off run is determined from the suggested formula in Roskam and Lan (1997):

$$\bar{T} = \frac{3}{4} \cdot \frac{(5+BPR)}{(4+BPR)} \cdot T_{static}$$

The maximum take-off lift coefficient is the minimum C_L associated with $V_2 = 1.2V_{\mathrm{stall}}$ or the C_L for the tail scrape angle. C_{Lstall} is read in through the input file and is independent of configuration. The tail scrape lift coefficient is:

$$\mathrm{C_{Lscrape}} = \mathrm{C}_{\mathrm{L}\alpha=0} + \mathrm{C}_{\mathrm{L}\alpha} \cdot (\mathrm{Angle_{scrape}} - \mathrm{Margin_{scrape}})$$

where $\mathrm{C}_{\mathrm{L}\alpha=0}$ and $\mathrm{C}_{\mathrm{L}\alpha}$ are found from LMAS take-off lift curves and drag polars. Currently the tail scrape C_L is the most critical. A 0.5-degree scrape margin is used to match the LMAS C_L.

Roskam and Lan (1997) methods are also used to determine the landing distance. Three legs are defined. The air distance is the distance from clearing the 50 ft. object to the point of wheel touchdown, including the flare distance. The free roll distance is the distance between touch-down and application of brakes. And finally, the brake distance is the distance covered while braking.

The air distance is given by:

$$S_A = \frac{h_f}{\gamma} + \frac{V_F^{\,2}\gamma}{2g(n-1)}$$

where h_f is the 50-foot obstacle height, V_F is the velocity at flare, n is the number of g's at flare, and γ is the glide slope. n is assumed to be 1.2. γ is set to the radian conversion of 2-3 degrees as suggested in Roskam and Lan (1997) since the throttle can be arbitrarily set to match this value. The flare velocity is assumed to be equal to the approach velocity. The lift coefficient is the least of the C_L associated with $V=1.3*V_{stall}$ or the C_L to meet the tail scrape requirement. The drag coefficient is calculated with gear down.

The free roll distance is given by:

$$S_{FR} = t_{FR} \cdot V_{TD}$$

where t_{FR} is the time which the aircraft is in free roll, and V_{TD} is the touch-down velocity which is assumed to be the approach velocity.

The braking distance is found by:

$$S_B = \frac{W}{2g} \cdot \frac{V_{TD}^{\ \ 2}}{F_m}$$

where F_m is the mean braking force. The first step in calculating the mean braking force is to calculate the static braking force:

$$F_{Static} = \mu_{Brake} \cdot W_{Landing}$$

Next, the initial braking force is:

$$F_{Initial} = \mu_{Brake} \cdot W_{Landing} - \frac{1}{2} \cdot \rho \cdot V_{TD}^2 \cdot \left(\mu_{Brake} \cdot C_{LGround} - C_{DGround}\right)$$

The braking factor is:

$$K_{Brake} = \frac{\left(1 - F_{Initial} / F_{Static}\right)}{Log\left(F_{Static} / F_{Initial}\right)}$$

And finally, the mean braking force is:

$$F_m = K_{Brake} \cdot F_{Static}$$

Corrections must be made to the landing lift curves and landing drag polars in ground effect during the braking segment of landing using equations found in Roskam and Lan (1997). First, the effective aspect ratio in ground effect is:

$$AR_{Weffective} = AR_W \cdot \left(0.2 + 0.7855 \cdot \left(\frac{Clearance}{b_W / 2}\right)^{0.468945} - 0.07164 \cdot \left(\frac{Clearance}{b_W / 2}\right)^{2.0033}\right)$$

The ratio of the lift curve slopes in and out of ground effect is:

$$\frac{C_{L\alpha}}{C_{L\alpha Ground}} = \frac{AR_W}{AR_{Weffective}} \cdot \frac{2+\sqrt{AR_{Weffective}^2\left(1+\frac{TAN^2\left(\Lambda_{W,c/2}\right)}{1-M_{Landing}^2}\right)+4}}{2+\sqrt{AR_W^2\cdot\left(1+\frac{TAN^2\left(\Lambda_{W,c/2}\right)}{1-M_{Landing}^2}\right)+4}}$$

The effective angle of attack in ground effect is:

$$\alpha_{GroundEffect} = \left(0.6\cdot t/c_{inboard} + 0.4\cdot t/c_{outboard}\right)\cdot\left(3.5655\cdot\left(\frac{\bar{c}}{Clearance}\right) - 0.177\cdot\left(\frac{\bar{c}}{Clearance}\right)^2\right)$$

Now the lift coefficient in ground effect becomes:

$$C_{LGround} = \frac{C_L}{C_{L\alpha}/C_{L\alpha Ground}} - \frac{C_{L\alpha}}{C_{L\alpha}/C_{L\alpha Ground}}\cdot\alpha_{GroundEffect}$$

The ground roll drag coefficient is:

$$C_{DGround} = C_{DoApproach} + \frac{f}{\pi\cdot AR_W}\cdot\left(C_L^2 + \left(\frac{1}{f_{Approach}} - 1\right)\cdot\left(C_{LBreak,Approach} - C_L\right)^2\right) - \frac{f\cdot\sigma'\cdot C_{LGround}^2}{\pi\cdot AR_W}$$

where *f* is the wingtip-mounted engine lift dependent drag factor. The ground effect factor for the drag polar, σ', is given by:

$$\sigma' = \frac{\left(1-\frac{1.32\cdot Clearance}{b_W}\right)}{\left(1.05+\frac{7.4\cdot Clearance}{b_W}\right)}$$

Note that ground effect is not considered at take-off. The balanced field length equation does not require aerodynamic information for conditions other than second segment climb.

The missed approach climb gradient is calculated in the same way as the second segment climb gradient with few exceptions. First, the weight of the aircraft at landing is assumed to be 73% of the take-off gross weight, as specified by LMAS. Second, all engines are operational. Third, the landing drag polar is used, which is distinct from the take-off drag polar. Minimum missed approach climb gradients for aircraft having 2-4 engines are presented in Table 3.3. The FAR minimum missed approach climb gradient constraint and landing distance constraint are never violated in this study.

Table 3.8. Minimum Second Segment and Missed Approach Climb Gradients.

Number of Engines	Minimum Second Segment Climb Gradient	Minimum Missed Approach Climb Gradient
2	0.024	0.021
3	0.027	0.024
4	0.030	0.027

The drag polars take the general form:

$$C_D = C_{Dm} + f \cdot k \cdot (C_L - C_{Lm})^2 + f \cdot k_{Break} \cdot (C_L - C_{LBreak})^2$$

Where

$$k = \frac{1}{\pi \cdot AR_W \cdot e} \qquad \text{and} \qquad k_{Break} = \frac{1}{\pi \cdot AR_W \cdot e_{Break}}$$

when $C_L > C_{LBreak}$, and k_{Break}=0 otherwise. The factors e and e_{Break} are read in from the input file. The minimum drag coefficient, C_{Dm}, is found by:

$$C_{Dm} = C_{DmFactor} \cdot \frac{S_{Wet}}{S_{ref}}$$

where $C_{DmFactor}$ is read in from the input file. All factors are based on LMAS drag polars for aircraft take-off and landing configurations.

The wing aspect ratio used for the take-off and landing drag polars, AR_W, takes a different form than the wing aspect ratio used for wing weight estimation. The wing aspect ratio used by FLIPS.F is the square of the wingspan divided by the reference area. The reference area is the wing area minus the Yehudi flap area. AR_W is the square of the wingspan divided by the wing planform area. The drag polar correlation made with LMAS data is unaffected because the LMAS drag polars were for single taper wings without Yehudi flaps. The reason for using a different aspect ratio for these drag polars (k and k_{break} terms) is that the reference area based aspect ratio becomes very large for the cantilever wing. In this case the wing root chord is restricted if the wingtip chord and wing break chord are both small. This is because the reference area is the area enclosed by the leading and trailing edges of the outboard panel and their inboard projections. The balanced field length and second segment climb constraints are so difficult to meet that the cantilever wing aircraft would manipulate this geometry specification to give wings with very narrow outboard panel chords. Obviously, this is an artificial effect, because aircraft do not reduce the wing break chord to meet field performance requirements.

Chapter 4

Results

4.1 Summary

The results of this study include minimum take-off gross weight and minimum fuel weight designs at various technology levels and range requirements. The cases are arranged in three parts: point optima (Figure 4-1a-c), sensitivity analysis, and range investigations. A total of 75 cases are presented.

Figure 4-1a is a matrix of the 14 primary cases of interest. The columns are arranged by configuration and the rows by mission. . Each element in the matrix is a half-wing planform of an optimum design. The configurations from left to right are the cantilever, T-Tail SBW with fuselage-mounted engines, SBW with wingtip-mounted engines, and the SBW with underwing engines outboard of the strut. The missions from top to bottom are the 2010 technology full mission minimum TOGW, 2010 technology full mission minimum fuel, 2010 technology economic mission minimum TOGW, and 1995 technology full mission minimum TOGW. Each element in Figure 4-1a will be described in greater detail later. Figure 4.1b shows how a given configuration can change with various missions. Vicki Johnson (1990) presented her cost optima results in a similar format. Figure 4.1c demonstrates how varied the final planform of a given mission are for the configurations.

Note that a color-coding representation of the various configurations has been introduced in Figure 4.1a-c. The cantilever wing is black, T-tail fuselage mounted engine SBW is red, the wingtip-mounted engine SBW is blue and the underwing-engine SBW is green. This color convention is used in figures and tables from this point forward.

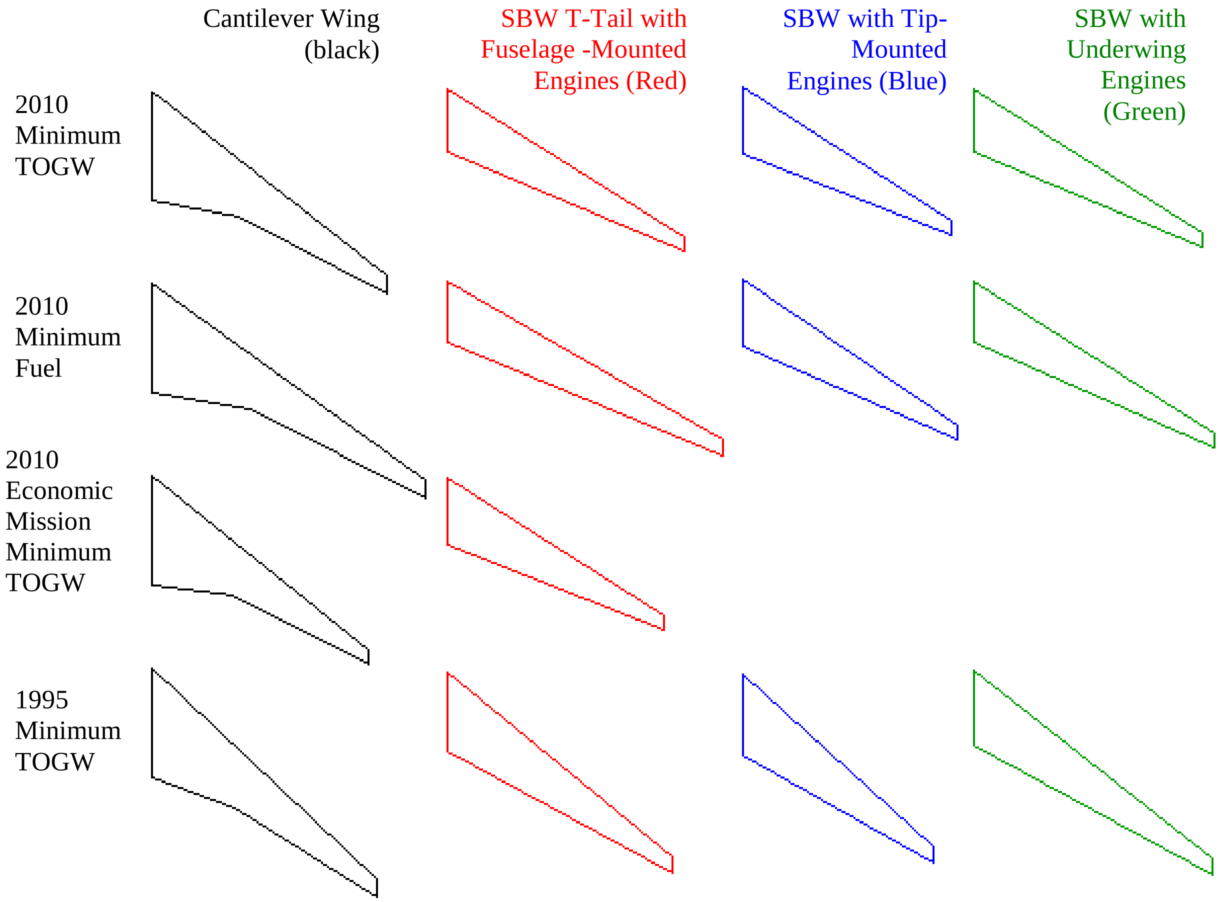

a) Study Matrix.

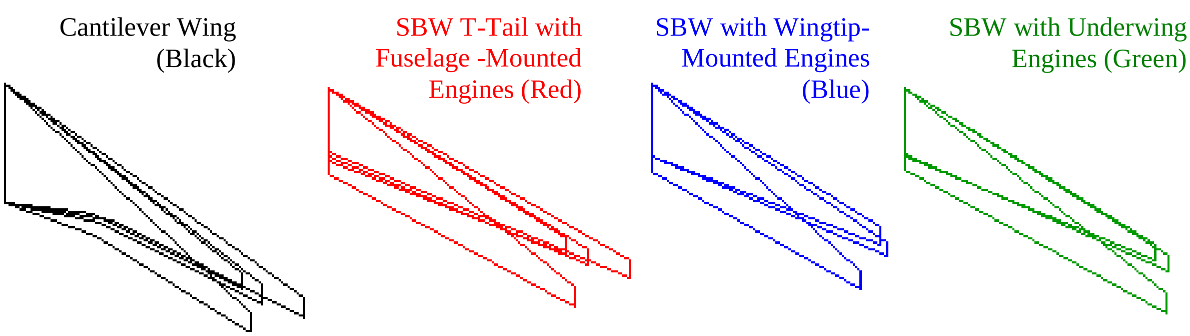

b) Variations within a Single Configuration for Different Objective Functions.

Figure 4.1. Wing Planforms for Different Configurations and Objective Functions.

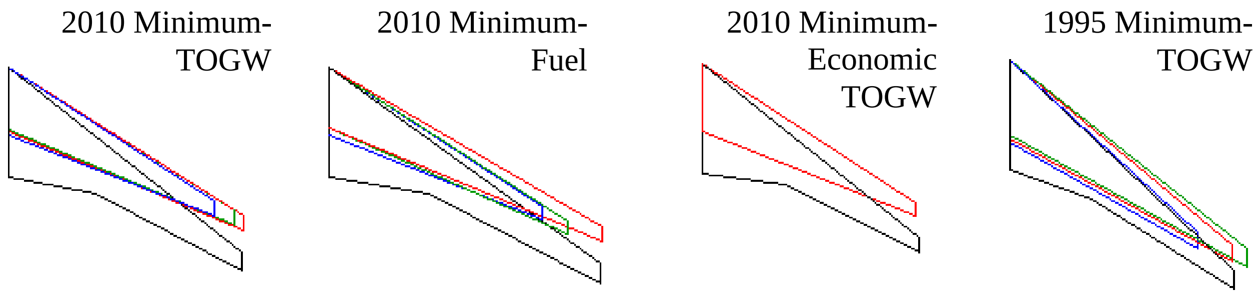

c) Variations within a Single Objective Function for Different Configurations.

Figure 4.1. Continued.

4.2 Minimum Take-Off Gross Weight Optima

Table 4.1 lists the results of the minimum-TOGW cantilever, fuselage-mounted engine T-Tail SBW, wingtip-mounted engine SBW and underwing engine SBW with the engines mounted either inboard or outboard of the strut. Figures 4.2a-c show the graphical output of the four main cases. The SBW is superior to the cantilever configuration for the minimum-TOGW objective function. While the SBW has between 9.2-17.4% decrease in TOGW for minimum TOGW designs, the savings in fuel consumption are even more impressive. A SBW has between 14.3-21.8% lower fuel burn than a cantilever configuration when optimized for minimum-TOGW, and between 16.2-19.3% lower fuel weight when both are optimized for minimum fuel weight.

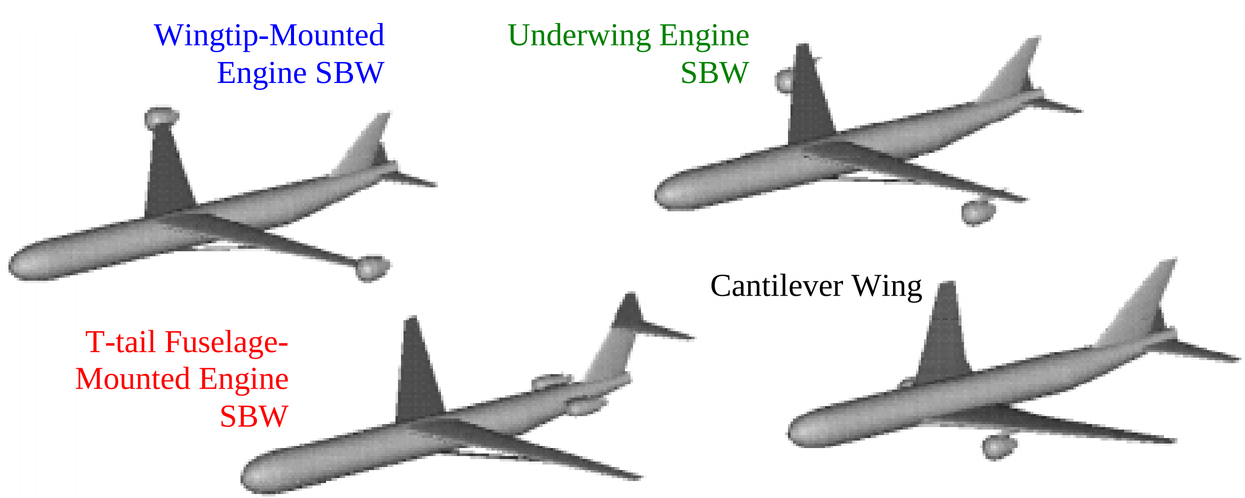

a) Isometric Views.

Figure 4.2. 2010 Minimum-TOGW Designs.

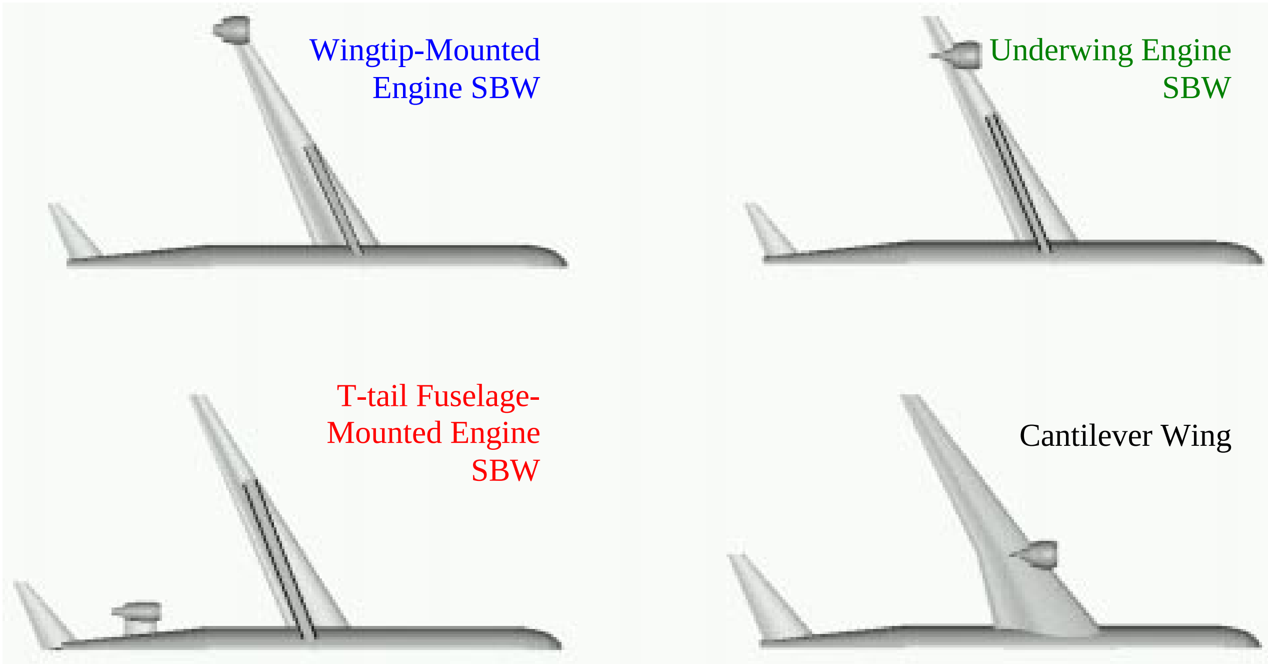

b) Planview from Below.

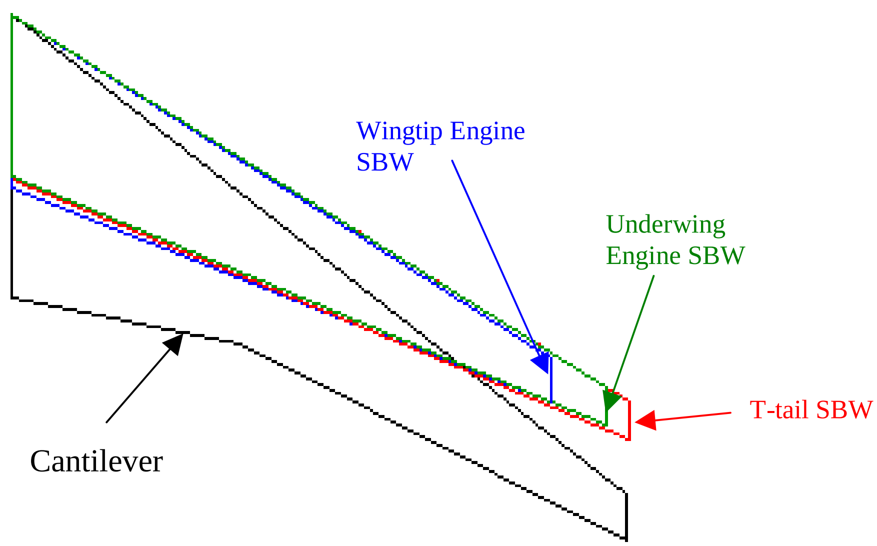

c) Wing Planform Comparison.

Figure 4.2. Continued.

Table 4.1. 2010 Minimum-TOGW Designs.

Cantilever Wing-Eng.	SBW T-Tail	SBW Tip Engines	SBW Underwing	
225.3	226.0	198.6	220.1	Span (ft)
52.0	30.2	31.8	29.4	Root Chord (ft)
5307	4205	3907	3970	S_w (ft^2)
9.57	12.15	10.10	12.20	AR
15.14%	14.28%	14.36%	14.00%	Root t/c
10.55%	6.58%	7.56%	7.15%	Break t/c
7.40%	6.56%	6.85%	7.37%	Tip t/c
34.2	29.9	30.2	29.8	Wing $\Lambda_{1/4}$ (deg)
	20.5	23.5	21.6	Strut $\Lambda_{1/4}$ (deg)
	68.8%	56.8%	62.4%	η Strut
37.0%		100.0%	83.8%	η Engine
75793	59463	51851	56562	T_{max} (lbs)
42052	40429	40736	40097	Cruise Altitude (ft)
23.38	25.33	25.25	25.30	L/D
63706	59581	41854	50287	Wing Wt. (lbs)
47266	42473	25213	33335	Bending Matl (lbs)
186295	159629	145618	151342	Fuel Wt. (lbs)
540230	**490312**	**446294**	**464556**	TOGW (lbs)
1563.24	1507.06	1461.97	1480.44	Total Cost ($M)
87.49	82.69	76.70	79.01	Acquisition Cost ($M)
583.68	538.49	504.86	518.75	DOC ($M)
892.07	885.88	880.41	882.68	IOC ($M)
	9.2%	17.4%	14.0%	% TOGW Improvement
	14.3%	21.8%	18.8%	% Fuel Improvement
	21.5%	31.6%	25.4%	% Thrust Reduction
	3.6%	6.5%	5.3%	% Cost Reduction
ACTIVE	ACTIVE	ACTIVE	ACTIVE	Shock Cl Constraint
ACTIVE	ACTIVE		ACTIVE	2nd Segment Climb
	ACTIVE	ACTIVE	ACTIVE	Balanced Field Length
				Initial Cruise ROC
		ACTIVE	ACTIVE	Wingtip Deflection
ACTIVE				Engine Out
				Approach Velocity
				Fuel Volume

Some trends can be observed from these results which will be found in most cases to follow. In general, the T-tail fuselage-mounted engine SBW has nearly the same span as the cantilever wing configuration. The underwing engine SBW cases have less span than either the T-tail fuselage-mounted engine SBW or the cantilever wing due to the wingtip deflection constraint. Similarly, the wingtip deflection constraint limits the span of the wingtip-mounted engine SBW such that it has the least span of all arrangements. The configurations, from lightest to heaviest, are the wingtip-mounted engine SBW, underwing engine SBW, T-tail fuselage-mounted engine SBW and cantilever wing. At a 7500 nautical mile range, the same order applies for fuel weight, moving from least to most fuel burned. Figure 4.2c shows the wings of the four main configurations for the 2010 minimum-TOGW cases. Note that there is a break in the trailing edge of the cantilever wing, and the SBW cases generally have much less sweep and less wing area.

As discussed in Chapter 1, the SBW sweep reduction is largely due to a reduction in *t/c* (5.2-7.5% lower for 2010 minimum-TOGW SBW cases), which reduces transonic wave drag. The *t/c* reduction allows the SBW wing to have less sweep than a cantilever wing for the same amount of wave drag. The sweep reduction promotes natural laminar flow. It also decreases the wing structural weight. The combination of these effects drives the SBW wing sweep to lower values than for the cantilever wing configuration (usually around 4^o less sweep).

4.3 Minimum-Fuel Optima

Table 4.2 lists the results of the minimum-fuel cases, and Figures 4.3a-c show the corresponding graphical outputs. These aircraft have greater wingspans to increase the *L/D* and for flight at higher altitudes. The cantilever wing uses 4.62% less fuel, the minimum-fuel T-tail SBW uses 6.76% less fuel than its minimum-TOGW counterpart, the wingtip-mounted engine SBW uses 2.19% less fuel and the underwing engine SBW uses 2.41% less fuel. The fuel reduction for the wingtip-mounted engine and the underwing engine SBW cases are relatively small because the wingtip deflection constraint limits the wingspan. The minimum-fuel-SBW TOGWs are 9.7-19.9% lower than an equivalent cantilever design. The cantilever wing configuration *L/D* increases from 23.4 to 26.4 going from the minimum-TOGW to the minimum fuel objective function, from 25.3 to 29.2 for the T-tail fuselage mounted engine SBW, from 25.3 to 26.1 for the wingtip-mounted engine case and from 25.3 to 26.3 for the underwing engine SBW. The *L/D* increase for the wingtip-mounted engine and underwing engine SBW configurations from changing the objective function from TOGW to fuel weight is very small, because the wingspan experiences little change. Improved aerodynamic efficiency for all configurations except for wingtip-mounted engine and underwing engine cases is achieved by increasing the wing span, but this incurs a cost in structural weight. The increase in TOGW when the objective function is changed from TOGW to fuel weight is 16,915 pounds for the T-tail SBW and 21,663 pounds for the cantilever wing. TOGW changes for the underwing engine SBW and wingtip engine SBW cases are small.

Fuel burn is likely to be an increasingly important factor in aircraft design from two perspectives. First, as the Earth's petroleum resources are depleted, the cost of aviation fuel will rise. Any reduction in fuel demand will be welcome if the fuel price becomes a larger part of transport life cycle cost. Second, strict emissions regulations stemming from environmental concerns will limit the amount of pollutant discharge permitted by an aircraft. Beyond engine design, reducing the overall amount of fuel consumed for a given flight profile by improved configuration design will also reduce the total amount of emissions.

Airport noise pollution can limit the types of aircraft permitted to use certain urban airfields and impose operational restrictions on those that do. Simply speaking, minimizing engine size can also be expected to reduce the noise generated if the engine is of similar design. Minimum-TOGW SBW engine thrust is reduced by 21.5-31.6% over the equivalent cantilever design. Perhaps the noise pollution at an airport can be reduced by a similar amount.

Table 4.2. Minimum Fuel Optimum Designs.

Cantilever Min Fuel	SBW T-Tail Min F	SBW Tip Eng Min F	SBW Wing Eng	
260.9	262.1	204.3	230.6	Span (ft)
52.0	28.4	32.0	29.1	Root Chord (ft)
5793	4723	3933	4113	S_w (ft^2)
11.75	14.54	10.61	12.92	AR
12.97%	12.20%	14.07%	13.78%	Root t/c
9.27E-02	6.22%	7.52%	7.12%	Outboard t/c
5.21E-02	5.95%	6.88%	7.52%	Outboard t/c
32.5	28.3	31.7	30.5	Wing $\Lambda_{1/4}$ (deg)
	22.0	24.3	22.3	Strut $\Lambda_{1/4}$ (deg)
	65.9%	53.8%	60.2%	η Strut
37.0%		100.0%	82.9%	η Engine
71032	56304	52285	54973	T_{max} (lbs)
43783	42723	40765	40518	Cruise Altitude (ft)
26.37	29.23	26.08	26.34	L/D
92991	85558	47120	56488	Wing Wt. (lbs)
78456	68276	30914	39593	Bending Matl (lbs)
177692	**148838**	**143425**	**147695**	Fuel Wt. (lbs)
561893	507227	449926	466858	TOGW (lbs)
1578.38	1518.53	1464.85	1481.49	Total Cost ($M)
92.66	87.54	77.76	80.12	Acquisition Cost ($M)
590.96	543.02	506.22	518.41	DOC ($M)
894.76	887.98	880.87	882.96	IOC ($M)
	9.7%	19.9%	16.9%	% TOGW Improvement
	16.2%	19.3%	16.9%	% Fuel Improvement
	20.7%	26.4%	22.6%	% Thrust Reduction
	3.8%	7.2%	6.1%	% Cost Reduction
ACTIVE	ACTIVE	ACTIVE	ACTIVE	Shock Cl Constraint
ACTIVE				2nd Segment Climb
	ACTIVE	ACTIVE	ACTIVE	Balanced Field Length
	ACTIVE			Initial Cruise ROC
		ACTIVE	ACTIVE	Wingtip Deflection
				Engine Out
				Approach Velocity
				Fuel Volume

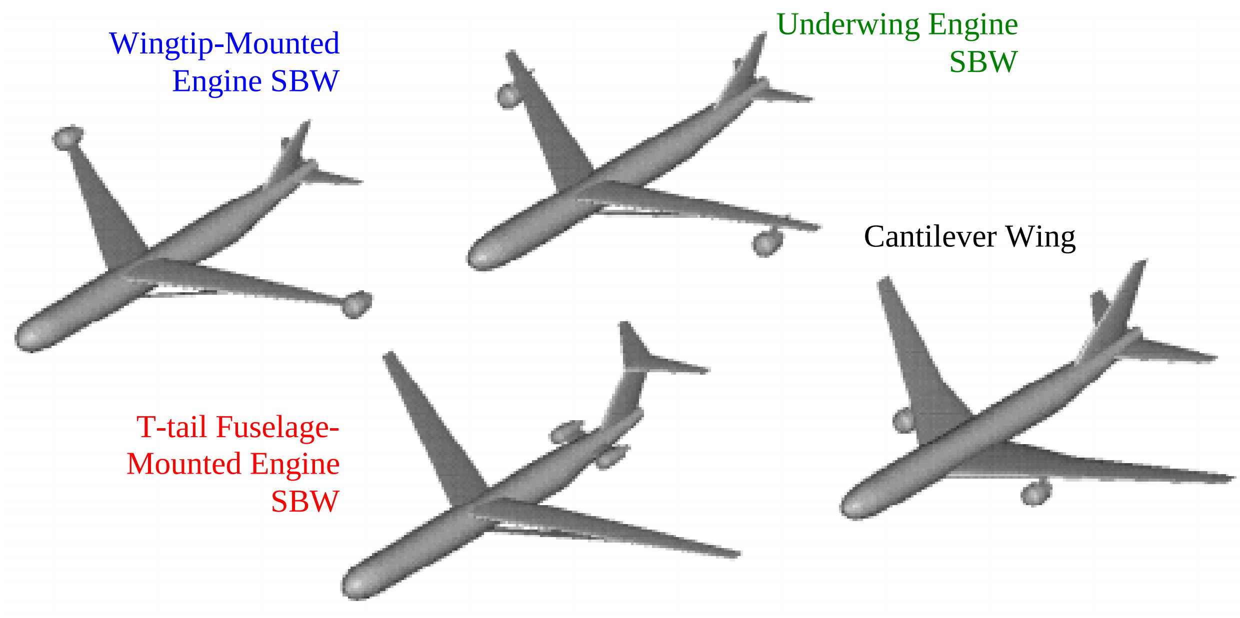

a) Isometric View.

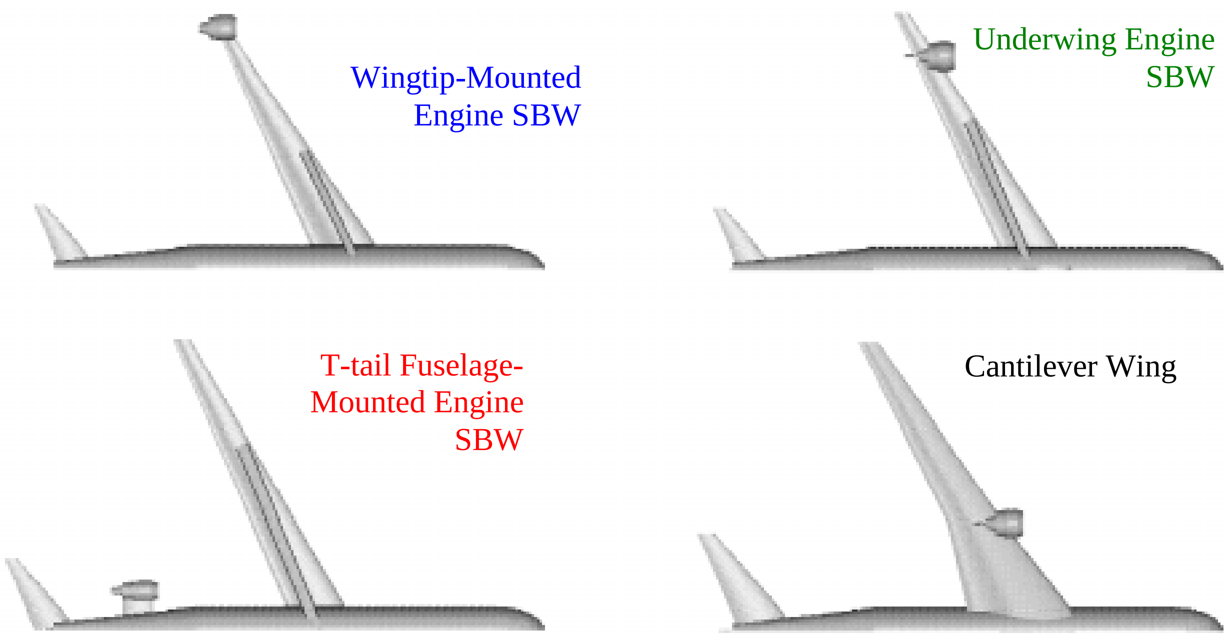

b) Planview from Below.

Figure 4.3. 2010 Minimum-Fuel Designs.

Figure 4.3c shows the overlay of the four 2010 minimum-fuel optima. Again, the cantilever wing has a break in the trailing edge, greater sweep and more area than the SBW designs. Similar wingspan trends are found in the minimum-fuel and minimum TOGW cases. The T-tail

SBW has the largest wingspan, the cantilever concept is slightly less, and then the underwing engine SBW, followed by the wingtip-mounted engine SBW.

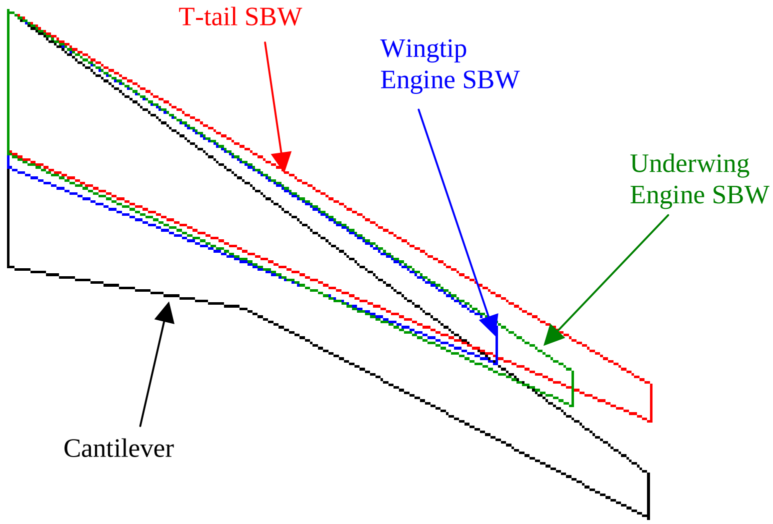

c) Wing Planform Comparison.

Figure 4.3. Continued.

4.4 Economic Mission Analysis

Table 4.3 shows the results of the economic mission analysis. It is important to realize that while the economic mission aircraft is optimized for the minimum economic mission TOGW, the aircraft must also be capable of performing the full mission. Only the cantilever wing and T-tail fuselage-mounted SBW cases are considered. The economic mission analysis did not yield any strikingly different results except for the unexpected similarity in aircraft TOGW when optimized for either the full 7500 nautical mile mission or the 4000 nautical mile economic mission (see Table 4.3). The economic mission and full mission optima have little in common for a given configuration except for the similar TOGW at a design condition. The economic mission aircraft have 16.9-20.5 feet less span (see Figure 4.4), cruise at lower altitudes, and have a lower L/D than their full mission equivalents for both the SBW and cantilever cases. By decreasing the wing span at a reduced passenger and fuel load, the wing bending material weight is less and so is the resulting economic TOGW. Apparently, the *L/D* decrease associated with the span reduction at the full mission scenario adversely affects the full mission TOGW for the minimum economic TOGW optimum. The TOGW at the 7500 nautical mile range is negligibly increased (0.8-1.3%) for those vehicles optimized for the economic mission compared to those optimized for the full mission. The economic mission TOGW is slightly lower for the full mission optimized cantilever wing case, but the difference is very slight. In other words, the weights at the economic mission condition for the cantilever wing economic mission optimum and the full mission optimum are about the same within the fidelity level of the analysis.

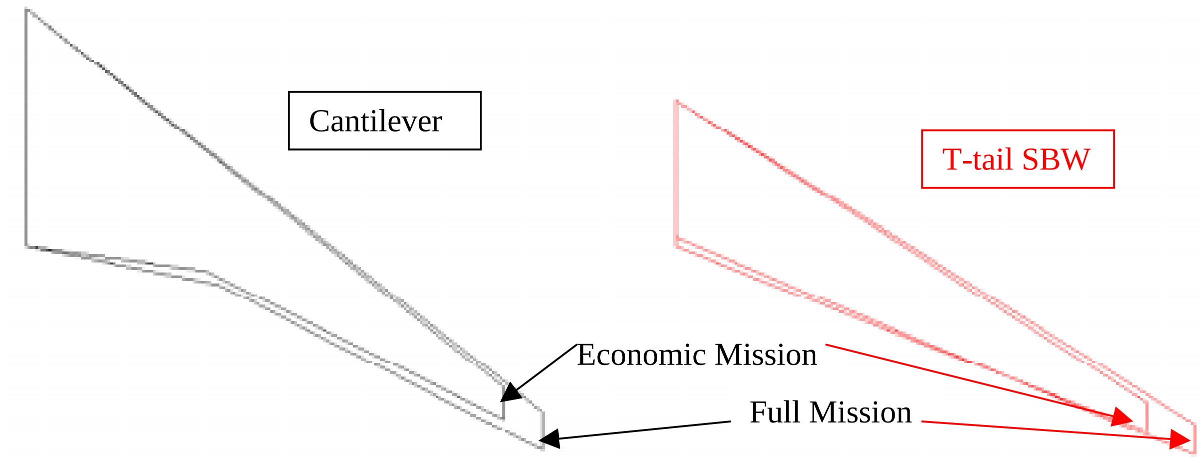

Figure 4.4. Economic Mission Minimum-TOGW and Full Mission Minimum-TOGW Wings.

Table4.3. Economic Mission Results.

Cantilever Wing-Eng.	Cantilever Econ Mission	SBW T-Tail	SBW T-Tail Econ	
225.3	208.4	226.0	205.5	Span (ft)
52.0	52.0	30.2	32.1	Root Chord (ft)
5307	4611	4205	3948	S_w (ft^2)
9.57	9.42	12.15	10.70	AR
15.1%	15.3%	14.3%	14.4%	Root t/c
10.6%	10.8%	6.6%	7.2%	Outboard t/c
7.4%	7.0%	6.6%	6.6%	Outboard t/c
34.2	34.5	29.9	30.2	Wing $\Lambda_{1/4}$ (deg)
		20.5	20.3	Strut $\Lambda_{1/4}$ (deg)
		68.8%	69.0%	η Strut
37.0%	37.0%			η Engine
75793	80909	59463	64846	T_{max} (lbs)
42052	38151	40429	38182	Cruise Altitude (ft)
23.38	21.90	25.33	23.27	L/D
63706	57360	59581	50244	Wing Wt. (lbs)
47266	41585	42473	33536	Bending Matl (lbs)
186295	197896	159629	171022	Fuel Wt. (lbs)
540230	547499	**490312**	494374	TOGW (lbs)
	-0.2%		0.7%	% Econ TOGW Improv.
421276	**422124**	384220	**381707**	Econ TOGW
ACTIVE	ACTIVE	ACTIVE	ACTIVE	Shock Cl Constraint
ACTIVE	ACTIVE	ACTIVE	ACTIVE	2nd Segment Climb
		ACTIVE	ACTIVE	Balanced Field Length
				Initial Cruise ROC
				Wingtip Deflection
ACTIVE	ACTIVE			Engine Out
				Approach Velocity
				Fuel Volume

4.5 Range Investigations

Figures 4.5 and 4.6 show the effects of range on TOGW and fuel weight. In each graph, minimum TOGW is the objective function. The SBW becomes increasingly desirable as the design range increases. The T-tail fuselage-mounted engine SBW TOGW reduction relative to the cantilever configuration steadily improves from 6.0% at a 4,000 nautical mile range up to 12.9% at 11,000 nautical miles. Similarly, the TOGW for the wingtip-mounted engine SBW steadily improves from 11.8-23.7% from 4,000 to 11,000 nautical miles, and the underwing engine SBW improves from 9.5-19.2% over the same range span. The T-tail SBW fuel weight savings fluctuates within about 11.3-16.8%, but it generally improves as the design range increases. The wingtip-mounted engine SBW fuel weight savings generally improves with range with values ranging from 17.6-25.8%. Similar trends are found for the underwing engine SBW with values ranging from 16.0-24.6%. The wingtip-mounted engine SBW is superior at all ranges in TOGW, but the underwing engine SBW burns less fuel as range increases. This shows that much of the wingtip-mounted engine SBW TOGW reduction is due to low structural weight rather than fuel consumption benefits relative to the underwing engine SBW case. Maximum fuel weight is set at 400,000 pounds. The T-tail SBW maximum range is 13,304 nautical miles at this fuel weight, whereas the cantilever configuration can only reach 11,906 nautical miles, or the SBW has 11.7% greater maximum range. To orient the reader, an aircraft can reach any destination on Earth with a 12,000-nautical mile range. The maximum range of the underwing engine SBW is 17.4% greater than the cantilever wing at the same maximum fuel weight. The wingtip-mounted engine SBW can not attain the same range as the other cases because the wingtip deflection severely limits the wingspan. The underwing engine SBW can move the engines inboard to meet the wingtip deflection constraint. At the maximum range condition, the underwing engine SBW engine location actually moves slightly inboard of the strut. In general, the SBW can either have a reduced fuel weight for a given range or an increased range for a given fuel weight relative to the cantilever configuration. Range case data tables can be found in the Appendix 2.

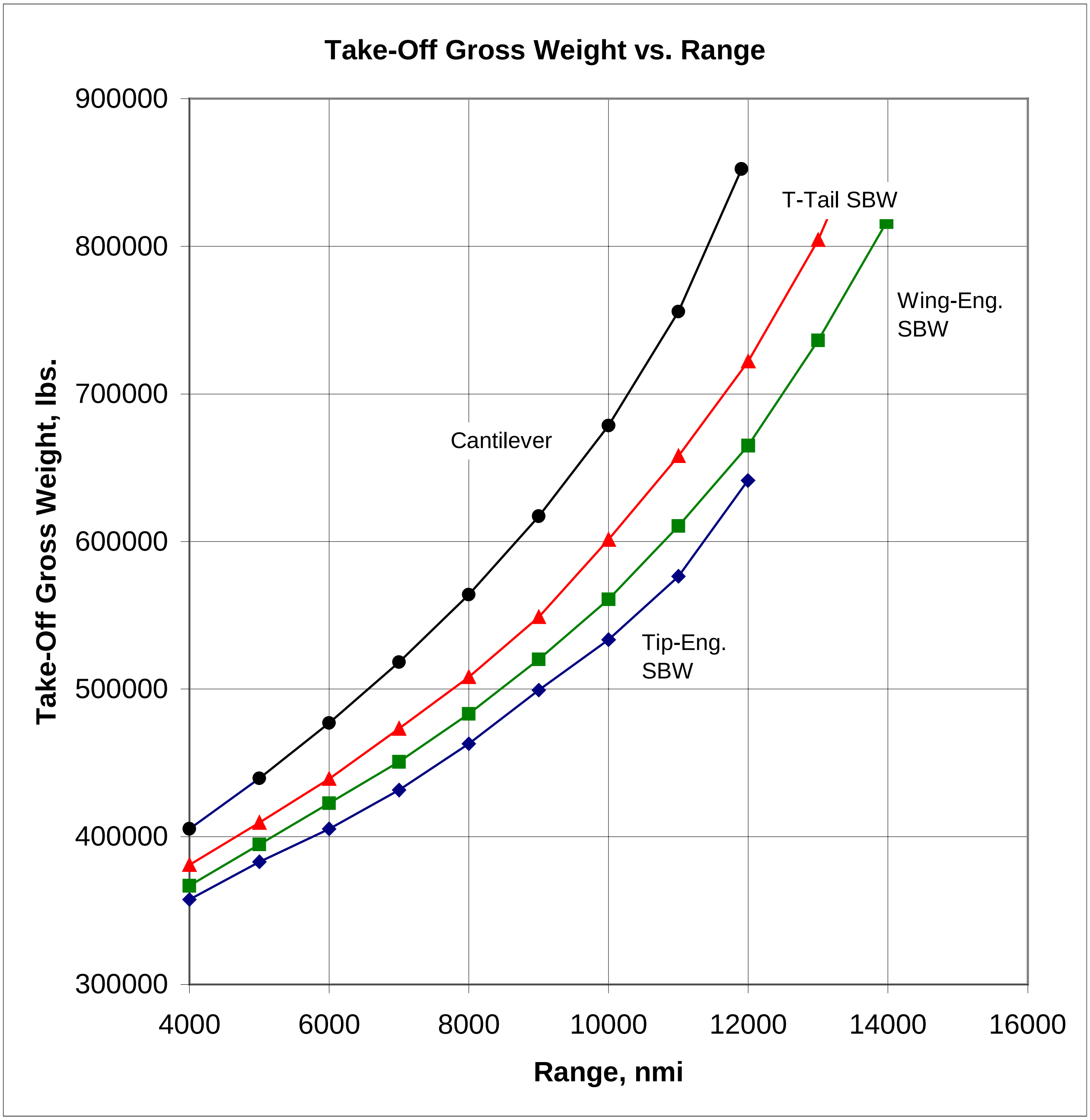

Figure 4.5. Effect of Range on TOGW for All Configurations at Minimum-TOGW.

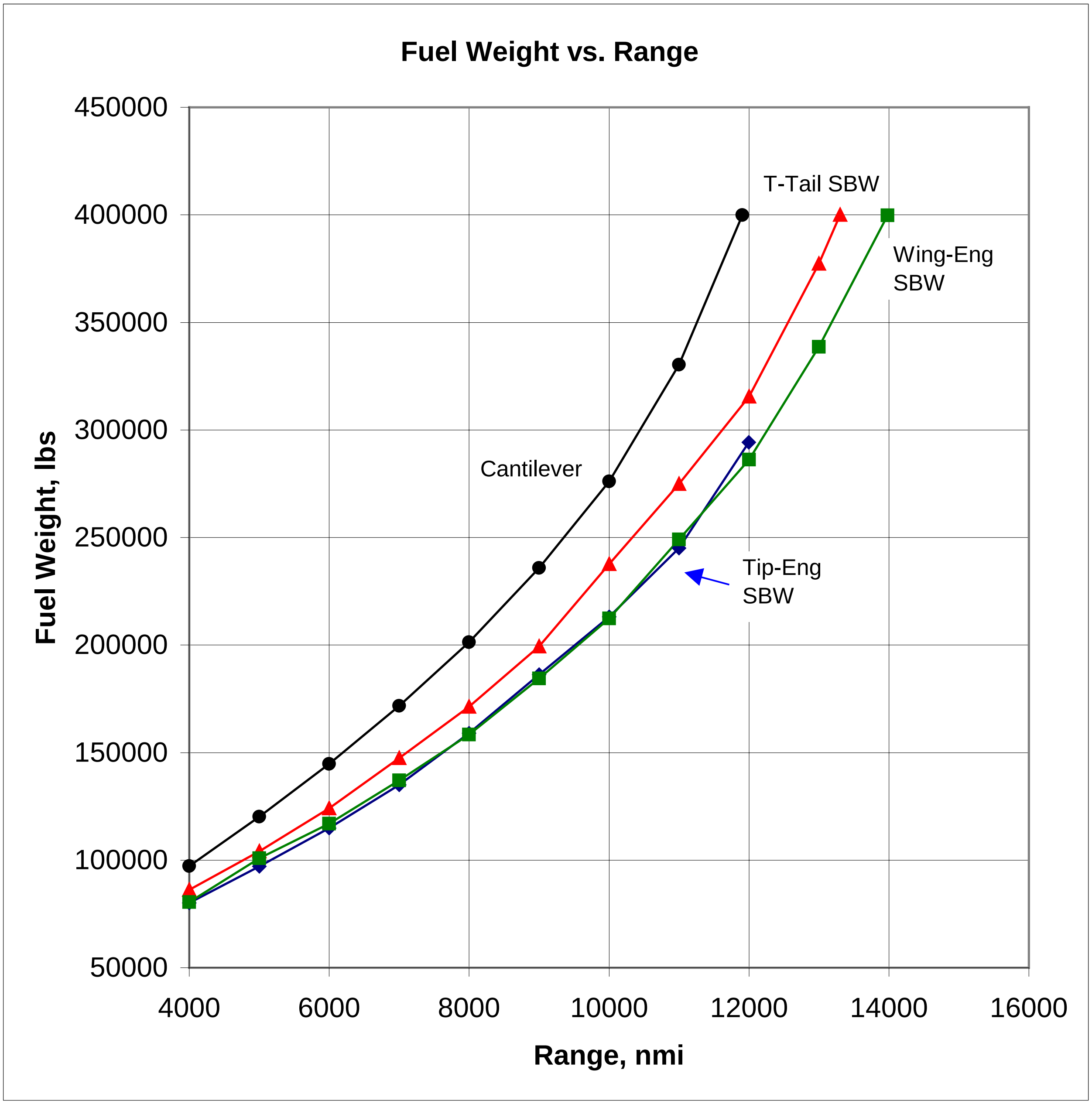

Figure 4.6. Effect of Range on Fuel Weight for All Configurations at Minimum-TOGW.

4.6 Technology Impact Study

The first step in performing the technology impact study is to find 1995 minimum-TOGW optima for all configurations. All weights technology factors are set to 1.0, no natural laminar flow is allowed, the wave drag airfoil technology factor is reduced and the tail volume coefficient is increased. Figures 4.7a-c show the graphical output of the 1995 minimum-TOGW designs. Note that the wing sweep is greatly increased over the 2010 technology equivalents. SBW wing quarter chord sweeps increase by 6-7 degrees, and the cantilever wing sweep increases by about 5.5 degrees at the 1995 technology level. The sweep is increased to reduce the transonic wave drag, which is more critical with the lower airfoil technology factor. Also, there is no aerodynamic benefit in having low sweep when natural laminar flow is not permitted.

Figure 4.7c shows an overlay of the four 1995 minimum-TOGW wings. Like other cases, the T-tail SBW and cantilever wing have approximately the same wingspan, and the wingtip-mounted engine SBW has the least wingspan. Unlike earlier cases though, the underwing engine SBW has the greatest wingspan. This span increase helps increase the L/D by reducing the induced drag. The associated structural penalties are offset by the ripple-through effect of the fuel reduction due to increased aerodynamic efficiency. The 1995 technology level wingtip-mounted engine SBW wingspan is reduced by about 16.4 feet to meet the wingtip-deflection constraint with the higher engine weight.

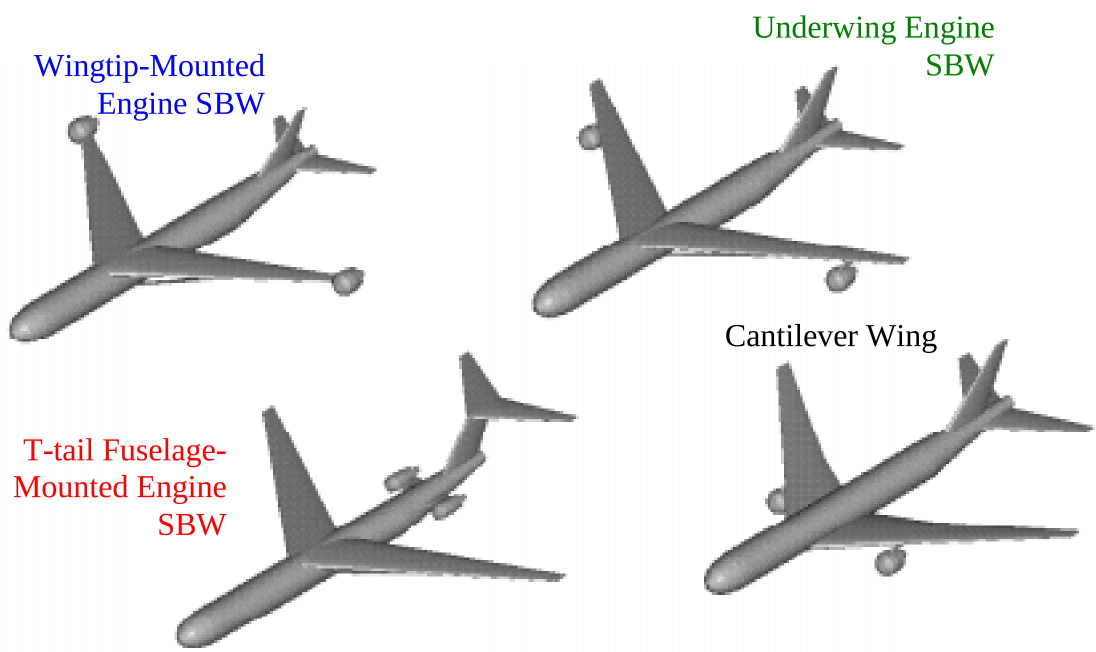

a) Isometric View.

Figure 4.7. 1995 Minimum TOGW Designs.

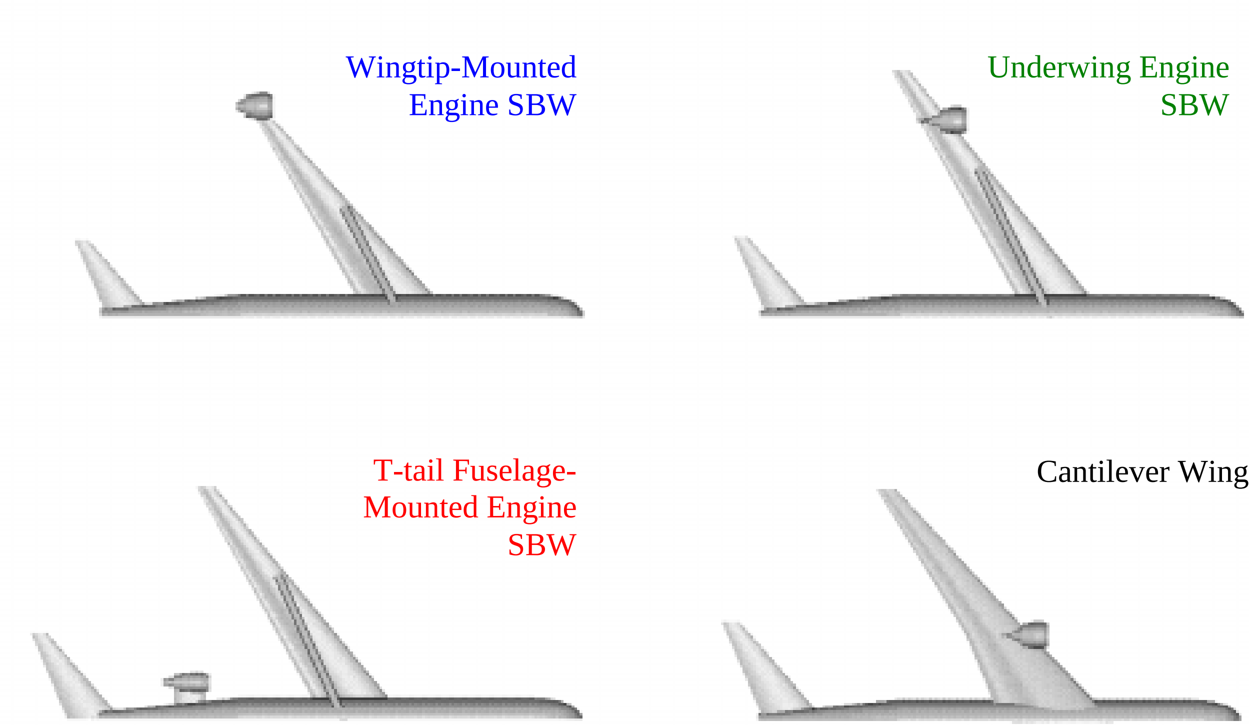

b) Planview from Below.

Figure 4.7. Continued.

Figures 4.8-4.11 show the results of the technology impact study. The top of the left figure is the 1995 technology level aircraft and the bottom is the 2010 technology level aircraft. Each step represents the resulting change in TOGW when a technology group is applied to the 1995 technology level aircraft. The sum of the TOGW changes of the technology groups when applied individually is on the left of the figure, and the overall change in TOGW between 1995 and 2010 technology level is presented on the right of the figure. The right figures show the TOGW and selected weight components of each aircraft.

The technology impact study shows that SBW configurations are more sensitive to improvements in natural laminar flow than the cantilever wing configuration. The sum of the changes made in each technology group is less than the total difference between the 1995 and 2010 SBW designs for all cases, showing that there is generally no overall synergism in the technology group application. The cantilever wing configuration is more responsive to all technology groups except for natural laminar flow than any of the SBW cases, suggesting that the cantilever wing aircraft will benefit more from development of these technologies than the SBW. However, the SBW is superior to the cantilever wing in TOGW and fuel consumption for all technology levels investigated here. Technology impact study data tables can be found in Appendix 3.

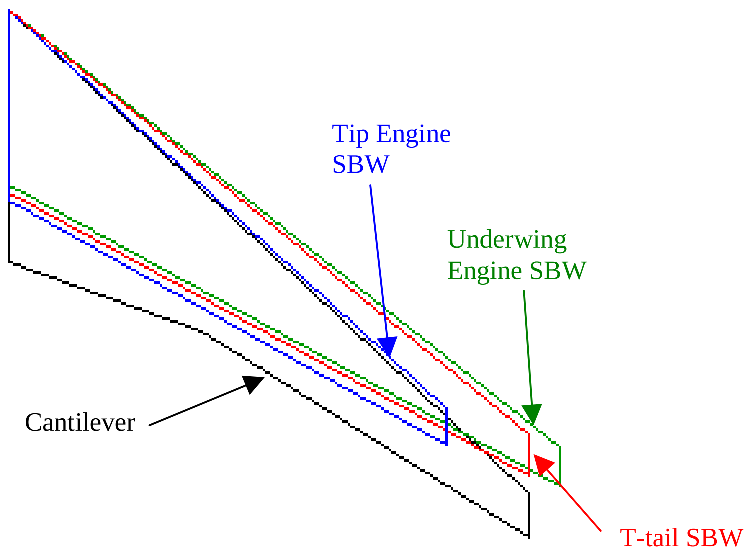

c) Wing Planform Comparison.

Figure 4.7. Continued.

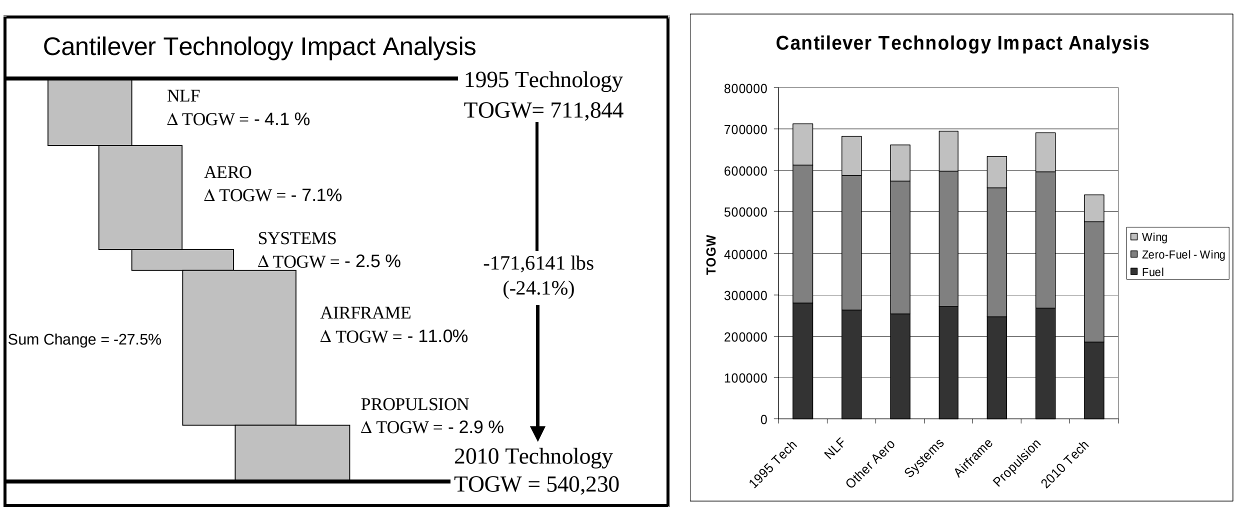

Figure 4.8. Cantilever Sensitivity Analysis.

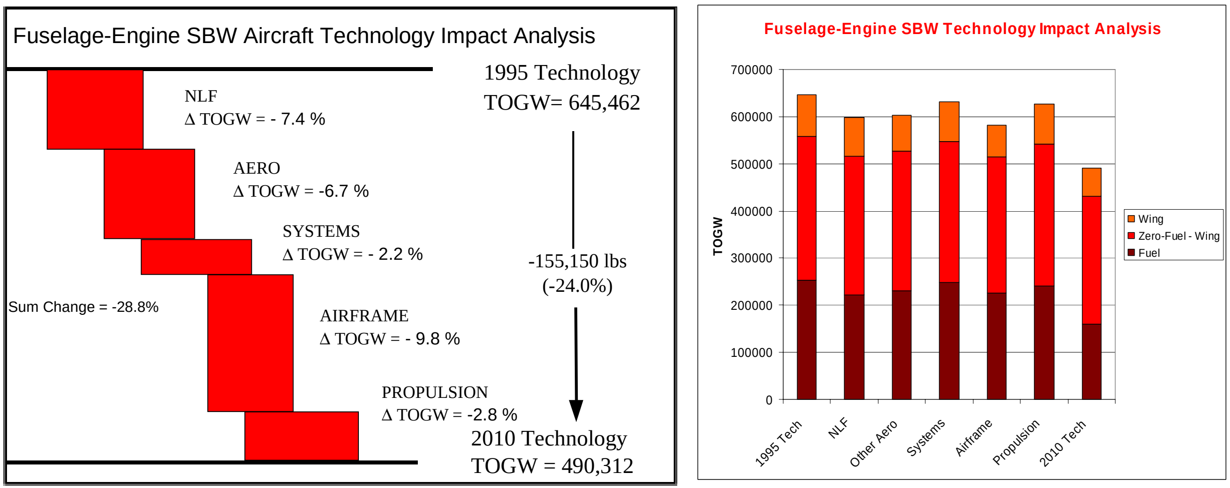

Figure 4.9. T-Tail SBW Sensitivity Analysis.

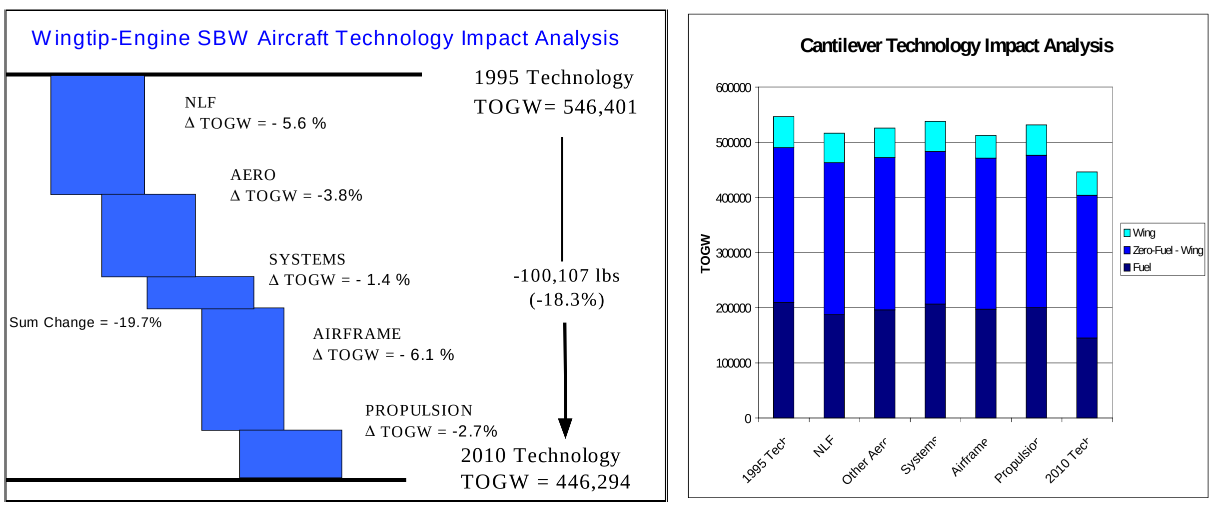

Figure 4.10. Tip-Mounted Engine SBW Sensitivity Analysis.

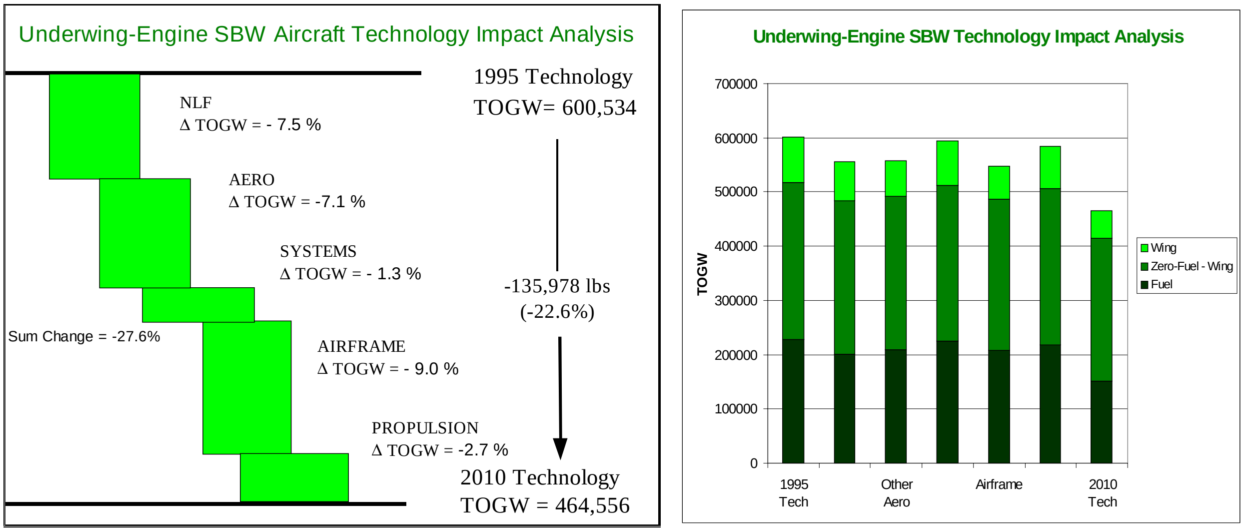

Figure 4.11. Underwing-Engine SBW Sensitivity Analysis.

4.7 Cost Analysis

The FLOPS cost module [McCullers] was used to determine the acquisition cost, direct operating cost and indirect operating cost of all vehicles. The acquisition and direct operating costs are less for the SBW cases than for the cantilever wing cases. The acquisition cost is a function of zero fuel weight. Typical acquisition cost reductions of the SBW designs range from 5.5-16.0%, with the wingtip-mounted engine SBW offering the greatest improvement. Direct operating cost is a function of fuel weight, so naturally the SBW cases offer improvements. SBW direct operating cost improvements over the cantilever wing configuration range from 8.1-14.3%, again with the wingtip-mounted engine case offering the greatest benefits. The indirect operating cost is a weaker function of TOGW, and the SBW has 0.8-1.6% improvement in this area. With this formulation, the total aircraft cost is the sum of the acquisition cost, direct operating cost and indirect operating cost. The total aircraft cost reductions for the SBW cases range from 3.8-7.2%. The SBW cost reductions are not as impressive as the fuel consumption and TOGW, because the costs are also strong functions of the number of passengers and other parameters that do not vary.

4.8 General Configuration Comparisons

The tip-mounted engine SBW is lighter than the fuselage mounted engine SBW because of engine inertia relief on the wing and induced drag reduction at take-off and cruise. Field performance constraints largely dictate the engine size, so any drag reduction produces large benefits. Although the tip-mounted engine vehicle is the lightest of the SBW cases, this configuration raises important issues. LMAS noted that the resultant net thrust and vertical tail lift at the engine-out condition would be at a 45-degree angle to the flight path. Obviously, this is not a practical flight condition. Even when circulation control is allowed, the engine-out constraint imposes severe limitations on the wing span, so the relative benefits are reduced as the TOGW increases.

The underwing engine SBW is a compromise between the wingtip-mounted engine SBW and the fuselage-mounted engine SBW. By not forcing the engines to remain at the tip, the wing can extend beyond the engines freely without running into the engine-out constraint. Because the height of the pylon plus the diameter of the nacelle is considered in the wingtip deflection constraint, it is often more difficult to satisfy than on the wingtip-mounted engine case. This constraint often forces the engines inboard towards the strut.

An underwing engine SBW case with the engines inboard of the strut is generally heavier than if the engines were located outboard of the strut. Engines provide inertia relief to the wing and are more effective for reducing the bending moment at the wing root as they move farther outboard. Thus, it is not surprising to see that the inboard engine case is heavier than the outboard engine case. The inboard engine case does offer the advantage of not requiring circulation control on the vertical tail, and may be a more viable candidate design solution. This configuration still offers advantages over the T-tail fuselage-mounted engine SBW. The T-tail fuselage-mounted engine case has no inertia relief on the wing due to the engine placement. Problems arise when engine/strut interference is considered, because the engine exhaust will blow on the strut when the underwing engine is located inboard of the strut. As a result, this case is not given further consideration.

One can learn much about an optimum design by noting the active constraints. In every optima presented here, the section lift coefficient limit constraint is active. This indicates that the aircraft do not fly at the altitude for best *L/D* and are thus penalized. Typically, the engines are sized based on balanced field length, second segment climb or rate of climb at initial cruise altitude. The wingtip-mounted SBW engine sizing is dictated by the balanced field length and sometimes by rate of climb at initial cruise altitude. This is because the field performance requirements are greatly relaxed by the induced drag reductions from the tip engines. Other cases generally have the engines sized based on balanced field length and second segment climb.

One of the early concerns regarding the SBW configuration is the large increase in wingspan compared to cantilever wings seen in previous studies [Grasmeyer (1998A,B)]. More refined modeling of the wing structure and added realism brought about through work with LMAS has lessened the earlier trend. Indeed, now the T-tail SBW has about the same span as the cantilever configuration for the minimum TOGW and minimum fuel designs. The underwing engine SBW span is either slightly more or less than the cantilever wing, depending on the case. Part of the reason for the reduced underwing engine SBW span reduction is that the engine deflection is now part of the wingtip deflection constraint, making it much harder to satisfy. The optimum wingspans fall within the FAA 80-meter gate box limitation for all designs.

Chapter 5

Conclusions

Virginia Tech transport studies have shown the potential of the SBW over the traditional cantilever configuration. After much added realism by a major airframe manufacturer, the MDO analysis shows that the SBW still demonstrates major improvements over the cantilever wing configuration. Significant reductions in TOGW and cost were found, but the greatest virtues of the SBW may be its improved fuel consumption and smaller engine size. The SBW TOGW is reduced 9.2-17.4% for minimum-TOGW designs. The minimum-fuel optimum SBW aircraft burn 16.2-19.3% less fuel than an equivalent cantilever wing aircraft. Minimum-TOGW SBW aircraft engines are 21.5-31.6% smaller than a similar cantilever wing engine. These results indicate that the SBW will be more economically viable, reduce the consumption of natural resources, limit pollutant discharge and reduce noise pollution for urban airports. Advantages of the SBW increase with range, suggesting that this configuration may be ideal for larger, long-range transports.

The SBW exhibits a strong sensitivity to natural laminar flow technology. This implies that greater emphasis should be placed on laminar flow than on other systems and technologies in the development of the SBW. An investment in natural laminar flow technologies will give a greater return for the SBW than the cantilever wing configuration. Although the cantilever wing configuration shows more sensitivity to all other technology groups, the SBW is still lighter for every case.

The cooperative relationship with LMAS focussed on adding realism to the SBW design effort for direct comparisons with the cantilever design. Realism often takes the form of weight penalties and expanded performance analysis, which inevitably detracts from SBW theoretical potential. Presently efforts are underway to identify technologies and strut/truss arrangements to exploit the strengths of the strut. In other words, limiting the SBW design arrangements so that the aircraft takes the appearance of a cantilever wing with a strut may not be the most appropriate approach to realize the full potential of the SBW. Some possible design modifications are discussed in the recommendations section.

Finally, the SBW is likely to have a more favorable reaction from the public and aircrews than other competing configurations, especially for those who suffer from a fear of flying.

Affirmative passenger and aircrew acceptance is probable because other than the addition of a visually innocuous strut and a high wing, there is little to distinguish the SBW from the existing airliner fleet. Radical appearances of the blended-wing-body, joined wing, twin-fuselage, C-wing or other candidate configurations may cause apprehension in many flying patrons.

Chapter 6

Recommendations

One can envision a number of extensions to the general SBW layout studied here, with some ideas more daring than others. Such concepts include variations of analysis, configuration, or mission. This limited study demonstrates only a few of the advantages of the strut-braced wing.

Configuration changes may allow the SBW to exhibit further benefits. The strut vertical offset thickness has been assumed as identical to that of the strut. However, the strut offset must take much greater bending loads. Imposing drag penalties as a function of offset thickness but also allowing the thickness to vary will likely yield lower total weights.

One possible way to counter the engine-out problem for the tip-mounted engine configuration would be to add a more powerful engine on the centerline (Figure 6.1). If one of the tip engines fail, the other can be shut off and the centerline engine would provide the necessary thrust for the critical cases. This may raise unique dilemmas when attempting to certify this configuration because it is essentially a two engine aircraft from an engine failure point of view, but there are physically three engines. The FAA would have to decide if the vehicle should meet the two or three-engine requirements.

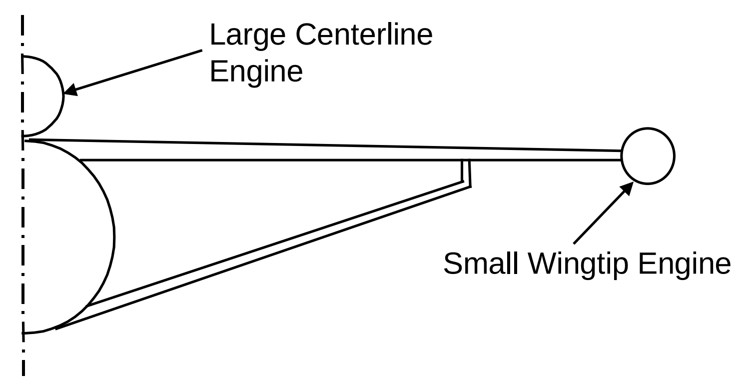

Figure 6.1. SBW with Large Centerline Engine and Small Wingtip Engines.

An arch strut, first suggested by Dr. Joseph Schetz, will eliminate many complex and heavy moving parts by allowing the strut to bend. By eliminating the threat of strut buckling, the demanding -2 G taxi bump case will no longer place such critical demands on the strut.

The vertical distance between the strut and the wing at the fuselage plays a significant role in strut effectiveness. As the vertical separation increases, a smaller component of the strut force causes compression on the main wing. This lessens the wing skin thickness required to counteract buckling, and reduced the overall wing weight. A double-deck fuselage would greatly increase the vertical separation of the wing and strut at the fuselage. Other means of achieving a greater separation include using a parasol wing (Figures 6.2-6.3) or attaching the strut to downward-protruding landing gear pods (Figure 6.3). These arrangements may facilitate underwing engines inboard of the strut/wing intersection without unwanted exhaust interference effects with the strut.

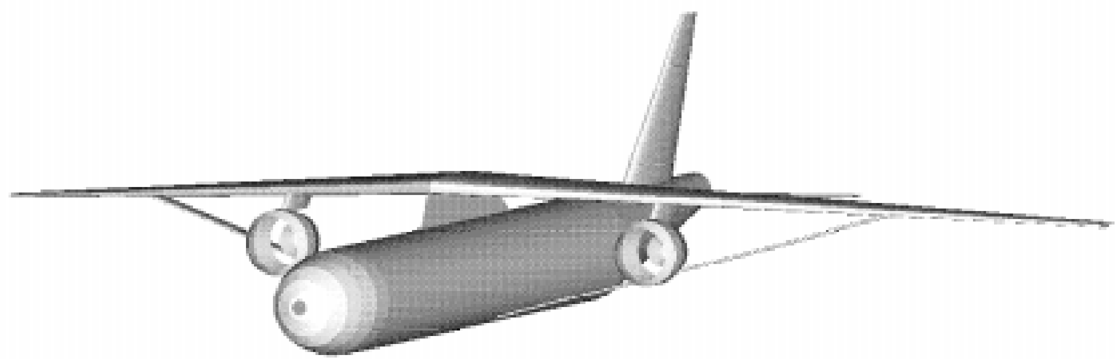

Figure 6.2. Parasol SBW Layout.

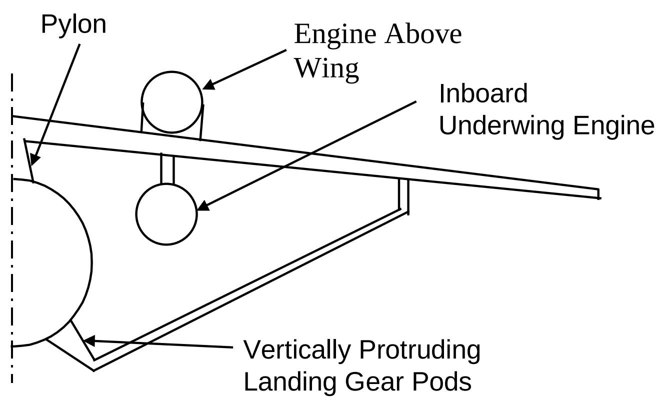

Figure 6.3. Parasol SBW with Landing Gear Pod Extensions.

Locating engines above the wings (Figure 6.3) can add inertia relief without interfering with the strut. Blowing over the upper wing surface will help decrease the take-off distance. Furthermore, inboard engines will not demand exotic schemes like vertical tail blowing to meet the engine-out constraint.

Perhaps the most fanciful of strut variations is to make the SBW a hydrofoil flying boat

(Figure 6.4). The FAA may be concerned that the SBW aircraft cabin may flood more quickly with its high-wing after a water landing than a low wing cantilever configuration. Virtue may be found in addressing this concern. Landing gear pods could extend out from the fuselage to act as sponsons, while the strut then extends up towards the wing. The fuselage and strut are partially submerged while the aircraft is at rest in the water. The strut is effectively a hydrofoil, lifting the aircraft out of the water as it accelerates. Retractable steps may be necessary to break rear fuselage suction. Imagine a luxury airliner flying from one port of call to the next in the nostalgic tradition of the Pan Am clippers of old. McMasters (1999) developed a similar concept for a C-wing configuration. Such a vehicle could also be used for cargo or utility for island nations or in major ports.

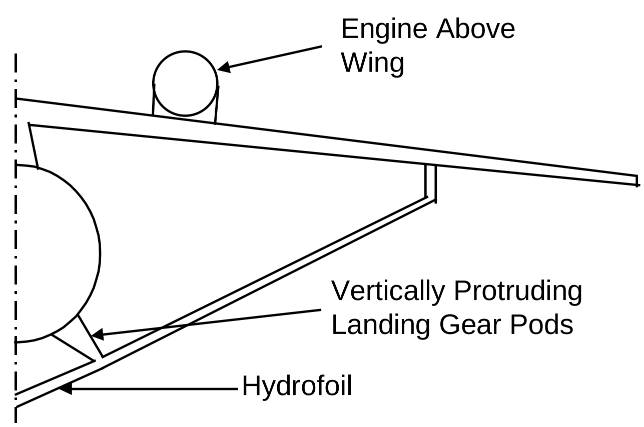

Figure 6.4. Hydrofoil SBW Configuration.

References

Braslow, A.L., Maddalon, D.V., Bartlett, D.W., Wagner, R.D., and Collier, F.S., "Applied Aspects of Laminar-Flow Technology," *Viscous Drag Reduction in Boundary Layers*, AIAA, Washington D.C., 1990, pp. 47-48.

Dollyhigh, S.M., Monta, W.J., and Sangiorgio, G., "Longintudinal Aerodynamic Characteristics at Mach 0.60 to 2.86 of a Fighter Configuration with Strut-Braced Wing," NASA-TP-1102, December 1977.

Grasmeyer, J.M., "Multidisciplinary Design Optimization of a Strut-Braced Wing Aircraft", MS Thesis, Virginia Polytechnic Institute & State University, April 1998A.

Grasmeyer, J.M., Naghshineh_Pour, A., Tetrault, P.-A., Grossman, B., Haftka, R.T., Kapania, R.K., Mason, W.H., and Schetz, J.A., "Multidisciplinary Design Optimization of a Strut-Braced Wing Aircraft with Tip-Mounted Engines", MAD 98-01-01, 1998B.

Grasmeyer, J., "Stability and Control Derivative Estimation and Engine-Out Analysis", VPI-AOE-254, January 1998C.

Grasmeyer, J., "A Discrete Vortex Method for Calculating the Minimum Induced Drag and Optimimum Load Distribution of Aircraft Configurations with Noncoplanar Surfaces," VPI-AOE-242, January 1997.

Hilton, W.F., *High Speed Aerodynamics*, Longmans, Green & Co., London, 1952.

Hoerner, S.F., *Fluid Dynamic Drag*, published by Mrs. Hoerner, 1965. Current address: P.O. Box 65283, Vancouver, WA 98665, pp. 8-1 – 8-20.

Jobe, C.E., Kulfan, R.M., and Vachal, J.D., "Wing Planforms for Large Military Transports," AIAA-78-1470, 1978.

Johnson, Vicki, "Minimizing Life Cycle Cost for Subsonic Commercial Aircraft", *Journal of Aircraft*, Vol. 27, No. 2, February 1990, pp. 139-145.

Kulfan, R.M., and Vachal, J.D., "Wing Planform Geometry Effects on Large Subsonic Military Transport Airplanes," Boeing Commercial Airplane Company, AFFDL-TR-78-16, February 1978.

Liebeck, R.H., Page, M.A. and Rawdon, B.K., "Blended-Wing-Body Subsonic Commercial Transport," AIAA Paper 98-0438, January 1998.

Loftin, L.K., *Subsonic Aircraft: Evolution and the Matching of Size to Performance*, NASA RP 1060, Hampton, VA, 1980, pp. 152-153.

Malone, B. and Mason, W.H., "Multidisciplinary Optimization in Aircraft Design Using Analytic Technology Models," *Journal of Aircraft*, Vol. 32, No. 2, March-April 1995, pp. 431-438.

Martin, K.C., and Kopec, B.A., "A Structural and Aerodynamic Investigation of a Strut-Braced Wing Transport Aircraft Concept", LG98ER0431, November 1998.

Mason, W.H., *FRICTION Code Documentation*, available on the World Wide Web at: http://www.aoe.vt.edu/aoe/faculty/Mason_f/CatxtAppD5.pdf

Mason, W.H., "Analytic Models for Technology Integration in Aircraft Design," AIAA-90-3262, September, 1990.

Mattingly, J.D., Heiser, W.H., and Daley, D.H., *Aircraft Engine Design, AIAA*, Washington, D.C., 1987, pp. 36.

McCullers, L.A., *FLOPS User's Guide*, Release 5.81. Text file included with the FLOPS code, NASA Langley Research Center.

McMasters, J.H., and Kroo, I.M., "Advanced Configurations for Very Large Transport Airplanes", *Aircraft Design* Vol. 1, No. 4, 1999, pp. 217-242.

Miranda, L.R., and Brennan, J.E., "Aerodynamic Effects of Wingtip-Mounted Propellers and Turbines," AIAA-86-1802, 1986.

Naghshineh-Pour, A.H., Kapania, R., and Haftka, R., "Preliminary Structural Analysis of a Strut-Braced Wing", VPI-AOE-256, June 1998.

Park, P.H., "The Effect on Block Fuel Consumption of a Strutted vs. Cantilever Wing for a Short Haul Transport Including Strut Aerolastic Considerations," AIAA 78-1454, 1978.

Patterson, J.C., and Bartlett, G.R., "Evaluation of Installed Performance of a Wing-Tip-Mounted Pusher Turboprop on a Semispan Wing," NASA Technical Paper 2739, 1987.

Pfenninger, W., "Design Considerations of Large Subsonic Long Range Transport Airplanes with Low Drag Boundary Layer Suction," Northrop Aircraft, Inc., Report NAI-54-800 (BLC-67), November 1954.

Roskam, J., and Lan, C.-T. E. *Airplane Aerodynamics and Performance*, DARCorporation, Lawrence, KS, 1997, pp. 100-104, 435-508.

Smith, P.M., DeYoung, J., Lovell, W.A., Price, J.E., and Washburn, G.F., "A Study of High-Altitude Manned Research Aircraft Employing Strut-Braced Wings of High-Aspect Ratio," NASA CR-159262, February, 1981.

Spearman, M.L, “A High-Capacity Airplane Design Concept Having an Inboard-Wing Bounded by Twin Tip-Mounted Fuselages,” AIAA-97-2276, June 1997.

Tetrault,P.-A., Private Communications, July-October, 1998.

Torenbeek, E., *Synthesis of Subsonic Airplane Design*, *Delft University Press*, Delft, 1981, pp. 63, 459.

Turriziani, R.V., Lovell, W.A., Martin, G.L., Price, J.E., Swanson, E.E., and Washburn, G.F., “Preliminary Design Characteristics of a Subsonic Business Jet Consept Employing an Aspect Ratio 25 Strut-Braced Wing,” NASA CR-159361, October 1980.

Vanderplaats Research & Development, Inc., *DOT User’s Manual*, Version 4.20, Colorado Springs, CO, 1995.

Wolkovitch, J. “The Joined Wing – An Overview,” AIAA-85-0274, January, 1985.

Appendix 1. Tail Geometry

This appendix details the calculation procedure for finding the distance from the wing leading edge to the leading edge of the two tail surfaces given their tail moment arms used for stability and control analysis. The input variable *dx_htail* and *dx_vtail* no longer represent the distance from the leading edge of the wing to the leading edge of the respective tail surface. Now these variables represent the distance from the aircraft center of gravity to the aerodynamic center of the tail surface in question. Figure A1.1 shows the new convention. The center of gravity is assumed to be at the wing aerodynamic center. So *dx_htail* and *dx_vtail* are tail moment arms used for tail volume coefficient sizing. The tail areas are:

$$S_{HT} = \frac{TVC_{HT} \cdot S_w \cdot MAC_w}{dx\_htail} \quad \text{and} \quad S_{VT} = \frac{TVC_{VT} \cdot S_w \cdot b_w}{dx\_vtail}$$

where S is the planform area of a tail surface, *TVC* is tail volume coefficient, S_w is the wing planform area, MAC_w is the wing aerodynamic chord and b_w is the wing span. The input file has an integer variable tvc_flag to control whether or not to use the tail volume coefficient sizing method or to simply input a constant tail area. If the tail volume coefficient flag is set to 1 in the input file, then the tail volume coefficient method is employed. Otherwise, if it is set to 0, then input tail areas are used.

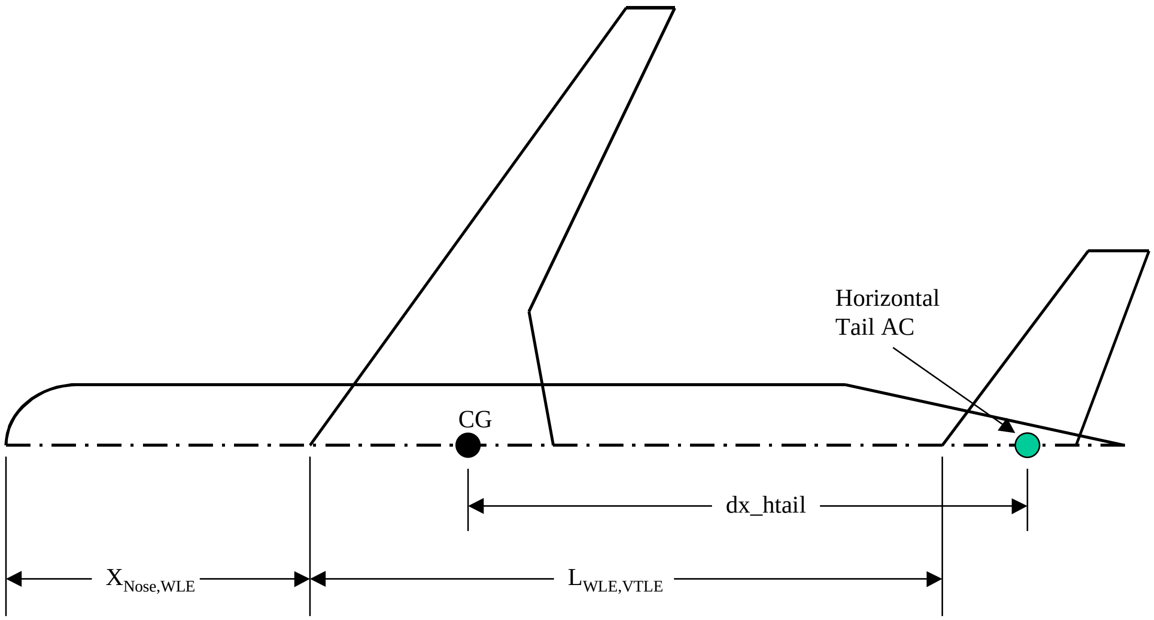

Figure A1.1. Length Definitions.

Previously, the span, root chord and tip chord of the horizontal and vertical tail surfaces, and the rudder span and average chord were input directly. This was the most convenient way to handle the tail geometry if the tail size remains constant. In studies by Grasmeyer (1998A-C), the tail size and geometry were held fixed at the value of the Boeing 777. Because the tail volume coefficient method allows the tail size to vary with the wing geometry, defining tail lengths is no longer convenient. To remedy this, the tail geometry was parameterized in terms of aspect ratio, taper ratio, sweep, and percentage chord and span of the rudder. The lengths are found from the dimensionless parameters and areas by:

$$C_{HTroot} = \frac{2 \cdot \sqrt{\dfrac{S_{HT}}{AR_{HT}}}}{(1-\lambda_{HT})} \quad \text{and} \quad C_{VTroot} = \frac{2 \cdot \sqrt{\dfrac{S_{VT}}{AR_{VT}}}}{(1-\lambda_{VT})}$$

$$AR_{HT} = \frac{b_{HT}^2}{S_{HT}} \quad \text{and} \quad AR_{VT} = \frac{b_{VT}^2}{S_{VT}}$$

where b_{HT} and b_{VT} are the spans of the respective tail surfaces including their projections into the fuselage.

$$C_{HTtip} = C_{HTroot} \cdot \lambda_{HT} \quad \text{and} \quad C_{VTtip} = C_{VTroot} \cdot \lambda_{VT}$$

$$b_{HT} = \frac{AR_{HT}}{2} \cdot C_{HTroot} \cdot (1 - \lambda_{HT}) \quad \text{and} \quad b_{VT} = \frac{AR_{VT}}{2} \cdot C_{VTroot} \cdot (1 - \lambda_{VT})$$

$$C_{rudder} = \%C_{rudder} \cdot \frac{(C_{VTroot} + C_{VTtip})}{2}$$

$$b_{rudder} = \%b_{rudder} \cdot b_{VT}$$

Once the lengths are calculated, they are used in the same way as before for the stability and control analysis and for drag calculations. Since the variables *dx_htail* and *dx_vtail* no longer represent the distance from the wing leading edge to the leading edge of the respective tail surfaces, this value must be found for the DXF file generator. Figure A1.2 shows the wing geometry and terms used to define the wing.

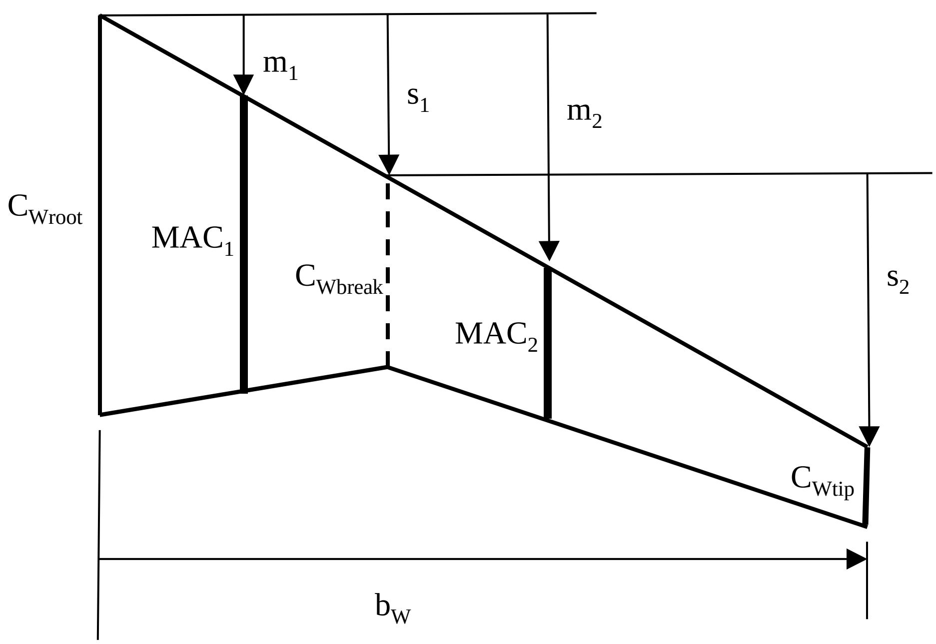

Figure A1.2. Wing Geometry for Tail Length Calculations.

The first step in this procedure is to find the mean aerodynamic chords (MAC) of the inboard and outboard wing panels.

$$MAC_1 = \frac{2}{3}\left(C_{Wroot} + C_{Wbreak} - \frac{C_{Wroot} \cdot C_{Wbreak}}{C_{Wroot} - C_{Wbreak}} \right) \quad \text{and} \quad MAC_2 = \frac{2}{3}\left(C_{Wbreak} + C_{Wtip} - \frac{C_{Wbreakt} \cdot C_{Wtip}}{C_{Wbreak} - C_{Wtip}} \right)$$

Then the leading edge sweep of the leading edge is found, assuming that the leading edge sweep for the inboard panel is the same as the outboard panel.

$$\Lambda_{W,LE} = TAN^{-1}\left(\frac{2}{b_W}\left(-\frac{1}{4}C_{Wtip} + \frac{1}{4}C_{Wbreak} + \frac{b_W}{2}TAN\left(\Lambda_{W,c/4}\right)\right)\right)$$

The streamwise-distance from the leading edge of the segment root to the leading edge of the segment tip is:

$$s_1 = \frac{b_W}{2} \cdot \eta_{break} \cdot TAN\left(\Lambda_{W,LE}\right) \quad \text{and} \quad s_2 = \frac{b_W}{2} \cdot \left(1 - \eta_{break}\right) \cdot TAN\left(\Lambda_{W,LE}\right)$$

Now, the streamwise-distance from the leading edge of the wing root chord to the leading edge of the mean aerodynamic chord of each segment can be found by:

$$m_1 = s_1 \cdot \frac{\left(C_{Wroot} + 2 \cdot C_{Wbreak}\right)}{3} \cdot \left(C_{Wroot} + C_{Wbreak}\right) \quad \text{and}$$

$$m_2 = s_1 + s_2 \cdot \frac{\left(C_{Wbreak} + 2 \cdot C_{Wtip}\right)}{3} \cdot \left(C_{Wbreak} + C_{Wtip}\right)$$

The areas of each segment are:

$$S_{W1} = \frac{b_W}{4} \cdot \eta_{break} \cdot \left(C_{Wroot} + C_{Wbreak}\right) \quad \text{and} \quad S_{W2} = \frac{b_W}{4} \cdot \left(1 - \eta_{break}\right) \cdot \left(C_{Wbreak} + C_{Wtip}\right)$$

Now the overall MAC and distance from the leading edge of the root chord to the leading edge of the MAC are calculated as the area weighted average of the components:

$$MAC_W = \frac{(MAC_1 \cdot SW_1 + MAC_2 \cdot SW_2)}{(SW_1 + SW_2)}$$

$$m_W = \frac{(m_1 \cdot SW_1 + m_2 \cdot SW_2)}{(SW_1 + SW_2)}$$

The same general procedure is duplicated for the tails. Calculations are simplified, because the each tail surface consists of only one component. The procedure for calculating the MAC and distance form the root leading edge to the mean aerodynamic chord of each tail surface is as follows:

$$MAC_{HT} = \frac{2}{3} \cdot \left(C_{HTroot} + C_{HTtip} + \frac{C_{HTroot} \cdot C_{HTtip}}{C_{HTroot} + C_{HTtip}} \right)$$

$$MAC_{VT} = \frac{2}{3} \cdot \left(C_{VTroot} + C_{VTtip} + \frac{C_{VTroot} \cdot C_{VTtip}}{C_{VTroot} + C_{VTtip}} \right)$$

$$\Lambda_{HT,LE} = TAN^{-1}\left(\frac{2}{b_{HT}} \cdot \left(-\frac{1}{4} C_{HTtip} + \frac{1}{4} C_{HTroot} + \frac{b_{HT}}{2} \cdot TAN(\Lambda_{HT,c/4}) \right) \right)$$

$$\Lambda_{VT,LE} = TAN^{-1}\left(\frac{1}{b_{VT}} \cdot \left(-\frac{1}{4} C_{VTtip} + \frac{1}{4} C_{VTroot} + b_{VT} \cdot TAN(\Lambda_{VT,c/4}) \right) \right)$$

$$m_{HT} = \frac{b_{HT}}{2} \cdot TAN(\Lambda_{HT,LE}) \cdot \frac{(C_{HTroot} + 2 \cdot C_{HTtip})}{3 \cdot (C_{HTroot} + C_{HTtip})}$$

$$m_{VT} = b_{VT} \cdot TAN(\Lambda_{VT,LE}) \cdot \frac{(C_{VTroot} + 2 \cdot C_{VTtip})}{3 \cdot (C_{VTroot} + C_{VTtip})}$$

Finally, the distance from the leading edge of the wing to the leading edge of the each tail surface now becomes:

$$L_{WLE,HTLE} = dx\_htail + m_W + \frac{1}{4}MAC_W - m_{HT} - \frac{1}{4}MAC_{HT}$$

$$L_{WLE,VTLE} = dx\_vtail + m_W + \frac{1}{4}MAC_W - m_{VT} - \frac{1}{4}MAC_{VT}$$

For a conventional tail, the horizontal root trailing edge is farther aft than the vertical tail root trailing edge, and there is a nominal separation of 3 feet from the aft end of the fuselage. The corresponding distance between the nose of the aircraft and the leading edge of the wing root for a conventional tail is:

$$X_{Nose,WLE} = L_{Fuselage} - 3 - C_{HTroot} - L_{WLE,HTLE}$$

For a T-tail aircraft, a similar argument applies except the vertical tail root trailing edge is a nominal distance of 3 feet from the aft end of the fuselage. The distance from the nose of the aircraft to the wing root leading edge now becomes:

$$X_{Nose,WLE} = L_{Fuselage} - 3 - C_{VTroot} - L_{WLE,VTLE}$$

The values $X_{Nose,WLE}$, $L_{WLE,HTLE}$, and $L_{WLE,VTLE}$ are passed to DXF.F and calculations proceed as before. One new modification is that T-tail flag is now passed to DXF.F and the leading edge of the root chord of the horizontal tail is automatically attached to the tip chord leading edge of the vertical tail, regardless of the *dx_htail* value.

Appendix 2. Range Analysis

These tables summarize the results of minimum-TOGW optima designed to fly at the specified ranges. Each of the four configurations have separate tables.

Table A2.1. Cantilever Wing Range Effects.

Cant 4000	Cant 5000	Cant 6000	Cant 7000	Cant 8000	Cant 9000	Cant 10000	Cant 11000	Cant Max	
4000	5000	6000	7000	8000	9000	10000	11000	**11906**	Range (nmi)
196.4	202.4	211.2	220.2	231.0	239.8	248.9	249.4	250.2	Span (ft)
52.0	52.0	52.0	52.0	52.0	52.0	52.0	52.0	52.0	Root Chord (ft)
4343	4498	4757	5121	5534	5746	6223	6160	6480	Sw (ft^2)
8.88	9.10	9.37	9.47	9.64	10.01	9.96	10.09	9.66	AR
15.61%	15.17%	15.12%	15.04%	15.14%	14.99%	15.01%	14.87%	14.69%	Root t/c
10.75%	10.58%	10.63%	10.48%	10.62%	10.61%	10.62%	10.62%	9.83%	Outboard t/c
5.49%	5.28%	5.00%	5.02%	5.21%	5.36%	5.01%	5.25%	6.20%	Outboard t/c
34.1	34.0	34.1	33.8	34.1	34.2	33.9	34.2	33.4	Wing L1/4 (deg)
60655	64883	68917	73499	78184	83986	91426	103085	118178	Tmax (lbs)
42573	41919	41814	42094	42127	41058	41188	38992	36987	Cruise Altitude (ft)
21.69	22.13	22.68	23.17	23.68	24.03	24.29	23.97	23.30	L/D
41461	46610	53031	59970	68424	78424	88661	98142	108286	Wing Wt. (lbs)
27223	31882	37653	43901	51539	61269	70703	80205	90005	Bending Matl (lbs)
97179	120225	144765	171752	201312	235901	276144	330385	399848	Fuel Wt. (lbs)
405310	**439630**	**477044**	**518210**	**563994**	**617150**	**678548**	**755682**	852366	TOGW (lbs)
78.07	80.43	83.09	85.98	89.22	92.70	96.74	100.82	105.57	Acquisition Cost ($M)
543.38	550.63	561.32	575.50	592.71	614.34	641.19	677.05	857.95	DOC ($M)
941.93	920.42	906.02	895.97	888.84	883.97	880.82	879.57	930.78	IOC ($M)
ACTIVE	ACTIVE	ACTIVE	ACTIVE	ACTIVE	ACTIVE	ACTIVE	ACTIVE	ACTIVE	Shock Cl Constraint
ACTIVE	ACTIVE	ACTIVE	ACTIVE	ACTIVE	ACTIVE	ACTIVE	ACTIVE	ACTIVE	2nd Segment Climb
								ACTIVE	Balanced Field Length
	ACTIVE	ACTIVE	ACTIVE	ACTIVE	ACTIVE	ACTIVE	ACTIVE	ACTIVE	Engine Out
								ACTIVE	Approach Velocity
									Fuel Volume

Table A2.2. T-Tail SBW Range Effects.

SBW-fuse 4000	SBW-fuse 5000	SBW-fuse 6000	SBW-fuse 7000	SBW-fuse 8000	SBW-fuse 9000	SBW-fuse 10000	SBW-fuse 11000	SBW-fuse 12000	SBW-fuse 13000	SBW-fuse Max	
4000	5000	6000	7000	8000	9000	10000	11000	12000	13000	**13304**	Range (nmi)
198.8	208.5	215.0	220.9	228.1	234.3	233.6	244.9	261.2	257.9	262.5	Span (ft)
27.3	28.3	28.2	30.1	30.4	32.0	34.6	36.9	38.7	42.0	43.3	Root Chord (ft)
3334	3648	3763	4137	4344	4683	4983	5495	6126	6509	6807	S_w (ft^2)
11.86	11.92	12.29	11.80	11.97	11.73	10.95	10.91	11.14	10.22	10.12	AR
13.94%	13.78%	13.71%	13.78%	13.80%	13.88%	13.60%	13.10%	13.20%	13.23%	13.21%	Root t/c
7.54%	7.13%	7.12%	6.95%	7.15%	7.17%	6.75%	7.09%	7.14%	6.83%	6.68%	Outboard t/c
6.86%	6.53%	6.79%	6.36%	6.72%	6.65%	5.69%	6.58%	6.92%	6.25%	6.08%	Outboard t/c
27.5	28.7	29.1	29.9	30.2	31.1	31.0	30.1	31.0	31.1	30.6	Wing $\Lambda_{1/4}$ (deg)
20.7	20.6	21.0	20.8	21.1	21.2	21.6	22.6	22.9	22.1	21.8	Strut $\Lambda_{1/4}$ (deg)
66.1%	67.2%	67.4%	68.7%	68.4%	68.5%	68.6%	63.2%	67.2%	66.0%	66.7%	η Strut
48134	50840	53778	58187	61843	66897	75658	82100	88492	103686	108450	T_{max} (lbs)
40025	40697	40263	40951	40859	40943	40415	40540	40881	41571	41656	Cruise Altitude (ft)
23.50	24.47	25.01	25.23	25.64	25.80	25.30	25.61	26.07	25.34	25.22	L/D
41236	47042	52298	56970	62689	68530	73411	83976	97297	103034	108225	Wing Wt. (lbs)
6493	7343	8019	9023	9912	11107	12413	12612	15855	15227	15688	Strut Wt. (lbs)
2231	2540	2835	3247	3478	3801	4646	5614	6333	7025	7109	Offset Wt. (lbs)
27104	31950	36805	40184	45501	50321	53544	63953	75851	79733	84097	Bending Matl (lbs)
86202	104107	124129	147456	171325	199396	237726	274929	315517	377323	399999	Fuel Wt. (lbs)
380952	**409516**	**439224**	**473298**	**508164**	**548776**	**601136**	**657972**	**721974**	**804260**	837288	TOGW (lbs)
11.3%	13.4%	14.3%	14.1%	14.9%	15.5%	13.9%	16.8%				% Fuel Reduction
6.0%	6.8%	7.9%	8.7%	9.9%	11.1%	11.4%	12.9%				% TOGW Reduction
75.14	77.46	79.43	81.73	83.92	86.44	89.20	92.99	97.39	101.24	103.01	Acquisition Cost ($M)
512.07	515.17	521.51	533.11	544.32	560.02	584.19	608.56	636.00	674.93	759.17	DOC ($M)
936.54	914.97	900.24	890.03	882.32	876.83	873.52	871.14	869.73	869.87	895.99	IOC ($M)
ACTIVE	ACTIVE	ACTIVE	ACTIVE	ACTIVE	ACTIVE	ACTIVE	ACTIVE	ACTIVE	ACTIVE	ACTIVE	Shock Cl Constraint
ACTIVE	ACTIVE	ACTIVE	ACTIVE	ACTIVE	ACTIVE	ACTIVE	ACTIVE				2nd Segment Climb
				ACTIVE	ACTIVE	ACTIVE	ACTIVE	ACTIVE	ACTIVE	ACTIVE	Balanced Field Length
											Engine Out
											Approach Velocity
											Fuel Volume

Table A2.3. Tip Engine SBW Range Effects.

SBW-tip 4000	SBW-tip 5000	SBW-tip 6000	SBW-tip 7000	SBW-tip 8000	SBW-tip 9000	SBW-tip 10000	SBW-tip 11000	SBW-tip 12000	SBWtip maxr	
4000	5000	6000	7000	8000	9000	10000	11000	12000	**12114**	Range (nmi)
178.6	191.1	191.9	195.8	198.5	198.5	198.4	209.0	222.0	215.2	Span (ft)
30.2	30.9	30.8	31.6	33.6	35.7	36.1	40.4	47.9	51.2	Root Chord (ft)
3305	3640	3643	3812	4049	4176	4349	4966	6043	6413	S_w (ft^2)
9.65	10.03	10.11	10.06	9.73	9.44	9.05	8.79	8.16	7.22	AR
14.39%	14.37%	14.33%	14.34%	14.31%	14.14%	14.24%	13.97%	13.70%	13.62%	Root t/c
7.34%	7.55%	7.46%	7.51%	7.49%	7.29%	7.37%	7.04%	6.80%	6.80%	Outboard t/c
6.85%	6.87%	6.85%	6.83%	6.85%	6.76%	6.82%	6.90%	6.67%	6.40%	Outboard t/c
28.9	30.0	30.0	30.1	30.6	31.4	31.4	32.0	32.3	32.6	Wing $\Lambda_{1/4}$ (deg)
23.6	23.5	23.6	23.5	23.6	24.1	23.8	25.5	25.9	25.2	Strut $\Lambda_{1/4}$ (deg)
56.2%	56.6%	56.6%	56.6%	56.8%	55.5%	56.3%	56.5%	57.0%	57.9%	η Strut
45000	46292	47626	49813	53814	60390	66005	67753	69668	73316	T_{max} (lbs)
40708	40708	40708	40708	40357	39557	40557	40257	40257	39057	Cruise Altitude (ft)
23.84	24.55	24.91	25.10	24.99	24.88	24.94	24.98	24.26	22.75	L/D
30879	35660	37578	40260	42667	45642	47014	52999	60860	59913	Wing Wt. (lbs)
4125	4918	4873	5021	5235	4807	5260	6112	6873	6630	Strut Wt. (lbs)
3113	3837	3834	3976	4181	4186	4406	5078	5566	5969	Offset Wt. (lbs)
16695	20301	21961	24014	25580	28026	28499	32902	37963	35638	Bending Matl (lbs)
80057	97131	114874	134991	158957	186235	213127	245034	294200	326248	Fuel Wt. (lbs)
357540	**383050**	**405305**	**431677**	**462911**	**499382**	**533471**	**576456**	**641327**	677111	TOGW (lbs)
17.6%	19.2%	20.6%	21.4%	21.0%	21.1%	22.8%	25.8%			% Fuel Reduction
11.8%	12.9%	15.0%	16.7%	17.9%	19.1%	21.4%	23.7%			% TOGW Reduction
71.48	73.45	74.44	75.84	77.46	79.34	80.87	83.35	86.98	87.93	Acquisition Cost ($M)
490.32	492.56	494.14	500.44	511.38	525.80	537.57	554.51	585.55	627.26	DOC ($M)
931.36	910.19	895.06	884.52	877.03	871.67	867.11	864.11	863.36	872.78	IOC ($M)
ACTIVE		ACTIVE	ACTIVE	ACTIVE	ACTIVE		ACTIVE	ACTIVE	ACTIVE	Shock CI Constraint
										2nd Segment Climb
			ACTIVE	ACTIVE	ACTIVE	ACTIVE	ACTIVE	ACTIVE	ACTIVE	Balanced Field Length
	ACTIVE	ACTIVE	ACTIVE	ACTIVE	ACTIVE	ACTIVE	ACTIVE			Wingtip Deflection
						ACTIVE	ACTIVE	ACTIVE	ACTIVE	Engine Out
										Approach Velocity
ACTIVE	ACTIVE	ACTIVE							ACTIVE	Initial Cruise ROC

Table A2.4. Underwing Engine SBW Range Effects.

SBW-win 4000	SBW-win 5000	SBW-win 6000	SBW-wing 7000	SBW-win 8000	SBW-win 9000	SBW-wing 10000	SBW-win 11000	SBW-win 12000	SBW-win 13000	SBW-wing maxr	
4000	5000	6000	7000	8000	9000	10000	11000	12000	13000	**13979**	Range (nmi)
204.5	207.8	224.5	229.9	236.8	242.3	249.6	249.9	259.9	262.3	262.5	Span (ft)
28.1	30.2	29.5	29.4	29.8	31.4	32.8	34.8	36.8	39.7	42.5	Root Chord (ft)
3447	3778	4022	4117	4312	4651	4989	5304	5795	6258	6712	S_w (ft^2)
12.13	11.43	12.53	12.83	13.01	12.63	12.49	11.78	11.65	11.00	10.27	AR
13.07%	13.31%	12.95%	12.88%	12.76%	12.79%	12.79%	12.84%	12.81%	12.84%	12.89%	Root t/c
6.59%	7.55%	6.73%	6.47%	6.38%	6.47%	6.89%	6.86%	6.86%	6.89%	7.46%	Outboard t/c
8.49%	9.05%	8.39%	8.25%	8.18%	8.12%	8.41%	8.25%	8.32%	8.21%	8.43%	Outboard t/c
27.0	28.4	27.4	27.0	27.5	27.6	28.8	29.3	29.8	30.3	31.4	Wing $\Lambda_{1/4}$ (deg)
24.9	25.9	25.3	25.1	25.3	25.6	26.3	26.0	26.2	26.2	26.6	Strut $\Lambda_{1/4}$ (deg)
62.9%	59.2%	63.8%	64.4%	63.2%	62.8%	61.6%	63.9%	64.3%	65.5%	63.3%	η Strut
86.6%	87.5%	82.9%	82.5%	80.7%	79.5%	79.5%	72.4%	72.5%	67.5%	60.7%	η Engine
45208	49335	51172	52913	56209	60796	65416	73022	79275	90162	103557	T_{max} (lbs)
40728	41282	41987	41622	41444	41715	41672	41425	41510	41042	40519	Cruise Altitude (ft)
24.50	24.26	25.74	26.09	26.66	26.70	26.92	26.50	26.66	26.11	25.47	L/D
38381	40276	48720	53247	59849	64850	71711	76620	85929	93477	100744	Wing Wt. (lbs)
5419	6091	7844	7811	8908	10141	9786	12120	13159	14486	14607	Strut Wt. (lbs)
2263	2620	2810	2648	3161	3866	3890	4929	5597	6500	6666	Offset Wt. (lbs)
23714	24525	32417	36669	42753	46945	53006	56997	65162	71401	77267	Bending Matl (lbs)
80520	100938	116978	137046	158367	184422	212310	249139	286181	338617	399824	Fuel Wt. (lbs)
366842	**394693**	**422759**	**450678**	**483205**	**520031**	**560812**	**610516**	**664945**	**736297**	816265	TOGW (lbs)
17.1%	16.0%	19.2%	20.2%	21.3%	21.8%	23.1%	24.6%				% Fuel Reduction
9.5%	10.2%	11.4%	13.0%	14.3%	15.7%	17.4%	19.2%				% TOGW Reduction
73.25	75.06	77.49	79.08	81.30	83.52	86.06	88.61	91.98	95.61	98.84	Acquisition Cost ($M)
496.57	503.48	506.98	513.44	523.50	537.60	553.40	575.30	598.23	631.16	833.68	DOC ($M)
933.40	912.29	897.72	887.03	879.40	873.83	869.70	867.05	865.21	864.88	926.32	IOC ($M)
ACTIVE	ACTIVE	ACTIVE	ACTIVE	ACTIVE	ACTIVE	ACTIVE	ACTIVE	ACTIVE	ACTIVE	ACTIVE	Shock Cl Constraint
	ACTIVE		ACTIVE	ACTIVE	ACTIVE	ACTIVE	ACTIVE	ACTIVE	ACTIVE	ACTIVE	2nd Segment Climb
				ACTIVE		ACTIVE	ACTIVE	ACTIVE	ACTIVE	ACTIVE	Balanced Field Length
	ACTIVE		ACTIVE	ACTIVE	ACTIVE						Wingtip Deflection
									ACTIVE	ACTIVE	Engine Out
											Approach Velocity
ACTIVE	ACTIVE	ACTIVE									Initial Cruise ROC
										ACTIVE	Fuel Volume

Appendix 3. Technology Impact Study Results

These tables summarize the results of the technology impact study of minimum-TOGW optima with various technologies. Results for each of the four configurations are presented in separate tables.

Table A3.1 Cantilever Wing Sensitivity Analysis.

1995 Conv Wing Eng.	1995 Conv NLF	1995 Conv Aero	1995 Conv Airframe	1995 Conv Propulsion	1995 Conv Systems	2010 Conv Wing-Eng.	Tot Change **-171614** Sum Change **-27.5%**
7500.1	7496.5	7500.1	7500.1	7500.0	7500.1	7499.8	Range
214.9	211.5	217.9	215.2	210.4	213.9	225.3	Span (ft)
52.0	52.0	52.0	52.0	52.0	52.0	52.0	Root Chord (ft)
8.8	8.3	8.6	8.2	8.5	8.6	8.5	Root Chord (ft)
5413	5213	5198	4959	5254	5415	5307	S_w (ft^2)
8.53	8.58	9.13	9.34	8.43	8.45	9.57	AR
15.61%	15.27%	16.36%	15.26%	15.39%	15.65%	15.14%	Root t/c
10.65%	10.32%	11.73%	10.83%	10.28%	10.61%	10.55%	Break t/c
6.20%	5.78%	6.66%	5.52%	5.75%	5.25%	7.40%	Tip t/c
39.8	39.0	36.7	40.4	39.3	39.8	34.2	Wing $\Lambda_{1/4}$ (deg)
37.0%	37.0%	37.0%	37.0%	37.0%	37.0%	37.0%	η Engine
108861	104599	98437	94274	106772	105789	75793	T_{max} (lbs)
35640	35598	37253	36112	35519	35943	42052	Cruise Altitude (ft)
19.94	20.68	20.83	20.39	19.79	20.15	23.38	L/D
98791	93734	87267	75388	94109	96260	63706	Wing Wt. (lbs)
280900	262535	253180	246252	268265	271935	186295	Fuel Wt. (lbs)
430948	420028	408324	387600	422738	422209	353928	Zero Fuel Wt. (lbs)
711844	**682770**	**661501**	**633848**	**691004**	**694142**	**540230**	TOGW (lbs)
1745.56	1714.78	1693.33	1666.17	1723.94	1722.98	1563.24	Total Cost ($M)
102.51	100.54	98.56	94.81	101.02	99.55	87.49	Acquisition Cost ($M)
729.68	704.50	687.65	667.66	712.13	712.26	583.68	DOC ($M)
913.37	909.74	907.12	903.69	910.78	911.17	892.07	IOC ($M)
	-4.1%	-7.1%	-11.0%	-2.9%	-2.5%	-24.1%	% TOGW Reduction
	-1.8%	-3.0%	-4.5%	-1.2%	-1.3%	-10.4%	% Fuel Reduction
ACTIVE	ACTIVE	ACTIVE	ACTIVE	ACTIVE	ACTIVE	ACTIVE	Shock Cl Constraint
ACTIVE	ACTIVE	ACTIVE	ACTIVE	ACTIVE	ACTIVE	ACTIVE	2nd Segment Climb
							Balanced Field Length
							Wingtip Deflection
ACTIVE	ACTIVE	ACTIVE	ACTIVE	ACTIVE	ACTIVE	ACTIVE	Engine Out
ACTIVE	ACTIVE			ACTIVE			Approach Velocity
							Initial Cruise ROC
							Fuel Volume

Table A3.2. T-Tail Fuselage-Mounted Engine Sensitivity Analysis.

T-Tail SBW 1995	T-Tail SBW NLF	T-Tail SBW AERO	T-Tail SBW Airframe	T-Tail SBW Propulsion	T-Tail SBW Systems	T-Tail SBW 2010	Tot Change -155150 Sum Change -28.80%
7500.0	7499.5	7499.2	7499.5	7498.9	7497.8	7499.9	Range
214.4	210.9	208.4	212.7	211.8	212.2	226.0	Span (ft)
37.7	36.3	35.9	35.1	37.1	37.5	30.2	Root Chord (ft)
8.1	7.3	8.1	7.6	7.9	7.8	7.0	Tip Chord (ft)
4910	4598	4581	4541	4770	4805	4205	Sw (ft^2)
9.37	9.68	9.48	9.96	9.41	9.37	12.15	AR
13.68%	13.36%	14.19%	13.65%	13.74%	13.64%	14.28%	Root t/c
7.07%	6.61%	7.13%	6.72%	6.82%	6.85%	6.58%	Break t/c
7.48%	6.93%	7.55%	7.43%	7.39%	7.33%	6.56%	Tip t/c
36.9	35.6	32.9	37.1	36.4	36.6	29.9	Wing $\Lambda_{1/4}$ (deg)
23.7	24.5	21.6	26.4	24.6	24.4	20.5	Strut $\Lambda_{1/4}$ (deg)
65.5%	67.6%	67.5%	66.1%	64.5%	68.8%	68.8%	η Strut
89515	81836	83553	78461	86991	87404	59463	Tmax (lbs)
36700	36576	37851	37046	36628	36648	40429	Cruise Altitude (ft)
20.10	21.89	20.88	20.48	20.07	20.10	25.30	L/D
88200	81346	75472	67152	85143	84196	59581	Wing Wt. (lbs)
50794	46012	41735	48129	48876	47679	42500	Bending Matl (lbs)
253141	220879	230181	225527	241120	247624	159629	Fuel Wt. (lbs)
392000	377036	372286	356850	386141	383556	330683	Zero Fuel Wt. (lbs)
645000	**597922**	**602480**	**582378**	**627268**	**631176**	**490312**	TOGW (lbs)
1675.30	1624.60	1631.86	1611.11	1656.17	1656.34	1507.31	Total Cost ($M)
95.30	92.40	91.70	88.90	94.10	92.30	82.70	Acquisition Cost ($M)
675.00	633.00	640.00	625.00	659.00	661.00	538.00	DOC ($M)
905.00	899.00	900.00	897.00	903.00	903.00	886.00	IOC ($M)
	7.3%	6.6%	9.7%	2.7%	2.1%	24.0%	% TOGW Reduction
	12.7%	9.1%	10.9%	4.7%	2.2%	36.9%	% Fuel Reduction
ACTIVE	ACTIVE	ACTIVE	ACTIVE	ACTIVE	ACTIVE	ACTIVE	Shock Cl Constraint
ACTIVE	ACTIVE	ACTIVE	ACTIVE	ACTIVE	ACTIVE	ACTIVE	2nd Segment Climb
ACTIVE	ACTIVE	ACTIVE	ACTIVE	ACTIVE	ACTIVE	ACTIVE	Balanced Field Length
							Wingtip Deflection
							Engine Out
ACTIVE		ACTIVE		ACTIVE	ACTIVE		Approach Velocity
							Initial Cruise ROC
							Fuel Volume

Table A3.3. Wingtip-Mounted Engine SBW Sensitivity Analysis.

Tip SBW	Tip SBW	Tip SBW	Tip SBW	Tip SBW	Tip SBW	Tip SBW	Tot Change -100107
1995	NLF	AERO	Airframe	Propulsion	Systems	2010	Sum Change **19.7%**
7499.7	7496.1	7499.9	7495.5	7499.6	7499.9	7499.7	Range
182.2	181.9	182.6	176.5	183.0	181.1	198.6	Span (ft)
38.8	38.1	38.4	37.1	40.8	38.7	31.8	Root Chord (ft)
7.6	7.0	7.2	7.4	6.8	7.3	7.5	Tip Chord (ft)
4221	4099	4165	3931	4360	4171	3907	S_w (ft^2)
7.86	8.07	8.01	7.93	7.68	7.87	10.10	AR
14.17%	14.09%	14.37%	14.16%	14.14%	14.23%	14.36%	Root t/c
7.71%	7.17%	7.78%	7.81%	7.03%	7.77%	7.56%	Break t/c
7.49%	6.99%	7.39%	7.55%	6.97%	7.58%	6.85%	Tip t/c
39.2	38.2	36.7	39.9	39.5	39.7	30.2	Wing $\Lambda_{1/4}$ (deg)
26.5	26.9	25.2	26.3	27.6	26.9	23.5	Strut $\Lambda_{1/4}$ (deg)
58.7%	58.6%	58.5%	58.0%	63.9%	57.3%	56.8%	η Strut
100.0%	100.0%	100.0%	100.0%	100.0%	100.0%	100.0%	η Engine
71302	65587	66961	67511	65621	70164	51851	T_{max} (lbs)
38540	38376	38650	38513	38567	38301	40736	Cruise Altitude (ft)
20.68	22.38	21.53	20.57	20.65	20.81	25.25	L/D
55668	53356	52426	42179	54596	55190	41854	Wing Wt. (lbs)
25462	24475	23606	23555	24543	25279	25213	Bending Matl (lbs)
210173	187580	196448	197894	200271	206309	145618	Fuel Wt. (lbs)
336228	328318	329010	314928	331191	332432	300676	Zero-Fuel Wt. (lbs)
546401	**515984**	**525459**	**512826**	**531463**	**538821**	**446294**	TOGW (lbs)
1574.13	1540.89	1551.70	1540.12	1558.07	1562.00	1462.46	Total Cost ($M)
84.84	83.30	83.49	80.74	84.02	82.80	76.70	Acquisition Cost ($M)
596.45	568.37	577.87	570.59	582.99	587.28	504.86	DOC ($M)
892.84	889.05	890.24	888.67	890.98	891.89	880.41	IOC ($M)
	5.6%	3.8%	6.1%	2.7%	1.4%	18.3%	% TOGW Reduction
	10.7%	6.5%	5.8%	4.7%	1.8%	30.7%	% Fuel Reduction
ACTIVE	ACTIVE	ACTIVE	ACTIVE	ACTIVE	ACTIVE	ACTIVE	Shock Cl Constraint
							2nd Segment Climb
ACTIVE	ACTIVE	ACTIVE	ACTIVE	ACTIVE	ACTIVE	ACTIVE	Balanced Field Length
ACTIVE	ACTIVE		ACTIVE	ACTIVE		ACTIVE	Wingtip Deflection
ACTIVE	ACTIVE	ACTIVE	ACTIVE	ACTIVE	ACTIVE		Engine Out
			ACTIVE				Approach Velocity
							Initial Cruise ROC
							Fuel Volume

Table A3.4. Underwing Engine SBW Sensitivity Analysis.

Wing SBW 1995	Wing SBW NLF	Wing SBW AERO	Wing SBW Airframe	Wing SBW Propulsion	Wing SBW Systems	Wing SBW 2010	Tot Change -135978 Sum Change **27.6%**
7498.2	7498.0	7499.9	7498.9	7498.5	7497.3	7499.3	Range
227.1	217.1	212.7	217.9	223.0	226.8	220.1	Span (ft)
36.0	34.7	33.8	33.8	35.7	35.9	29.4	Root Chord (ft)
7.9	7.7	7.6	7.5	7.9	7.9	6.6	Tip Chord (ft)
4981	4601	4412	4501	4860	4969	3970	S_w (ft^2)
10.36	10.25	10.26	10.54	10.23	10.35	12.20	AR
13.81%	13.89%	14.22%	13.60%	13.81%	13.82%	14.00%	Root t/c
7.26%	7.50%	7.00%	6.62%	7.21%	7.29%	7.15%	Break t/c
7.64%	8.08%	7.32%	7.21%	7.65%	7.66%	7.37%	Tip t/c
36.2	35.4	31.1	36.1	36.1	36.3	29.8	Wing $\Lambda_{1/4}$ (deg)
24.9	27.0	24.3	25.3	25.3	24.9	21.6	Strut $\Lambda_{1/4}$ (deg)
63.7%	62.5%	64.1%	62.7%	63.2%	63.7%	62.4%	η Strut
79.5%	82.6%	83.9%	80.7%	80.7%	79.5%	83.8%	η Engine
77745	72939	73927	70892	76285	76530	56562	T_{max} (lbs)
38536	38481	38891	38446	38561	38682	40097	Cruise Altitude (ft)
21.03	22.57	21.48	21.00	20.90	21.17	25.30	L/D
82685	71738	65728	60285	78471	82048	50287	Wing Wt. (lbs)
45999	38202	34038	40883	42893	45638	33335	Bending Matl (lbs)
228225	200881	208875	207958	218235	224112	151342	Fuel Wt. (lbs)
372222	354888	348929	338608	365947	368511	313214	Zero-Fuel Wt. (lbs)
600534	**555770**	**557802**	**546574**	**584174**	**592442**	**464556**	TOGW (lbs)
1627.49	1580.68	1584.22	1573.58	1610.57	1614.87	1480.44	Total Cost ($M)
91.40	88.16	87.07	85.28	90.24	89.30	79.01	Acquisition Cost ($M)
636.54	598.53	602.89	595.45	622.80	626.99	518.75	DOC ($M)
899.55	894.00	894.25	892.86	897.53	898.57	882.68	IOC ($M)
	7.5%	7.1%	9.0%	2.7%	1.3%	22.6%	% TOGW Reduction
	12.0%	8.5%	8.9%	4.4%	1.8%	33.7%	% Fuel Reduction
ACTIVE	ACTIVE	ACTIVE	ACTIVE	ACTIVE	ACTIVE	ACTIVE	Shock CI Constraint
ACTIVE	ACTIVE	ACTIVE	ACTIVE	ACTIVE	ACTIVE	ACTIVE	2nd Segment Climb
		ACTIVE				ACTIVE	Balanced Field Length
ACTIVE	ACTIVE	ACTIVE		ACTIVE		ACTIVE	Wingtip Deflection
							Engine Out
							Approach Velocity
							Initial Cruise ROC
							Fuel Volume

Benefits of Dual Wings over Single Wings for High-Performance Business Airplanes

Mark D. Rhodes* and Bruce P. Selberg†
University of Missouri, Rolla, Missouri

An investigation was performed to compare closely coupled dual-wing aircraft and swept-forward swept-rearward (SFSR), dual-wing aircraft to corresponding single-wing aircraft to judge the advantages offered by aircraft designed with multiple-wing systems. The optimum dual-wing geometry used on the dual-wing designs were determined in an analytical study which investigated the two- and three-dimensional aerodynamic behavior of a wide range of dual-wing configurations in order to find the wing geometry that created the minimum cruise drag. This analysis used a multielement inviscid vortex panel program coupled to a momentum integral boundary-layer analysis program to calculate the two-dimensional aerodynamic data, which was then used as input for a three-dimensional vortex-lattice program, which calculated the three-dimensional aerodynamic data. The low drag of the dual-wing configurations is due to a combination of two- and three-dimensional drag reductions, and the structural advantages of the two wings, which permitted higher aspect ratios for the two wing systems, because of the wing tip structural connections.

Nomenclature

$A\!R$	= aspect ratio, b^2/S_{ref}
b	= wing span
C_D	= total drag coefficient
$C_{D_{cr}}$	= cruise drag coefficient
C_{D_i}	= induced drag coefficient
C_d	= sectional drag coefficient
C_L	= total lift coefficient
$C_{L_{cr}}$	= cruise lift coefficient
C_l	= sectional lift coefficient
C_l/C_d	= sectional lift-to-drag ratio
C_{l_α}	= sectional lift curve slope
C_p	= pressure coefficient, $(p-p_\infty)/q_\infty$
c	= wing chord
D	= decalage angle
D_{cr}	= cruise drag
G	= gap (in chord lengths)
L/D	= total lift-to-drag ratio
$(L/D)_{cr}$	= cruise lift-to-drag ratio
P_{cr}	= cruise power
R	= Reynolds number, per meter or foot
R_c	= Reynolds number based on wing chord
S	= stagger (in chord lengths)
V_{cr}	= cruise speed
W_{cr}	= cruise weight
x/c	= nondimensional chordwise location
α	= wing angle of attack
ΔD_i	= percent reduction in induced drag
λ	= taper ratio, $c_{\text{tip}}/c_{\text{root}}$

Introduction

WITH the advent of the all-metal aircraft wing, the biplane and triplane wing designs used on most of the early aircraft were replaced by a single-wing surface which was structurally stronger and aerodynamically "cleaner" than the multisurface wings it replaced. Progressively lighter and more powerful aircraft engines and higher flight speeds obviated the need for the additional wing area provided by the multisurface wings. However, more recent studies have shown that closely coupled dual-wing systems possess aerodynamic advantages over the single-wing configuration that could lead to dual-wing aircraft designs that are more fuel efficient than single-wing designs by virtue of the lower drag of the dual wings.

The three main factors affecting the performance of a closely coupled dual-wing system with the same airfoils and equal chords are stagger S, the longitudinal separation of the wings; gap G, the vertical distance between the wings; and decalage D, the relative angle between the two wings. Both stagger and gap are measured from midchord to midchord and nondimensionalized with respect to chord length c. Gap is always positive, stagger is positive when the upper wing is ahead of the lower wing, and decalage is positive when the upper wing is at a higher angle of incidence than the lower wing. Figure 1 illustrates these geometric relationships.

Several researchers have investigated dual-wing systems,[1-4] however, Nenadovitch[5] was the first investigator to discover improved aerodynamics. Nenadovitch conducted two-dimensional tests with dual-wing configurations and with the equivalent single wing. His tests showed that a stagger of 1.0, a gap of 0.33, and a decalage of -6 deg achieved the greatest increase in performance over the equivalent single wing. All three of these optimum configuration parameters were at the extreme end of the range of values investigated.

In 1974, Olson and Selberg[6] compared dual wings and single wings of the same lift capacity in experiments with three-dimensional models. Their findings showed that dual-wing configurations could achieve substantially higher lift-to-drag ratios than a single wing at lift coefficients below $C_{l_{\max}}$. In 1979, Wolkovitch[7] investigated tandem wing configurations for VSTOL applications. All of his configurations had negative stagger and the experimental results illustrated the lower induced drag predicted by the Munk-Prandtl-Tietjens theory.[8-10] His results also indicated that at the higher lift coefficients the span efficiency of the dual-wing configuration was higher than the single-wing configuration. Addoms and Spaid[11] did an aerodynamic analysis of high-performance dual wings where they tailored the wing's

Received Dec. 10, 1982; revision received June 28, 1983.

*Former Graduate Student, Mechanical and Aerospace Engineering Department.

†Professor of Aerospace Engineering, Mechanical and Aerospace Engineering Department. Member AIAA.

camber to compliment the induced flowfield of the dual wings in order to maintain the same $C_{l_{max}}$ as the single-wing configuration. Their final dual-wing design configuration gave superior low-speed maneuverability, short field performance, load carrying capability, and lower cost than their single-wing aircraft comparison.

Several authors have recently modified the original analysis of Munk-Prandtl-Tietjens[8-10] for canard wing or tandem wing configurations. Laitone[12] modified Prandtl's induced drag equation to account for nonelliptical span lift distributions. However, he presented results for only constant and elliptically loaded cases. Kroo[13] has solved for the minimum induced drag of canard configurations by extending Prandtl's analysis. His results assume the canard is elliptically loaded and his results add one additional correction to the classical result. Butler[14] analyzed canard wing configurations of infinite span for the purpose of calculating induced drag. His results showed an induced thrust that increased as gap decreased and was a maximum for canard span to wing span ratios of one-half. With the exception of Butler's work all of the induced drag results are for relatively large gap-to-span ratios, whereas Butler's is for infinite stagger.

Several investigators have analytically studied dual-airfoil effects. Most of the early work investigated slat-airfoil effects of airfoil-flap effects. In 1972, Liebeck[15] investigated the aerodynamics of slat-airfoil combinations. This study was attempting to maximize the lift coefficient through the use of slats. No drag data was presented, moreover, no discussion or maximizing took place at cruise-type conditions. Lissaman and O'Pray[16] developed a semi-inverse technique to design optimum slats for a given airfoil. They did not discuss drag morslat orientation with respect to reported results. In 1974, Smith,[17] in the Wright Brothers Lecture, gave an extensive discussion of high-lift aerodynamics. He discussed slats, flaps, and multielements all with respect to high lift. He proved that a two-element airfoil can produce more lift than a single-element airfoil. However, he did not consider the drag benefits or penalties of multielement airfoil systems. Moreover, he did not consider typical cruise conditions and the lift-to-drag ratio at these conditions.

In 1980, Rokhsaz,[18] also using analytical methods, determined that dual-airfoil systems could reduce two-dimensional drag by 13-20% over an equivalent single-airfoil system. In addition, he discussed the mechanisms which caused this phenomenon.

The current study is intended first to find the dual-wing and SFSR wing which attains the greatest performance improvements over a single wing, using two state-of-the-art airfoil sections, the MS(1)-0313[19] and the laminar NL(S)-0715F,[20] which has recently been given the official NASA designation of NLF-0215F. The second phase of this study involves the design and performance comparison of several single-wing "baseline" aircraft and of corresponding dual-wing and SFSR-wing aircraft to determine the advantages and disadvantages of these dual-wing aircraft designs. All dual-wing studies will consider only dual wings of equal chord length.

Dual-Airfoil, Two-Dimensional Tradeoff Studies

A detailed parametric study was conducted to analytically determine the combination of stagger, gap, and decalage which resulted in the greatest improvement in the wing lift-to-drag ratio, L/D, in terms of both two-dimensional viscous drag and three-dimensional induced drag results. For small staggers the results of Rokhsaz[18] indicated that the most favorable configuration, on the basis of two-dimensional performance only, was a stagger of 1.0, a gap of 0.26, and a decalage of -6 deg for the NACA 63_2-215 airfoil. Using this placement of the airfoil system as the starting point for the two airfoils considered in this study [the MS(1)-0313 and the NL(S)-0715F], the parametric investigation was performed by holding the initial values of two of these parameters constant while changing the value of the third variable.

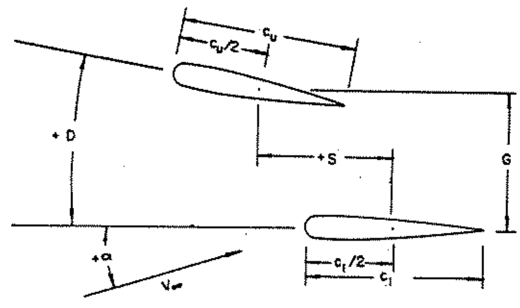

Fig. 1 Dual-airfoil geometric relationships.

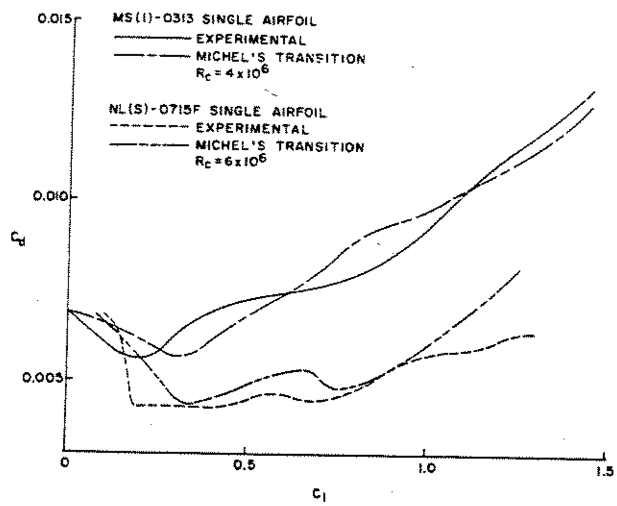

Fig. 2 Comparison of theoretical with experimental results.

The parametric study utilized an inviscid vortex panel multielement airfoil program[18] where the airfoils are represented by polygon approximations. Typical cases involved using 48 panels per airfoil. The inviscid multielement program was joined to a momentum integral boundary-layer analysis program to compute theoretical two-dimensional viscid and inviscid data. The laminar flow portion of the momentum integral program predicts the behavior of the boundary layer with Thwaites' method[21] and uses Michel's transition criterion[22] to determine the point of laminar-turbulent transition. The turbulent flow solution is then obtained by Head's momentum integral method[23] and the viscous drag is calculated with the Squire-Young formula.[24] This program set allows computation of complete multielement aerodynamic coupling, including thickness effects which become important at small gaps. Viscous drag predictions from the combined vortex panel viscous boundary-layer program were compared to experimental results[19,20] at the same Reynolds numbers to determine the degree of correlation between experimental and analytical results. Figure 2 compares the theoretical and experimental data for the MS(1)-0313 airfoil at a Reynolds number R_c of 4×10^6 and for the NL(S)-0715F at a Reynolds number of 6×10^6. This good agreement was achieved by using a Young's factor of 2.4 for the MS(1)-0313 and 2.2 for the NL(S)-0715F in the Squire-Young equation. Similarly good results were obtained at other Reynolds numbers for both airfoils.

Initial investigation of the performance of various dual-wing configurations covered a wide range of staggers to confirm the observations of previous dual-wing research.[5,6,18] Figures 3 and 4 present the findings of this investigation and a comparison with the single-wing data for the MS(1)-0313 airfoil. In Fig. 3, the negative-stagger runs (curves E through H) invariably exhibited flow separation at relatively low lift

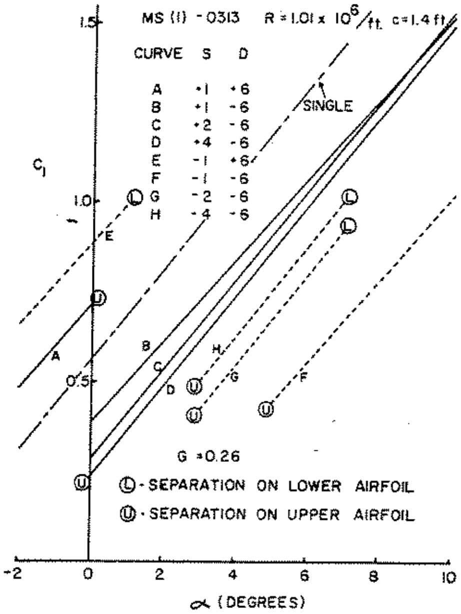

Fig. 3 Dual-wing two-dimensional lift curves.

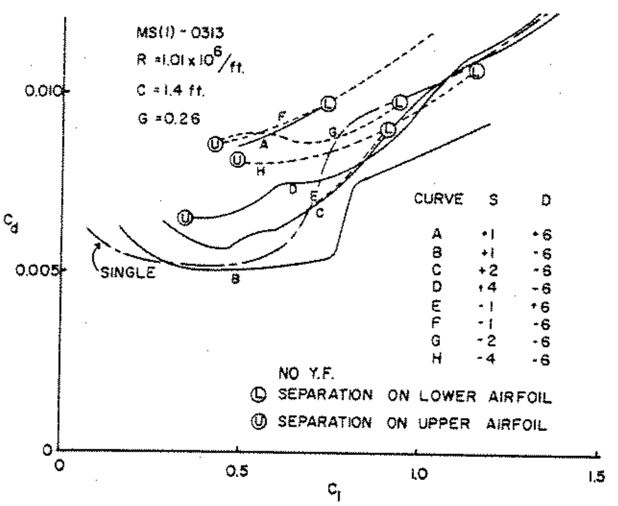

Fig. 4 Dual-wing two-dimensional drag polars.

coefficients, while the positive-stagger, negative-decalage cases (curves B through D) delayed the separation point to lift coefficients of 1.5 or greater. The positive-stagger, positive-decalage run (curve A) separated at a lift coefficient of less than 0.8, and produced an excessive amount of drag, as shown in Fig. 4. Likewise, the negative-stagger configurations created large amounts of drag in relation to the positive-stagger, negative-decalage cases. All of these findings supported the conclusions reached by Norton,[1] Nenadovitch,[5] and Olson and Selberg,[6] who determined that both the negative-stagger and the positive-decalage configurations performed poorly compared with the positive-stagger, negative-decalage condition. The NL(S)-0715F airfoil displayed similar behavior.

With the negative-stagger and positive-decalage cases rejected for their poor performance, the stagger, gap, and decalage angle changes were varied to find the optimum positive-stagger configuration.

Figure 5 shows the pressure distribution for two airfoil sections that are closely coupled; a stagger of 1.0, a gap of 0.26, and a decalage of −6 deg. For this case, the lower wing at a geometric angle of attack α of 1 deg obtained a lift coefficient C_l of 0.439, comparable to that of a single wing at a −1 deg angle of attack. The upper wing produced a lift

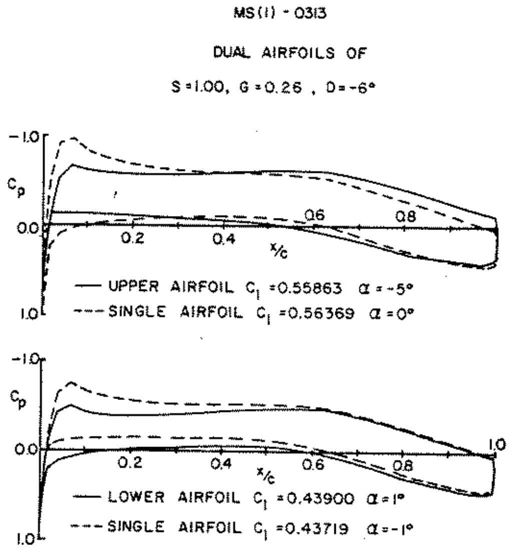

Fig. 5 Single- and dual-wing pressure distributions.

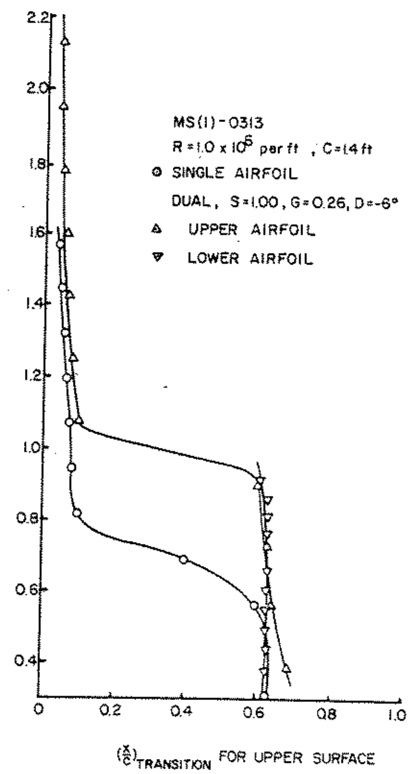

Fig. 6 MS(1)-0313 transition points.

coefficient of 0.559 at a geometric angle of attack of −5 deg, which is approximately equal to the lift on a single wing at a 0 deg angle of attack. Thus, the upper and lower wings receive a +5 and −2 deg induced angle of attack, respectively, indicating that the flow about each wing is significantly affected by the presence of the other wing. Figure 5 also illustrates the reduced leading-edge pressure peak and the reduced adverse pressure gradient experienced by the dual wings, both of which inhibit boundary-layer separation. Smith[17] refers to the dual-airfoil aerodynamic coupling in terms of five effects: slat effect, circulation effect, dumping effect, off-the-surface pressure recovery, and fresh boundary-layer effect. The "slat" effect reduces the pressure peak at the leading edge. The downstream airfoil causes the trailing edge of the upstream airfoil to be in a region of high velocity, thereby increasing the "circulation" on the forward airfoil. Since the

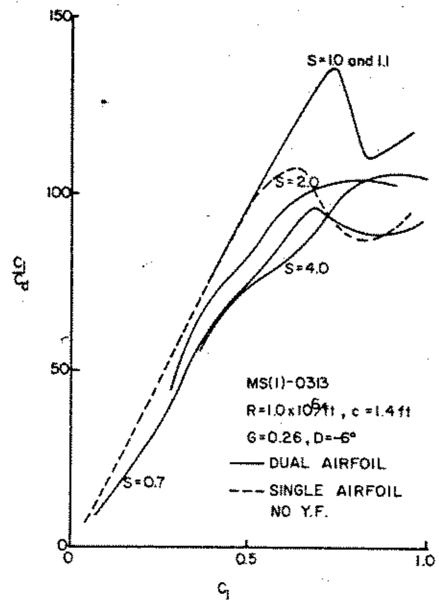

Fig. 7 MS(1)-0313 two-dimensional stagger study results.

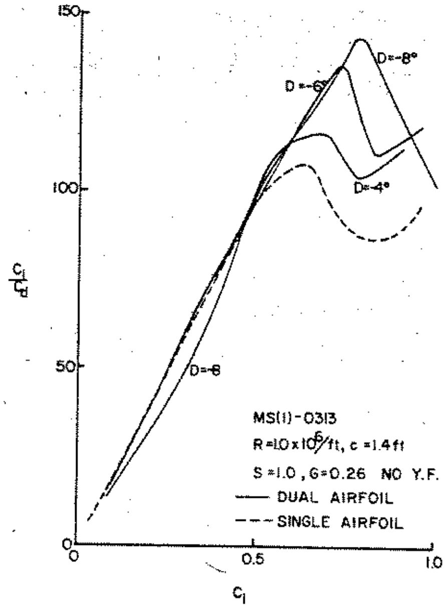

Fig. 9 MS(1)-0313 two-dimensional decalage study results.

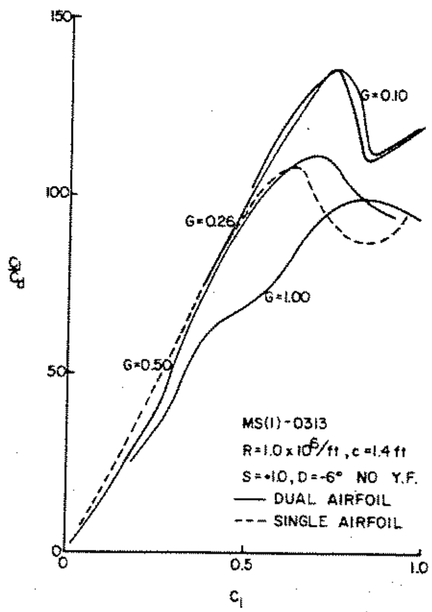

Fig. 8 MS(1)-0313 two-dimensional gap study results.

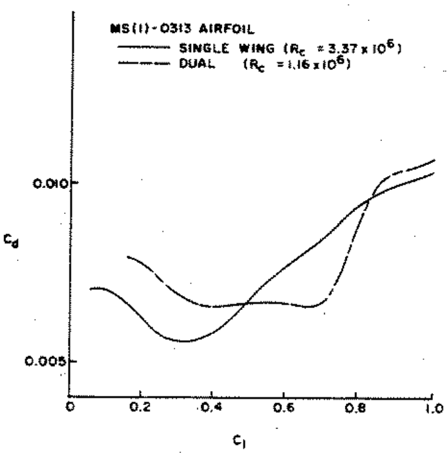

Fig. 10 Two-dimensional drag comparison.

trailing edge of the forward airfoil is in a region of high velocities the boundary layer "dumps" at a very high velocity. The boundary layer is dumped at velocities higher than freestream allowing the "off-surface pressure recovery." Finally each new airfoil starts with a "fresh new boundary layer."

Upper surface transition location for a stagger of 1.0, a gap of 0.26, and a decalage of −6 deg is shown in Fig. 6. The transition points for both the dual- and single-wing configurations were at about 60% and 10% chord for low- and high-lift coefficients, respectively. However, the shift from transition at 60% chord to transition at 10% chord occurred at lift coefficients of 0.6-0.8 for the single wing, as opposed to 0.9 to 1.1 for the dual-wing configuration. The essence of this behavior is that the dual wing benefits from a considerably longer period of laminar flow between lift coefficients of 0.6 and 1.1 and a corresponding decrease in viscous drag.

Results of the parametric study for the MS(1)-0313 airfoil are shown in Figs. 7-9. These figures illustrate relative comparisons at the same Reynolds number and do not contain the Young's factor correction. Figure 7 depicts the two-dimensional results of the constant-gap, constant-decalage, variable-stagger runs and, for comparison, the single-wing performance. A significant increase over the single-wing C_l/C_d curve was obtained with staggers of 1.0 and 1.1. Performance fell off as stagger was increased or decreased from this optimum stagger range.

The two-dimensional, variable-gap analysis is summarized in Fig. 8. With stagger and decalage held at 1.0 and −6 deg, respectively, the highest performance was obtained at gaps of 0.10 and 0.26. Lift-to-drag ratios dropped considerably as gap increased beyond 0.26. The 0.1 gap case was not used to avoid any flow blockage which might occur.

Figure 9 presents the data for the variable-decalage, two-dimensional runs. Overall, the best small stagger performance was obtained with a −6 deg decalage. An −8 deg decalage produced a higher maximum lift-to-drag ratio than did the −6 deg decalage case, but the latter held the performance edge at lift coefficients of 0.5 and below.

A typical dual-wing configuration would have a lower chord Reynolds number than the single wing. Figure 10 shows the two-dimensional drag of the dual and single airfoils. $S=1.0$, $G=0.26$, and $D=-6$ deg for the dual airfoils. The Reynolds number of the dual is 1.16×10^6, whereas the single is double the dual, or 3.37×10^6. The drag bucket has been

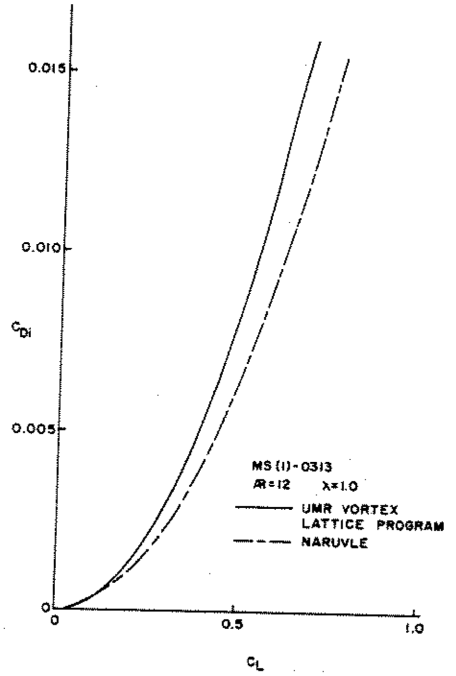

Fig. 11 Induced drag comparisons.

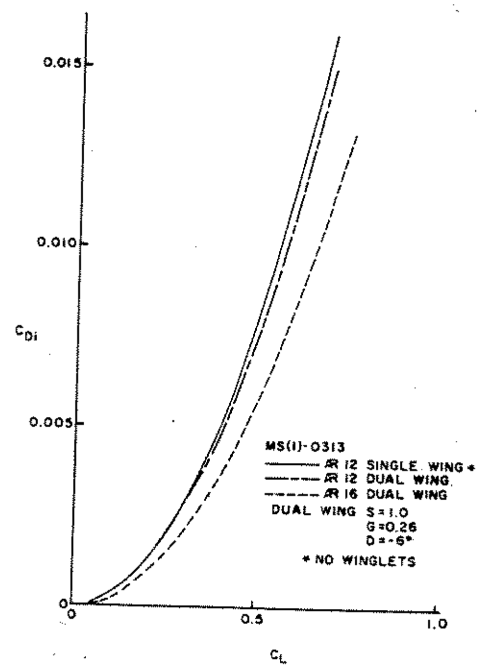

Fig. 13 Typical induced drag curves for the MS(1)-0313 airfoil.

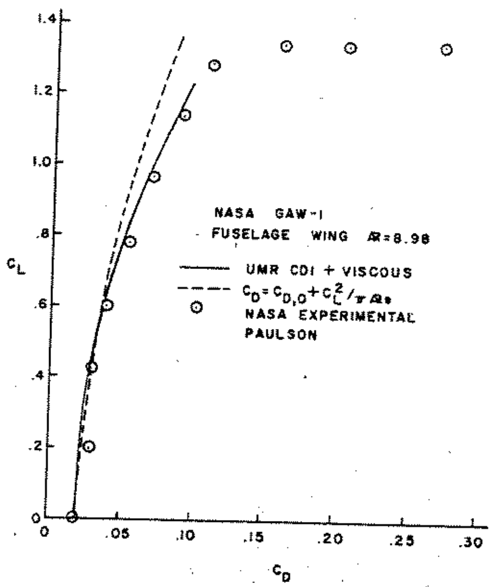

Fig. 12 Vortex-lattice program comparison.

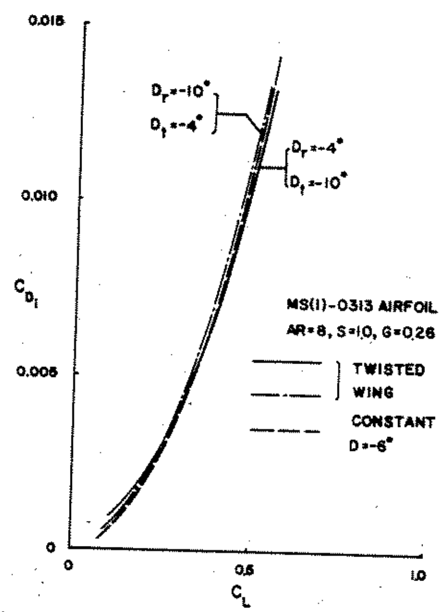

Fig. 14 Dual-airfoil twist effects on induced drag.

shifted to the right giving the dual airfoil lower drag at the higher lift coefficients.

This optimal dual-airfoil placement, $S=1.0$, $G=0.26$, and $D=-6$ deg was used for the SFSR configuration at the tip with the remainder of the wing geometry being varied to give the lowest total drag. Due to the sweep of the wings on the SFSR configurations it was necessary to determine if spanwise contamination was significant, hence negating the two-dimensional boundary-layer results. Calculation of Re based on momentum thickness which were made after Beasley[25] verified that spanwise contamination was not important for conditions under consideration.

Dual-Airfoil, Three-Dimensional Tradeoff Studies

The two-dimensional results indicated that the maximum l/d improvement for the dual airfoils occurred at a small gap, $G=0.26$. At this gap there is strong aerodynamic coupling and the differences in C_{l_0} predictions using vortex panel results which include thickness vs vortex-lattice results which ignore thickness is about 60%.[26] Since all the methods discussed earlier[8-10,12-14] did not account for thickness, and since the gaps are such that thickness is important, a vortex-lattice method, which utilized C_{l_α} and C_{l_0} data from the vortex panel program,[22] was used to predict induced drag. Figure 11 shows the results of this program compared to NARUVLE[28] a vortex-lattice program without a thickness correction. The University of Missouri-Rolla (UMR) vortex-lattice program predicts higher values of induced drag than NARUVLE. A comparison of the UMR vortex-lattice program with a wing fuselage NASA model $Æ=8.9$ after Paulson[29] is shown in Fig. 12. There is excellent agreement up to the beginning of boundary-layer separation.

Aspect ratio, taper, stagger, gap, decalage, and twist studies were conducted for the closely coupled dual wing configurations and the SFSR configuration. Figure 13 shows the effect of aspect ratio for the closely coupled dual wing as compared to the single wing illustrating the slight induced

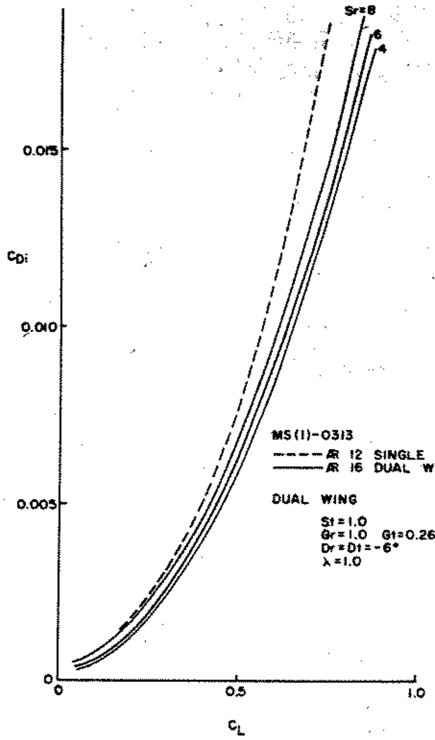

Fig. 15 Effects of stagger on induced drag for SFSR configuration.

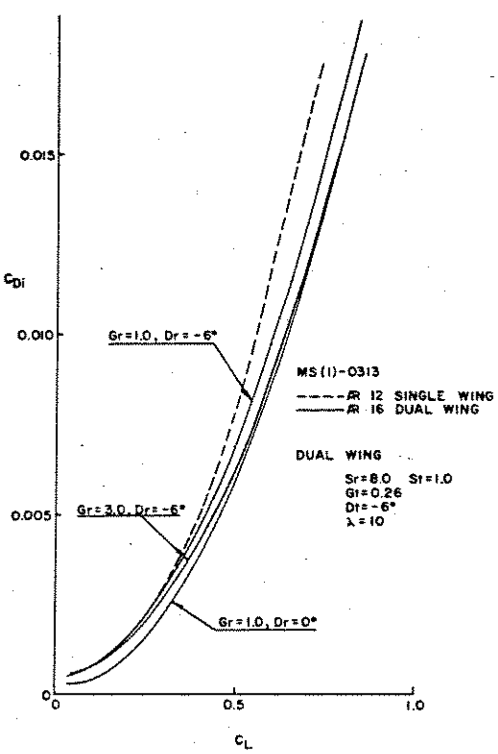

Fig. 16 Gap and decalage effects on induced drag for SFSR configuration.

drag advantage of the dual wing over a single wing of equivalent aspect ratio, i.e., a single airfoil with the same span, b, and area, S_{ref}, as the dual wing, and whose chord is equal to the sum of the two dual wing chords. The figure also indicates the significantly lower induced drag of the aspect ratio 16 wing compared to the wing of aspect ratio 12. Taper ratio studies were conducted for closely coupled dual wings, $S=1$, $G=0.26$, and $D=-6$ degrees. The results indicated minimum drag was obtained for taper ratios of 0.4 and 0.6. A taper ratio of 0.6 was used because it allowed a larger chord. Twist studies were also conducted. An example of these results is shown in Fig. 14 for the MS(1)-0313 airfoil. There is a slight reduction in induced drag for geometric washout and a slight increase for geometric washin. On the basis of the two-dimensional viscous drag and the three-dimensional induced drag results, the optimum closely coupled dual-wing configuration was determined to be a stagger of 1.0 and a gap of -6 deg with a taper ratio of 0.6.

Induced drag studies were also conducted for the SFSR configuration. Figure 15 shows the effect of stagger on induced drag for the SFSR configuration with the lowest stagger configurations having the least induced drag. Figure 16 shows the effects of gap and decalage variation with span for a fixed stagger at the wing root. The geometry at the tip was chosen to be that which gave the optimum improvements in the closely coupled two-dimensional study. As the figure illustrates, the best configuration has a gap of 1.0 at the wing root and a decalage of zero at the root.

The two-dimensional parametric study was also conducted with the NL(S)-0715F airfoil section. The same transition and lift-over-drag trends were found to occur except at much higher lift coefficients. The NL(S)-0715F dual-airfoil transition delay did not occur until lift coefficients greater than 1.0 were realized. This is because below lift coefficients of 1.0 most of the surface has laminar flow, hence, the coupling can not produce a significantly greater laminar run. Above lift coefficients of 1.0 most of the surface has laminar flow, hence, the coupling can not produce a significantly greater laminar run. Above lift coefficients of 1.0 the dual-airfoil improvements were again realized, although not to as great an extent. From the two-dimensional results for the NL(S)-0715F airfoil section the optimum configuration for the wing was a stagger of 1.0, a gap of 0.26, and a decalage angle of -6 deg. All induced drag trends followed those of the MS(1)-0313 airfoil section.

Design of the Baseline and Dual-Wing Configurations

The performance figures produced by this parametric study were used to design 12 aircraft: a six-place and a twelve-place "baseline" aircraft, a six-place and a twelve-place closely coupled dual-wing aircraft, and a six-place and a twelve-place SFSR aircraft. Each of these six configurations were evaluated with the MS(1)-0313 and the NL(S)-0715F airfoil sections, making a total of 12 designs. The two baseline aircraft were of conventional single-wing, aft-tail configuration and were used as reference points. The dual-wing aircraft and SFSR wing aircraft, which used the same fuselage, tail, and power plant as the corresponding baseline aircraft, were compared to these reference points to ascertain the merits of these dual-aircraft designs.

The 12 aircraft in this study were designed for a 563 km/h (350 mph) cruise speed at altitudes of 9,144-12,192 m (30,000-40,000 ft) and a range of 2414 km (1500 miles) or more. The baseline aircraft were limited to aspect ratios of 6-12 and wing loadings of 1197-2873 N/m^2 (25-60 psf). However, due to the structural advantages gained by connecting the two wings at their wing tips, the dual-wing designs were limited to aspect ratios of 16 or less, rather than 12, as was the case with the baseline aircraft. Aspect ratio was defined as the square of the wing span divided by the total projected area of the two wings. For each wing configuration, two separate aircraft designs were required, both a six- and twelve-place airplane. The six-place aircraft was designed for 5338 N (1200 lb) payload and was intended as a personal or small business airplane, while the twelve-place aircraft, with twice the payload of the six-place, was meant to compete in the business aircraft market. All of the aircraft in this study were designed with lifting surfaces made of composite materials.

The fuselage was sized first. The height and width of the six- and twelve-place fuselages were sized to present minimum frontal area, and thus create minimum drag, while providing interior volume for pilot, passengers, and luggage. The width of the twelve-place fuselage also was influenced by the requirement for a 30.5 cm (12 in.) aisle between the seats. The seat pitch, or the distance between adjacent rows of seats, was set at 91.4 cm (36 in.) for both versions. The passenger and luggage compartments for each version were then enclosed in a pressure vessel designed to provide a cabin pressure altitude of 2,438 m (8,000 ft) at an actual altitude of 12,192 m (40,000 ft). The rest of each fuselage was sized to provide space for the landing gear, power plant, avionics, and environmental control unit. No space was required for the fuel, since the fuel tanks were placed in the wings.

The six-place fuselage was built around a 132-cm (52-in.) high, 112-cm (44-in.) wide, 4.42-m (14.5-ft) long pressure cabin containing the six seats (in three rows of two seats each) and a luggage area aft of the last row of seats. The fuselage was designed for a conventional tricycle landing gear arrangement, with the nose gear housed below and forward of the pressure cabin and with the main gear located below and aft of the luggage compartment. The main gear retract aft into the fuselage. The gear arrangement exceeds the FAR overturning criteria. The single-turboprop engine was buried in the aftmost section of the fuselage tail cone. Air inlets for the engine were situated on either side of the fuselage and the propeller shaft was extended through the aft fuselage. The avionics and the environmental control unit were also housed in the fuselage aft of the pressure cabin.

The twelve-seat fuselage consisted of six rows of two seats and a baggage compartment aft of the last seat row. A 30.5 cm (12 in.) center aisle was also provided. The passenger and cargo areas were enclosed by a 163-cm (64-in.) high, 163-cm (64-in.) wide, and 7.37-m (24.2-ft) long pressure vessel. The tricycle gear were placed in approximately the same relative positions with respect to percentage of fuselage as were the landing gear for the six-place fuselage. The two turbofan engines were mounted on horizontal pylons attached to the aft fuselage. The avionics and environmental control units were placed in the aft fuselage. The dual-wing designs used the same fuselage as the baseline except for minor modifications, such as the addition of a fuselage fuel tank and minor rearrangement of internal systems. The wing fuel tanks of the dual wing were able to hold only about 50% of the required fuel.

The six-place aircraft used a scaled version of the Pratt and Whitney PT6-A45A turboprop engine[30] with a 2.29-m (90-in.)-diam four-bladed propeller. Specified fuel consumption was assumed to be a constant 0.344 kg/kW-h (0.55 lb/hp-h). The twelve-place aircraft used twin turbofan engines scaled from engines from a General Aviation Turbine Engine (GATE) study.[31] A 0.061 kg/N-h (0.6 lb/lb-h) thrust specific fuel consumption was assumed. The turboprop engine weight was scaled by the ratio of required power to production power, while the turbofan engine weight was scaled by the ratio of required thrust to reference engine thrust.

All aircraft were designed to utilize winglets to reduce the induced drag. A computer winglet study was conducted on a wing of aspect ratio 12 with taper ratios of 0.2-1.0, using the NARUVLE vortex-lattice program to compute the induced drag of the various configurations. Using a NASA winglet study[32] as a guide, the dihedral and incidence of the winglets were varied to find the configuration that provided the greatest reduction in induced drag. The optimum configuration agreed with Ref. 32 in terms of dihedral and incidence, although the magnitude of the predicted drag reduction was less. Because of the high degree of correlation between the current study and the NASA study, it was decided to use the standard NASA winglet design of Ref. 32. To be conservative, the drag reduction value obtained from NARUVLE was used, rather than that of Ref. 32. A taper ratio of 0.8 was chosen for the baseline.

For both dual-wing aircraft, because of the absence of information on the effectiveness of winglets on dual wings, it was conservatively assumed that the addition of winglets on dual wings would reduce the induced drag by approximately half the percentage of drag reduction achieved by winglets on a single wing. A taper ratio of 0.6 was found to create the least induced drag for the closely coupled dual-wing configuration, while a taper ratio of 1.0 gave the least induced drag for the SFSR configuration.

For the SFSR configuration all longitudinal control forces must be exerted by the wings, which implies a large stagger. Thus, the minimum root stagger which provided a $C_{m\delta_E}$ equal to the baseline was chosen. This occurred at $S_{root} = 8$. A gap of 3 was chosen to put the wings at the top and bottom of the fuselage.

Aircraft weight estimates were obtained with the aid of equations from Nicolai[33] and Torenbeek[34,35] and from a UMR design project,[36] a four-place, high-speed general aviation aircraft that utilized NASTRAN prediction methods.

Using equations from Nicolai with the UMR four-place design as a reference aircraft, the fuselage and empennage weights were determined for the six- and twelve-place aircraft under consideration. Nicolai's equations were used as scaling factors on the above reference weights. Wing weights were obtained for the six-place MS(1)-0313 configurations from NASTRAN-SEMOBEAM[37] computer optimization results. Wing weights for the six-place NL(S)-0715F configurations and all twelve-place configurations were obtained from a modification of Torenbeek's formula to account for the composite wings, and, for the dual-wing aircraft, Torenbeek's formula was calibrated using the six-place MS(1)-0313 configuration results. It was decided to structurally connect the dual wings only at the tip and the first bending moment location to minimize the added drag due to these structural connections. The NASTRAN-SEMOBEAM results demonstrated that the connection at the first bending moment location was not needed. With the structural connection only at the wing tip in the form of a structural winglet any additional drag would occur only at this location. This possible additional drag was accounted for by reducing the induced drag due to the structural winglets by one-half the winglet induced drag savings on the single wing. While lighter dual wings could have been designed using more structural connections, the uncertainty in the added strut drag would have overshadowed the structural savings. An ultimate load factor of 5.7, calculated from a 3.8 g load with a safety factor of 1.5, was used. Engine weight was obtained by scaling up the reference aircraft engine weight, using as a scaling the ratio of required thrust to the references aircraft required thrust. Miscellaneous weights were obtained with Nicolai's equations.

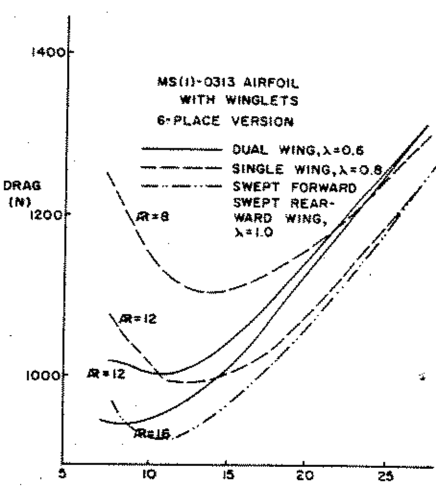

Fig. 17 Six-place aircraft, sample optimization curves.

Estimates of total aircraft drag coefficient were obtained by the component buildup method. The drag coefficients of each component, weighted by the ratio of the component area to the aircraft reference area, were totaled and multiplied by 1.1 to account for interference effects, as suggested in Ref.35.

The drag of the lifting surfaces, the wing and horizontal tail, was predicted with the programs described above. For each cruise lift coefficients being investigated, the viscous drag at the proper Reynolds number and the induced drag at the desired aspect ratio, taper ratio, and sweep angle were added to get a total wing drag coefficient. A factor of 0.0005, or 5-10% of the zero-lift drag coefficient for the airfoils under consideration, was added to this wing drag coefficient to account for interference.

Graphs and equations for turbulent flow about streamlined bodies from Roskam,[38] Hoerner,[39] and Crawford[40] were used to estimate the drag contributions of essentially nonlifting components. These drag coefficients, separately weighted by the ratio of component reference area to the aircraft reference area, were then added to get the total drag coefficient due to nonlifting components. To account for interference drag, this drag coefficient was increased by 10%.

The wing area was then optimized. A computer code would scan through a range of wing areas to find the area which created the least cruise drag. For each wing area in the desired range, the program computed the total aircraft cruise weight W_{cr} assuming constant engine weight, which determined the cruise lift coefficient. The program then searched through the two- and three-dimensional drag polars to find the viscous and induced drag coefficients of the wing at the desired lift coefficient for the specified conditions; namely, cruise Reynolds number and aspect ratio. Engine weight was then recalculated based on required cruise power before the final drag minimization which was the criteria by which the program selected the optimum wing area. All aircraft were optimized for cruise performance only with no attempt to take into account takeoff, climb, or landing performance. However, all aircraft were designed and checked to assure takeoff rotation.

Figure 17 shows a sample of the results of the optimization program for the six-place aircraft with wings of MS(1)-0313 section and aspect ratios of 8 and 12 for the single wing and aspect ratios of 12 and 16 for the dual and SFSR configurations. Over a wing area range of 7-28 m^2 (75-301 ft^2), the minimum cruise drag for the single-wing aircraft was obtained at an area of 12.9 m^2 (140.0 ft^2) for the case of $\mathcal{R} = 12$. For the closely coupled dual-wing aircraft the minimum drag was obtained at an area of 7.7 m^2 (84.0 ft^2) for the case of $\mathcal{R} = 16$. The SFSR wing aircraft obtained a minimum drag at an area of 10.5 m^2 (114.8 ft^2) for the case of $\mathcal{R} = 16$.

On the basis of the results of the optimization program, a cruise altitude of 12,192 m (40,000 ft) was selected to be the best cruise altitude. Since the study was limited to aspect ratios of 12 or less for the single wing, the $\mathcal{R} = 12$ case was chosen. For the closely coupled dual wing and the SFSR wing with their enhanced wing structural capability due to the wing connections an aspect ratio of 16 was selected.

After the optimum wing areas were determined, a final sizing of the horizontal and vertical tails was required to provide longitudinal, lateral, and directional stability. With the center of gravity placed at its most unfavorable position, the horizontal and vertical tail areas were varied until each aircraft was statically stable. The degree of static stability attained was comparable to that found in typical light and business aircraft. The static stability analysis was performed using the techniques of Roskam.[41,42]

Once the horizontal tail size was known, the trimmed performance of each aircraft was estimated. The required tail lift coefficient for zero pitching moment in cruise was computed, and this tail lift coefficient was used to find the tail drag coefficient at the trimmed condition, using the momentum integral boundary-layer and vortex-lattice programs described previously. This additional trim drag was calculated and the untrimmed data obtained from the optimization program was modified accordingly. Drag penalties due to train were less than 3% of the total drag.

Table 1 gives the final results for the six-place, single- and dual-wing aircraft. For both airfoil sections, Table 1 gives the cruise weight, wing weight, engine weight, drag, power, and lift coefficients at trimmed cruise conditions. Also shown is the lift-to-drag ratio in cruise wing area and range for each aircraft.

The lift-to-drag ratios achieved by these baseline aircraft were markedly higher than most contemporary light and business aircraft. Holmes and Croom[30] indicate that current technology six-place aircraft have maximum lift-to-drag ratios of about 14 at 556 km/h (300 knots) cruise speeds. The baseline six-place aircraft in the current study attained cruise lift-to-drag ratios of more than 19 at 563 km/h (350 mph), or 36% improvement. This greatly improved performance can be attributed to the superior airfoil sections used on the baseline aircraft as well as to the higher aspect ratios found on the aircraft of this study. The dual-wing and SFSR six-place aircraft both attained cruise lift-to-drag ratios of more than 20 at 563 km/h, which is a 48% improvement. The addition of winglets to these aircraft also contributed to their superior performance.

Figure 18 shows the exterior projected view of the finished six-place baseline, dual-wing, and SFSR aircraft.

Table 2 gives the final modified trimmed results of the single-, dual-, and SFSR design process for the twelve-place aircraft. Again, the dual-wing and SFSR wing configurations outperform the single wing for both airfoil sections.

For both the six- and twelve-place aircraft the dual-wing configurations with their higher L/D ratios are operating

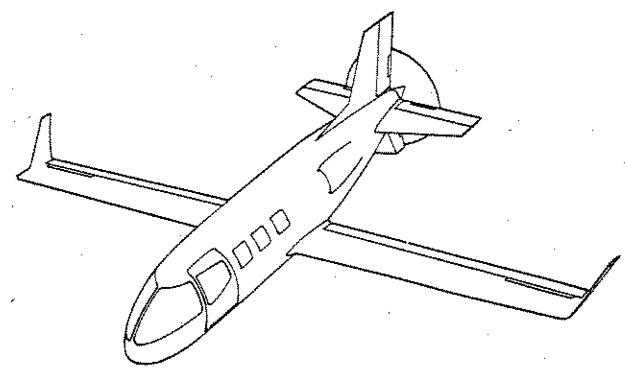

Fig. 18a Baseline-exterior view.

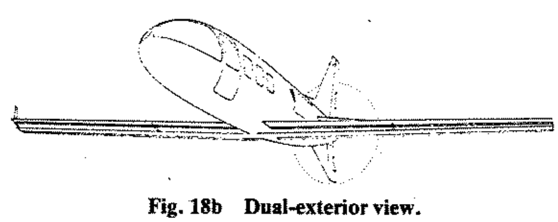

Fig. 18b Dual-exterior view.

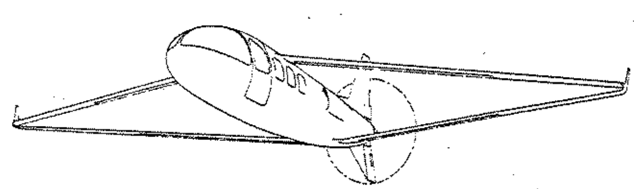

Fig. 18c Swept forward/swept rearward-exterior view.

Table 1 Design performance—Minimum Cruise Drag (trimmed six-place with winglets)

	W_{cr}, N (lb)	W_{eng}, N (lb)	W_{wing}, N(lb)	$C_{L_{cr}}$	D_{cr}, N (lb)	P_{req}, kw (hp)	$\frac{\Delta P_{req}}{P_{req}}$, %	$\left(\frac{L}{D}\right)_{cr}$	S_{ref}, m^2 (ft^2)	$\left(\frac{W}{S}\right)_{wing}$, N/m^2(lbf/ft^2)	R, km (miles)	$\frac{\Delta R}{R}$, %
						MS(1)-0313						
Single-wing[a] baseline	19,673 4,423	3,483 (783)	1,806 (406)	0.41	1,018 (229)	159 (213)		19.28	12.9 (140.0)	1,534 (31.6)	2,757 (1,713)	
Dual wing[a]	18,241 (4,271)	3,260 (733)	1,419 (319)	0.66	943 (212)	148 (198)	−7.3	20.13	7.7 (84.0)	2,461 (50.8)	2,981 (1,852)	8.1
SFSR[a]	18,827 (4,339)	3,154 (709)	1,503 (338)	0.49	908 (204)	142 (190)	−10.8	21.23	10.5 (114.8)	1,831 (37.8)	3,095 (1,923)	12.3
NL(S)-0715F												
Single-wing[b] Baseline	19,091 (4,292)	3,363 (756)	1,383 (311)	0.42	974 (219)	152 (204)	−4.2	19.66	11.2 (121.6)	1,710 (35.3)	2,899 (1,801)	5.4
Dual wing[b]	18,628 (4,316)	3,260 (733)	1,548 (348)	0.55	943 (212)	148 (198)	−7.0	20.39	9.2 (100.2)	2,093 (43.2)	2,983 (1,853)	8.2
SFSR[b]	17,140 (4,140)	3,047 (685)	1,245 (280)	0.63	872 (196)	136 (182)	−14.5	21.32	7.9 (86.0)	2,355 (48.6)	3,231 (2,007)	17.2

[a]NASTRAN weights. [b]Scaled NASTRAN weights.

Table 2 Design performance—Minimum Cruise Drag (trimmed twelve-place with winglets)

	W_{cr}, N (lb)	W_{eng}, N (lb)	W_{wing}, N(lb)	$C_{L_{cr}}$	D_{cr}, N (lb)	P_{req}, kw (hp)	$\frac{\Delta P_{req}}{P_{req}}$, %	$\left(\frac{L}{D}\right)_{cr}$	S_{ref}, m^2 (ft^2)	$\left(\frac{W}{S}\right)_{wing}$, N/m^2(lbf/ft^2)	R, km (miles)	$\frac{\Delta R}{R}$, %
						MS(1)-0313						
Single-wing[a] baseline	33,809 (7,601)	3,856 (867)	2,953 (664)	0.46	1,797 (404)	281 (376)		18.79	19.7 (214.0)	1,720 (35.5)	2,971 (1,846)	
Dual wing[a]	33,671 (7,570)	3,607 (811)	3,065 (689)	0.57	1,761 (369)	256 (343)	−8.8	20.45	15.8 (171.8)	2,137 (44.1)	3,250 (2,019)	9.4
SFSR[a]	32,941 (7,406)	3,572 (803)	2,904 (653)	0.48	1,601 (360)	250 (335)	−10.9	21.71	19.0 (207.0)	1,735 (35.8)	3,467 (2,154)	16.7
NL(S)-0715F												
Single-wing[b] Baseline	33,458 (7,522)	3,736 (840)	2,722 (612)	0.46	1,788 (402)	279 (374)	−0.5	18.71	19.5 (212.0)	1,720 (35.5)	2,989 (1,857)	0.5
Dual wing[b]	33,778 (7,594)	8,589 (807)	3,189 (717)	0.49	1,619 (364)	253 (339)	−9.8	20.83	18.4 (200.6)	1,836 (37.9)	3,306 (2,054)	11.3
SFSR[b]	32,453 (7,296)	3,483 (783)	2,504 (563)	0.60	1,503 (338)	235 (315)	−16.2	21.65	14.5 (158.2)	2,233 (46.1)	3,565 (2,215)	20.0

[a]NASTRAN weights. [b]Scaled NASTRAN weights.

Table 3 Design performance—constant wing loading (trimmed six-place with winglets)

	W_{cr}, N (lb)	W_{eng}, N (lb)	W_{wing}, N(lb)	$C_{L_{cr}}$	D_{cr}, N (lb)	P_{req}, kw (hp)	$\frac{\Delta P_{req}}{P_{req}}$, %	$\left(\frac{L}{D}\right)_{cr}$	S_{ref}, m^2 (ft^2)	$\left(\frac{W}{S}\right)_{wing}$, N/m^2 (lbf/ft^2)	R, km (miles)	$\frac{\Delta R}{R}$, %
						MS(1)-0313						
Single-wing[a] baseline	19,949 (4,485)	3,683 (828)	1,623 (365)	0.54	1,081 (243)	169 (226)		18.81	10.1 (109.6)	1,982 (40.9)	2,654 (1,649)	
Dual wing[a]	19,513 (4,387)	3,309 (744)	1,552 (349)	0.54	956 (215)	149 (200)	−11.5	20.09	9.5 (103.7)	2,049 (42.3)	2,897 (1,800)	9.2
SFSR[a]	18,948 (4,260)	3,136 (705)	1,437 (323)	0.54	898 (202)	140 (188)	−16.8	20.81	9.3 (101.0)	2,044 (42.2)	3,092 (1,921)	16.5
NL(S)-0715F												
Single-wing[a] Baseline	19,665 (4,421)	3,416 (768)	1,592 (358)	0.54	992 (223)	154 (207)	−8.4	19.59	9.7 (105.2)	2,035 (42.0)	2,802 (1,741)	5.6
Dual wing[a]	19,487 (4,381)	3,269 (735)	1,561 (351)	0.54	943 (212)	147 (197)	−12.8	20.40	9.6 (104.0)	2,040 (42.1)	2,946 (1,830)	11.0
SFSR[a]	18,566 (4,174)	3,109 (699)	1,334 (300)	0.54	890 (200)	139 (186)	−17.7	21.02	9.3 (100.8)	2,006 (41.4)	3,187 (1,980)	20.0

[a]NASTRAN weights.

Table 4 Design performance—constant wing loading (trimmed twelve-place with winglets)

	W_{cr}, N (lb)	W_{eng}, N (lb)	W_{wing}, N(lb)	$C_{L_{cr}}$	D_{cr}, N (lb)	P_{req}, kw (hp)	$\frac{\Delta P_{req}}{P_{req}}$, %	$\left(\frac{L}{D}\right)_{cr}$	S_{ref}, m^2 (ft^2)	$\left(\frac{W}{S}\right)_{wing}$, N/m^2 (lbf/ft^2)	R, km (miles)	$\frac{\Delta R}{R}$, %
						MS(1)-0313						
Single-wing[a] baseline	33,516 (7,535)	3,754 (844)	2,762 (621)	0.51	1,806 (406)	282 (378)		18.63	17.7 (192.2)	1,899 (39.2)	2,967 (1,843)	
Dual wing[a]	33,698 (7,576)	3,612 (812)	3,087 (694)	0.51	1,646 (370)	257 (344)	−9.0	20.46	17.4 (189.0)	1,943 (40.1)	3,282 (2,039)	10.6
SFSR[a]	32,826 (7,380)	3,527 (793)	2,833 (637)	0.51	1,552 (349)	243 (325)	−14.2	21.03	17.2 (186.8)	1,914 (39.5)	3,427 (2,129)	15.5
NL(S)-0715F												
Single-wing[a] Baseline	33,333 (7,494)	3,745 (842)	2,589 (582)	0.51	1,797 (404)	281 (376)	−0.5	18.58	17.5 (190.4)	1,909 (39.4)	2,988 (1,856)	0.7
Dual wing[a]	33,742 (7,586)	3,594 (808)	3,149 (708)	0.51	1,623 (365)	254 (340)	−10.0	20.82	17.8 (193.3)	1,899 (39.2)	3,297 (2,048)	11.1
SFSR[a]	32,666 (7,344)	3,501 (787)	2,700 (607)	0.51	1,521 (342)	237 (318)	−15.9	21.54	17.2 (187.3)	1,899 (39.2)	3,519 (2,186)	18.6

[a]Scaled NASTRAN weights.

closer to their maximum L/D ratios. The wing loadings for these dual-wing aircraft under these conditions are also higher. This could cause stall speed problems relative to the single-wing aircraft. Although only cruise conditions were analyzed herein, Smith[17] has shown that two-element airfoils can achieve higher maximum lift coefficients than a single-element airfoil which will alleviate the problem.

The performance of these aircraft also can be compared at constant wing loading. Tables 3 and 4 present the performance results at constant wing loading. Wing loadings between the optimum single- and dual-wing cases were chosen for comparison.

Design Comparison and Recommendations

Comparing Tables 1 and 2, one notices the lower cruise drag of the dual- and SFSR-wing configurations. The drag of the closely coupled dual-wing cases was lower than that of the baseline aircraft by 7.3-8.8% for the MS(1)-0313 airfoil and 7-9.8% for the NL(S)-0715F airfoil. In terms of range, this means that for the same fuel, the closely coupled dual-wing aircraft achieved 9.4-12.3% more range than the baseline aircraft with the MS(1)-0313 airfoil and up to 8.2-11.3% more range with the NL(S)-0715F airfoil. The drag of the SFSR-wing configuration was 10.8-10.9% lower than that of the baseline aircraft for the MS(1)-0313 airfoil and 14.5-16.2% lower for the NL(S)-0715F airfoil. The range of the SFSR aircraft was 9.4-12.3% greater than the baseline for the MS(1)-0313 airfoil and 17.2-20.0% greater for the NL(S)-0715F airfoil.

The difference in optimum cruise lift coefficient is also outstanding. The optimum cruise lift coefficients for the baseline aircraft ranged between 0.41 and 0.46, while the dual- and SFSR-wing designs optimized at much higher lift coefficients, from 0.48 to 0.66, with correspondingly lower wing areas. Both dual-wing configurations are operating closer to their respective L/D maxima. The dual- and SFSR-wing aircraft also have lower engine weights than the baseline, which translates into lower engine acquisition costs. The wing weights of the dual-wing configurations that employed NASTRAN-SEMOBEAM weight predictions were also lower than their baseline configurations.

Comparing Tables 3 and 4, where essentially constant wing loading is maintained, the same basic trends occur for the dual and SFSR configurations; lower cruise drag and greater ranges. The actual magnitudes are also very close.

Some potential problems were noted with the dual-wing designs. The wing volume available for fuel was insufficient, requiring the fuel to be carried aft of the pressurized cabin. The possibility also exists that the dual-wing configuration have aeroelastic problems not experienced by the conventional single-wing configuration.

In outperforming the baseline aircraft, the dual designs had to overcome some disadvantages. The greatest disadvantage was the increase in drag coefficient as Reynolods number decreased. Since the wing chords of the dual aircraft were half that of the single-wing aircraft, the dual designs were penalized by higher drag coefficients due to the reduced Reynolds number. This disadvantage would be reduced or eliminated by using an airfoil section designed for very low Reynolds numbers, (from about 10^6 to 2×10^6). The two airfoil sections investigated in this study were designed for Reynolds numbers of $6\text{-}9\times10^6$, and suffer from a degradation of performance at lower Reynolds number.

A second disadvantage was the conservative structural approach taken in designing the dual wings. The utilization of more bracing could offer an optimized aerodynamic-structural configuration.

Third, to be conservative, the winglets on the dual-wing aircraft were given only half of the induced drag reduction achieved by the single-wing winglets. This last disadvantage may be removed by extensive research on winglet designs for the dual-wing configuration, as has been done for single-wing configurations in the past.

Also, no effort was made to reduce the fuselage weight of the dual-wing configurations due to the multiple attachment points and hence lower stress levels.

In spite of these conservative estimates used in the design process, the baseline aircraft designs offer a significant improvement in cruise performance as compared to current technology aircaft. The dual-wing designs, aside from all of their disadvantages, offer still higher cruise performance, and a corresponding decrease in fuel consumption. With further research into the multiwing aircraft system, such as static and dynamic structural testing, low Reynolds number airfoil design, specifically for dual-wing applications and dual-wing winglet research, the dual-wing aircraft should prove to be even more attractive.

Acknowledgments

The results presented in this paper were obtained from research funded by NASA Research Grant NAG1-26 administered by Langley Research Center under the direction of Dr. Bruce Holmes.

References

[1] Norton, F.H., "Effect of Staggering a Biplane," NACA TN-710, 1918.

[2] Knight, M. and Noyes, R.W., "Wing Tunnel Test on a Series of Biplane Wing Models, Part I. Effects of Changes in Stagger and Gap," NACA TN-310, 1929.

[3] Knight, M. and Noyes, R.W., "Wind Tunnel Tests on a Series of Biplane Wing Models, Part II. Effects of Changes in Decalage, Dihedral, Sweepback, and Overhand," NACA TN-325 1929.

[4] Knight, M. and Noyes, R.W., "Wind Tunnel Tests on a Series of Biplane Wing Models, Part III. Effects of Changes in Various Combinations of Stagger, Gap, and Decalage," NACA TN-330, 1929.

[5] Nenadovitch, M., "Recherches sur les Cellules Biplane Rigides d'Envergure Infine" Publications Scientifiques et Techniques du Minister de L'Air, Institut Aero'-technique de Saint-Cyr, Paris, 1936.

[6] Olson, E.C. and Selberg, B.P., "Experimental Determination of Improved Aerodynamic Characteristics Utilizing Biplane Wing Configurations," *Journal of Aircraft*, Vol. 13, April 1976, pp. 256-261.

[7] Wolkovitch, J., "Subsonic V/STOL Configurations with Tandem Wings," *Journal of Aircraft*, Vol. 16, Sept. 1979, pp. 605-611.

[8] Munk, M.M., "General Biplane Theory," NACA 151, 1921.

[9] Prandtl, L., "Induced Drag of Multiplanes," NACA TN-182, March 1924.

[10] Prandtl, L. and Tietjens, O.G., *Applied Hydro- and Aeromechanics*, Dover Publications, Inc., New York, 1957, pp. 213-216.

[11] Addoms, R.B. and Spaid, F.W., "Aerodynamic Design of High Performance Biplane Wings," McDonnell-Douglas Corporation Report, McDonnell-Douglas Corporation, St. Louis, Mo., 1975.

[12] Laitone, E.V., "Prandtl's Biplane Theory Applied to Canard and Tandem Aircraft," *Journal of Aircraft*, Vol. 17, April 1980, pp. 233-237.

[13] Kroo, I.M., "Minimum Induced Drag of Canard Configurations," *Journal of Aircraft*, Vol. 19, Sept. 1982, pp. 792-794.

[14] Butler, G.F., "Effect of Downwash on the Induced Drag of Canard-Wing Combinations," AIAA Paper 72-221, 1972.

[15] Liebeck, R.H., "Theoretical Studies on the Aerodynamics of Slat Airfoil Combinations," AIAA Paper 72-221, 1972.

[16] Lissaman, P.B.S. and O'Pray, J.E., "Slat Design by a Semi-Inverse Technique," AIAA Paper 71-11, 1971.

[17] Smith, A.M.O., "High Lift Aerodynamics-37th Wright Brothers Lecture," 13th AIAA Aerospace Sciences Meeting, Pasadena, Calif., 1975.

[18] Rokhsaz, K., "Analytical Investigation of the Aerodynamic Characteristics of Dual Wing Systems," Thesis, University of Missouri, Rolla, Mo., 1980.

[19] McGhee, R.J., "Wind Tunnel Results for a 13-Percent-Thick Medium Speed Airfoil Section," (NASA TM in publication).

[20] Sommers, D.M., "Design and Experimental Results for a Flapped Natural-Laminar-Flow Airfoil for General Aviation Applications," NASA TR-1865, June 1981.

[21] Thwaites, B., "Approximate Calculation of the Laminar Boundary Layer," Aeronautical Quarterly, Vol. 1, pp. 245-280, 1949.

[22] Michel, R., "Etude de la Transition sur les Profiles d' Aile; Establissement d'un Critere de Determination de Point de Transition

et Calcul de la Trainee de Profile Incompressible," ONERA Rept. 1/1578A, 1951.

[23]Cebeci, T. and Bradshaw, P., *Momentum Transfer in Boundary Layers*, Hemisphere Publishing Corp., Washington, 1977, pp. 192-194.

[24]Cebeci, T. and Smith, A.M.O., "Calculation of Profile Drag of Airfoils at Low Mach Numbers," *Journal of Aircraft*, Vol. 5, Nov.-Dec. 1968, pp. 535-542.

[25]Beasley, J.A., "Calculation of the Laminar Boundary Layer and Prediction of Transition on a Sheared Wing," R.A.E. Rept. 3787, Oct. 1973.

[26]Rokhsaz, K. and Selberg, B.P., "Disadvantages of Thin Airfoil Formulations for Closely Coupled Airfoils," *Journal of Aircraft*, Vol. 20, June 1983, pp. 574-576.

[27]Rokhsaz, K., Internal correspondence, University of Missouri, 1981.

[28]Tulinius, J., "Unified Subsonic, Transonic, and Supersonic NAR Vortex Lattice," North American Rockwell, Los Angeles, Calif., TFD-72-523, 1972.

[29]Paulson, J.W., "Application of Vortex Lattice Theory to Preliminary Aerodynamic Design," NASA TN-D-8236 1976.

[30]Holmes, B.J. and Croom, C.C., "Aerodynamic Design Data for a Cruise-Matched High Performance Single Engine Airplane," SAE Paper 810625, 1981.

[31]Benstein, E.H. and Smith, R., "Advanced General Aviation Turbine Engine (GATE) Study," NASA CR-159624, 1979.

[32]Whitcomb, R.T., "A Design Approach and Selected Wind-Tunnel Results at High Subsonic Speeds for Wing-Tip Mounted Winglets," NASA TN D-8260, 1976.

[33]Nicolai, L.M., *Fundamentals of Aircraft Design*, METS, Inc., San Jose, Calif., 1975, pp. 5.1-5.24 and 20.1-20.24.

[34]Torenbeek, E., *Synthesis of Subsonic Airplane Design*, Delft University Press, Delft, Holland, 1976, pp. 27-76, 263-302, 352.

[35]Torenbeek, E., "Prediction of Wing Group Weight for Preliminary Design," *Aircraft Engineering*, Vol. 43, July 1971, pp. 17-21.

[36]Hayes, B., Lopez, R., and Rhodes, M., "General Aviation Light Turbo-Powered Aircraft," Senior Design Project, University of Missouri, Rolla, 1980.

[37]Somnay, R.J., "Design of Dual Wing Structures," Thesis, University of Missouri, Rolla, Mo., 1983.

[38]Roskam, J., *Methods for Estimating Drag Polars of Subsonic Airplanes*, published by the author, Lawrence, Kan., 1971, p. 2.3.

[39]Hoerner, S.F., *Fluid Dynamic Drag*, published by the author, 1965, pp. 6.15-6.19.

[40]Crawford, D.R., *A Practical Guide to Airplane Performance and Design*, 1st Ed., Crawford Aviation, Torrance, Calif., 1979, p. 174.

[41]Roskam, J., *Methods for Estimating Stability and Control Derivatives of Conventional Subsonic Airplanes*, published by the author, Lawrence, Kan., 1971, pp. 2.1-12.2.

[42]Roskam, J., *Airplane Flight Dynamics and Automatic Flight Controls, Part I*, Roskam Aviation and Engineering Corp., Lawrence, Kansas, 1979, pp. 243-377.

2001-01-3031

High Performance Executive Transport Design Employing Twin Oblique Lifting Surfaces

Askin T. Isikveren
Department of Aeronautics
Royal Institute of Technology (KTH)

ABSTRACT

This paper presents a new Trans-Atlantic high performance executive transport suitability equipped to offer accommodation for 19 first class passengers. The unique feature of this conceptual design is application of Twin Oblique Lifting Surfaces or TOLS configuration. Minimum goals for the design included: similar maximum takeoff gross weight; satisfactory field performance; good stalling characteristics; and, competitive fuel burn qualities at high-transonic and low-supersonic speeds, i.e. M0.90-1.20, compared to contemporary M0.75-0.85 large and super-large business jets. The vehicle is to be powered by two medium by-pass derivative engines based on the BMW-Rolls Royce BR715 in an effort to maximize the likelihood of availability, ensure adequate en route performance efficiency and fulfillment of yet to be ratified Stage 4 noise compliance requirements.

INTRODUCTION

The oblique wing concept has fallen in and out of favour over the latter half of the Twentieth Century. It gathered notoriety with Vogt's variable sweep oblique wing aircraft design proposal in the 1940s designated as the Blohm and Voss P202[1]. This unconventionally asymmetric aircraft design was one of the first concerted attempts to reconcile conflicting conditions of wing sweep optimality for low and high speed performance of an aerospace vehicle. Around the same period, Campbell and Drake[2] at NACA conducted experimentation on similar layouts. It was subsequently championed by Jones[3,4] who found interest in such a configuration because analysis and windtunnel testing indicated that elliptical oblique wings would provide minimum wave drag in supersonic flow.

Notwithstanding the potential offered by oblique wings, there exists a distinct absence of such aircraft in both the military and civilian operational arenas. From a programme perspective, it is potentially a large risk venture. Historically, difficulties have included the following: problems with low-speed aeroelastic divergence associated with a high aspect ratio, forward swept semi-wing; in the absence of a mature automatic control systems technology knowledge-base, the adequate handling of longitudinal and lateral motion coupling produced by the interaction of highly non-linear aerodynamic and inertial moments; lack of rigid body and wing structural mode coupling; the drawback of having an obligatory wing pivot mechanism; and, the sense it is a highly exotic configuration.

Alternative configurations that challenge the traditional cantilevered single wing have also been examined. As a follow on from experimentation done by Olson and Selberg[5], studies by Rhodes and Selberg[6] showed that both closely coupled dual-wing and swept forward swept rearward (connected at the wingtip) systems exhibit aerodynamic advantages over single wing configurations. They found the low drag of multi-surfaces were due to a combination of two and three dimensional drag reductions, tailoring the three dimensional drag for the swept forward swept rearward design, and improved structural efficiency through connection thus permitting higher aspect ratios.

Another example of unconventional planform design is the strut-braced wing (SBW) and origins of this concept can be traced back to Pfenninger's research of a long-range transonic transport truss-braced wing study[7] done in the mid-1950s. Proponents of SBWs cite as a result of favourable interaction between structures, aerodynamics and propulsion, potential for higher aerodynamic efficiency and lower Maximum Takeoff Weight (MTOW) can be realised. Encouraging results from design studies of the 2010 SBW transonic transport completed by Virginia Polytechnic (Gundlach et al[8]) show a potential to shave up to 10% of MTOW defined by design mission requirements.

In view of the significant potential for performance enhancement and with due regard given to the difficulties discussed above, a new hybrid concept is proposed here which comprises two independent, fixed, oblique (or skewed) wings linked by a wing-pylon-engine bracing structural system (WPEBS). This configuration, coined as Twin Oblique Lifting Surfaces or TOLS (Figure 1), is intended to produce a new aircraft design perspective that will afford acceptable en route efficiency at high-transonic and low-supersonic speeds with an unconventional operational flexibility of satisfactory field performance and stalling characteristics.

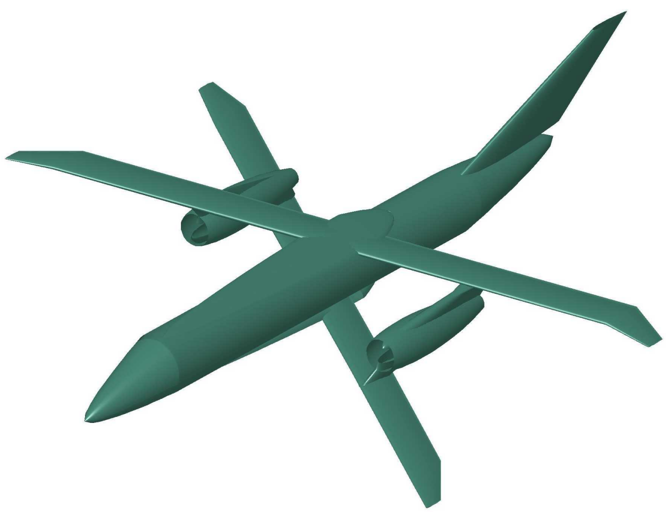

Figure 1. Introducing the TOLS configuration.

Even though commercial aviation and the charter industry provide transportation at more competitive rates for the upper echelon of customers, they have proven to be both inefficient and unreliable. Due to a growing dissatisfaction with commercial airliner services, there are strong indications demand will shift towards business aviation. There are some newly emerging business and corporate aviation concepts to improve affordability and quality of contemporary air travel. Today, prospective customers can choose from five distinct methods of owning or chartering business jets:

- Traditional ownership – outright ownership and complete responsibility for operation;
- New and used fractional ownership – allotment of time based on a given fractional ownership of a new or used business jet;
- Branded charter – privately owned fleet of similarly outfitted business jets offering chartered service;
- "By-the-seat" charter – chartered seats sold in scope similar to commercial operators; and,
- Business airline charter – regularly scheduled flights using business jets between city pairs deemed profitable.

Traditional business jet ownership is the most dependable means of travel, but comes at an appreciable expense. As a result, the charter services and fractional ownership have demonstrated to be schemes attracting the majority of commercial aviation customers as well as enticing clientele who would normally not purchase business jets to consider fractional ownership. In view of the great potential of growth, a new conceptual aircraft design targeting this market niche is taken to be a potentially lucrative venture.

UNIQUE CONCEPTUAL DESIGN PREDICTION INFERENCES FOR THE TOLS CONFIGUATION

Almost all conceptual design synthesis methods rely on empirical or handbook methods based on datasets of similar aircraft. In effect, the analysis methods assume a level of weights, aerodynamics and performance within the bounds of the aircraft survey dataset. With regards to the unconventional nature associated with TOLS configurations, a series of unique conceptual design prediction algorithms must be formulated in order to ensure consistent account of weight and aerodynamics, and to establish minimum goals with confidence. The main considerations that ideally would be reviewed for study of this unique configuration are addressed below.

WING WEIGHT RELIEF – With respect to SBWs, Gundlach et al[8] reason the vertical force of the strut produces a shear force discontinuity along the wing span creating a break in the bending moment slope, thus reducing the magnitude of bending moment inboard of the strut. Also, the strut vertical offset generates a favourable moment that creates a spanwise bending moment curve discontinuity further alleviating the bending moment inboard of the strut. For SBWs, this condition translates into a significant rationalisation of weight and thus allows for thinner wing sections promoting a decrease in zero-lift and transonic wave drag. It also gives scope to decrease vortex-induced drag via an increase in wing aspect ratio; combining to yield an improved aerodynamic efficiency.

Even though TOLS configurations employ dual-wing planforms skewed in opposite sense to each other, a legitimate parallel to SBWs and the associative benefits therein can be drawn. The WPEBS system which links individual oblique lifting surfaces is akin to the bracing effect produced by an offset strut – in this context, the offset strut height being equivalent to each of the four engine pylon heights.

INTERFERENCE DRAG DUE TO WING-ENGINE-PYLON BRACING SYSTEM – To quantify the interference drag between the wings and WPEBS intersections, a combination of form factors[9] and a wing-strut interference drag model developed using Computational Fluid Dynamics (CFD) techniques by Tetrault (reproduced in the 2010 SBW transonic transport study by Gundlach et al[8]) was employed. Tetrault shows the wing-strut interference drag (ΔC_{Dint}) model is best described utilising a hyperbolic fit to the CFD results because interference drag was found to vary inversely with arch radius (or offset strut height), viz.

$$\Delta C_{D\,int} = \frac{18}{h_{os}} \tag{1}$$

where h_{os} is the offset strut height in feet, and, ΔC_{Dint} is expressed in drag counts.

For the final TOLS configuration selected in this study, a total increment of drag due to dual-wings, WPEBS and empennage interference effects was predicted to be 40 drag counts, or, typically 10% of the total en route drag. This contrasts as proportionately 2-3 times greater constituent contribution compared to contemporary subsonic transport aircraft.

MULTIPLANE VORTEX-INDUCED DRAG – The shortcoming of contemporary reference wing definition conventions (ESDU, Boeing Wimpress, Airbus Gross and Net) is an inadequacy to appropriately and consistently represent multi-surface wing designs. These methods are only suited to the single cantilevered wing premise, thus producing a geometric to aerodynamic qualities disconnect. One objective was to derive an expression that quantifies the TOLS equivalent reference wing aspect ratio (AR_E) with consistency so that the vortex-induced drag factor to be used for ensuing calculations can be based directly on the geometric attributes of an equivalent single reference wing.

To address this requirement, a starting point is Prandtl's "two-surface" vortex-induced drag equation as presented by Kendall[10]. Prandtl indicates that, "The total [induced] drag (of a multi-surface) consists of the sum of all the separate drag and of as many mutual drags as there are combinations of the wings in twos". For speeds greater than M0.40 and with no account of compressibility effects, the elliptically loaded two-surface vortex-induced drag factor equation can be related to an analytical expression derived by Obert[11]:

$$\frac{dC_D}{dC_L^2} = \frac{1}{\pi S_W}\left[\frac{S_1^2}{b_1^2} + 2\sigma\frac{S_1 S_2}{b_1 b_2} + \frac{S_2^2}{b_2^2}\right] \equiv \frac{\alpha}{\pi AR_E} + \beta \tag{2}$$

where Prandtl's mutual drag factor σ accounts for gap effect as presented by Kerber and can be found in Durand[12], S and b are the constituent area and span respectively for wings 1 (lower) and 2 (upper), S_W is the reference wing area, and, α and β are coefficients of proportionality equal to 1.05 and 0.0070 respectively as derived by Obert.

To round off, Munk's stagger theorem states no change in the vortex-induced drag will occur due to longitudinal location as long as the surface loads remain unchanged. This means Prandtl's mutual drag factor may be applied to any multi-surface configuration without any consideration given to the longitudinal location of the semi-wing surfaces relative to each other.

DESIGN SPECIFICATIONS

A business jet aeroplane design must concurrently fulfil a number of requirements as dictated by today's discerning clientele: a premium on passenger comfort, a high degree of operational readiness and exceptional performance characteristics. High passenger comfort levels are paramount since the cabin living volume can act as an executive office or conference room. Also, a business jet is viewed as an aid to saving time and increasing productivity, and so, dispatch-reliability should be maintained at very high levels. Superior performance attributes afford a great deal of operational flexibility. The ability of operating in and out of relatively short airfields, of expediently climbing to cruising altitudes above inclement weather or avoiding congested airways altogether, and cruising at significantly faster speeds than conventional aircraft at comparable en route efficiencies would all combine to produce a vehicle with unmatched appeal.

In view of the mission role discussed above, the hard specifications that were deemed necessary for the success of this proposal are defined below.

- The vehicle must accommodate at least 19 passengers seated with a 1.40 m (55 in.) pitch;
- Takeoff field length less than 1830 m (6000 ft) at ISA, sea level conditions;
- Effective operation at 5000 ft (1524 m) airport pressure altitude and at ISA+20°C conditions;
- Initial cruise altitude of at least FL 470;
- Time to climb to typical bandwidth of cruise flight levels in around 15-25 minutes;
- Service ceiling not less than FL 510 and High-Speed Cruise (HSC) Mach number not less than 1.20;
- Maximum range not less than 4000 nm (7408 km) at Typical Speed Cruise (TSC) of M0.95, and, 3500 nm (6482 km; this represents a westbound Trans-Atlantic flight between LHR and JFK with 85% probability winds) at Maximum Cruise (MCRZ) assuming NBAA IFR mission rules and reserves, and, a maximum passenger complement;
- Landing reference speed to be not greater than 135 KCAS at Maximum Landing Weight (MLW) and ISA, sea level conditions;

- A competitive en route Specific Air Range (SAR) efficiency at TSC compared to similarly sized contemporary large and super-large business jets;
- Low parts count and relatively simple construction, avoidance of complex double curvature in fuselage geometry;
- Should fit into existing Air Traffic Control (ATC) patterns, and noise levels should comply to current version of yet to be ratified Chapter 4 definition;
- The vehicle shall be certified according to FAR 25 and JAR 25 transport category aircraft requirements.

In addition to these, a soft specification was set to provide for a suitable cargo hold, i.e. a target total volume of 0.28 m^3 (10 cu.ft) per passenger.

DESIGN PREAMBLE

FUSELAGE DESIGN – The design cycle began by establishing the fuselage size in isolation. The height, width and resulting fineness basically catered to providing ample volume in accommodating the necessary 1.40 m (55 in.) seat pitch for passengers. Ancillary attention was paid to minimizing frontal area as well as producing a lower $Volume^2/Length^4$ (or volume-reference length ratio) for minimum zero-lift and wave drag respectively. The width of the fuselage was also influenced by the requirement of allowing at least 610 mm (24 in.) of aisle width between passenger seats. Finally, consideration was also given to ensure space for landing gear, avionics, supporting systems and fuel was sufficient. The geometric layout of the fuselage was loosely based on the 50 PAX Saab 2000 high-speed turboprop[13]. Apart from catering to a higher pressure differential, the cylindrical cabin has mostly been retained, however, extensive modifications have been introduced to the forward fuselage to meet the requirements imposed by operating in the high transonic and low supersonic speed regime.

ENGINE SIZING AND SELECTION – Even though this design study involves a hypothetical or "paper" engine using methods conceived by the author[14] and investigations made by Svoboda[15], the results derived from initial analysis were used to propose a plausible engine the market could conceivably design and manufacture. As expected, the engine optimisation process focused on the cruise condition for sizing. Preliminary investigations showed a suitable engine should meet the following criteria:

- Target maximum static thrust of 71.2 kN (16000 lb.f) at sea level standard conditions;
- Cruise By-Pass Ratio (BPR) of around 3.0 to reduce the thrust lapse rate at given speed and altitude;
- Overall Pressure Ratio (OPR) of at least 30 to keep the overall engine efficiency as high as possible;
- Relatively high engine Turbine Entry Temperature (TET) to maintain required specific thrust characteristics.

The BMW Rolls-Royce BR715 is identified as an ideal candidate for future derivative development work. With the current configuration of 1 fan, 2 boosters, 10 compressors, 2 low pressure turbines and 3 high-pressure turbines, the basic layout can be retained but the requirement of an en route design BPR decrease from 4.8 to 3.0 will have with it an associative reduction in fan diameter from 1.53 m (60 in.) to approximately 1.25 m (49 in.). This has a beneficial effect of reducing the engine empty weight by almost 454 kg (1000 lb). The design point Thrust Specific Fuel Consumption (TSFC) degrades somewhat from 0.63 at M0.76 and 35000 ft to approximately 0.73 at 45000 ft and M0.95.

Operation at low supersonic speeds will reduce the possibility of maintaining an exceptionally high pressure recovery. Nonetheless, the axisymmetric intake was found to be satisfactory for speeds slower than M1.50. Providing due consideration is given to applying sharper lip geometry, the single normal shock wave of a pitot intake would yield only about a 2% reduction compared to the two-dimensional shock intake as cited by Whitford[16]. Also, this design ensures efficient structural shape for low duct weight and minimum wetted area for given stream-tube flow area.

EMPENNAGE SIZING – With variation of wing geometry and placement, associated changes to the empennage were made accordingly. Approximate dimensioning was based on the inequality constraint of keeping the vertical tail volume coefficient greater than or equal to 0.090.

AEROFOIL AND PLANFORM GEOMETRY – The selection of aerofoil section thickness and general wing design characteristics were based on studies presented by Kroo[17]. Numerical optimisation techniques have shown that a wing thickness (t/c) of up to 14.0% is acceptable for oblique wing design proposals. Indeed, van der Velden and Torenbeek[18] have taken this notion further by employing a higher t/c of 15.0% for their supersonic oblique wing transport design. With respect to planform geometry design, taper ratio and wing twist needs to be selected such that unbalanced lift loads are avoided. This circumstance fortuitously gives scope to approximate the elliptical load distribution ideal as well.

DESIGN PREDICTION

SYNTHESIS CODE – To perform the required parametric calculations, the QCARD-MMI software package developed by Royal Institute of Technology (KTH) Department of Aeronautics was utilised. QCARD-MMI, or Quick Conceptual Aircraft Research and Development Version 2001, is a MATLAB based computer program and embodies the quasi-analytical conceptual design prediction methods developed by the author[14]. The system places an emphasis on assisting the user to interactively draft, predict and optimise coherently during the conceptual aircraft design generation process.

A variety of known regional aircraft were input and QCARD-MMI predictive powers were inspected against each respective vehicle's manufacturer Performance Engineers' Handbook (PEH) or its equivalent. Indications have shown very good agreement against published results[9] with typical errors frequently falling within a bandwidth of ±5% for weight; engine performance - TSFC and thrust lapse; aerodynamics - total drag for All Engines Operational (AEO) and One Engine Inoperative (OEI) at low and high speed, maximum lift for clean wing and for given flap setting; and, operational performance - takeoff including minimum control speed limitations and initial climb, en route climbing, cruise, complete mission and landing. Additionally, QCARD-MMI methodology was benchmarked against the General Aviation Synthesis Program (GASP) developed by NASA-Ames Research Centre[19]. To ascertain consistency of the high-speed aerodynamics and engine thrust-burn modules, QCARD-MMI was tested on a supersonic design completed by van der Velden and Torenbeek[18] and was found to be in good agreement in the high transonic and low supersonic regime. The only significant discrepancy was observed in the friction drag component with a conservative prediction of +24%.

The points to follow outline the prediction algorithm methodology for a select array of core disciplines analysed by QCARD-MMI.

Drag – Drag calculations are partitioned into three distinct groups, namely, friction, vortex-induced and wave. Friction drag that is independent of lift is predicted using the component build-up method at a representative Mach number and altitude (generally Long Range Cruise [LRC] and optimum altitude) and subsequently used to derive an equivalent characteristic length for off-reference conditions. This approach is coined Equivalent Characteristic Length Method (ECLM) and a full treatment can be found in the author's previous work[9]. This component also accounts for interference, 3-dimensional effects, roughness and excrescences using the conventional form factor approach. The vortex-induced drag is calculated using an analytical expression derived by Obert[11], which approximates vortex-induced drag factors computed for a wide variety of commercial transport aircraft. Wave drag accounts for the presence of significant compressibility effects. The Critical Mach number (M_{CR}) is approximated with the Korn equation[20] modified to include simple sweep theory with adjustments made using empirical data given by Obert[11]. The total wave drag is estimated using the zero-lift and lift related components (representing geometric difference) from the total drag equation for supersonic cruise drag given by Jones[21]. Using this as a basis, an exponential drag rise and divergence model originating from Torenbeek's[22] proposed algebraic structure is dynamically constructed employing empirical guidelines for drag divergence properties presented by Raymer[23].

Maximum Lift – The clean wing maximum lift is computed for any original planform geometric definition using a MATLAB module developed by KTH called TORNADO[24]. The TORNADO software with a 3-dimensional Vortex-Lattice Method (VLM) calculates aerodynamic properties of multi-wing designs that are swept (symmetric or otherwise skewed), tapered, cambered, twisted and cranked with dihedral. Unlike the classical VLM approaches, TORNADO models the wake coming off the trailing edge of every lifting surface as flexible and changing shape according to the flight state considered. With a distorting wake, non-linear effects such as the interaction of multiple surfaces can be simulated more consistently.

Since the primary assumption of any VLM is linearity, the prediction of maximum lift coefficient (C_{Lmax}) is taken from empirical data describing the relative increment of C_L with change in angle of attack between the beginning of lift non-linearity and C_{Lmax}. Even though thickness effects are neglected, the slope of the mean camber surface is accommodated. Camber data is sourced from a comprehensive aerofoil library compiled for another MATLAB based program developed by KTH called PABLO[25] (low-speed aerofoil analysis using one-way coupled inviscid and boundary layer model). High-lift produced by flap and slat deflection is estimated based on methods presented by Young[26]. This reference uses empirical correlation from assorted accumulated data and predicts with adequate accuracy the aerodynamic characteristics of high lift devices.

Propulsion – An engine model taken from previous work done by the author[14], based on the premise of exponential decay and proportional to variation of flight level and speed was expected to generate an adequate description of thrust lapse and TSFC variation. For accuracy, two distinct models describing takeoff-climb, and, maximum cruise thrust characteristics are employed. Linear performance deterioration models to account for effects of off-ISA temperature deviations are also considered. Since these expressions do not permit direct sensitivities to more pertinent working parameters like BPR and OPR, a new hybrid model was developed to include this aspect using research compiled by Svoboda[15].

Weight – Aircraft constituent weight estimates of wings, vertical tail, fuselage, landing gear, avionics, electrical, hydraulic, environmental control system (ECS), anti-icing, auxiliary power unit (APU) and other equipment on board were obtained with the aid of methods developed by Linnell[27], Scott and Nguyen[28] and the author[14]. Formulae to account for weight relief due to presence of fixed masses on the wing (to be discussed in the Optimisation section) were also introduced into the MTOW transcendental algorithm. Owing to the absence of a consistent conceptual prediction method, wing weight estimation for this study did not include account of the TOLS configuration structural efficiency due to WPEBS inter-wing connection. This produced a prediction almost 8% greater than that of a single wing with the same area, aspect ratio and strength.

Estimates for engine weight, and, complement of pylons and nacelles were obtained using methods detailed by the author[14]. A completion allowance of 2170 kg (4785 lb) was predicted from estimated interiors for contemporary large and super-large business jets. This figure did not intentionally include a crew rest area (saving almost 400 kg; 880 lb) as standard since it was assumed almost all missions would be completed within an 8-hour duty cycle.

Weight of fuel is estimated using a quasi-analytical procedure developed by the author. The integral wing and centre tanks are described by a series of truncated pyramid geometries with adjustments made to reconcile an over-estimated volume compared to the more elliptical face of aerofoil sections. Elliptic paraboloids more accurately describe volume encased by the forward fuselage fairing and saddle tanks. The aft fuselage auxiliary tank is simply predicted assuming a cylinder with segment cutout bounded by the circular cross-section and chord. All tank volume constituents were further reduced in volume to account for presence of structure based on recommendations made by Torenbeek[22].

<u>Performance Definitions</u> – A series of guidelines were adhered to when evaluating the operational performance attributes of each design candidate. Since the design engine sizing requirements for this exercise was understood to focus on en route cruise, it was surmised that both takeoff and climbing performance would still be acceptable even with a significant amount of engine de-rate for each of these two mission phases. The takeoff performance was defined using engine de-rate for normal takeoff thrust, with no facility for Automatic Power Reserve (APR), as a free variable. The selection of an appropriate de-rate level was based on one that yielded a minimum (twin engine) OEI second segment climb gradient of 2.4% at takeoff flaps of 30°, an airport pressure altitude of 5000 ft, ISA+20°C ambient conditions and MTOW at brakes release. A philosophically similar set of criteria were also employed for AEO en route climbing; in this instance, maximum climb thrust de-rate for the engines was determined by a vehicle candidate clearing FL 510 with residual climb rate of 300 fpm at the fastest forward speed technique assuming ISA still air and MTOW at brakes release.

The Optimum Trajectory-Profile Algorithm (OTPA) in QCARD-MMI utilises an interval halving numerical scheme with climb distance as the free variable for given flight level. The algorithm caters to a myriad of objective function evaluations, including unconstrained maximum SAR, constrained maximum SAR at given speed technique and unconstrained minimum time (maximum block speed) flight technique evaluation. For accuracy, a default of 5 segments is assumed for the entire mission profile. In this particular study, each of the numerically integrated en route mission computations was limited to a maximum of three cruise-steps to simulate actual operational procedures. As a margin for establishing the validity of en route cruise speed minimum goals, a residual of 100 fpm was imposed to identify the engine thrust limit. Even though consideration for altitude capability constrained by high-speed buffet (1.3g margin) is important, owing to the lack of a coherent conceptual method to determine this aspect, experience dictated that engine thrust limited altitude would be the most likeliest of constraints for the interim. Finally, all en route mission computations adhered to flight techniques, reserves and contingency policies stipulated by NBAA IFR guidelines including 200 nm alternate and 30 minutes hold.

DESIGN OPTIMISATION

A very limited scope of multivariate optimisation was undertaken in this study. The objective here was to ascertain in a relatively quick manner if the TOLS configuration exhibits feasibility. Many of design variables were systematically bounded for the global optimisation process after formulating the best objective function result for that given sub-space. For example, once initial estimates yielded an idea of the most likely engine candidate dimensions and weight, a generic trade study between engine lateral coordinate wing placement and aircraft empty weight was examined. To assist in this process, weight relief factors were drawn from semi-analytical methods of contemporary transport aircraft wing weight estimation done by Torenbeek[29].

CANDIDATE SELECTION – Various combinations of wing area, complementary wing skew angles, thickness and aspect ratio were analysed to determine an acceptable trade off between good field and en route performance. Each candidate MTOW design point was defined as one in which 19 PAX at 100 kg (220 lb) can be accommodated with maximum fuel load. A myriad of possible performance constraint criteria to inspect for sensitivity and subsequently identify feasible solutions were reviewed.

The hard specification takeoff field length (TOFL) constraint of 1830 m (6000 ft) was initially found to be a limiting condition. Further scrutiny revealed the engine inoperative decision speed (V_1) should be considered as a primary parameter because a combined effect of high wing loading and minimum control speed (V_{MC}) limitations produced reference speeds that became quite high. As an orthogonal delineation to the V_1 decision speed trade, two separate en route performance inequality constraints were examined: maximum PAX range at MCRZ speed technique, and, range with maximum payload assuming constrained maximum SAR technique at M0.95. The first choice, which proved to be the most limiting, of maximum range at MCRZ speed technique assuming a payload of 19 PAX at 100 kg (220 lb) each with NBAA IFR flight guidelines and reserves, 200 nm alternate and 30 minutes hold was finally designated as the primary en route constraint criterion. Consequently, the selection process focused on maximising range, and, minimising takeoff field length as well as lowering the V_1 takeoff safety speed.

In terms of final selection in this study, thrust-to-weight (T/W) and wing loading (W/S) needed to be maximised in order to rationalise the gross weight, thereby theoretically reducing the equipped price. This is explained by the presence of a fixed powerplant (hence thrust level) and the fact decreasing reference wing area allows less available space for fuel. In stark contrast, reference wing area and aspect ratio needed to be maximised (minimise W/S) in order to minimise takeoff and landing distances as well as the respective reference speeds. For given reference wing area, aspect ratio needed to be reduced to increase available fuel volume thence to maximise range performance. To reconcile these conflicting effects, the requirements were plotted on a series of charts that allowed definition of bounded geometric regions in which freedom of selection existed. An example of a simplified final T/W and W/S trade study for the high-performance executive transport is given in Figure 2. Note the final candidate for selection was subsequently given the designation of TOLS-X.

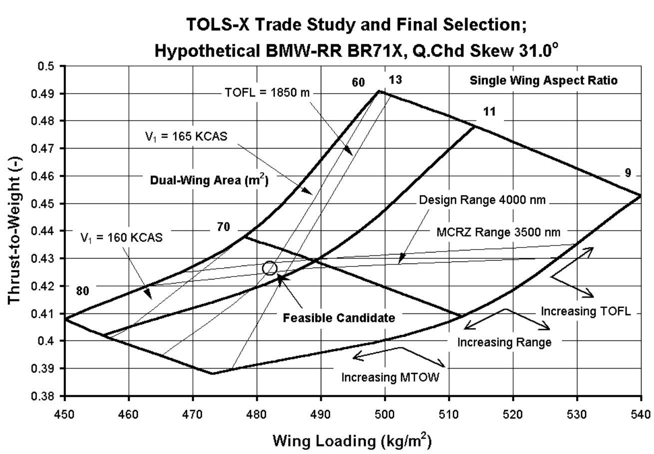

Figure 2. Simplified representation of final selection for TOLS-X design.

It can be discerned for an optimal wing skew of 31.0°, the T/W and W/S sensitivity study indicates that approximately 482 kg/m^2 (98.7 lb/sq.ft) and T/W of 0.426 are appropriate. This design candidate with MTOW equal to 34493 kg (76043 lb) and reference wing area of 71.6 m^2 (771 sq.ft) produces a vehicle which can operate out of runways less than 1830 m (6000 ft), and is capable of completing 3500 nm (6480 km) range at MCRZ speeds of up to M1.22.

AIRCRAFT DESIGN DESCRIPTION

OVERVIEW - The TOLS-X vehicle is a tricycle, employs dual-winged planforms with relative skew, and, twin turbofan using podded engine installations connected with pylons between the upper and lower skewed planforms. The vehicle is pressurised and incorporates only a vertical tail for empennage. The landing gear is retractable and each leg is twin wheeled. The vehicle accommodates a flight crew of two and an optional flight attendant. The standard configuration seats a maximum of 19 passengers. The powerplant is a medium BPR derivative of the BMW Rolls-Royce BR715 turbofan designated as BMW Rolls-Royce BR71X. It is projected the engines shall comply with the yet to be determined Chapter 4 noise levels. The vehicle shall be configured in a manner such that Extended Twin Operations (ETOPS) approval shall be granted with minimal modifications. The vehicle is designed to comply with FAR 25 U.S airworthiness regulations and the European JAR 25 rules. Table 1 supplies a synopsis of TOLS-X design weights, merit values and geometry data. Figure 3 (overleaf) shows a three view general arrangement of the TOLS-X high performance executive transport design.

Table 1. Design weights, merit values and geometry data for TOLS-X vehicle.

Weights		
Maximum Ramp Weight	34593 kg	76264 lb
Maximum Takeoff Weight	34493 kg	76043 lb
Maximum Landing Weight	31000 kg	68343 lb
Maximum Zero Fuel Weight	20660 kg	45547 lb
Basic Operating Weight	17968 kg	39612 lb
Maximum Payload	2693 kg	5937 lb
Maximum Usable Fuel	14729 kg	32472 lb
Merit Parameters		
Wing loading	482 kg/m^2	98.7 lb/sq.ft
Thrust-to-weight	0.426	
External Dimensions		
Overall span	20.5 m	67 ft 2 in.
Height	7.48 m	24 ft 7 in.
Overall length	29.6 m	97 ft 1 in.
Wheel base	14.2 m	46 ft 7 in.
Wheel track	2.74 m	9 ft
Fuselage Dimensions		
Length	27.3 m	89 ft 6 in.
External diameter	2.31 m	7 ft 7 in.
Wing Geometry		
Total reference area	71.6 m^2	771 sq.ft.
Reference wing aspect ratio	8.79	
Quarter chord skew	±31.0°	
Vertical Tail Geometry		
Area	15.0 m^2	162 sq.ft.

INTERIOR ARRANGEMENT – The pressurised vessel of the fuselage includes the cockpit, passenger cabin and baggage compartment. The cockpit accommodates a crew of two. Facility for one flight attendant is also to be available.

The standard layout of the cabin permits 19 passengers to be accommodated in sleeper-seats arranged 9 rows to

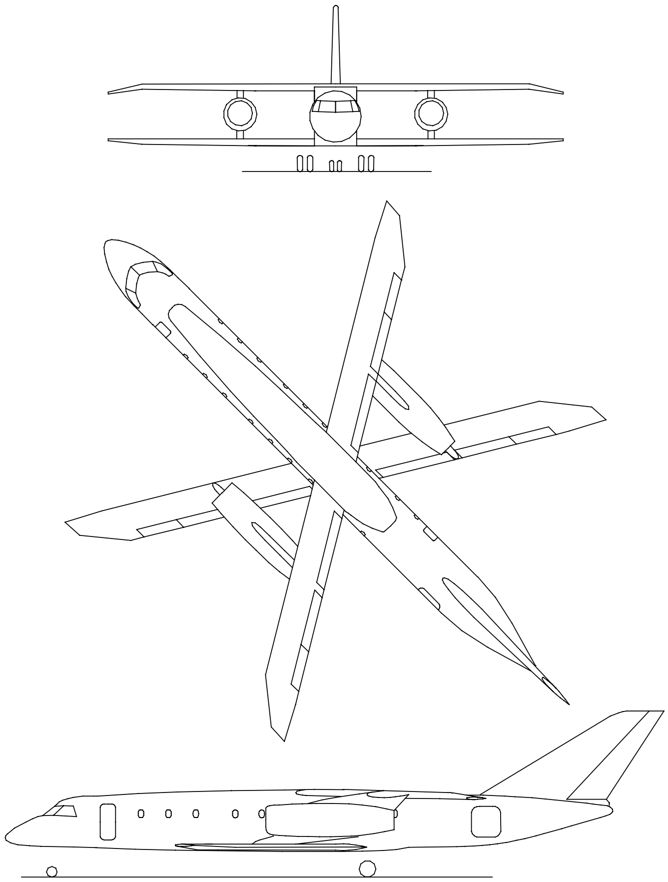

Figure 3. TOLS-X general arrangement.

port (left) and 10 rows to starboard (right) of the centre aisle with a seat pitch of 1.40 m (55 in.). Each seat extends out to 1.83 m (72 in.) when fully reclined and with the footrest deployed. Overhead baggage bins running the entire seating length of the passenger cabin are installed on the starboard side. Provision is also made for a forward stowage and closet compartment located starboard, and galley located aft of the cabin on the port side of the aisle. The toilet is located at the front of the cabin. The standard cabin allows no provision for a crew rest area since almost all TOLS-X missions will last less than 8 hours in duration. A baggage compartment with approximately 5.35 m^3 (189 cu.ft) of volume is located rear of the cabin. Figure 4 elucidates the interior arrangement of the cabin with 19 seats, toilet, stowage-wardrobe and galley.

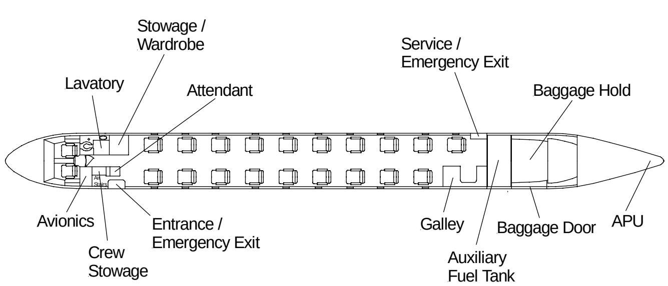

Figure 4. TOLS-X standard interior for 19 PAX.

The main door, 1.60 m x 0.69 m (63 in. x 27 in.) with sill height of 1.68 m (66 in.), is located on the port side of the fuselage front section to permit crew and passengers to have access to the cabin. An aft, starboard service door, 1.22 m x 0.61m (48 in. x 24 in.) permits unobstructed passage to the galley. Access to the baggage compartment is only from the port side of the rear fuselage section through an up-and-over baggage bay door with dimensions 1.32 m x 1.35 m (52 in. x 53 in.).

WING CHARACTERISTICS – The wing t/c variation of 15.0% at the root and 12.0% near the tip, complementary wing quarter chord skew of $\pm 31.0°$ and reference wing aspect ratio of 8.79 generates an optimal speed schedule which varies between M0.80-0.98 at altitudes above FL 410. Each skewed wing is separated by almost one fuselage diameter or non-dimensional gap (with respect to local wing chord) of 1.06, hence, based on results posted by Rhodes and Selberg[6], flow blockage effects are not surmised to be significant. The wing thickness distribution assists in housing more volume for fuel, and, promotes structural efficiency thus rationalising weight and increasing stiffness.

The wing profile is designed for high-speed natural laminar flow (HSNLF)[30], and tentatively chosen to be HSNLF-1-0213, with a t/c of approximately 14.8% at each semi-wing MAC spanwise locale. Built-in wing washout was designed to optimise the wing lift distribution for low-speed flight (to assist the control-configured system in promoting satisfactory stall progression) with consideration given to minimising penalties incurred to high-speed aerodynamic qualities. The semi-wings have no leading edge devices and high-lift is effected by two panels of simple plain flaps, or flaperons, that extend out to 65% of each wing semi-span. High-speed buffet and flutter problems are not envisaged at faster speed flight since the bow shock wave emanating from the forward fuselage does not coincide with the forward TOLS wingtips until approximately M1.26. To assist in minimising the detrimental effects in this regime, modifications are envisaged for the TOLS-X wing such that the leading edge becomes akin to (more rounded nose) super-critical wing sections.

CONTROL SURFACES – Longitudinal and lateral-roll control are produced by three distinct surfaces, namely, the upper and lower fixed skewed wings and the vertical tail. Each of the four semi-wings employ the use of three simple plain flaps tasked to act in the duplicitous role of flaperon. The wing mounted flaperon relative chord length is 25% of the local swept wing chord. The maximum deflection is set at 30° TEU (-) and 75° TED (+). Symmetric flaperon deflection provides pitch control; while asymmetric deflection of the flaperons coordinated with rudder-assist provides roll control authority through an aileron to rudder interconnect. It would be desirable to minimize out-of-trim rolling moments on each of the oblique wings - for this reason some amount of positive and negative dihedral for the upper and lower planforms respectively have been considered at the wingtips.

FLIGHT CONTROL SYSTEM – The design is to be control-configured with longitudinal, roll and lateral control accomplished via a full 6 degrees-of-freedom Stability Augmentation System (SAS). This approach will assist handling qualities and shall negate any questions on how the onboard pilot will react to an asymmetric highly coupled aircraft. Vehicular manoeuvring and trim is to be effected with differential combinations of aileron and flap deflection (flaperons). Each upper and lower semi-wing will have three segment flaperons. The common primary and secondary control surfaces located on the wings will be simply flapped arrangements thus reducing complexity with an added benefit of allowing for a cleaner wing free of flap fairings and blisters.

For each upper and lower wing planforms, application of a TOLS configuration avoids the problem of pronounced aerodynamic centre (a.c.) shifting since wing chords are not as large as conventional symmetric swept layouts. Also, due to the fact lift produced by each respective forward and aft semi-wing panel is countered in a complementary fashion, a collective a.c. locale forward of the aft-swept semi-wing panels is fortuitously established. For oblique wing aircraft, aerodynamic coupling of the pitch, roll and yaw axes produces a condition where trim in roll predominates with increasing angle of attack. This effect also has a tendency of influencing the pitching moment and the asymmetric lift is also responsible for a yawing effect as well. With TOLS configurations, a less pronounced result of simultaneous disturbances around pitch, roll and yaw is expected since the four semi-wing panels will collectively offset each other. It is emphasized that aerodynamic coupling due to the asymmetric layout of the upper and lower wing in side-view will still be an issue but is postulated to be at a more manageable (therefore at more easily solvable) level.

TOLS-X flight control is to be a triplex fly-by-wire with two digital modes (a primary and backup) and an analog mode. Trim for this configuration requires the equilibrium of six highly non-linear forces and moments. In view of the longitudinal and lateral motions being coupled, a good deal of research will need to take place on identifying optimal combinations of control surface deflection. One method is to decouple the dynamic modes so that handling quantities are similar to those of a conventional symmetric swept wing aircraft. With respect to oblique wing aircraft designs, Kroo[17] indicates that several approaches to address this control law definition problem are under investigation. One area of research suggested by Kroo is to compile data about the correlation of aerodynamic coupling to handling qualities and pilot ratings. In principle, the results and conclusions drawn from these studies would be relevant to aircraft employing TOLS configurations.

In an attempt to exploit benefits from control-configured vehicles, a possibility exists to reduce structural weight via manoeuvre load alleviation. For vehicles operating in the transonic speed regime and for those having high aspect ratio wings, this function reduces the wing root bending moment by re-orienting the spanwise lift distribution so that the magnitude of outboard loading is minimized. This effect is achieved by scheduling the flaperon deflections in a relative manner using advanced control laws. A technology factor to reflect benefits associated with manoeuvre load alleviation was not employed for this particular study.

EMPENNAGE – The empennage consists of a single surface vertical tail with no provision given for a horizontal stabiliser. A vertical fin and rudder constitutes the vertical tail. The rudder comprises one segment, is supported by two hinges attached to the rear of the vertical stabiliser and the deflection range is 30° for both TE left (+) and TE right (-). The vertical tail has an aspect ratio of 1.0 and taper ratio of 0.35. With a quarter chord sweep of 48°, increased moment arm due to sweepback of the fin is beneficially generated.

UNDERCARRIAGE – The landing gear is a tricycle type arrangement consisting of two main gear assemblies mounted on the fuselage lower portion just aft of the lower oblique wing root centre-section, and a nose gear mounted on the forward fuselage beneath the flight deck. Extension and retraction is hydraulically actuated and electrically controlled. The nose gear retracts forward into the nose gear bay while the main gears shall retract rearward into the main landing gear bay located in the fuselage fairing aft of the lower oblique wing. For the main landing gear, a trailing arm design shall be adopted. All shock absorbers are of the oleo-pneumatic type, and each gear strut is equipped with two wheels. The main gears shall be equipped with two power operated carbon brake assemblies that provide anti-skid performance. The nose gear shall have a hydraulically powered steering system with shimmy damping.

STRUCTURAL DESIGN – Fore and aft variation of the TOLS planforms distributes volume uniformly with that of the fuselage thus negating the need for fuselage cross-section reduction and complex double curvature. The skewed wingbox structure is to become continuous between regions close to the wingtips, and, both upper and lower assemblies shall be mated to the fuselage in one piece. Individual ribs and other sub-assemblies such as constituents that make up the wingtips are to be duplicated as much as possible. Advantages include greater parts commonality between each of the four semi-wing panels and much simpler construction compared to symmetrically swept aircraft wings.

<u>Fuselage</u> – The structure of the fuselage consists of three major assemblies: front - nose with cockpit; centre - cabin; and, aft - rear section including the aft fuselage auxiliary fuel tank and cargo compartment. With the

exception of fore and aft sections, the fuselage is cylindrical with a 2.31 m (7.6 ft) maximum diameter cross-section.

The front section comprises the radome, nose landing gear attachments, electronics/avionics, the hydraulic bay and pilot compartment. The centre section constitutes the passenger cabin including windows, entrance/emergency exits, overhead baggage racks, stowage compartments and seat attachments. Plug type doors are standard. The floor is capable of withstanding a maximum floor loading of 732 kg/m^2 (150 lb/sq.ft). Two specially reinforced frames are to be incorporated for upper and lower wing interface. Space has been provided below the floor and within the region of the wing-fuselage attachment fairing for fuel storage as well as systems and equipment installation, and, landing gear housing. The aft section consists of: a rear pressure bulkhead; auxiliary fuel tank; baggage compartment; compartments for ancillary electrical/electronic systems; and, empennage supporting structure. The baggage compartment floor area and volume are 2.55 m^2 (27.5 sq.ft) and 5.35 m^3 (189 cu.ft).

The fuselage maximum pressure differential is 64.2 kPa (9.3 psi). The pressurised area is confined by a flat bulkhead located forward of the flight deck and a flat rear bulkhead located forward of the aft fuselage auxiliary fuel tank. In the regions cut by the upper and lower wings, the pressurised area maintains integrity by way of a pressure floor and ceiling outside the wing carry-through sections.

<u>Wing</u> – The upper and lower wing structures are complete and continuous assemblies and interfaced to the fuselage top and belly by two reinforced frames. The structure accommodates flaperons or simple plain flaps, integral fuel tanks, one centre fuel tank and the main landing gear attachment assembly. Each wing structure consists of two spars, upper and lower skins, stringers and ribs. Air loads are carried by the front and rear spars that are located at 15% and 60% of local swept chord respectively. Each of the rear spars from outer wing to WPEBS interface, then towards the wing-fuselage interface closes out the flaperon bay and supports control systems therein. This spar also closes out the integral fuel tanks as well; the entire box beam encloses two distinct integral fuel tanks. The central wing torsion box consists of two beams that run in the same sense as wing skew. Aft of the lower wing planform centre wingbox, a box beam yielded from a Keelson and closed by a beam perpendicular to the fuselage contour houses the main landing gear as well as various equipment and systems.

The wing leading edges are detachable parts, made of metal and facilitate anti-icing. The flaperons are each a mono-spar structure hinged on four supports attached to the wing rear spar and collectively extend out to 80% of wing semi-span. The two most inboard flaperons that extend out to 65% semi-span also act as the secondary flight control surface group, i.e. high-lift arrangement, in-flight spoilers, speed-brakes and ground spoilers with interconnected controls to prevent asymmetric operation. The entire flaperon system acting as spoilers can be deployed in unison during rejected takeoff procedures and landing ground-roll.

<u>Aeroelasticity</u> – A structural divergence problem or lack of structural stiffness of the forward semi-wings (lower wing to port and upper wing to starboard) was initially surmised by the author as causing greatest potential for difficulties with TOLS configurations. However, Jones and Nisbet[31] have shown analytically and experimentally that due to lift load alleviation during rolling motion when the forward wing is deflected, oblique wing aircraft could be flown at speeds faster than the clamped divergence speed without instability. This result established the notion that structural divergence for TOLS would probably be a mute point in relation to the other primary consideration of upward bending for instance.

Wing deformation demonstrates the importance of bending for the forward semi-wings since there exists a direct influence on wing aerodynamic qualities and formulation of a consistent control system protocol suitable for the entire flight envelope. The undesirable traits of this phenomenon are postulated as being minimised by virtue of the WPEBS integration. A somewhat reduced cantilever ratio from the WPEBS juncture point to each of the four respective wingtips is perceived as countering any weight penalties incurred compared to the equivalent cantilevered wing premise. As another avenue to improve structural efficiency, consideration might be given to aeroelastic tailoring[31]. This would involve entertaining the notion of employing carbon fibre materials technology for TOLS-X even though this particular study adheres to application of metal alloys only.

FUEL TANKS AND SYSTEM – Similar to the Gulfstream G200, Embraer Legacy, Bombardier CL-604 Challenger, Dassault F900EX and Bombardier Global Express business jets, fuel is stored in multiple cells within the wing and fuselage. Locales include: an integral tank in the lower wing centre section (capacity 867 litres; 229 USG); one in each of the four semi-wings (totalling 5712 litres; 1509 USG); saddle and underfloor tanks forward of the lower wing centre-section (capacity of 8564 litres; 2262 USG); and, an auxiliary tank located aft of the fuselage (3223 litres; 851 USG); the projected maximum usable fuel capacity is 18366 litres (4851 USG). All auxiliary tanks located in the fuselage were required to supplement the four wing fuel tanks, which were too small to hold more than 31% of required fuel. To improve balance and loadability, a selective fuel management system shall be incorporated.

To limit centre of gravity shifts with changes in aircraft attitude and restrict fuel sloshing, wing ribs act as integrated baffles in each wing tank. Access doors to the fillers are installed in upper wing panels for each semi-wing. Gravity refuelling is made possible via these fillers. A single point pressure refuelling facility is located rear of the aft fuselage auxiliary tank. Gravity de-fuelling is accomplished via dump valves installed on the wing tanks' lower surface. Fuel is to be supplied to each engine by an engine driven integral fuel pump. A DC electrically powered positive displacement pump in each fuel tank is to be provided for redundancy.

PROPULSION SYSTEM - The powerplant installation consists of two hypothetical BMW Rolls-Royce BR71X turbofans and is a derivative based on the BMW Rolls-Royce BR715 turbofan. The engines are to be flat-rated to ISA+20°C ambient conditions. The nacelles are located at 42% semi-span and do facilitate thrust-reversing capability. Each podded installation is a pylon-nacelle-pylon arrangement in which the pylon provides redundant support. Each pylon has two spars (longerons) - upper and lower major bulkheads, and is attached to the wing at four primary points through the use of two mid-spar fittings, an upper link and a diagonal brace (drag strut). Each nacelle adopts a long ducted shape, measures 5.70 m (18.7 ft) in length and is vertically aligned between each upper and lower wing stations such that the pylon heights are congruent.

AERODYNAMIC DESIGN QUALITIES

High-lift Characteristics – In a concerted effort to avoid undue sophistication for the sake of promoting improved dispatch reliability, reducing zero-lift drag increments incurred from flap supports; avoiding the structural complications of multi-track supports and extension mechanisms, and, the associative weight penalties of utilising chord extending leading edge and trailing edge flaps, the TOLS-X design utilizes a simple plain flap for high-lift. The array of flap settings available for field performance is designated as 0°, 15°, 30° and 60°.

Experimental data had shown that this arrangement is characterized by an optimum flap deflection angle of 60° and an optimum flap chord ratio of approximately 0.25. The TORNADO VLM module within QCARD-MMI software package was executed to set minimum goals for TOLS-X high-lift performance. For a takeoff flap setting of 30º, the incremental contribution was estimated to be ΔC_{L30} = 0.51. Similarly, for a landing flap setting of 60°, a ΔC_{L60} of 1.03 resulted, thus giving a predicted maximum lift coefficient of 2.26. The landing C_{Lmax} compares favourably with contemporary large and super-large business jets; the TOLS-X minimum goal is approximately 0.09 or 4% less than the best performing high-lift configuration employing both double slotted trailing edge flaps and leading edge slats. Notwithstanding comparable lift coefficients between TOLS-X and contemporary business jets with flaps deployed, one undesirable trait is the higher wing loading does translate into somewhat higher stalling speeds and hence reference speeds.

Subsonic En route Drag – The greatest disadvantage TOLS configurations have is a noticeable zero-lift drag penalty – attributable to shorter wing chords being approximately half of single wing vehicles. This generates a lower magnitude of Reynolds number and in conjunction with a very preliminary assumption of 5% chordwise flow transition for wing surfaces only, a correspondingly higher value of skin friction results. In this study, TOLS-X was predicted to produce a vehicular skin friction coefficient of between 0.0040 and 0.0042, which can be considered to be towards the much higher threshold of modern transport aircraft. Even though the possibility was not thoroughly investigated in this study, it is highlighted that using HSNLF aerofoil sections designed specifically for a lower Reynolds number operation to draw out the extent of chordwise laminarisation could reduce such a drag penalty.

Transonic Wave Drag Increment – The difference in zero-lift drag coefficient between the fastest Mach number and the Critical Mach (M_{CR}; where compressibility effects become significant) is defined as transonic wave drag. Figure 5 shows the breakdown of drag constituents for M0.80, M0.95 and M1.20 forward speeds. M_{CR} was found to occur around M0.73 for an operational C_L range of between 0.3-0.5. This value is similar to the M_{CR} speeds found on contemporary turbofan transport designs employing the now mainstay super-critical wing sections. Based on wing reference area, the total wave drag coefficient (volume and lift dependent) increment at M1.20 was predicted to be 146 counts. The maximum cross-section area was derived from the cross-section area development plot generated by QCARD-MMI and is shown in Figure 6. Note that the streamtube area has been subtracted from the cross-sections, i.e. 10% of the nacelle inlet capture area was retained to account for an inlet mass-flow ratio of 0.90.

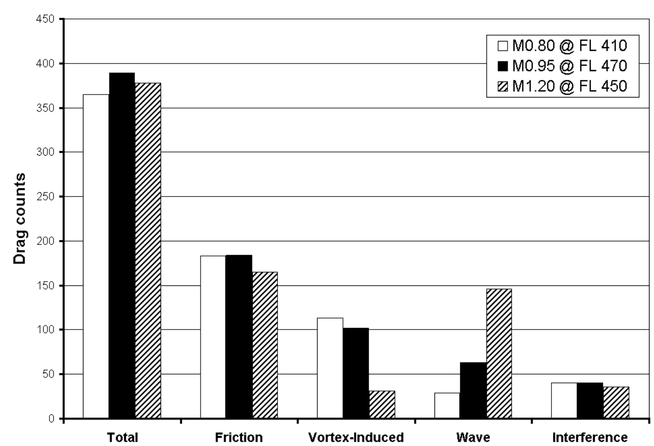

Figure 5. Total and constituent breakdown of TOLS-X drag at various cruise speeds (85% MTOW).

Because wave drag is more a function of cross-section area than reference wing area, it is appropriate to consider the wave drag coefficient based on cross-section area. Figure 7 presents transonic aerodynamic performance of TOLS-X plotted against results obtained

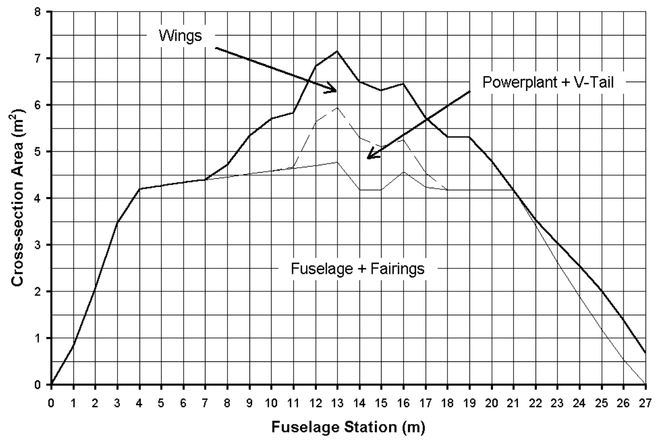

Figure 6. Cross-section area development plot of TOLS-X configuration at sonic speed.

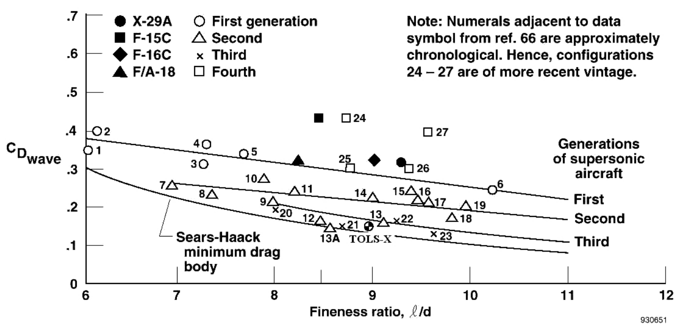

Figure 7. Historic correlation of wave drag sourced from Jobe[33], and, Saltzman and Hicks[34] compared to TOLS-X concept.

for military and experimental aircraft published by Jobe[33], and, Saltzman and Hicks[34]. The ordinate is referenced to maximum cross-section area from which the equivalent diameter is derived for the fineness ratio merit function on the abscissa. It is discernable that the TOLS-X configuration in keeping with satisfactory area-ruling practise exhibits quite desirable transonic wave drag traits; showing qualities in step with significantly older and aerodynamically efficient transonic configurations than contemporary military and experimental aircraft.

<u>Lift-to-Drag Ratio and Aerodynamic Efficiency</u> – Figure 8 shows the variation of lift-to-drag (L/D) with Mach number for three operating lift coefficients of 0.3, 0.4 and 0.5. A bounded speed range is presented for each operating C_L and this is attributable to limitations in instantaneous gross weight as dictated by the TOLS-X vehicular definition.

At a typical commercial Trans-Atlantic operation altitude of FL 370, TOLS-X can achieve an operating Long Range Cruise (LRC) M*L/D (or aerodynamic efficiency merit function) value of 10.9; this figure is approximately 22% lower than contemporary single-aisle long-range transports flying at an LRC speed schedule of M0.80. If one considers a TOLS-X typical cruise speed technique of M0.95 (corresponding to an operating C_L of 0.475 at FL 470), M*L/D values close to 12.0 are predicted, and this contrasts as +12% over the single-aisle long-range transports flying at MCRZ speed schedule of M0.85 (12% slower). In addition, TOLS-X displays an M*L/D advantage of anywhere between +4% to +25% compared to the super-large business jets at M0.85. At a cruise speed of M1.22, M*L/D parity occurs between TOLS-X and super-large business jets at MCRZ. Even though, en route efficiency is somewhat lacking at contemporary business jet LRC speed schedules and altitudes, it is evident that TOLS-X is optimized specifically for missions above FL 410 and speeds greater than M0.90.

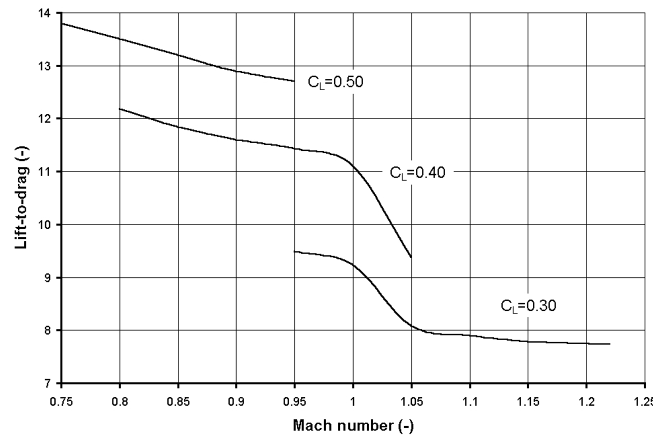

Figure 8. Variation of L/D ratio with Mach number for operating lift coefficients of 0.3, 0.4 and 0.5.

FLIGHT ENVELOPE, PERFORMANCE SYNOPSIS AND COMPETITIVE ANALYSIS – The unique aerodynamic design behind TOLS and WPEBS integration allows for a much broader flight envelope compared to contemporary large and super-large business jets. Flight at FL 510 and speeds up to M1.26 (723 KTAS) are achievable. The flight envelope is presented in Figure 9.

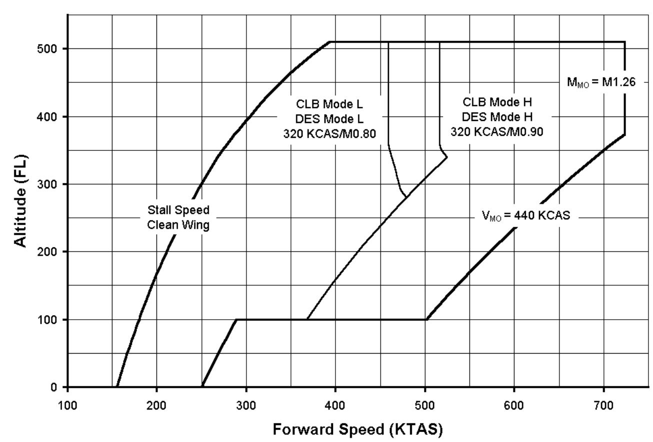

Figure 9. Flight envelope for TOLS-X business jet transport.

Figure 10 shows the predicted TOLS-X payload-range capabilities, whilst Table 2 (overleaf) summarises estimates of the major performance characteristics and compares these with current market equipment.

Comparison of TOLS-X to these vehicles is based on technically analysed data taken from originally published marketing information.

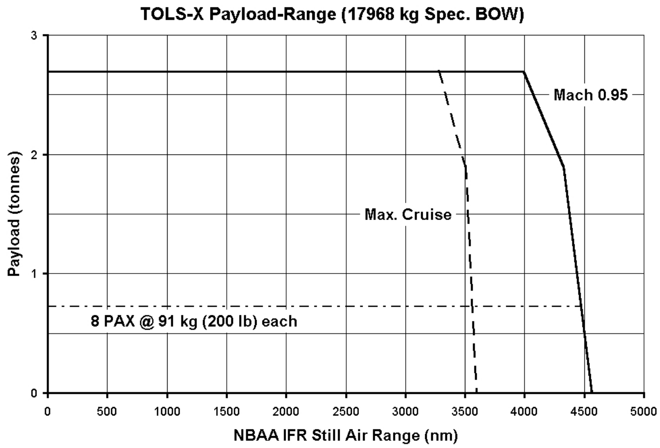

Figure 10. Payload-range envelope for TOLS-X business jet transport.

Cabin – TOLS-X cabin and baggage volume is the biggest in the class of large and super-large business jets. The gross cabin volume less baggage is superior by at least 30%, and the baggage compartment is at least 11% larger than competitor aircraft. The 190-220 mm (7-9 in.) difference in maximum internal and floor width between Dassault products and Gulfstream GIV-SP and the TOLS-X design produced in this study indicates the superiority of F2000 and F900EX in terms of cabin cross-section.

Takeoff and Landing – Takeoff distance for TOLS-X is approximately 4-12% longer (maximum +192 m; +630 ft) compared to the F2000, F900EX and GIV-SP. This can be regarded as satisfactory because the hard specification limit of 1830 m (6000 ft) has not been violated. One unsavory aspect of TOLS-X takeoff field performance is the reference speeds. A decision speed of 165 KCAS is quite fast, approximately +15 KCAS to +35 KCAS upon comparison to the large and super-large business jets. Further scrutiny showed this speed is equivalent to a B737-400 at Flaps 5, but since the TOLS-X V_2 speed does not violate an upper threshold exhibited by contemporary commercial transports, was considered to be within the realm of tacit acceptability. Nonetheless, one suggestion might be to investigate ways in reducing this without compromising the global design considerations. The landing distance at MLW is estimated to be 881 m (2890 ft) with corresponding landing field length equal to 1468 m (4820 ft) at ISA, sea level ambient conditions. TOLS-X displays better attributes in this respect compared to the large and super-large business jets. A landing reference speed of 133 KCAS is another positive trait comparable to that of the F900EX. In view of the above analysis, it can be surmised intentions of producing a vehicle to conduct effective operations in and out of relatively short airfields has been realised with TOLS-X.

Table 2. Parametric review of TOLS-X against contemporary large and super-large business jets.

	TOLS-X	Falcon 2000	Falcon 900EX	GIV-SP
External Length (m)	29.6	20.2	20.2	26.9
External Height (m)	7.48	7.07	7.56	7.44
Fuselage Diameter (m)	2.31	2.50	2.50	2.38
Engines	2 x RR-BMW BR71X	2 x CFE CFE738-1-1B	3 x Honeywell TFE731-60	2 x RR Tay Mk 611-8
Unit Output (kN)	71.2	26.3	22.3	61.6
Span [Excl. Winglets] (m)	20.5	19.3	19.3	23.2
Ref. Wing Area (m^2)	71.6	47.8	47.8	88.3
Ref. Aspect Ratio (-)	8.79	7.80	7.82	6.08
Q.Chd Sweep (deg.)	31.0	25.6	25.6	26.8
Wing loading (kg/m^2)	482	347	465	383
Thrust-to-Weight (-)	0.426	0.324	0.306	0.371
Cabin Seating Length (m)	14.0	5.73	7.70	7.77
Internal Height (m)	1.83	1.89	1.89	1.89
Max. Internal Width (m)	2.16	2.35	2.35	2.23
Cabin Floor Width (m)	1.70	1.92	1.92	1.68
Cabin Vol. Less Bagg. (m^3)	49.9	25.2	35.8	38.4
Baggage Volume (m^3)	5.35	3.80	3.60	4.79
MRW (kg)	34593	16647	22317	34020
MTOW (kg)	34493	16556	22226	33838
MLW (kg)	31000	14969	19051	29937
MZFW (kg)	20660	13000	14000	22226
Spec. BOW (kg)	17968	9730	11204	19278
BOW/MTOW (-)	0.521	0.588	0.504	0.570
Max Payload (kg)	2693	3270	2796	2948
Max Fuel (kg)	14729	5513	9526	13381
Payload @ Max Fuel (kg)	1896	1404	1588	1361
M_{MO} (Mach)	1.26	0.870	0.870	0.880
V_{MO} (KCAS)	440	370	370	340
Certified Ceiling (ft)	51000	47000	51000	45000
TOFL, sl ISA, MTOW (m)	1823	1760	1631	1661
LD, sl ISA, MLW (m)	881	953	1073	972
V_{REF} at MLW (KCAS)	133	122	132	149
CLB Schedule Initial Cruise Altitude (ft)	320KCAS/M0.80 51000	260KCAS/M0.75 41000	260KCAS/M0.72 39000	300KCAS/M0.75 41000
LRC Speed (Mach)	0.90	0.75	0.77	0.77
Max Cruise (Mach)	1.22	0.83	0.85	0.85
Range(1) @ LRC (nm)	4460	3110	4320	4125
SAR(1) @ LRC (nm/kg)	0.336	0.656	0.509	0.348
Range(1) @ MCRZ (nm)	3560	NA	3549	3200
SAR(1) @ MCRZ (nm/kg)	0.268	NA	0.417	0.271

(1) 8 PAX @ 200 lb per PAX, NBAA mission and IFR reserves.

Climb – TOLS-X maximum rate of climb of 5340 fpm at sea level is around 30-56% higher than contemporary large and super-large business jets. It is common practise to assign at least two distinct climb modes, or more specifically, two different speed schedules for climb control that complements cruising techniques. A slow climb speed technique (CLB Mode L) and faster climb speed schedules (CLB Mode H) are also formulated with regards to optimal climb trajectory profile state and time function adherence and designated divergence criteria respectively. Owing to the considerable amount of specific excess power available at maximum climb thrust, a 33% de-rate was invoked by setting the criterion TOLS-X should cruise initially at maximum service ceiling or FL 510 using CLB Mode H speed techniques. Notwithstanding the significant maximum climb thrust de-rate, this still translates into exceptional time-to-climb to altitude FL 370 and maximum service ceiling of FL 510 in 13 minutes and 23 minutes respectively assuming MTOW at brakes release. Even though TOLS-X frequently flies in the drag rise and divergence regime that promotes optimum (or maximum SAR) altitudes below the service ceiling, further increases in de-rate were disregarded to permit operator flexibility of slotting into higher altitudes if traffic congestion at lower airways becomes an issue.

Cruise – LRC, TSC and HSC show an appreciable difference between the TOLS-X and contemporary large and super-large business jets. LRC is at least 75 KTAS and TSC (at M0.95) is 85 KTAS faster than the F900EX and GIV-SP business jets above the tropopause. The maximum cruise speed capability of up to +210 KTAS for TOLS-X has opened up a totally new regime of lower block times. It is evident that the Dassault range of aircraft display quite superior en route performance efficiency characteristics compared to TOLS-X; as exemplified by a greater than 50% better SAR (at 14% and 30% slower speeds for LRC and HSC respectively) of the F900EX. The GIV-SP however, has SAR attributes more in-line with TOLS-X consistently demonstrating a +4% to +1% advantage but again at 14% and 30% slower speeds for LRC and HSC respectively. Even though the F900EX has more desirable en route burn attributes, TOLS-X has fulfilled the main objective of matching en route efficiency characteristics to a primary competitor, namely the GIV-SP, whilst permitting a marked increase in block speed performance.

CONCLUSION

The TOLS-X vehicle proposal is an executive jet concept that accommodates a maximum of 19 passengers and affords excellent comfort through speed, spaciousness and amenities not paralleled by contemporary large and super-large business jets. This business/corporate jet works off a contemporary turbofan technology level, i.e. by virtue of being a derivative of the BMW Rolls-Royce BR715. The marked increase in block speed of TOLS-X does require a trade off in higher fuel flow as denoted by lower Specific Air Range (SAR) values compared to the smaller and lighter Dassault F2000 and F900EX business jets. However, upon comparison to an equivalent airframe in size and weight, such as the Gulfstream GIV-SP, it was found that comparable SAR values are produced at speeds that are 17-44% faster. Irrespective of the dramatic increase in cruising speeds, effective field performance has been maintained and permits the original hard specification of operations in and out of relatively short airfields.

Various issues needed to be addressed with the Twin-Oblique Lifting Surfaces (TOLS) design. One drawback was the greater structural weight of TOLS integrated with the wing-pylon-engine bracing structural system (WPEBS) compared to a cantilevered single wing equivalent. It was appreciated from the outset that the TOLS configuration would possess some benefit from a structural efficiency perspective. Ideally, a piece-wise linear beam model would have been employed in estimating the bending material weight. Unfortunately, owing to an absence of this functionality, and even an equivalent conceptual method, possibilities of investigating for leaner structural weight was not realised. The higher wing loading and modest lift increments at lower flap deflections using the assumed plain flapping arrangement translates into higher stall speeds and hence reference speeds during takeoff. Another disadvantage was an increase in zero-lift drag due to a significantly lower Reynolds number generated by the smaller local wing chords characteristic of TOLS configurations and a preliminary assumption of 5% chordwise laminarisation on wing surfaces only. This aspect can be enhanced with application of aerofoils specially optimised (such as modified HSNLF-1-0213 section) for low Reynolds number thus promoting further aft chordwise flow transition. As a final note for improvement, since this particular investigation concentrated on a very limited scope of multivariate optimization, it is suggested that application of Multi-Disciplinary Optimisation (MDO) techniques would be an advantageous step. This procedure should realise the most efficient vehicular candidate when considering all the primary disciplines concurrently.

This paper has shown the potential of the TOLS layout integrated with WPEBS for high-speed mission capability compared to the conventional wisdom of delta wing designs employed on all modern supersonic business jet proposals. It is granted the highly exotic nature of the TOLS configuration will be met with less than a favourable reaction from crews and passengers alike. Notwithstanding this negative aspect, it must be highlighted that unless a radical shift in vehicle configuration design is entertained, significant strides in performance will not come to fruition - not even incremental increases in speed up to the high transonic to low supersonic regime. The results in this study demonstrate there exists a feasibility, and if the abovementioned areas of conservative assessment can be rationalised through future research, it is projected the TOLS layout will become even more of an appealing proposition.

REFERENCES

1. Taylor, J., Munson, K., “History of Aviation”, Crown Publishers Inc., 1978.
2. Campbell J.P., Drake, H.M., “Investigation of Stability and Control Characteristics of an Airplane Model with Skewed Wing in the Langley Free-Flight Tunnel”, NACA TN 1208, 1945.
3. Jones, R.T., “New Design Goals and a New Shape for the SST”, Astronautics and Aeronautics, Vol. 10, No.12, December 1972.
4. Jones, R.T., Nisbet J.W., “Transonic Transport Wings – Oblique or Swept?”, Astronautics and Aeronautics, January 1974.
5. Olson E.C., Selberg, B.P., “Experimental Determination of Improved Aerodynamic Characteristics Utilising Biplane Wing Configurations”, Journal of Aircraft, Vol. 13, April 1976.
6. Rhodes, M.D., Selberg, B., “Dual Wing, Swept Forward Swept Rearward Wing, and Single Wing Design Optimisation For High Performance Business Airplanes”, ICAS-82-1.4.2, 1982.

7. Pfenninger, W., “Design Considerations of Large Subsonic Long Range Transport Airplanes with Low Drag Boundary Layer Suction,” Northrop Aircraft, Inc., Report NAI-58-529 (BLC-111), 1958. (Available from DTIC as AD 821 759).
8. Gundlach IV, J.F., Naghshineh-Pour, A., Gern, F., Tetrault, P.-A., Ko, A., Schetz, A., Mason, W.H., Kapania, B., Grossman, B., Haftka R.T. (University of Florida), “Multidisciplinary Design Optimisation and Industry Review of a 2010 Strut-Braced Wing Transonic Transport”, MAD 99-06-03, Department of Aerospace and Ocean Engineering, Virginia Polytechnic Institute and State University, June 1999.
9. Isikveren, A.T., ” Methodology for Conceptual Design and Optimisation of Transport Aircraft”, Report 98-8, Royal Institute of Technology, Department of Aeronautics, Sweden, 1998.
10. Kendall, E.R., “The Minimum Induced Drag, Longitudinal Trim and Static Longitudinal Stability of Two-Surface and Three-Surface Airplanes”, AIAA-84-2164, 1984.
11. Obert. E., “Some Aspects of Aircraft Design and Aircraft Operation”, Lecture Series, Sweden, 1996.
12. Durand, W.F., “Aerodynamic Theory”, Vol. V, January 1943.
13. Saab 2000 Type Specification, 73VPS010, Revision F, Saab Aerospace AB, November 1996.
14. Isikveren, A.T., ”Methodology for Conceptual Design and Optimisation of Transport Aircraft”, ICAS 98-7.8.2, September 1998.
15. Svoboda, C., “Turbofan Engine Database as a Preliminary Design Tool”, Aircraft Design 3 (2000) 17-31, Aircraft Design Journal, 2000.
16. Whitford, R., “Design for Air Combat“, Jane’s Information Group Ltd., date not available.
17. Kroo, I., “The Aerodynamic Design of Oblique Wing Aircraft”, AIAA Paper 86-2624, October 1986
18. van der Velden, A.J.M, Torenbeek, E., “Design of a Small Oblique-Wing Transport Aircraft”, Journal of Aircraft, Vol. 26, No. 3, March 1989.
19. Isikveren, A.T., ”The PD340-2 19 Passenger Turbofan Regional Transport- Feasibility Study”, Report 98-5, Royal Institute of Technology, Department of Aeronautics, Sweden, 1998.
20. Mason, W.H., “Analytical Models for Technology Integration in Aircraft Design”, AIAA-90-3262-CP, 1990.
21. Jones, R.T., “The Oblique Wing – Aircraft Design for Transonic and Low Supersonic Speeds”, Acta Astronautica, Vol. 4, Pergammon Press, 1977.
22. Torenbeek, E., ”Synthesis of Subsonic Airplane Design”, Delft University Press, 1988.
23. Raymer, D.P., ”Aircraft Design: A Conceptual Approach”, AIAA Educational Series, 1992.
24. Melin, T., “A Vortex-Lattice MATLAB Implementation for Linear Aerodynamic Wing Applications”, Masters Thesis, Royal Institute of Technology, Department of Aeronautics, Sweden, December 2000.
25. Wauquiez, C., Rizzi, A., “PABLO – Potential Flow Around Airfoils with Boundary Layer coupled One-way”, Royal Institute of Technology, Department of Aeronautics, Sweden, 1999.
26. Young, A.D., ”The Aerodynamic Characteristics of Flaps”, Aeronautical Research Council, Technical Report No. 2622, 1953.
27. Linnell, R., “Weight Estimation Methods”, FKHV-1-RL790724:01, Saab AB, July 1979.
28. Scott, P.W., Nguyen D., ”The Initial Weight Estimate”, SAWE Paper No. 2327, Index Category No. 11, MDC 96K0030.
29. Torenbeek, E., “Development and Application of a Comprehensive, Design-sensitive Weight Prediction Method for Wing Structures of Transport Category Aircraft”, Report LR-693, Delft University of Technology, Faculty of Aerospace Engineering, The Netherlands, October 1994.
30. Sewall, W.G., McGhee, R.J., Viken, J.K., Waggoner, E.G., Walker, B.S., Millard, B.F., “Wind tunnel results for a high-speed, natural laminar-flow airfoil designed for general aviation aircraft”, NASA-TM-87602, NASA Langley Research Centre, November 1985.
31. Jones, R.T., Nisbet J.W., “Aeroelastic Stability and Control of an Oblique Wing”, The Aeronautical Journal of the Royal Aeronautical Society, August 1986.
32. Weisshaar, T., Zeiler, T., “Dynamic Stability of Flexible Forward Swept Wing Aircraft”, Journal of Aircraft, December 1983.
33. Jobe, C.E., “Prediction of Aerodynamic Drag”, AFWAL-TM-84-203, Flight Dynamics Laboratory, Air Force Wright Aeronautical Laboratories, Wright-Patterson Air Force Base, OH 45433, July 1984.
34. Saltzman, E.J., Hicks, J.W., “In-Flight Lift-Drag Characteristics for a Forward-Swept Wing Aircraft (and Comparisons with Contemporary Aircraft)”, NASA Technical Paper 3414, December 1994.

ADDITIONAL SOURCES

1. Abbott, I.H., Von Doenhoff, A.E., ”Theory of Wing Sections”, Dover Publications, 1959.
2. Clancy, L.J., ”Aerodynamics”, Longman Scientific & Technical, 1975.
3. Currey, N., ”Aircraft Landing Gear Design: Principles and Practises”, AIAA, 1988.
4. Gillette, W.B., ”Nacelle Installation Analysis for Subsonic Transport Aircraft”, AIAA Paper 77-102.
5. Graham, A., Jones, R.T., Boltz, F., “An Experimental Investigation of Three Oblique Wing and Body Combination at Mach Numbers Between 0.6 and 1.4”, NASA TM X-62256, April 1973.
6. McCormick, B.W., ”Aerodynamics, Aeronautics and Flight Mechanics”, John Wiley & Sons, 1979.
7. Nelms, Jr., W.P., “Applications of Oblique-Wing Technology – An Overview”, AIAA Paper 76-943, September 1976.

8. Niu, M.C.Y., ”Airframe Structural Design”, Conmilit Press Ltd., 1989.
9. Roskam, Dr. J., ”Airplane Design”, Vol. I-VII, 1986.
10. Schippers, K.A., ”Cowl Design Methodology”, D6-41800 TN (unreleased), Boeing Airplane Company.
11. Tipton, B.J., Dudley E.S., “The Preliminary Design Analysis of a Unique Semi-Tailless Aircraft Configuration”, AIAA Paper 952053, 1995.

ACRONYMS AND ABBREVIATIONS

a.c.	Aerodynamic centre
AEO	All Engines Operational
BOW	Basic Operating Weight
BPR	By-Pass Ratio
CFD	Computational Fluid Dynamics
CLB Mode H	Climb Mode High speed technique
CLB Mode L	Climb Mode Low speed technique
FAR	Federal Aviation Regulations
FL	Flight Level
HSC	High-Speed Cruise
HSNLF	High-Speed Natural Laminar Flow
IFR	Instrument Flight Rules
JAR	Joint Airworthiness Regulations
KTH	Royal Institute of Technology (KTH), Stockholm, Sweden
LD	Landing distance
LRC	Long Range Cruise
MCRZ	Maximum Cruise
MLW	Maximum Landing Weight
MRW	Maximum Ramp Weight
MTOW	Maximum Takeoff Weight
MZFW	Maximum Zero-Fuel Weight
NACA	National Advisory Committee for Aeronautics
NBAA	National Business Aviation Association
OEI	One Engine Inoperative
OPR	Overall Pressure Ratio
PAX	Passengers
SAR	Specific Air Range
SBW	Strut-Braced Wing
TE	Trailing Edge
TED	Trailing Edge Down
TEU	Trailing Edge Up
TOFL	Takeoff field length
TOLS	Twin Oblique Lifting Surfaces
TSC	Typical Speed Cruise
TSFC	Thrust Specific Fuel Consumption
USG	U.S. gallons
VLM	Vortex-Lattice Method
WPEBS	Wing-Pylon-Engine Bracing Structural system

Transonic Transport Wings—Oblique or Swept?

By ROBERT T. JONES
NASA Ames Research Center
and
JAMES W. NISBET
Boeing Commercial Airplane Co.

In terms of gross weight, fuel consumption, and aircraft noise, an oblique-wing aircraft looks best, and it shows acceptable aeroelastic stability; but its design characteristics and economic implications need further study

In transonic-aircraft design, one naturally thinks of highly swept arrow or delta-wing shapes. An article in the December 1972 *A/A*, however, proposed a radically different wing form for such aircraft[1]: a conventional unswept subsonic wing that can be turned to different oblique angles for different flight speeds. Tests in the 11-ft supersonic wind tunnel at NASA Ames Research Center confirmed the superior aerodynamic efficiency of the oblique wing.

While it seems clear that the oblique wing can generate higher lift-to-drag ratios in the transonic speed range, it is not clear that such an unusual arrangement could be successfully adapted to a real airplane. Factors such as increased structure weight, aeroelastic instability, or other configurational considerations might nullify a purely aerodynamic advantage.

To answer such practical questions, a comparative study of transonic and low-supersonic transport aircraft was undertaken by the Boeing Commercial Airplane Co. under NASA contract. The study covered five different wing designs (see the sketches in F-1 at right).

1. Swept wing; fixed geometry.
2. Swept wing; variable sweep.
3. Fixed delta wing.
4. Oblique wing with two bodies.[2]
5. Oblique wing with single body.

The study covered aerodynamic and engine performance analysis, preliminary structural calculations and weight estimates, and dynamic-stability and aeroelastic-stability analysis, as well as configurational work. (Aerodynamic and performance considerations: R. M. Kulfan, E. C. Noble, J. R. Stalter, and J. K. Murakami. Propulsion and noise characteristics: defined by M. B. Sussman. Weight and balance estimates: J. P. McBarron. Flight stability of the unsymmetrical configurations: A. R. Mullally. Structural and aeroelasticity studies: J. W. Nisbet and D. W. Gimmestad. The general arrangements were worked out by F. D. Neumann.)

It was found that the assigned flight mission could be performed by any one of the five design concepts, although airplane size and weight varied considerably.

ROBERT T. JONES (F), (far left), a senior staff scientist at NASA-Ames, played a major part in raising the speed of aircraft through developing theory for swept and slender delta wings. In 1946 the AIAA gave him its Sylvanus Albert Reed Award. He has been with NACA and NASA since 1934, except for seven years with the AVCO Everett Research Laboratory, where he directed work on cardiac-assist devices. Besides aerodynamics, he has maintained a professional interest in optics. JAMES W. NISBET, during 13 years at Boeing, has worked on nearly all of the current jet airplanes as well as in preliminary design and research. Currently responsible for aeroelastic loads in airplane exploratory design, he has long been involved in analysis, wind-tunnel testing, and airplane testing regarding aeroelasticity and structural dynamics. Before joining Boeing, he spent four years with Canadian Westinghouse on the design of electrical system controls.

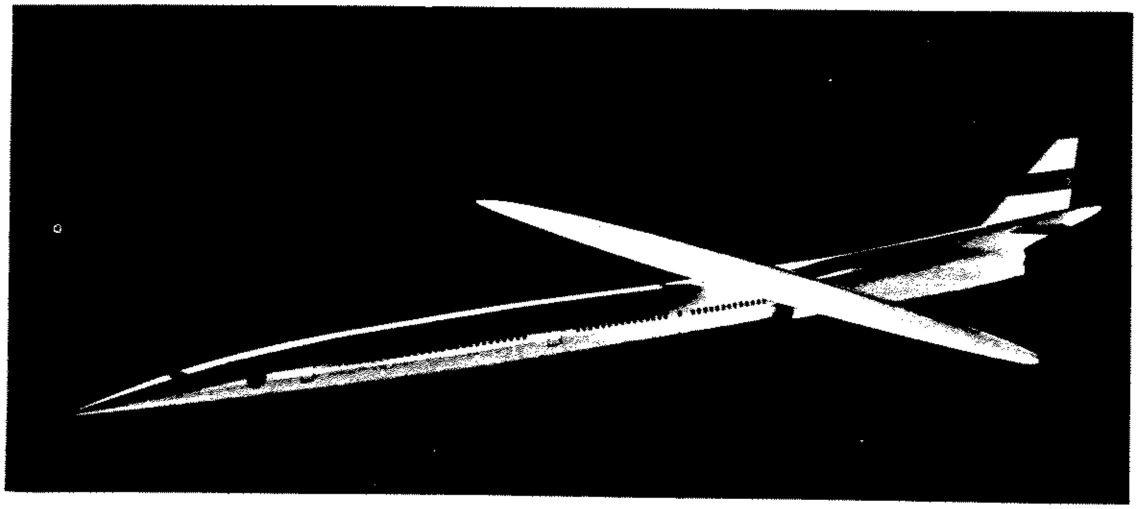

F-1 CONFIGURATION CONCEPTS

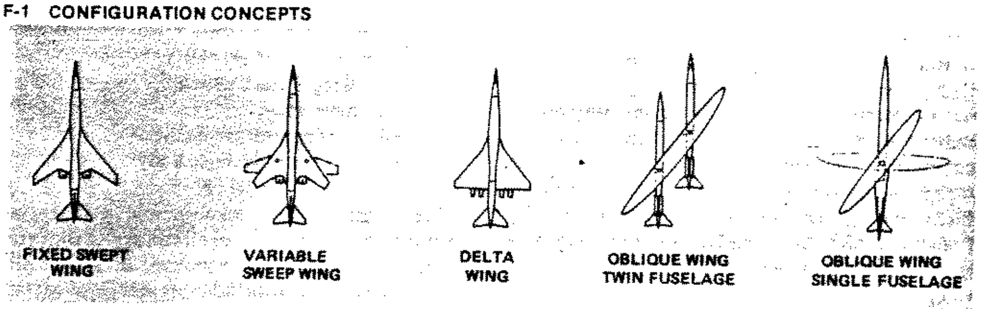

Complete results and the assumptions employed in the study are contained in NASA CR 114658.[3] This article emphasizes certain results characterizing oblique-wing designs.

Each airplane was designed to carry 195 passengers 3000 n. mi. at a speed near the sonic ground speed. Operation just below sonic ground speed eliminates the sonic boom associated with overland supersonic flight. As shown in F-2 (from Ref. 4) the shock fronts curve slightly as they progress to lower altitude. This curvature, caused by the change in speed of sound with temperature, establishes the maximum speed at which a transonic transport can fly without producing a boom at ground level. When the shock front becomes vertical the boom does not extend to the ground; this would permit boom-free flight at speeds nearly 50% greater than subsonic jets make today—*a saving of some 2 hr on east-to-west and 1 hr on west-to-east transcontinental U.S. flights.*

The aerodynamic characteristics of all five configurations were developed using similar procedures. The planform parameters were selected to exploit the aerodynamic benefits of each concept. The wing thickness distributions were derived from past weight-drag tradeoff studies on transonic transports. The camber and twist distributions were developed by linear theory. The body designs for all configurations were area-ruled to yield minimum cruise drag. The nacelle shape and location was strongly influenced by the engine size and the configurational arrangement.

Engine performance, size, and weight characteristics were consistent with the results of the Advanced Transport Technology (ATT) study.[5] Engine selection was based on an engine-bypass-ratio tradeoff study. The penalty of reducing the jet noise by increasing bypass ratio was compared to the penalty associated with jet suppression of lower-bypass-ratio installations. A bypass-ratio-of-1 engine with jet suppression was selected for all configurations as the most efficient means of achieving low noise levels.

The swept-wing, variable-sweep wing, and delta-wing configurations had the advantage of considerable previous study; and it seems probable that the arrangement of landing gear, engine, etc. was near the optimum in those cases.

The oblique-winged aircraft introduced some new problems, and considerable effort was devoted to finding a good general arrangement. The emphasis was on the engine and landing-gear placement. There was considerable flexibility in locating the landing gear because takeoff rotation and high-angle landing flare were not required. F-3 shows the arrangement adopted in the final stage of the study.

A balance and loading analysis of the oblique-wing configuration indicated the need for a center-of-gravity range of 25% MAC (mean aerodynamic

F-2 AVOIDING SONIC BOOM

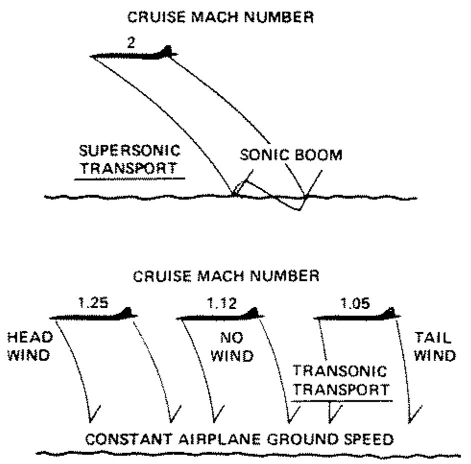

NO SONIC BOOM—SHOCK WAVES DO NOT REACH GROUND

chord). Forward body ballast was required for low payloads. Selective fuel management with an aft body fuel tank allowed minimizing cruise trim-drag.

Control, trim, and aerodynamic stability characteristics were evaluated with the wing in the oblique position. Aerodynamic coupling between the longitudinal and lateral motions does exist and was considered. The effect of wing flexibility on this coupling is currently being evaluated. It appears that the flight characteristics do not present any insurmountable problems, although modified control techniques will be required.

Structural weight of the oblique wing received considerable attention because of the concern over aeroelastic stability. This phase of the study will be presented in some detail because of its potential impact on oblique-wing performance and because of the unique oblique-wing aeroelastics.

Wind-tunnel results given last January in *A/A* represented an elliptic wing having an aspect ratio of 12.7 (10:1 ellipse) with airfoil sections of 10% thickness/chord ratio.[1] The beam slenderness ratio (length/max thickness) in that case ran 50 to 1, whereas 17 to 1 might typify current transport aircraft. It was discovered rather early in the studies reported here that such proportions would lead to excessive structural weight. Reducing the aspect ratio to 10.2 (8:1 ellipse) and increasing the wing root thickness to 12% improved the situation considerably, and for the remainder of the studies these proportions characterized the oblique wing.

Structural materials were selected for all configurations based on the Advanced Transport Technology (ATT) study results.[5] F-4 identifies the materials selected for the single-fuselage oblique-wing configuration and gives an estimate of the percent weight savings of the advanced materials relative to conventional aluminum skin-stringer construction.

Graphite-epoxy honeycomb was selected for the wing, fuselage, and vertical-tail primary structure. Titanium was selected for the wing pivots and pivot-support structure. For configurations other than the oblique wing, the primary wing-structure weightsaving was estimated to be 25%. Primary-structure weight savings for the oblique wing was determined by analysis of both an aluminum and a graphite-epoxy structure. The aluminum oblique wing was stiffness- rather than strength-critical: the graphite-epoxy oblique wing was strength-critical. This resulted in a weightsaving of 35% for the advanced material as compared to aluminum.

Structural analysis of the graphite-epoxy oblique wing involved these conditions:

A ply arrangement—considering external load distributions and the bending stiffness required for aeroelastic stability.

Isotropic structural parameters (such as ultimate strength and stiffness modulus) simulating the anisotropic ply arrangement.

An estimated compression-buckling curve for built up panels.

Allowables and stiffness moduli were determined from material data in the Air Force Advanced Composites Design Guide.[6] High-modulus graphite was used. Fiber orientations were selected to enhance wing-bending strength and stiffness, while retaining adequate strength in the other directions. Ply orientation in the graphite-epoxy face sheets was 60% (0°), 30% ($\pm 45^{\circ}$) and 10% (90°). An allowance of 15% for aluminum and 25% for graphite-epoxy was added to the wing's primary structural weight to account for fittings, fasteners, and joints.

In F-5 you see a conceptual design (cross section) for the oblique-wing pivot. It differs significantly from a variable-sweep wing pivot. A variable-sweep wing pivot must transfer wing-bending moments through the pivot bearings. This was avoided on the oblique-wing pivot by placing the bearings below the wing and maintaining continuous upper and lower wing-surfaces to transfer the bending moments. In addition, the pivot diameter was made as large as possible to keep the bearing loads low. Vertical loads, rolling moments, and pitching moments were transferred through the bearings on the circumference of the pivot. Drag loads and side loads were transferred through bearings on the pin in the middle of the pivot. Systems going from the body to the wing were routed through the center of the pivot.

As is well known, swept-forward wings show a tendency for aeroelastic divergence. Bending of a swept-forward wing panel creates an aerodynamic force which acts to increase the deflection in opposition to the structural stiffness. At a sufficiently high flight speed or dynamic pressure the aerodynamic destabilizing force can overpower the structural stiffness, leading to aeroelastic divergence.

The behavior of the oblique wing differs from the bilaterally symmetric swept-forward wing's: the coupled rolling motion exerts a *stabilizing influence.* Aeroelastic instability of the oblique wing occurs as an oscillatory instability; there is a progressive lengthening of the period and loss of damping of the elastic bending oscillations of the wing combined with rolling motion.

F-6 illustrates the dynamic model used to study the aeroelastic stability of the oblique wing. The wing mass was represented by a series of point masses. The aerodynamic lift distribution was represented by a section lift coefficient for each of the wing panels. Wing flexibility was represented by beam bending and beam torsion, although it was found in the analysis that torsional stiffness had little effect on the stability of a wing with an oblique angle of 45 deg. Airplane roll was treated as a separate degree of freedom in the analysis.

F-7 shows the results of the analysis of a wing with an aspect ratio of 12.7 (10:1 ellipse) designed for strength alone. For comparison, it also shows stability with the fuselage clamped to prevent rolling (as in a wind-tunnel test). At zero flight speed (or, equivalently, zero dynamic pressure) the frequency of the unrestrained airplane as well as both wings of the restrained airplane was 0.93 Hertz. As the speed was increased, the damping ratio initially increased.

With the fuselage clamped, the frequency of the forward wing decreased while the frequency of the aft wing increased. The damping ratio of the forward wing decreased rapidly at higher speeds. (The so-called "static" divergence speed is the speed at which both the frequency and damping ratio become zero.)

F-3 OBLIQUE-WING AIRPLANE

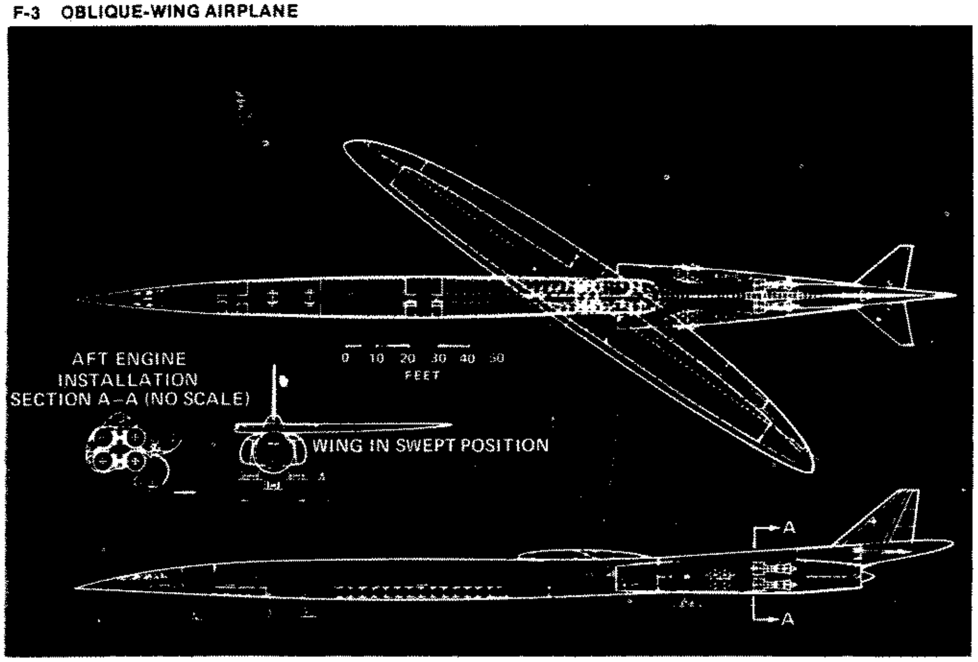

F-4 MATERIALS SELECTION FOR AN ADVANCED-TECHNOLOGY OBLIQUE-WING AIRCRAFT

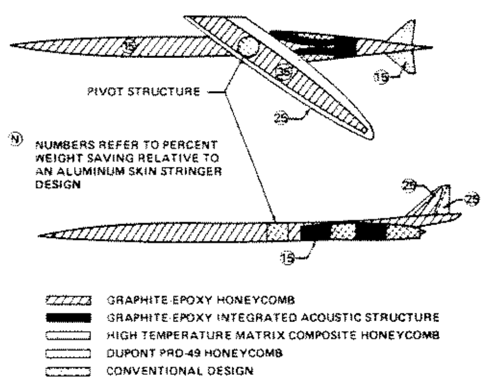

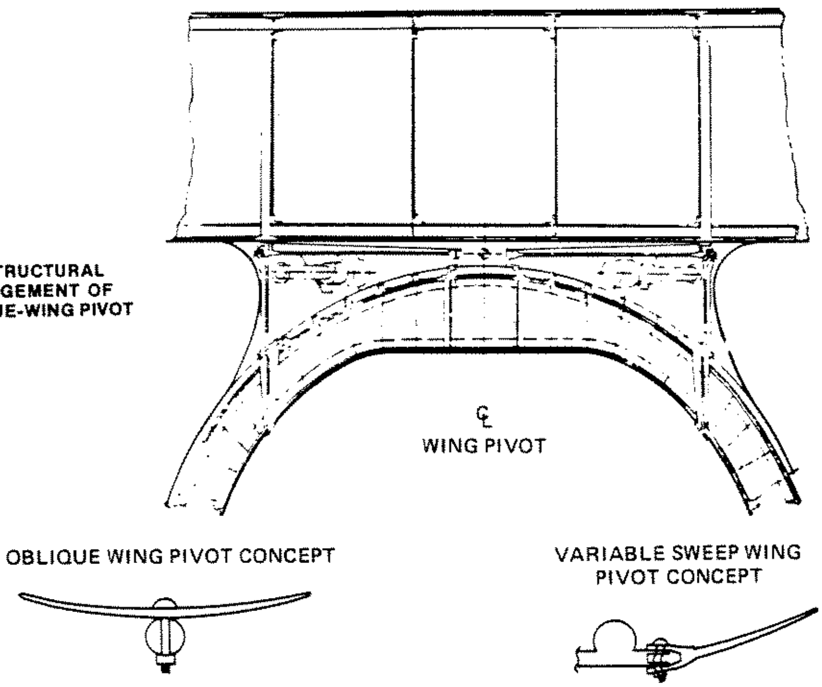

F-5 STRUCTURAL ARRANGEMENT OF OBLIQUE-WING PIVOT

The unrestrained airplane did not exhibit this static instability. As speed was increased, the frequency decreased and the bending deflection of the forward wing increased relative to the aft wing. The wing-bending deflections introduced roll participation into the oscillation. The oscillatory aeroelastic instability occurred at a higher speed than the speed at which the clamped fuselage static instability occurred.

Analyses of aeroelastic behavior which assume that the fuselage is clamped at the wing root appear to be conservative for most oblique-wing configurations. The aspect-ratio-12.7 oblique wing designed for strength alone became unstable at about 90% of the airplane's speed. FAA criteria require stability up to 120% of the design speed. It is evident that a wing of this high an aspect ratio would require considerable additional structure for stiffness.

F-6 STABILITY - ANALYSIS MODEL

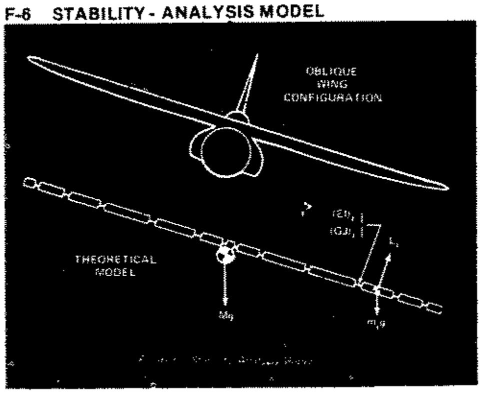

Reducing the aspect ratio to 10.2 (8:1 ellipse) improved this situation considerably. F-8 compares the stability of *strength*-designed aluminum and graphite-epoxy wings of aspect ratio 10.2. The aluminum wing designed for strength alone still did not satisfy the requirement for aeroelastic stability; it would have to be stiffened with more material to improve the stability. On the other hand, the graphite-epoxy wing designed for strength alone had adequate stability.

The advantage of using graphite-epoxy rather than aluminum for construction of an oblique wing, and the importance of aspect ratio, can be seen in F-9. A graphite-epoxy wing satisfying only the strength requirements offers about 20% weight advantage. Considering the aeroelastic stability indicated, the graphite-epoxy should have an even greater advantage over aluminum. Reducing the aspect ratio of the wing gave lower weight and improved stability. These results, however, should not be considered as the last word since only an elliptic planform was included in this study.

F-7 ELASTIC STABILITY: ASPECT-RATIO-12.7 OBLIQUE WING

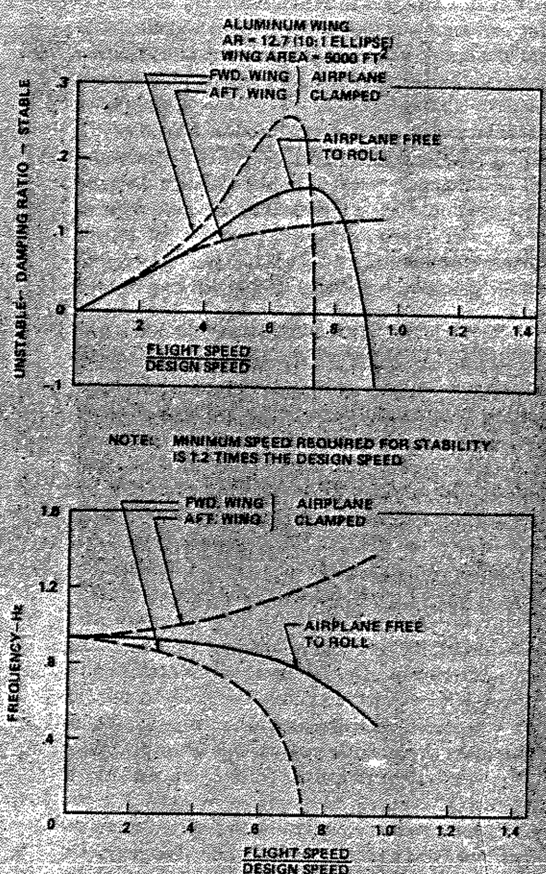

F-8 ELASTIC STABILITY: ASPECT-RATIO-10.2 OBLIQUE WING

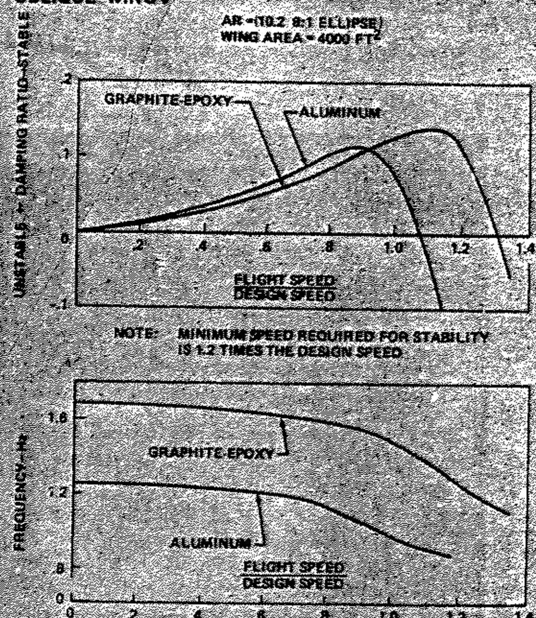

F-9 WEIGHT EFFECT OF ASPECT RATIO AND STRUCTURAL MATERIALS ON OBLIQUE WING

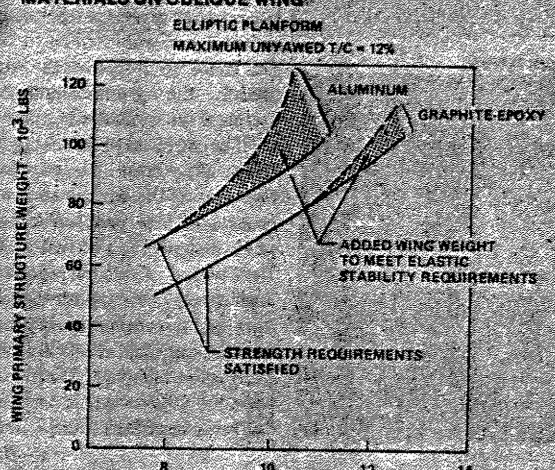

F-10 GROSS-WEIGHT SUMMARY

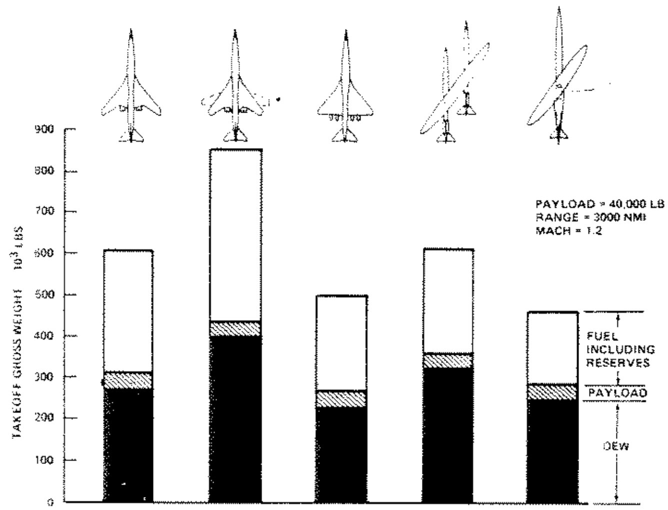

F-11 WEIGHT COMPARISON

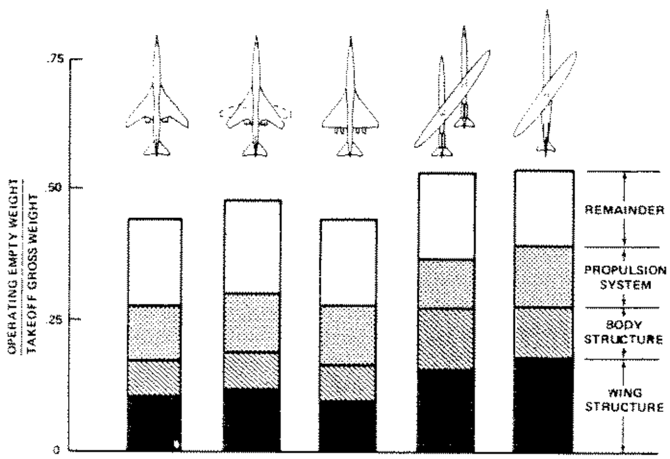

F-12 CRUISE-DRAG COMPARISON

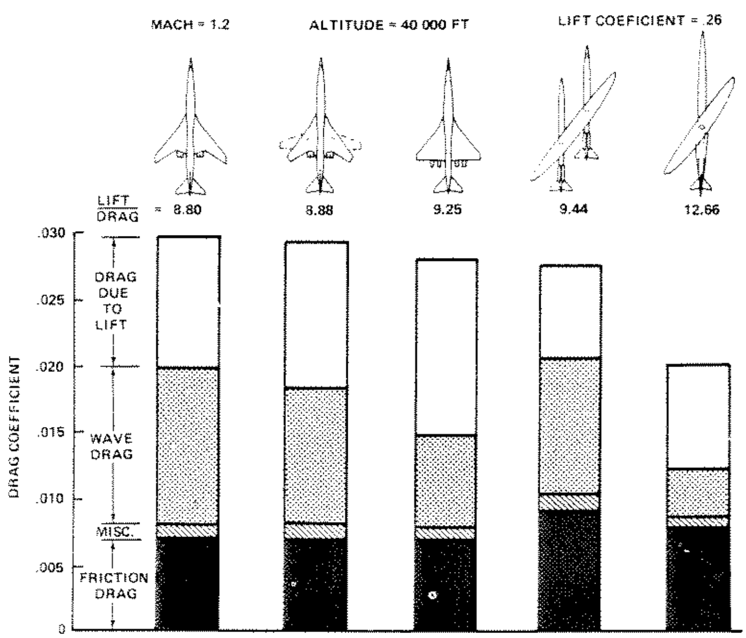

Further planform studies considering the distribution of mass and stiffness as well as the aerodynamic characteristics of the wing would seem to be most important.

Minimum gross weight (F-10) required to perform the 3000-n. mi. mission was determined for airplanes based on the five configurational concepts in this study. Additional work established the gross weight penalty for noise reduction.

Substantially lower gross weights were required for the delta-wing and single-body, oblique-wing configurations than for any of the others. The delta-wing configuration had the advantage of a low structural weight and thus a low operating empty weight, as shown in F-11. The single-body, oblique-wing airplane (F-10) had a smaller gross weight because of its lesser fuel requirements. It is interesting to note that the structural weight penalty of the oblique wing was not primarily associated with the peculiar features of the design nor the variable geometry, but rather it was the result of the basic strength requirements of a high-aspect-ratio wing.

The single-body oblique wing has the advantage in aerodynamic efficiency, as shown by the cruise-drag comparison in F-12. The effect of the higher aspect ratio in reducing drag due to lift is quite evident for the oblique-wing configurations. Another major difference in drag of the configurations was found to be the wave drag due to volume. The double-pod installation was primarily responsible for the high wave drag on the fixed- and variable-sweep-wing configurations. The low wave drag of the single-body oblique wing reflects the integrated body-nacelle arrangement and the inherent characteristics of the oblique wing.[2]

F-13 describes the impact on takeoff gross weight of achieving lower noise levels by engine-nacelle treatment. The takeoff-gross-weight increase reflects weight added for acoustical treatment and the associated engine-performance losses. Only the oblique-wing configurations could achieve a noise level of FAR 36 minus 15 EPNdB.

This technically orientated study has yielded, we believe, a realistic performance comparison of the five wing-planform concepts and gives insight into areas unique to the oblique-wing configuration. The oblique wing offers desirable performance, but further analysis and wind-tunnel work will be needed to develop a rounded picture of its potential. In particular, future work should include an economic evaluation of the consequences of oblique wing's ability to increase today's cruise speeds 50%.

In terms of the transonic concepts it covers, the most significant conclusions of this study might be summarized as follows:

F-13 IMPACT OF NOISE TREATMENT ON TAKEOFF GROSS-WEIGHT

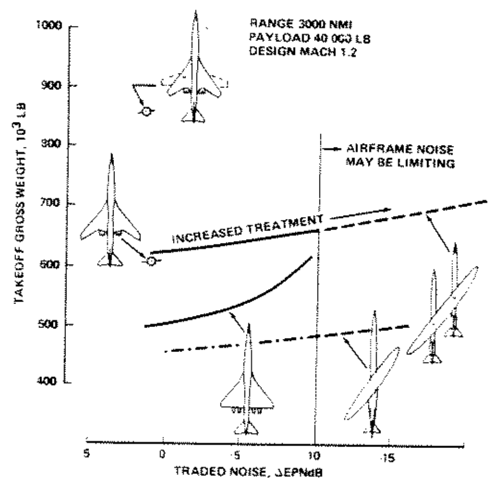

1. The oblique-wing airplane had the smallest gross weight and the lowest fuel consumption.

2. Only the oblique-wing airplane could achieve a noise level of FAR 36 minus 15 EPNdB.

3. The oblique wing is aeroelastically less stable than a sweptback wing but more stable than a swept-forward wing. For the designs considered, an aluminum oblique wing would require a moderate amount of additional stiffness to meet stability requirements. For graphite-epoxy no additional stiffness would be required.

4. Further development studies supported by wind-tunnel tests will be needed to develop the full potential of the oblique-wing concept. This should be followed by an economic evaluation treating productivity.

References

1. Jones, R. T., "New Design Goals and a New Shape for the SST," *Astronautics & Aeronautics*, Vol. 10, No. 12, Dec. 1972, pp. 66-70.

2. Jones, R. T., "Reduction of Wave Drag by Antisymmetric Arrangement of Wings and Bodies," *Astronautics & Aeronautics*, Vol. 10, No. 2, Feb. 1972, pp. 171-176.

3. Kulfan, Robert M., et al., "High Transonic Speed Transport Aircraft Study," NASA CR-114658, Sept. 1973.

4. Goodmanson, Lloyd T., "Transonic Transports," *Astronautics & Aeronautics*, Vol. 9, No. 11, Nov. 1971, pp. 46-56.

5. NASA Contracts NAS1-1071, NAS1-1072, NAS1-1073, "Study of the Application of Advanced Technologies to Long-Range Transport Aircraft".

6. "Advanced Composites Design Guide," Advanced Composites Division, Air Force Material Laboratory, Air Force Systems Command, Wright-Patterson Air Force Base, Ohio, Nov. 1971. ■

Design of a Small Supersonic Oblique-Wing Transport Aircraft

Alexander J. M. van der Velden*
Stanford University, Stanford, California
and
Egbert Torenbeek†
Delft University of Technology, Delft, the Netherlands

Previous work in the early 1970's has shown the merits of a (large) transonic oblique-wing transport. In this paper, the suitability of the oblique-wing planform for a small supersonic transport aircraft will be shown. The aircraft is designed to transport 24 passengers with first-class accommodations at a cruising speed of 1500 km/h over a distance of 5800 km. It complies to the JAR 25 and FAR 25 airworthiness requirements and the FAR 36 stage 3 noise regulations and is powered by two medium bypass turbofan engines. The proposed aircraft offers a typical increase in blockspeed of 53% at ranges of 4000–7000 km compared with similar small transport aircraft, with comparable fuel efficiency, range, and field performances.

Nomenclature

C_D	= drag coefficient
C_L	= lift coefficient
D	= drag
L	= lift
M	= flight Mach number
q	= dynamic pressure
S	= gross area (no index: wing)
T_{to}	= total engine thrust at SLS, ISA
t/c	= wing thickness-to-chord ratio
W_p	= design payload weight
W_{to}	= aircraft takeoff weight
$(W/S)_{to}$	= takeoff wing loading
$(W/T)_{to}$	= takeoff thrust loading
Λ	= sweepback angle at 25% chord of wing
ϵ	= ellipse ratio of wing
η	= overall engine efficiency

Subscripts

n	= normal to wing leading edge
h	= horizontal tail plane
to	= takeoff
v	= vertical tail plane

Introduction

TEN years after the introduction of the Concorde into commercial service, it is generally concluded that, despite its relatively high maintenance costs, its technology generally satisfies or exceeds the expectations at the start of the project. However, economically it does not fit into the current structure of air traffic due to its high fuel costs, and the high research and development costs cannot be negotiated by the small number of aircraft in operation. And though Concorde's high cruise speed reduces the time to travel drastically, the sonic boom it produces makes overland flights impossible at supersonic speeds.

Nevertheless, the Concorde's high load factors have shown that a market exists for faster and more comfortable passenger transport than is currently available. Present-day first-class, long-range, high-subsonic transportation does offer good spatial comfort and catering service, but the high-priced tickets do not result in reduced traveling times due to the moderate cruise speed and the long boarding times of large, wide-body aircraft.

A new type of aircraft with a maximum cruise speed of about 1500 km/h (Mach 1.4) and a maximum capacity of 24 passengers could have some advantages over both high-subsonic transports and the Concorde:

1) The cost of developing a low-supersonic aircraft is considerably less than that for a Mach 2 aircraft, especially when the aircraft has a limited passenger capacity.

2) A low-supersonic aircraft can be designed in such a way that supersonic overland flights become acceptable from an environmental point of view.

3) The low-speed performance of such an aircraft can be comparable to the low-speed performance of high-subsonic aircraft, in particular when the configuration is selected, which is proposed in the present article.

4) Such an aircraft could more easily be fitted into the present-day structure of holding patterns, approach speeds, and noise regulations.

Choice of the Configuration

Mascitti[1] showed some of the problems associated with the application of a symmetrical fixed wing to small supersonic transports:

1) Applying area ruling to the symmetrical wing/body configuration results in severely waisted fuselage contours at the fuselage center sections.

2) In view of the low lift-to-drag (L/D) ratios over the entire speed range, very low payload fractions could be achieved, resulting in high takeoff, empty weights and costly aircraft.

3) The poor low-speed aerodynamics do not allow the aircraft to operate from small airfields, thus significantly reducing operational flexibility and increasing the passenger's overall traveling time.

The oblique-wing configuration proposed by Jones[5] has the advantage that a near-cylindrical passenger cabin can be used, since the equivalent area distribution of the wing is better spread out longitudinally. The resulting higher L/D ratios increase the payload fraction significantly. The low-speed aerodynamic qualities of the aircraft can be made comparable to efficient subsonic transports, provided the wing is unswept at subsonic speeds.

Received April 5, 1987; revision received Feb. 15, 1988.

*Ph.D. Student, Department of Aero-Astro.

†Professor of Aircraft Design.

A disadvantage of such a concept is the need for a pivot structure and the limited data base available on oblique-wing designs. One of the main objections to the large oblique-wing transport designs of the early seventies[2]—that its cruise speed does not allow it to fit into the current transatlantic operations of the major airlines—may not apply to a low-supersonic transport operating at altitudes above 15,000 m.

The medium bypass ratios that will be required to fulfill the FAR 36 stage 3 noise requirements pose serious problems to a successful airframe-propulsion integration. For transonic aircraft, the wave drag of podded engines may be the single largest contribution to the total zero-lift drag due to the low engine mass-flow ratios in the transonic regime. Burying the engines in the rear fuselage section allows area ruling of the fuselage in such a way that there is virtually no extra spillage drag due to engine installation in subsonic cruise[2] and low extra wave drag in transonic flight.

The horizontal tail must be designed and located in such a way that good control over the aircraft and minimum trim drag are realized in all flight conditions. It is, therefore, objectionable to locate the tail close to the engine exhaust flow. For this reason, it was decided to select a T-tail configuration. The complexity of the T-tail structure is clearly a disadvantage, but its low drag and good control qualities make it superior to other positions. A long-coupled canard configuration was rejected because of the expected unfavorable aerodynamic interference with the flow over the high-mounted wing and through the engine inlet.

Baseline Design

A layout drawing of the proposed Small Supersonic Oblique-Wing Transport Aircraft (SSOTA) is shown in Fig. 1. During the design process, this configuration adapted many of the features of the earlier Boeing 5-3a design.[2] The oblique wing planform is mounted to the top of the fuselage by means of a pivot. It has an elliptic planform with an elliptic spanwise distribution of the thickness-to-chord ratio, resulting in minimum wave drag for a given volume.[3] For high-aspect-ratio oblique wings, the chordwise thickness distribution appears to have only a secondary effect on the equivalent body shape.

The provisionally selected NLR supercritical airfoil sections[4] achieve a high cruise C_l with very limited drag rise, allowing a buffet-free cruise L/D ratio near the unconstrained maximum value. The wing is designed for a normal lift coefficient of 0.9 and a normal Mach number of 0.7, allowing for a 1.3-g pull-up maneuver. The high t/c ratio of the supercritical wing (the root section has a t/c ratio of 15%) reduces wing weight and creates a sufficiently large fuel tank to contain all the fuel in the wing.

To obtain an elliptic spanwise lift distribution, the elliptic wing planform must obtain a uniform distribution of lifting pressures, even at large angles of yaw. This can be realized by giving the wing an upward curvature along the span. For the oblique wing with an ellipse ratio of 10, the optimum wing warp is described in Ref. 5.

The wing is swept during acceleration and cruise, maintaining a constant M_n of 0.7, resulting in a 60-deg sweep at a cruise Mach number of 1.4.

The minimum cruise altitude of 14,500 m at Mach 1.4 sets a maximum structural design equivalent airspeed of 170 m/s. The wing beam structure is based on graphite-epoxy honeycomb panels. This material is plied in such a way that the wing possesses enough stiffness to accommodate static and dynamic bending moments that result from aeroelastic deformation.

The wing is located on top of the center fuselage frame with load-bearing rings in between. These rings are integrated into the wing and the body without interrupting their carry-through structures. Vertical loads and rolling and pitching moments are transferred via the bearings at the circumference of the pivot. Shear forces are carried through the bearings and the pivot joint. Hydraulic and flight-control systems, running from the body to the wing, are routed through the center of the pivot. A gear drive attached to the fuselage and a rim fastened to the wing ribs actuate the sweep mechanism. It remains to be investigated whether such a configuration would be acceptable from a safety point of view.

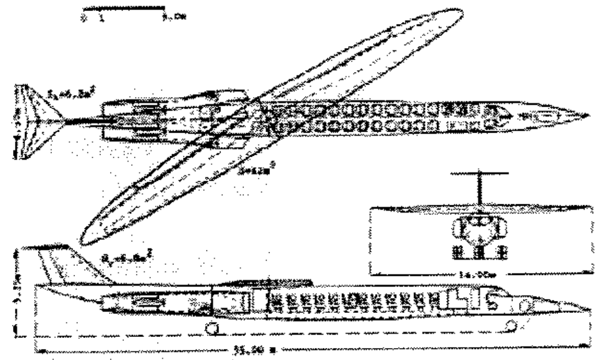

Fig. 1 Small, supersonic, oblique-wing transport aircraft layout.

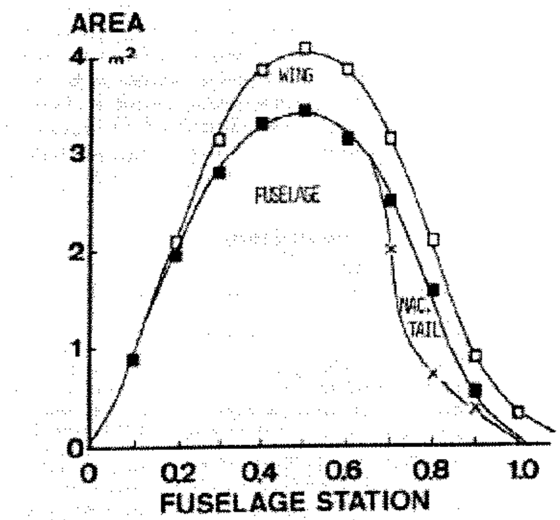

Fig. 2 Equivalent area distribution for the SSOTA configuration at Mach 1.4.

The external shape of the fuselage is to a great extent determined by the area distribution of the other aircraft components. However, the components locations have been chosen carefully in order to create a near-cylindrical cabin for maximum cabin-layout flexibility. The equivalent area distribution at Mach 1.4 is depicted in Fig. 2, which clearly illustrates that insertion of any substantially cylindrical fuselage section will seriously impair the area distribution.

Compared with small supersonic aircraft with fixed wings, and using a considerable waisting of the cabin, the resulting fuselage structural design problem is quite moderate in the proposed oblique pivoting wing configuration. It is now possible to design a near-cylindrical cabin with a minimal internal cross-sectional diameter of 1.70 m for the front row and up to 1.90 m for the center rows. There is very limited double curvature.

The cockpit layout is essentially similar to the one in the Gates-Learjet 35. Though not very spacious, this cockpit will accommodate two pilots with dual controls side by side. In combination with a suitable nose section it has a low-drag geometry.

The pressurized cabin, to be constructed of aramid reinforced aluminum laminate (ARALL) material, stretches from the rear of the baggagehold to the front bulkhead of the cockpit. Preliminary investigations have shown a typical 20%

weight reduction when ARALL is used in comparison to conventional materials.[5] Added to this comes the shielding effect of the fuselage to the wiring and avionics from electromagnetic interference.

To provide the aircraft undercarriage with adequate wheel track, the main gear hinge is mounted to an extension frame at about 75 cm distance from the rear bulkhead frame. The upper part of the gear leg is located in the nacelle structure aft of the inlet scoop. The wheels are retracted into the fuselage behind the rear pressure bulkhead. The nose gear hinge is mounted to the front pressure bulkhead.

Power-Plant Installation

The design goals for the engines were high cruise and climb efficiency, minimal power-plant weight, and acceptable development costs in case of selection of a new or modified engine. To comply to the FAR 36 stage 3 noise regulations, medium bypass ratio turbofan engines are required to reduce the exhaust jet velocity. To satisfy the thrust requirements during cruise, a turbine entry temperature (TET) in excess of 1600 K will have to be used.

To minimize wave drag, the engines are buried in the rear fuselage section. The utilization of this space for the power-plant installation is not penalized by any decrease in passenger cabin volume. The fixed-intake geometry is of the two-dimensional shock type. The air is compressed by one oblique and one normal shock. This will provide a good intake shock efficiency at the design Mach number 1.4 without the necessity of a variable geometry inlet. The intake is S shaped and separated from the sides of the fuselage to capture the undisturbed free air. Behind the straight diffusor section the inlet ducts are bent toward the aircraft centerline, and the duct area gradually diffuses, decelerating the air to an intake Mach number of about 0.50.

There are auxiliary air intake doors in the diffusor section. These doors guarantee sufficient inlet airflow and minimal compressor face distortion at takeoff. In addition, there are outlet doors to cope with excessive intake air in low power conditions. The rear nacelle structure houses the convergent-divergent nozzles. To avoid the complexity of a variable nozzle geometry, the SAAB-VIGGEN exhaust concept was used. During takeoff, an extra air inlet just behind the nozzle throat sucks the air into the divergent nozzle section, thereby avoiding overexpansion of the flow. At Mach 1.4 the exhaust gases can expand fully inside the condi-nozzle, thus providing maximum thrust and fuel efficiency.

Optimization of the Design

While complying with the specifications and additional geometric, airworthiness, and technological constraints, the wing ellipse ratio, thrust-to-weight ratio T/W, wing loading W/S, engine cycle, and bypass ratio have been optimized for maximum payload fraction (W_p/W_{to}). Reference 10 shows that this parameter will yield an optimum configuration that is sufficiently close to the configuration for minimum direct operating costs (DOC).

The optimization was carried out by means of the program AVSAD, developed by the first author. Based on the methodology of Refs. 7 and 10, this program uses parametric input and available technological information to generate realistic aerodynamic, weight, and performance data for supersonic aircraft. The AVSAD program was tested for seven supersonic designs by NASA, Boeing, and MDD, as well as Concorde, with cruise Mach numbers ranging from 1.2–2.7 and W_{to} ranging from 360–3400 kN. It was found that the major aerodynamic weight and performance data were typically within a 15% error margin from the data generated by the various design teams.

A typical plot used to select T/W, W/S, and the ellipse ratio is shown in Fig. 3. After comparing plots for different ellipse ratios, it was concluded that $\epsilon = 10$ represents the optimum value. Reducing ϵ decreases the payload fraction, whereas increasing it results in violation of the various design constraints indicated in Fig. 3:

1) The initial cruise altitude of at least 14,500 m.

2) The bow shock wave from the fuselage nose must not hit the forward wing tip at $M = 1.5$ to avoid flutter problems.

3) Excessive additional engine nacelle wave drag should be avoided by restricting the engine mass flow to 50 kg/s.

4) The wing must have enough volume to contain all the fuel for the transatlantic flight.

5) A buffet-limited cruise lift coefficient of 0.23 has been assumed.

From Fig. 3, it can also be derived that it is not useful to increase the C_L constraint, unless the t/c limit would also be

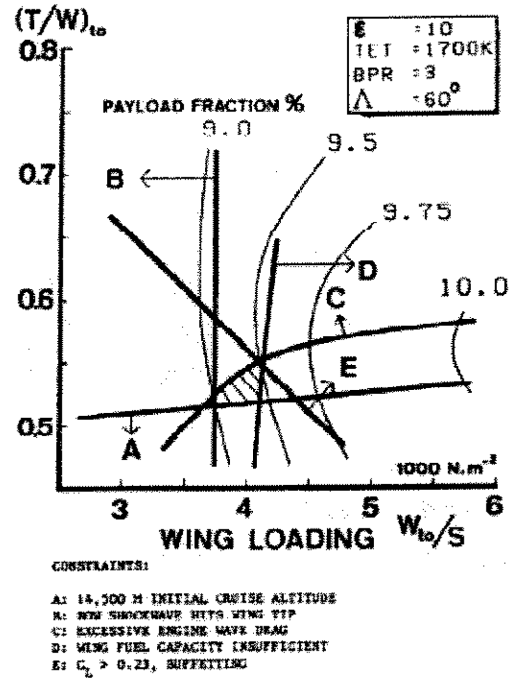

Fig. 3 Wing- and thrust-loading optimization.

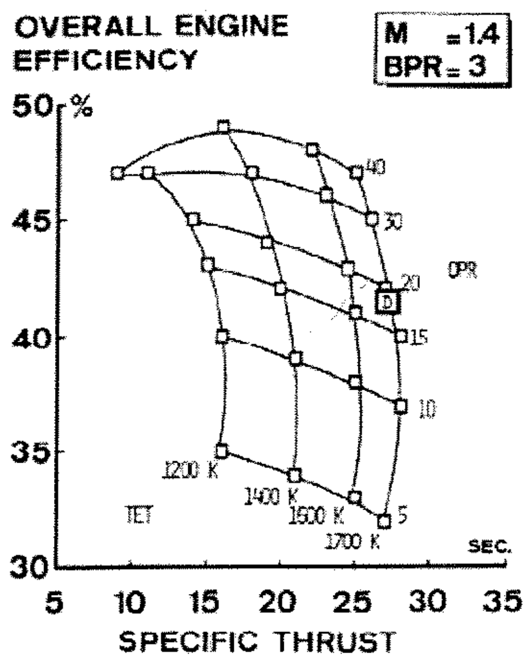

Fig. 4 Engine cycle optimization.

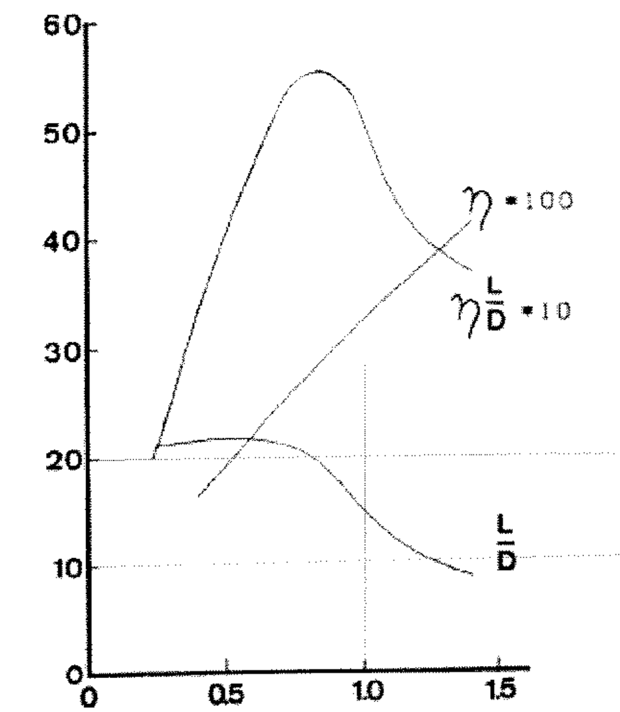

Fig. 5 Variation of L/D and overall engine efficiency with Mach number.

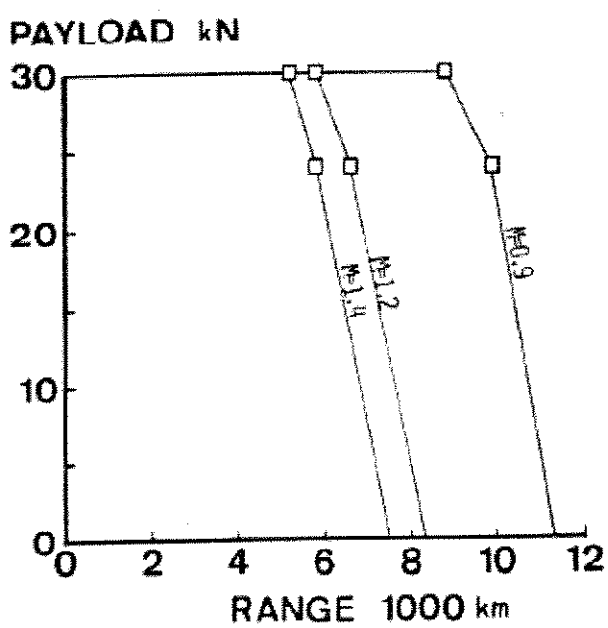

Fig. 6 Payload-range diagram.

relaxed. Inside the feasible region the best design is obtained for a T/W of 0.55 and a wing loading of 4.1 kN/m^2.

The engine optimization is concentrated on the design condition (cruise). The TET and overall pressure ratio (OPR) were optimized for maximum overall efficiency at sufficient thrust. In Fig. 4, it is shown that, for a bypass ratio (BPR) of 3, a TET of 1400 K, and an OPR of 40, an overall engine efficiency of 48% can be achieved. However, at this TET only 50% of the 27-s initial specific thrust requirement at cruise is met. Maximum specific thrusts are typically reached at OPR

Table 1 Drag breakdown at $M = 1.4$, $C_L = 0.23$, $h = 15{,}200$ m

Drag Component	Drag coefficient
Friction	
Wing	0.0052
Fuselage	0.0038
Tail/nacelle	0.0019
Wave	
Wing	0.0011
Fuselage	0.0028
Tail/nacelle	0.0028
Roughness	0.0015
Lift	
Induced	0.0062
Wave	0.0011
Total	
Drag coefficient	0.0264

Table 2 Weight breakdown for the harmonic range (5800 km/3130 nm)

Weight component	Weight, kN
Structure	
Wing	21.4
Fuselage	30.6
Tail	4.8
Undercarriage	10.0
Nacelles	9.8
Power plant	23.9
Systems and equipment	32.3
Operational/miscellaneous items	8.5
Payload	
18 Passengers	18.0
Baggage	6.0
Fuel	
Trip	78.0
Reserve	11.0
Maximum takeoff weight	254.3 kN (57,150 lb) 25923 kg

values of 15. A good design compromise appears to be point D, with an OPR of 18 and a TET of 1700 K.

To keep the engine development costs as low as possible, the core of the RB 199 with a BPR of 3 fan was selected. The RB 199 is used in the Tornado fighter and is still being improved further. With a BPR of 3, only limited acoustical lining will be necessary, while a high overall efficiency and sufficient thrust can be obtained.

Design Characteristics

In Fig. 5, the effects of Mach number variation on maximum L/D and engine efficiency are shown; in Table 1, the drag breakdown for Mach 1.4 cruise is given. The maximum aerodynamic efficiency at cruise is not more than 8.7, whereas at Mach 0.7 a value in excess of 20 can be reached. The reason for this lies primarily in the high value of the sweep angle during cruise, compared with the high-aspect-ratio subsonic configuration.

The weight breakdown for the transatlantic range and design payload is given in Table 2. This shows the relatively low fuel weight fraction, which is obtained because the relatively low L/D ratio is compensated by a high engine efficiency. In addition to this, the oblique-wing configuration significantly reduces the reserve fuel fractions necessary for holding and flight to an alternate airport. The high cruising speed will enable the aircraft to operate under ETOPS regulations over the North Atlantic routes.

The takeoff and climb performance is such that the aircraft is able to take off from almost all international airports. At W_{to}, the aircraft requires a balanced field length of only 1100 m and reaches the initial cruise altitude of 15,000 m in less than 15 min. The SSOTA is able to fly at blockspeeds that are on average 53% higher compared to existing aircraft, at ranges between 4000 and 7000 km. Figure 6 gives the payload vs range diagram.

Though the sonic boom overpressures (47 N/m^2 at initial cruise) are significantly lower than those for the Concorde, it is very doubtful whether this value will be acceptable to the public, so the overland cruise Mach number may have to be limited to a value near Mach 1.2, allowing boomless supersonic flight in a standard atmosphere.

Aeroelastic Aspects and Stability and Control

The SSOTA has a sufficient tail volume to maneuver and control the aircraft in all conditions. For the entire speed and center of gravity (c.g.) envelope, adequate static stability can be shown to exist.

After significant simplification of the problem, a method was derived to determine the stability derivatives and the motion matrix of all medium- and high-ellipse-ratio oblique wing/body configurations in subsonic flow. It was found that the natural frequencies of both the short-period longitudinal oscillation and the dutch roll were typically 1 rad/s for all sweep angles. According to MIL requirements,[8] the aircraft can be controlled for $C_L > 0.3\cos\Lambda$ without stability augmentation.

A lateral stability augmentation system will have to be designed for normal flight. In the asymmetric configuration, all oscillations will involve simultaneous pitching, rolling, and yawing motions, making it very difficult for the pilot to control the aircraft. In view of the cross-coupling effects involved, design of such an augmentation system will be more difficult than that for a symmetrical aircraft.

If the automatic unsweeping mechanism fails during approach, the aircraft cannot be landed on small airfields. To cope with this problem, a manual backup system is installed to unsweep the wing.

The oblique wing of the SSOTA does not show aeroelastic divergence up to values of 4 q at cruise, i.e., twice the Federal Aviation Administration (FAA) limit. Stabilized bank angles will originate after excitation of the leading or trailing wing. It will therefore be necessary to install an active stability augmentation system to correct the bank angle continuously. This system may use the outboard placed ailerons as a control surface, since they do not increase the aeroelastic instability once they are used both to the same deflection. The fact that aileron effectiveness is not influenced by aeroelastic effects renders high-speed inboard ailerons unnecessary.[9]

Conclusions

1) The oblique-wing configuration is very suitable for small transport and executive aircraft flying at transonic and low-supersonic speeds.

2) The performance of the present aircraft design in terms of fuel efficiency, range, and comfort is comparable to existing subsonic aircraft, whereas the maximum cruise speed is increased by 75%. The block speed increment is in excess of 50%.

3) The technology to manufacture this aircraft exists today, and it can therefore be expected that the costs of developing, manufacturing, and operating such an aircraft will be acceptable.

References

[1]Mascitti, V. R., "A Preliminary Study of the Performance and Characteristics of a Supersonic Executive Aircraft," NASA TM-74055, Vols. 1 and 2, 1977.

[2]Kulfan, R., McBarron, J. P., Mulally, A. R., Neumann, F. D., Gimmestad, D. W., Murakami, J. K., Nisbet, J. W., Noble, E. C., Stalten, J. L., and Sussman, M. B., "High Transonic Speed Transport Aircraft Study," NASA CR-114658, Sept. 1973.

[3]Smith, J. H. B., "Lift/Drag Ratios of Optimized Slewed Wings at Supersonic Speeds," *Aeronautical Quarterly*, Vol. 12, Aug. 1961, pp. 201–218.

[4]Sloof, J. W. and Voogt, N., "Aeronautical Design of Thick Supercritical Wings Through the Concept of Equivalent Subsonic Pressure Distribution," NLR MP 78001U, 1978.

[5]Graham, L. A., Jones, R. T., and Boltz, F. W., "An Experimental Investigation of Three Oblique Wing and Body Combinations at Mach Numbers Between 0, 60, and 1.40.," NASA TM-X-62256, April 1973.

[6]Vogelesang, L. B. and Gunnink, J. W., "ARALL, a Material for the Next Generation of Aircraft, a State of the Art," Delft Univ. of Technology, Rept. LR-400, Aug. 1983.

[7]Torenbeek, E., *Synthesis of Subsonic Airplane Design*, student ed., Delft Univ. Press/Nijhoff, Delft, The Netherlands, 1982.

[8]Anonymous, "Flying Qualities of Piloted Airplanes," MIL-F-8785B (ASG), Aug. 1969.

[9]Jones, R. T. and Nisbet, J., "Aeroelastic Stability and Control of an Oblique Wing," *Aeronautical Journal*, Vol. 20, Aug. 1976, pp. 365–369.

[10]Torenbeek, E., "Fundamentals of Conceptual Design Optimization of Subsonic Transport Aircraft," Delft Univ. of Technology, Dept. of Aerospace Engineering, Rept. LR-292, 1980.

FIGURE 1. "SMALL SUPERSONIC OBLIQUE WING TRANSPORT AIRCRAFT LAYOUT" BY AJM VANDERVELDEN

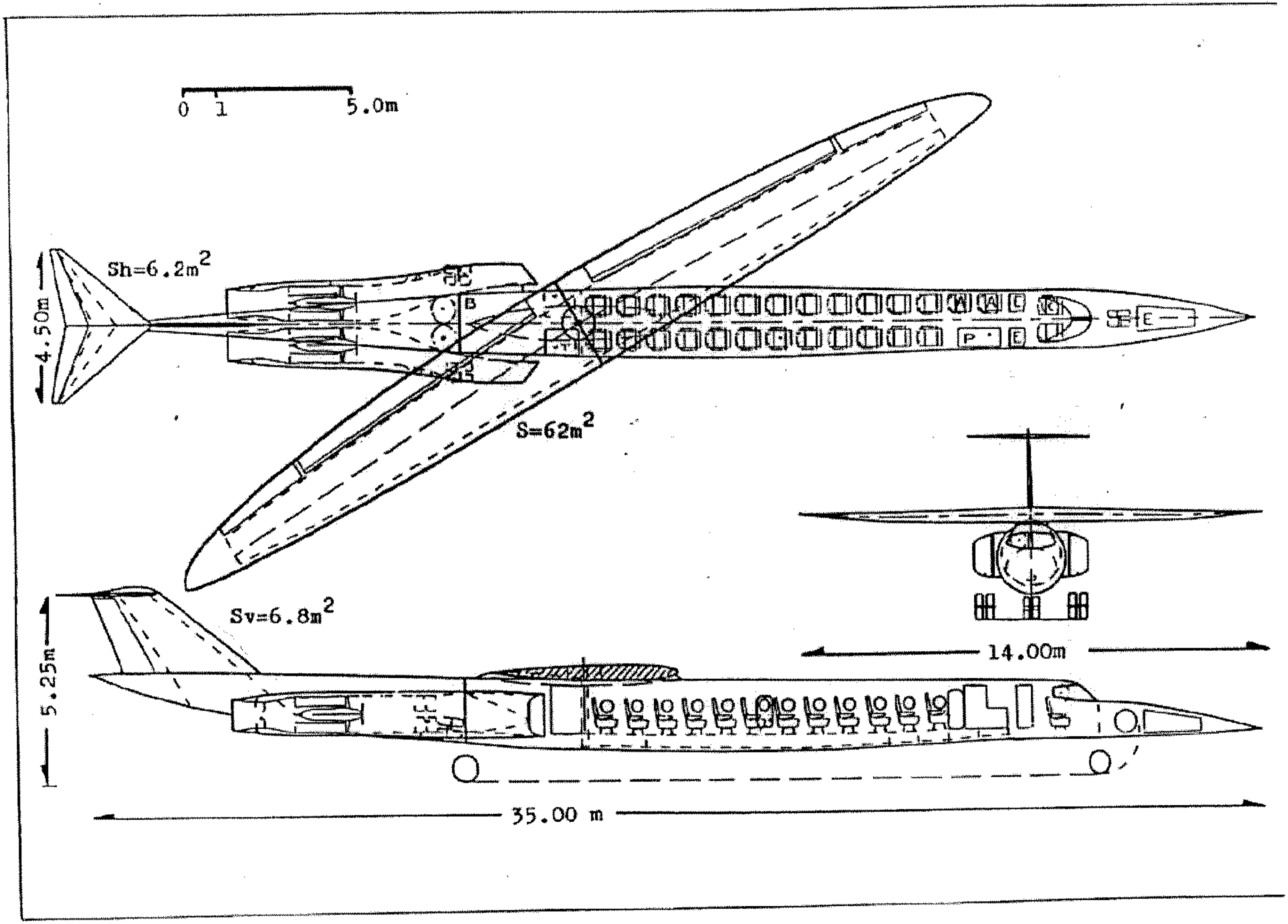

The Joined Wing: An Overview

Julian Wolkovitch
ACA Industries, Inc., Torrance, California

Nomenclature

A	= aspect ratio, b^2/S
B	= span ratio (rear wing/front wing)
b	= span
b'	= effective span (see Sec. II)
C	= chord ratio (rear wing/front wing)
C_D	= drag coefficient, drag/qS
C_L	= lift coefficient, lift/qS
C_m	= moment coefficient, pitching moment/$qS\bar{c}$
C_n	= yawing moment/qSb
C_l	= rolling moment/qSb
$\bar{c}$	= reference chord
d'	= effective beam depth (see Sec. II)
e	= span-efficiency factor
GPA	= gross projected area of all lifting surfaces on a plane containing the aircraft longitudinal axis and normal to the airplane's plane of symmetry
L	= lift
n	= load factor
q	= dynamic pressure
S	= reference area
W	= gross weight
W_w	= wing weight
α	= angle of attack
β	= sideslip angle
Γ	= dihedral angle
ϵ	= downwash angle
Λ	= sweep angle of quarter-chord line
λ	= taper ratio (tip chord/root chord)

Subscripts

F	= front wing
R	= rear wing

I. Introduction

THE joined-wing airplane may be defined as an airplane that incorporates tandem wings arranged to form diamond shapes in both plan and front views.[1-3] This general concept can take different forms, as shown in Figs. 1-4, which show joined-wing tunnel models. All the models obtain the desired diamond-shaped front view by locating the root of the rear wing at or near the top of the vertical tail(s). Figure 1 shows a transonic model[4] having wings joined by means of streamlined tip bodies. Figure 2 shows a wind tunnel model that combines a joined wing with a 60-deg sweep canard.[5] In both the configurations shown in Figs. 1 and 2, the wing-joining members are small bodies, but it is also possible to join the wings by lifting surfaces (winglets) as shown in Fig. 3. This configuration uses twin fins to support the center section of the rear wing. The interwing joint may also be located inboard of the tips as shown in Fig. 4; this shows a wind tunnel model of a design for an agricultural airplane.[6] In this design the pilot is located in the vertical tail, which has an airfoil of 18% thickness/chord ratio. Other joined-wing arrangements are possible, as described in Refs. 1-3.

Advantages claimed for the joined wing include:

1) Light weight.
2) High stiffness.
3) Low induced drag.
4) Good transonic area distribution.
5) High trimmed C_L max.
6) Reduced wetted area and parasite drag.
7) Direct lift control capability.
8) Direct sideforce control capability.
9) Good stability and control.

These claims have been supported by independent analyses, design studies and wind tunnel tests, as described later.

Joined wings differ from conventional wings in their internal structure as well as their external configuration. This important difference is illustrated in Figs. 5 and 6. Figure 5 shows how the lift loads acting on each wing can be resolved into components acting normal and parallel to the truss structure formed by the joined wings. The in-plane components are well resisted by the truss structure. The out-of-plane components tend to bend the wings about a tilted bending axis, as shown in Fig. 5. To resist this, the wing structural material must form a deep spar about this axis. This implies that the material must be concentrated near the upper leading edge and lower trailing edge, as shown in the lower portion of Fig. 5.

The above arrangement is different from that of a cantilever wing. Figure 6 portrays schematically a section of a typical subsonic transport wing. The lift loads on the wing are resisted by a box beam extending from typically 15% to 65% of the chord. The box beam also serves as a fuel tank. Over most of the span, the box beam employs upper and lower skins which,

---

Dr. Wolkovitch received his B.S., M.S., and Ph.D. degrees in Aeronautical Engineering from the University of London. Since 1954 he has been engaged in design and research in aerodynamics and control systems of airplanes, missiles, and helicopters. Initially he was employed by Folland Aircraft Ltd. in England. After immigrating to the U.S. in 1958, he joined the Convair Division of General Dynamics Corporation. Subsequently he was employed by Systems Technology Inc., Mechanics Research Inc., and Vought Corporation. Since 1982 he has been President of ACA Industries, Inc., a small research and consulting company. Much of his recent effort has been devoted to the joined wing, including research studies for the U.S. Navy, NASA, and other government agencies, and consulting for airframe manufacturers. He has authored numerous technical papers, and was awarded the Wright Brothers Medal of the Society of Automotive Engineers.

Presented as Paper 85-0274 at the AIAA 23rd Aerospace Sciences Meeting, Reno, NV, Jan. 14-17, 1985; received Jan. 29, 1985; revision received Oct. 18, 1985.

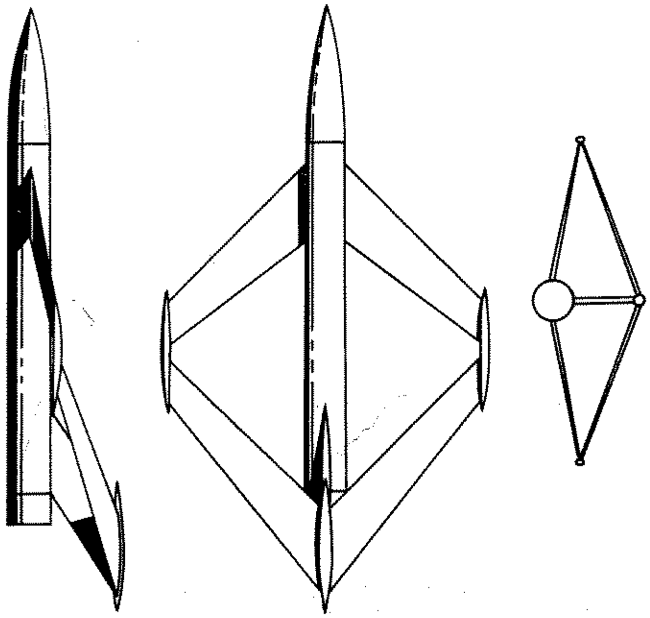

Fig. 1 Rockwell transonic wind tunnel model.

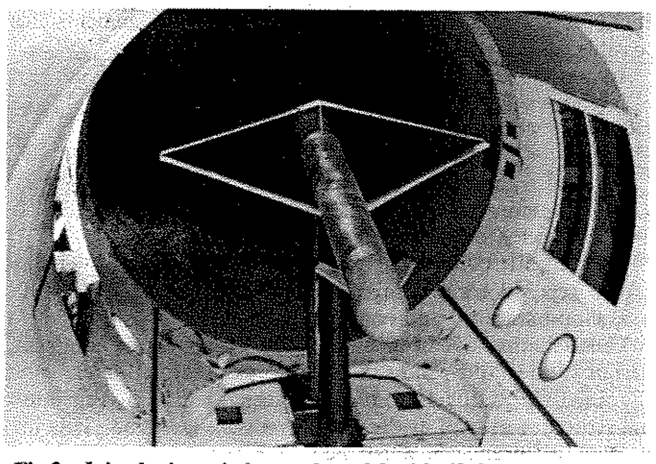

Fig.2 Joined-wing wind tunnel model with 60-deg sweep canard.

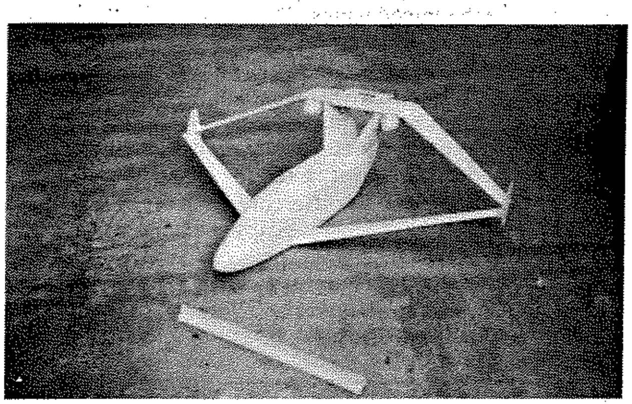

Fig. 3 University of Kansas wind tunnel model with twin fins and winglets.

at a given spanwise station, are of relatively constant thickness across the chord of the beam. This is expected because the maximum bending strength for a given weight of structural material is obtained by maximizing the second moment of area of the beam about its bending axis. Hence, it is not profitable to extend the structural box forward of 15% or aft of 65% of the airfoil chord since in these regions the airfoil thickness (beam depth) is less than in the midportion of the airfoil.

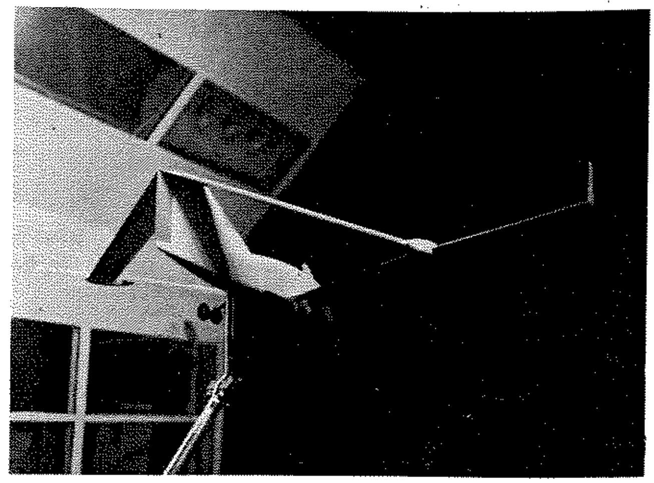

Fig. 4 NASA wind tunnel model of agricultural airplane design.

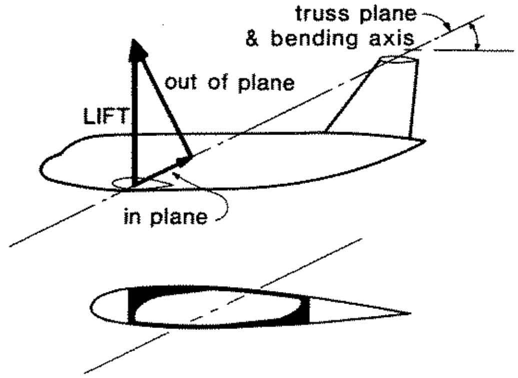

Fig. 5 Tilted bending axis of a joined wing.

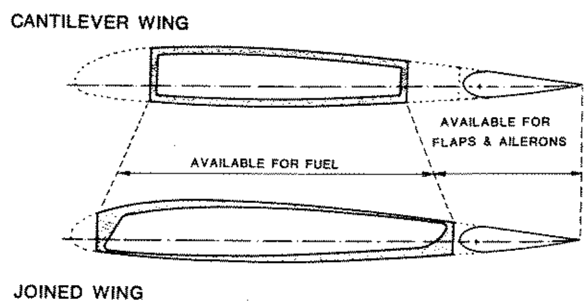

Fig. 6 Optimum wing structures.

As explained above and in Refs. 1,3, and 7, the joined wing's strength/weight ratio is maximized by concentrating the bending-resistant material near the upper leading edges and lower trailing edges. Consequently, an optimum joined-wing structure occupies large percentages of the chords of its airfoils. For both the front and rear wings, the structural box may extend from the leading edge to the trailing edge of the fixed part of the airfoil. The limits are set by the space needed for deicing systems, flaps, high-lift devices, and actuators. The effective beam depth of a joined wing is primarily determined by the chord of its airfoils; their thickness is secondary. Hence, thin airfoils may be employed with less weight penalty than for cantilever wings.

Finite element structural analyses[7] confirm that, except in certain limited regions (e.g., near the interwing joint), the optimum material distribution conforms to the above simple model.

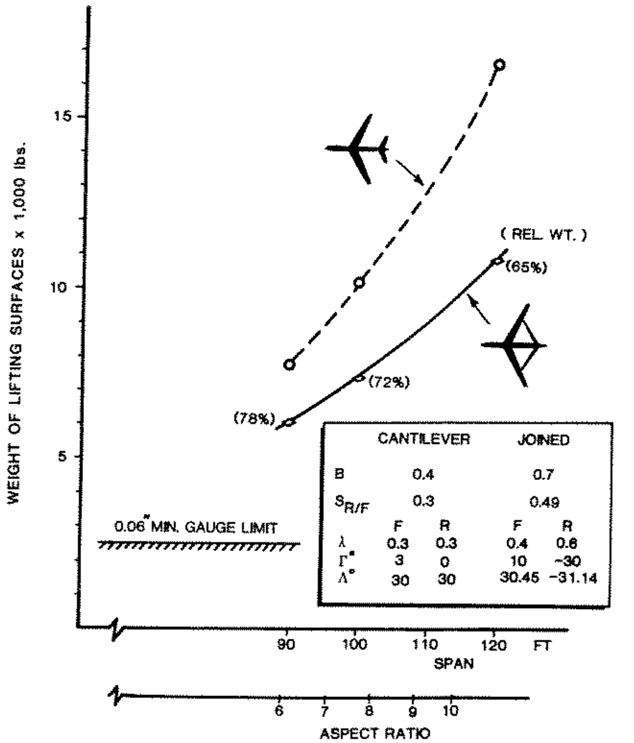

Fig. 7 Weight of lifting surfaces of turboprop transports vs aspect ratio.

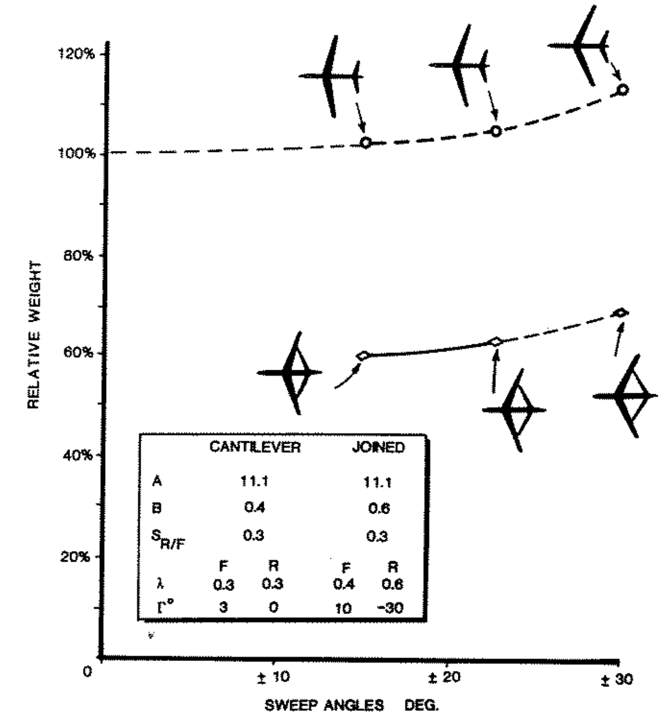

Fig. 8 Effect of sweep on relative weight of lifting surfaces of turboprop transports.

Organization of This Paper

It is important to understand that the joined wing is a highly integrated concept that links structural and aerodynamic features in novel ways. The present paper, therefore, first outlines the structural principles of the joined wing (in Sec. II). These principles must be understood in order to effectively perform joined-wing aerodynamic design, which is discussed in Sec. III. Stability and control aspects of joined wings are examined in Sec. IV. The close interaction of joined-wing structural and aerodynamic characteristics provides some novel problems of configuration design, which are discussed in Sec. V. Specific designs, projects, and concepts employing joined wings are presented in Sec. VI, together with a brief assessment of the performance benefits of the joined wing. Conclusions are given in Sec. VII, which is followed by an Appendix giving historical and technical information on other aircraft configurations related to the joined wing.

II. Results of Structural Analyses

Weight Comparisons

Shyu and Miura, of NASA Ames Research Center, have performed comprehensive structural analyses of joined wings, employing the EAL, SPAR, and NASTRAN finite element programs.[8] Reference 10 compares their results with the results obtained independently by Samuels[7] and Hajela,[11] who employed the SAP-5 and ACCESS-3 finite element programs, respectively. Reference 10 shows that the results obtained by Shyu and Miura are consistent with those of Samuels and Hajela.

By analyzing wider ranges of geometric parameters than were studied by Samuels or Hajela, Shyu and Miura found some joined-wing configurations that gave large weight savings. For example, Fig. 7 shows results of Refs. 8 and 9 showing the effect of sweep on the weights of transport wings. This figure compares the weights of joined vs conventional wing-plus-tail systems that are aerodynamically equivalent. That is, both systems have the same gross projected areas, equal taper ratios, equal magnitudes of sweep angles (sweepback for the wing and tail, sweepback and sweepforward for the joined wing), and equal ratios of front to rear lifting surface projected areas. The total design airloads and the structural material properties were also made equal in these comparisons, which employed identical optimization techniques. A streamwise thickness/chord ratio of 12% was employed for all lifting surfaces. Figure 7 shows that the joined wing typically weighs 65 to 78% of the weight of the aerodynamically equivalent cantilever wing-plus-tail. (The above comparison and the others cited here include all the nonmovable portions of the wing, including the inter-wing joint. Control surface weights are not included for either the joined or conventional configurations and are approximately equal for both types of wing systems.)

The above comparison did not exactly achieve the condition for aerodynamic equivalence since the quarter-chord sweep angles of the joined wing (30.45, −31.14 deg) were slightly larger than those of the cantilever wing and tail (30 deg on each surface). The relative advantage of the joined wing improves as sweep is reduced. This is shown in Fig. 8, which graphs further results of Shyu and Miura.[8,9] Figure 8 compares the weights of aerodynamically equivalent systems constructed from aluminum and employing a streamwise thickness/chord ratio of 12.0%. The relative weights are graphed vs the magnitude of the sweep angle employed on each lifting surface (positive and negative for the joined wing, positive for the conventional system). At least one surface of the joined wing must be swept, whereas the cantilever wing and tail can both be unswept. Nevertheless, the joined wing shows a large weight saving at all sweep angles. For example, at 15 deg sweep the joined wing weighs only 58% of the 15-deg sweep wing-plus-tail and approximately 60% of the unswept cantilever system.

Joined wings are not invariably lighter than aerodynamically equivalent conventional wing-plus-tail systems. Weight will be saved only if:

1) The geometric parameters of the joined wing such as sweep, dihedral, taper ratio, and joint location (as a fraction of the span) are properly chosen.

2) The internal wing structure is optimized, with the wing box occupying the section of the airfoil between 5 and 75% chord (or greater if possible).

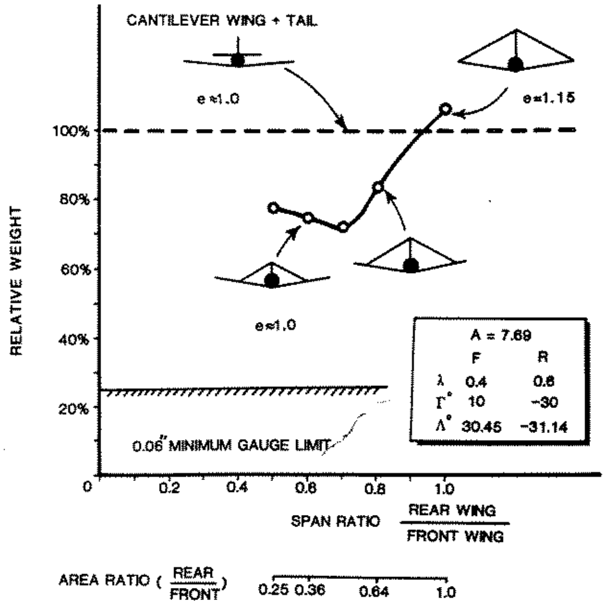

Fig. 9 Effect of span ratio on relative weight and span-efficiency factor.

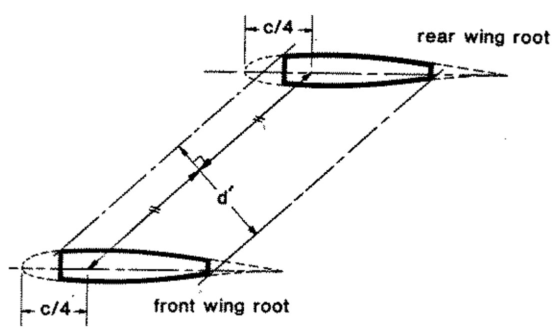

Fig. 10 Effective beam depth parameter.

Guidance on the selection of the geometric parameters for minimum weight is given below.

Effect of Joint Location

For a given span, GPA, and maximum lift, with constant sweep and dihedral angles, locating the interwing joint inboard provides a lighter wing system than joining the wings at their tips. However, the tip-jointed arrangement has some aerodynamic advantages (such as higher span-efficiency factor, suitability for winglets, and greater trimming moment capability). In general, joint locations of from 60-100% of the span must be considered to arrive at an overall optimum design.

The above considerations are illustrated in Fig. 9, which graphs results of Refs. 8 and 9 on the effect of span ratio on weight. Figure 9 shows that, for the particular taper ratios considered (0.3 for the cantilever surfaces, 0.4 and 0.6 respectively, for the front and rear joined wings), the lightest joined wing is obtained with a span ratio of 0.7, i.e., the tip of the rear wing structure connects to the front wing structure at 0.70 of the span of the front wing. Figure 9 also shows that the tip-jointed configuration is heavier than the cantilever system of the same span. Therefore, it might be thought that the tip-jointed configuration need not be considered further. However, this would not be correct: as noted in Fig. 9, the tip-jointed configuration has a span-efficiency factor e, which (as discussed later) is substantially higher than that of the inboard-jointed configuration or that of the cantilever configuration. Thus, to obtain true aerodynamic equivalence, the span of the tip-jointed joined-wing configuration should be reduced to give the same induced drag (at equal weight and speed) as the conventional configuration. If this is done, and if higher taper (taper ratio = 0.3) is employed on both the front and rear wings, it is found that the tip-jointed configuration weighs approximately 80% of the weight of the cantilever wing-plus-tail. This is still higher than the optimum achieved by the configuration having the wings joined at 70% span. However, the weight advantage of the latter is not so great that it could not be overriden by aerodynamic advantages of the tip-jointed configuration, such as higher trimming moments or suitability for winglets. This example emphasizes the need to consider several joint locations in determining an overall optimum design and to integrate structural and aerodynamic considerations.

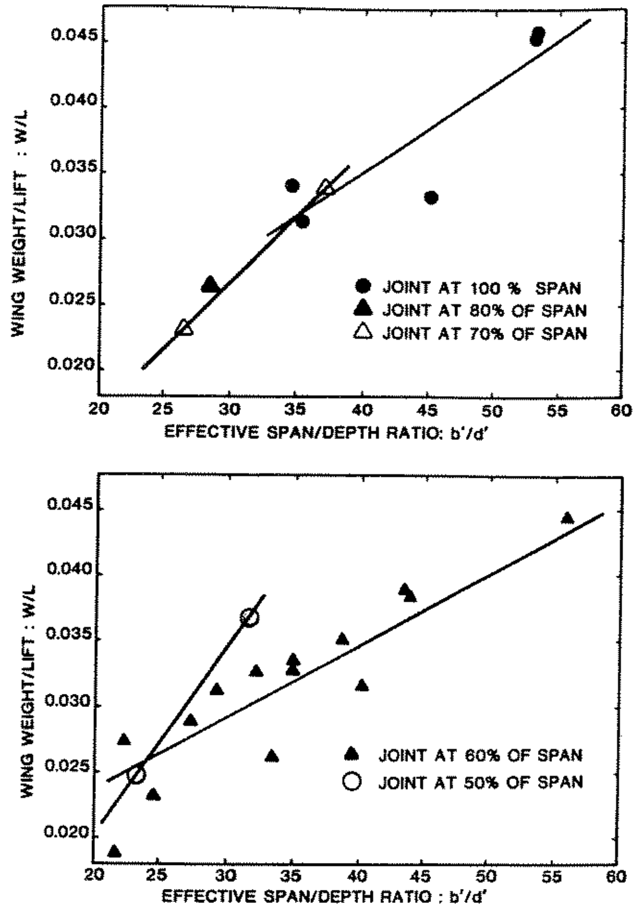

Fig. 11 Correlations of computed weights vs effective (depth/span) ratio parameter.

Weight Prediction

For conventional wings, weight data are frequently correlated in terms of span, maximum root chord thickness, and other geometric parameters, as well as material properties. Reference 10 shows that similar correlations can be produced for joined wings using two parameters denoted as effective depth (d') and effective span (b'). The effective depth parameter is defined from the root centerline chords of the front and rear wings as shown in Fig. 10. The effective span is defined as the mean of the true (not projected) lengths of the quarter-chord lines of the front and rear wings and is given by

$$b' = 0.5[(b_F/\cos\Gamma_F\cos\Lambda_F) + (b_R/\cos\Gamma_R\cos\Lambda_R)]$$

The ratio of b' to d' will be referred to as the effective span/depth.

Figure 11 shows the results of correlating W_W/L, $(=W_W/nW)$, wing system weight/lift with the effective span/depth for the joined wings considered in Ref. 8. These included variations of the parameters in Table 1.

The correlations of Fig. 11 show that the weight is minimized by decreasing the effective span/depth ratio. This requires: 1) Large dihedral (positive and negative), 2) Low sweep angles (positive and negative), and 3) High taper ratios (front and rear).

Reference 8 shows that the sensitivity of weight to the thickness/chord ratio is typically 30% less for joined wings than for cantilever wings. Joined wings are therefore particularly suitable for thin airfoils.

Special Structural Characteristics

Column Buckling Considerations

Under positive load factors, the rear wing of a joined-wing pair is in compression. Therefore, overall column buckling must be considered. In the work of Shyu and Hajela reported above, buckling was checked using the "differential stiffness" option of NASTRAN. Buckling was not found to be a constraint. The minimum wing thickness/chord ratio employed was 0.12; thinner wings would be more prone to exhibit column buckling phenomena. To avoid this, pin-joints with horizontal axes should not be used on joined wings. For ultrathin wings minimum weight may be obtained by employing a strut linking the leading edge of the rear wing to the trailing edge of the front wing. The column length of the rear wing can also be reduced by employing twin fins, as in Fig. 3, and/or an inboard location for the interwing joint.

The torsional stiffness of joined wings is high since torsion of one wing is resisted by flexure of the other (see Fig. 12). This leads to higher aileron effectiveness than is obtainable with cantilever wings of comparable weight. It also yields higher flutter speeds, as described below.

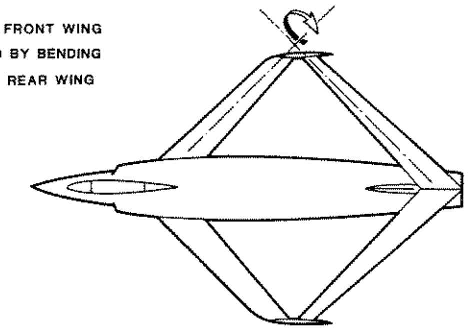

Fig. 12 Resistance of torsion of one wing by flexure of the other.

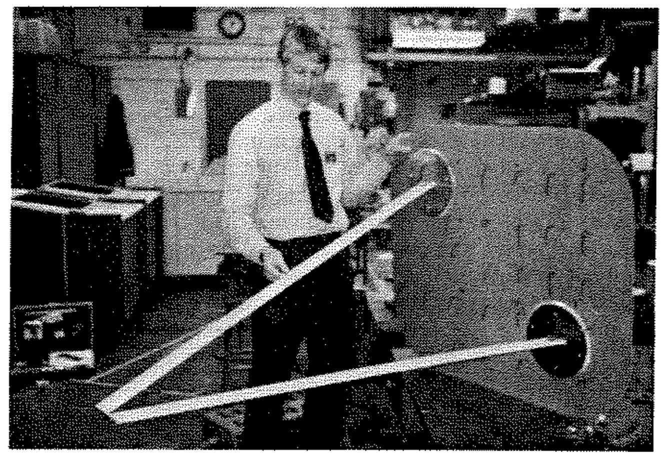

Fig. 13 NASA Langley joined-wing flutter model.

Aeroelasticity

Aeroelastic characteristics of joined wings have been studied by theoretical analyses[7,12] and also by tests performed on flutter models.[13] These tests were performed in the NASA Langley Research Center variable density transonic dynamics tunnel. Half-models of high-altitude RPV wing concepts were tested, comparing joined vs cantilever wings of equal span, weight, and GPA. Figure 13 shows the joined-wing model. The aspect ratios of the models were high ($A=21.6$ for both models, giving $A=43.2$ for each individual joined wing). The tests were performed at $M=0.4$ and 0.6. At each Mach number, the dynamic pressure for aeroelastic instability (q') was found to be approximately 1.6 times the value of q' for the cantilever wing. It should be noted that the internal structure of the joined-wing model did not employ the optimum leading-edge/trailing-edge (L.E./T.E.) spar arrangement of Fig. 6. Instead, a single spar was used, located at approximately 40% chord. It is possible that still better results would have been obtained if the spar arrangement had been optimized.

Other aeroelastic analyses of joined wings have been performed, e.g., Ref. 12. This reference predicts large gains in flutter speed for the joined wing, but does not compare aerodynamically equivalent systems and apparently neglects the fore-and-aft degree of freedom of joined wings. This is significant and was included in the other references cited. In general, flutter analyses of joined wings should consider the effects of horizontal as well as vertical displacements of wing elements.

Fuselage Structural Weight and Stiffness

In general, under maximum positive load factor, the front and rear wings of a joined-wing pair both lift upward. Thus, the fuselage is supported near both ends: by contrast, a conventional wing-plus-tail system supports the fuselage near its middle, with the tail applying a trimming download. The net result is that the fuselage bending moments produced by a joined wing are smaller than those produced by a comparable wing-plus-tail. Lateral and torsional fuselage loads may also be reduced since the joined wing provides additional load paths to withstand rolling and yawing moments applied by gusts or by control surfaces. The savings in fuselage structural weight obtainable through the joined wing depend on the extent to which the fuselage is designed by pressurization loads as opposed to airloads. However, for many fuselages it would appear that significant weight can be saved, and this aspect of the joined wing deserves further study.

Table 1 Parameter variations for joined wing (Refs. 8 and 9)

Parameter	Min.	Max.
Aspect ratio, $A=b^2/\mathrm{GPA}$	4.81	16.25
Span ratio, $B=b_R/b_F$	0.5	1.0
Area ratio, $B/C=S_R/S_F$	0.3	1.0
Taper ratio λ_F, λ_R	0.20, 0.25	0.75, 0.75
Sweep, Λ_F, Λ_R deg.	15.0-15.0	45.0-45.0
Dihedral Γ_F, Γ_R deg.	5.0-10.0	30.0-30.0
Thickness/chord ratio	0.12	0.15

Fin Structure

The fin must support symmetric and asymmetric loads transmitted via the rear wing root. This does not necessarily lead to a heavy fin structure because:

1) For a given overall sideslip angle, the total sideforce acting on the fin and wings is considerably less than would act on these components in isolation. This is due to the flow-straightening effect of each component on the others.

2) Due to the large anhedral of the rear wing, sideslip-induced rolling moments that it applies to the fin root op-

pose those due to fin sideforces. The rear wing also provides substantial inertia relief.

Twin fins having approximately 60-deg dihedral can be employed, as shown in Figs. 3 and 14. This arrangement reduces the unsupported column length of the rear wing and permits mounting the engines in the "armpit" formed by the fin and rear wing. In this location the engines are rigidly supported, and the pusher or tractor propellers produce little noise in the passenger cabin. The "armpit" mounting also eliminates some of the wetted area of the nacelles, fins, and rear wings. The twin-fin arrangement requires that the rear wing center section have little or no sweep and no dihedral. Since this portion of the wing is lightly loaded in cruise, these requirements may well be acceptable from an aerodynamic viewpoint.

Structure of Joined-Wing Wind Tunnel Models

The structural design of joined-wing wind tunnel models has been a recurring source of difficulty. The wings of wind tunnel models are typically machined from slabs of uniform (solid) material. Hence, they do not have the optimum concentration of structural material shown in Fig. 6. Relative to comparable "solid" cantilever wings, "solid" joined wings contain less volume of structural material, and it is not as well distributed to resist lift loads. The problem is compounded by the standard practice of using simple beam formulas to calculate stresses in wind tunnel models. This is adequate for cantilever wings but is not acceptable for joined wings. Any wind tunnel program involving joined wings must include adequate stress analyses by finite-element methods to check model safety and predict aeroelastic deflections.

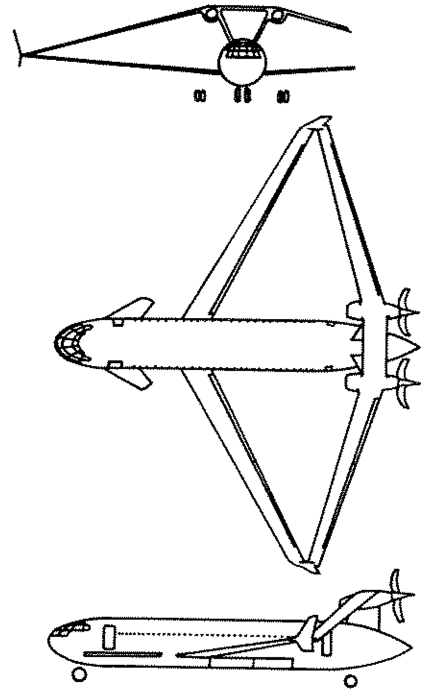

Fig. 14 Turboprop transport configuration with aft-mounted engines.

III. Joined-Wing Aerodynamics

Induced Drag

This subsection presents results relating to induced drag computed by standard Prandtl-Munk biplane theory. This theory assumes that the vortex sheet shed by the front lifting surface remains undistorted (no roll-up) and parallel to the freestream (no downward drift). Munk[14] noted that the latter assumption overestimates the induced drag of back-staggered configurations because it overpredicts the downwash induced on the rear wing by the front wing. This error is of little consequence for the biplane configurations that were of interest to Prandtl and Munk because their stagger is small compared to their span. For joined-wing configurations, the stagger is large, and wind tunnel test data indicate that the span-efficiency factors computed by the Prandtl-Munk theory are too low. Accordingly, we first present the theoretical span-efficiency factors for various joined-wing configurations and then give correction factors based upon experimental data.

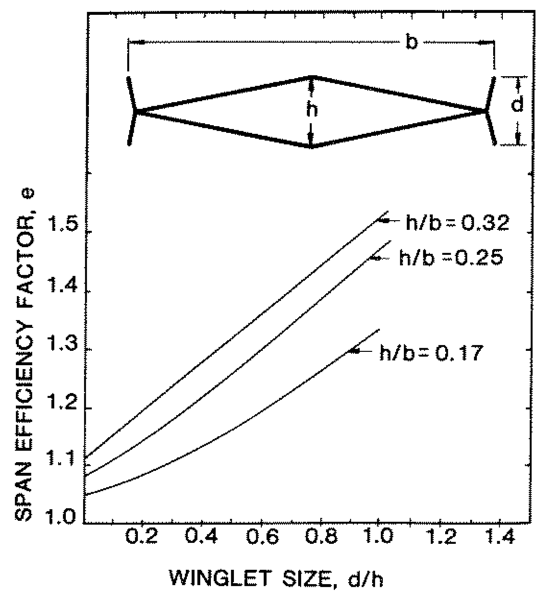

Fig. 15 Theoretical span-efficiency factor for joined wing with or without symmetric inclined winglets.

Figure 15 shows the span-efficiency factor e for optimally loaded joined wings with winglets inclined at 90 deg to the chord plane of each wing. Note that e may be expressed in terms of induced-drag coefficient, lift coefficient, and aspect ratio as

$$e = C_L^2/\pi A C_{D_i} \tag{1}$$

or in terms of induced drag, lift, and span as

$$e = L^2/\pi q b^2 D_i \tag{2}$$

The numerical value of e resulting from Eq. 2 is identical to that given by Eq. 1, but Eq. 2 has the advantage of showing that the value of e is independent of the choice of reference area.

Figure 15 is based upon theoretical analyses of Letcher[15] and Kuhlman.[16] Letcher obtained a solution for e for diamond-shaped wings without winglets; by Munk's stagger theorem this solution applies for all wings having the same Trefftz-plane configuration; hence, it includes tip-jointed joined wings. Letcher's analytic solution was subsequently verified by Kuhlman, using numerical optimization procedures. Kuhlman also showed that the optimal span-loading is almost elliptic for joined wings without winglets.

Reference 10 presents similar data on span-efficiency factor computed for inboard locations of the interwing joint. Moving the joint inboard causes a considerable loss of span efficiency; typically it falls to a level only 2 or 3% greater than the monoplane value.

Trim Drag

In general, it is not possible to obtain optimal span-loading at all lift coefficients while still maintaining trim.

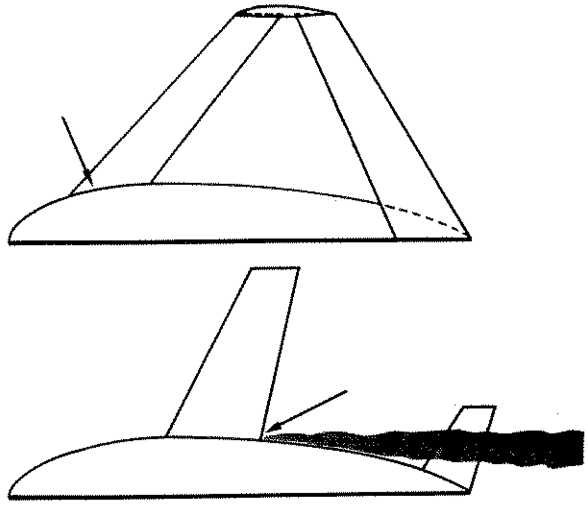

Fig. 16 Schematic comparison of wing-fuselage interference.

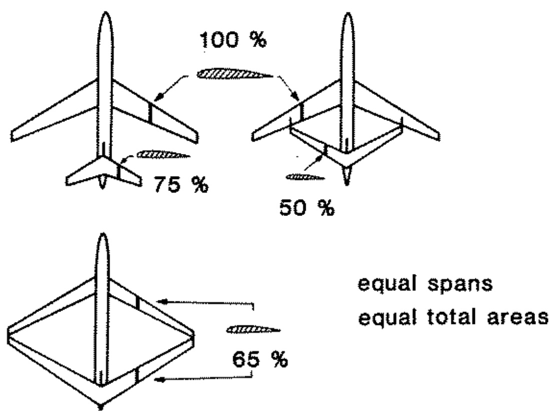

Fig. 17 Relative Reynolds numbers of mean geometric chords of front and rear lifting surfaces, for equal spans and equal gross projected areas.

The additional induced drag due to trim is generally slight for tip-jointed configurations because relatively small changes in loading of the center sections of the front and rear wings produce large moments. Furthermore, the winglets are typically located within a small longitudinal distance of the c.g.; hence, they can be optimally loaded without inducing unwanted pitching moments. Typically the trim drag in cruise is estimated at 1% of the induced drag calculated from the values of span-efficiency factor given above. For inboard-joint configurations, trim drag is comparable to that of conventional aircraft.

Experimental Corrections to Theoretical Induced Drag

In the tests described in Ref. 5, joined-wing and conventional-wing models were tested using the same fuselage. One of the principal objectives of this test was to examine the relative induced-drag characteristics of joined vs monoplane wings. Care was taken to compare the wings at equal chord Reynolds numbers and to subtract out fuselage drag measured at the appropriate angle of attack and Reynolds number. Wing spans and areas were matched, and the wing-joining member was made as small as possible to eliminate its endplate effect. Both wings were optimally twisted for the same design C_L of 0.645 (with the reference area S equal to the GPA).

The joined-wing model was similar to that shown in Fig. 2 but had a shorter nose and no canard. The joined-wing model had 10.8-deg (front) and -9.2-deg (rear) dihedral and, by the analytical method of Ref. 15, was predicted to

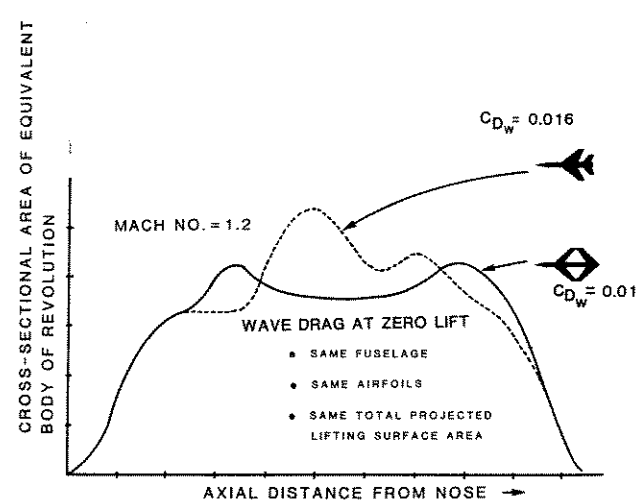

Fig. 18 Transonic wave drag comparison.

have a span-efficiency factor 1.0486 times that of the monoplane. The test results indicate that this ratio is actually 1.09. Thus, this particular joined wing achieves a span-efficiency factor 4% higher than the standard theory predicts. This occurs because the theory neglects the downward drift of the vortex sheet shed by the front wing.

Reference 17 describes similar comparative tests on monoplane vs nonjoined tandem wings, which showed a span-efficiency factor 14% higher than predicted by the theory. One would expect a higher gain for a tandem-wing system than for a joined-wing system since the tip regions on the former have a higher gap and stagger and are therefore more sensitive to vortex sheet drift.

Extensive free-vortex computations would be necessary to resolve the question of how much additional benefit to span-efficiency factor derives from the back-stagger of the joined wing. Pending such computations, it is tentatively recommended that the span-efficiency factors should be multiplied by the following ratio, which has been derived by considering the sweep angles of the quarter-chords of the wings of the model of Ref. 5 (+29 and -20 deg):

$$\frac{e_{\text{actual}}}{e_{\text{theoretical}}} = 1 + \frac{0.04(\tan\Lambda_F + \tan\Lambda_R)}{(\tan 29\ \text{deg} + \tan 20\ \text{deg})} \tag{3}$$

Offset Drag Polars

For an isolated lifting surface that is twisted and/or incorporates spanwise variations in camber, it has been shown[18] that the induced drag is described by an equation of the following form:

$$C_{D_i} = [(C_L - C_{LX})^2/\pi A e_x] + (C_{D_i})_{\min} \tag{4}$$

where C_{LX} and e_x are constants.

This form of drag polar is offset along both axes from the classical form of induced drag polar:

$$C_{D_i} = C_L^2/\pi A e \tag{5}$$

Note that the offset form arises even if the parasite drag is zero or invariant with C_L. Also, note that at a given lift coefficient the minimum achievable induced drag, corresponding to uniform downwash, is the same regardless of which form of polar is used. This minimum is obtained only at the design C_L if the polar is offset, but, for a wide range of off-design C_L, the drag increase over the nonoffset value is negligible.

The tests of Refs. 5 and 17 indicate that, for a given twist, the offsets along both axes are increased by combining airfoils in tandem or as joined wings. It is probable, therefore, that the offset effect is relatively large for joined and tandem wings. Unfortunately, no theoretical analysis is available at present and no general guidelines can be given. An empirical correlation is given in Ref. 5 for the particular airfoils tested in that reference, but no basis for extrapolation to more general airfoils is yet known. A complicating factor is the fact that viscous effects add an additional offset, which is critically dependent on the extent to which leading-edge suction is developed.[19]

For joined wings that are optimally twisted to give minimum induced drag at a specified C_L, the induced drag at this "design" C_L may be computed from Eq. (5). For off-design conditions the following approach is tentatively suggested, based on Ref. 5 (p. 43): Increase C_{LX} by 0.15 above the two-dimensional viscous airfoil value; put e_x equal to $e-0.255$, and equate the induced drag computed by the offset polar to the nonoffset value at the design C_L.

Fuselage Interference

As with any airplane, the presence of the fuselage causes a loss in span-efficiency factor. This is generally less severe for a joined wing than a conventional wing because the rear wing is clear of the fuselage. Additionally, the rear wing may be able to reduce the nonuniformity of the downwash of the front wing so that the Trefftz-plane downwash distribution more nearly approaches its ideal uniform value. Empirically it is suggested that these factors should be taken into account by reducing the fuselage intereference penalty on e to one-half its value for a monoplane of the same ratio of fuselage diameter to wing span.

Wing Interference

None of the wind tunnel tests performed to date have shown any significant drag penalty due to adverse interference in the region of the wing joint. For example, the Rockwell model of Fig. 1, tested over the Mach number range of 0.4-0.95, displayed drag polars of normal appearance, with a minimum drag value only 7% greater than the computed drag of its isolated components.[4,21] For the model of Fig. 4, the measured minimum drag was 92% of the value computed by standard NASA drag prediction methods.[23] The major reasons for the absence of adverse interference are:

1) The airfoils do not overlap in plan view.

2) Each airfoil is designed to operate in the curved flowfield generated by lift on the adjacent airfoil (as will be discussed in the Section titled Airfoil Design).

Parasite Drag of Joined-Wing Aircraft

The following rules should be followed for low parasite drag:

1) Do not overlap the front and rear wings in plan view. This is likely to induce a venturi effect, which will increase drag. (None of the joined-wing wind tunnel tests performed to date have indicated any significant penalty due to interference at the joint, and it is believed that this has resulted from the absence of overlap.)

2) Locate the front wing root forward on the fuselage in a region of favorable pressure gradient. As shown in Fig. 16, this reduces the tendency to separation that occurs with conventional configurations where the wing root is located at the maximum width portion of the fuselage. (Although such separation can be reduced by fillets, these increase the wetted area of the configuration.)

3) Fillet the junction of the rear wing undersurface and the vertical tail to minimize separation. A T.E. "bullet" fairing of semicircular cross section should be used to anchor the fillet.

4) As shown in Fig. 17, for tip-jointed configurations, wing Reynolds numbers are lower than for comparable cantilever wings. Therefore, for tip-jointed configurations, consider the use of natural laminar flow airfoils. (Inboard-jointed configurations operate at Reynolds numbers similar to conventional wings; see Fig. 17).

Wave Drag

At low supersonic Mach numbers, joined wings have less zero-lift wave drag than conventional wings of similar L.E. sweep and total area. Figure 18 illustrates this for the Rockwell configuration of Fig. 1. Due to its smoother area progression, the joined wing has only 69% of the zero-lift wave drag of a conventional configuration of equal gross projected area and thickness/chord ratio.

Wave drag at finite lift is also low for joined-wing aircraft because the total lift is carried over a large fraction of the length of the vehicle. The self-bracing of the joined wing permits the use of very thin airfoils, giving further wave drag savings.

Airfoil Design

The lift on each airfoil of any joined-wing pair causes the other airfoil to be immersed in a curved flowfield (see Fig. 19). Because of this induced flow curvature, fair comparisons between joined wings and isolated wings cannot be made if the airfoils are constrained to be identical. This point has been demonstrated for biplanes by Addoms.[20] Thus, the design of airfoils for joined wings must consider the induced flow curvature, and design methods similar to those used for multielement airfoils should be employed, particularly for airfoils in the vicinity of the interwing joint.

For a full account of airfoil design for a transonic joined wing, see Ref. 21, which has been published in an abbreviated form as Ref. 4. For subsonic aircraft, some preliminary discussion of joined-wing airfoil design is given in Ref. 1, but much more remains to be done. The vortex-lattice program of Ref. 22, which yields optimum joined-wing twist and camber lines for specified pressure distributions, has proven to be useful in airfoil selection. This program typically leads to the camber/incidence relations shown in Fig. 20, for chordwise pressure distributions with a uniform pressure over the first 50% of the chord and a design C_L of 0.3. (Figure 20 is merely illustrative and may not be optimum or near-optimum for different configurations. For similar configurations, the camber and twist required for minimum trimmed induced drag at C_L other than 0.3 can be obtained by ratioing the camber and twist proportionately to C_L.) It is not essential to attain the optimum twist and camber exactly; linear or bilinear spanwise variations may be used instead. However, it is essential to "wash out" the front wing so that its tip has less incidence than its root, and the rearwing should be "washed in" with less incidence at its root than at its tip. The rear wing should also incorporate less camber than the front wing.

Simple model gliders of 12 to 24-in. span are of value in understanding the joined wing's structural and aerodynamic characteristics. Readers are encouraged to build such models, which should follow the above recommendations on twist and camber. The following approximate rules may also

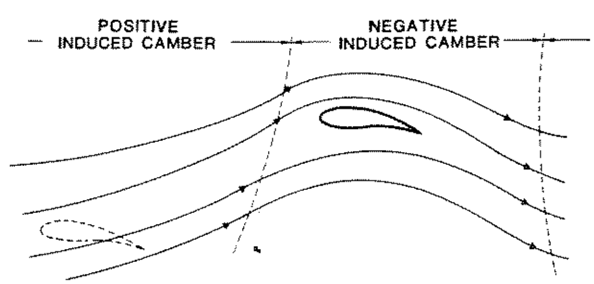

Fig. 19 Curvature of flowfield induced by rear wing on front wing, showing effective change of camber induced on front wing.

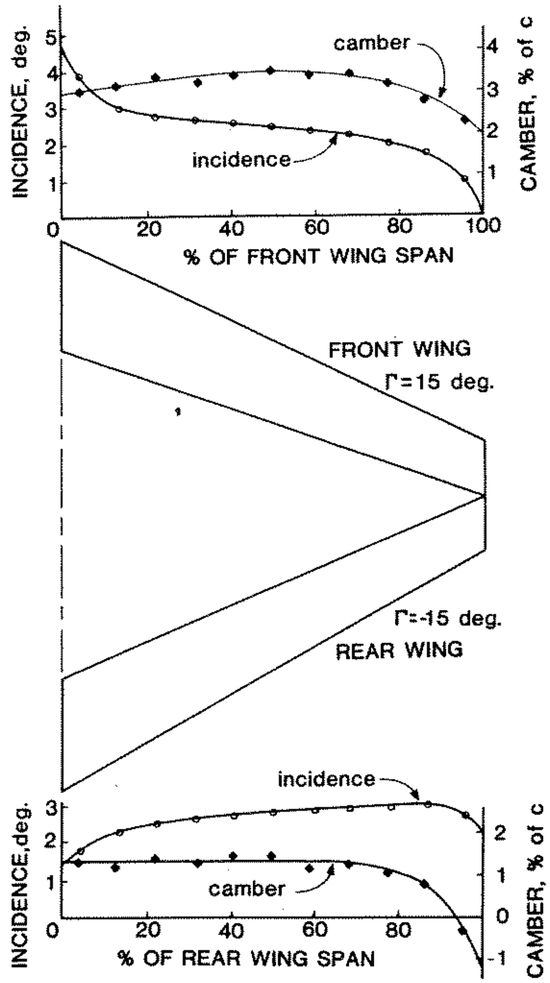

Fig. 20 Twist and camber for minimum induced drag at $C_L = 0.3$ (incompressible flow).

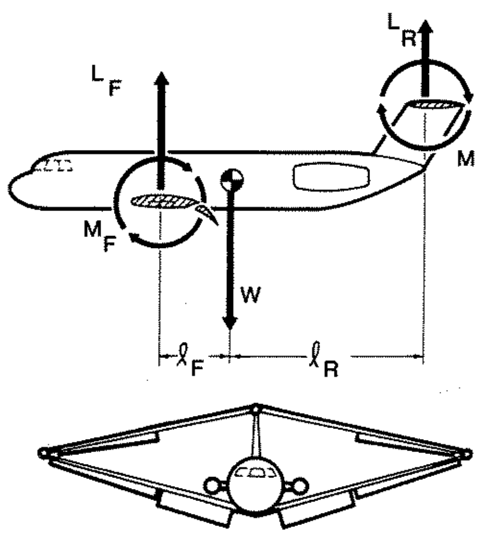

Fig. 21 Trimming for maximum lift coefficient.

be helpful. Typically the front wing root incidence should be 8 deg, decreasing linearly to zero at the tip, and the rear wing tip incidence should be zero to -1.0 deg at the tip, decreasing to -3.5 deg at the root. Relative to the type of curved plate airfoil that would normally be employed on the wing of a conventional model of this size, the front wing camber should be increased by 50% and the rear wing camber decreased by 50%. Both wings should be tapered, with approximately equal magnitudes of positive and negative dihedral.

For inboard-joint configurations there is an abrupt decrease in total (front-plus-rear) chord at the joint. A correspondingly abrupt increase in wing incidence just outboard of the joint is desirable, to maintain a smooth span-load distribution across the joint. Typically, a 1-deg jump in incidence of the front wing is required.

Further research is needed on joined-wing airfoil design. This should include consideration of very thin airfoils. For some applications these are desirable aerodynamically but not feasible with cantilever wing structures. Additional comments on airfoils are given at the end of the next subsection.

Planform and Airfoil Considerations for High Lift Coefficients

Certain guidelines must be followed to enable the joined wing to obtain high lift without excessive wing area. These guidelines include considerations of trim, as well as flow separation.

Trim Equations and Their Consequences for Airframe Geometry

Figure 21 shows the lift forces L_F and L_R acting at the aerodynamic centers of a joined-wing pair. When each wing (individually) is producing zero net lift, it produces a pitching couple M_O, as indicated. For 1-g steady flight, the lift and moment equations about the c.g. become (with notation as in Fig. 21)

$$L_F l_F + M_{OF} + M_{OR} = L_R l_R \tag{6}$$

$$L_F + L_R = W \tag{7}$$

It will be found for almost all statically stable joined-wing configurations that when the front wing attains its $C_{L\max}$, the rear wing lift required to maintain trim is less than the rear wing could generate, were trim not required. In other words, the front wing stalls first. This provides good stall recovery, but it is nevertheless undesirable for the front wing to stall while the rear wing is still far from stalling. If this occurs, it implies that the rear wing area is oversized from the viewpoint of generating the total maximum lift to meet the requirements of $1g$ and maneuvering flight. One would prefer the front wing to stall when the rear wing is almost at its $C_{L\max}$. To achieve this, certain principles must be followed in designing the overall airframe geometry, especially the planform. These principles can be derived by manipulating Eqs. (6) and (7) as follows. From Eq. (6),

$$L_R = L_F(l_F/l_R) + (M_{OF} + M_{OR})/l_R \tag{8}$$

whence

$$\frac{C_{LR}}{C_{LF}} = \frac{S_F}{S_R} \cdot \frac{l_F}{l_R} + \frac{(M_{OF} + M_{OR})}{C_{LF} S_R l_R} \tag{9}$$

The quantity $(S_F l_F)/(S_R l_R)$ in Eq. (9) is always less than unity for a statically stable aircraft. Even for identical front and rear wing areas and equal (positive and negative) sweep angles, $l_F/l_R < 1$ because the overall vehicle aerodynamic center (a.c.) is nearer to the a.c. of the (isolated) front wing than the a.c. of the (isolated) rear wing. This is because the C_{L_α} of the rear wing is $(1 - d\epsilon/d\alpha)$ times its own isolated C_{L_α}. The following principles should be followed to obtain the highest possible value of the first term in Eq. (9).

1) Decrease the ratio of front wing lift-curve slope to rear wing lift-curve slope by employing less sweep on the rear wing.

2) Increase the ratio of rear wing/front wing chord to move the a.c. aft.

3) Reduce the effective $d\epsilon/d\alpha$ at the rear wing by using a large centerline gap (i.e., make the fin tall). It is also

beneficial to employ winglets since these reduce the average $d\epsilon/d\alpha$ at the rear wing.

4) Take advantage of the large pitch damping of the joined-wing configuration to move the c.g. aft without sacrificing maneuver margin. (Generally maneuver margin, not static margin, is the key stability parameter.) If control configured vehicle (CCV) technology is allowable, it should certainly be employed so that the maneuver margin can be made negative. This increases trimmed $C_{L\max}$.

Turning now to the second term in Eq. (9), the key consideration is to make the M_O terms large and positive. This leads to the following guidelines:

1) Do not employ equal flap deflections across the span of each wing. Instead, employ maximum flap deflections on the inboard front wing and outboard rear wing, as shown in the upper half of Fig. 21, to make each wing's M_O as nose-up as possible.

2) Leading-edge devices near the root of the front wing are beneficial.

3) A low-aspect ratio canard can provide appreciable nose-up moment with little forward a.c. shift.

4) Where practicable, the fuselage should be shaped (i.e., cambered) and the wing incidence selected to provide positive C_{mO}.

The foregoing recommendations have emphasized overall airframe geometry rather than local aerodynamic design (e.g., of airfoils and flaps). It is, however, particularly important that the front wing root airfoil be selected to give a high local $C_{L\max}$, as discussed below.

Airfoil Considerations for High Lift

Figure 22 (redrawn from Ref. 24, Sec. 16, p. 4) shows that a swept-back wing obtains a high $C_{L\max}$ near its root. This effect is doubly beneficial for the joined wing since, besides increasing $C_{L\max}$ directly on the front wing, it also provides a nose-up moment that allows the rear wing to be trimmed at a higher C_L.

As described later, wind tunnel tests on joined wings (Refs. 4-6, 21) show no indications of the pitch-up associated with swept wings, possibly because the joined wing tips are only a short distance aft of reasonable c.g. locations. There may also be a beneficial slat effect of the rear wing, which delays stalling of the front wing tips. Design of joined-wing airfoils for high lift should include considerations of the induced angle of attack and the flow curvature induced by each wing on the other. This may require the use of multielement or biplane airfoil design techniques.

Effect of Canard on Maximum Lift

The configuration of Fig. 2 was tested with and without the 60% sweep canard, and also with a conventional wing and tail. The canard exposed area was 11.7% of the GPA of the front plus rear joined wings. Strakes were also tested (see Fig. 23). These had an exposed area of 2.3% of the GPA. Comparisons of $C_{L\max}$ were made at equal Reynolds numbers for each configuration. It was found that the L.E. vortex shed by the canard induced considerable augmentation of the lift of the front wing. A full description of the comparison is given in Ref. 5. The essential points are summarized below.

For fair comparison of lifting capabilities of alternative wing systems, the reference areas employed to define lift coefficient must be equitable. Reference 5, therefore, compares measured trimmed C_L of joined vs conventional wings by referring each C_L to the total exposed area of the appropriate lifting surfaces, including the canard and strake when present. This lift coefficient will be denoted as C_{LE}. At equal dimensional static margins and equal Reynolds numbers, with essentially identical airfoils, the relative trimmed C_{LE} values determined from wind tunnel tests compared as follows: conventional, 100%; joined wing, 104-107%; joined wing plus canard, >119%.

The > sign indicates that, as shown in Fig. 23, the C_L-alpha graph was still rising at the highest angle of attack tested (22 deg).

As noted in Ref. 10, the wind tunnel data of Ref. 5 show that the above ratios are maintained over a wide range of stable static margins. At forward c.g.s the vortex lift generated at the front wing root and on the canard provides the required nose-up trimming moment. If this effect can be maintained at full scale, the joined wing should be able to trim over a wide c.g. range without significant loss of maximum lift.

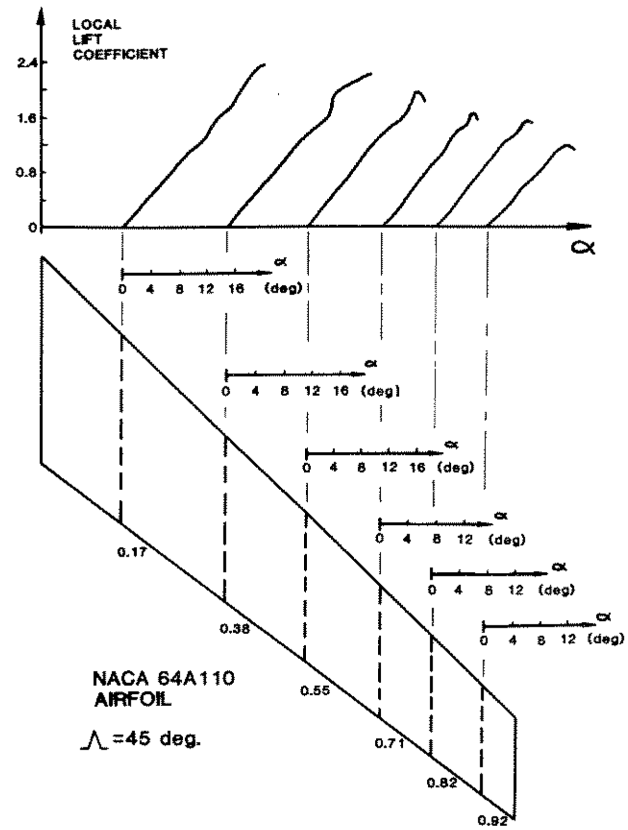

Fig. 22 Measured sectional lift vs angle of attack of a swept wing with no flaps.

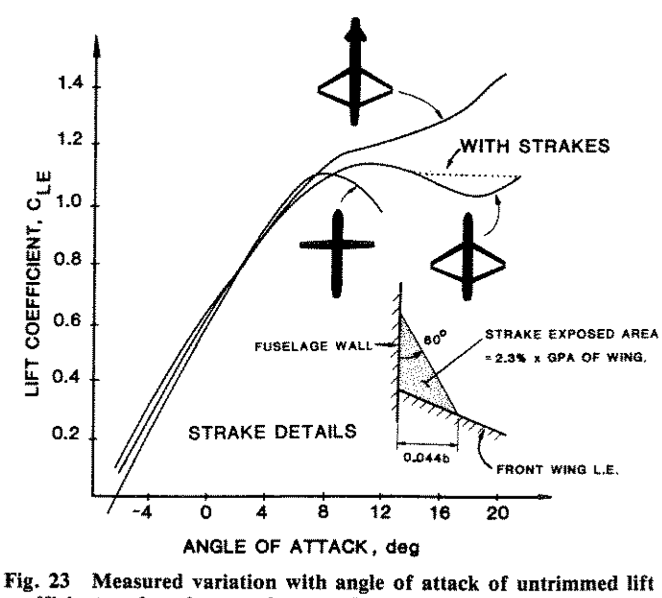

Fig. 23 Measured variation with angle of attack of untrimmed lift coefficients referred to total exposed areas of all lifting surfaces.

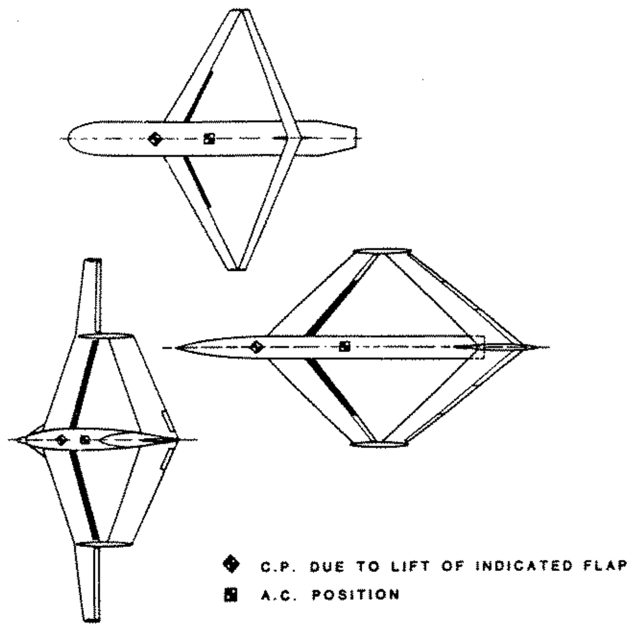

Fig. 24 Aerodynamic center and flap c.p. locations from low-speed wind tunnel tests.

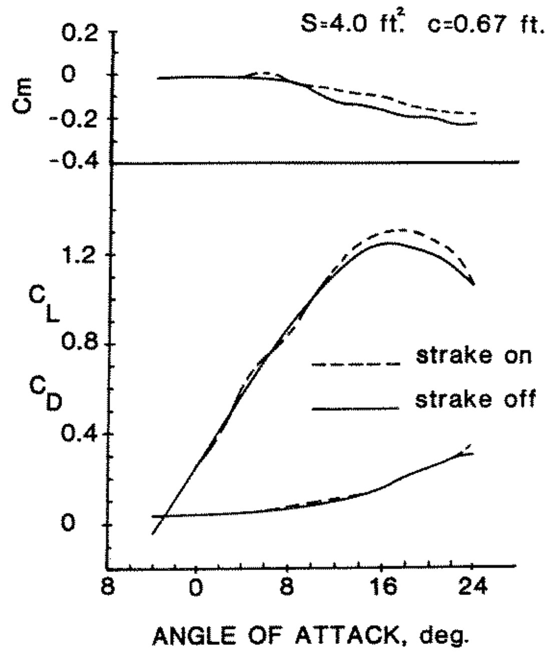

Fig. 25 Effect of strakes on longitudinal characteristics of agricultural airplane model.

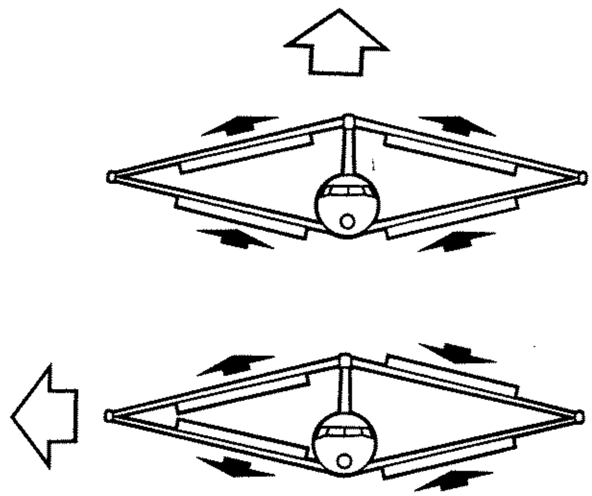

Fig. 26 Direct lift and sideforce capabilities.

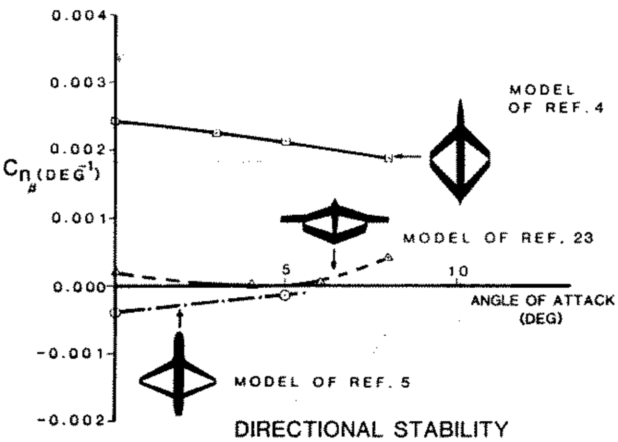

Fig. 27 Yawing moment due to sideslip from low-speed wind tunnel tests.

IV. Stability and Control

Longitudinal Stability

Because of the large number of combinations of geometric parameters possible for a joined-wing pair, it is not feasible to give handbook-type formulas for aerodynamic center location. However, Ref. 10 presents a series of DATCOM style charts showing a.c. location as a function of front/rear sweep, dihedral, taper, and other geometric parameters, as well as Mach number. These charts were computed by vortex-lattice methods, which have demonstrated good agreement with measured a.c. locations, such as the typical a.c. locations shown in Fig. 24.

As discussed below, for some configurations this procedure predicts an a.c. location that is accurate at low angles of attack but is slightly too far forward at high angles of attack below the stall.

Nonlinear Pitching Moment

Some, but not all, of the wind tunnel tests that have been performed on joined-wing configurations have shown a mildly nonlinear pitch-down characteristic at moderate and high angles of attack below the stall. At these conditions the a.c. tends to move aft of its low-angle-of-attack position. This phenomenon is clearly shown in Fig. 25, from Ref. 23, which shows low-speed test results for the configuration of Fig. 4 with and without strakes. These strakes, shown in Fig. 24, employ 55-deg leading-edge sweep of the wing GPA. At angles of attack above 8 deg, with strakes off, the a.c. shifts aft by 13% of the distance between the front and rear wing quarter-chords. With strakes on, this shift is only 6%. Similar trends occurred in tests of a tandem-wing nonjoined configuration.[17] The joined-wing model of Fig. 2 also exhibited this tendency with the canard off,[5] but the model of Fig. 3 (unpublished data) showed an extremely linear pitching moment variation with lift up to the stall. The model of Fig. 1, tested over a Mach range of 0.4-0.95, showed only a very slight pitch-down effect at all Mach numbers.[4, 21]

Reference 23 ascribes the pitch-down to partial stalling of the front wing. This causes the lift-curve slope of the front wing to reduce, and it also reduces the downwash on the rear wing, so its lift increases. The net result is that the overall configuration lift-curve slope remains approximately constant, but the pitching moment slope becomes more negative, because of the large moment arms of the front and rear wings about the moment center. Since such partial stalling (or partial loss of leading-edge suction) is highly dependent on Reynolds number and on model configuration details and surface condition, it is hard to predict. However, one would expect it to decrease as Reynolds number is increased, so it should be less apparent at full scale.

Strakes

The model of Fig. 4 was tested with and without small strakes. The strakes reduced the pitch-down tendency, although they did not eliminate it. This is illustrated in Fig. 25. Small strakes with wetted area equal to 2.5% of the joined-wing wetted area were also tested on the model of Fig. 2 (canard off). They increased $C_{L\max}$ slightly but did not affect the pitching moments. The model of Fig. 2 employed a 9%-thick airfoil, whereas that of the Fig. 4 model was 19% thick. The strakes would be expected to produce larger changes when fitted to the thicker wing since it does not generate as much vortex lift as the thinner wing. The strake-induced vortex lift provides a pitching moment that opposes the pitch-down caused by partial loss of leading-edge suction on the front wing.

Canard

Adding the 60-deg sweep canard to the configuration of Fig. 2 caused the pitch-down tendency to be replaced by a pitch-up due to the vortex-lift generated on the canard and the effect of the canard vortices in delaying the stall of the front wing. It appears that rear wing elevators (not tested) would have been adequate to control the pitch-up and would have increased the total lift still further. For the model as tested, trim was obtained by canard incidence.

Longitudinal Control

Pitch Attitude Control

Elevators may be mounted on either or both the front and rear wings and also on the canard, if one is employed. The center of pressure of the additional lift generated by front wing elevators is generally located some distance forward of the elevators, as illustrated on Fig. 24. This figure shows the c.p. locations for three configurations as determined from wind tunnel tests. (These c.p. locations are close to the locations predicted by vortex-lattice methods.) The c.p. locations are further forward than the elevator because of the downwash induced on the rear wing. This reduces the total lift generated by downward elevator deflection but increases the nose-up pitching moment. This moves the c.p. forward because the distance of the c.p. ahead of the moment center is equal to the incremental pitching moment divided by the incremental lift.

In general, rear wing elevators produce negligible effects on the lift of the front wing, and their c.p. location can be predicted by standard methods, considering the rear wing in isolation. The large number of parameters involved precludes simple formulas for the c.p. location and effectiveness of front wing elevators, but Fig. 24 provides some guidance.

Direct Lift Control

As indicated from Fig. 26, if front wing and rear wing elevators are deflected downward by equal angles measured about the appropriate hinge lines, the resultant lift acts close to the moment center. Thus, by combining front and rear wing elevators, direct lift control is obtained. In general, the elevator deflections required for direct lift control will not be equal on both wings. For the wind tunnel model of Fig. 1, equal elevator deflections provided direct lift because the configuration employed equal sweep angles on front and rear wing leading edges. This gave a large sweep angle to the hinge line of the rear wing elevator (54 deg vs 26 deg for the front elevator). As a result, the pitching moment effectiveness of the rear elevator was reduced to a level comparable to that of the front elevator in the presence of the rear wing.

The optimum form of pitch control is not known, but one would expect that some combination of front elevator and direct lift control would be desirable to facilitate takeoff rotation and liftoff. Such a control arrangement would also improve flying qualities by reducing the lag between the application of pitch control and the buildup of normal acceleration in the desired direction.

Lateral—Directional Stability

The variation of yawing moment with sideslip for the model of Fig. 1 was found to be very linear. As shown in Fig. 27, the model attained a normal level of directional stability ($C_{n\beta} = 0.0025$ per deg). The earlier models of Fig. 2 (canard off) and Fig. 4 did not have satisfactory directional stability. This was unexpected, since both of these models were expected to derive a substantial directional stability contribution from the anhedraled rear wing, which presents considerable side area. However, Ref. 10 has recently explained the phenomenon. Reference 10 analyzes this effect and shows how the low $C_{n\beta}$ stems from the "vane" effect of the vertical tail on the rear wing. The anhedral of the rear wing augments $C_{n\beta}$, but the vertical tail decreases the local sideslip angle at the rear wing to approximately 50% of the overall sideslip angle of the aircraft. The effect was counteracted in the tests of Ref. 23 on the model of Ref. 4 by adding a vertical tail extension above the rear wing. The net conclusion is that, because of the above-mentioned vane effect, the anhedraled rear wing is only about 50% effective in providing directional stability. If directional stability proves to be low, either fin area and/or rear wing anhedral should be increased. As indicated by the Fig. 1 configuration, the fin area required for directional stability is not excessively large.

The rolling moment due to sideslip can be set to normal levels by tailoring the front and rear wing dihedral angles. Since the rear wing is immersed in the sidewash of the front wing, it is less effective in generating rolling moments. Hence, with equal and opposite dihedral and sweep angles, the front wing dominates, and the net $C_{l\beta}$ is markedly negative. References 4, 5, 10, 21, and 23 provide data on joined-wing rolling moments due to sideslip.

Roll Control

Figure 28, from Ref. 5, shows wind tunnel data on the ratio of yawing moment to rolling moment induced by ailerons mounted on the rear wing of the model of Fig. 2 (canard off). No aileron differential was employed; nevertheless, the ailerons generate only a small yawing moment. This desirable result occurs because (as shown by the inset diagram on Fig. 28) the aileron sideforces produce a yawing moment that opposes the yawing moment due to differential aileron drag. Conversely, it was found in Ref. 5 that front wing ailerons produced severe adverse yaw. Front wing ailerons appear to be less desirable than rear wing ailerons and may require considerable differential if the front wing has a large dihedral angle.

The selection of aileron geometry for joined wings must take into account the above factors and must also allow for the high rigidity of joined wings, which improves aileron effectiveness.

For aircraft requiring a high roll rate it may be desired to fit ailerons on both the front and rear wings. This is permissible if the front wing has little dihedral. The greatest roll control power is obtained by mounting the front wing ailerons slightly inboard so that their upwash/downwash increases the rolling moment on the outboard sections of the rear wing. This is discussed in Refs. 10 and 25.

Yaw Control

Rudder effectiveness was examined in Ref. 23 for the agricultural airplane configuration of Fig. 4 and was found to be low. Contributing factors were the 18%-thick airfoil of the vertical tail and the low Reynolds number of the test (approximately 50,000 based on mean chord of the rudder). Reference 23 suggests that the rudder effectiveness may be low because of its enclosure within the channel formed by the front and rear wings. However, flight tests on several radio-controlled joined-wing models have shown adequate rudder effectiveness, so this question remains open.

Direct Sideforce Control

Direct sideforce capability is inherent in the joined wing and requires no vertical surfaces, as shown in Fig. 26. The transonic wind tunnel tests described in Refs. 10 and 21 have verified this capability but have not explored it in detail or optimized the ratio of front to rear wing control surface deflections to minimize rolling and yawing moments.

V. Design Integration

The Importance of Design Integration

Having described the aerodynamic and structural principles of joined wings, their use in complete airframes will now be discussed. Although it is possible to take an existing fuselage for a conventional wing-plus-tail and mate it to a joined wing, this rarely produces the best results. It is better to design a completely new airframe. The preliminary design of this new airframe involves some novel considerations with regard to fuel tankage, landing gear, wing/fuselage geometry, and the use of a canard in addition to the joined wing. These and other aspects of design, such as crashworthiness and wing folding, are discussed below.

Fuel Volume

Figure 29 compares the wing fuel tank volume available from conventional and joined wings of the same span, GPA, and thickness/chord ratio. To match the fuel capacity of the conventional wing, a tip-joined joined wing must employ the extended box spar that is also needed for minimum structural weight (see Fig. 6). The comparative fuel volumes shown in Fig. 29 assume that the fuel occupies the space between the wing shear webs, i.e., 5-75% of the joined-wing chord, vs 15-65% of the cantilever-wing chord. This reduces the chord available for flaps on the joined wing. The tip-jointed configuration should also carry fuel in both the front and rear wings. This is not necessary for an inboard-jointed configuration which, as indicated in Fig. 29, can accommodate more fuel than a conventional wing due to its use of an extended box spar in the joined portion of the wings, with a normal box spar in the cantilever portion.

Landing Gear

Reference 10 describes several alternative landing gear concepts for joined-wing transports. Figure 30 illustrates one concept; this can employ three main wheels, a single main wheel with outriggers, or dual main wheels that retract into the interwing fairing. Whatever landing gear arrangement is selected, the main wheel location and ground angle should be tailored to permit easy nosewheel raising. A positive ground angle may be necessary.

Propulsion System Integration

The joined-wing structure is well suited to pusher or tractor engines located in the "armpit" formed by the rear wing and twin fins as shown in Fig. 14. This engine location has several advantages. It provides a rigid engine mounting and moves the propellers aft of the passenger cabin, thus minimizing cabin noise. It permits short landing gear and allows the engines to be lowered to the ground for servicing, although the local wing and fin structure must be protected from engine components in the event of disintegration. The principal disadvantage is the high thrust line, which causes power-induced trim changes. The prospects of countering these trim effects by local twisting of the wing and/or downthrust deserve investigation. If this location is not acceptable, wing- or fuselage-mounted engines may be employed.

Wing Folding

Figure 31 illustrates a wing folding system employing front and rear wing hinges on a common axis. Reference 1 describes other systems of folding for missile applications, where the folded wing must be accommodated within the missile fuselage.

Crashworthiness

The joined-wing airplane offers a potential advantage in this regard. Placing the front wing root toward the nose of the fuselage enables the joined wings to brace the passenger compartment so that it is less likely to buckle in a crash. The front wing becomes the major energy-absorbing structural element.

Ditching characteristics of joined-wing aircraft are expected to be satisfactory since the airplane floats supported by the front wing, winglets and tip tanks.

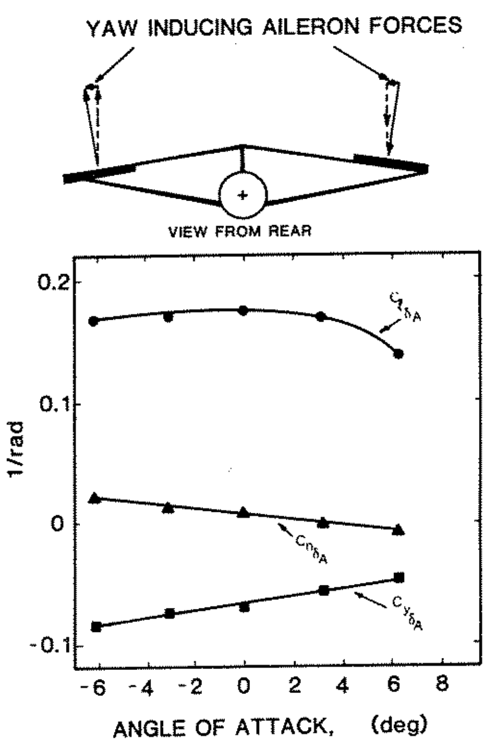

Fig. 28 Measured aileron roll, yaw, and sideforce with zero aileron deflection and rear wing ailerons only.

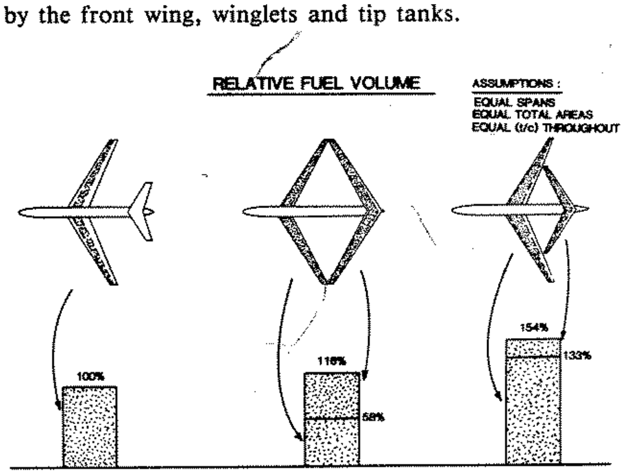

Fig. 29 Fuel volume comparison.

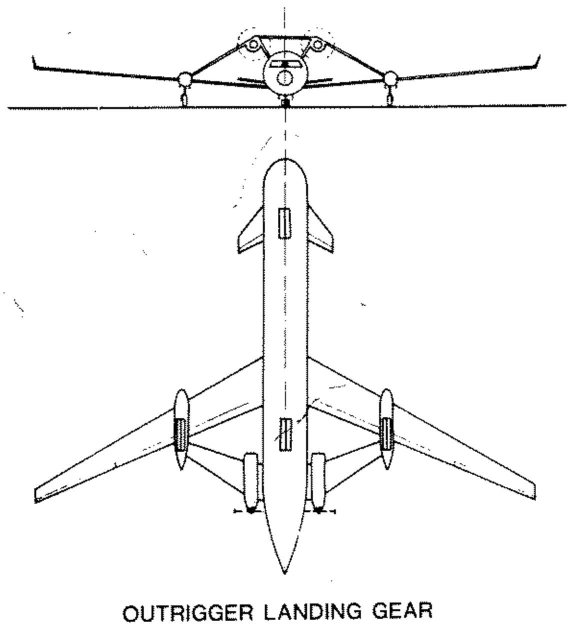

Fig. 30 Configuration employing landing gear with three main wheels.

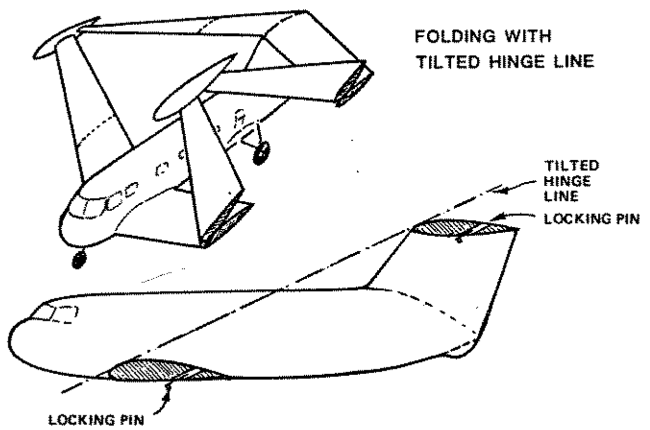

Fig. 31 Wing folding system employing front and rear wing hinges with a common axis.

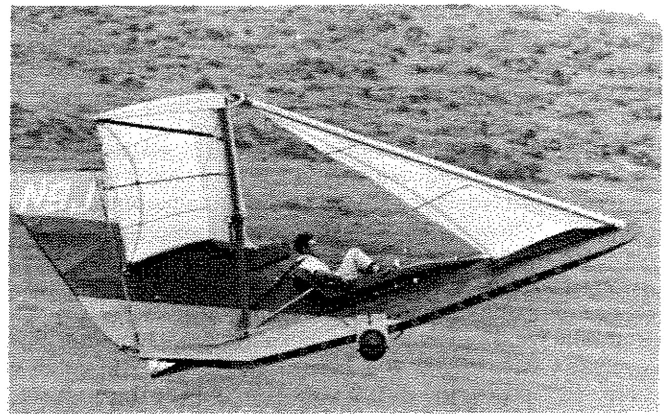

Fig. 32 The author's 1974 primary glider.

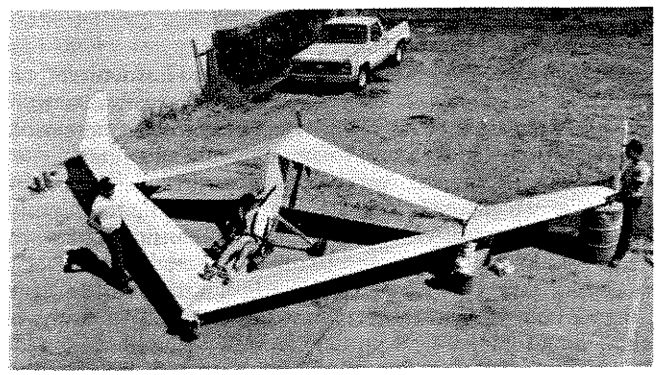

Fig. 33 Summit Aircraft Corp. Trident ultralight airplane.

Wing/Fuselage Geometry

As described in Secs. I and II, the structural weight savings of the joined wing are greatest for wings having 1) moderate sweep and 2) large dihedral angles (positive and negative). This combination is most compatible with a fuselage having relatively low fineness ratio and a tall vertical tail. For many applications, fuselages of low fineness ratio are desirable from the viewpoint of passenger comfort, landing gear accomodation, and minimum weight. If a long, slender fuselage must be employed, it may be best to combine it with a joined wing plus a canard. This combination provides adequate pitch trim capabilities while avoiding too low a ratio of sweep to dihedral for the joined wing. Figure 14 illustrates such a configuration, incorporating a highly swept canard that is retracted in cruise. The canard serves as a high lift system, allowing the wing leading edges to remain free of high lift devices, thus facilitating laminar flow.

VI. Joined Wing Applications

Example Designs

The joined wing has a wide spectrum of applications, ranging from hang gliders to space shuttles. Some selected designs are briefly discussed below.

Figure 32 shows a primary glider (the Skyrider), designed, built, and flown in the early 1970s by the writer, assisted by Mr. Dana Lake and others.[2, 26] The original goal of joining the wings on this glider was to obtain crash resistance and pilot protection. It became apparent that the joined-wing principle also offered other, more general advantages, as described earlier in this paper. Therefore, the Skyrider glider was not developed further, and the main effort of joined-wing research shifted to fairly general structural analyses and exploration of joined-wing aerodynamics via theory and wind-tunnel models. Following the validation of the basic concept by such research, the effort is currently turning toward design studies, construction, and flight testing of prototype manned aircraft.

Figure 33 shows an ultralight airplane (the Trident T3), produced by Summit Aircraft Corp., Denton, Texas.[27-29] This aircraft is largely of composite construction and incorporates extremely thin, highly cambered airfoils, made possible by the self-bracing joined wing. Pilot protection and good flying qualities were prime design goals for this aircraft, which was designed by Mr. David Lund of ACA Industries, Inc., and first flew in January 1985.

Figure 34 illustrates a concept for a high-altitude RPV designed for long endurance flight at altitudes above 60,000 ft. Structure weight is of extreme importance for such aircraft, yet the drag of bracing wires and struts is undesirable. The joined wing meets the weight requirement while providing the robustness required for rough landings in addition to climbs and descents through turbulence.

Figure 35 presents an artist's concept of another application. This figure illustrates the application of a joined wing to an executive jet. Applications to cruise missiles, ASW patrol-type naval aircraft, and agricultural aircraft have been shown in Figs. 2, 3, and 4, respectively, and various transport concepts (e.g., Fig. 14) are discussed in Ref. 10.

The joined wing has outstanding potential for V/STOL aircraft because it offers light structure weight and a convenient location for the lift engines near the c.g. yet distant from the lifting surfaces, so that suck-down and interference are minimized. This is illustrated in Fig. 36.

Figure 37 shows a radio-controlled model of a manned research airplane (the JW-1), intended to gain experience of joined-wing flying qualities. This aircraft employs the fuselage and engines of the existing NASA AD-1 oblique-wing research airplane to provide a low-cost research and demonstrator vehicle. Reference 25 provides a full discussion of this aircraft.

To conclude this brief sampling of joined-wing applications, Fig. 38 shows a space shuttle orbiter concept. Reductions in both structure weight and induced drag were prime design goals. Leading-edge heating is estimated to be similar to existing orbiter configurations.

The above list of concepts and designs provides only a small selection of the possible applications of the joined wing.

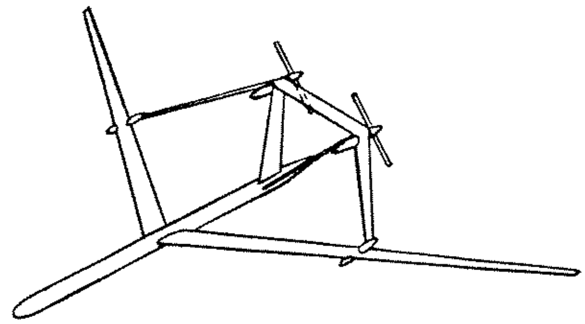

Fig. 34 High-altitude remotely piloted vehicle.

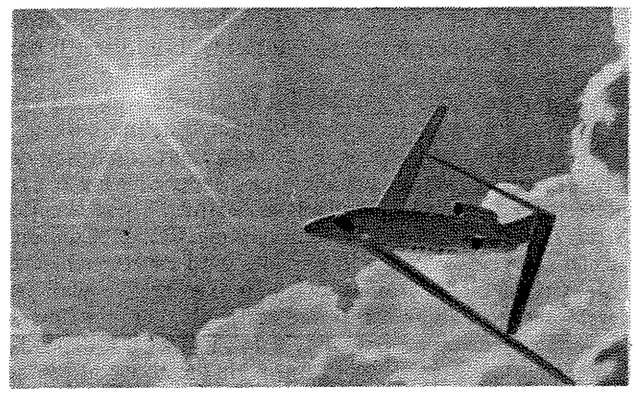

Fig. 35 Concept for an executive jet airplane.

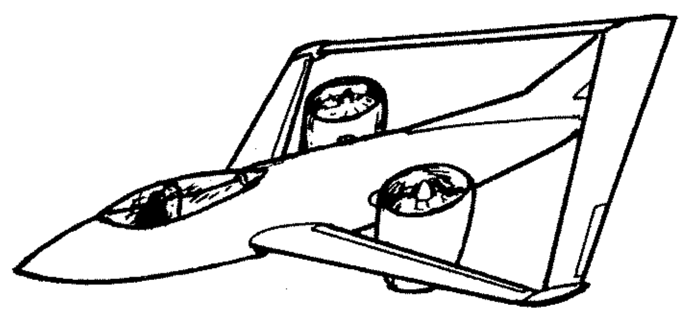

Fig. 36 Schematic Drawing of joined-wing V/STOL aircraft.

Performance Benefits of the Jointed Wing

The benefits provided by the joined wing depend on its application and the design goals. For some applications, weight saving may be of prime importance; for others, low wave drag and suitability for thin airfoils may be decisive. Since the joined wing can provide both aerodynamic and structural advantages, a full assessment requires the use of an aircraft design synthesis program to size an optimal design. For rapid assessments of the impact of the joined wing on performance, a number of shortcut methods may be used. For example, one may assume that no aerodynamic advantage is taken from the joined wing and that it is employed only to save structure weight. The weight saved may be traded for an equal weight of payload or fuel. Leaving the aerodynamic characteristics unchanged, the effect on range can then be assessed by the Breguet formula. To illustrate this approach, we consider a 155-passenger propfan transport design from Ref. 30.

Reference 30 describes a twin-engine transport having a gross weight of 140,000 lb, which consumes 19,552 lb of fuel to fly its maximum range of 1479 n. mi. The wing weight plus horizontal tail weight total 17,431 lb. From Figs. 7 and 8, 40% of this weight (i.e., 6972 lb) could be saved through replacing the wing and tail by an aerodynamically equivalent joined wing. If this weight is replaced by an equal weight of fuel, the relative range is given by the Breguet formula as

$$\frac{\text{Range of joined wing airplane}}{\text{Range of conventional airplane}} = \frac{\ln\left\{1+\dfrac{19{,}522+6{,}972}{120{,}478-6{,}972}\right\}'}{\ln\left\{1+\dfrac{19{,}522}{120{,}448}\right\}} = 1.396$$

Thus, in this application, the joined wing gives an increase in range of 39.6%.

If desired, the joined wing could be used to increase span at the same weight, thus reducing induced drag. It could also be employed to permit thinner airfoils, giving faster cruise speeds. For unchanged range the joined wing could be used to increase the number of passengers. Allowing 300 lb per passenger to include fuselage structure, seats, and baggage, and an allowance for fuel used to overcome the drag of the enlarged fuselage, the number of passengers would increase by 23, from 155 to 178. With a break-even load of 110 passengers, this would change the potential airline profit on direct operations by a factor of $(178-110)/(155-110)=1.51$, i.e., an increase of 51% in potential profit. (Even allowing as much as 400 lb per passenger for fuselage structure, etc., the number of passengers would increase by 17 and the potential profit by 38%.

The joined-wing is at an early stage in its development and much data are still unpublished. In addition, the space available for this paper has not permitted discussion of many of the subtleties and refinements of joined-wing design. Therefore, the reader who wishes to evaluate the potential benefits of the joined wing for any specific application should contact the writer to obtain the most up-to-date information.

New Technology and the Joined Wing

Recent advances in aircraft design have developed new technology, e.g., composite materials, laminar flow airfoils, and control configured vehicles having relaxed static stability. The joined wing does not depend upon any of these new developments although it can make good use of all of them. For example, laminar flow is more easily obtained at the lower Reynolds numbers characteristic of tip-jointed joined wings. Composite materials are well suited to the non-uniform chordwise distribution of structural material that is optimum for joined wings (Fig. 6). Relaxed static stability permits higher rear wing loadings, decreasing the total wing area required to lift the aircraft at takeoff and landing. The above examples show that the joined wing is synergistic with new technology.

The results obtained to date on the joined wing have not assumed any new technology. This restriction has been imposed so that comparisons between joined-wing and existing conventional aircraft could be made on a fair basis. In practical aircraft design, full advantage should be taken of new technology, and this is particularly true for the joined wing, because of its synergy with the technology advances cited above.

VII. Conclusions

1) The joined wing provides advantages over a conventional wing-plus-tail arrangement, including: a) lighter weight and higher stiffness, b) less induced drag, c) reduced transonic and supersonic drag, and d) built-in direct lift and sideforce capability.

2) Experimental data show that the joined wing has good stability and control in normal flight and at the stall.

3) The joined wing can provide reductions in parasite drag through smaller lifting surface areas, reduced wing-fuselage interference, and suitability for thin airfoils. These beneficial effects offset the effects of lower wing Reynolds numbers such that overall savings in parasite drag can be achieved.

4) Although the joined wing is synergistic with new developments such as composite materials, laminar flow airfoils, and control configured vehicles, it does not depend on new technology. Hence, it can provide the above advantages with short development times and low risk.

5) The joined wing is a highly integrated concept involving structures and aerodynamics. Coordinated efforts in both these technical areas are required to maximize the advantages of the joined wing.

Appendix: Related Configurations

Aircraft configurations having connected tandem wings have been proposed since the earliest days of aviation, (e.g., the Henson and Warren-Young projects of Refs. 31 and 32). Most of these proposals did not progress to the stage of flying manned aircraft, and none of them included the special geometric and structural features of the type of joined wing that is the principal subject of this paper. Therefore, they will be referred to as connected-wing rather than joined-wing configurations. A full historical summary would far exceed the space limitations of the present paper, so details will be given of only the two connected-wing airplanes known to have flown successfully. These are the 1922 Platz glider and the 1932 Brown airplane.

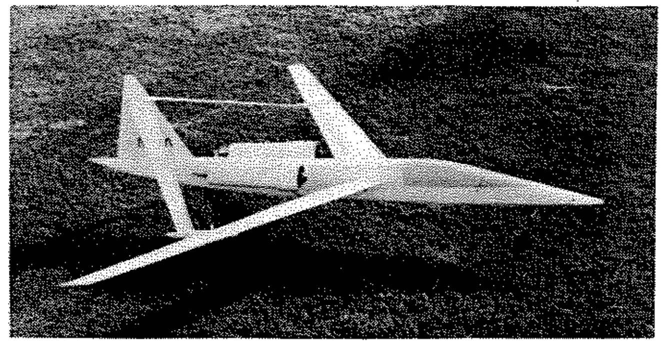

Fig. 37 Radio-controlled model of JW-1 research airplane design.

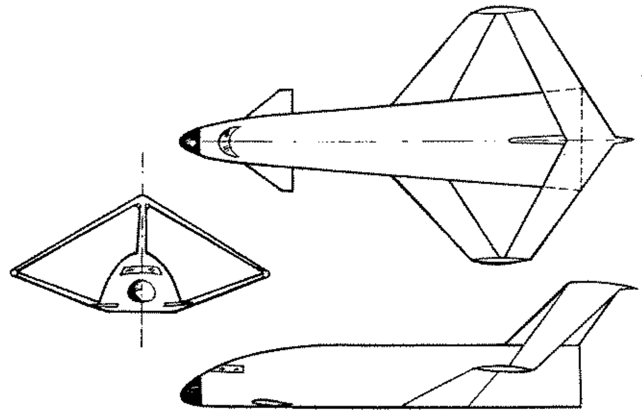

Fig. 38 Joined-wing space shuttle orbiter concept.

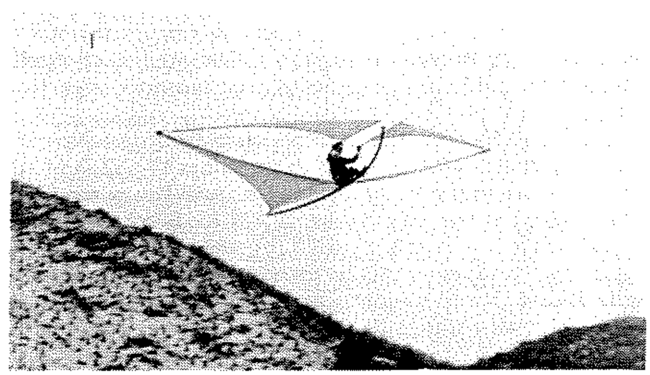

Fig. 39 1922 Platz glider.

The Platz Glider

Figure 39 shows the Platz glider. This has been described in various references. The primary source of information is Ref. 33, but Ref. 34 is more accessible. The glider was designed by Fokker's chief designer, Reinhold Platz, and appeared in two versions during the early 1920s. Platz also constructed a modern version in 1963. The glider employed a structure in the form of a cross, consisting of a transverse spar, which formed the leading edge of the rear wing, attached to a longitudinal spar, which served as a fuselage. To these spars Platz attached for-and-aft sails, forming tandem wings. The root of each foresail was attached to a pivoted root rib, the trailing edge of which was held by the pilot. By moving these trailing edges in unison, the pilot obtained pitch control; roll control was obtained by differential movements. No fin or rudder was fitted. Approximate dimensions of the glider are: span, 24.6 ft; length, 16.2 ft.

The Platz glider flew well but did not influence glider design and passed into obscurity. One reason for this may have been that the unbraced spar arrangement was relatively heavy compared to the strut-braced gliders of its era. The gap between the front left and right wings also would have caused considerable induced drag. Regardless of these deficiencies, the Platz design deserves admiration for its originality and remarkable simplicity.

The Brown Airplane

This unnamed aircraft was designed by Ben Brown of the University of Kansas around 1932. It is shown in Fig. 40.[34] It employed swept-back and swept-forward wings arranged to form a diamond shape in plan view but (unlike the joined wing) not in front view. A third wing, equal in chord to each of the others, acted as a strut. The Brown airplane made cross-country flights and performed loops. The only flying qualities deficiency of which the writer is aware is that the rudder was relatively ineffective for taxiing, due to its location ahead of the slipstream of the pusher propeller. The drive shaft system included a dry clutch to absorb torsional vibration and performed well. The Brown airplane faded away without influencing other airplane designs. The design can be criticized because of the low Reynolds number of each of the three equal-chord wings, but the major reasons for its lack of impact on the trend of aviation history are probably not technical but relate to the adverse economic environment of the early 1930s.

The Boxplane

Turning now to configurations related to the joined wing that have been wind tunnel-tested but not flown full-scale, mention must be made of the boxplane concept invented by Luis Miranda of Lockheed Corporation. Figure 41 illustrates a boxplane transport configuration studied by Lockheed.[35] Low-speed and transonic tests were also performed on a lower aspect-ratio boxplane representative of a fighter design.[36]

Compared to the joined wing, the boxplane differs in that the wings do not form a diamond shape in front view. An additional difference is that the boxplane internal wing structure does not follow the special form employed for the joined wing. The prime motivation of the boxplane was to obtain a high span-efficiency factor. Standard induced-drag theory predicts that, for a given height and span, the boxplane arrangement achieves the maximum possible span-efficiency factor. For example, Ref. 36 shows that with a height/span ratio of 0.3, the boxplane produces only 60% of the induced drag of an elliptic monoplane wing of the same span, operating at the same airspeed and air density and generating the same lift as the total lift of the front plus rear wings of the boxplane.

The low-speed wind tunnel tests verified the predicted savings of induced drag, but the transonic tests and the transport design studies uncovered some problems that led to the abandonment of U.S. Government sponsorship of boxplane research. The transport design studies revealed an unacceptably low flutter speed and also showed no saving in wing-plus-tail weight relative to a baseline conventional configuration. The transonic tests showed several problems, discussed below. These included high minimum drag coefficient and premature separation on the front wing at subsonic Mach numbers, leading to an increase in lift-dependent drag and lower maximum lift coefficient than that of a reference conventional configuration. With the benefit of hindsight, it appears that at least some of the aerodynamic problems noted in Ref. 36 could have been overcome, as discussed below.

There were three causes of the apparently disappointing results of the Ref. 36 boxplane tests. First, the airfoils of the boxplane were not designed with consideration to the flow curvature induced by the neighboring airfoil. Instead, standard monoplane airfoils were chosen. As was later shown by Addoms,[37] biplane configurations must employ airfoils having substantially different camber from those of competitive monoplanes. A fair comparison between monoplanes and multiwing configurations cannot be obtained if all the configurations are forced to use the same airfoils. As noted by Addoms, typically the use of monoplane airfoils on biplanes causes premature separation and unnecessarily low maximum lift.

The importance of the above point cannot be overstated for configurations such as boxplanes and joined wings. The use of "off-the-shelf" monoplane airfoils for such configurations is disadvantageous and is no longer necessary in view of the current state of airfoil design technology.

The second cause of the apparently disappointing performance of the boxplane in the tests of Ref. 36 was improper selection of reference areas. The reference area for the boxplane model was selected to be the same as that for the reference baseline model of conventional wing-plus-tail layout. The latter had 20% more total horizontal lifting surface area (due to its tail, which was not included in the reference area). Hence, the monoplane would be expected to produce a higher maximum lift coefficient because it has a higher ratio of lifting surface area to reference area. The third reason for the poor showing of the boxplane vs the monoplane in the tests of Ref. 36 was that the data were not corrected to full-scale Reynolds numbers. Although at $M=0.5$ the boxplane had a trimmed maximum L/D of 12.2 vs 11.1 for the conventional configuration trimmed at a dimensionally equal static margin, this result is less favorable than would be achieved at full-scale conditions. This is because, at model test Reynolds numbers, the short chord lengths of the boxplane wing increase its minimum drag over that of the reference monoplane by a larger proportion than at full scale.

In summary, the aerodynamic problems of the boxplane may be less severe than has been believed, and may be partly curable with proper airfoil design. The low Reynolds numbers of its short-chord wings may be acceptable for laminar flow airfoils. Low flutter speed and lack of weight saving are probably more serious drawbacks to the boxplane than any aerodynamic factors.

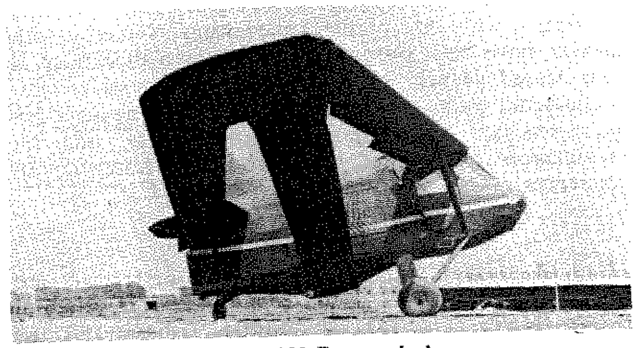

Fig. 40 1932 Brown airplane.

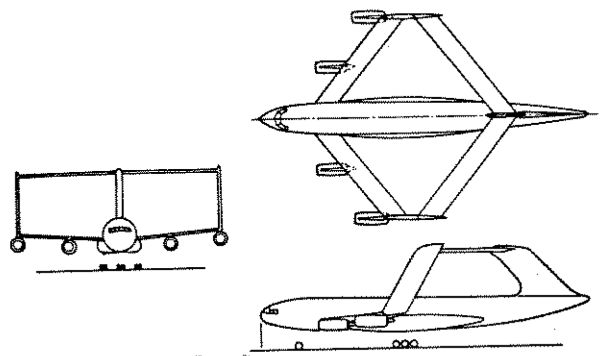

Fig. 41 Lockheed boxplane transport design.

Other Concepts

A brief summary of other connected-wing concepts that are of research interest is given below.

Henderson and Huffman[38] present low-speed test data on a modified boxplane in which the rear wing root is mounted on top of the fuselage. Rhodes and Selberg,[39] Cahill and Stead,[40] and Zimmer[41] describe configurations in which a swept-back wing is connected at its tips to a second wing that is either swept forward or less highly swept-back than the first wing. Other examples of this category are the Warren-Young rhomboidal wing designs.[32] For all these configurations, the root of the front wing is higher than the root of the rear wing, and the fin is not directly connected to the rear wing. In these and other respects, the above configurations differ from the joined wing.

The wind tunnel models tested by Cahill and Stead were unsophisticated in some respects (one had flat-plate airfoils) and, as a result, had high induced drag. The Zimmer configuration was more refined but retained a separate horizontal and vertical tail, which did not connect with its front or rear wings. The Warren-Young, Cahill, Henderson, and Zimmer concepts do not detail any internal wing structure comparable with that of the joined wing. Numerous other concepts have been proposed from time to time (e.g., the "ring wing," which forms a circle in front view and a parallelogram in side view), but data on these related configurations are fragmentary and incomplete, and their resemblances to the joined wing are less significant than their differences.

Acknowledgments

Part of the work reported herein was performed under NASA Contracts NAS2-11255 and NAS2-11725 and also under Navy Contracts N00014-79-C-0953 and N00014-82-C-0607. NASA Project Monitors were Mr. Thomas J. Gregory and Mr. George H. Kidwell. The Navy Project Monitor was Dr. Robert E. Whitehead.

References

[1]Wolkovitch, J., "Application of the Joined Wing to Cruise Missiles," Phase I, ONR-CR-212-266-1, Nov. 1980.

[2]Wolkovitch, J., Joined Wing Aircraft, U.S. Patent 3,942,747, March 1976.

[3]Wolkovitch, J., Joined Wing Aircraft, U.S. Patent 4,365,773, Dec. 1982.

[4]Clyde, J.A., "Transonic Design and Wind Tunnel Testing of a Joined Wing Concept," AIAA Paper 84-2433, 1984.

[5]Wolkovitch, J. and Bettes, W.H., "Low-Speed Wind Tunnel Test on Joined Wing and Monoplane Configurations, Vol. I: Analysis of Results, Vol. II: Test Data," ACA Industries, Inc., Rancho Palos Verdes, CA, ACA Report 82-2, 1984.

[6]White, E.R., "Preliminary Force Test Data for a Joined Wing Aircraft Configuration," NASA Langley Research Center, Hampton, VA, Internal Memo File V-19100/OLTR-094, April 8, 1980.

[7]Samuels, M.F., "Structural Weight Comparison of a Joined Wing and a Conventional Wing," *Journal of Aircraft*, Vol. 19, June 1982, pp. 485-491.

[8]Shyu, A., "Analysis of Structural Weights of Joined and Cantilever Wing Systems for Transports," forthcoming NASA Ames Research Center Report.

[9]Miura, H., Shyu, A., and Wolkovitch, J., "Parametric Weight Evaluation of Joined Wings by Structural Optimization," AIAA Paper 85-0642-CP, April 1985.

[10]Wolkovitch, J. and Lund, D.W., "Application of the Joined Wing to Turboprop Transport Aircraft," forthcoming NASA CR-22187.

[11]Hajela, P., "Weight Evaluation of the Joined Wing Configuration," Final Report, Department of Engineering Sciences, University of Florida, Gainesville, FL, 1983.

[12]Turner, C.D. and Ricketts, R.H., "Aeroelastic Considerations for Patrol High Altitude Surveillance Platforms," AIAA Paper 83-0924-CP, 1983.

[13]Durham, M.H., "Flutter Tests on High-Aspect-Ratio Model Joined and Cantilever Wings for High Altitude Platforms," Kentron International Corp., Hampton, VA.

[14]Jones, R.T., "Classical Aerodynamic Theory," NASA Reference Publication 1050, 1979.

[15]Letcher, J.S., "V-Wings and Diamond-Ring Wings of Minimum Induced Drag," *Journal of Aircraft*, Vol. 9, Aug. 1972, pp. 605-607.

[16]Kulhman, J.M. and Ku, T.J., "Numerical Optimization Techniques for Bound Circulation Distribution for Minimum Induced Drag of Non-Planar Wings: Computer Program Documentation," NASA CR-3458, 1982.

[17]Wolkovitch, J., "Subsonic VSTOL Aircraft Configurations with Tandem Wings," *Journal of Aircraft*, Vol. 16, Sept. 1979, pp. 605-611.

[18]Igoe, W.B., Re, R.J., and Cassetti, M.D., "Transonic Aerodynamic Characteristics of a Wing-Body Combination Having a 52.5 Deg Sweptback Wing of Aspect Ratio 3 and Conical Camber and Designed for a Mach Number of $\sqrt{2}$," NASA TN D-817, May 1961.

[19]DeLaurier, J., "Drag of Wings with Cambered Airfoils and Partial Leading-Edge Suction," *Journal of Aircraft*, Vol. 20, Oct. 1983, pp. 882-886.

[20]Addoms, R.B. and Spaid, F.W., "Aerodynamic Design of High Performance Biplane Wings," *Journal of Aircraft*, Vol. 12, Aug. 1975, pp. 629-630.

[21]Clyde, J.A., Bonner, E., Goebel, T.P., and Spacht, L., "Joined Wing Transonic Design and Test Validation," Rockwell International Corp., NAAO Div., Los Angeles, CA, Rept. 84-1434, June 1984.

[22]Lamar, J.E., "A Vortex-Lattice Method for the Mean Camber Shapes of Trimmed Noncoplanar Planforms with Minimum Vortex Drag," NASA TN D-8090, 1976.

[23]White, E.R., "Low-Speed Wind-Tunnel Investigation of a Joined-Wing Aircraft Configuration," forthcoming NASA Report.

[24]Hoerner, S.F. and Borst, H.V., "Fluid-Dynamic Lift," Hoerner Fluid Dynamics, Brick Town, NY, 1975.

[25]Wolkovitch, J., "Joined-Wing Research Airplane Feasibility Study," AIAA Paper 84-2471, 1984.

[26]Bulot, C., "Joined Wings: Modernizing an Old Concept," *Homebuilt Aircraft*, Vol. 10, March 1983, pp. 20-23, and 70.

[27]Levy, H., "Oshkosh 84," *Flight International* (U.K.), Sept. 15, 1984, pp. 680-681.

[28]"Microlights Join Together," *Flight International* (U.K.), Nov. 10, 1984, pp. 1237.

[29]"Trident T 3 Brochure," Summit Aircraft Corp., Denton, TX.

[30]Goldsmith, I.M., "A Study to Define the Research and Technology Requirements for Advanced Turbo/Propfan Transport Aircraft," Douglas Aircraft Company, Long Beach, CA, NASA CR-166138, 1981.

[31]"An Original All-British Aeroplane," *Flight*, (U.K.), Feb. 5, 1910, pp. 87-90.

[32]Hall-Warren, N., "Design of Tailless Aircraft," *Flight* (U.K.), Aug. 10, 1950, pp. 179-181.

[33]Platz, R., "Ein neuartiges Segelflugzeug," *Zeitschrift fur Flugtechnik und Motor Luftschiffahrt*, Vol. 13, 1922.

[34]Bowers, P.M., *Unconventional Aircraft*, Tab Books, Inc., Blue Ridge Summit, PA, 1984.

[35]Lange, R.H. et al., "Feasibility Study of the Transonic Biplane Concept for Transport Aircraft Application," NASA CR-132462, 1974.

[36]Miranda, L.R. and Dougherty, G.L., "Transonic Wind Tunnel Testing of a Low Induced Drag Lifting System, Vols. I and II," Lockheed Aircraft Corp., Burbank, CA, Feb. 1974.

[37]Addoms, R.B. and Spaid, F.W., "Aerodynamic Design of High Performance Biplane Wings," *Journal of Aircraft*, Vol. 12, Aug. 1975, pp. 629-630.

[38]Henderson, W.P. and Huffman, J.K., "Aerodynamic Characteristics of a Tandem Wing Configuration at a Mach Number of 0.30," NASA TM X-72779, Oct. 1975.

[39]Rhodes, M.D. and Selberg, B.P., "Benefits of Dual Wings over Single Wings for High-Performance Business Airplanes," *Journal of Aircraft*, Vol. 21, Feb. 1984, pp. 116-127.

[40]Cahill, J.F. and Stead, D.H., "Preliminary Investigation at Subsonic and Transonic Speeds of Aerodynamic Characteristics of a Biplane Composed of a Swept-Back and Swept-Forward Wing Joined at the Tip," NACA RM L53L34B, March 1954.

[41]Zimmer, H., "Das Hochauftribsverhalten beim Rautenflugelkonzept," Dornier GMBH, Friedrichshafen, Germany, DGLR Rept. No. 78-114, 1978.

PERGAMON

Aircraft Design 1 (1998) 217–242

AIRCRAFT DESIGN

Invited Paper

Advanced configurations for very large transport airplanes

John H. McMasters[a,]*, Ilan M. Kroo[b]

[a]The Boeing Company, MC GY-93, P.O. Box 3707, Seattle, WA 98124, USA
[b]Department of Aeronautics and Astronautics, Stanford University, Stanford, CA, USA

Abstract

Recent aerospace industry interest in developing subsonic commercial transport airplanes with at least 50% greater passenger capacity than the largest existing aircraft in this category (e.g. the Boeing 747-400 with approximately 400–450 seats) has generated a number of proposals based primarily on the configuration paradigm established 50 years ago with the Boeing B-47 bomber. While this classic configuration has come to dominate subsonic commercial airplane development since the advent of the Boeing 707/Douglas DC-8 in the mid-1950s, its extrapolation to the size required to carry more than 600–700 passengers raises a number of questions, including:

- How large can an airplane of 707/747 configuration be built and still remain economically and operationally viable?
- What configuration alternatives might allow circumvention of practical size limitations inherent in the basic 707/747 configuration?
- What new and/or dormant technology elements might be brought together in synergistic ways to resolve or ameliorate very large subsonic airplane problems?

To explore these and a number of related issues, a team of Boeing, university and NASA engineers was formed under the auspices of the NASA Advanced Concepts Program during 1994. The results of a Research Analysis contract (NAS1-20269) focused on a large, unconventional (C-wing) transport configuration for which Boeing and the authors were granted a design patent in 1995 is the subject of this paper which is based on information contained in McMasters et al. (NASA CR 198351, October 1996).

* Corresponding author.

PII: S1369-8869(98)00018-4

Return now to a new Golden Era of complete customer satisfaction in commercial aviation

1. Introduction

A fascination for very large airplanes, transmitted to a certain population of the aircraft design community via the "Russian gene" for many decades, has penultimately manifested itself in the realization of a class of subsonic transports typified by the Boeing 747, the Lockheed-Martin C-5, and the Ukrainian Antonov An 124 and An 225 "*Mriya*". In an industry that has existed for less than a century and which already has experienced several "Golden Ages" of remarkable achievements, the *Mriya* (Dream) with a maximum take-off weight approaching 6 MN ($\sim$ 1.3 M lb) and wing span of 88.4 m (290 ft) remains an impressive engineering accomplishment. It should be noted here for later reference in this paper that each of these giants is a reasonable evolutionary extrapolation of the basic configuration for such aircraft established 50 years ago by the Boeing B-47 bomber and characterized by a cylindrical fuselage mated to a "high" aspect ratio wing with pod-mounted engines distributed across its span and an aft-mounted empennage.

Ever dynamic and marked by a restless curiosity the international aircraft industry (and even its commercial component despite its supposed maturation) has found its products so successful in transforming the global transportation system in recent decades that it has become necessary to contemplate the development of giants even beyond the size of machines like the An 225. The reasons for this are several but come down to two simple factors: airport capacity is limited and has become a severely constricting bottleneck at several key "hubs" around the world; and, everything else being equal, the economics of flying devices tend to improve in direct proportion to their increasing size. These two factors are demonstrated in Fig. 1 (which shows that at a "typical" airport like JFK in New York traffic growth is once again approaching airport capacity), and in Fig. 2 (from Ref. [2]) which shows very general empirical evidence of the value of increasing size on devices that travel in a variety of modes.

The final decade of this century has presented us with a very different world than that which experienced the protracted ebb and flow of the Cold War with all the fantastic developments in military technology that went with it, and which to varying degrees spilled over into the development of civil aircraft which are finally capable flying more-or-less anywhere on the earth on a non-stop basis. The rising emergence of Asia as an economic power and as an extremely rich potential marketplace has greatly contributed to a steady increase in air traffic to the Far East.

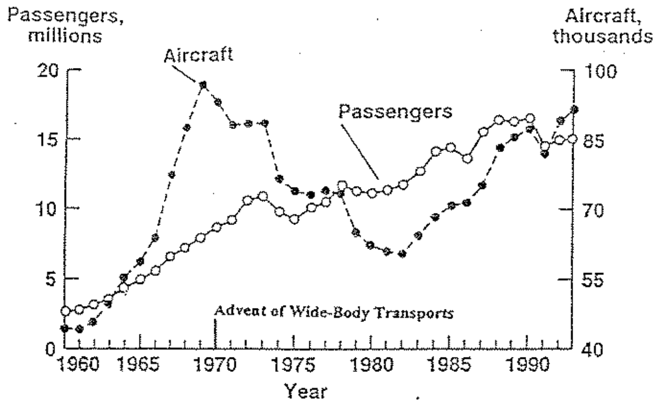

Fig. 1. Traffic growth and aircraft arrival/departure data for Kennedy International Airport, New York (NASA data via H. Fuhrmann).

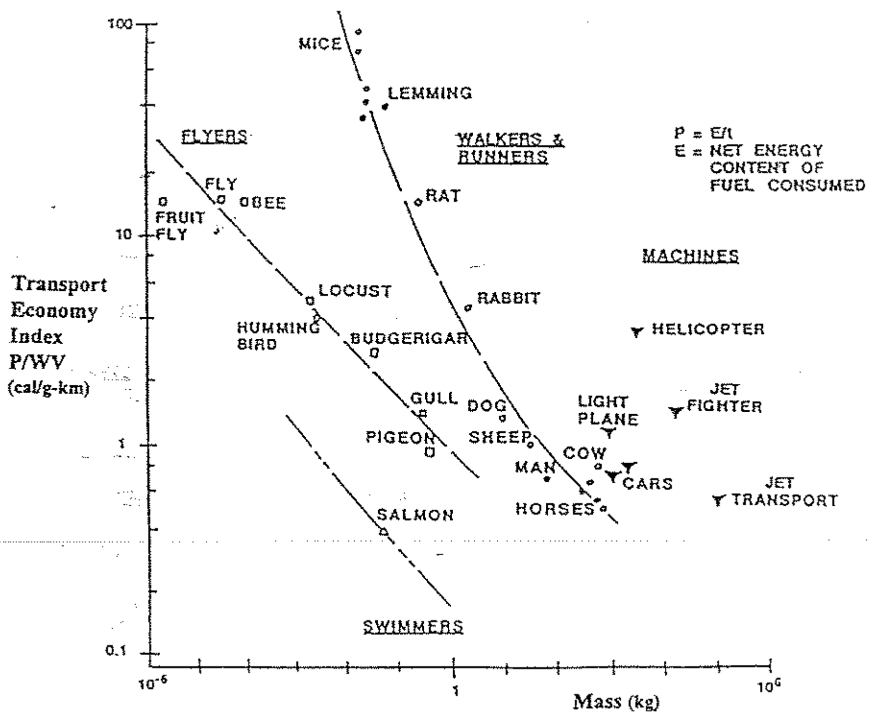

Fig. 2. Variation in minimum transport economy index [power(P)/weight(W) × speed(V)] with increasing size (mass) for various modes of travel (after V. Tucker as discussed in [2]).

Independent of arguments for or against the development of a supersonic transport, given the previously cited airport capacity limitations at destinations such as Tokyo and Hong Kong continued traffic growth has been thought to be limited unless ways were found to either increase take-off and landing frequency or increase passenger count for a given arrival-departure frequency.

The latter approach being "simpler" to achieve than the former, despite the anticipated enormous development cost, a good deal of enthusiasm was generated in the early 1990s for a class of aircraft capable of carrying at least half again as many passengers as the existing Boeing 747.

The basic *very* large subsonic transport airplane design problem revolves around accommodating over 600 passengers in an efficient airframe which is compatible with existing airports (terminal gates, taxiways, runaways, etc.), and meets customer requirements (cost, performance, operating economics, etc.), expected noise regulations, safety standards, and others of a myriad of operational and economic constraints. An obvious (traditional) approach to all this has been to take a proven aircraft configuration, increase the size to that required, and then refine it until it works. The Boeing 747 has worked very well for about 30 years based on the original Boeing B-47/B-52/707/C-135 paradigm. The evolution of this basic configuration and its merits relative to an alternative classic are shown in Fig. 3 and have been well documented by Schairer [3], Cook [4] and Roskam [5] following Torenbeek [6]. This approach thus represents a logical point of departure for very large (600 passenger) airplane configuration studies. Typical of what one gets by this approach is shown in Figs. 4 and 5. It also suffers from quite a list of often mundane but potentially very serious problems as listed in Fig. 5. In the end it may be considered perhaps the ultimate limit of extrapolation of a long line of highly successful recapitulations by Boeing (and its competitors) on a good basic scheme. A question, which is the subject to be addressed in this paper, that thus arises is: Is this basic, 50-year old configuration paradigm really the appropriate (or best) one for an

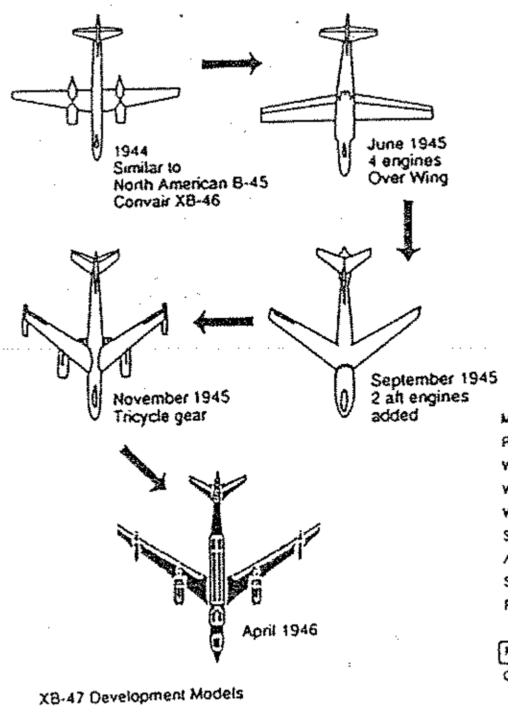

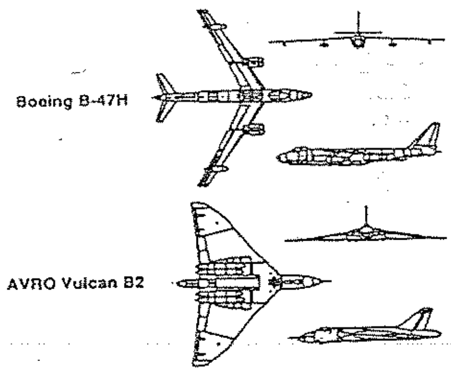

		Boeing B-47H	AVRO Vulcan B2
Max. take-off weight	W_{TO}	202,000	200,000
Ref. wing area	S	1,400	3,964
Wetted surface area	S_{wet}	11,300	9,600
Wing span	b	116	111
Wing loading	$(W/S)_{TO}$	144	50.5
Span loading	$(W/b)_{TO}$	1,741	1,801
Aspect ratio	AR	9.6	3.1
Skin friction coefficient	Cf (assumed)	0.0030	0.0030
Parasite drag area	$f(C_f{}^*S_{wet})$	34.0	29.0
	$dC_D/dC_L{}^2$ (e=0.8 assumed)	0.041	0.128
Max. lift-drag ratio	$(L/D)_{max}$	15.8	16.4
C_L at L/D Max.	$CL(L/D)_{max}$	0.77	0.24

Fig. 3. Evolution of the Boeing B-47 configuration and a comparison with a very different airplane configuration designed for the same mission.

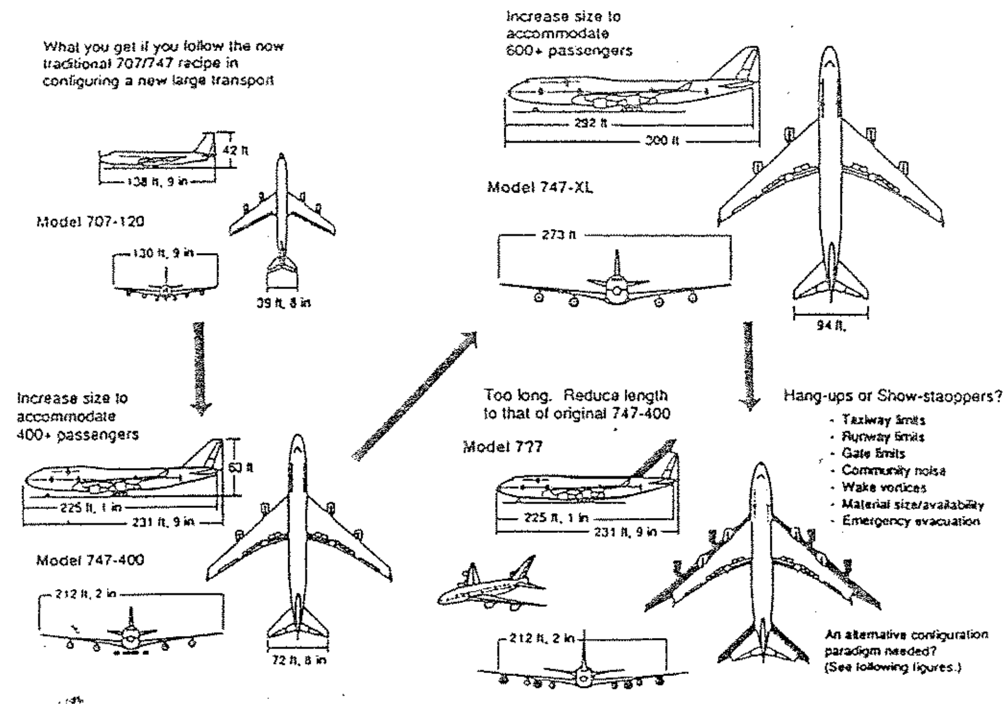

Fig. 4. A demonstration of a classic evolutionary process in transport airplane design.

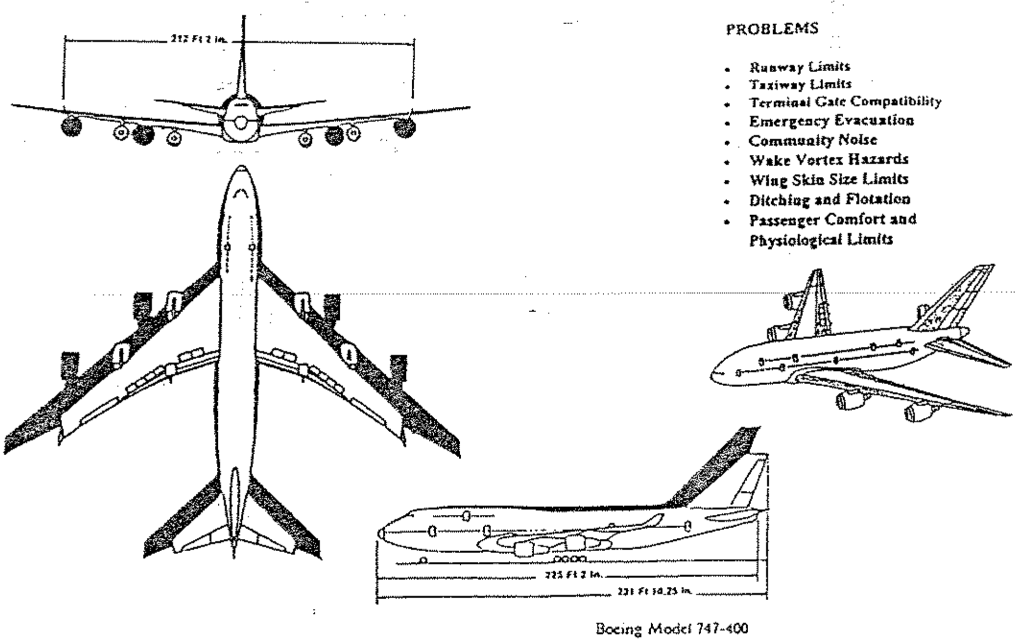

Fig. 5. A conventional configuration for a possible very large (600 passenger) subsonic commercial transport airplane (ca. 1992) shown in comparison with a Boeing 747-400.

airplane substantially larger than a 747? Before addressing this issue however, the more general question of the effect of increasing size beyond current limits on the economics of a conventional transport airplane configuration is worth further evaluation.

2. The effects of aircraft size on performance and cost

A very simple study of the effect of aircraft size on performance and cost produces some interesting results. It has been suggested that the square-cube law [9,10] may limit the feasible size of aircraft in a given category and that proposed 600–800 passenger transport aircraft may be approaching this limit. There is, of course reason to suppose that the square-cube law will at some (highly technologically dependent) point limit the feasible size of aircraft (cf. [10]). For example, for geometrically similar configurations wing weight can be expected to grow as WbAR from bending strength considerations alone, and thus wing weight of the aircraft as size and weight increase. As it turns out, however, wing and fuselage weight remain a *relatively* modest fraction of the total airplane weight, and to explore the issue of the net effects of size increase requires a more detailed quantitative evaluation. The details of the analysis that one of us (Kroo) conducted in the context of the topic of the present paper are outlined in [1] using methods (an empirically enriched and extended square-cube law analysis) described in [11] to which the interested reader is encouraged to refer.

To permit a rapid trade study, many parameters that would be optimized in a more refined design were held constant to obtain the result to be reported here. Thus, in addition to specifying certain fixed performance parameters (initial cruise altitude, cruise Mach number and range), a number of geometric parameters (wing aspect ratio, sweep, thickness–chord ratio, airfoil geometry, fuselage fineness ratio, tail area ratio, etc.) were held constant. Computations were then performed for a family of "conventionally configured" aircraft ranging in size from a 4-abreast "commuter-size" dwarf to a triple deck monster with approximately 1500 passengers in 29-abreast seating. The results for a common 5000 nautical mile mission flown at a cruise Mach number of 0.8 at an initial cruise altitude of 32,000 are shown in Fig. 6. While highly simplified, the analysis can be seen to have produced results that are at least first-order correct with respect to existing aircraft for which such comparisons are valid.

To some degree the results shown in Fig. 6 are surprising. The expected square-cube law trend showing the largest aircraft to be uneconomical is not demonstrated. Rather direct operating cost (DOC) is seen to decrease even for the largest aircraft although the data also shows that for machines with more than 600 passengers, the improvement is very slight for these conventional configurations. The fundamental conclusion to be drawn from this exercise is that basic aerodynamic and structural considerations do not inherently limit the size of a subsonic aircraft that can be operated economically – at least in the case where there are no externally imposed limits. In practice, however, issues such as airport compatibility, scheduling, passenger loading and servicing, emergency egress and other very practical, if seemingly mundane or "trivial", matters become the principal concerns to be dealt with and, if solutions cannot be found, may become show-stoppers.

As a matter of interest, as design work commenced ca 1992–93 on 600+ passenger transports in several companies, the overlooming issues that most profoundly tended to limit airplane

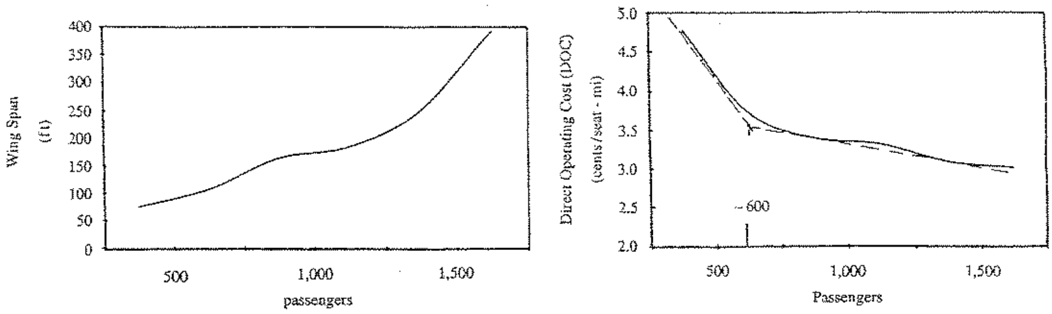

Seats in cross-section	Fuse. width (ft)	Fuse. ht (ft)	No. Seats Total	Take-off Wt (klb)	Wing span (ft)	Wing area (sq ft)	L/D	DOC (cents/ seat-mi)	Relative price	
4	8.7	8.7	68	92	75	707	16.1	4.77	0.58	Cruise $M = 0.8$
5	10.6	10.8	100	137	92	1054	16.4	4.13	0.77	Range = 5000 n.mi
6	12.3	12.3	138	190	108	1461	16.8	3.73	1.00	Init. Cr. Alt. = 32 kft
7	16.5	18.1	217	336	144	2585	16.9	3.66	1.65	AR = 8.0
8	18.5	18.5	280	435	164	3346	17.4	3.49	2.07	Wing Sweep = 30 deg.
9	20.3	20.3	351	558	185	4292	17.7	3.50	2.87	SLT/W = 0.3
12	21.3	25.7	492	770	218	5923	18.2	3.32	3.63	
16	22.2	28.0	672	1025	251	7885	18.7	3.10	4.78	
19	25.6	31.1	931	1460	300	11231	19.4	3.06	6.83	
29	27.9	33.6	1537	2500	392	19231	20.0	3.03	6.66	

Fig. 6. Results of a "square-cube law" analysis of the effects of size increase on a subsonic transport airplane of conventional configuration (cf. Fig. 5).

size were airport compatibility (both in terms of terminal gate clearances, a variety of awkwardly placed "immovable" obstructions around runways or taxiways at certain key airports, and various pavement loading constraints which imposed severe restrictions on landing gear placement and design), emergency evacuation requirements as mandated by various national and international airworthiness regulations, and the always looming spectre of wake vortex hazards and ever more stringent community noise limitations. After considerable pencil sharpening and negotiations, it was eventually concluded that if the proposed new airplanes could be designed to fit within the confines of an "80 m ($\sim$260 ft) box", most of the more serious airport compatibility issues could be resolved. The emergency egress problem for conventional (usually double-deck) aircraft configurations has remained a central challenge, however.

3. Alternative large subsonic transport airplane configurations

Having concluded on the basis of a first-order/first principles analysis that with respect to the technical portion of the problem pure size increase *alone* does not appear to limit airplane performance and economics, the question of what configuration(s) may be "best" for an unconventionally large subsonic transport airplane may be addressed. The primary purpose in this is to explore possible opportunities to exploit the unconventionally large *physical size* of a "Jumbo 747" (or its major components parts) which, when coupled with advances in technology available in various disciplines, might allow a designer to

1. obtain significant improvements in airplane performance and economics compared to those aircraft currently in operation, or
2. find ways to circumvent practical operational and infrastructure-related problems encountered in increasing the size of an orthodox configuration beyond current limits without incurring significant performance or economic penalties.

The first option has been the traditional target for most classes of aircraft developed since the beginning of our enterprise. It has simply been what we did in a general quest to fly farther, higher, faster, and more economically. A good example of this approach is reflected in the recent work of our colleagues Bob Liebeck and Mark Page reported in a companion paper [11], early results of which were to some degree the genesis for the large airplane configuration studies to be reported here. As our work progressed, however, the second objective listed above very quickly became the central focus of our investigations. Thus, the Liebeck/Page approach to the very large airplane problem and our own represent almost diametrical opposites to each other, with some interesting convergences in conclusions to be drawn from our largely independent work. Neither result looks much like a Boeing 747 with a watermelon-proportional fuselage (cf. Figs. 4 and 15) – thank fortune.

3.1. *Innovative airplanes – a digression into generalities*

The authors, as teachers and thus students of airplane design, are as different (and opinionated) as is characteristic of our breed. Each of us was drawn to the commercial airplane design problem for different reasons, and to varying degrees, reluctantly. At this rather late stage in an admittedly very high stakes game, we seem to find what is widely *perceived* to be a "mature" technology characterized by continuing development of "cookie-cutter" airplanes superficially almost identical in outward appearance to each other (though varying in size) with all the romance of "flying Greyhound buses". Can there really be nothing new from now on to excite a future generation of our own students as one of us (John) was once enthralled by "Spitfires" and Messerschmitts (or F-15s and Sukhois in more recent times)?

All this is of course nonsense, and the continued challenge of developing viable transports in an ever more complex international environment is as demanding, rewarding and intellectually stimulating as it has ever been. Continuing the previous line of philosophic maundering a bit farther, however, a student of the history of airplane design may observe that while most of the airplane designs of the past were a mixture, there are two basic flavors to the approach taken in their conception. In this artificial differentiation, one class of designer had in mind arranging the best state-of-the-art components of the airplane so that the result "best" met a given set of mission or performance requirements and constraints. The aesthetic consequences of this might be more or less pleasing, but were generally a derivative by-product of the designer's art. Ever mindful of the maxim "innovation for innovation's sake can be a great waste of time", this class of designer recognized that form must generally follow function as dictated by the often counterintuitive imperatives of physics and economics. The results of this first approach might best be described as "Mission Driven" designs.

A second fundamental approach to the design problem may be characterized as "Concept Driven". In this case the designer either: (1) had some preconceived notions of what he wanted his airplane to look like and then did every thing possible to produce a practical machine that preserved the pristine purity of the "aesthetic ideal" thus envisioned, and/or (2) had some mechanical or design concept around which a practical airplane was to be build and did every thing possible to achieve this end. Examples of the former were many of the designs by Jack Northrop, the Horten brothers, and Alexander Lippisch. The latter are represented by machines such as the Custer "Channel Wings", the "lifting bodies" of Vincent Burnelli, and a large portion of the various schemes developed to provide aircraft with a vertical take-off and landing capability. Somewhere in the middle of this whole class of concept airplanes are the now numerous products of the fertile mind of Burt Rutan and his colleagues. A large proportion of the results of this class of design have been either failures or only marginally successful for some of the reasons outlined by Roskam [5]. Others were essentially ahead of their time, and while "failures" at the time of their original embodiments, such concept airplanes are occasionally worth revisiting on the basis of what new enabling technology may have been developed in the intervening time period that might transform failure into success. A now classic example of this is the advent of the Northrop B-2 bomber (aided by active controls and composite structures technology) with its partial genesis in the original dreams of Jack Northrop, ca. 1940–50. Thus we are reminded of the immortal words of the famous aerodynamicist Dietrich Kuchemann [13], which have been a running thread through much of the subsequent discussion of *very* large airplane configuration alternatives: "To prove that a pig cannot fly is not to design a machine that can do so".

It may also be noted that, once conceived, the traditional approach to developing a new airplane was to divide the overall problem into bits and parts that individuals or small groups could deal with. Then, organized within fairly strict discipline boundaries, work each problem separately assuming that after being passed back and forth between various hands in sequential steps, the sum of these discrete parts would somehow add up to a good airplane system. In many cases this process worked – witness, for example, Boeing's commercial transport sales record over the 30-year period ca. 1960–90. At the same time it may be argued that much of our industry had become organizationally and intellectually "muscle bound" by past successes. A partial solution to this has been the more recent use of multidisciplinary "integrated product teams" which has proven successful in the development of products such as the Boeing 777. Members of these IPTs still retain a high degree of discipline specificity in their outlook and it may be argued that, if we are to advance beyond our present limits, the future may lie in the hands of individuals who can be characterized as "deep generalists". Such individuals would have a sufficient depth of knowledge in more than one technical discipline to allow them (working in teams with necessary discipline-specific experts) to more fully exploit possibly unorthodox synergisms in the creation of very highly integrated systems. It is a purpose of this paper to demonstrate (albeit primitively) a possible result of such an approach to the airplane design problem.

3.2. Innovative very large airplane configurations

A "conventional approach" to innovation in dealing with a very large airplane is to examine various forms of wing-alone or tail-less configurations with the disposable loads (payload and fuel) distributed over the span of the wing with the overall system optimized for maximum cruise efficiency. As described above, while the pristine purity of this sort of approach can produce very aesthetically appealing results [12,14,15], past examples have generally failed to pass one or more critical tests of operational or manufacturing suitability, and thus have seldom found favor when decisions regarding what to offer for sale are made. The appeal to some of this class of configuration remains, however, and the following line of reasoning may be pursued:

- The ideal cruising airplane (at least from an aerodynamicist's point of view) wants to be a simple, elegant flying wing. Everything that does not contribute to the efficient generation of lift should be placed in or on the wing *provided* that in so doing no significant weight, cost or other penalties are incurred.
- A typical business-class passenger may be assumed to be approximately 6 ft tall. A typical transonic cruise airfoil section is currently about 12% of the wing chord in thickness. Thus if the inboard wing chord exceeds about 70 ft (~ 20 m), it becomes feasible to *imagine* placing the payload in a wing of only moderate sweep rather in a drag and weight producing fuselage. When 3 dimensional considerations are included, such an arrangement is possible with substantially smaller chords.
- Contrary to popular myth, aerodynamics is not yet a sunset technology and there are still a number of items have yet to be exploited in a subsonic transport airplane: These include:
    - Active and hybrid laminar flow control schemes.
    - Active (e.g. Griffith/Goldschmied [16]) and passive (e.g. slotted cruise [17]) boundary layer control airfoils.
    - "Extremely" non-planar wings (i.e. far beyond "visible technology" winglets).
- There are similar opportunities in other disciplines, including:
    - The advent of high-bypass ratio turbofan engines in the 400 kN thrust class
    - Fly-by-wire/fly-by-light active control systems
    - Composite (anisotropic) structural materials
    - Computational tools to deal with "designed aeroelastics", increasingly powerful multi-disciplinary optimization (MDO) routines, etc.

The train of thought this list generated led one of the authors (John) to begin a series of informal and unofficial (i.e. outside any Boeing product development organization) concept scoping exercises aimed at exploring configuration concepts that might resolve or ameliorate the very large airplane problems identified in Fig. 5. Again, the very large size of any greater-than-600 passenger airplane immediately suggests a flying'wing/span-loader configuration, a candidate (ca. 1991) example of which is shown in Fig. 7. Serendipitously, this sort of (mostly) all wing configuration is a promising candidate for laminarization. A quick calculation suggested that using conventional airfoil technology (cf. Fig. 8), the required wing would not be thick enough until it became large

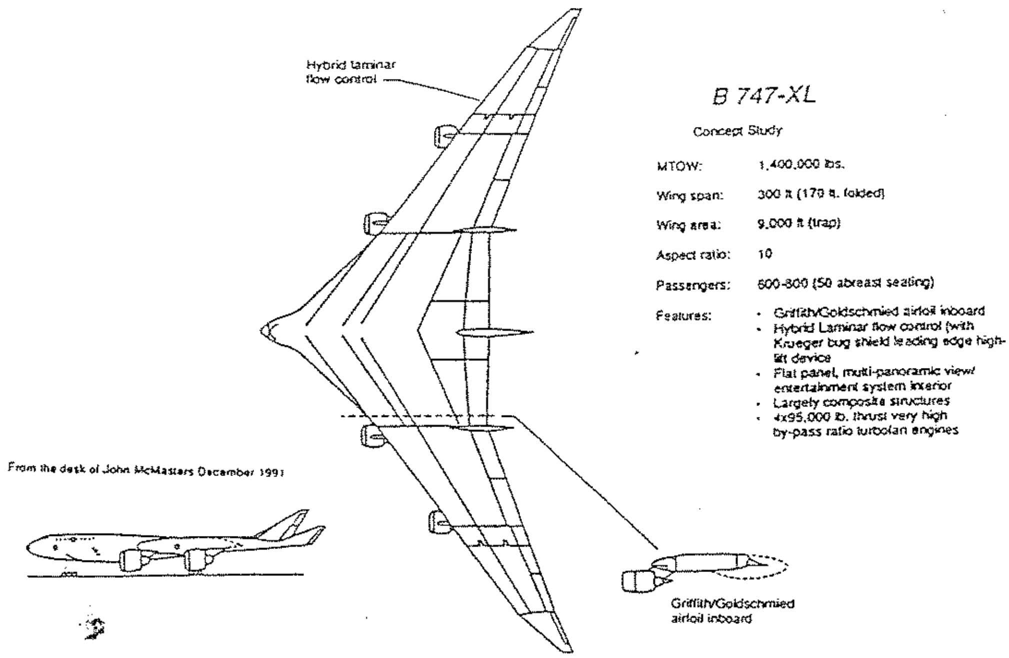

Fig. 7. A preliminary concept for a very large span-loader subsonic transport.

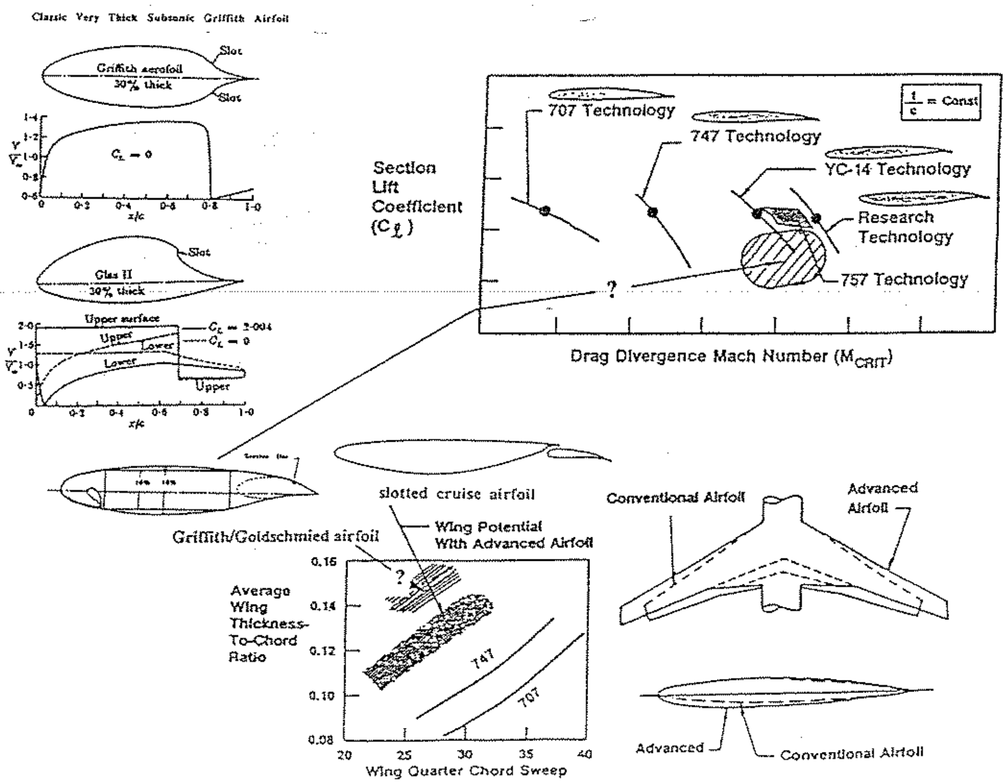

Fig. 8. Prospects for advances in transonic airfoil technology.

enough to carry around 800 passengers; or was swept exorbitantly, which is of course antithetical to the requirements for establishing laminar flow.

A "conventional flying wing" of this sort also has its own suite of problems both in the air and on the ground, most particularly with respect to airport/terminal compatibility, emergency egress and the perennial question: "Where do you put the passenger windows on a thing like that?" The precedent of using folding wing tips on the Boeing 777 and the use of seat-back video entertainment systems suggest ways to address some of these issues within the current state-of-the-art in commercial aircraft. More fundamentally, in order to reduce the size to that required to carry *only* 600 passengers what is wanted is an unconventionally thick cruise airfoil and an obvious candidate is the Griffith section invented in Britain over 50 years ago and more recently advocated in this country by Fabio Goldschmied and others ([16], Fig. 8). Limited (low-subsonic) test data and calculations indicate that it may work provided enough suction is provided, although this has yet to be demonstrated at transonic conditions. It should also be noted that a span-holder is likely to have a lot of wing area which means in turn that at cruise conditions, airfoil section lift requirements will be rather low, thereby offering an opportunity to trade section lift for thickness while retaining adequate critical Mach number capability on a wing of acceptable (for LFC purposes) sweep angle. High-lift requirements are similarly reduced, at least in principle. As a final side benefit, the rather unorthodox geometry of a classic (subsonic) Griffith/Goldschmied airfoil suggests the possibility that when it exceeds a given *physical* thickness, the entire aft wing spar/pressure-bulkhead area becomes available at a location for the necessary emergency escape system, thus potentially ameliorating a major problem with any large airplane configuration. Thus despite its problems and limitations, the concept shown in Fig. 7, and the technology incorporated in it, might contain the germs of a promising idea.

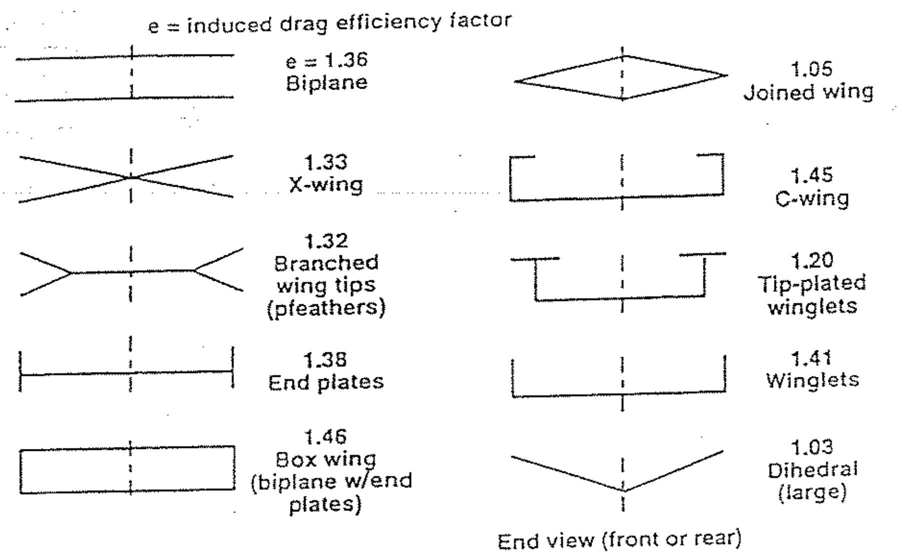

Fig. 9. Theoretical values of the induced drag efficiency factor (e) for various non-planar wing configurations of the same projected wing span, area, and height-to-span ratio ($=0.2$).

3.3. Alternate alternative large airplane configurations

While the airplane shown in Fig. 7 is less boldly imaginative (and aesthetically pleasing) than its Liebeck/Page counterpart as these machines existed ca. 1991–92, they all shared the common problem of having enormous (greater than 80 m) wingspans. To address the wing span issue(s) a study by one of the authors (Kroo) is of considerable interest. In this study, the results of which are summarized in Fig. 9, the theoretical induced drag span efficiency factors (e) for a wide range of non-planar (when viewed from the front or rear) wing configurations were calculated in a Treffetz plane analysis [18]. The results demonstrate the obvious advantage of a wing with very large winglets compared to an optimally loaded planar wing ($e = 1.0$) of the same projected area and span. While this result is well known, a bit more intriguing from his menu of unorthodox wing configurations is the "C-wing" which amounts to adding a pair of smaller horizontal winglets on the tips of the ordinary vertical winglets. While this configuration shows only a small increase in span efficiency factor compared to simpler wingleted configuration, quite a different picture emerges when one contemplates sweeping such an arrangement by a conventional amount (say, about 35° on all surfaces). This arrangement puts the horizontal "winglets-lets" in roughly the longitudinal position of a T-tail horizontal stabilizer relative to the rest of the wing. When optimally loaded, the winglet-lets are lifting *downward*, just as the horizontal tail on a conventional airplane during cruise.

From this point it does not take much imagination to transform the simple span loader in Fig. 7 into the C-wing configuration shown in Fig. 10, the principal features of which are

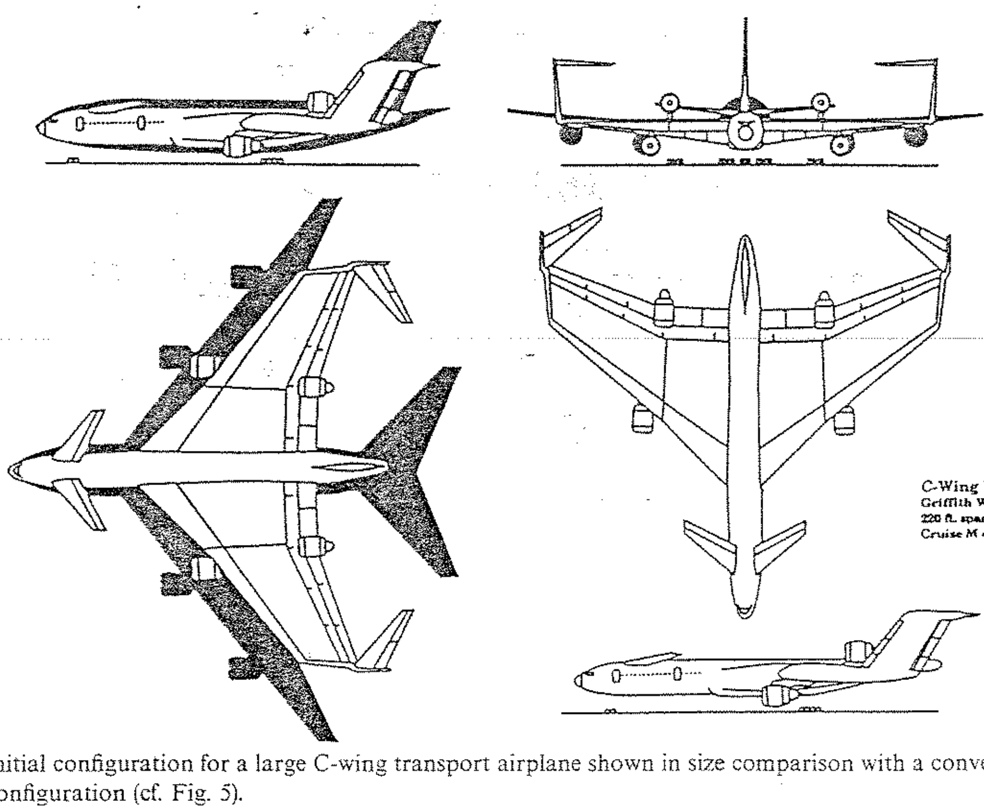

Fig. 10. Initial configuration for a large C-wing transport airplane shown in size comparison with a conventional large airplane configuration (cf. Fig. 5).

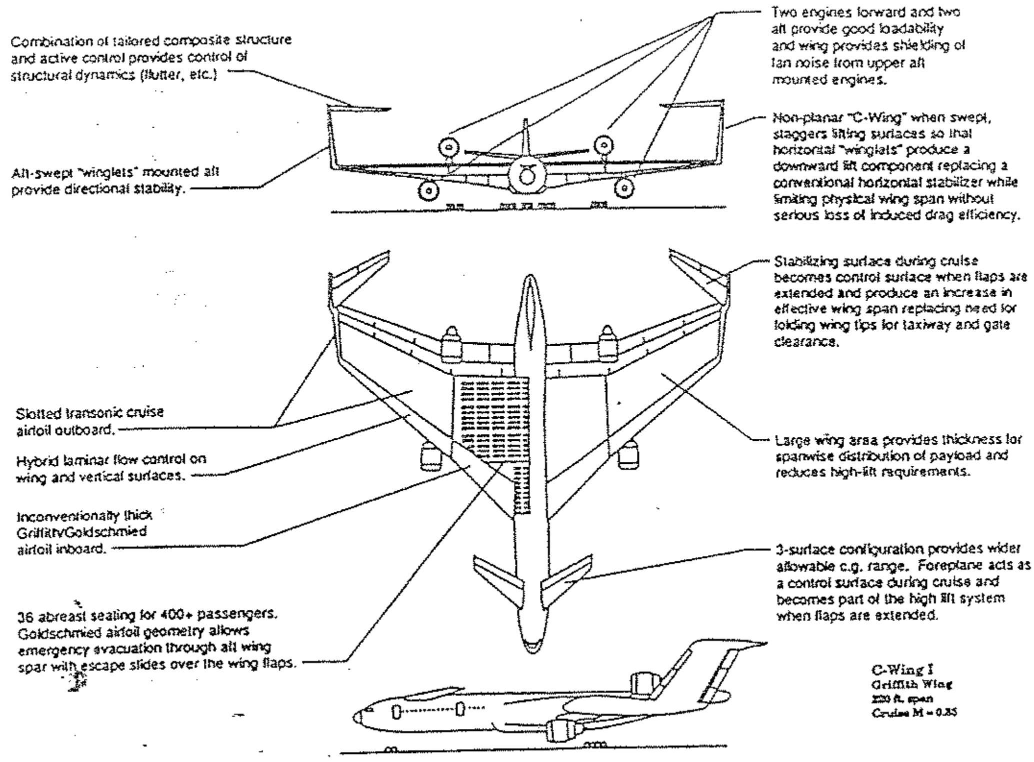

Fig. 11. Principal design features of the initial large C-wing transport airplane configuration.

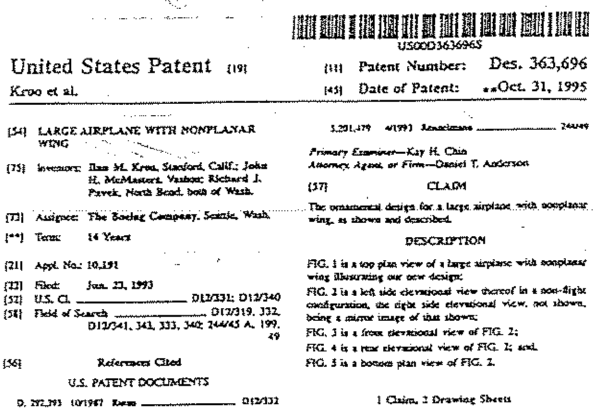

US00D363696S

United States Patent [19] — Kroo et al.

[11] Patent Number: Des. 363,696
[45] Date of Patent: **Oct. 31, 1995

[54] LARGE AIRPLANE WITH NONPLANAR WING

[75] Inventors: Ilan M. Kroo, Stanford, Calif.; John H. McMasters, Vashon; Richard J. Pavek, North Bend, both of Wash.

[73] Assignee: The Boeing Company, Seattle, Wash.

[**] Term: 14 Years

[21] Appl. No.: 10,191

[22] Filed: Jun. 23, 1993

[52] U.S. Cl. D12/331; D12/340

[58] Field of Search .... D12/319, 332, D12/341, 343, 333, 340; 244/45 A, 199, 49

[56] References Cited

U.S. PATENT DOCUMENTS

D. 292,393 10/1987 Kroo D12/332
5,201,479 4/1993 Renzelmann 244/49

Primary Examiner—Kay H. Chin
Attorney, Agent, or Firm—Daniel T. Anderson

[57] CLAIM

The ornamental design for a large airplane with nonplanar wing, as shown and described.

DESCRIPTION

FIG. 1 is a top plan view of a large airplane with nonplanar wing illustrating our new design;
FIG. 2 is a left side elevational view thereof in a non-flight configuration, the right side elevational view, not shown, being a mirror image of that shown;
FIG. 3 is a front elevational view of FIG. 2;
FIG. 4 is a rear elevational view of FIG. 2; and
FIG. 5 is a bottom plan view of FIG. 2.

1 Claim, 2 Drawing Sheets

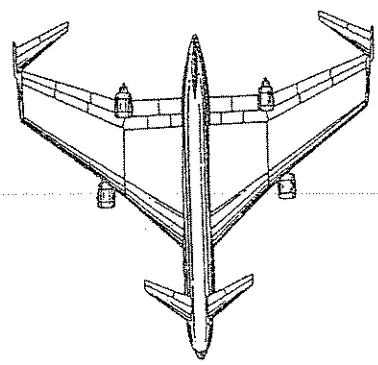

Fig. 12. Design patent issued [10/31/95] for the initial C-wing transport.

shown in Fig. 11. Along the way this became a quasi-three surface (rather than canard) airplane for reasons outlined in [18,19]. This new configuration, for which a patent was applied for in June 1993 and granted to Boeing and the authors in October 1995 (Fig. 12), retains many of the features of a *single deck* span loader with the projected wing span reduced to that of a ca. 1992 conventional very large (600 passenger) airplane with its wing tips folded (i.e. to fit into a terminal gate compatible with a Boeing 747), while retaining approximately the same (on paper) induced drag characteristics of the baseline configuration with 280 ft of span. The price is a pair of winglets which are *each* roughly the size of the vertical stabilizer on a 747, which still results in airplane with a tail height about 20 ft less than that of the conventional airplane (cf. Fig. 10).

It should be noted here that the work done to this point in developing the C-wing configuration was done in parallel with and independently of the official program within Boeing to develop what was being called the New Large Airplane (NLA) [7,8]. No Boeing NLA-specific data and configuration drawings other than what has been published in the open literature has been used in the work reported in this paper. Other than allowing one of the authors to seek a NASA contract for further study of the concept (and to apply for a patent for it), and authorizing the use of proprietary generic preliminary design methodology (e.g. ahighly modified version of the sizing routine ACSYNT [20]), the configuration development work has never had much official status within Boeing. That work was able to continue beyond the point described so far was due to the interest of a few individuals within NASA, Boeing and the team of individuals from several universities which we put together to conduct a limited "research analysis" under the auspices of the then new NASA Advanced Concepts Program in 1994. The subsequent work done by our team under NASA contract (NAS1-20269, awarded in August 1994) is reported in [1] and need only be summarized in the remainder of this paper.

4. The NASA sponsored phase of C-wing configuration development

4.1. Basic configuration objectives

As noted earlier, the primary purpose in developing the alternative configuration concepts described in this paper was to investigate ways to directly address the problems to be anticipated in increasing the size of a Boeing 747-like configuration to that required to produce an economically and operationally satisfactory 600–700 passenger airplane, rather than to explore opportunities to significantly improve airplane performance. In particular, the following issues were the primary focus of attention:

1. To meet large airplane economic and performance goals, a conventional planar wing of very large span (260–280 ft) is required. To meet ground handling and terminal area operating restrictions it was originally thought that some sort of folding wing tip arrangement would be required with concomitant weight penalties, complexity and safety concerns. Further, if a conventional podded, underwing engine location is to be used, the mandatory high-bypass ratio turbofans, when optimally located across the span, present potentially major runway/taxiway compatibility problems. In the configuration show in Fig. 5, for example, the outboard engines of a typical vintage NLA are located at about the wing tip stations of an existing Boeing 747. While the C-wing configuration "looks strange" and represents some potentially formidable structural dynamics and stability and control problems, it also offers the promise of significantly ameliorating the worst of the large airplane "wing span problems" without incurring

a significant induced drag penalty. A very preliminary analysis also indicated that the C-wing might be potentially advantageous in reducing wake vortex hazards, although much work remains to be done to verify this.

2. A conventional double-deck, quasi-circular cylindrical fuselage works well enough until airplane capacity, constrained by acceptable maximum body length, reaches the point where meeting safety requirements for emergency evacuation becomes an overriding concern. The double-deck 600-plus passenger airplane is at that limit. Thus a central objective was to devise a configuration that directly addresses the emergency evacuation problem, preferably with a single-deck configuration that met all other NLA galley, lavatory, etc., requirements in a normal tri-class passenger arrangement. The huge wetted area and volumetric efficiency of very large conventional cylindrical fuselages also seemed to offer opportunities for improvement. The possible synergisms with the unorthodox geometry of a Griffith airfoil offered some intriguing opportunities (and new problems) in connection with these issues.
3. While not a central consideration, the possible advantages of a span loader/flying wing configuration as a laminar flow control airplane compared to a conventional NLA were magnified by the large percentage of airplane total wetted area represented by the huge cylindrical fuselage in the latter. Conceptually, it was imagined that if some of the fuselage wetted area could be transformed into wing (lifting surface) area without excessive penalty, then a larger percentage of total airplane wetted area would be available for effective laminarization. This benefit might then be used to improve performance or to off-set other potential penalties imposed by employing the unusual wing configuration selected. Lack of budget precluded serious analysis of this potential in our subsequent investigations, however, and the quantitative results to be reported later are for conventional "turbulent flow" aircraft.

As these basic factors were weighed and the overall C-wing configuration reached a better level of definition, a more interesting (than the airplane itself) factor began to emerge. It became increasingly clear that the preferred configuration concept was a highly complex system of interlocking parts with several very unconventional interrelationships between the concerns of what, in the past, have been more-or-less independent disciplines. The clearest example of this is in the inextricable relationship between the performance and geometry of the Griffith airfoil, details of a high-lift system compatible with it, and the payloads issues of passenger compartment layout and emergency evacuation. Likewise the use of the highly non-planar C-wing involves the judicious balancing of its characteristics as a means to potentially reduce wing span while maintaining the desired level of induced drag, while at the same time making it an intrinsic part of the airplane stability and control system about all three axes of the airplane – in addition to consideration of its possible effect on wake vortex hazards. In short, almost every aspect of this airplane becomes more-or-less unconventionally multi-disciplinary, opening opportunities for new synergisms and/or exacerbating the difficulty of making the trades and compromises like those which are now well understood in developing viable systems configured along traditional lines. In several important areas, existing analysis methods (calibrated to a very large base of past data) are not capable of providing firm answers on sizing and performance questions of central importance. In profound ways, the whole design approach for such highly integrated unconventional configurations needed to be rethought.

It was for some of these reasons that as the already controversial C-wing configuration was evolving, we stopped short of going even farther by incorporating the highly integrated propulsion scheme originally envisioned for the blended wing-body concept. Early on, it was decided to build our concept around the use of a conventional single-deck cylindrical body core (in the case shown, that of a Boeing 777). This more conservative approach has several advantages. Most importantly, a significant portion of the payload compartment thus remains "independent" of the complex airfoil contour-constrained inner wing passenger compartment. Therefore a significant portion of the weight, etc. of the passenger compartment can be estimated reliably using well established data; much of the emergency evacuation, interior layout (overhead bins, gallery placement, etc.) can be dealt with in a conventional manner; first class and some business class passengers can be provided

Table 1
Summary of results of a preliminary sizing analysis of C-wing airplane configuration using the Boeing vesion of ACSYNT

Geometry summary	Baseline: (Conventional) 259 ft span, Cruise $M = 0.85$	C-Wing I Griffith wing 220 ft span Cruise $M = 0.85$	C-Wing II Griffith wing 240 ft span Cruise $M = 0.85$	C-Wing III conventional wing 240 ft span Cruise $M = 0.80$
Engine				
Number	4	3	3	3
Diameter (ft)	9.5	10.7	10.2	10.2
Weight (lbs)	13,310.3	18,098.2	16,374.5	16,374.5
TSLS (1bs)	77,200.0	105,000.0	95,000.0	95,000.0
SFC (TSLS)	0.313	0.313	0.313	0.313
Fuselage				
Length (ft)	226.5	205.9	205.9	205.9
Diameter (ft)	24.4	20.3	20.3	20.3
Wing				
Reference area (sq. ft.)	8,000.0	12,000.0	12,000.0	12,000.0
Total area (sq. ft.)	8,379.3	12,315.4	12,385.0	12,385.0
Wetted area (sq. ft.)	14,724.2	21,353.5	21,574.5	21,632.6
Span (ft)	258.7	220.0	240.0	240.0
C/4/Sweep (deg)	38.9	34.0	34.7	34.7
Aspect ratio	8.37	4.03	4.80	4.80
Taper ratio	0.23	0.41	0.41	0.41
T/C root (ft)	0.130	0.160	0.160	0.180
T/C tip (ft)	0.100	0.100	0.100	0.100
Root chord (ft)	70.5	99.1	97.2	97.2
RAC (ft)	31.9	56.7	51.1	51.1
Weight				
Structure	297,001	369,602	382,723	380,595
Propulsion	62,093	67,809	61,671	62,077
Fixed equipment	96,780	88,866	88,665	88,906
Minimum empty weight	455,874	526,277	533,059	531.578
STD & OPR items	50,335	47,026	46,506	46,921
Operating empty weight	506,209	573,303	579,565	578,499

Table 1. *Continued*

Performance summary	Baseline: (Conventional) 259 ft span, Cruise $M = 0.85$		C-Wing I Griffith wing 220 t span Cruise $M = 0.85$		C-Wing II Griffith wing 240 ft span Cruise $M = 0.85$		C-Wing III conventional wing 240 ft span Cruise $M = 0.80$	
Airport elevation (ft)	0		0		0		0	
Airport temperature (deg F)	59		86		86		86	
Range (Nautical miles)	7400.0		7399.8		7399.9		7399.9	
Block time (h)	15.709		15.621		15.642		16.555	
Ramp weight (lbs)	1,086,132		1,214,497		1,190,786		1,219,284	
Takeoff weight (lbs)	1,084,782		1,213,120		1,189,540		1,218,038	
Landing weight (lbs)	678,535		752,482		756,056		756,594	
OEW (lbs)	506,209		573,303		579,565		578,499	
Payload (lbs)	126,000		126,000		126,000		126,000	
Passengers (600)	105,000		105,000		105,000		105,000	
Baggage	21,000		21,000		21,000		21,000	
Total fuel (lbs)	453,923		515,115		485,324		514,720	
Block fuel	409,347		462,780		435,422		463,383	
Reserve fuel	45,326		53,100		50,595		52,030	
Fuel/seat	682.2		771.3		725.7		772.3	
Takeoff field length (ft)	8795.4		9505.6		10,151.9		10,688.5	
Landing field length (ft)	6459.3		5.424.3		5408.6		5367.8	
Approach speed (kt)	141.3		123.9		123.7		123.0	
ICAC (buffet limited) (ft)	38292.6		44373.1		44,810.2		41,855.6	
	Req'd	Actual	Req'd	Actual	Req'd	Actual	Req'd	Actual
Initial segment climb gradient (does not include ground effect)	0.017	0.099	0.015	0.031	0.015	0.021	0.015	0.032
Transition segment climb gradient	0.005	0.084	0.003	0.031	0.003	0.003	0.003	0.014
Second segment climb gradient	0.030	0.099	0.027	0.031	0.027	0.021	0.027	0.032
En-route climb gradient	0.017	0.077	0.015	0.036	0.015	0.027	0.015	0.034
Landing approach climb gradient	0.027	0.183	0.024	0.091	0.024	0.078	0.024	0.079
Landing climb gradient	0.032	0.299	0.032	0.248	0.032	0.215	0.032	0.222

with conventional windows; and finally, growth can be readily provided for by the simple, traditional expedient of lengthening of the fuselage with cylindrical body "plugs" (without the necessity of major redesign of the wing). All of this is incorporated in the initial C-wing baseline design shown in Figs. 10 and 11.

This baseline was the beginning point for sizing analyses conducted independently by Monica Fetty at NASA-Langley Research Center (using NASA methods) and at Boeing using the aforementioned company version of ACYSNT. In both the NASA and Boeing analyses generic conventional "NLA-like" airplane configurations were also analyzed to provide a direct basis for comparision. The results of the Boeing analysis are contained in Table 1. Here four cases are

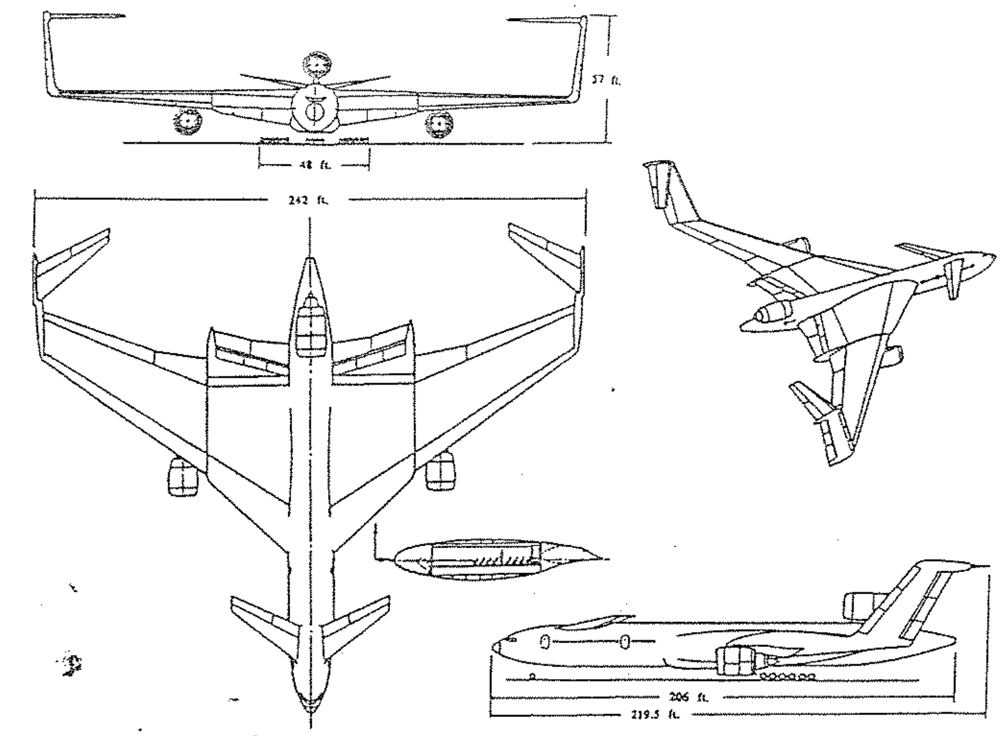

Fig. 13. Final 600 passenger C-wing transport configuration [C-wing II].

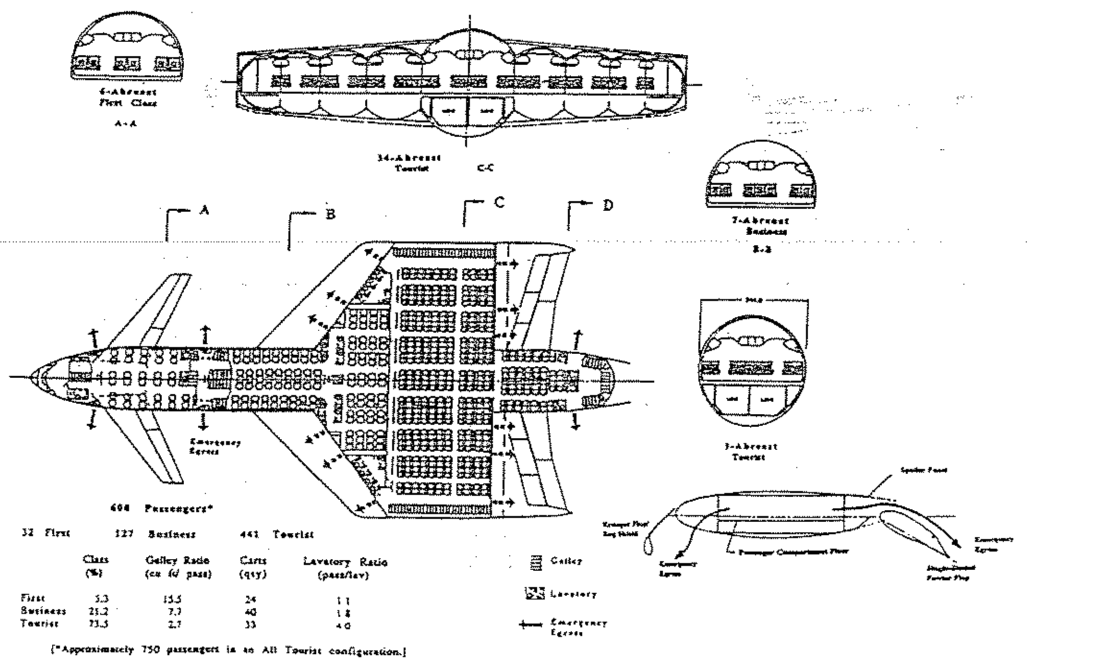

Fig. 14. Layout of passenger accommodations (LOPA) for the final 600 tri-class passenger C-wing II configuration.

summarized, each airplane carrying 600 passengers in a tri-class arrangement flying a common 7400 n.mi. range mission with necessary fuel reserves, etc., according to standard international mission rules. The cases shown were:

- A conventional-configuration baseline with cruise $M = 0.85$.
- A 220 ft span C-wing with cruise $M = 0.85$.
- A 240 ft span C-wing with cruise $M = 0.85$.
- A 240 ft span C-wing with cruise M reduced to 0.80 (to evaluate the possible consequences of eliminating the need to use the Griffith airfoil).

It should be noted that while certain of the initial assumptions were very different and the weights predicted by the NASA and Boeing analyses showed substantial differences (cf. [1]), the *trends* predicted independently by the two methods were generally quite similar and both sizing routines produced "optimum" C-wings with spans of about 73 m (240 ft). The final C-wing configuration (C-wing II) developed on the basis of these analyses is shown in Figs. 13–15 and may be compared to a later (ca. 1994) version of the Boeing NLA with span reduced to about 80 m [7] and the competing Airbus A 3XX [8] shown in Fig. 16.

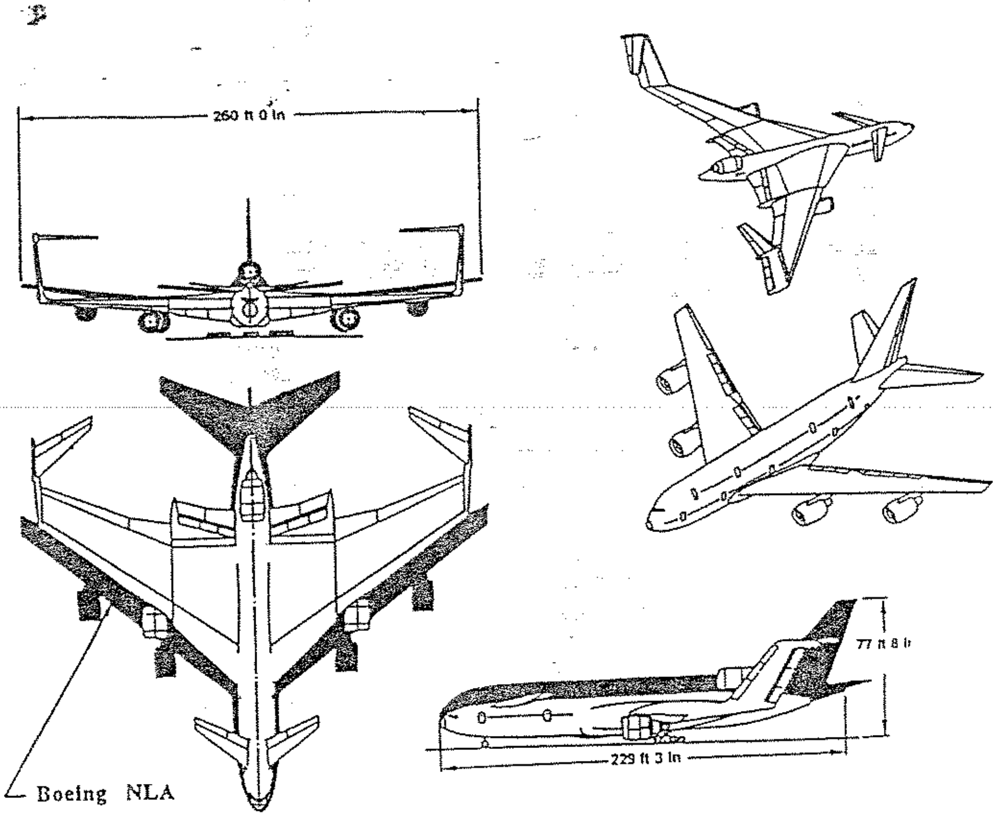

Fig. 15. Size and configuration comparison of the C-wing II with a later version of the Boeing new large airplane [NLA] ([7], Fig. 16).

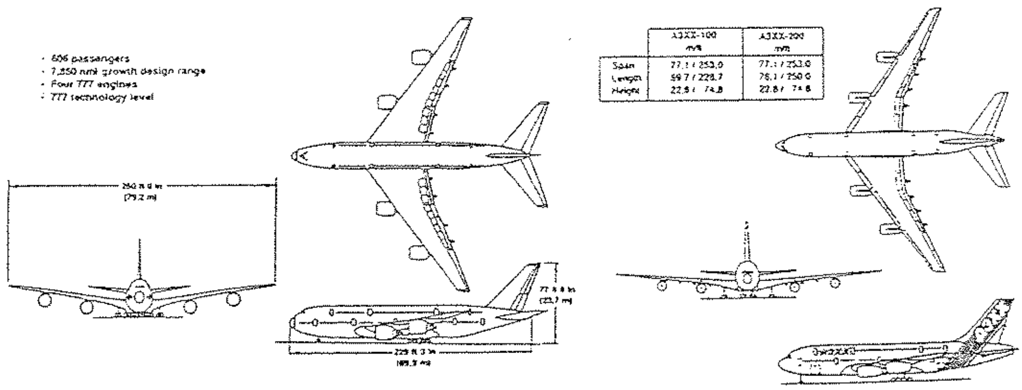

Boeing NLA

Fig. 16. Boeing NLA and Airbus A3XX very large transport airplanes [7, 8].

5. Conclusions and future possibilities

Based on the use of preliminary design methods with limited capabilities for dealing with highly unconventional configurations, and with no well-established databases for key technology items (e.g. transonic Griffith/Goldschmied airfoils, structural dynamic and hence weight characteristics of extremely non-planar wings), both the NASA and Boeing preliminary sizing results present a mixed (and perhaps too pessimistic) view of the potential of the C-wing configuration for very large airplane development. Clearly (within the limits of the available data), all the analysis results presented seem to dash a central hope that use of the highly non-planar wing could very significantly reduce the wing span requirement compared to that for an "optimized" giant 747. It may be emphasized here, however, that this conclusion seems to hold for subsonic transports carrying *up to* about 600 passengers in a tri-class arrangement.

As pointed out earlier, even a simplified square-cube law analysis (unconstrained by airport infrastructure and other practical operational considerations) suggests that the performance and economic improvements to be expected from simple size increase diminish significantly for a conventionally configured aircraft capable of carrying more than about 600 passengers. This further suggests that even if one sharpens one's pencil and negotiates an approximately 80 m span limit for a large airplane without the need for folding wing tips when operating from a significant number of (but not all) existing airports of interest world-wide, an approximately 600 tri-class passenger airplane of conventional configuration is approaching a practical upper bound. Even at this level, such an aircraft represents a formidable developmental challenge.

Against this situation and within the limits the available data, it was demonstrated in our conceptual study that:

1. There is nothing in the results presented which indicates that, with sufficient further effort, the C-wing configuration proposed cannot be made to work – and perhaps even reasonably well.
2. Most of the really difficult problems encountered in attempting to converge on an acceptable 600 passenger C-wing were related in most cases to the slightly *too small* size of the airplane as presently configured. In short the design problem becomes easier to deal with conceptually as

the size of the C-wing increases, with considerable apparent further growth potential even within the limits of an "80 m box".

Viewed from a second perspective, the objective of devising what might be a viable *single-deck* 600-plus passenger large airplane configuration concept which could meet necessary constraints on emergency egress, etc.; and which may have some advantages as a laminar flow control configuration have been achieved in principle. These same advantages could be claimed for any of a variety of span-loader airplane concepts (e.g. as shown in Fig. 7 and as described in [12,14]), but it can be further claimed that the C-wing configuration has advantages beyond those of traditional "flying wing (tail-less)" configurations and particularly those in which the payload/passenger compartment is fully integrated into the basic wing structure. The basic wing-fuselage concept embodied in the C-wing configuration investigated in our study has the potential virtues of providing some conventional windows for high fare passengers and some growth potential by simple body stretch is naturally accommodated. In this latter connection, it is also possible to imagine the same basic configuration concept being built up around a Boeing 747 center body core, the passenger layout and emergency egress features from the forward upper deck of which are well established. This approach could allow development, at least in principle, of a really large airplane within the dimensional limits of the basic 80-m box.

The most striking difference between the semi-span loader C-wing and a conventional flying wing is the opportunity the C-wing (perhaps augmented with a foreplane to produce a quasi-three surface airplane) offers to deal with the stability and control problems and limitations inherent in even an actively controlled tail-less airplane. Since the basic features needed to deal with the pitching moment increments associated with very heavily aft-loaded cruise airfoils (especially transonic versions of the Griffith section) and a proper chamber changing flap high-lift system come as an intrinsic part of the span-reducing characteristics of the C-wing, there is a unique natural synergism in this arrangement. If in fact a hoped for improvement in wake vortex hazard alleviation could be realized from the use of such unconventional wing configurations, the *sum* of a number of small C-wing virtues may add up to a sufficient reason to pursue further development and testing. It may also be added that until the structural dynamic characteristics of the C-wing have been evaluated in some detail (a task beyond the resource limits available for the work reported here), no firm weight estimates can be made. Until such work is done all arguments either for or against further evaluation of the C-wing remain largely speculative.

In this same vein, the value of the Griffith airfoil has become more ambiguous as more specific information on the appropriate geometry of transonic variants have become available. While no test data on an airfoil of this type exists, the limits of how thick such a section could be at a given set of Mach number and lift conditions have been clarified somewhat by analysis. If the earlier discussion on "how big an airplane can be" is valid, our sizing analyses suggest that when the C-wing becomes large enough (i.e. with somewhat more than 600 passengers) the use of a Griffith section becomes an unnecessary complexity. Similarly, if cruise Mach number requirements are relaxed slightly (e.g. to around $M_c = 0.8$), a "conventional" airfoil may be sufficient to meet physical wing thickness requirements (without excessive sweep) even for the "smaller" 600 passenger variant of the airplane. Ironically, this substitution of a more conventional airfoil contour for the Griffith section does not interfere (conceptually) with the emergency egress scheme (Fig. 14) evolved to deal with the evolving shape of the Griffith section from its classic low-subsonic to transonic form (cf. Fig. 8). Despite this, the Griffith section remains much more than an intriguing curiosity and good answers to the many questions surrounding the practical implementation of it in transonic wings could be of significant value since they remain a potentially important "enabling technology" for a variety of moderate sized large airplanes where wing thickness may be critical.

5.1. Some opportunities for further study

The work reported here has been highly conceptual and limited by the non-availability of key pieces of technical data needed to provide definitive answers to important questions regarding the advantages and disadvantages of the C-wing concept. To advance beyond our present understanding of the limits on large airplane size and possible conventional airplane configurations which might allow current limits to be extended, at least the following items need to be investigated in considerably more detail:

- The geometry, performance and power requirements for transonic Griffith/Goldschmied airfoils and wings need to be established and supported by experimental data.
- The aerodynamic and structural dynamic characteristics of the C-wing need to be investigated in far more detail analytically and validated experimentally. Data required include induced drag, wake vortex and both static and dynamic stability and control characteristics; and weight estimations for candidate structural concepts employing both metal and composite materials.
- Good structural concepts for minimum weight penalty "flat pressure vessels" need to be developed and validated. These concepts have potential application to a variety of unconventional airplane configurations beyond the C-wing discussed here (e.g. an oblique wing HSCT) and availability of validated practical schemes for such components would be of real value to designers of future innovative airplane concepts.
- Tools and database development to support evaluations of unconventional airplane configuration concepts are an on-going need. The use of multidisciplinary optimization (MDO) methodology is a particularly promising approach to dealing with the type of highly integrated configuration discussed here. Configurations such as the C-wing pose a real test of the merits of MDO methodology.

6. Postscript – further flights of fancy in very large airplanes

Having completed the initial NASA contract work on our C-wing concept, the authors had hoped to continue more detailed investigations of portions of it under the Advance Concepts Program or similar auspices. Alas, the Advanced Concepts Program was terminated shortly after the work reported here was completed, which also coincided roughly with a waning interest in the United States in development of NLA-class airplanes due in part to an ambiguous market for, and the likely huge development cost of, such monsters. Even the cost of developing further higher capacity derivatives of the proven Boeing 747 has more recently been judged prohibitive. In the meantime, strategies have been developed to at least (in principle) temporarily resolve the airport capacity problem on Asian routes and thus buy the time necessary to make future new very large airplane development an acceptable business case for any potential manufacturer – either here or abroad.

Ever optimistic, the authors had already observed that the 600 passenger C-wing "didn't look like any kind of Boeing" and wasn't likely to go anywhere further within the company except in the unlikely event that the conventional configuration layout being worked on officially ran into uncircumventable technical barriers. Having in the meantime discovered and read with relish the ancient paper by Dravid Keith-Lucas [10], a strategy for gaining some increased interest and/or plausibility for the C-wing quickly came to mind – based in part on the results of square-cube law analysis described earlier. It should first be observed that even a 747 is a mind-bogglingly large airplane when one stands under one and an airplane 30% larger in physical dimensions as the NLA was to be was a real strain on the imagination. On the other hand, except for some niggling infrastructure problems, our square-cube analysis indicated that there was nothing fundamental stopping one from developing a 1500 passenger airplane if a shed large enough to do the construction could be found. Thus the strategy was to go a leap further and design a *really* large airplane – one so magnificently huge (and at least vaguely plausible to the untutored eye) that it would make a 600-passenger jumbo 747 seem almost ordinary. Thus rather than thinking of a Boeing NLA (or our C-wing) as a bold *extrapolation* from a 747 baseline, it could be seem as almost prosaic *interpolation* between the 747 and what might ultimately be.

The result of this little exercise was the 1250–1500 passenger "Super Clipper" shown in Fig. 17. Following the old path laid down by Keith-Lucas, such a machine is of course configured as a flying boat for the same reasons he argued forty years earlier. Having done this bit of frivolous mischief, it came as something of a surprise that some individuals thought it not entirely a joke. This was in part because, in designing the thing in the first place, inadequate attention had been paid to a high level of nostalgia that still seems to exist for the romantic Golden Age of the great flying boats that were the public's first flying entree into the vast mysteries of the East. Thus, reevaluating the concept in this new light, it can be seen that there are least three modern, possibly even practical uses for such a machine:

- Develop it as an alternative to either a high subsonic speed or a supersonic transport for very long distance routes between two coasts. A non-stop flight in an Airbus A 340 between San Francisco and Hong Kong is a *very* long ride even at a *high* subsonic Mach number, and it is not made all that much easier by passively sitting confined in one's seat watching various-in-flight entertainments, etc. An HSCT could potentially halve the trip time, but at a cost in both a fare surcharge and wear and tear on the environment. In this third scheme, the traveler would have the opportunity to recapture some of the elegance and glory (at a reasonable fare) of the great flying boats or zeppelins of a by-gone era, while enjoying activities (e.g. dancing, drinking in a real lounge, working out, sleeping in a real berth) which are almost unfeasible to arrange in a conventional "slim" tubular fuselage. If such a trip were to take a bit longer than that required for the other two alternatives, what difference would it really make when one is having such a good time.
- It could serve as the mobile headquarters of multi-national corporations, with most of the amenities (conference rooms, recreational facilities, etc.) such enterprises might reasonably require.

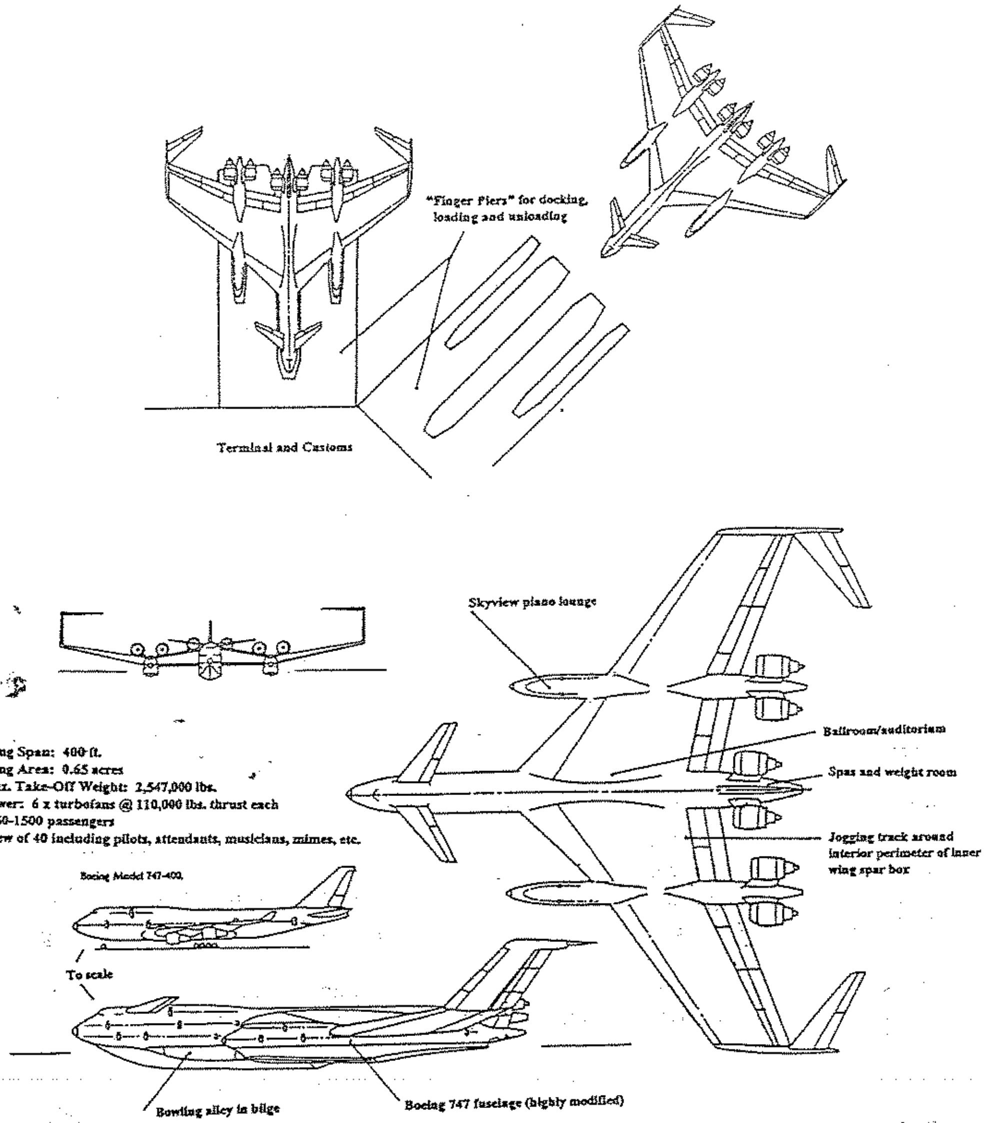

Fig. 17. A concept for a very large subsonic transport airplane configured as a flying boat.

- As cargo carriers to fill a niche between existing air freighters (Boeing 747s, MD [Boeing]-11s) and fast container freight ships for both civil and military purposes. In this latter category, operating in a wing-in-ground-effect mode there would be no requirement for pressurizing the unfortunately contoured freight compartment, power requirements could be greatly reduced if speeds of only 200 kts or so are acceptable, and the economics of operation could thus be entirely favorable.

And then there is the possibility of reducing ferry runs from minutes to seconds, and so on. Those who argue that the airplane business is now "mature" and thus no more interesting for a future generation of designers than the tractor business simply have not understood the full range of remaining possibilities.

Acknowledgements

The authors owe a considerable debt to the members of the team who participated in the contract work reported in this paper: John Sullivan, Purdue University; Mark Drela, MIT; Kwasi Bofah, formerly of Tuskegee University; David Paisley and Richard Hubert of Boeing; Monica Fetty, J.R. Elliot, S.J. (Jack) Morris, and Henri Furhmann, NASA-LaRC; and John Gallman, NASA-ARC. Other charter members of *John's Really Big After Hours Airplane Design Club* include: Dennis Bushnell, NASA-LaRC; R.W. (Toby) Halbert, Ron Bengelink and Bob Kelley-Wickemeyer of Boeing; and Tamaira Ross. While all of these people contributed something very significant to the work reported here, all errors and opinions are those of the authors, and do not necessarily reflect the official position of The Boeing Company.

References

[1] McMasters JH, Kroo IM et al. Advanced configurations for very large subsonic transport airplanes'. NASA (LaRC) CR 198351, October 1996.
[2] McMasters JH. Reflections of a paleoaerodynamicist. Perspectives in Biology and Medicine. University of Chicago, Spring, 1986:3–70.
[3] Schairer GS. The 707 revolution. AIAA Paper, June 20, 1989.
[4] Cook WmH. The Road to the 707, 1992.
[5] Roskam J. What drives unique configurations? SAE Technical Paper Series 881353, Aerospace Technology Conference and Exposition, Anaheim, CA, Oct 3–6, 1988.
[6] Torenbeck E. Synthesis of subsonic airplane design. Delft: Delft University Press, 1976.
[7] Proctor P. Boeing refines designs for a 600-seat NLA. Aviation Week and Space Technology, November 21, 1994:48–53.
[8] Sparaco P. Airbus paves way for A-3XX megajet. Aviation Week and Space Technology, May 22, 1995:26–7.
[9] Cleveland FA. Size effects in conventional aircraft design. J Aircraft 1970;7:483–511.
[10] Keith-Lucas D. The relative efficiencies of large landplanes and flying boats. In Jarck BH, editor, Proceedings of the 2nd International Aeronautics Conference, New York, May 24–27, 1949.
[11] Kroo IM. An interactive system for aircraft design and optimization. AIAA 92-1190, February 1992.
[12] Liebeck R, Page M. Blended wing body technology study (invited paper). AIAA 98-0438, AIAA 36th Aerospace Sciences Meeting, Reno, Nevada, January 13, 1998.
[13] Kuchemann, D. The Aerodynamic design of aircraft, New York: Pergamon, 1978.
[14] Sweetman Wm, Brown SF. Megaplanes. Popular Science, April 1995:54–74.
[15] Woolridge ET. Winged wonders (The story of the flying wing). Washington, DC: Smithsonian Institution Press, 1993.
[16] Farrah, JM. Boundary layer controlled thick suction airfoils. Final Co-Op Report, NASA-LaRC, August 1994.
[17] Drela M. Design and optimization method for multi-element airfoils. AIAA 93-0969, AIAA/AHS/ASEE Aerospace Design Conference, Irivine, CA, February 16–19, 1993.
[18] Kroo IM. A general approach to multiple lifting surface design and analysis. AIAA 84-2507, October 1984.
[19] Kendall, ER. The aerodynamics of three surface airplanes. AIAA 84-2508, October 31, 1984.
[20] Myklebust A, Gelhausen P. Putting the ACSYNT on airplane design. Aerospace America 1994;32(9):26–30.

NASA/TM-1998-207644

Synergistic Airframe-Propulsion Interactions and Integrations

A White Paper Prepared by the 1996-1997 Langley Aeronautics Technical Committee

Steven F. Yaros, Matthew G. Sexstone, Lawrence D. Huebner, John E. Lamar, Robert E. McKinley, Jr., Abel O. Torres, Casey L. Burley, Robert C. Scott, and William J. Small
Langley Research Center, Hampton, Virginia

March 1998

The NASA STI Program Office . . . in Profile

Since its founding, NASA has been dedicated to the advancement of aeronautics and space science. The NASA Scientific and Technical Information (STI) Program Office plays a key part in helping NASA maintain this important role.

The NASA STI Program Office is operated by Langley Research Center, the lead center for NASA's scientific and technical information. The NASA STI Program Office provides access to the NASA STI Database, the largest collection of aeronautical and space science STI in the world. The Program Office is also NASA's institutional mechanism for disseminating the results of its research and development activities. These results are published by NASA in the NASA STI Report Series, which includes the following report types:

- TECHNICAL PUBLICATION. Reports of completed research or a major significant phase of research that present the results of NASA programs and include extensive data or theoretical analysis. Includes compilations of significant scientific and technical data and information deemed to be of continuing reference value. NASA counter-part or peer-reviewed formal professional papers, but having less stringent limitations on manuscript length and extent of graphic presentations.

- TECHNICAL MEMORANDUM. Scientific and technical findings that are preliminary or of specialized interest, e.g., quick release reports, working papers, and bibliographies that contain minimal annotation. Does not contain extensive analysis.

- CONTRACTOR REPORT. Scientific and technical findings by NASA-sponsored contractors and grantees.

- CONFERENCE PUBLICATION. Collected papers from scientific and technical conferences, symposia, seminars, or other meetings sponsored or co-sponsored by NASA.

- SPECIAL PUBLICATION. Scientific, technical, or historical information from NASA programs, projects, and missions, often concerned with subjects having substantial public interest.

- TECHNICAL TRANSLATION. English-language translations of foreign scientific and technical material pertinent to NASA's mission.

Specialized services that help round out the STI Program Office's diverse offerings include creating custom thesauri, building customized databases, organizing and publishing research results . . . even providing videos.

For more information about the NASA STI Program Office, see the following:

- Access the NASA STI Program Home Page athttp://www.sti.nasa.gov

- Email your question via the Internet to help@sti.nasa.gov

- Fax your question to the NASA Access Help Desk at (301) 621-0134

- Phone the NASA Access Help Desk at (301) 621-0390

- Write to:
  NASA Access Help Desk
  NASA Center for AeroSpace Information
  800 Elkridge Landing Road
  Linthicum Heights, MD 21090-2934

NASA/TM-1998-207644

Synergistic Airframe-Propulsion Interactions and Integrations

A White Paper Prepared by the 1996-1997 Langley Aeronautics Technical Committee

Steven F. Yaros, Matthew G. Sexstone, Lawrence D. Huebner, John E. Lamar, Robert E. McKinley, Jr., Abel O. Torres, Casey L. Burley, Robert C. Scott, and William J. Small
Langley Research Center, Hampton, Virginia

National Aeronautics and
Space Administration

Langley Research Center
Hampton, Virginia 23681-2199

March 1998

Available from the following:

NASA Center for AeroSpace Information (CASI)
800 Elkridge Landing Road
Linthicum Heights, MD 21090-2934
(301) 621-0390

National Technical Information Service (NTIS)
5285 Port Royal Road
Springfield, VA 22161-2171
(703) 487-4650

Executive Summary

This white paper documents the work of the NASA Langley Aeronautics Technical Committee from July 1996 through March 1998 and addresses the subject of Synergistic Airframe-Propulsion Interactions and Integrations (SnAPII). It is well known that favorable Propulsion Airframe Integration (PAI) is not only possible but Mach number dependent -- with the largest (currently utilized) benefit occurring at hypersonic speeds. At the higher speeds the lower surface of the airframe actually serves as an external precompression surface for the inlet flow. At the lower supersonic Mach numbers and for the bulk of the commercial civil transport fleet, the benefits of SnAPII have not been as extensively explored. This is due primarily to the separateness of the design process for airframes and propulsion systems, with only unfavorable interactions addressed. The question ‘How to design these two systems in such a way that the airframe needs the propulsion and the propulsion needs the airframe?’ is the fundamental issue addressed in this paper. Successful solutions to this issue depend on appropriate technology ideas.

In order for a technology (idea) to be applicable it must successfully pass through the two filters of technical and technological. The technical filter addresses the questions: Does it violate any fundamental laws?, Does it work as envisioned?, Can it successfully be demonstrated?; whereas, the technological filter addresses the question: Does it make any sense in the real world?

This paper first details ten technologies which have yet to make it to commercial products (with limited exceptions) and which could be utilized in a synergistic manner. Then these technologies, either alone or in combination, are applied to both a conventional twin-engine transonic-transport and to an unconventional transport, the Blended Wing Body. Lastly, combinations of these technologies are applied to configuration concepts to assess the possibilities of success relative to five of the ten NASA aeronautics goals. These assessments are subjective but point the way in which the applied technologies could work together for some break-through benefits.

The following recommendations are made to continue the work initiated in this document:

(1) Based upon the evaluation presented herein of the potential benefits of applying SnAPII technologies in achieving the Agency's aeronautics goals, we recommend that system studies be initiated to independently assess our findings and perhaps provide the basis for future research in the SnAPII arena to be incorporated into new and existing programs. Those concepts that successfully pass the systems analyses could also be reasonable candidates for small-scale flight testing.

(2) Not withstanding recommendation number one, it is recommended that all future systems studies in aeronautics consider the application of SnAPII technologies (identified in the first part of this paper), in addition to the technologies currently funded in the aeronautics program for the evaluation of system benefits. This is an appropriate time to re-look at these with advancements in such areas as computational fluid dynamics, materials, manufacturing, as well as new methods to further optimize these technologies. Furthermore, many of these technologies have been adequately tested in wind tunnel settings, but lack flight test verification. Remotely-piloted small-scale flight testing could conceivably be utilized to provide data for these technologies in a flight airframe system to reduce risk and bring them to a higher level of application readiness.

(3) The idea of investigating a combined propulsion/airframe design using a minimum entropy production method may be a good analytical approach, complementing the systems analyses and experimental studies, to exploiting SnAPII technologies. Presently, this method has been applied to only aerodynamic drag-reduction problems, but extending this to SnAPII is a next logical step.

Contents

Preface

This document provides a compendium of technologies that use propulsive power to affect/enhance vehicle aerodynamics. The results generated in the second part of this paper are based on simplified performance equations and conceptual ideas. No effort has been made to optimize or even define a vehicle concept. Instead, it is hoped that a flavor for the potential benefits that may exist from these technologies in synergy has been brought forward. It is the intent of this document to provide the impetus for systems analysis studies in synergistic airframe-propulsion interactions and integrations and, if justified, a complementary research program.

The creation of this document required the concerted efforts of the entire Committee. Listed below are the responsible individuals for particular sections of the paper; the reader is referred to these individuals for more information on a specific topic.

Casey Burley	Circulation Control Wing
Lawrence Huebner	Favorable Shock/Propulsive Surface Interference and Interactions, Revolutionary Vehicle Concepts
John Lamar	Goldschmied Airfoil
Robert McKinley	Thrust Vectoring
Robert Scott	Blown Flaps, Wing-Tip Blowing
Matthew Sexstone	Augmentor/Jet Wing, Evolutionary Vehicle Concepts
William Small	Laminar Flow Control, Natural Laminar Flow, Pneumatic Vortex Control
Abel Torres	Boundary Layer Inlet
Steven Yaros	Wing-Tip Engines/Turbines

I take this opportunity to acknowledge the essential contributions of a number of individuals. Thanks go to Chris Gunther, Dee Bullock, and Bill Kluge for their graphics expertise for the second part of this paper. Thanks also to LATC member emeritus, Scott Asbury, for providing a thorough review of the draft version of this paper. A special thanks to Steven Yaros for serving as the compiling editor of this paper. Receiving text and figures from eight other authors and organizing all of the information into a consistent style was truly a formidable task. Finally, on behalf of the entire committee, I thank the sponsor of this Technical Committee, Dennis Bushnell, NASA Langley Senior Scientist, for his support, encouragement, and constructive comments.

Lawrence Huebner
Chairman
1996-97 Langley Aeronautics Technical Committee

Introduction

Historically, the benefits of propulsion-airframe integration (PAI) have been shown to be highly dependent upon the cruise Mach number [ref. 1]. At hypersonic speeds, an airbreathing engine is totally integrated to the airframe. The vehicle forebody serves as an external precompression surface for the inlet flow; the midbody contains the internal inlet, combustor, and internal nozzle; and the aftbody serves as an external expansion surface for the combustion flow. Thus, the complete engine flowpath is made up of the entire vehicle lower surface. At supersonic speeds, it is possible to utilize the flow fields off of engine nacelles to provide favorable interference drag reductions and interference lift. Conversely, the airframe (body or wings) can be used to precompress the flow entering the engine inlets for improved engine performance. However, at subsonic speeds, few appreciable beneficial interactions are being exploited. PAI research and analysis is only used to reduce or eliminate problems or unfavorable interactions. Exploiting PAI at lower speeds may lead to more efficient aircraft and/or entirely new vehicle designs.

In particular, this paper deals with airframe and propulsion technologies and how beneficial interactions and integrations can result in synergistic effects. This led to the titling of the present work as Synergistic Airframe-Propulsion Interactions and Integrations (SnAPII). One basis for this effort can be attributed to a 1966 report by Rethorst, et al. on the elimination of induced drag [ref. 2]. The authors state that, "the most expedient means to eliminate induced drag . . . is to exchange the energy otherwise dissipated in the trailing vortex system into nonuniform energy level flows in the aircraft." They cited three possible methods for achieving this, namely, by exchanging this energy to (1) a lower energy level system in the boundary layer, converting vorticity or angular velocity into pressure on the back of the wing, (2) an extended uniform energy level system to spread the vorticity over a larger wake, and (3) a higher energy level system to integrate the vorticity with the propulsion system to recover trailing-edge vortex energy as pressure. It is the last of these methods that provides the connection with the present study.

Induced drag minimization is an inherent part of aircraft design and is carried out not only by experimental methods, but by using several different analyses, which usually involve simplifications such as a planar wake assumption. Greene [ref. 3] has approached this problem from a different direction, basing his "viscous lifting line" method on the principle of minimum entropy production. He has analyzed wing configurations with tip extensions, winglets, and in-plane wing sweep, with and without a constraint on wing-root bending moment. The approximate closed-form solutions obtained by Greene could possibly be extended to numerical optimizations including propulsive effects and their interaction with the external aerodynamic flow. Such an approach could also include structural and geometric constraints and might be valuable in the analyses of SnAPII configurations.

Some of the technologies that were studied use the additional energy added to the airplane system via the combustion of fuel (stored chemical energy) in the propulsion system in a way that provides beneficial airframe-propulsion interaction. Other technologies use more passive methods of extracting energy, such as wing-tip turbines. It is the intent of this paper to unbound the typical constraints imposed on basic performance metrics, such as high lift, cruise efficiency, and maneuver, by exploiting these technologies in a SnAPII way. One process for doing this is to address the full degrees of freedom for certain aspects of aircraft design. These degrees of freedom include: the type of propulsion system utilized; engine geometric design and placement; interactions between the engine(s) and the body, engine(s) and wings, engine(s) and empennage, and engine(s) with other engine(s); engine inlet ducting and nozzle shaping; and interactions of engine-generated flow phenomena.

Combined with the potential technology applications of PAI, one must also address the current airplane design philosophy to identify an important perspective on the realistic impact of this effort. New technologies and airplane designs are currently guided by "the economics of air travel." [ref. 4] They must meet the needs of the customer, and focus on utilization, maintenance, and airplane price. The technologies for new airplane designs need to be focused on solving real problems that make good economic sense for those that buy airplanes. Rubbert [ref. 5] adds that new strategy is market- or customer-driven, not technology driven. Furthermore, he states that “the driving factor is economic performance, the ability of the airplane to do its job at less overall cost, with the utmost in safety and reliability.”

In order to have a good technical idea applied to a new aircraft, it must pass through two filters. The first filter addresses the questions: Does it violate any fundamental laws?, Does it work as envisioned?, Can it be successfully demonstrated?; whereas the second filter addresses real world concerns, such as economics [ref. 6], regulations, and the various operational ‘-ilities’ [ref. 1]. The technology ideas discussed subsequently make an effort to address the status of readiness for aircraft application.

The objectives of this white paper are to present a concise summary of available technologies that provide synergistic interactions and integrations of the propulsion and airframe systems. This includes brief descriptions of the concepts, current and/or past utilization, technology benefits, and issues for incorporating them into aircraft design. Following this, the paper describes the potential application of these technologies, including quantification of benefits, where possible. The paper will conclude with a summarization of the salient points of the paper and recommendations for future research. It is the intent of the paper to address the future research recommendations with respect to the latest report from NASA Headquarters on aeronautics [ref. 7]. Where appropriate, we will take into account the goals underlying the three pillars of aeronautics and space transportation success. These pillars are: (1) to ensure continued U. S. leadership in the global aircraft market through safer, cleaner, quieter, and more affordable air travel, (2) to revolutionize air travel and the way in which aircraft are designed, built, and operated, and (3) to unleash the commercial potential of space and greatly expand space research and exploration. In support of these pillars are ten goals. They are to: improve safety by reducing aircraft accident rates, reducing emissions and noise, increase air travel capacity while maintaining safety, reducing the cost of air travel, reducing intercontinental travel time, increase production of general aviation aircraft, provide next-generation design tools and experimental aircraft to increase the confidence in future aircraft design, and reduce payload cost to orbit by one, then two, orders of magnitude.

References.

1. Bushnell, Dennis M.: “Aerodynamics/Aeronautics in an Open Thermodynamic System.” Presented to the Langley Aeronautics Technical Committee, July 11, 1996.

2. Rethorst, Scott; Saffman, Philip; and Fujita, Toshio: Induced Drag Elimination on Subsonic Aircraft. U.S. Air Force, AFFDL-TR-66-115, December 1966.

3. Greene, George C.: An Entropy Method for Induced Drag Minimization. SAE Technical Paper Series 892344. Aerospace Technology Conference and Exposition, Anaheim, CA, September 1989.

4. Condit, Philip M.: Performance, Process, and Value: Commercial Aircraft Design in the 21st Century. 1996 Wright Brothers Lectureship in Aeronautics, presented at the World Aviation Congress and Exposition, Los Angeles, California, October 22, 1996.

5. Rubbert, Paul E.: CFD and the Changing World of Airplane Design. ICAS-94-0.2, pp. LVII-LXXXIII, Copyright © 1994 by ICAS and AIAA.

6. Bushnell, Dennis M.: “Application Frontiers of ‘Designer Fluid Mechanics,’ Visions vs. Reality.” Presented to the Langley Aeronautics Technical Committee, November 1, 1996.

7. NASA Office of Aeronautics and Space Transportation Technology: Aeronautics & Space Transportation Technology: Three Pillars for Success. March 1997.

Bibliography.

Ferri, Antonio, Lecture Series Director: Airframe Engine Integration. AGARD Lecture Series No. 53, AGARD-LS-53, May 1972.

Technology Reviews

Powered Lift Technology

Powered lift refers to a concept of utilizing secondary airflows, typically supplied by means of an aircraft's propulsion system, to increase lift (and thus $C_{L,max}$) through an increase in wing circulation above that which is theoretically possible for unpowered wings. Numerous concepts have been explored over the past sixty years to accomplish this goal and several experimental aircraft have been built and flown for experimental testing (figure 1). However, to date, only one production fixed-wing aircraft, the McDonnell Douglas C-17 Globemaster, incorporates powered lift into its design (this ignores direct-lift thrust designs intended for vertical takeoff, as this topic is considered separately for purposes of this report). The performance, environmental, and safety benefits that may be derived through the use of powered lift (short takeoff and landing, reduced terminal area noise footprints, increased payload and range capability, and decreased landing speeds) necessitate an effort to understand the other factors arising in the decision to either include these concepts in future aircraft designs or not.

Three powered lift concepts are covered herein: a circulation control wing, blown flaps, and an augmentor/Jet wing. Most other concepts are slight deviations of these three with the exception of direct-lift thrust which is reserved for discussion as thrust vectoring technology. The concepts are discussed separately due to their unique technical characteristics, historical background, benefits and penalties, and configuration integration issues.

Reference.

1.Nielson, J. N.; and Biggers, J. C.: "Recent Progress in Circulation Control Aerodynamics", AIAA 87-0001, January 1987.

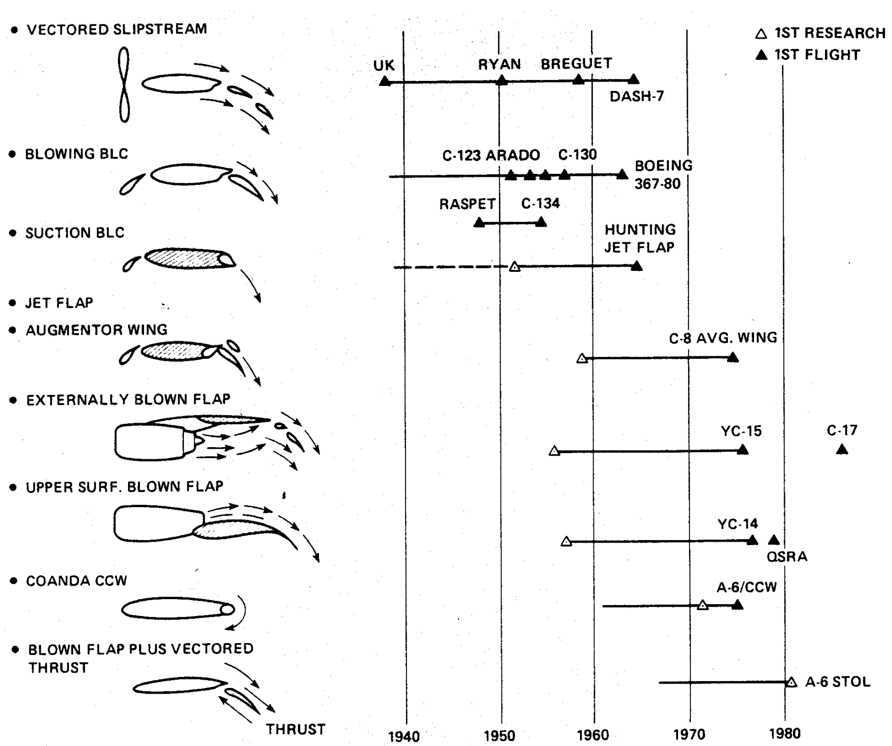

Figure 1. Powered Lift Chronology, from ref. 1

Circulation Control Wing

Technical Description. Circulation control refers to an aerodynamic configuration that incorporates an airfoil with a rounded trailing edge, an internal duct, and a slot on the upper surface near the trailing edge.

On a typical airfoil, the flow from the upper surface cannot turn around the sharp trailing edge without the velocity becoming infinite and, since this is impossible, the flow instead separates from the trailing edge. For a given airfoil angle of attack, separation at the trailing edge occurs for a particular value of the circulation and, hence, for a particular lift coefficient. A circulation control airfoil [ref. 1], on the other hand, has a rounded trailing edge, as shown in figure 1. Without blowing, a circulation control airfoil will have a separation point S1 on the upper surface. With blowing, the separation point S1 can move around the trailing edge onto the bottom surface. A slot is provided near the trailing edge such that the flow from the slot is tangent to the airfoil surface. The slot flow is at a higher speed than that of the local outer-flow and thus energizes the mixing boundary. This action permits the upper flow to remain attached until it reaches the separation point S1. From inviscid theory, the separation point S2 for the boundary layer on the lower surface coincides with S1; however, for a viscous fluid a “dead air” region can exist, with S1 and S2 at its extremities. The important principle to note is that there is a strong interaction between the outer inviscid flow and the jet flow, and that interaction determines airfoil circulation which thus determines its lift.

The lift of a circulation control airfoil is a direct function of turbulent mixing between the upper surface boundary layer and the slot jet. This turbulence mechanism is one of the major controlling factors in the process, and a good model of this mechanism is required for the rational prediction of flow about circulation control airfoils. Much effort has been focused on understanding this mechanism and in designing optimum circulation control wings (CCW). In 1986, a Circulation Control Workshop [refs. 2 and 3] was held at NASA Ames to establish the status of CCW for commercial and military applications and to identify research goals that are essential to its implementation for future fixed- and rotary-wing aircraft. The workshop was well attended by representatives from government agencies, industry and academia. The workshop resulted in a compilation of fundamental CCW research needs as well as specific research needs for CCW technologies for the X-wing, fixed-wing, NOTAR and tiltrotor applications. Since then numerous numerical [refs. 4 to 8] and experimental [refs. 9 to 14] studies have been conducted and knowledge of the CCW mechanisms have been greatly enhanced. The design of CCW wings, with optimum slot placement and size, airfoil shape, and performance is now possible [ref. 8].

Recently (1996) Dr. B. McCormick (Boeing Professor Emeritus) made a presentation titled, “Synergistic Effects of Propulsion for Aircraft” at LaRC [ref. 15]. In his talk Dr. McCormick presented a brief summary of high lift systems (mainly pertaining to V/STOL applications), some of which included circulation control concepts and their integration into the design of an aircraft. His concluding remarks included a rather strong statement: there are reams of test results in the literature on high lift systems and that further generic studies of high lift systems are not needed. What is needed, however, is application studies leading to design and construction of large scale models and an assessment of the net effect of integrating high lift systems with propulsion systems.

The basic concept of circulation control (CC) was developed at the David Taylor Naval Ship Research & Development Center (DTNSRDC) and has continued to be developed since the late 1960s. Many of these early developments are documented in references 16 and 17. The unique qualities of this concept are very attractive for many applications in the fields of aerodynamics and hydrodynamics.

To evaluate high lift potential, a Navy A-6/CCW demonstrator aircraft program was initiated in 1968 by DTNSRDC [ref. 18]. The aircraft configuration showing the CCW airframe changes is shown in figure 2. The principal aircraft modification included the incorporation of a circular trailing edge, attached to the existing flap, which forms both the Coanda surface, as well as bleed ducting. Existing flow fences were removed and outboard flow fences added. The leading edge radius was increased and a fixed Krueger leading edge flap was added. A CCW air system powered by bleed air from the two engines was added. The bleed flow was controlled by throttle valves operated by the pilot.

The flight test of the A-6 confirmed previous wind tunnel predictions that the CCW could double the aircraft lifting capabilities while utilizing bleed air from the engines. A summary of the A-6/CCW aircraft performance as compared to the conventional A-6 is presented in figure 3. Following this test an advanced high lift system was developed that combined CCW and upper surface blown (USB) flaps to produce lift for STOL operations by Navy aircraft [refs. 19 and 20]. This combined system (USB/CCW) was found to be a very effective, yet simple method to control wing lift augmentation and vertical/horizontal force components. The original airfoil was modified at the trailing edge in order to have minimal impact on cruise efficiency. Several other modifications are documented in reference 21. The experimental results confirm thrust turning through angles up to 165 degrees and associated benefits as a STOL and thrust reverser system. Significant improvements in performance as compared to CTOL were found, since the maximum trimmed lift coefficient increased on the order of 200 percent. High-lift, vertical thrust, and thrust reversing were shown to be generated directly from the cruise configuration instantaneously and without external moving parts. Control of the thrust on takeoff and landing is directly controlled by the pilot (via bleed air) which is highly desirable for low speed lateral control. When compared to other high lift systems involving flaps and actuators, the USB/CCW system has significantly less moving parts. This contributes to increased reliability, maintainability, aircraft lifespan, and affordability (to first order; cost is proportional to weight and part count)..

The NASA Quiet Short-haul Research Aircraft (QSRA) is a high performance STOL powered lift research aircraft for which extensive low-speed wind-tunnel, flight simulation, and flight research testing has been conducted. In 1981 and 1983 the QSRA was reconfigured with a USB/CCW system and ground tested for the Navy to verify deflected engine thrust [refs. 22 and 23]. Circulation control capabilities were added and combined with the existing USB capability and are shown in figure 4; results of a study conducted on this configuration are documented in reference 24. A conclusion of the study was that flight verification is required to assess overall performance and control characteristics with fully integrated airframe, propulsion, and control system.

A program applying CCW to a Boeing 737 subsonic transport aircraft was planned and initiated in 1993 [refs. 19, 25, and 26]. The goal was to determine the feasibility and potential of pneumatic circulation control technology to increase high-lift performance while reducing system complexity and aircraft noise in the terminal area. (Terminal area noise is dominated by airframe noise, i.e., landing gear, flaps, non-streamlined protrusions). The study was four-phased and included experimental development and evaluation of advanced CCW high-lift configurations, development of pneumatic leading edge devices, computation evaluation of CCW airfoil designs, and evaluation of terminal-area performance employing CCW.

Figure 5 shows the high-lift and control surfaces for a conventional B737 and the B737/CCW aircraft. In its production version, the B737 employs a triple-slotted mechanical flap with leading edge slat. This sketch shows both this arrangement and the modified B737/CCW configuration. In the absence of actual full-scale flight test data for this aircraft, 1/8-scale wind tunnel results were used. The effect of including CCW was then computed. A comparison of lift coefficient (cl) vs. angle of attack (Alp) for the conventional and CCW configuration is presented in figure 6, along with a drag polar. The study verified previous results showing the benefits of CCW.

McDonnell Douglas Helicopter Company (MDHC) has actually employed a circulation control device on a production helicopter. The anti-torque system of a helicopter has a major impact on the weight, performance, agility, reliability, flight and ground crew safety, and vehicle survivability. MDHC has been working on the No-Tail Rotor (NOTAR) concept for the past 20 years. This anti-torque system is in production and exists on current MD 500 series and Explorer vehicles. MDHC used a structured approach to the development of this system. First, the performance of the individual NOTAR system components was measured and evaluated by experiment. Then, integrated system performance was investigated in ground testing, powered model rotor wind tunnel testing, and flight testing of 3 different aircraft: OH-6 Demonstrator, MD 520N/530N and MD 900 [refs. 9 and 10].

Currently, commercial utilization of circulation control on production aircraft is limited to rotorcraft. The McDonnell Douglas 500 series and the Explorer employ circulation control as an anti-torque device replacing the tail rotor. This application has also reduced the overall noise levels of the rotorcraft. For fixed wing the utilization is limited to experimental aircraft programs, such as the Navy/ Grumman A-6 and the NASA QSRA, discussed above.

Current and/or Past Utilization. No current nor past production (unclassified) aircraft utilize circulation control wing for powered lift. Experimental aircraft programs have utilized the concepts with results discussed in the previous section.

Technological Benefits and Penalties. The primary benefit of circulation control is currently focused on providing high-lift on the order of C_L of 8 at zero angle of attack [ref. 26]. This magnitude of performance would greatly reduce takeoff and landing speeds, reduce runway lengths, and increase safety of flight in terminal areas. The resulting steep climbout and approach flight paths due to the STOL capability would also reduce the noise exposure to surrounding communities, thus increasing airport capacity. In addition, greatly increased liftoff gross weight and landing weight provided by the smaller wing area would allow transport wing designs that are more optimized for cruise and fuel efficiency. Compared to other high-lift wing/flap systems, the pneumatic CCW configurations reduce complexity and offer the opportunity to combine high-lift, roll control, and direct-lift-control surfaces into a single multipurpose pneumatic wing/control surface. Many of these identified benefits are concluded from component studies and/or studies where the effects on the total system were not fully investigated. In addition, the benefits do not fully account for the economics of design change costs which would be incurred if implemented on a production type aircraft.

Benefits of a circulation control wing are:

1. potential increase in $C_{L,max}$ by a factor of 4
2. reduction in part count which directly reduces overall cost
3. improved maneuverability and control
4. performance is primarily inviscid, thus reduces Reynolds number sensitivity
5. increased runway productivity by altering wake vortex and allowing several aircraft on same runway

Penalties and concerns for circulation control airfoils/wings are:

1. potential for increased base drag in cruise
2. decrease in thrust (estimated 5%) due to bleed flow requirement from engine compressor
3. asymmetric failure
4. system reliability
5. increased complexity and potential weight increase
6. cost/benefits analysis needed
7. true benefits unevaluated thus far.

Configuration Integration. There are several factors that need to be considered in designing a circulation control STOL aircraft, including:

1. Characteristics of the circulation control airfoil aerodynamics.
2. The relationship between the engine thrust lost and the bleed air requirement.

3. The lift loss associated with trimming unusually large pitching moments from circulation control aerodynamics.
4. Why is the locally obtainable lift coefficient about 6? What are the factors and design parameters that limit this?
5. CCWs may have abrupt wing-stall characteristics.
6. Rounded trailing edges, typical for CCW, must be retracted or modified for good cruise efficiency. (Note: the amount of "rounding" of the trailing edge can be very small to gain advantage, ref. 13)

References.

1. Nielson, J. N.; and Biggers, J. C.: "Recent Progress in Circulation Control Aerodynamics," AIAA 87-0001, January 1987.

2. Riddle, D. W.; and Eppel, J. C.: "A Potential Flight Evaluation of an Upper-Surface-Blowing/Circulation-Control-Wing Concept," Proceedings of the Circulation-Control Workshop 1986, NASA Ames Research Center, Moffett Field, CA, NASA CP 2432, February 19-21, 1986.

3. Nielson, J. N.: Proceedings of the Circulation-Control Workshop 1986, NASA Ames Research Center, Moffett Field, CA, NASA CP 2432, February 19-21, 1986.

4. Williams, S. L.; and Franke, M. E.: "Navier-Stokes methods to predict circulation control airfoil performance," *J. Aircraft*, Vol. 29, Mar.-Apr. 1992, p. 243-249.

5. Witherspoon, L. S.: "The Numerical Simulation of Circulation Controlled Airfoil Flowfields," Ph.D. Thesis, Stanford University, CA., 1993.

6. Himeno, R.; Kuwahara K.; and Kawamura, T.: "Computational Study of Circulation Control with Suction," AIAA 85-0042, January 1985.

7. Englar, R. J.; Smith, M. J.; Kelley, S. M.; and Rover III, R. C.: "Development of Circulation control Technology for Application to Advanced Subsonic Transport Aircraft," AIAA 93-0644, January 1993.

8. Wood, N. J.: "A New Class of Circulation Control Airfoils," AIAA 87-0003, January 1987.

9. Spaid, F. W.; and Keener, E. R.: "Boundary-Layer and Wake Measurements on a Swept, Circulation-Control Wing," *J. Aircraft*, Vol. 28, No.11, November 1991.

10. Dawson, S.; and Thompson, T.: "Recent NOTAR Anti-Torque System Research and Testing at MDHC," 49th AHS Annual Forum, Saint Louis, MO, May 19-21, 1993.

11. Kozachuk, A. D.: "Experimental Studies of Air Flow in the Channel of a Circulation-Control Rotor Blade," Problems in the design of helicopter rotors (A93-32173 12-05), Izdatel'stvo Moskovskogo Aviatsionnogo Instituta, Russia.

12. Franke, M. E.; Pelletier, M. E.; and Trainor, J. W.: "Circulation Control Wing Model Study," AIAA 93-0094, January 1993.

13. Englar, R. J.; Nichols, J. H., Jr.; Harris, M. J.; and Huson, G.: "Experimental Development of an Advanced Circulation Control Wing System for Navy STOL Aircraft," AIAA 81-0151, January 1981.

14. McLachlan, B. G.: "A Study of a Circulation Control Airfoil with Leading/Trailing Edge Blowing," AIAA 87-0157, January 1987.

15. McCormick, B. W.: "Synergistic Effects of Propulsion for Aircraft," Presentation made at NASA LaRC, Sept. 12, 1996.

16. Englar, R. J.; Stone, M. B.; and Hall, M.: "Circulation Control - An Updated Bibliography of DTNRDC Research and Selected Outside References," DTNSRDC Report 77-076, September 1977.

17. Englar, R. J.; and Applegate, C. A.: "Circulation Control - A Bibliography of DTNSDRC Research and Selected Outside References," DTNSRDC Report 84-052, October 1984.

18. Pugliese, A. J.; and Englar, R. J.: "Flight Testing the circulation Control Wing," AIAA 79-1791, August 1979.

19. Englar, R. J.: "Development of the A-6/Circulation Control Wing Flight Demonstrator Configuration," DTNSRDC Report ASED-79/01, January 1979.

20. Nichols, J. H.; and Englar, R. J.: "Advanced Circulation Control Wing System for Navy STOL Aircraft," AIAA 93-0094, August 1980.

21. Nichols, J. H.; and Harris, M. J.: "Fixed Wing CCW Aerodynamics With and Without Supplementary Thrust Deflection," N88-17607, presentation only, no paper.

22. Eppel, J. C.; Shovlin, M. D.; Janes, D. N.; Englar, R. J.; and Nichols, J. H.: "Static Investigation of the Circulation-Control-Wing/Upper-Surface-Blowing Concept Applied to the Quiet Short-Haul Research Aircraft," NASA TM 84-232, 1982.

23. Englar, R. J.; Nichols, J. H.; Harris, M. J.; Eppel, J. C.; and Shovlin, M. D.: "Circulation Control Technology Applied to Propulsive High Lift Systems," SAE Paper 84-1497, October 1984.

24. Englar, R. J.; Hemmerly, R. A.; Moore, W. H.; Seredinsky, V.; Valckenaere, W. G.; and Jackson, J. A.: "Design of the Circulation Control Wing STOL Demonstrator Aircraft," AIAA 79-1842, August 1987.

25. Englar, R. J.; Smith, M. J.; Kelley, S. M.; and Rover III, R. C.: "Application of Circulation Control to Advanced Subsonic Transport Aircraft, Part II: Transport Application," *J. Aircraft*, Vol. 31, No. 5, September-October 1994.

26. Englar, R. J.; Smith, M. J.; Kelley, S. M.; and Rover III, R. C.: "Application of Circulation Control to Advanced Subsonic Transport Aircraft, Part I: Airfoil Development," AIAA 93-0644, January 1993.

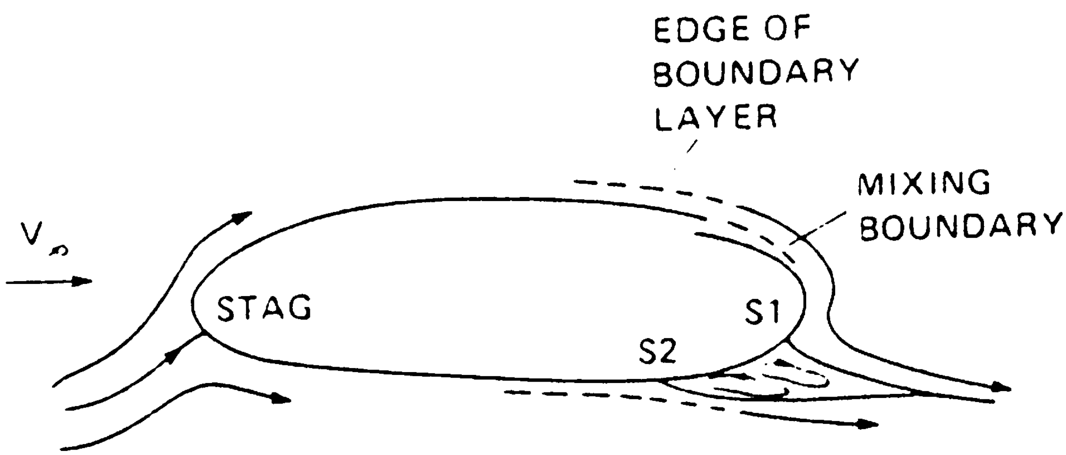

Figure 1. Flow circulation about a circulation control aircraft, from ref. 1.

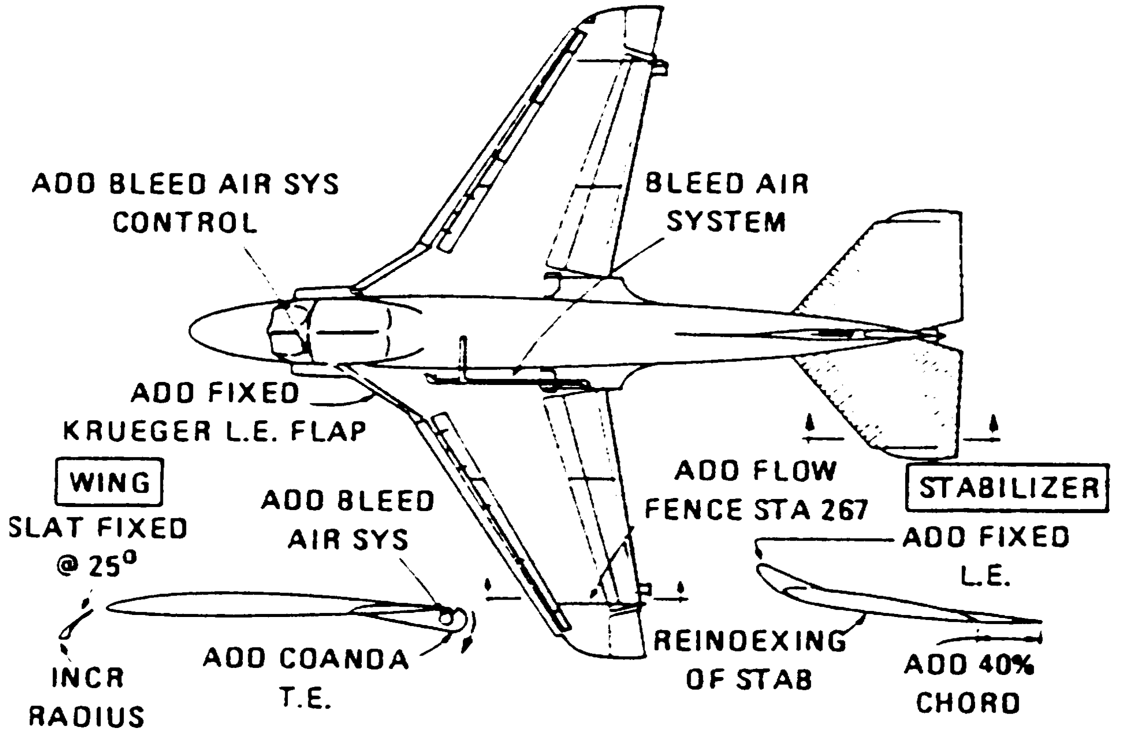

Figure 2. CCW airframe modifications, from ref. 19.

	A-6 (30 FLAPS) (REF)	A-6/CCW
85% INCREASE IN $C_{L_{MAX}}$	2.1	3.9 (C_μ = 0.30)
35% REDUCTION IN POWER-ON APPROACH SPEED	118 knots (C_L = 1.49)	76 knots (0.75 P_{MAX}, C_μ = 0.14, C_L = 2.78)
65% REDUCTION IN LANDING GROUND ROLL	2450 ft	900 ft
30% REDUCTION IN LIFT OFF SPEED	120 knots (C_L = 1.41)	82 knots (0.6 P_{MAX}, C_μ = 0.04, C_L = 2.16)
60% REDUCTION IN TAKEOFF GROUND ROLL	1450 ft	600 ft
75% INCREASE IN PAYLOAD/FUEL AT TYPICAL OPERATING WEIGHT (EW = 28,000 lb)	45,000 lb	58,000 lb

BASED ON FLIGHT DEMONSTRATION RESULTS
TOGW = 35,700 lb, LGW = 33,000 lb
CORRECTED TO SEA LEVEL, STANDARD DAY

Figure 3. A-6/CCW STOL performance, from ref. 15.

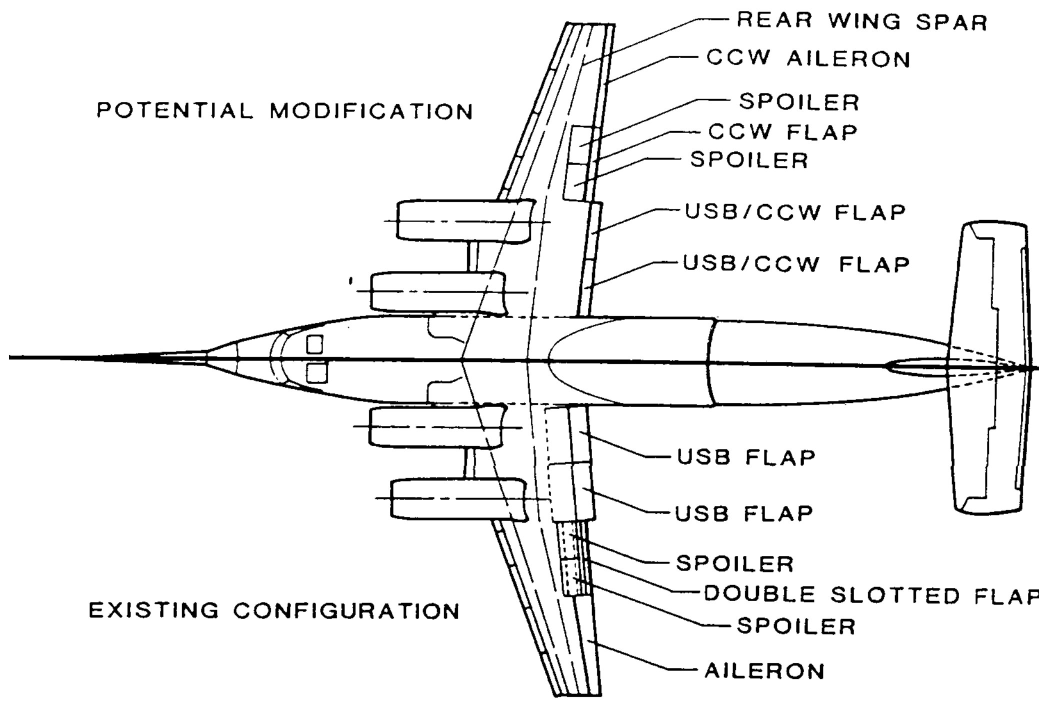

Figure 4. Comparison of existing QSRA wing to a USB/CCW modification, from ref. 14.

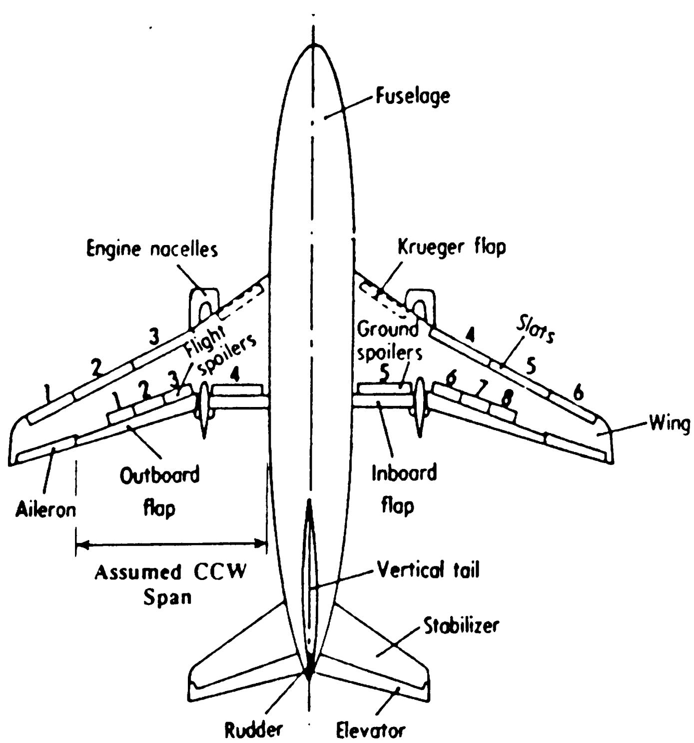

Figure 5. High-lift and control surfaces for conventional B737 and B737/CCW aircraft, from ref. 26.

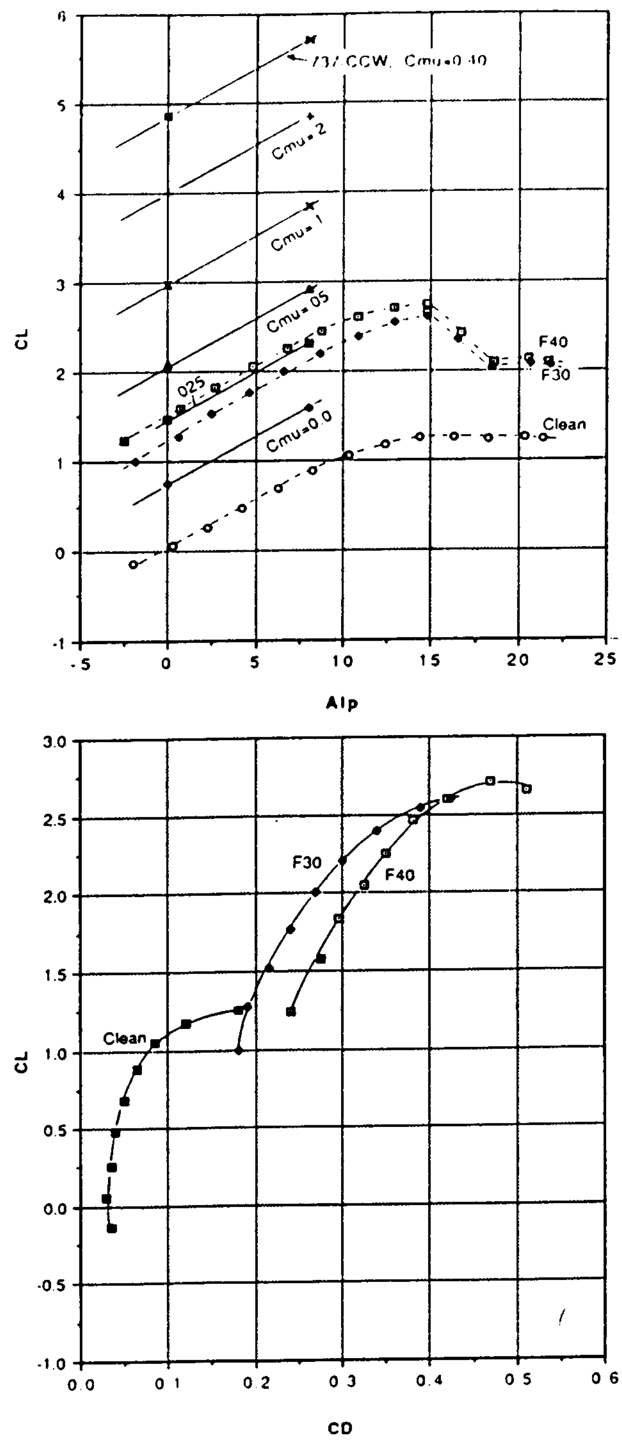

Figure 6. 1/8-scale wind tunnel lift and drag data for B737 (clean) aircraft compared with predicted B737/CCW (F30, F40) data, from ref. 26.

Blown Flaps

Technical Description. Blown flaps are a subset of powered lift technology where the vehicle lift is augmented by blowing over, under, or through wing trailing-edge flaps using either engine bleed air or engine exhaust flows. These systems achieve increased lift by increasing wing circulation and, to some extent, by deflecting thrust downward. These systems can significantly increase the maximum lift coefficient ($C_{L,max}$) of the aircraft and thus, provide STOL capability. Figure 1 shows the range of $C_{L,max}$ values possible by various techniques as a function of wing aspect ratio. Plain wings are limited to values well below 1.5. Mechanical flaps increase $C_{L,max}$ to around 2.0. Blowing boundary layer control (BLC) is limited to values around 4.0. For $C_{L,max}$ values above 4.0, forced circulation is required; further increases require the addition of direct thrust. Blown flap systems can be grouped into two general categories, internal flow systems and external flow systems. The internal flow systems utilize internal ducts to eject air over the flap(s), and the external flow systems exploit favorable placement of the engine and flap(s). The flap systems described herein are categorized in the manner of references 1 and 2.

There are at least four varieties of internal flow blown flap systems. They are blowing boundary layer control, the circulation control wing (discussed earlier), the jet flap, and the augmentor wing. These systems are shown in figure 2. In all four systems bleed air is ducted to and ejected over the flap upper surface.

Blowing boundary layer control (BLC) was first explored in the 1920s; systematic studies were performed in the 1940s and 1950s. This system makes use of engine bleed air to energize the boundary layer on the upper surface of the wing and delay flow separation. This allows a much higher maximum lift coefficient to be achieved. The Boeing 367-80 (707) prototype airplane demonstrated a BLC high lift system [ref. 3]. During flight testing, lift coefficients of at least 3.3 at a speed of 73 knots were obtained. For comparison, the maximum lift coefficient for a Boeing 707 is approximately 1.7 at a speed of 102 knots.

The internal flow jet flap is unique in that a large percentage of the engine exhaust is deflected through trailing-edge slots and over the flap. This system was initially proposed and tested in 1932, and it was demonstrated on the Hunting jet flap research airplane in the 1960s. For this configuration, lift coefficients greater than 6.0 were measured in the Langley 7x10-Foot Low Speed Wind Tunnel, and coefficients as high as 9.0 were measured during flight tests of the full scale vehicle [ref. 5]. The augmentor wing is a variation of the jet flap. It has a shroud assembly over the flap to create an ejector system which augments the thrust of the nozzle by entraining additional air. A DeHavilland C-8A was modified to include the augmentor wing design [ref. 6]. For this configuration lift coefficients of up to 5.5 were obtained.

There are two varieties of external flow blown flaps systems shown in figure 3. They are the externally blown flap (EBF) and the upper surface blown (USB) flap. Both approaches utilize relatively conventional flap designs. The EBF approach uses conventional pod-mounted engines which blow exhaust on the lower surface of the flaps [ref. 7]. The USB design has engines mounted on the upper surface of the wings and blow exhaust over the upper surface of the wing and flaps [ref. 8]. These two systems have similar aerodynamic characteristics, and demonstrated operational performance. During the 1970s the EBF design was first demonstrated on the YC-15 research aircraft and the USB system was first demonstrated on the YC-14 research aircraft. The USB approach has somewhat better noise characteristics than the EBF approach as the wings tend to shield engine exhaust noise from the ground [ref. 9].

The general performance characteristics of the internal and external flow systems are compared with deflected thrust approaches in figure 4. This plot provides an indication of the amount of thrust used to produce a direct lifting force versus the amount used to increase wing circulation. Deflected thrust is another powered lift concept in which the engines are used directly to produce a lifting force and wing circulation is not augmented. Internal flow systems are the most aerodynamically efficient because they provide the greatest increase in wing circulation for a given level of thrust, followed by external flow systems. While this implies that internal flow systems are superior, this result is tempered by the fact that engines appropriate for use with externally blown flaps have a relatively low fan pressure ratio and provide more static thrust than engines for internally blown flaps designed for the same cruise thrust. This difference in engine fan pressure ratio tends to balance out the difference in flap efficiency so that overall performance is not greatly different for the two flap systems. Clearly the choice between the various systems needs to be considered in the context of the entire aircraft design.

A unique implementation of the USB concept is the channel wing [refs. 10, 11, 12, and 13]. The channel wing, often referred to as the Custer Channel wing after its promoter Willard Custer, integrates the propeller flow with the wing aerodynamics by using the wing as a "shroud" in front of and below the propeller (Figure 5). The propeller draws its flowstream over the wing, inducing high upper-surface flow velocities at low airspeeds. This increases the circulation of the wing and provides a powered-lift capability similar to that of jet-powered USB systems.

It is possible for aircraft to employ more than one of these concepts to achieve greater STOL capability. One such aircraft is the NASA Quiet Short-haul Research Aircraft (QSRA), first mentioned in the Circulation Control discussion. This aircraft was originally configured with inboard USB flaps and blown BLC ailerons which can be drooped during flight to effectively provide a nearly full-span blown flap system. In addition, the wing had a leading-edge flap with blowing BLC [refs. 14 and 15]. This aircraft was able to obtain maximum lift coefficients as high as 10.

One final point needs to be made regarding high lift systems. With an increase in the operational lift coefficient comes a reduction in the vehicle airspeed and a reduction in the effectiveness of conventional control surfaces. Consequently, jet reaction control or blowing BLC for roll, yaw, and pitch control may be required. In addition, increased reliance on powered lift systems also increases the difficulty of achieving a design that can tolerate engine failures, which increases system complexity.

Current and/or Past Utilization. The McDonnell Douglas C-17 is the only transport currently in production employing powered lift technology. The design employs an externally blown, double-slotted, trailing-edge flap. Lift augmentation is achieved by deflecting the flap into the exhaust from engines mounted under the wing. An unusual aspect of the C-17 is the fact that it is the first powered-lift airplane to demonstrate the value of increased lift capability from powered-lift for increased payload rather than for emphasis on increased takeoff and landing performance.

Technological Benefits and Penalties. STOL aircraft have enhanced in-flight capabilities that include steep-gradient and curved-flight departures and approaches, high rates of climb, steep final descents, high maneuverability, rapid response for aborted landing, and low landing-approach speeds. These characteristics yield aircraft that require less airspace in the near-terminal area, require less ground space at the terminal, operate with less noise, and have improved crashworthiness and survivability because of their low speed capability at near-level fuselage attitudes. Thus, the use of existing airport infrastructure could be enhanced by utilizing vacant airspace, operating from separate short runways, minimizing time on the runway, and operating from presently underutilized small terminals. Also, the cost of new terminals could be minimized, and new modes of operation such as high-speed transportation directly to and from corporate headquarters and factories could be stimulated. Application to military missions include supply at more desirable, forward sites, operation on damaged runways, and enhanced operations from naval vessels.

All of the technologies discussed in the preceding section have the benefit of increasing the maximum lift coefficient of the aircraft. This effect allows all of these technologies to effectively reduce noise by allowing the aircraft to climb faster and achieve a higher altitude prior to overflying populated areas. This is in spite of the fact that source noise of these concepts generally increases due to the interaction of the propulsion system with the wing and flaps. The equivalent noise footprint of a STOL vehicle may be an order of magnitude less than that of comparable conventional aircraft [ref. 16]. Thus, resistance to new terminal projects can be minimized due to greater public acceptance.

Two penalties for employing these lift augmentation technologies are increased integration difficulties and mechanical complexity. The internal flow systems are the most efficient in terms of required thrust to weight ratio, but they suffer the largest penalties. They are complex, require more maintenance, have a higher initial cost, have engine performance penalties, and have structural and weight problems as compared with their external flow counterparts. The external flow systems do not experience these difficulties, but have lower aerodynamic efficiency and have higher required thrust-to-weight ratios.

Configuration Integration. Five primary issues for integrating blown flaps into an aircraft design are:

1. Engine placement relative to wing (EBF, USB, internal flow)
2. Engine air ducting and routing (internal flow only)
3. Structural layout of the wing box, movable flaps, and ducts
4. Flight control effectors for low-speed or vertical flight
5. Stealth

Engine placement relative to the wing is extremely important to EBF concepts due to the close interaction of emitted thrust flows with the wing and flap aerodynamics and optimization for both STOL operations and cruise. USB concepts require careful attention to wing/engine integration to ensure acceptable cruise performance of the wing aerodynamics. Internal flow designs require the consideration of engine placement for the integration of ducting from the engine exhaust path to the wing locations desired for blowing. The ducting itself encounters trade-offs between a desire for short duct lengths for minimum weight and a desire for large radii of curvature for maximum internal flow efficiency. Both the engines and the ducting must consider their volume impacts on the wing box structural design and possible load path implications. As mentioned, at very low STOL speeds, traditional control surfaces lose effectiveness, requiring unconventional configurations or control devices. Stealth issues are important in determining the flap arrangement and engine exhaust locations for military vehicles. Additionally, the acoustic qualities of STOL operations produce inherent, non-traditional stealth applications for covert insertions.

References.

1. Johnson, J. L.: “Review of Powered Lift Technology, Aerodynamic Considerations,” Eagle Engineering, Inc., Hampton Division. October 1991.

2. Deckert, W. H.; and Franklin, J. A.: “Powered -Lift Aircraft Technology,” NASA SP-501, December 1989.

3. Grazter, L. B.; and ODonnell, T. J.: “Development of a BLC High-Lift System for High-Speed Airplanes,” *J. Aircraft*, November-December 1965.

4. Englar, Robert J.: “Development of the A-6/Circulation Control Wing Flight Demonstrator Configuration,” DTN SRDL/ASED-7901, January 1979.

5. Harris, K. D.: “The Hunting H.1326 Jet-Flap Research Aircraft. Assessment of Lift Augmentation Devices,” AGARD, LS-43-71, 1971.

6. Quitley, Hervy, C.; and Innis Robert C.: “A Flight Investigation of the STOL Characteristics of an Augmented Jet Flap STOL Research Aircraft,” NASA TM X-62334, 1974.

7. Campbell, John P.; and Johnson, Joseph L., Jr.: “Wind-Tunnel Investigation an External Flow Jet-Augmented Slotted Flap Suitable for Application to Airplanes With Pod-Mounted Engines,” NASA TN-3898, 1956.

8. Turner, T. R.; Davenport, E. E.; and Riebe, J. M.: “Low-Speed Investigation of Blowing From Nacelles Mounted Inboard and on the Upper Surface of an Aspect Ratio 7.0 35^{o} Swept Wing With Fuselage and Various Tail Arrangements,” NASA Memo 5-1-59L, 1959.

9. Maglieri, D. J.; and Hubbard H. H.: “Preliminary Measurements of the Noise Characteristics of Some Jet-Augmented-Flap Configurations,” NASA Memo 12-4-58 L, 1959.

10. Young, D. W., "Test of Two Custer Channel Wings Having a Diameter of 37.2 Inches and Lengths of 43 and 17.5 Inches", Army Air Forces Technical Report 5568, April 1947.

11. Pasamanick, J.; "Langley Full-Scale Tunnel Tests of the Custer Channel Wing Airplane", NACA Research Memorandum L53A09, April 1953.

12. Anderton, D. A.; "Vertical Lift is Claimed for Channel Wing", Aviation Week, December 17, 1951.

13. Blick, E. F. and Homer, V.; "Power-On Channel Wing Aerodynamics", Journal of Aircraft, Vol. 8, No. 4, April 1971, pp. 234-238.

14. Eppel, J. C.; Shovlin, M. D.; Jaynes, D. J.; Englar R. J.; and Nichols, J. H., Jr.: “Static Investigation of the Circulation-Control-Wing/Upper Surface-Blowing Concept Applied to the Quiet Short-Haul Research Aircraft,” NASA TM-84232, 1982.

15 Stephens, V. C.; Riddle, D. W.; Martin, J. L.; and Innis, R. C.: “Powered-Lift STOL Aircraft Shipboard Operations - A Comparison of Simulation, Land-Based and Sea Trial Results for the QSRA,” AIAA 81-2480, November 1981.

16. Brown, D. G.: “The Case for V/STOL Aircraft in Short-Haul Transportation,” SAE National Air Transportation Meeting, Paper No. 700333, April 1970.

Bibliography.

Langford, John S., III: “The NASA Experience in Aeronautical R&D: Three Case Studies With Analysis,” IDA Report R 319, March 1989.

Englar, R. J.; Niebur, C. S.; and Gregor, S. D.: “Pneumatic Lift and Control Surface Technology Applied to High Speed Civil Transport Configurations,” AIAA 97-0036, January 1997.

Johnson, W. G.: “Aerodynamic Characteristics of a Powered, Externally Blown Flap STOL Transport Model With Two Engine Simulator Sizes,” NASA TN D-8057, November 1975.

Powered-Lift Aerodynamics and Acoustics. Conference held at Langley Research Center, Hampton, VA, NASA CP-406, May 24-26, 1976.

Antinello, John S.: “Design and Engineering Features of Flap Blowing Installations,” *Boundary Layer and Flow Control*, Pergamon Press, 1961, pp. 462-515.

Davidson, I. M.: “The Jet Flap,” *J. Royal Aeronautical Society*, Vol. 60, January 1956.

Malavard, L.; Poisson-Quinton, P.h.; and Joussenandot, P.: “Theoretical and Experimental Investigation of Circulation Control,” Princeton University Report No. 358, July 1956.

Lockwood, Vernard E.; Turner, Thomas R.; and Riebe, John M.: “Wind Tunnel Investigation of Jet-Augmented Flaps on a Rectangular Wing to High Momentum Coefficients,” NACA 3865, 1956.

Cone, Clarence D., Jr.: “A Theoretical Investigation of Vortex-Sheet Deformation Behind A Highly Loaded Wing and Its Effect on Lift,” NASA TN D-657, 1961.

Nichols, J. H., Jr.; Englar, R. C.: “Advanced Circulation Control Wing System for Many STOL Aircraft,” AIAA 80-1825, August 1980.

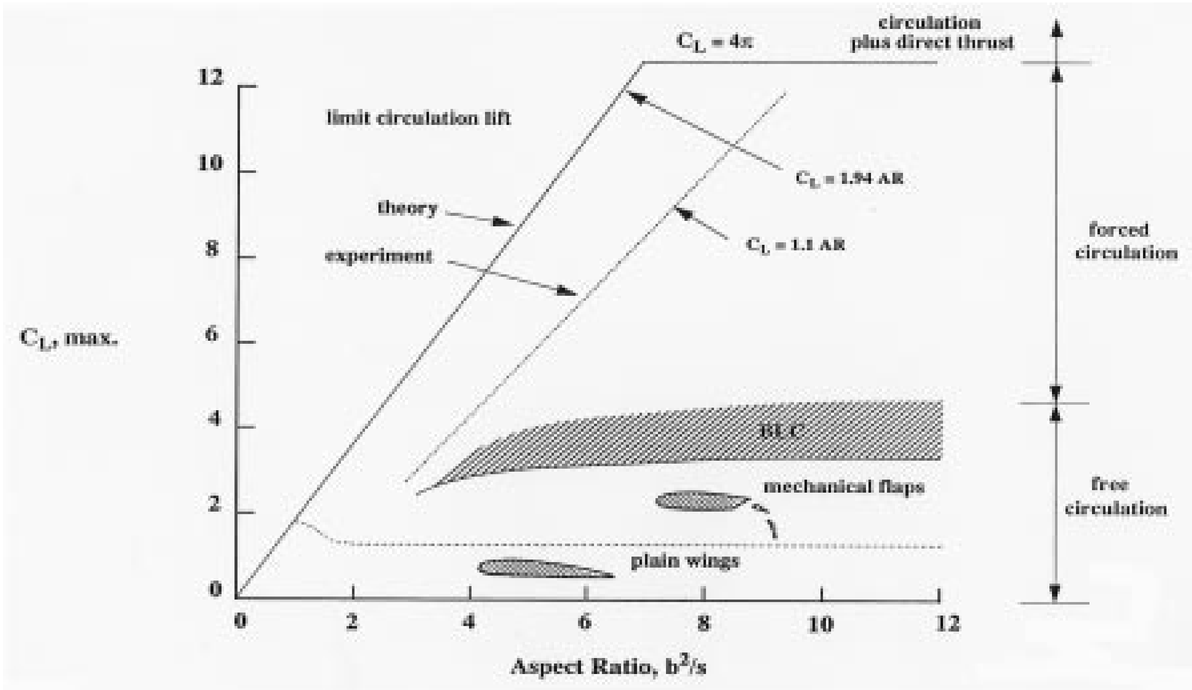

Figure 1. Maximum lift coefficient as a function of aspect ratio.

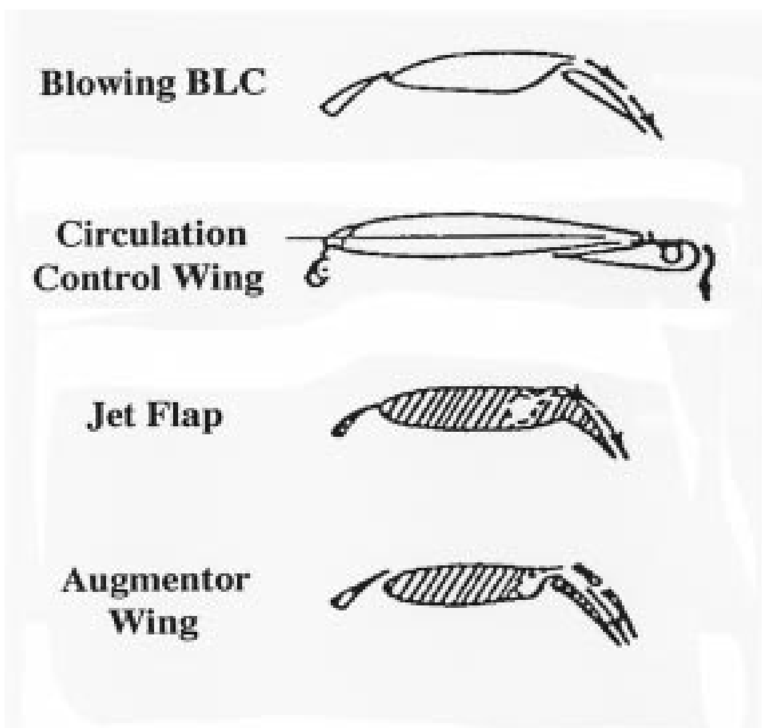

Figure 2. Internal flow, blown flap systems.

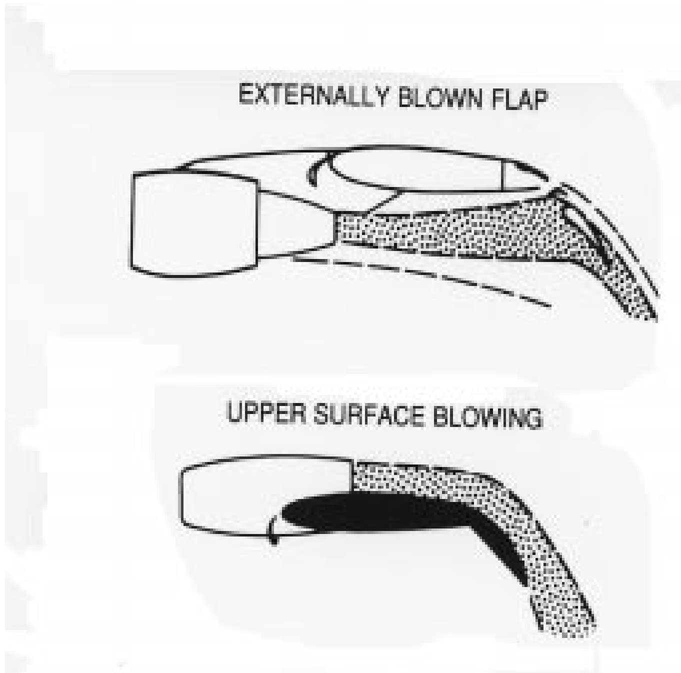

Figure 3. External flow, blown flap systems.

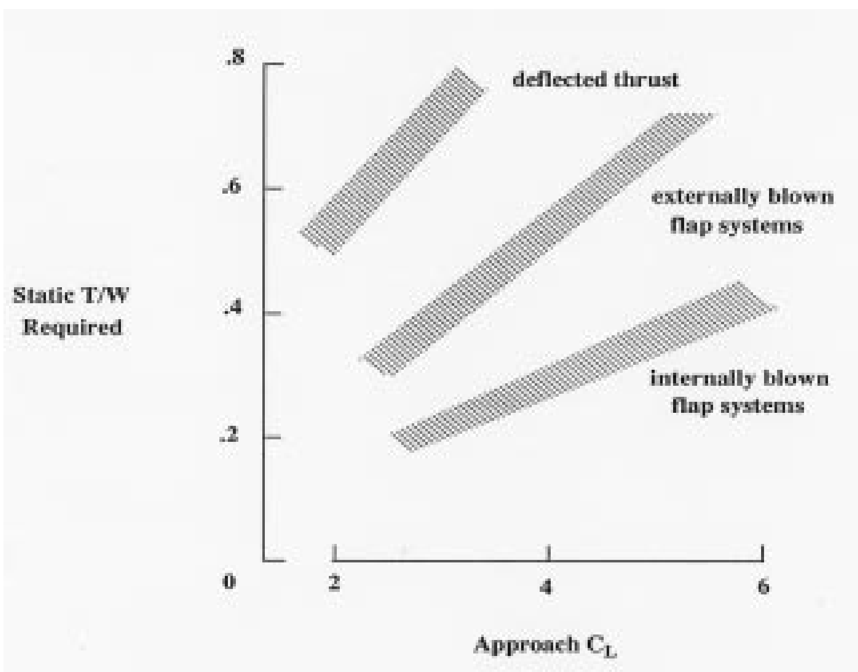

Figure 4. Comparison of thrust requirements of internally and externally blown flaps with deflected thrust approaches.

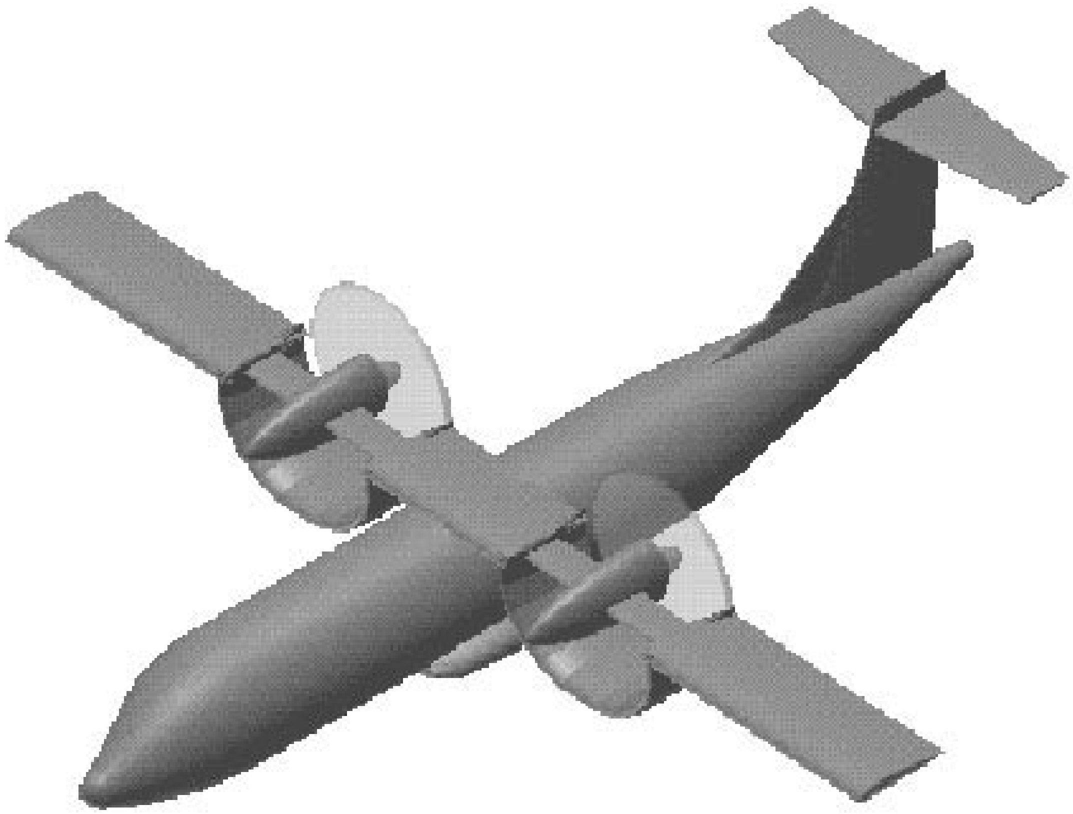

Figure 5. The Channel Wing

Augmentor/Jet Wing

Technical Description. The ejector/augmentor wing and Jetwing are two examples of powered lift technology. Other examples of powered lift include internally and externally blown flaps, upper surface blowing, thrust vectoring, and lift-fan or direct-lift engines. Envisioned as a means of achieving good V/STOL performance for military aircraft, these technology concepts have been investigated experimentally and computationally since the 1950's.

Powered lift technologies utilize propulsion bleed and/or exhaust flows to increase wing circulation. This is accomplished through various means: entrainment of external flows, super-velocity acceleration of flows, and direct vectoring of propulsive flows in the lift vector orientation. Cross-sectional wing schematics for various powered lift technologies are shown in figure 1.

There are two general approaches to the ejector/augmentor concept which will be referred to as the XFV-12A and E-7A concepts due to their usage within those experimental aircraft test programs. The XFV-12A concept for ejector/augmentor wings is a V/STOL application that typically consists of three trailing-edge flap elements arranged as shown in figure 2. The center flap element contains ejector augmentors which blow propulsive air in the lift direction. The jet created by these ejectors serves to entrain airflow over the surface of the other two flaps which act to form a diverging nozzle. In addition, the two lower flaps contain Coanda surfaces to further assist in flow entrainment. The concept results in a lift force greater than the propulsive force utilized, thus “augmenting” the power output by the engines. An internal layout drawing of the XFV-12A is shown in figure 3. Note that both the main wing and the canard are configured as ejector/augmentor wings and that the vehicle is a single engine, supersonic aircraft.

The E-7A ejector/augmentor concept is also a V/STOL application and consists of a channel through each wing, near the root, where a series of deflectable ejector vanes are arranged (figures 4 to 6). Fan air is diverted to these ejectors as well as through an aft centerline nozzle fixed in both a forward thrust and lift contributing axis. The ejector/augmentors serve to entrain flow from over the wing surface through the channel and thus create a thrust augmentation through supercirculation. The bottom portion of the wing channel is opened into a nozzle through a complex mechanism and closes to form a sealed, supersonically viable configuration.

The Jetwing concept, developed by the Bell-Bartoe Aircraft Company, is a STOL concept with two basic configurations. Figure 7 shows a concept utilizing a second wing, forming an ejector between it and the main wing. The leading edge section of the main wing contains a duct and plenum through which air is blown over the upper surface of the wing. This blown flow entrains additional flow through the ejector area. A Coanda surface on the trailing edge flap serves to create high flow turning angles and completes the high-lift concept. Figure 8 shows the other version of the concept without the ejector that utilizes only upper surface blowing and the Coanda flap. An internal layout of the engine and ducting of the Bell-Bartoe Experimental Jetwing Aircraft is shown in figure 9. Note that all of the airflow, including both the fan and core flows, are directed entirely to the wing.

Current and/or Past Utilization. No current nor past production (unclassified) aircraft utilize either the ejector/augmentor wing or Jetwing design concepts for powered lift. Experimental aircraft programs have utilized the concepts with results discussed in the previous section. V/STOL technology is generally viewed as most valuable in military applications where short field capabilities or carrier-based operations are required. Future civilian requirements in community noise restriction, air traffic congestion, airport layout design constraints, and the business transportation market may present the possibility of new markets for V/STOL technologies.

Technological Benefits and Penalties. Studies have demonstrated that the ejector/augmentor wing and Jetwing concepts have benefits in performance, noise, emissions, and safety. There may be additional benefits in life-cycle cost savings and air traffic throughput achieved through the usage of these concepts.

There appears to be little publicly available performance data on the ejector/augmentor wing, probably due to the classification on the Navy/Rockwell XFV-12A program. However, figure 10 shows the split between circulation lift and jet lift for the ejector/augmentor concept in the XFV-12A at various flight speeds without indicating the lift coefficient. Note that the lift generated by circulation is zero for no forward flight, indicating vertical takeoff, and that the ejector/augmentor lift goes to zero at 140 knots. Figure 11 shows the mechanical transition of the XFV-12A ejector/augmentor wing from hover to cruise.

The proponents of the XFV-12A concept wing demonstrated in laboratory tests that the augmentation ratio, defined as the ratio of the total thrust generated to the primary thrust injected at the ejector/augmentor, could exceed 2.0. If such performance was attainable in a flight article, the takeoff and climbing benefits would be capable of offsetting the additional weight of necessary flow diverters and ducting.

The General Dynamics E-7A incorporates a very different concept of ejector/augmentors but the physics of the thrust augmentation procedure are the same. The primary implementation distinction is that the E-7A utilizes a secondary nozzle for vectored engine core thrust while a portion of the fan-diverted flow exits through a 2-D afterburning nozzle (figure 5). Figure 12 depicts the thrust distribution for hovering, transitional, and forward flight. The concept was tested in static and free-flight wind-tunnel tests during the late 1980's and early 1990's and appeared to be feasible. There may possibly have been some issues with both design complexity and stealth configuration that prevented the Lockheed Martin JAST team from proposing the concept for use in what is now the Joint Strike Fighter (JSF) program.

The V/STOL performance capabilities afforded through powered lift generate possible overall aircraft weight savings through reductions in fuel burn during takeoff, climb, descent, and landing operations. This reduction in fuel burn is possible due to higher vertical climb/descent rates used to reach or descend from cruise altitude in a shorter time than otherwise possible. This fuel savings results in an overall smaller (and lighter) aircraft, possibly costing less to manufacture and certainly costing less to fuel, and producing reduced emissions through reduced fuel burn. Accelerated climbouts additionally hold the potential for increased airport operations due to a decrease in necessary aircraft spacing, a variety of climb and descent profiles available to pilots and controllers, and through achieving community noise footprints likely superior to conventional aircraft due to shorter dwell times, higher altitudes, and reduced jet velocities.

In addition to the V/STOL capabilities afforded by the ejector/augmentor wing, these concepts hold key advantages in noise and “hot footprint” which translate directly to human safety benefits when compared to other V/STOL fixed wing aircraft. Figure 13 depicts noise levels for various powered lift concepts with ejector/augmentor wings and the Jetwing (Upper Surface Blown or USB in that figure) shown as the minimal noise producing concepts. A V/STOL aircraft produces patterns of hot exhaust which have two major effects: 1) limiting the proximity and type of materials/objects which can be present in the landing and takeoff area and 2) causing “hot day” performance and engine damage through ingestion of exhaust flows. Due to the superior flow mixing and resultant cooling of exhaust flows in the ejector/augmentor wing and the Jetwing, neither of these issues is a serious performance limiter. Hot and blast jet exhaust zones are severely decreased for these aircraft, increasing the safe maintenance and operations area available to personnel conducting pre- and post-flight servicing.

In addition to V/STOL capabilities for takeoff and landing operations, the performance capabilities of these propulsion integration concepts hold the potential to increase the survivability of military aircraft due to superior maneuvering capabilities. The University of Tennessee Space Institute published a paper [ref. 1] including a conceptual design study indicating maneuvering performance enhancements due to the Jetwing concept. Figures 14 and 15 show the reported benefits in turn rate and sustained normal load factors at sea level and combat altitude. The resulting configuration is shown in figure 16. Battle damage survivability can be poor depending on the exhaust arrangement of V/STOL aircraft. For example, Harriers tend to take heat seeking missiles amidship.

Three significant penalties inhibit the adoption of augmentor and Jetwing concepts: additional weight due to ducting and mechanical systems, constraints on design integration (see configuration integration) due to ducting and balance considerations, and the expense of system complexity. No data was publicly available on the details of system weight for any of the experimental vehicles and studies investigating the penalties associated with design of augmentor and Jetwing concepts must overcome the large uncertainties associated with systems weight and ducting losses. The associated life cycle cost -- especially in maintenance -- is a significant unknown with little applicable data existing either within the public domain or industry proprietary data.

Configuration Integration. Five primary issues for integrating either of these concepts into an aircraft design are:

1. Center of gravity location
2. Engine air ducting and routing
3. Structural layout of the wing box, movable flaps, and ducts
4. Flight control effectors for low-speed or vertical flight
5. Stealth

Center of gravity location is critical for thrust balance in a VTOL aircraft. It is the major factor in tail design for STOL aircraft. Engine air ducting allowances must be made in both the fuselage and wing for fuselage embedded engine aircraft. Significant turn radii are required for diverting the flow forward in these ducts while preventing separation. The ducts must fit within the thickness of the wing section making supersonic aircraft much more difficult to integrate while limiting wave drag. Finally, the ducts will take up volume normally used for fuel. The structural layout options greatly impact the weight of the wing due to positioning of primary structural members and carrying the structural loads from numerous, highly aerodynamically loaded flight controls and flaps. Flight control is a critical element of a V/STOL design due to limitations on the available effectiveness of primary flight controls. Many ejector/augmentor concepts for hovering and transitioning flight utilize pneumatic controls functioning off of the diverted propulsion flow. STOL flight controls concepts include both pneumatics and enlarged main control surfaces. The ability to include powered lift technologies in stealth designs is debatable. The required geometry and material treatment are difficult to achieve with concepts requiring large numbers of moving parts, internal chambers, and exposure to engine exhaust gases.

References.

1. Kimberlin, R. D.; and Sinha, A. K.: “STOL Attack Aircraft Design Based upon an Upper Surface Blowing Concept,” AIAA 83-2535, 1983.

2. Andrews, H.; Murphy, R.; and Wilken, I.: “The North American Rockwell XFV-12A - Reflections and Some Lessons,” AIAA 90-3240, 1990.

3. Whitley, D. C.; and Gilbertson, F. L.: “Recent Developments in Ejector Design for V/STOL Aircraft,” SAE Paper 841498, January 1984.

4. Kimberlin, R. D.: “An Investigation of the Effects of a Thrust Augmenting Ejector on the Performance and Handling Qualities of an Upper Surface Blown Research Aircraft,” Flight testing technology: A state-of-the-art review, Proceedings of the Thirteenth Annual Symposium, New York, NY, September 19-22, 1982 (A84-44451 21-01). Lancaster, CA, Society of Flight Test Engineers, 1982, p. 67-72.

5. Riley, D. R.; Shah, G. H.; and Kuhn, R. E.: “Low-Speed Wind-Tunnel Study of Reaction Control-Jet Effectiveness for Hover and Transition of a STOVL Fighter Concept,” NASA TM 4147, December 1989.

Bibliography.

Kimberlin, R. D.: “Performance Flight Test Evaluation of the Ball-Bartoe JW-1 Jetwing STOL Research Aircraft,” Flight testing in the Eighties; Proceedings of the Eleventh Annual Symposium, Atlanta, GA, August 27-29, 1980. (A82-20751 08-05) Lancaster, CA, Society of Flight Test Engineers, 1980, p. 16-1 to 16-20.

Kimberlin, R. D.; Solies, U. P.; and Sinha, A. K.: “A Flight Test Evaluation and Analytical Study of the Ball-Bartoe Jetwing Propulsive Lift Concept Without Ejector,” University of Tennessee Space Institute Report UTSI-82/17, Oct. 1, 1982.

Sinha, A. K.; Kimberlin, R. D.; and Wu, J. M.: “Equivalent Flap Theory: A New Look at the Aerodynamics of Jet-Flapped Aircraft,” AIAA 84-0335, 1984.

Woolard, H. W.: “Thin-Airfoil Theory of an Ejector-Flapped Wing Section,” AIAA 74-187, February 1974.

Proceedings of the NASA/NADC/AFFDL Workshop on Thrust Augmenting Ejectors, NASA CP-2093, September 1979.

Summary Report, XFV-12A Diagnostic and Development Program, Rockwell International, October 1981.

Catalano, G. D.; Nagaraja, K. S.; Wright, H. E.; and Stephens, D. G.: “Turbulence Measurement in an Ejector Wing Flow Field,” AIAA 81-1712, August 1981.

Porter, J. L.; and Squyers, R. A.: “Ejector Wing Design,” Air Force Wright Laboratories Report AFWAL-TR-82-3011, September 1981.

Anderson, S. B.; and Faye, A. E. Jr.: “Flight Investigation of the Low Speed Characteristics of a 35 Degree Swept-Wing Airplane Equipped with an Area-Suction Ejector Flap and Various Leading Edge Devices,” NACA-RM-A57G10, September 1957.

Fishbach, L. H.: “Performance of Ejector Wing Aircraft for Navy VTOL Fighters,” NASA TM X-68237, May 1973.

Squyers, R. A.; Porter, J. L.; Nagaraja, K. S.; and Cudahy, G. F.: “Ejector Powered Propulsion and High Lift Subsonic Wing,” ICAS 82-6.5.2.

Domalski, J. T.: “Theoretical Determination of the Lift of a Simulated Ejector Wing,” M.S. Thesis, Air Force Institute of Technology, December 1982.

Flinn, E.: “Tests of Ejector Pump Configurations Designed for Use in the Ejector Flap Boundary Layer Control System,” WADC Technical Note 55-29, Wright Air Development Center, Dayton, OH, August 1957.

Lowry, J. G.; Riebe, J. M.; and Campbell, J. P.: “The Jet-Augmented Flap,” Institute of the Aeronautical Sciences Paper No. 715, January 1957.

Deckert, W. H.; and Franklin, J. A.: “Powered-Lift Aircraft Technology,” NASA SP-501, 1989.

Deckert, W. H.; and Franklin, J. A.: “Powered Lift Technology on the Threshold,” *Aerospace America*, Vol. 23, No. 11, November 1985.

Riley, D. R.; Croom, M. A.; and Shah, G. H.: “Wind-Tunnel Free-Flight Investigation of an E-7A STOVL Fighter Model in Hover, Transition, and Conventional Flight,” NASA TP 3076, April 1991.

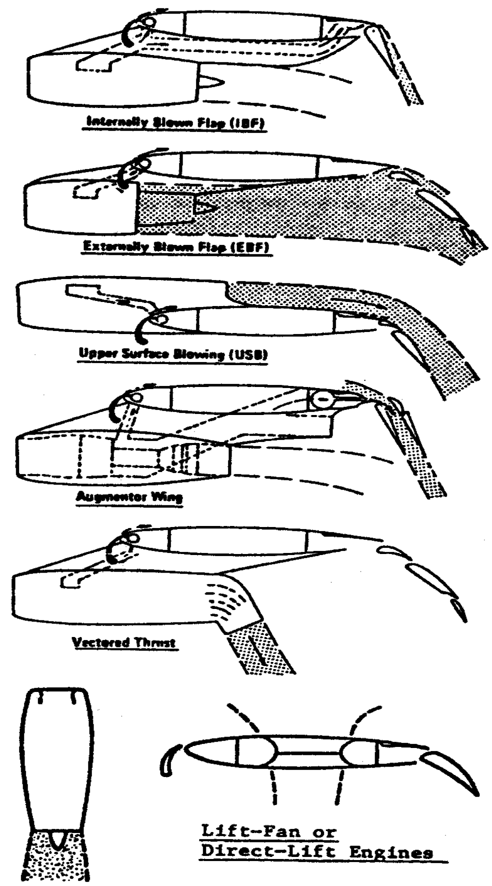

Figure 1. Powered Lift Concepts, from ref. 1.

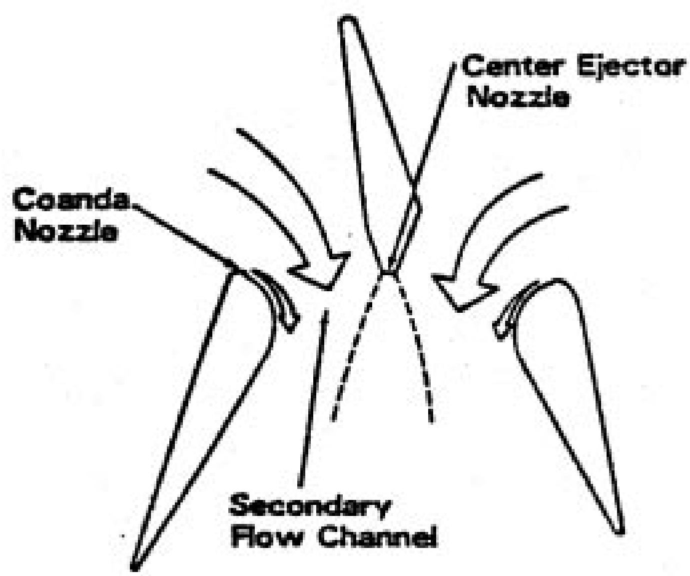

Figure 2. Typical ejector augmentor cross section for augmentor wing, from ref. 2.

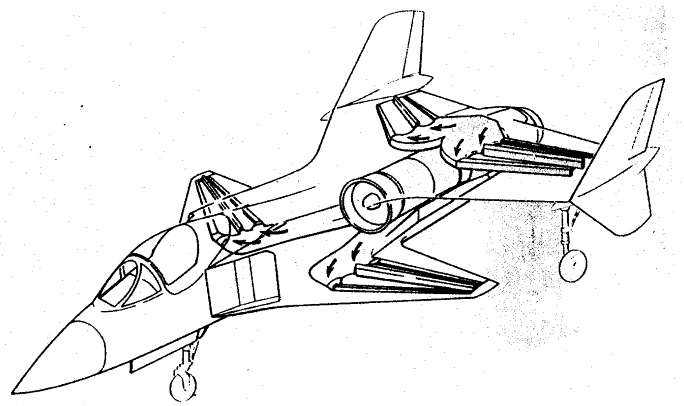

Figure 3. Propulsion system and augmentor flow for vertical lift, from ref. 2.

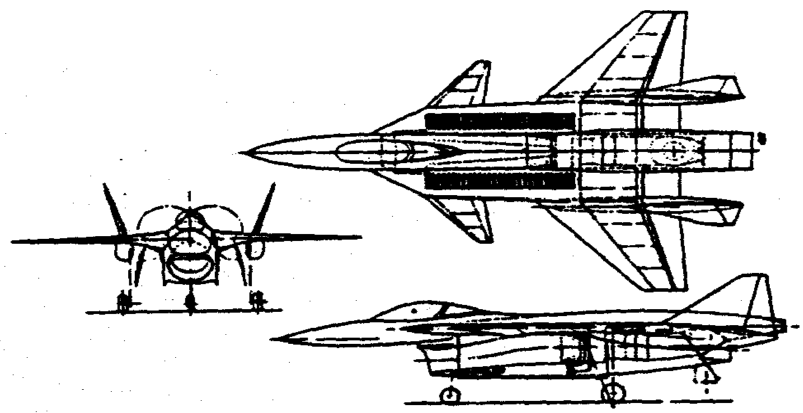

Figure 4. Ejector lift/vectored thrust concept combat aircraft, from ref. 3.

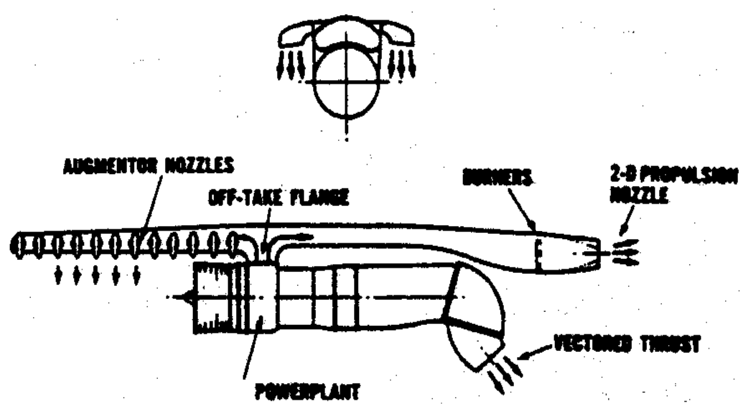

Figure 5. Deployment of jet flow for short takeoff, from ref. 3.

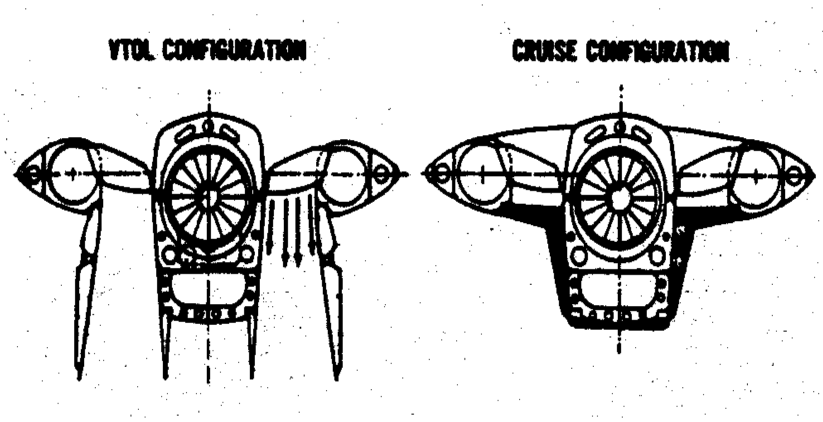

Figure 6. Cross section of ejector system, from ref. 3.

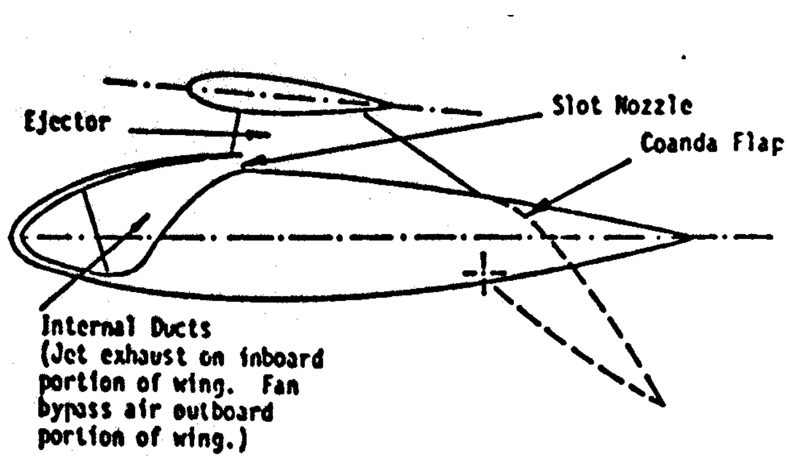

Figure 7. Two dimensional view of Jetwing concept with ejector installed, from ref. 4.

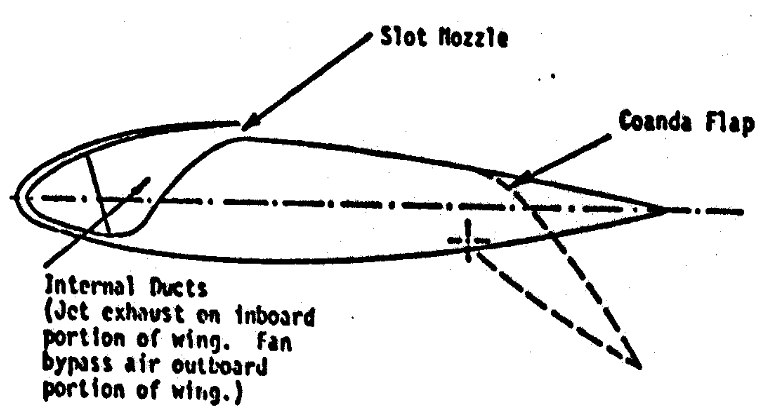

Figure 8. Two dimensional view of Jetwing concept without ejector installed, from ref. 4.

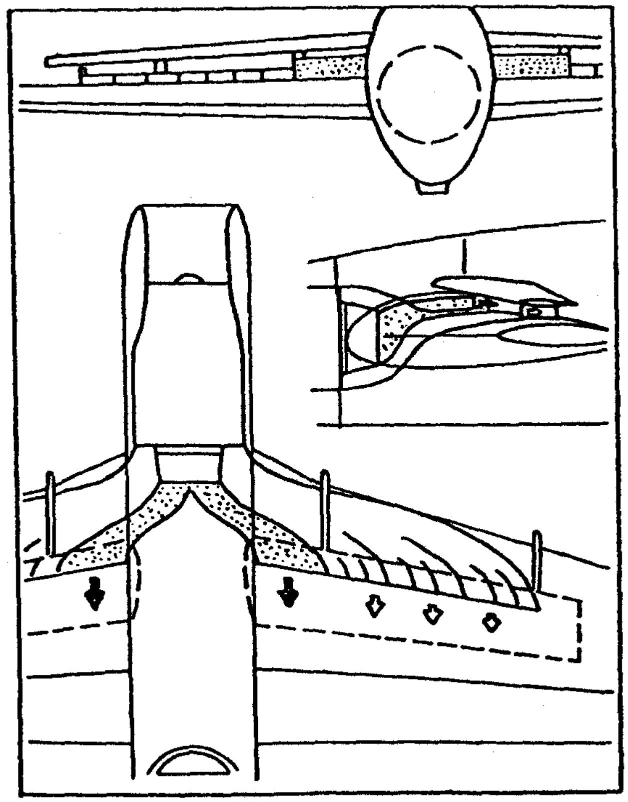

Figure 9. Jetwing ducting arrangement, from ref. 1.

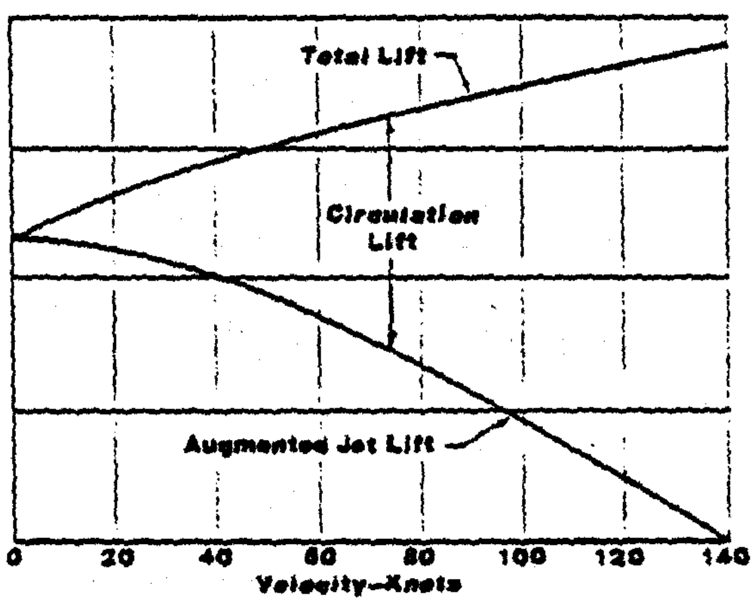

Figure 10. Increased STOL total lift with vectored augmentor, from ref. 2.

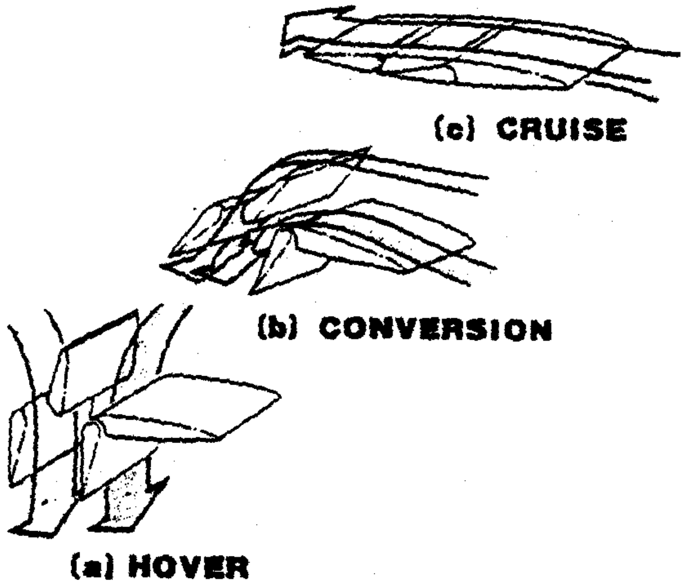

Figure 11. Thrust augmented wing in hover, transition/STOL, and conventional flight, from ref. 2.

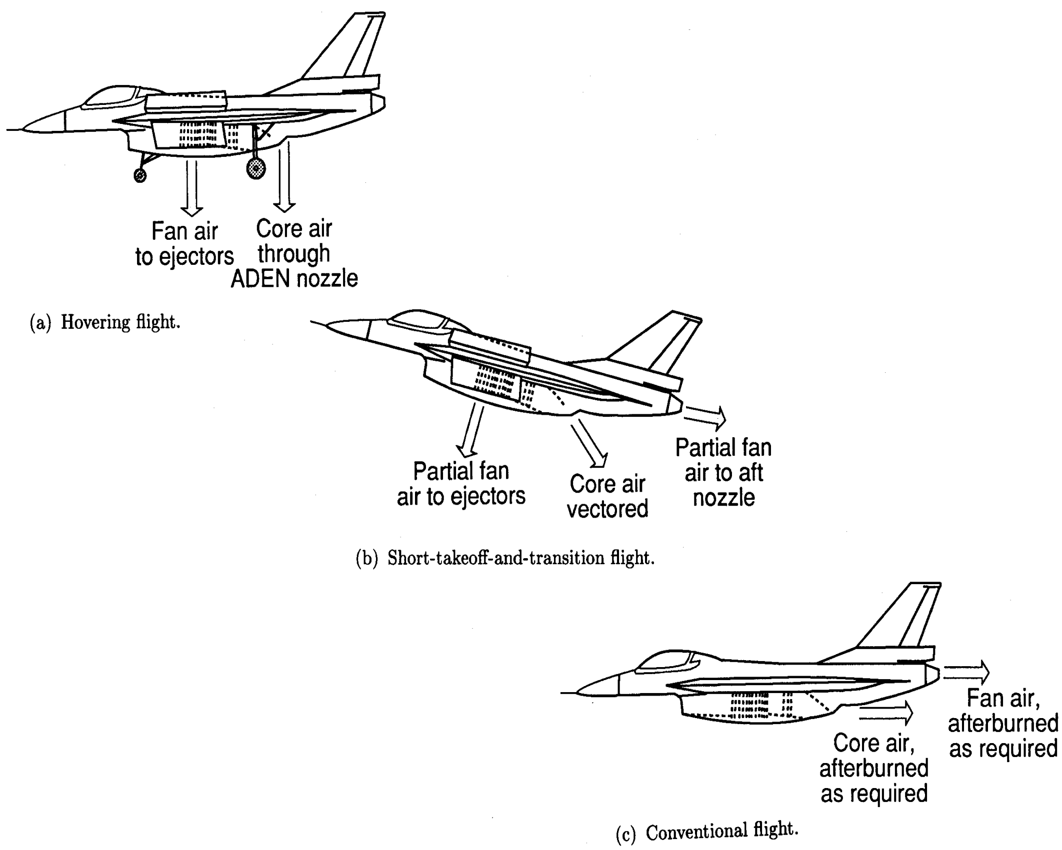

Figure 12. Modes of operation of the E-7A, from ref. 5.

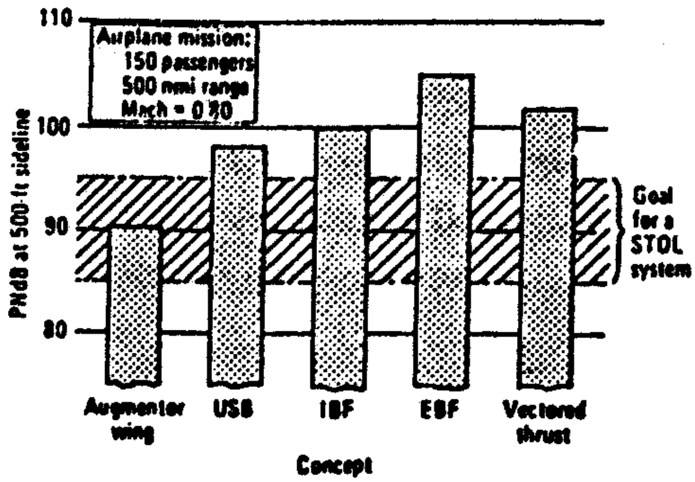

Figure 13. Noise levels for powered lift concepts, from ref. 1.

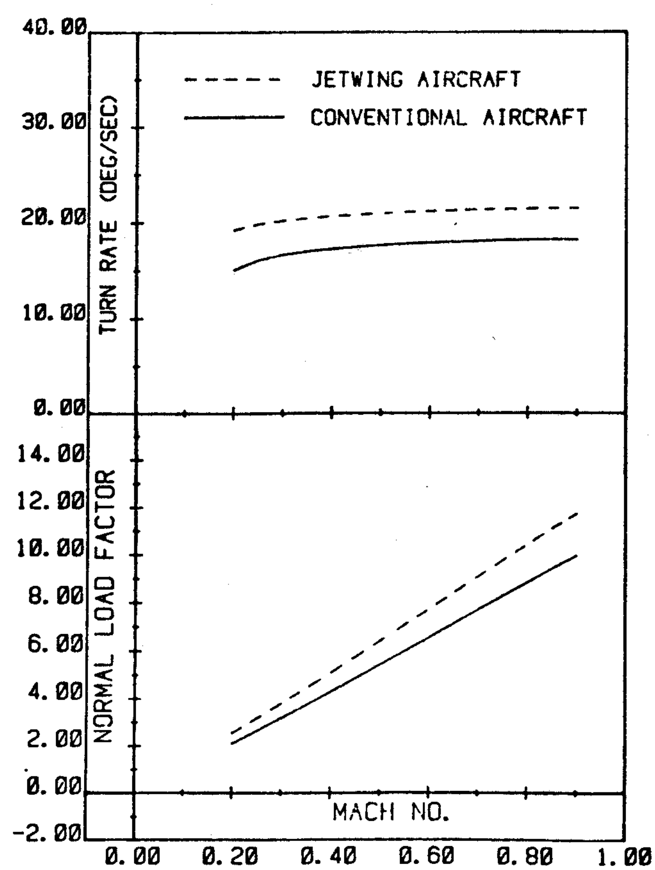

Figure 14. Sustained maneuver performance with afterburner at sea level, from ref. 1.

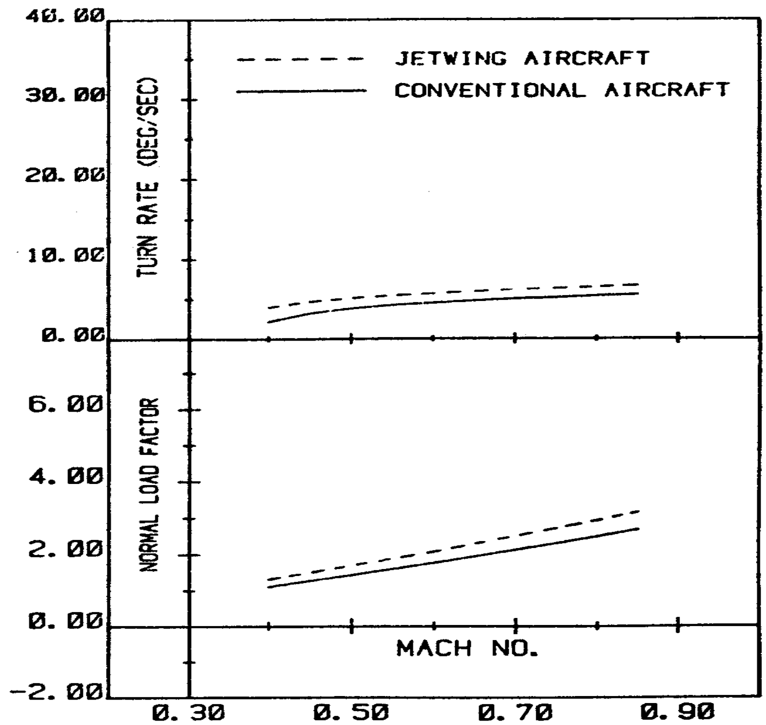

Figure 15. Sustained maneuver performance with afterburner at 35000 ft. altitude, from ref. 1.

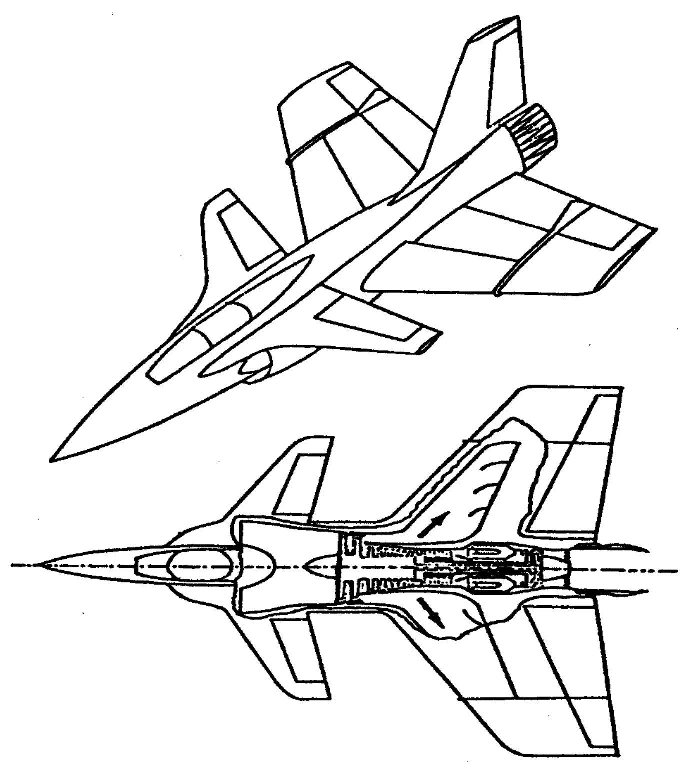

Figure 16. Attack aircraft based upon Jetwing concept, from ref. 1.

Wing-Tip Modifications

Blowing

Technology Concept. Wingtip blowing entails exhausting one or more jets of air from the wingtip in a generally spanwise direction. Air for the jet can be bled from the propulsion system, removed from the flow at the aircraft surface by a laminar-flow-control system, or ducted from the region of the stagnation line along the wing leading edge. Figure 1 shows two different blowing configurations, blowing from a long-chord slot and blowing from multiple short-chord slots. This figure and much of the following discussion is summarized from reference 1.

References 2 to 5 describe some early work in this area. Theses studies considered low-aspect-ratio wings, large jet momentum coefficients, and jet chords that were a large fraction of the wingtip chord. The results of these studies were that lift-curve slope could be increased and that blowing increased the loading across the span with the largest increases occurring near the tip. Blowing also increased the maximum lift coefficient. Flow surveys downstream of the wing with and without blowing indicated that blowing displaced the primary wingtip vortex outward and upward, diffused the vortex over a larger area, and reduced maximum vorticity at the center of the vortex. These studies used jet momentum coefficients ranging from 0.10 to 1.75. These values were much larger than the typical thrust to dynamic pressure-wing area ratios of transports of 0.04.

The more recent work found in references 6 to 8 made use of several short-chord jets, more realistic blowing coefficients typically between 0.001 and 0.008, and low aspect-ratio wings. These studies found that blowing from several short-chord jets can produce results similar to those obtained with a single continuous jet. The magnitude of the effects are proportional to the blowing coefficient.

One of the most recent and exhaustive investigations into this concept is presented in reference 1. This study differed from earlier efforts in that a larger aspect-ratio wing was tested and corresponding Navier-Stokes analyses were performed. The findings of this study were that for moderate aspect-ratio wings at high subsonic Mach numbers the benefits of spanwise blowing were quantifiable.

Benefits. Wing tip blowing can improve the aerodynamic performance of wings. The main effects of spanwise blowing are to increase the wing effective aspect ratio and to increase the loading towards the wing tips. Thus, wing tip blowing provides effects that are similar to those of winglets, but the blowing can be tailored to improve performance of the aircraft throughout its mission instead of just one design point. In addition, wingtip blowing can be used asymmetrically to provide roll and lateral control of the aircraft. Finally, wing-tip blowing may help to diffuse the wingtip vortex which can potentially make airport operations more efficient by allowing reduced aircraft separation.

Wing tip blowing has some limitations and penalties. It provides the greatest benefit for low aspect-ratio wings. Consequently, it may not be applicable to subsonic transports. It adds complexity and weight like other internal flow blowing systems, and the jet momentum coefficients required to achieve aerodynamic benefits may impose large engine performance penalties.

Applications. Wing tip blowing has not been applied to any aircraft, production or experimental. The concept performs better on low aspect ratio configurations so single stage to orbit or high speed civil transport vehicle designs may benefit from this technology. If wing tip blowing were considered as part of a larger system like suction boundary layer control, then it may have potential in other configurations.

References.

1. Mineck, R. E.: “Study of Potential Aerodynamic Benefits From Spanwise Blowing at the Wingtip,” NASA TP 3515, June 1995.

2. Tavella, D. A.; Wood, N. J.; Lee, C. S.; and Roberts, L.: “Two Blowing Concepts for Roll and Lateral Control of Aircraft,” NASA CR 180478, October 1986.

3. Ayers, R. F. and Wilde, M. R.: “An Experimental Investigation of the Aerodynamic Characteristics of a Low Aspect Ratio Swept Wing with Blowing in a Spanwise Direction from the Tips,” The College of Aeronautics Cranfield, September 1956.

4. Smith, V. J.; and Simpson, G. J.: “A Preliminary Investigation of the Effect of a Thin High Velocity Tip Jet on a Low Aspect Ration Wing,” Note ARL/A.163, Australia Dep. of Supply, June 1957.

5. Lloyd, Adrian: “The Effect of Spanwise Blowing on the Aerodynamic Characteristics of a Low Aspect Ratio Wing,” von Karman Institute for Fluid Dynamics Project Report 1963-90, 1963.

6. Wu, J. M.; Vakili, A. D.; and Chen, Z. L.: “Wing-Tip Jets Aerodynamic Performance,” 13th Congress of the International Council of the Aeronautical Sciences, AIAA Aircraft Systems and Technology Conference, Seattle, Washington, August 1982.

7. Wu, J. M.; Vakili, A. D.; and Gilliam, F. T.: “Aerodynamic Interactions of Wingtip Flow with Discrete Wingtip Jets,” AIAA 84-2206, August 1984.

8. Wu, J. M.; Vakili, A.; Chen, Z. L.; and Gilliam, F. T.: “Investigation on the Effects of Discrete Wingtip Jets,” AIAA 83-0546, January 1983.

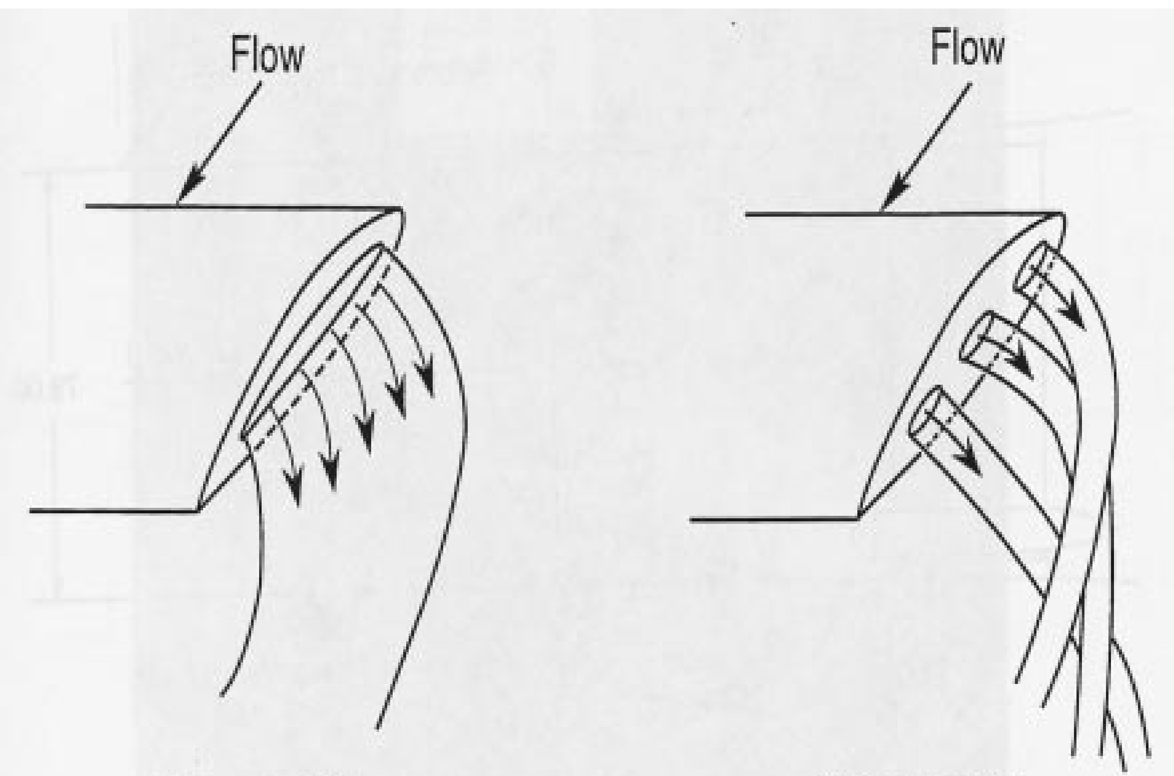

Long-chord jet Short-chord jet

Figure 1. Wingtip blowing configurations.

Engines/Turbines

Background and Technical Description. There has been an awareness for a long time of the large amount of energy present in the tip vortex that is shed from an aircraft wing during flight, as shown in figure 1. Devices to harness this energy usually come in three main forms: static, propulsive, and generative. Although the detailed analyses involved in the flow phenomena are quite complex, the basic concepts are straightforward.

Many static additions, some of which are shown in figure 2, have been proposed for the wing tips. These devices interrupt the formation of the wing-tip vortex, thus reducing the induced drag of the configuration. The most well-known example of the static device, however, is the winglet. In addition to reducing the formation of the wing-tip vortex, the design and placement of the winglet utilizes the local components of lift and drag at the wing tip to create a net increase in aircraft thrust. That winglets are successful in this task is apparent in the number of aircraft that now use them. For this reason, they are not covered in this summary of wing-tip devices.

Mounting propulsive devices on the wing tips has been considered since the early 1960’s for purposes of extracting additional energy from the tip vortex. Devices that have been analyzed and tested in the past include tractor propellers [refs. 1 and 2], pusher propellers [refs. 3 and 4], and fan-jets [ref. 5]. All of them rely on using the already-rotating vortex to lessen the necessary rotation of the engine to provide a certain level of thrust, and it is for this reason they all rotate counter to the direction of the vortex, figure 3.

In the 1980’s there appeared a great deal of interest in the third type of device, generative, which is usually referred to as a wing-tip vortex turbine [ref. 6]. These devices are essentially passive, as they are driven by the wing-tip vortex flow, with the resulting energy of the turbine to be used for pneumatic, hydraulic, or electrical purposes. As they are driven by the wing-tip vortex, they rotate in the same direction, figure 4.

Benefits. If propellers are mounted on the aircraft wing tips, rotating in a direction opposite to that of the wing-tip vortex, there is an increase in the net thrust minus drag of the configuration. According to reference 7, the reduction in the power required to maintain a given flight condition is the same for both tractor and pusher configurations, but for different reasons. In the case of a tractor propeller, the thrust of the propellers will be the same as an isolated propeller, but the induced drag of the wing behind the propeller will be less than the induced drag of the wing in isolation. In the case of pusher propeller, the induced drag of the wing will remain the same, but the thrust of the propeller will be greater than the thrust produced in isolation. Both improvements are essentially equal. The amount of thrust increase and drag decrease is highly configuration-dependent, but it can be significant.

If the fan-jet is mounted on the wing tip, then the effect of its rotating parts interacting with the vortex flow is significantly reduced because of the recessed location of the rotating parts within the nacelle and the forward placement of the fan-jet relative to the wing tip. In addition, the nacelle shape itself may actually increase the vortex strength. The prime benefit from a fan-jet installation on the wing tip is due to its non-rotating engine exhaust, which tends to dissipate the wing-tip vortex, thus reducing induced drag.

When considering the wing-tip vortex turbine, it is interesting to consider this passive device in the limiting case of zero rotation (if it is locked into position) as a static device, like an end plate. In this configuration, reduction of the induced drag is the only effect of the turbine. In normal operation the pitch of the turbine blades can be changed, altering the percentage of energy extracted that goes to the turbine. The wing-tip turbine is thus capable of a continuous trade-off of rotational energy extracted from the flow versus reduction of induced drag. This capability makes it a convenient device for supplying power or reducing drag, whatever is needed within the flight envelope. Flight test data [ref.8] from a small aircraft, a Piper PA-28 shown in figure 5, scaled theoretically to the size of a medium transport, have shown that the amount of vortex energy recovered by the wing-tip vortex turbine may be sufficient to generate the power required by an all electric aircraft system or a boundary layer control system [ref. 8]. The energy extracted from the wing-tip vortex does not need to be converted to electric power necessarily, as it may be used to develop pneumatic or hydraulic pressure directly.

All of the above devices that alter the vortex motion also have the advantage that, by doing so, they reduce the hazard to other aircraft due to this vortex. This is especially true near airports, where tip vortex effects and airplane traffic are at a maximum. Propulsive devices mounted on the wing tips, farther away from the fuselage than usual, would also be useful in reducing cabin noise levels.

Present and/or Past Utilization. There are no examples of any production configurations that have utilized either propeller or fan-jet engines at the wing tip for the purposes of altering the wing-tip vortex structure and extracting flow energy more efficiently. Current tilt-rotor designs tend to have their engines more outboard than usual, but this is done to ensure the clearance between the inordinately large propellers and the fuselage. The general feeling seems to be that putting the engines so far out would reduce the engine-out safety capabilities of the aircraft, as well as introduce a number of stability and control, aeroelasticity, structural design, and fabrication problems. The structural design problems may be alleviated using the concept of a truss-braced wing, which is currently being studied [ref. 9].

Although the wing-tip vortex turbine has not been used on a production aircraft, there seems to be more interest in this concept recently. Fairly recently, Airbus Industrie showed some interest in this device to be used as a winglet in the locked position during normal flight. It would then be released to provide electrical power in an emergency [ref. 10]. It was calculated that the vortex turbine could provide more than twice the power of a conventional ram-air turbine. This effort has been joined recently by Sundstrand Aerospace [ref. 11].

Applications and Configuration Integration. Although propulsive wing-tip devices have been shown to possess several advantages over their more conventionally-mounted counterparts, it remains to be seen whether the stability and control, aeroelasticity, structural design, and fabrication problems can be overcome. By far the most optimistic approach, and one that future applications may be based on, is with the truss-braced aircraft. There may also be a synergism between the thick Blended-Wing-Body concept and the placement of the propulsive units. If such a thick airfoil becomes desirable, then the Goldschmied Airfoil concept might also fit well into an integrated configuration.

Wing-tip Vortex Turbines seem to be more easily integrated into existing aircraft and future concepts. The idea of getting power from energy that would normally be left in the airstream is attractive, not to mention that any power extracted would make air traffic that much safer in the area. This power could be used as electricity for routine, backup, or emergency purposes. Instead of converting the vortex energy into electrical power, however, it could be used as pneumatic power as a supply for a boundary layer control system, for example. If it is converted into hydraulic power, it could be used to power flaps or some sort of active airfoil shaping system. The relative simplicity of a generative wing-tip system compared to a propulsive wing-tip system makes it that much more attractive.

References.

1. Snyder, Melvin H., Jr.; and Zumwalt, Glen W.: “Effects of Wingtip-Mounted Propellers on Wing Lift and Induced Drag,” *J. Aircraft*, Vol. 6, No. 5, September-October 1969.

2. Loth, J. L.; and Loth, F.: “Induced Drag Reduction with Wing Tip Mounted Propellers,” AIAA 84-2149, August 1984.

3. Patterson, J. C.; and Bartlett, G. R.: “Effect of a Wing-Tip Mounted Pusher Turboprop on the Aerodynamic Characteristics of a Semi-span Wing,” AIAA 85-1286, July 1985.

4. Patterson, James C., Jr.; and Bartlett, Glynn R.: “Evaluation of Installed Performance of a Wing-tip-mounted Pusher Turboprop on a Semispan Wing,” NASA TP 2739, 1987.

5. Patterson, James C., Jr.; and Flechner, Stuart G.: "An Exploratory Wind-Tunnel Investigation of the Wake Effect of a Panel Tip-Mounted Fan-Jet Engine on the Lift Induced Vortex," NASA TN D-5729, 1970.

6. Patterson, James C., Jr.; and Flechner, Stuart G.: "Exploratory Wind-Tunnel Investigation of a Wingtip-Mounted Vortex Turbine for Vortex Energy Recovery," NASA TP 2468, 1985.

7. Miranda, Luis R.; and Brennan, James E.: "Aerodynamic Effects of Wingtip-Mounted Propellers and Turbines," AIAA 86-1802, June 1986.

8. Abeyounis, William K.; Patterson, James C., Jr.; Stough, H. Paul, III; Wunschel, Lt. Col. Alfred J.; and Curran, Patrick D.: "Wingtip Vortex Turbine Investigation for Vortex Energy Recovery," SAE Technical Paper 901936, 1990.

9. Asbury, Scott C.: "DDF Proposal for Truss-Braced Wing Aircraft (Phase II)," NASA Langley Research Center, June 1996.

10. Flight International, 21 October 1989, p. 31.

11. Kroll, William B.: *1995 Annual Report, Vortex Turbine.* Sundstrand Aerospace, October 1995.

Bibliography.

Schaffer, A.: "A Study of Vortex Cancellation," *J. Aerospace Sciences.* Vol. 27, No. 3, March 1960, p. 193.

Snyder, M. H.: "Effects of Wingtip-Mounted Propeller on Wing Lift Induced Drag and Shed Vortex Pattern," Ph.D. Thesis, Oklahoma State University, May 1967.

Patterson, James C., Jr.; Hastings, E. C., Jr.; and Jordan, F. L., Jr.: "Ground Development and Flight Correlation of a Vortex Attenuating Spline Device," NASA SP 409, September 1972.

Patterson, J. C., Jr.: "Lift-Induced Wing-tip Vortex Attenuation," AIAA 74-0038, January 1974.

Patterson, James C., Jr.: "Vortex Attenuation Obtained in the Langley Vortex Research Facility," *J. Aircraft,* Vol. 12, No. 9, September 1975, pp. 745-749.

Patterson, James C., Jr.; and Jordan, Frank L.: "Thrust-Augmented Vortex Attenuation," NASA SP-409, February 1976.

"Wingtip-Vortex Turbine Lowers Aircraft Drag," *NASA Tech. Briefs*, Summer 1981.

"Turbines Recover Power by Dissipating Induced Drag from Wingtip Vortices," *Aviation Week & Space Technology*, September 1, 1986, p. 199.

"Wing-tip dynamos spin out extra power," *Popular Science*, September 1987.

Patterson, J. C., Jr.; and Abeyounis, W. K.: "Wingtip Vortex Turbine Investigation Vortex Energy Recovery," Vu-graphs from a presentation at the International Aviation Convention; Lakeland, Florida; April 1991.

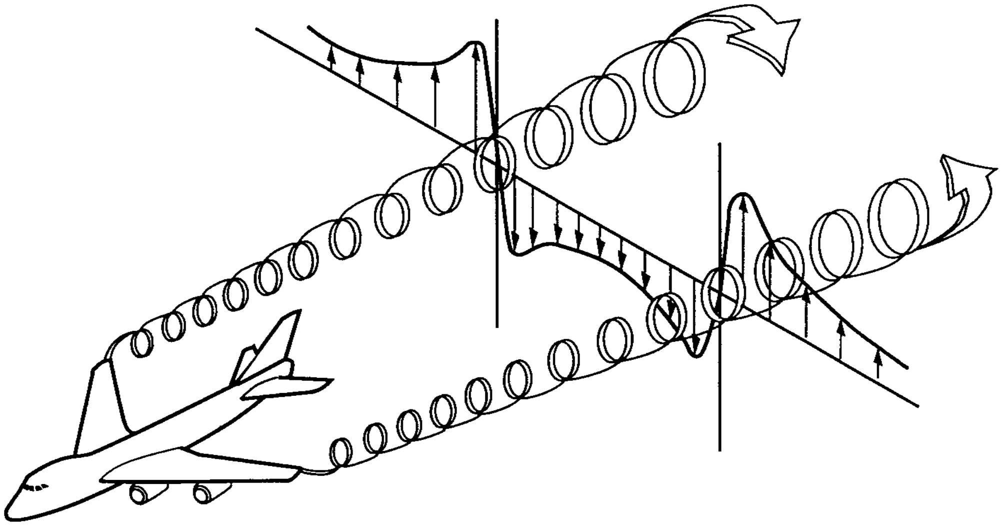

Figure 1. Downstream velocity distribution of an aircraft, from ref. 8.

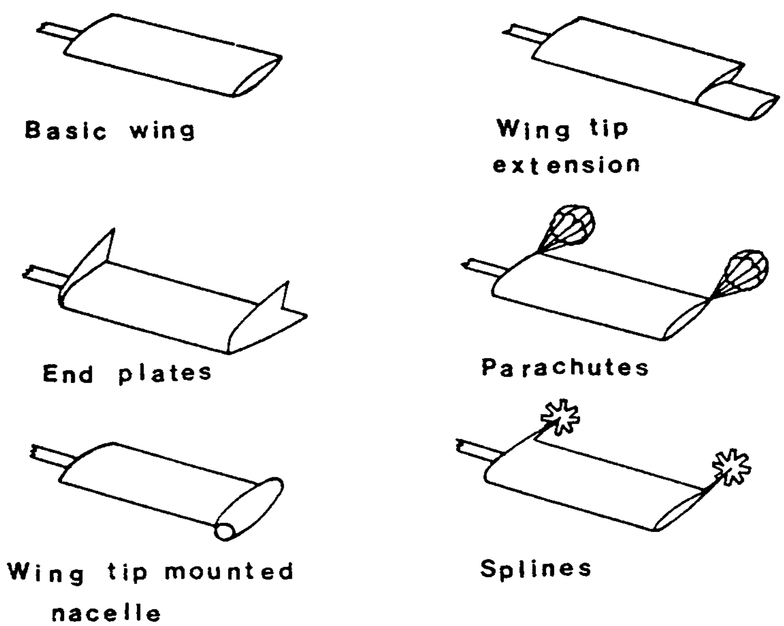

Figure 2. Techniques used to lower the trailing-vortex velocity, from ref. 2.

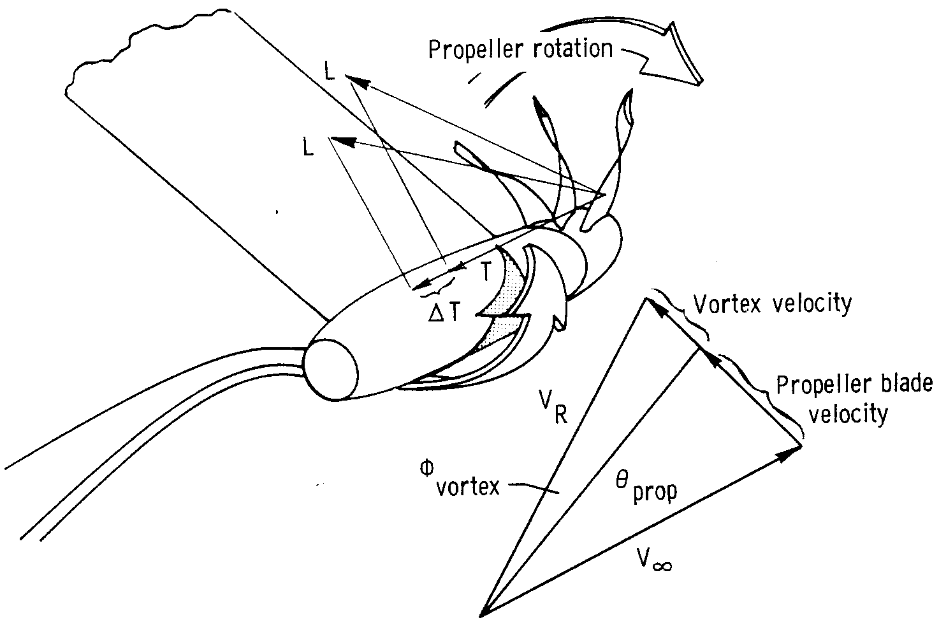

Figure 3. Change in velocity components due to vortex flow, from ref. 4.

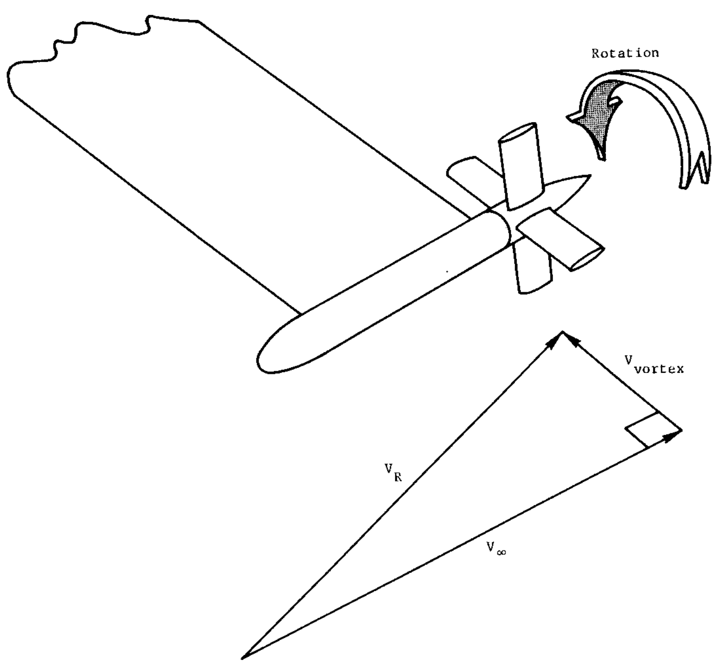

Figure 4. Vortex and stream flows and the resulting velocity, from ref. 6.

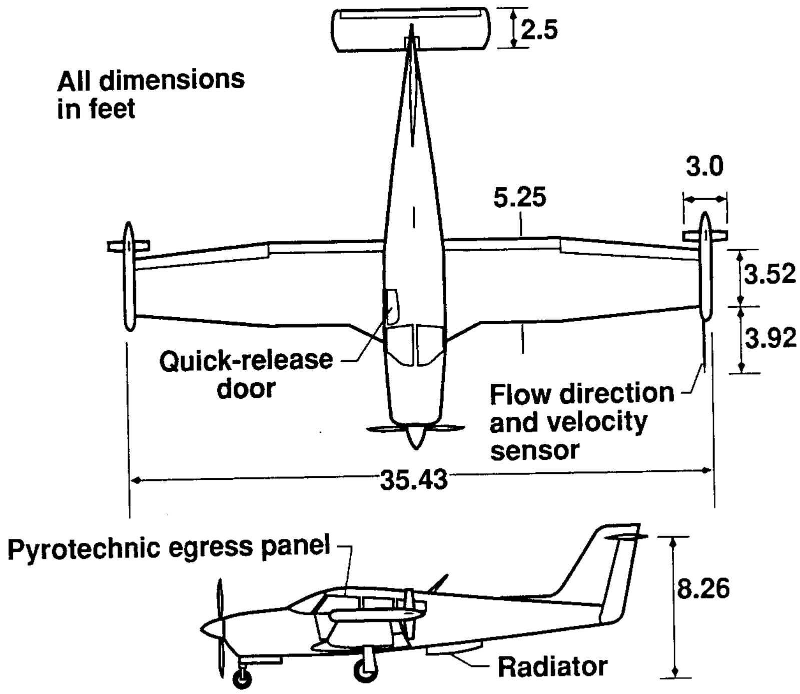

Figure 5. Test aircraft with vortex turbines on both wingtips, from ref. 8.

Methods of Increasing Cruise Efficiency

Goldschmied Airfoil

Background and Technical Description. (The final co-op report by J. M. (Farrah) Elliott [ref. 1] was used to extract much of the salient information presented below. That paper is to be consulted by the reader who is interested in a complete background summary of boundary-layer-controlled thick-suction airfoils.)

The idea of using laminar-flow airfoils with the associated low-drag benefit has been a long-held goal of aerodynamicists [ref. 2]. In fact, some recent flight studies of current business and commuter transport airplanes "suggest that significant regions of natural laminar flow exist and that this boundary-layer behavior is more persistent and durable on certain practical production airplane surfaces than previously expected" [ref. 3]. However, these regions are not full-chord and do not encompass the entire span. Early directed efforts at achieving natural laminar flow on aircraft was toward fighters [ref. 4] with thin airfoils of the NACA series of laminar-flow airfoils developed before and during World War II. However, applications of laminar flow to thicker section have also been considered. Among those doing this was A. A. Griffith of the Aeronautical Research Council in the U.K. in the 1940s, who suggested designing an airfoil with a velocity gradient along the chord that is boundary-layer stabilizing and favorable, except at one place along the airfoil where a velocity-discontinuity and a sharp-pressure-rise occur. (Some boundary-layer suction may be needed in order to achieve the extent of laminar flow desired on both thick- and thin-airfoil sections.) This suggestion has been experimentally investigated by Richards and Burge in reference 5 and an example is shown in figure 1. Applying boundary-layer suction in the required amount at a location just ahead of the occurrence of velocity discontinuity could result in a downstream flow which is not separated.

An application of boundary-layer suction was envisioned by Goldschmied in the 1950's as applied to airships. Later testing by Goldschmied [ref. 6] found that a self-propelled streamlined body with boundary-layer suction in the aft region worked well (see fig. 2); in particular, the combination of suction, a proper suction slot, an aft-mounted external-truncated-conical-ring (i.e., the Ringloeb cusp), and a tailboom. He also found that in order for the boundary-layer control to be integrated with the propulsion system of a vehicle, two conditions must be met. The levels of suction have to be the minimum to keep the flow attached, and the thrust of the stern jet must be equal to the sum of the wake drag and the suction momentum drag. In the tests with the integrated hull of a typical airplane, Goldschmied successfully showed that a large power gain could be achieved by integrating boundary-layer control with static-pressure propulsion [ref. 7]. He subsequently proposed the application of this concept to airfoils/wings [ref. 8].

Benefits and Research Opportunities. The use of boundary-layer suction for propulsion was put forward by Kuchemann and Weber [ref. 9] in that one could consider an "...extreme application of boundary-layer suction, which uses air from the boundary-layer on the aircraft surfaces as working air for the engine and restores it to full free-stream energy, instead of producing a thrust force to overcome the drag associated with the wake."

With the use of suction to control the boundary layer through slots and then using that air to provide static-pressure propulsion by means of a combination suction/blower, this concept will have a 50% reduction in power required for an integrated hull [ref. 10] at cruise. In addition, there will be a corresponding reduction in the thrust required and so the noise will also be reduced. This is because the air noise from a conventional fuselage can be reduced due to the propulsive system capturing most of the pressure fluctuations. Figure 3 shows how Goldschmied [ref. 11] proposed to do this on a small general aviation aircraft. He claims that by keeping the thrust coefficient about 0.025 and adjusting the gross weight of the aircraft against the speed and the volume of the fuselage, an aerodynamic efficiency index

[(Gross Weight)x(Free Stream Velocity)/(Fan Shaft Power x 550)] of at least 12.0 can be achieved. These large benefits need to be substantiated independently. Wings should also see reductions in wake drag with this system at cruise, but it needs to be validated. Moreover, there is research taking place to systematically quantify the aerodynamic benefits claimed. The recent work is being lead by J. P. Sullivan of Purdue University and has so far resulted in one paper [ref. 12]. This paper reports the results of a wind-tunnel experiment to test the suction portion of the idea and develop the detailed bookkeeping needed for thrust/drag. The resulting calculated section drag coefficients are reported to agree with past experiments [ref. 13]. Follow-on studies are planned to test the combination of suction/blowing.

Other areas to be researched and/or validated are ways to address the following items: high transonic drag on this thick wing; reduced critical Mach number; duct losses in the boundary-layer control system; details of how to integrate the suction/blower with the airframe; and details of how to integrate the external propulsion system with the airframe and suction/blower system.

Configuration Integration. Goldschmied [ref. 8] proposed for his spanloader (fig. 4) that the power source for the suction/blower be configuration integrated in the design. He envisioned using wing-tip mounted propellers which would rotate against the tip vortices and have a spanwise mechanical shaft that can be cross-connected between the two engines in case of engine failure.

Applications. There were/are numerous proposed applications contained in reference 1 to airships, to a glider, shown in figure 5 as taken from reference 14 to use an alternate single-slotted profile, to a spanloader/freighter, and to transonic passenger transports - of which the V-wing (fig. 6) of H. R. Chaplin [ref. 15] is an example. Other applications could be envisioned once the majority of uncertainties have been researched successfully with the risk both being more fully understood and managed.

References.

1. Elliott, J. M.: “Boundary Layer Controlled Thick Suction Airfoils,” Proposed NASA TM.

2. Shapiro, A. H.: *Shape and Flow: The Fluid Dynamics of Drag*, Anchor Books - Science Study Series, Doubleday & Company, Inc., 1961, p.167.

3. Holmes, B. J.; Obara, C. J.; and Yip, L. P.: “Natural Laminar Flow Experiments on Modern Airplane Surfaces,” NASA TP 2256, June 1984.

4. Anderson, J. D., Jr.: *Introduction to Flight*, McGraw Hill Book Co., 3rd ed., p.141.

5. Richards, E. J.; and Burge, C. H.: “An Airfoil Designed to Give Laminar Flow Over the Whole Surface with Boundary-Layer Suction,” A.R.C. R&M 2263, June 1943.

6. Goldschmied, F. R.: “Wind-Tunnel Test of the Modified Goldschmied Model with Propulsion and Empennage: Analysis of Test Results,” David W. Taylor Naval Ship R&D Center, Report ASED-CR-02-86, 1986.

7. Goldschmied, F. R.: “Aerodynamic Design of Low-Speed Aircraft with a NASA Fuselage/Wake-Propeller Configuration,” AIAA 86-2693, October 1986.

8. Goldschmied, F. R.: “Thick-Wing Spanloader All-Freighter: Design Concept for Tomorrow's Air Cargo,” AIAA 90-3198, September 1990.

9. Kuchemann, D.; and Weber, J.: *Aerodynamics of Propulsion*, McGraw Hill Book Co., 1953.

10. Goldschmied, F. R.: “Integrated Hull Design, Boundary-Layer Control and Propulsion of Submerged Bodies,” AIAA 66-658, June 1966.

11. Goldschmied, F. R.: “On the Aerodynamic Optimization of Mini-RPV and Small GA Aircraft,” AIAA 84-2163, August 1984.

12. Campbell, B. T.; White, G. R.; and Sullivan, J. P.: “Experimental Investigation of a Half-Span Boundary Layer Control Wing,” AIAA 96-2422, June 1996.

13. Preston, J. H.; Gregory, N.; and Rawcliffe, A. G.: “The Theoretical Estimation of Power Requirements for Slot-suction Aerofoils with Numerical Results for Two Thick Griffith Type Sections,” A.R.C. R&M 2577, June 1948.

14. Keeble, T. S.: “Development in Australia of a Thick Suction Wing,” In ‘Anglo-American Aeronautical Conference’, Brighton, 1951, pp. 45-76J.

15. Chaplin, H. R.: “Application of Very Thick BLC Airfoils to a Flying Wing Type Transport Aircraft,” SAE TP 901992, October 1990.

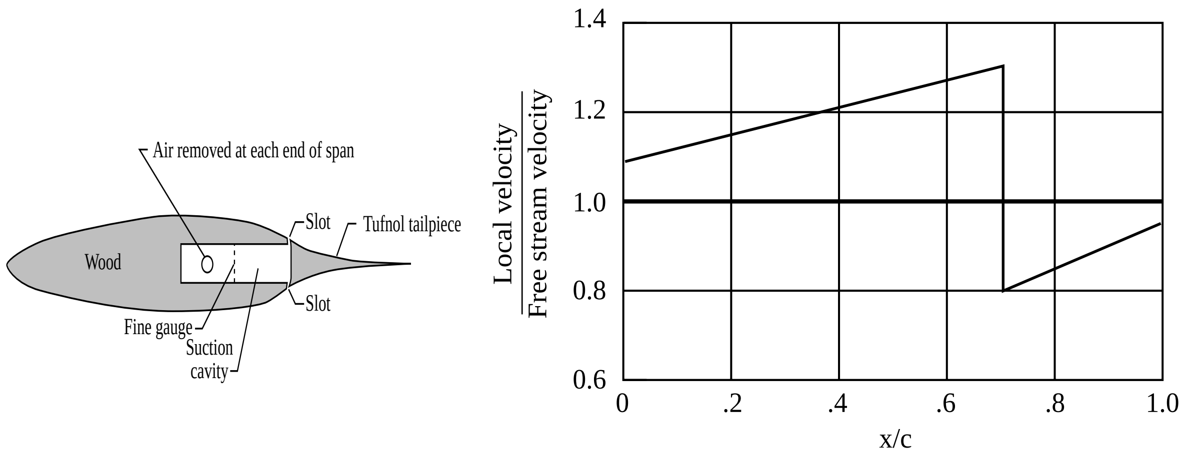

Figure 1. Profile and internal arrangement of Griffith type airfoil with boundary-layer suction and assumed airfoil velocity distribution over airfoil, from ref. 5.

Figure 2. Configuration 2 - Airship model with tailboom aftbody and empennage, from ref. 6.

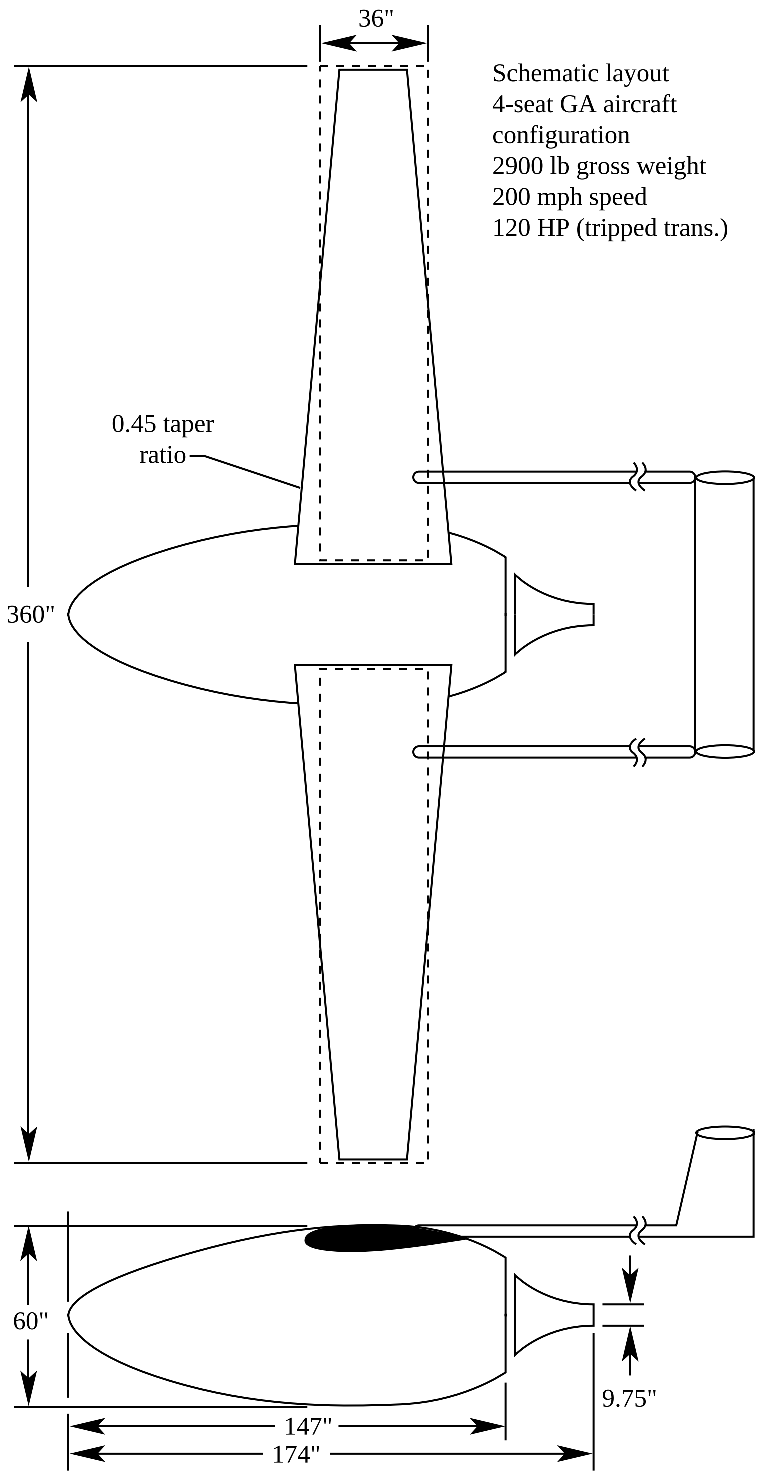

Figure 3. Four-seat GA aircraft layout, from ref.11.

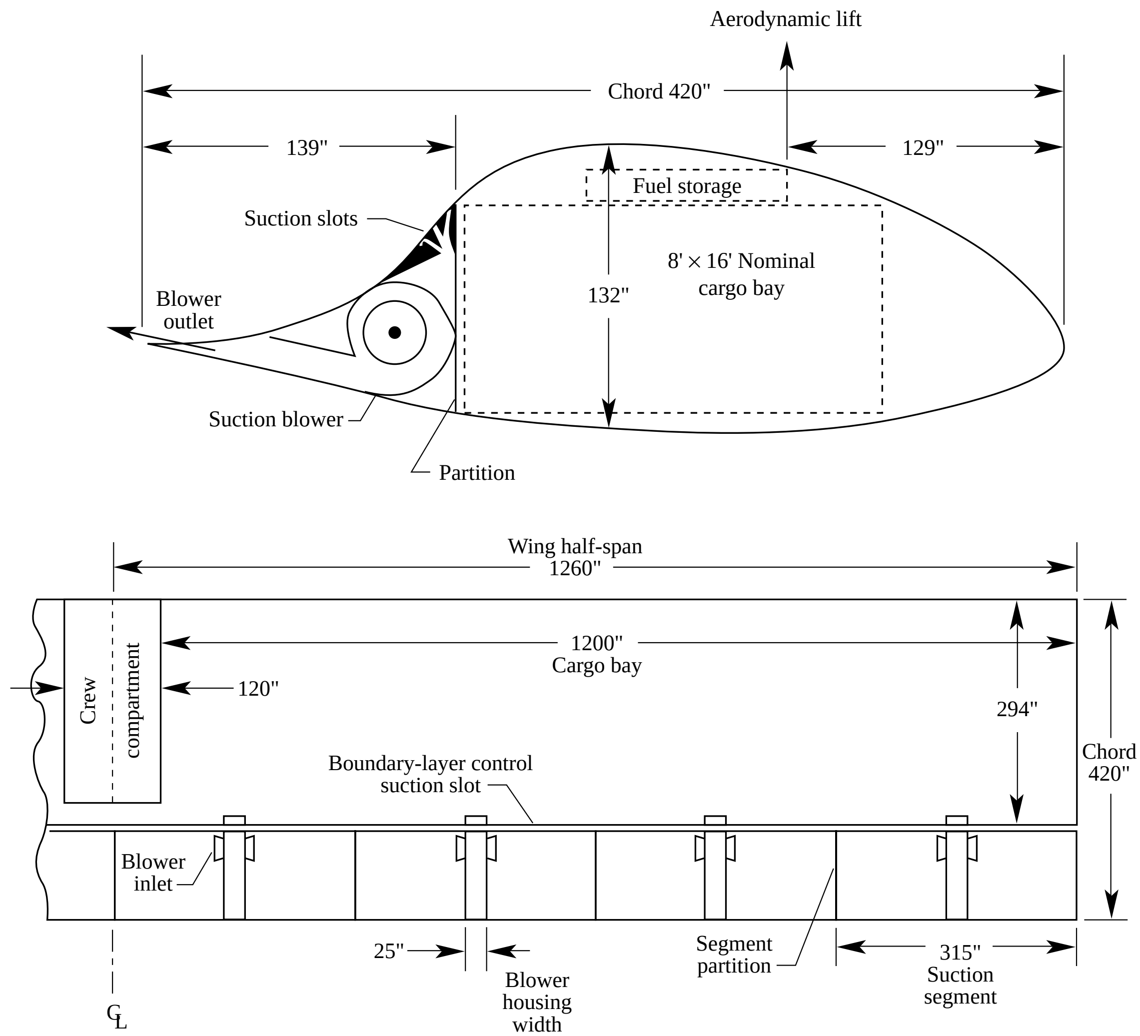

Figure 4. Goldschmied airfoil and plan view of right half of spanloader, from ref. 8.

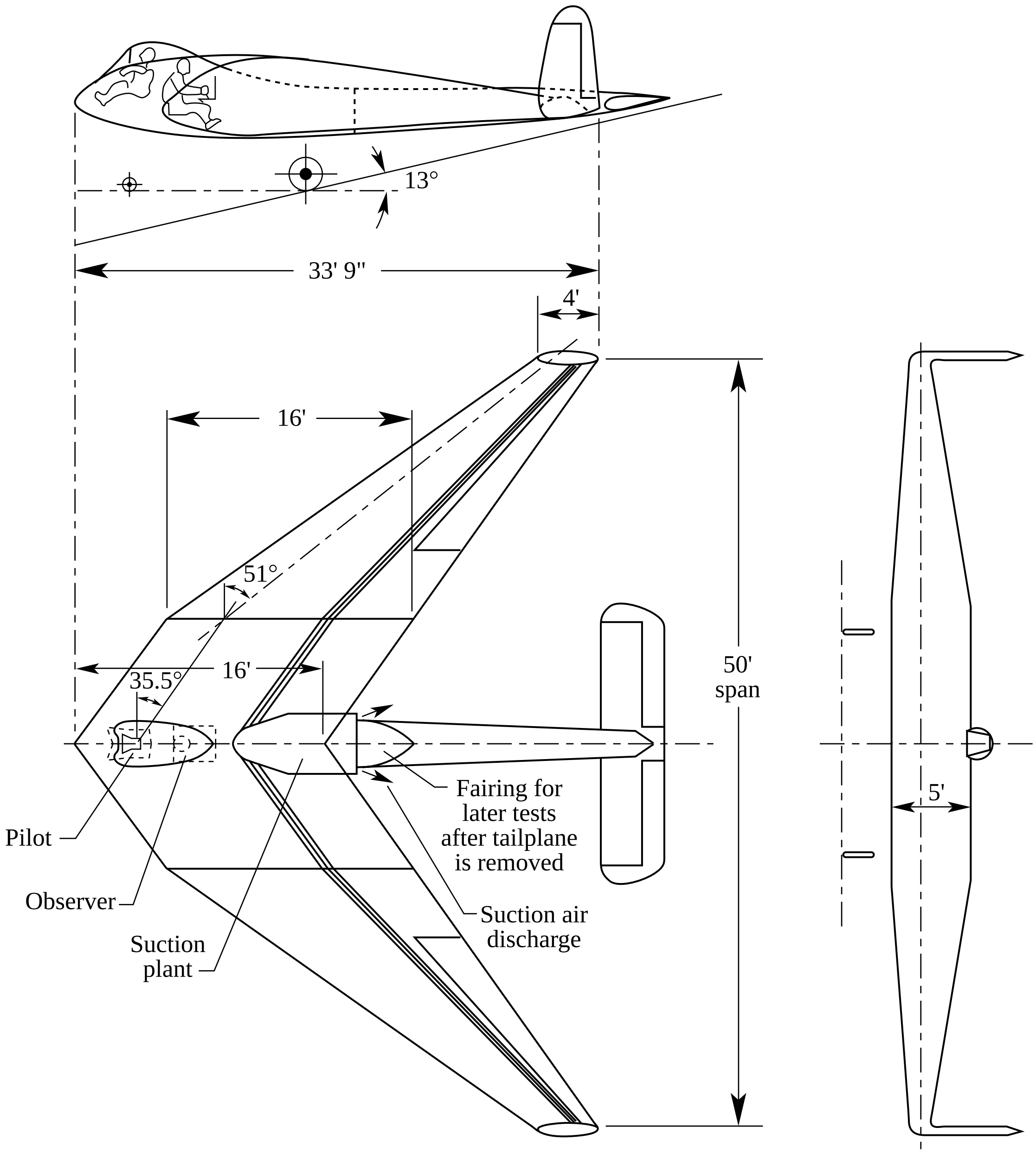

Figure 5. Proposed Australian suctioning glider with sweep-back, from ref. 14.

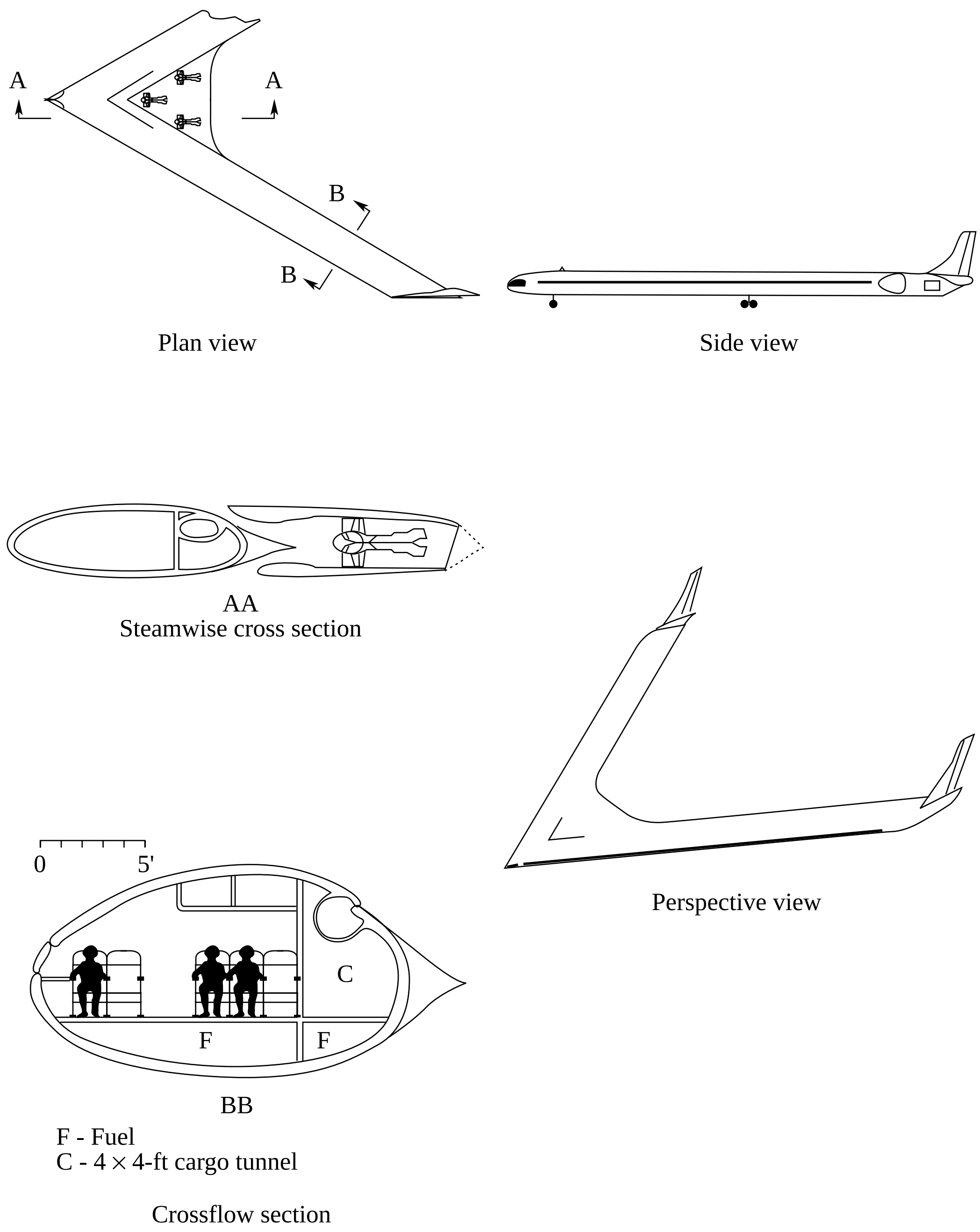

Figure 6. Chaplin V-Wing, from ref. 15.

Boundary Layer Inlet

Background and Technical Description. One of several examples of synergistic propulsion-aerodynamic interaction is the concept of the boundary layer inlet. Originally conceived for applications in marine propulsion (combat or cargo-carrying submarines, torpedoes) this approach involves the intake of the low momentum boundary layer generated on a body (fuselage or wing) to the propulsor (engine) in order to minimize losses in propulsive efficiency. Propulsive efficiency is a measure of the effectiveness of the propulsor in converting the energy of the fluid passing through the propulsor into thrust. In certain marine and in most aircraft applications it is desirable to have propulsors or engines with as high a thrust to weight ratio as possible. This requirement in turn leads to higher rotational speeds in the propulsor in order to provide a high level of thrust. The combination of small size (engine weight) and high rotational speed is connected with a corresponding loss in propulsive efficiency [ref. 1]. The boundary layer intake arrangement takes advantage of the use of the diminished inlet velocity (low momentum boundary layer fluid) to the propulsor in order to overcome some of these losses in propulsive efficiency. The amount of work required (shaft or compressor) is directly linked to the inlet velocity. Thus, by utilizing a lower inlet velocity, the amount of work required is diminished, and therefore, the propulsive efficiency of the engine is increased. The theoretical analysis of the boundary layer intake is presented in detail in references 1 and 2 where it is mainly applied to submerged bodies with a small propulsor unit. This approach can also be applied to aircraft or air-breathing propulsion missiles as suggested in reference 3. The boundary layer inlet concept, as applied to an airfoil, is illustrated in figure 1 [ref. 4]. The engine is shown mounted on the aft section of the wing swallowing the low incoming turbulent boundary layer momentum. Utilizing this arrangement, a beneficial trade-off between decrease in drag and increase in the fuel consumption of the engine (losses in compressor due to flow non-uniformity) is achieved.

Benefits. Recently, L. Smith [ref. 3] suggested that for aircraft propulsion, wake ingestion (low-momentum fluid intake) may be less beneficial, when compared to ship propulsion, because engines mounted on the aft section of wings only capture a small fraction of the total wetted flow over the wing. However, the application of this concept is suggested for cruise missiles because a single concentric aft-located propulsor can be used to swallow the boundary layer generated by the missile's fuselage while a bottom mounted inlet can be used to supply the core engine with distortion minimized flow. Benefits, in terms of gains in propulsive efficiency to the boundary layer intake engine, are of the order of 7-15% [refs. 3 and 5]. Recent studies [ref. 4] indicate possible reductions of 3-7% in aircraft take-off weight.

Present Utilization of Technology. No current or past production aircraft utilizes the boundary layer inlet concept. This technology has mainly been applied to torpedoes and other marine applications [ref. 3].

Configuration Integration. It is possible to extend this application to conventional aircraft by utilizing a boundary layer inlet engine mounted on the aft portion of the fuselage (to ingest the boundary layer) together with wing-mounted engines which take in distortion minimized flow. Additional applications may include the use of this technology in the Blended Wing Body aircraft concept taking advantage of the large wetted surface area of the fuselage. A major drawback of this concept is the control of separation (passively and/or actively) required in order to make the heavily distorted boundary layer flow more uniform. If flow distortion is too great, excessive loads can lead to fan blade fatigue/failure and rotating blade stall can occur.

References.

1. Wislicenus, G. F.: “Hydrodynamics and Propulsion of Submerged Bodies,” J. *American Rocket Society*, Vol. 30., December 1960, pp 1140-1148.

2. Gearhart, W. S.; and Henderson, R. E.: “Selection of a Propulsor for a Submersible System,” *J. Aircraft*, Vol. 3, No. 1, 1966, pp. 84-86.

3. Smith, Leroy H.: “Wake Ingestion Propulsion Benefits,” *J. Propulsion and Power*, Vol. 9, No. 1, January-February 1993, pp. 74-82.

4. “Megaplanes”, *Popular Science*, Vol. 246, No. 4, April 1995, p. 56.

5. Bushnell, Dennis M.: “Frontiers of the `Responsibly Imaginable' in (Civilian) Aeronautics,” 1998 AIAA Dryden Lecture.

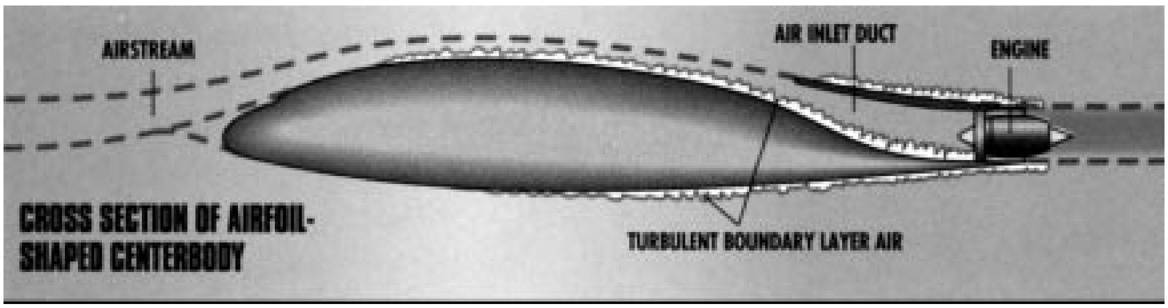

Figure 1. Boundary layer inlet concept, from ref. 5.

Laminar Flow Control

Background and Technical Description. Laminar flow control (LFC) refers to methods which artificially laminarize a boundary layer that, left to its own devices, would otherwise be turbulent. There are many reasons one may wish to have a laminar, rather than a turbulent, boundary layer. Such reasons generally involve significant reductions in skin friction and/or large reduced heat transfer rates possible with laminar (as compared to turbulent) boundary layers. Figure 1 illustrates the fundamental drag reduction potential of laminar contrasted to turbulent boundary layers as a function of Reynolds number. Because skin friction accounts for fully half of the total aircraft drag of a typical transport aircraft at cruise conditions, the appeal of laminar flow becomes obvious.

When applied to an aircraft, particularly an aircraft designed (sized) to cruise long distances, reductions in skin friction lead to significant reductions in fuel requirements. An aircraft requiring less fuel will have a lower structural and operating weight and reduced operating cost as compared to an all turbulent boundary layer aircraft carrying an equivalent payload an equal range. As will be discussed later, the basic technology exists to accomplish laminar flow control; however, uncertainty in cost and maintenance of equipment required to produce laminar boundary layers and manufacture's concerns of the risk of developing aircraft dependent on such new technology has so far prevented commercial application of LFC.

Engineers have worked since the 1930s on laminar flow control systems for aircraft. In the early 1960s Dr. Pfenninger and his team at the Northrop Company conducted full scale flight tests on the USAF sponsored X-21 experimental aircraft. Extensive regions of laminar flow up to Reynolds numbers on the order 20 to 25 million were routinely obtained by the end of the tests [ref. 1]. However, operational feasibility was not demonstrated. Because of the potential large skin friction drag reduction that can be obtained from laminar flow, research continued over the years and became particularly intense during the energy crises of the 1970s. Excellent technical and historical overviews of laminar flow control technology are contained in references 1 through 5.

Typically, LFC schemes place boundary-layer suction ports at and immediately behind the wing leading edge. This is a critical area in which to remove the low energy layers of the boundary layer due to large adverse pressure gradients that can easily amplify instabilities within the boundary layer, including crossflow disturbances that will lead to premature transition and turbulence. Cross flow disturbances become quite serious for wing sweep greater than about 20 degrees. Because most modern subsonic and supersonic cruise aircraft have swept leading edges for reasons of efficiency, the boundary layer at and near this swept edge develops a crossflow (spanwise) component to the general chordwise flow. Even after the boundary layer crossflow and other instabilities are removed, the flow will eventually become turbulent if left to its own devices. Before this occurs, another row of suction ports is introduced, and so on. Using this technique, the laminar boundary layer can be extended over a considerable chord length, perhaps in the case of a transonic aircraft to a trailing edge shock position. An experiment that proved transonic airfoils could be designed to take advantage of LFC was undertaken by NASA in the 1980s. In this experiment, the disposition and type of suction system and variation on the amount of suction was applied (parametrically) to an airfoil specially designed to promote laminar flow on the top and bottom surfaces. Reference 4 provides a summary of this experiment.

At the present time, the preferred method of controlling laminar flow at subsonic speeds is a technique called hybrid laminar flow control (HLFC). HLFC techniques place suction panels on the wing leading edge that can cover as much as the first 25 percent of the top side of the wing chord. Laminar flow is then maintained past this suction region by a favorable pressure gradient. The above mentioned transonic laminar flow airfoil experiment was modified for such a HLFC system. The experiment was very successful and the results are summarized in references 6 and 7.

NASA, Boeing, and the U. S. Air Force participated in a key flight experiment of a HLFC system on a modified Boeing 757 in the late 1980's [ref. 6]. In this experiment, a glove with a suction panel constructed of a microperforated (19 million holes) titanium surface and contoured to maximize laminar flow was mounted over a 22-foot section of the left wing of a Boeing 757. A Krueger high lift flap was integrated into the wing to serve as an insect shield during takeoff and low altitude flight. A thermal anti-ice system was also incorporated. Results showed extensive laminar flow was routinely achievable. NASA/Industry flight experiments of HLFC systems to reduce drag on engine nacelles have also shown promise. However, transonic wind tunnel tests of HLFC nacelles conducted by NASA LaRC in the mid 1990s indicated that a significant integration challenge exists to the successful implementation of HLFC nacelles on transonic transport configurations. With regard to supersonic HLFC, NASA has just completed an extensive flight experiment on a General Dynamics F-16XL aircraft. Again a section of the highly swept wing was modified with a glove designed to promote laminar flow with a microperforated leading-edge suction system to remove crossflow disturbances [refs. 8 and 9].

Results from these flight tests and experiments have been encouraging, but detailed results have been made accessible to U. S.-only sources due to the possible competitive advantage this technology may someday give American companies.

Reductions in heating rates across a laminar, compared to a turbulent, boundary layer can be particularly important for high speed aircraft where the kinetic energy of the air stream is converted to heat (as it decelerates within the boundary layer) that can significantly raise the temperature of the aircraft surface. For supersonic aircraft, the reductions in heating rates resulting from laminar flow may allow lower cost and lighter structural materials.

Studies have also shown the potential benefits of actively cooling hypersonic aircraft [ref. 10]. The cooled skin of such a vehicle may have extensive regions of laminar flow due to cool skin temperatures. Other cooling schemes for hypersonic aircraft have studied film cooling of the surface via slot injection of cool air with a laminar velocity profile.

Benefits. Commercial aircraft designs are driven by the requirements that their acquisition and operating costs allow them to make a profit for both the aircraft manufacturer and the airline companies. Profits are driven by aircraft operating costs, passenger appeal (including perceived aircraft safety issues), and any environmental factors imposed on commercial aircraft. These environmental factors can include noise regulations, possible emission reductions, and the ability to land and take off in adverse weather or congested traffic conditions. To be viable, a laminar flow control aircraft must generate greater profit than a comparable conventional (turbulent) aircraft. It could do this if it had significantly lower operating costs, including fuel usage and lower ownership costs. Obviously laminar flow technology can lower fuel usage if it reduces drag. Lower cruise drag translates into less fuel weight to carry and thus into a lighter weight aircraft which should be less expensive to manufacture. However, if the weight or cost of the laminar flow control system reverses these trends, the aircraft will become more expensive and non-competitive. Maintenance and safety issues raised by the laminar control system must also be carefully weighed. If, for example, a laminar flow aircraft is sized to complete its mission should the laminar system fail at the beginning of a trip, benefits of the system would be less than if the aircraft was sized for a failure halfway through the flight, or no failure of the laminar flow control system at all. The perception of risk can profoundly alter the design philosophy of the aircraft design and ultimately its profitability. In the following sections, a brief summary of five technical studies of the benefits of LFC applied to aircraft efficiency and operating cost are presented.

In a 1982 report [ref. 11] the Boeing Company reported on the design of a HLFC system for a Boeing 757 aircraft that laminarized 60% of the upper wing surface and 40% of the lower surface. Analysis showed it would reduce fuel consumption 8%. If the empennage was also laminarized fuel savings would increase to 12%. If the aircraft could be resized for this laminar system, there would be a further significant reduction in fuel consumption.

An unpublished study by the Mission Analysis Branch at NASA Langley Research Center [ref. 12] concluded that, with conservative assumptions, the direct operating costs of a modern long range transport aircraft would be reduced 6 percent (fuel price $1.00/gal) if it was designed with HLFC systems. The assumptions used in this analysis included increased development costs of a billion dollars for the aircraft calculated over a 500 aircraft fleet (two percent additional flyaway costs) and an additional 5 percent airframe maintenance cost above that of conventional concepts. The aircraft was sized with sufficient reserves to complete one-half the mission in a turbulent-flow mode should the HLFC system fail in flight.

A study of the benefits of HLFC by Arcara and Bartlett is reported in reference 13 for an aircraft sized for HLFC providing 50 percent chord laminar flow for the wing upper surface and 50 percent chord for both surfaces of the horizontal and vertical tails. Results showed a 15 percent reduction in cruise fuel and a 6.5 to 10 percent reduction in DOC depending on a fuel price variation from $0.65 to $2.00 per gallon.

ONERA studies from 1990 are reported in reference 14 which concluded HLFC applied to a 150 and a 300 passenger long range aircraft should reduce fuel consumption nearly 15 percent. HLFC was applied to the wing, the tail and fin and the engine nacelles.

An unpublished study entitled “Potential Economic Impact of Future Large Aircraft” by the Mission Analysis Branch [ref. 15] contains results of applying HLFC to a “conventional” 800 passenger aircraft. Laminar flow was postulated to cover 60 percent of the wing upper surface, 30 percent of the lower surface, and fifty percent of the empennage surfaces. A 6.5 percent reduction in seat mile cost was calculated for typical 65 percent load factors. Fuel costs were assumed at $0.60 per gallon.

Several studies of laminar flow applications to supersonic aircraft were sponsored by NASA as part of High Speed Civil Transport (HSCT) activity. A supersonic transport will consume more fuel per passenger mile than a conventional subsonic aircraft; thus, it might be assumed laminar flow would be particularly attractive to reduce fuel weight requirements. As an example, typical fuel fractions (fuel weight /gross weight) are on the order of 40 percent for a long range subsonic transport and can exceed 65 percent for an equivalent range supersonic transport. An additional bonus for supersonic transports is that transition Reynolds numbers are substantially higher at supersonic speeds than at subsonic speeds [ref. 8]; thus, a supersonic aircraft may require less suction than subsonic aircraft to achieve laminar flow.

The study of reference 16 by the Douglas Aircraft Company reports on a comprehensive analysis of HLFC applied to a Mach 3.2 supersonic transport. The analysis showed a distinct advantage for a full chord HLFC system as opposed to a partial chord suction system. A block fuel reduction of 14 percent and gross takeoff weight reduction of over 8 percent was obtained over a fully turbulent baseline design.

A Boeing Airplane Company study of HLFC application to a Mach 2.4 supersonic aircraft is documented in reference 17. Study results showed a block fuel reduction of 16 percent and a 12 percent reduction in gross takeoff weight.

Preliminary studies of the benefits of HLFC for supersonic aircraft was undertaken in the 1992 period and recorded in the unpublished study of reference 18. These studies sized supersonic transport concepts as a function of the amount of laminar flow assumed to cover wing, empennage and fuselage surfaces. Three cases were studied: a conventional concept with all turbulent flow; a concept resized for 30 percent laminar flow over wing/empennage surfaces and 12 percent over the fuselage; and third case with laminar flow covering 60 percent of the wing/empennage and 25 percent of the fuselage (see figure 2). Realistic weights for the suction systems were estimated from the previously mentioned Boeing and McDonnell Douglas studies. Results of the analysis showed a 9 and 16 percent reduction in gross takeoff weight and a reduction in operating cost of 8 and 10 percent for the two HLFC cases over the all turbulent vehicle.

Applications. Considering the large number of studies cited previously that showed a remarkable agreement on the advantages of laminar flow control concepts, why then has not a single commercial application of the technology been developed? The answer most likely can be traced to two factors: (1) risk and (2) the promise of larger performance gains from other more mature technologies. Both of these factors are addressed next.

(1) Risk: Current development cost for a new, large, long range subsonic transport may approach the net worth of an aircraft company. Development of a supersonic transport will undoubtedly cost much more. With such enormous sums at stake, aircraft manufacturers will not risk using technology, regardless of its promise, that has not been developed to a point that unmistakable benefits are clearly shown with real-world hardware systems in realistic airline environments. Analytical system studies have convinced most engineers that if laminar flow mechanical systems worked as well as assumed, the economic benefits are real. The experimental systems studied to date, however, consist of only small segments of the aircraft wing surface and not large complete systems that would lend confidence to building a commercial product. In previous decades, military aircraft proved new technologies often at great expense, of which the more successful ones were introduced into commercial use. In the absence of the large military programs of the past, what is needed now are large scale experimental laminar flow system technology demonstrations to reduce the risk to commercial airframe manufacturers.

(2) Alternate promising technologies: Aircraft companies are driven by the desire to increase their profits, and in large measure this is accomplished by improving the economics, safety, comfort, and environmental attractiveness of their aircraft to airlines and to the flying public (compared to a competitor's aircraft). In a sense, this pits technologies against one another as to which technology can deliver a competitive advantage at the lowest cost and the lowest risk. This can be illustrated by figure 3 from reference 18, which contains cost advantages for advances in three different technologies: laminar flow control, engine efficiency, and advanced composite construction. The advances shown are those that might reasonably be expected to be on operational aircraft in the next twenty years. Within the constraints of the study (e.g., fuel costs, aircraft configuration), it appears that larger performance gains will accrue to advances in propulsion systems and composite structures than due to laminar flow control. All things considered, engine and structure technology are thought of as more traditional, mature technologies while laminar flow control is not. For a given improvement in dollars per seat mile a manufacturer may find it more attractive to improve a more understood, less risky technology. Again the factor of risk and the level of maturity (or technical readiness) is the major issue for laminar flow control technology application. Large-scale integrated laminar-flow system demonstrations are most likely needed before airframers will consider designing laminar flow transport aircraft. Such demonstrations will have to eventually include major aircraft components such as complete wings and tail surfaces.

Looking Ahead. We can conjecture that as aircraft as we know them today become more and more efficient through conventional advances in propulsion and materials/structures technology; laminar flow control will become very attractive as one of the final remaining technologies that can deliver a large increment in performance. A more exciting scenario for the future, however, could be the advent of aircraft concepts that can take full advantage of laminar flow over major if not all aircraft surfaces, thus leading to much larger increases in performance than noted from the cases cited in this section. Perhaps the Blended Wing Body concept mentioned elsewhere in this document will lend itself to such "full coverage" laminar flow concepts. Perhaps, also, very short-chord, high-aspect-ratio wings supported by strut bracing will be able to take full advantage of laminar flow control, natural laminar flow, or a combination of the techniques. Another possibility may be that an increased environmental concern over global warming and restrictions on hydrocarbon emissions from aircraft will result in more fuel efficient aircraft designs. As noted in this paper, laminar flow control has a major impact on reducing fuel consumption and could be a major contributor to aircraft fuel efficiency.

References.

1. Wagner, R. D.; Maddalon, D. V.; Bartlett, S. W.; and Collier, Jr., F. S.: “Fifty Years of Laminar Flow Flight Testing,” SAE Technical Paper 881393, October 1988.

2. Joslin, Ronald D.: “Aircraft Laminar-Flow Control,” *Annual Reviews of Fluid Mechanics*, 1998, pp. 1-29.

3. Joslin, Ronald D.: “Overview of Laminar Flow Control,” NASA RP-97-1407, December 1997.

4. Barnwell, R. W.; Hussanini, M.Y.: “Natural Laminar Flow and Laminar Flow Control,” Spinger-Verlag, ICASE/LaRC Series, 1992.

5. “Research in Natural Laminar Flow and Laminar-Flow Control,” NASA CP-2487 Parts 1, 2, and 3. Procedings of a Symposium held at Langley Research Center, Hampton, Virginia, March 16-19, 1987.

6. Harvey, W. D.; and Bobbitt, P. J.: “Toward Lower Drag with Laminar Flow Technology,” Presented at the 16th Congress of the International Council of the Aeronautical Sciences, Jerusalem, Israel, August 28-September 2, 1988.

7. Bobbitt, Percy J.; Ferris, James C.; Harvey, William D.; and Goradia, Suresh H.: “Results for the Hybrid Laminar Flow Control Experiment Conducted in the NASA Langley 8-Ft. Transonic Pressure Tunnel on a 7-FT. Chord Model,” NASA TM 107582, March 1992.

8. “Laminar Flow Study Predicts $1 billion fuel saving,” *Air Transport World*, November 1990, p. 8.

9. Wilhite, Alan W.; and Shaw, Robert J.: “HSCT Research Picks Up Speed,” *Aerospace America*, Vol. 35, No. 8, August 1997, pp. 24-29, 41.

10. Becker, J. V.: “New Approaches to Hypersonic Aircraft,” Presented at the Seventh Congress of the International Council of the Aeronautical Sciences (ICAS), Rome, Italy, Sept. 1970

11. Boeing Commercial Airplane Company: “Hybrid Laminar Flow Control Study Final Technical Report,” NASA Contractor Report 165930, October 1982.

12. Memorandum to Mission Analysis Branch files, November 1990, from Head, Mission Analysis Branch, NASA Langley Research Center. Subject: Mission Analysis Branch Cost Study of Hybrid Laminar Flow Control.

13. Arcara Jr., P. C.; Bartlett, S. W.; and McCullers, L. A.: “Analysis for the Application of Hybrid Laminar Flow Control to a Long-Range Subsonic Transport,” Presented at the Aerospace Technology Conference and Exposition, Long Beach, California, Sept. 23-26, 1991.

14. Thibert, J. J.; and Reneaux, V. Schmitt: “ONERA Activities on Drag Reduction,” 17th ICAS Congress, Stockholm, Sweden, September 9-14, 1990, Proceedings, Vol. 1, ONERA TP No. 1990-114.

15. Small, W. J.; Morris Jr., Shelby J.; Harvey, W. Don; Martin, Glenn L.; Tice, David C.: “Economics of Advanced Subsonic and Supersonic Transports,” White Paper, February 25, 1992.

16. “HSCT Concept Development Group, Advanced Commercial Programs,” Douglas Aircraft Company, Long Beach, California: 1989 High-Speed Civil Transport Studies, NASA Contractor Report 4375.

17. Boeing Commercial Airplane Company: “Application of Laminar Flow Control to Supersonic Transport Configurations,” NASA CR-181917, 1990.

18. Small, William J.; Morris, Jr., Shelby J.; Harvey, W. Don; Martin, Glenn, L.; Tice, David C.: Unpublished Briefing entitled “Economics of Advanced Subsonic Transports and Supersonic Transports,” January 1992.

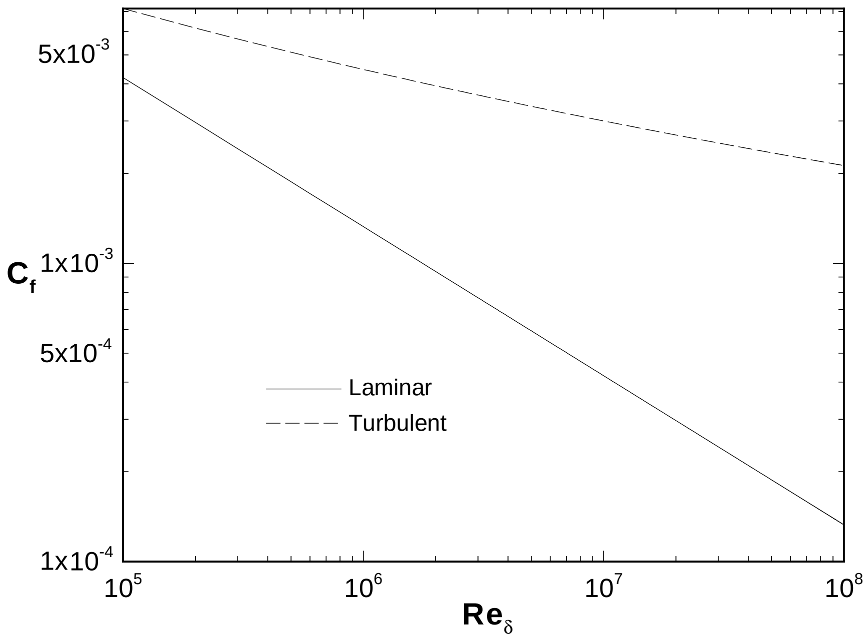

Figure 1. Effect of incompressible laminar and turbulent Reynolds Number on skin friction coefficient.

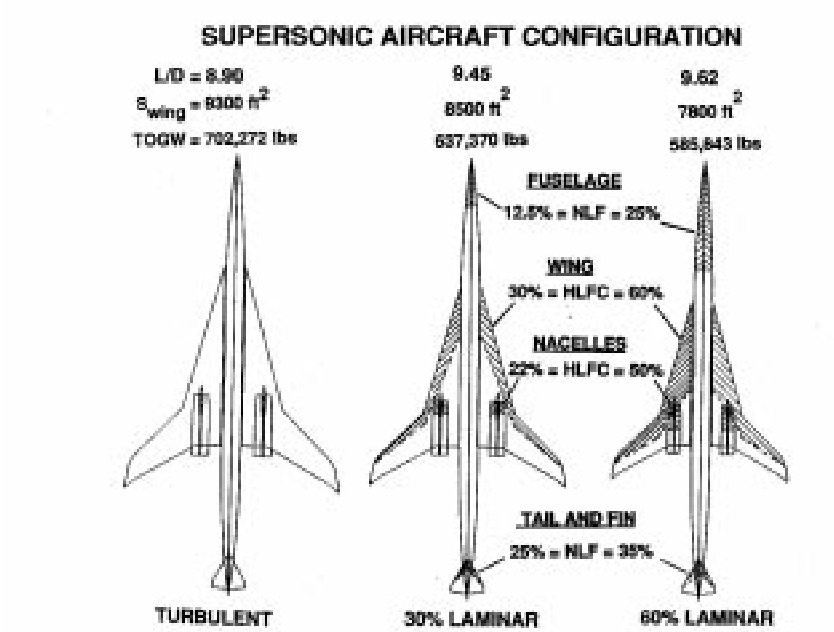

Figure 2. Parametric study of laminar flow control effects on supersonic transport sizing, from ref. 18.

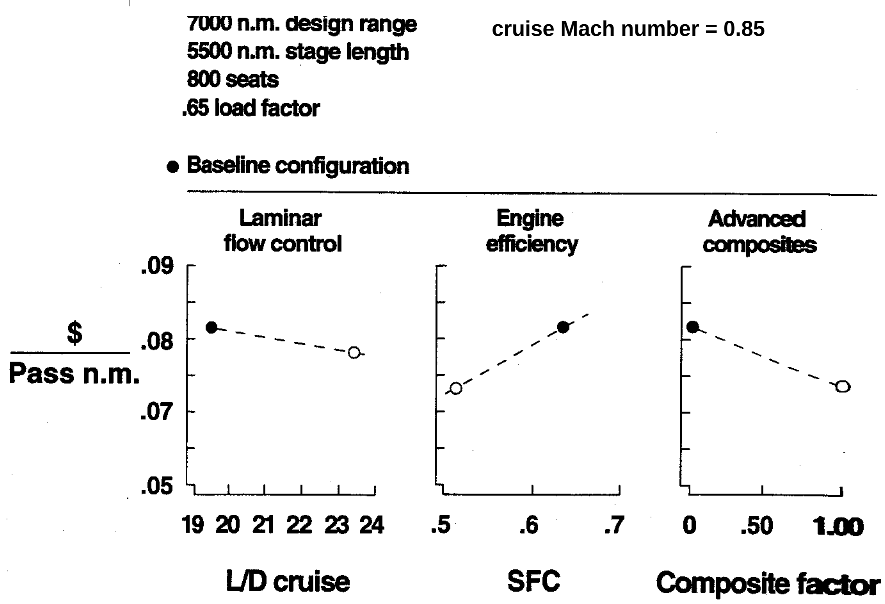

Figure 3. Sensitivity of passenger fare to advanced technology, from ref. 18.

Natural Laminar Flow

Background and Technical Description. Natural laminar flow (NLF) technology is designed to promote the advantages of laminar flow without the intercession of powered or mechanical means to extend the region of laminar flow. As discussed in the section entitled Laminar Flow Control, reasons that laminar flow is desired over an aircraft surface include reduced skin friction drag and reduced heating rates for high speed flight. Unlike the technology of laminar flow control, which has yet to find application on commercial aircraft, natural laminar flow is a technology now employed on an almost routine basis in the general aviation market. Potential benefits also are possible in the supersonic speed regime. References 1 and 2 provide a comprehensive treatment of the subject and extensive reference lists. The fairly recent successful application of NLF to general aviation aircraft was primarily the result of two factors. First, research activities have provided the understanding of the basic flow physics of laminar, transitional, and turbulent flow. This research began in the early days of NACA (mid 1930s) with studies of laminar flow airfoils as described in reference 1. A method of designing airfoil shapes to obtain desired pressure distributions was developed. This work led to the development of the NACA six-series NLF airfoils. Typically the concept that was pioneered involved tailoring the airfoil upper surface to maintain a favorable pressure gradient for as long as possible to maintain laminar flow [refs. 1-3]. Current analytical methods have extended these early ideas and allow the designer to tailor laminar airfoil design to the expected flight conditions [refs. 1 and 2]. Also, new classes of laminar flow airfoils have been extensively tested in wind tunnels and in flight [refs. 1 and 2].

The second major factor leading to the present use of NLF was the advent of very smooth metal and composite aircraft surfaces which provide the necessary smoothness to prevent disturbances causing premature transition to turbulent flow. General aviation aircraft such the Cessna Citation Jet, the Citation X, the Cirrus single engine pusher propeller light aircraft, and the Glasair single place light aircraft are just some examples of successful modern general aviation aircraft designed specifically with natural laminar flow airfoils. NLF has been applied to other specialized aircraft with short chord lengths such as gliders and modern long-duration reconnaissance aircraft. An instructive example of the methodologies employed for these low Reynolds number aircraft is contained in an informative description of the development of a low altitude RPV designed with laminar flow airfoils [ref. 4].

Although better categorized as a laminar flow control technology, other methods have been studied to determine their effect in increasing transition Reynolds number. Cooling of the boundary layer and suppression of turbulence-inducing disturbances with tailored acoustic energy [ref. 1] are two such advanced technologies which show promise.

Application of NLF concepts to large commercial subsonic and supersonic aircraft has been studied theoretically and experimentally; however, no application has entered the commercial market. An outstanding example of research directed towards large transport applications was the 757 wing noise and laminar flight tests conducted in the 1985 time period [ref. 1 and 2]. This experiment involved placing a fiberglass/foam core glove over a section of a 757 wing adjacent to and outboard of the left nacelle. This glove had somewhat less sweep than the 757 wing. Test results indicated that NLF could be maintained to between 20 and 30 percent chord over the top surface of the glove. Noise from a pylon mounted engine was found to have a minimal impact and then only on the lower surface of the glove. Means for protecting the surface against insects was also found to be important since laminar flow coverage was reduced when the test glove was not protected from insect contamination during takeoff and low-altitude operation. The dominant cause of transition, when it occurred, was believed to be crossflow disturbances.

Besides requiring careful design of the airfoil and close attention to surface smoothness, laminar flow wings must minimize cross-flow contamination. Crossflow disturbances cause premature transition and, to minimize this effect (for natural laminar flow airfoils), necessitate wings with low-sweep leading edges. Cross-flow disturbances become quite serious at angles of wing leading edge sweep greater than about 20 degrees. Figure 1 from reference 5 illustrates this point. On this figure a semiempirical curve is drawn at the approximate boundary between regions where NLF and Laminar Flow Control (LFC) are appropriate with current day technologies. Transition Reynolds numbers quickly decrease as wing sweep angles become larger than about 20 degrees. Almost no laminar flow can be expected at sweep angles above 50 to 60 degrees unless laminar flow control methods are employed.

Boundary layer transition Reynolds number has been found to increase with increasing supersonic Mach numbers [refs. 2, 6]. The fact that achieving laminar flow might be easier at supersonic speeds than at subsonic speeds has important implications for the use of both laminar flow and laminar flow control technology for supersonic aircraft. Applications of laminar flow technology to supersonic cruise aircraft can have a greater impact on performance than on subsonic aircraft. Refer to the Laminar Flow Control section in this document for more discussion on this point. An innovative theoretical application of natural laminar flow to a supersonic transport is described in reference 7. This study looked at a supersonic transport concept designed with a nouter cranked wing sweep of only 20 degrees instead of the typically moderately-swept (approximately 45 degrees) outboard wing sections of supersonic transport concepts. Chord Reynolds numbers appear low enough on this outer wing panel to support large regions of natural laminar flow.

Benefits. As mentioned in the previous section, general aviation aircraft are now using laminar flow airfoils for wing surfaces. Drag reductions up to 24 percent are claimed for business jet aircraft incorporating natural laminar flow over wings, fuselage, engine pods, and empennages [ref. 1 and 2]. For general aviation aircraft (especially business aircraft) speed is as important as efficiency. Laminar flow aircraft are thus capable of cruising at higher airspeeds for a fixed throttle setting than comparable turbulent designs.

Commuter aircraft with their moderate chord Reynolds numbers may be candidates for natural laminar flow technology. Reference 8 describes a study by ONERA and Aerospatiale for a short-haul commuter jet aircraft. Study results indicated a 10 percent drag reduction would be possible at cruise conditions through application of laminar flow. Current thinking is that large commercial transonic transport aircraft will rely on laminar flow control to achieve substantial benefits.

The study of reference 7 describes a supersonic transport concept that would develop laminar flow over an unswept outer panel wing. Depending on the extent of laminar flow achieved over the outboard wing, gross takeoff weight savings of over 10 percent are expected. This is a very significant savings, and can be appreciated by realizing that the entire payload weight of a supersonic transport is on the order of 6 percent. Figure 2 from reference 7 shows the weight reduction benefits of NLF. Subsequent studies by the Lockheed Aeronautical Systems Co. [ref. 9] have also looked at the possibilities of increasing the extent of supersonic laminar flow over outer wing panels of a supersonic transport and have concluded that significant gains in aircraft performance are possible.

Innovative studies by Gibson and Gerhardt [ref. 10] have looked at the possibilities of achieving laminar flow over the surface of a supersonic transport by actively cooling an entire (unswept) wing surface. Although the obvious integration problems of this cooled concept into a realistic supersonic transport configuration have yet to be resolved, the concept nonetheless remains attractive.

References.

1. Barnwell, R. W.; Hussanini, M. Y.: "Natural Laminar Flow and Laminar Flow Control," Springer-Verlag, ICASE/LaRC Series, 1992.

2. "Research in Natural Laminar Flow and Laminar-Flow Control," Proceedings of a Symposium held at Langley Research Center, Hampton, Virginia, March 16-19, 1987.

3. Harvey, W. D.; and Bobbitt, P. J.: "Toward Lower Drag with Laminar Flow Technology," ICAS-88-4.1.2. Presented at the 16th Congress of the International Council of the Aeronautical Sciences, Jerusalem, Israel, August 28- September 2, 1988.

4. Siddiqui, Shahid; and Kwa, Teck-Seng: "The Design and Flight Testing of a Long Endurance RPV," 17th ICAS Congress, Stockholm, Sweden, September 9-14, 1990, Proceedings, Vol. 2, ONERA TP No. 1990-11.

5. Harvey, W. Don; Forman, Brent: "Future Regional Aircraft Market Constraints, and Technology Stimuli," NASA TM 107669, 1992.

6. Jullie, Don W.; and Hopkins, Edward J.: "Effects of Mach Number, Leading-Edge Bluntness, and Sweep on Boundary-Layer Transition on a Flat Plate," NASA TND-1071, September 1961.

7. Fuhrmann, Henri D.: "Application of Natural Laminar Flow to a Supersonic Transport Concept," AIAA 93-3467, August, 1993.

8. Thibert, J. J.; and Reneaux, V. Schmitt: "ONERA Activities on Drag Reduction," 17th ICAS Congress, Stockholm, Sweden, September 9-14, 1990, Proceedings, Vol. 1, ONERA TP No. 1990-114

9. Harcrow, Aaron: "Part Span Natural Laminar Flow," Lockheed Aeronautical Systems Company; NASA contract NAS1-19348, Task 12, Oct 1994.

10. Gibson, Berry T.; and Gerhardt, Heinz A.: "Development of an Innovative Natural Laminar Flow Wing Concept for High Speed Civil Transports," Presented at the AIAA Applied Aerodynamic Conference , Aug. 9-11,1993, Monterey, CA.

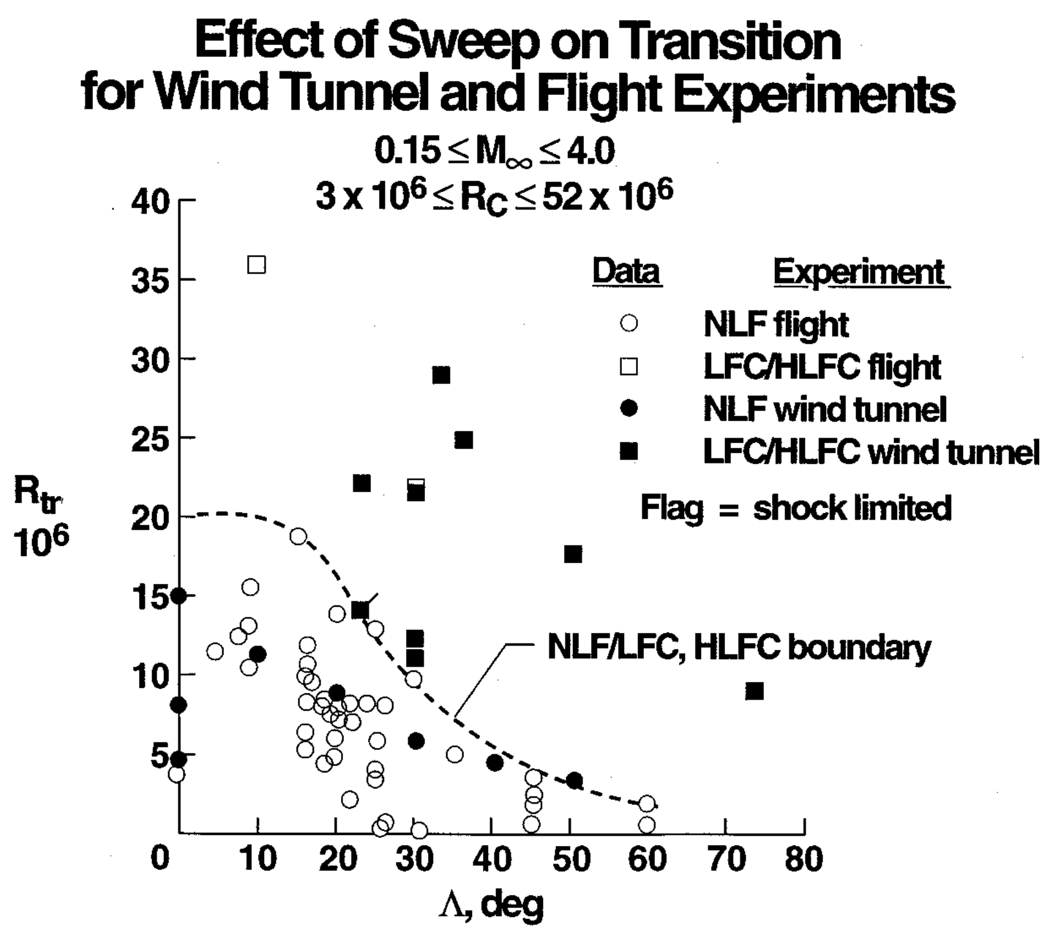

Figure 1. Effect of wing sweep on transition, from ref. 5.

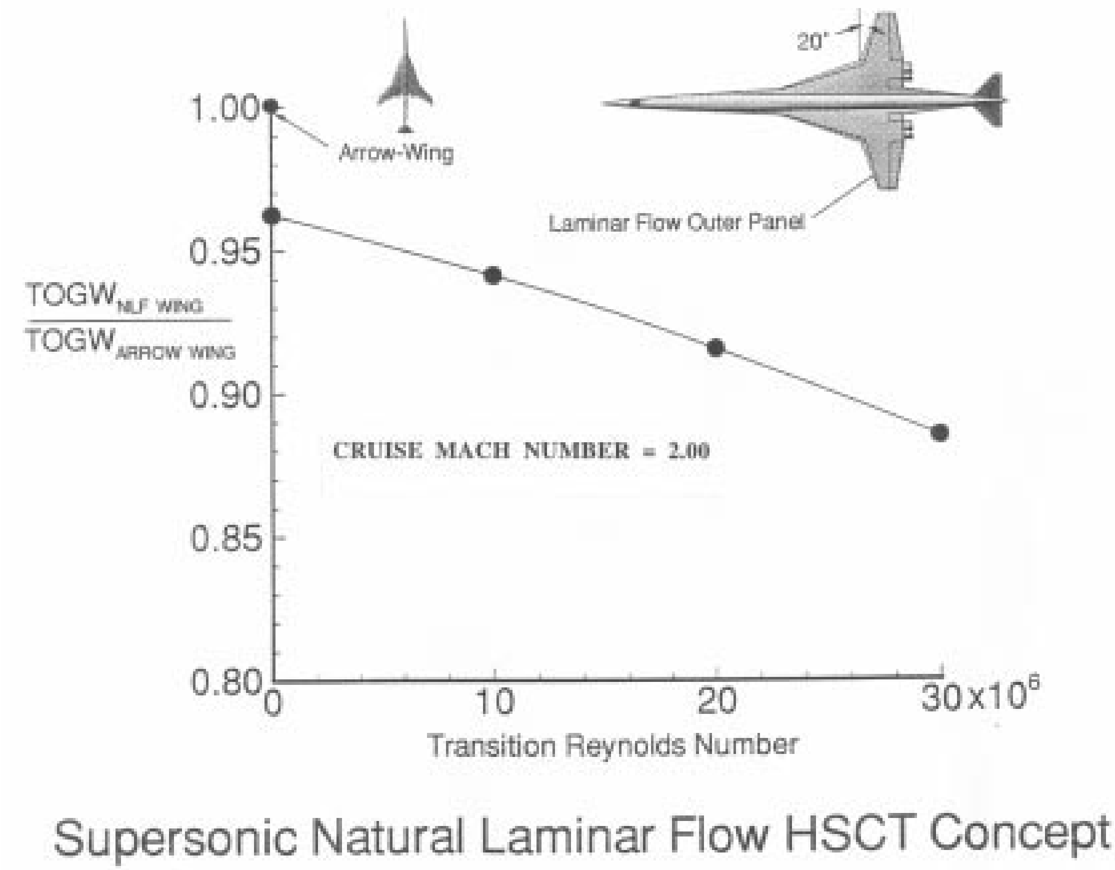

Figure 2. Takeoff weight reduction with natural laminar flow over outboard wing panels, from ref. 7.

Favorable Shock/Propulsive Surface Interferences and Interactions for Supersonic and Hypersonic Concepts

The open literature cites at least three different applications for the favorable use of shock waves to provide aeropropulsive performance benefits for supersonic and hypersonic concepts. The first two involve the tailoring of the external shape of vehicles to produce a beneficial shock wave when the vehicle is exceeding the speed of sound. The last one is a specialized application of localized supersonic flow for improved engine efficiency. Details of the three applications follow.

Supersonic Wing/Nacelle Integration and Favorable Aerodynamic Interference for Supersonic Airplane Design.

As far back as 1935, favorable interference was being addressed as a means of drag reduction. Busemann [ref. 1] theoretically described the judicious use of interfering flowfields to noticeably reduce wave drag due to thickness for two-dimensional wings. The idea, known as the Busemann biplane (see figure 1), was to establish a pattern in which the shock waves created at the leading edge of each wing are cancelled at the shoulders of the opposite wing where flow expansion occurs. For this set of wings, a symmetrical pressure distribution is produced, and the wave drag is zero. This is true only at the design Mach number; only partial cancellation occurs at off-design conditions. This concept was theoretically extended to three-dimensional systems by Ferri and Clarke [ref. 2].

The proper design and placement of propulsion nacelles and the design of the airframe were found to be mutually beneficial in three different ways. First, they can provide improved cruise aerodynamic efficiency. Second, the interference effects from the nacelle on the airframe can be made favorable. Lastly, the interference effects of the airframe flow structure can provide favorable effects on the flow going into the inlet of the propulsion system.

A report authored by Kulfan [ref. 3] addressed a variety of ways to achieve favorable aerodynamic interference for supersonic aircraft design. He concluded that a parasol wing concept had the greatest potential benefits for a small supersonic aircraft. The parasol wing concept is actually a three-dimensional application of the Busemann biplane wing cancellation concept, in which the forebody compression pressures are reflected off the wing onto the back of the body. This cancels part of the body wave drag and enhances the overall aerodynamic efficiency of the vehicle. The aerodynamic characteristics of the parasol wing are shown in figure 2. They include a favorable interference lift force and a partial wave drag cancellation on the body (which produces a thrusting force). A sketch of a body parasol-wing configuration is shown in figure 3. If a similar approach is taken with nacelles instead of a body, a double-parasol wing vehicle can be created (see figure 4). The planform shape of the wing is created to allow for the maximum nacelle interference lift per unit wing area. Analytical results (figure 5) for a Mach 3 small supersonic military aircraft showed that, when compared to a conventional aircraft with a reference flat wing design, the double-parasol wing vehicle has a 25% improvement in cruise L/D. When the nacelle area growth is optimized for the parasol wing, the potential L/D improvement increases to 37%. In fact, up to a 20% improvement in cruise L/D can still be achieved using a parasol wing over a conventional aircraft with an optimized wing designed for the cruise speed.

For the parasol wing concept, it is assumed that the inlets of the nacelles are still in the freestream part of the flow. Pritulo, et al. [ref. 4] addressed the benefits of locating the inlets inside of the airframe-altered flowfield. A sketch of the nacelle placement is shown in figure 6. They were able to show that proper inlet placement can improve the L/D at Mach 4 by 7% at AOA=8 degrees and up to 24% at AOA=0 degrees (figure 7). Furthermore, the ability to precompress the flow going into the inlets allows for higher values of mass capture than if they were in undisturbed flow. This actually allows the designer two choices: either accept the improved capability in the aircraft or reduce the size of the inlet capture area to make the engines more efficient.

Work at the University of Maryland [ref. 5] has developed a new class of waveriders that use predetermined flowfields from the leading edge of the vehicle (using an osculating-cone inverse design technique) to create a pre-compressed, uniform flow for capture by the engine inlets. While the aerodynamic performance of the new waveriders is similar to conical flow-derived waveriders, they possess advantages in inlet inflow properties that vary by less than one percent (see figure 8) and good volumetric efficiency. The inverse-design approach taken by the University of Maryland has been applied to a large class of supersonic and hypersonic Mach number forebody designs that maintain good aerodynamic performance and flow uniformity at off-design Mach numbers.

An historical application of this technology is the XB-70, which exploited favorable aerodynamic interference in its design. The reason why these types of systems have not been utilized in other aircraft designs is primarily because, aside from the HSCT, there are few aircraft designed for supersonic cruise efficiency. Furthermore, some of the designs pose a structural challenge because they do not contain long straight structural members. However, advances in materials may reduce the necessity for long, straight, structural members.

Each concept described above shows aerodynamic performance benefits over traditional design approaches, making them more cost effective. From an environmental standpoint, there is the potential that less fuel (and less exhaust) would be required because a precompressed inlet flow would require smaller engines for the same amount of thrust. Furthermore, some of the favorable aerodynamic interference may actually reduce noise signatures at cruise because of wave cancellation.

The integration of these concepts into configuration design requires that a rigorous approach be taken in the external shaping of wings, bodies, and nacelles. Off-design trades would have to be accomplished to ensure that performance is not significantly affected when not travelling at the design Mach number.

Thrust Deflection for Hypersonic Cruise.

In 1967, Krase published a note concerning the use of thrust deflection for hypersonic airbreathing vehicles [ref. 6]. By theoretically combining aerodynamic and propulsion parameters, the purpose of the note was to show that, with the moderate L/D ratios of hypersonic cruise vehicles and the low gross-thrust/ram-drag ratios of scramjet engines, there may be a substantial benefit to thrust deflection. A critical point is that the gross thrust (which can be much larger than the net thrust in an airbreather) is the part that is deflected. The deflected thrust can be used for decreasing wing size and weight at a constant altitude or to increase the cruise altitude of a prescribed configuration. For the latter, there would be an associated increase in capture area to maintain the air mass flow entering the engine. The analysis shows that for a vehicle with an L/D of 4 and a gross-thrust/ram-drag ratio of 1.1, a 14 deg., thrust deflection would provide a 34% greater range and fly 15,000 ft. higher than a vehicle without thrust deflection. It would also require a 52% larger capture area. The benefits are also evident at conditions corresponding to supersonic transport cruise conditions (L/D of about 8 and gross-thrust/ram-drag ratio of approximately 1.2), where a 7.1 deg. thrust deflection would provide about 4% greater range. At present, the topics of trim, stability, and control have not been addressed with respect to this type of thrust deflection.

There are a number of reasons why this concept has not been utilized. Most notably, there are very few research programs addressing supersonic and hypersonic cruise configurations. Second, the engines would be heavier because of the additional capture area required. This additional weight is countered by a reduction in the aerothermal loads on the vehicle and engine because of the higher cruise altitude.

As previously mentioned, there would be a tremendous range increase in the case of a hypersonic vehicle with thrust deflection.

Incorporation of this concept into vehicle design would involve either including the thrust deflection angle in the nozzle design or allowing for actuation of internal (and external) nozzle surfaces to allow for variable thrust deflection. This, of course, adds complexity and weight to the vehicle.

Shock Wave Engine.

Although this is purely an engine-only concept, the use of localized supersonic flow allows it to be discussed herein. The shock wave engine [ref. 7] is considered an unsteady flow device which uses a separate wave rotor along with the low and high pressure turbines to create a localized region of supersonic flow. The shock waves that are produced cause pressure ratio increases that are 2 to 10 times greater than pressures in a system using a conventional precompressor. An added benefit of the shock wave engine is considerable weight reduction based on two factors. First, shock compression takes place in significantly shorter distances than for steady flow compression, so size is reduced. Second, the compression pressure ratio across a single shock is much greater than in a steady flow diffuser for the same change in subsonic velocities.

There are no known configurations that currently use the shock wave engine. There have been problems in the past with fabrication of the wave rotor portion and the survivability of that portion at high rotation rates. However, Weber in reference 7 states, ". . . with careful design of the seals, the wave engine can greatly exceed the efficiency and be considerably lighter and more compact than conventional turbines or reciprocating internal combustion engines." This is a technology that is not quite ready for application today, but may be ready in 10-20 years with further research and development.

References.

1. Busemann, Adolf: *Atti del V. Convegno "Volta."* Rome, Reale Accademia d'Italia, 1935.

2. Ferri, Antonio; and Clarke, Joseph H.: "On the Use of Interfering Flow Fields for the Reduction of Drag at Supersonic Speeds," *J. of Aero. Sci.*, Vol. 24, No. 1, January 1957, pp. 1-18.

3. Kulfan, Robert M.: "Application of Favorable Aerodynamic Interference to Supersonic Airplane Design," SAE 901988, October 1, 1990.

4. Pritulo, T. M.; Gubanov, A. A.; and Voevodenko, N. V.: "Favorable Interference of Optimized Wing-Body Combination with Inlets at Supersonic Speed," AIAA 95-3946, September 1995.

5. Takashima, Naruhisa; and Lewis, Mark J.: "Waverider Configurations Based on Non-axisymmetric Flow Fields for Engine-Airframe Integration," AIAA 94-0380, January 1994.

6. Krase, W. H.: "Thrust Deflection for Cruise," *J. Aircraft*, Vol. 4, No. 2, March-April 1967, pp. 162-164.

7. Weber, Helmut E.: *Shock Wave Engine Design*. Wiley Interscience, 1994.

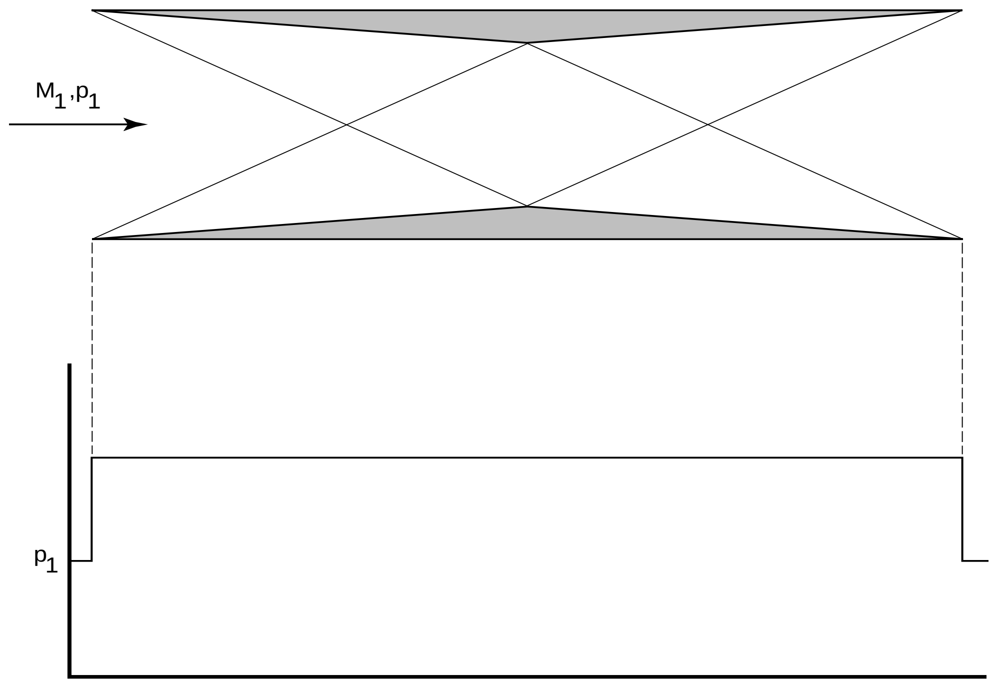

Figure 1. Busemann biplane concept with theoretical pressure distribution on an inside surface of the wing, from ref. 1.

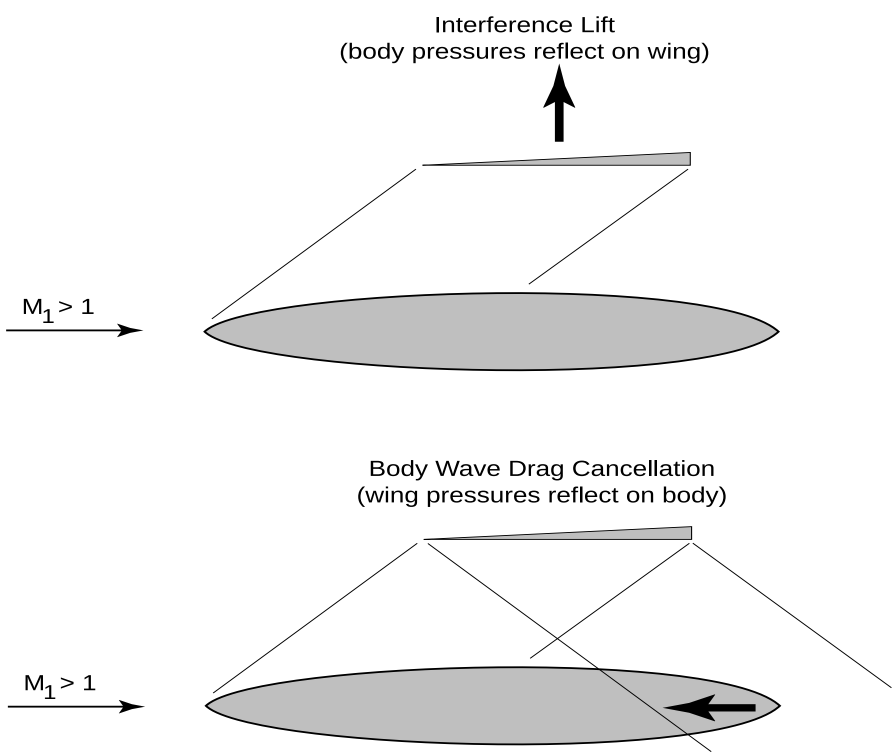

Figure 2. Parasol wing aerodynamic features, from ref. 3.

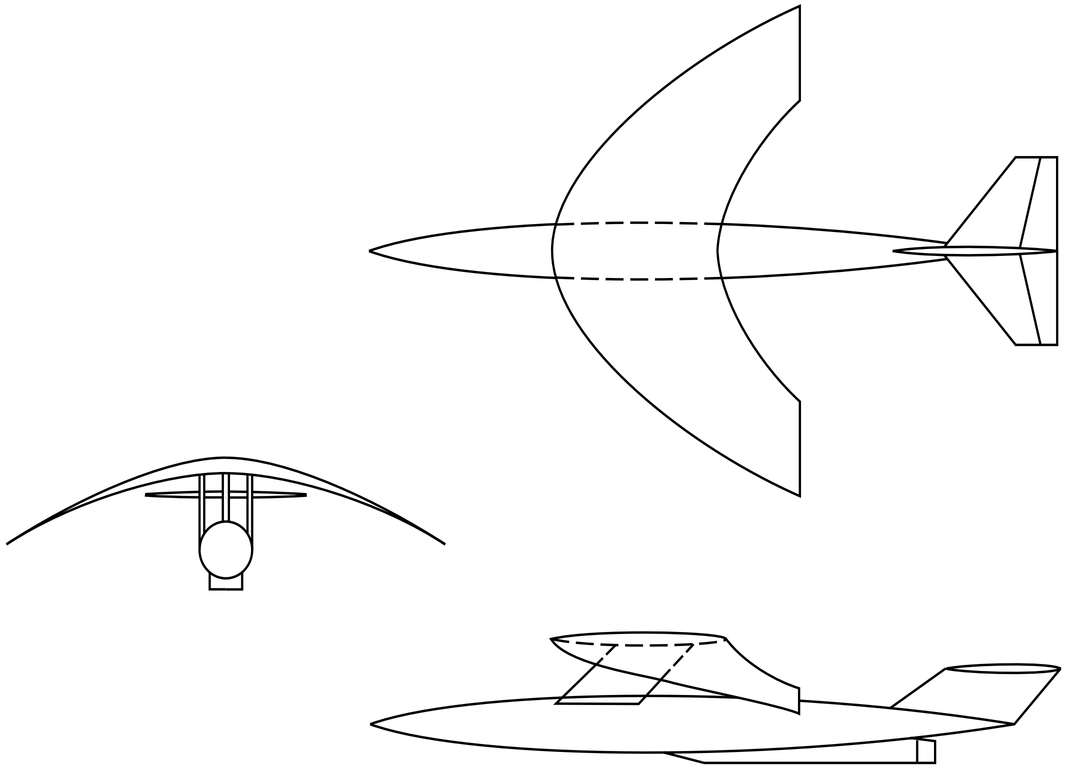

Figure 3. Body parasol-wing configuration features, from ref. 3.

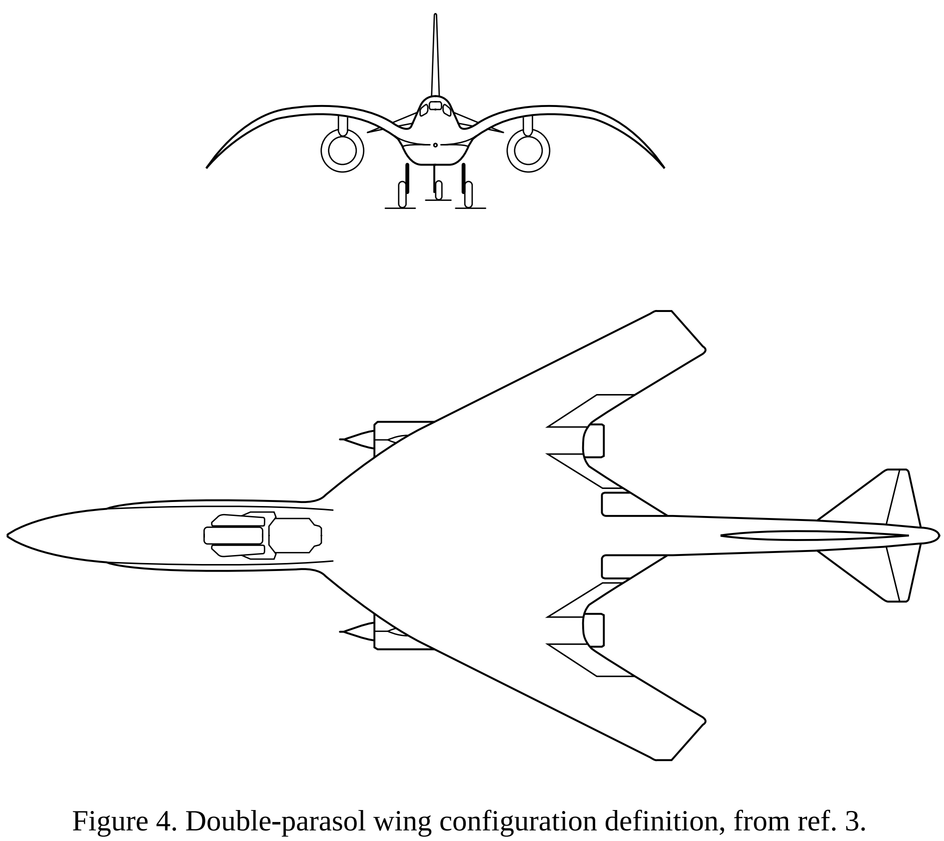

Figure 4. Double-parasol wing configuration definition, from ref. 3.

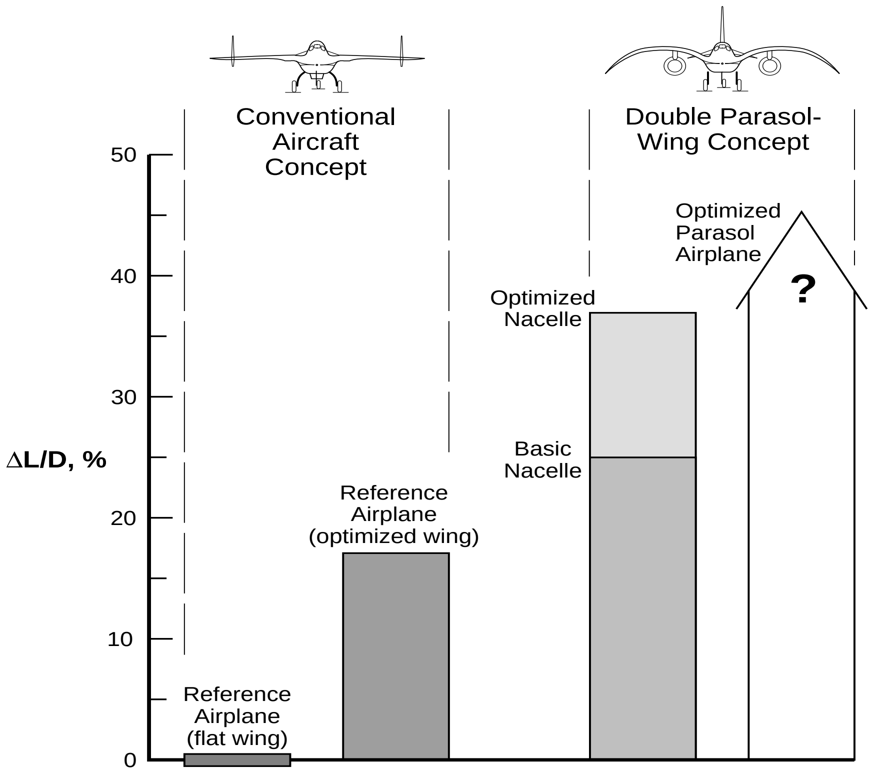

Figure 5. Improvement in maximum L/D improvement for a Mach 3.0 Double-Parasol Wing Configuration, from ref. 3.

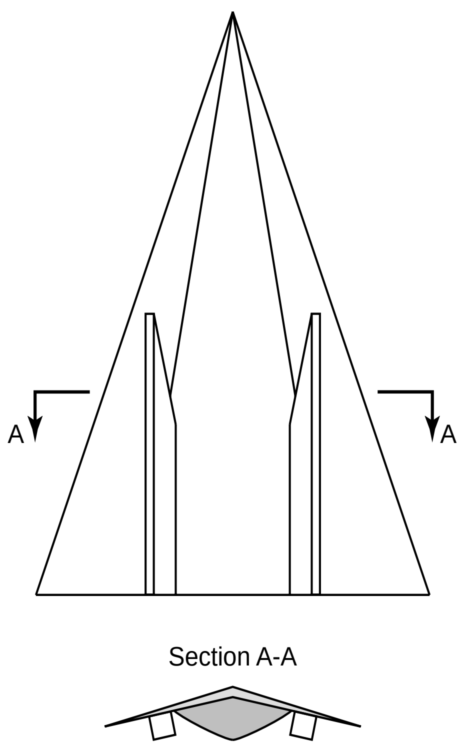

Figure 6. Airframe-Inlet configuration of Pritulo, et al., from ref. 4.

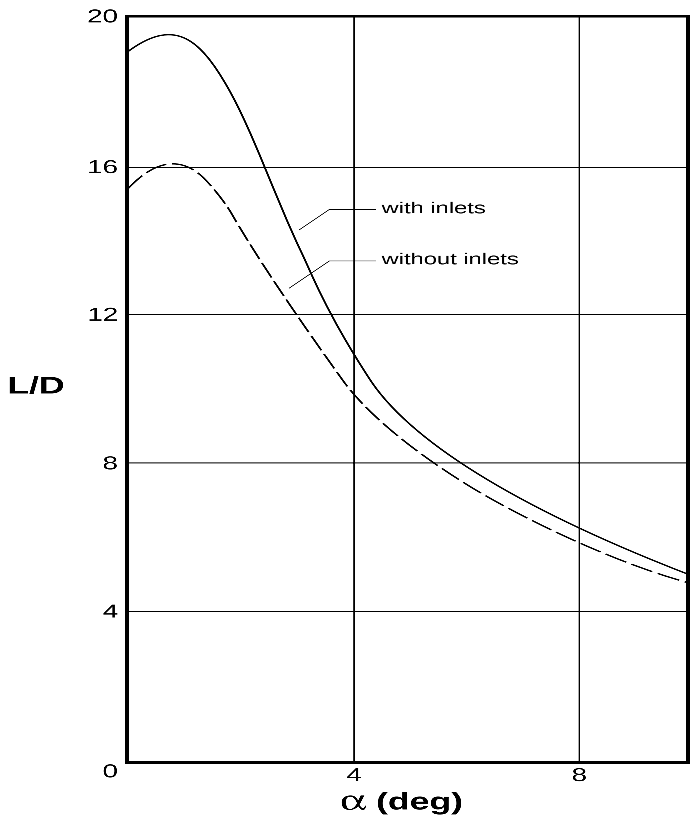

Figure 7. Favorable aerodynamic improvement from airframe-inlet interference, from ref. 4.

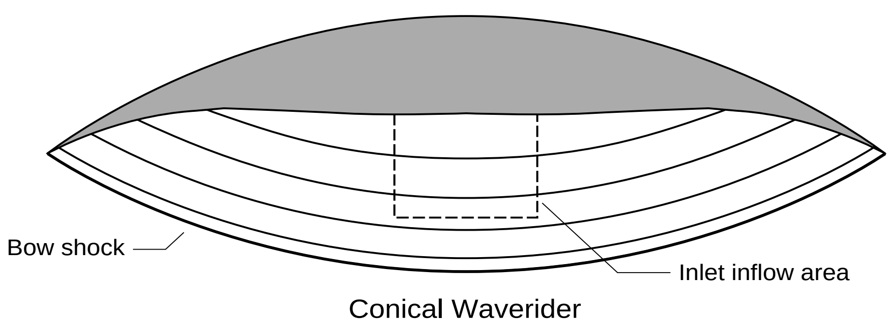

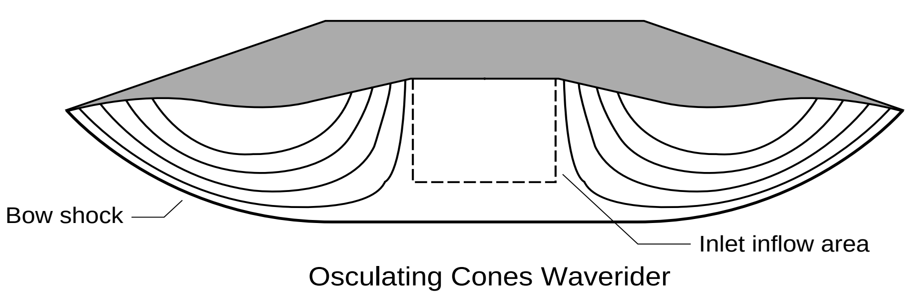

Figure 8. Pressure contours at the exit plane of two Mach 6 wave riders designed with conical and osculating cones methods, from ref. 5. (Typical inlet inflow area added for this report.)

Other Technologies

Thrust Vectoring

Technical Description. Thrust vectoring is exactly what its name implies; the thrust generated by an engine is turned (vectored) by the engines nozzle to create a force that is used to provide braking, lift, and/or control authority for an aircraft or missile. This technology has been investigated in various forms since the 1950s, mainly for use on military aircraft. The two basic methods used to accomplish the vectoring, mechanically actuated flaps in the exhaust flow and fluidic flow turning, are shown in Figures 1 and 2, respectively. Refer to reference 1 for a summary of aircraft thrust vectoring schemes. Thrust reversal for braking is the only widely used form of thrust vectoring in service to date; however, note that while thrust vectoring nozzles can provide both vectoring and reversing, thrust reversers as used in transport aircraft are not generally vectoring nozzles but dedicated thrust reverser systems. Also note that some High-Speed Civil Transport (HSCT) studies examined tilting nacelles for providing a lifting vector during cruise, but this survey will not address those studies.

Mechanical or fluidic thrust vectoring can be used to provide pitch vectoring, yaw vectoring, or a combination of the two (multi-axis vectoring). Nozzle design defines which of these functions are available for any given installation. Most of the following text describes mechanical thrust vectoring, which can be accomplished by several means. Little open literature describing fluidic thrust vectoring is available, and only a limited description of this technology is included below. In supersonic flow, fluidic nozzles have limited turning capability (less than 30^o, so far), although in subsonic flow, fluidic thrust reversers may be possible (i.e., reversing fan flow). Only mechanical nozzles can be used to provide thrust reversal of engine core flow or direct lift (for short/vertical takeoff and landing), and both require turning supersonic flow 90^o or more.

The most common use of mechanical thrust vectoring is thrust reversal. Jet transports have used this technology for decades to safely reduce landing rollout distances with something other than heavy, expensive and maintenance intensive wheel-mounted brakes. Thrust reverser systems add a margin of safety in terms of reduced stopping distances and increased directional control during landing rolls and rejected takeoffs on contaminated runways (e.g., water, snow, and/or ice). Flow is turned 135^o or more (from directly aft to forward) to provide braking power for the aircraft. Various mechanisms are used to effect the flow turning including clamshell (e.g., Boeing 737-100, see Figure 3) and cascade (Figure 4) reverser designs. Both designs physically block some or all of the engine core and/or fan flow. On a clamshell reverser, the blocked flow (efflux) is turned and vectored forward and concentrated into two large jets by the clamshell doors. This efflux must be oriented to avoid impingement on the aircraft, exhaust gas re-ingestion, foreign object damage (F.O.D.), and fuselage buoyancy effects, as well as to create a downforce. Cascade reversers operate in a different manner. Doors normal to the exhaust flow are used as blockers to the flow inside the nacelle (fan flow). Portions of the nacelle slide forward or aft to provide a flow exit and expose grid-like cascade vanes that direct the diverted flow. This type of reverser can distribute vectored flow more precisely than other reverser designs. Other thrust reversal techniques have been proposed to turn the fan flow of high-bypass ratio turbofans, including fabric parachutes deployed from the cowl of a pylon-mounted jet engine and blockerless reversers that use diverter jets (a fluidic technology) instead of blocker doors in a cascade-type reverser.

Thrust reversal as defined in the previous paragraph is almost exclusively used on the ground. In fact, reverser lockout systems are employed to ensure that the reversers are not inadvertently deployed in flight. Enormous forces can be generated by in-flight thrust reverser deployment, possibly causing loss of control and/or structural damage; however, some aircraft with cascade reversers are designed to use reverse thrust for emergency descents at idle thrust settings. The military fighter/attack aircraft community likes the idea well enough to consider using thrust reversing nozzles on future tactical aircraft. In this case, nozzles used for thrust vectoring functions would be modified to allow for thrust reversal as well. The aircraft would then have ground braking capabilities that would reduce field length requirements and an increase in airborne agility allowed by almost instantaneous airborne braking followed by acceleration, since thrust is used for both.

Pitch, yaw, and multi-axis vectoring nozzles are more complex than thrust reversers. Flow must be turned smoothly and efficiently to provide the proper thrust vector required for any given flight condition without significant thrust loss. Generally, nozzles with only pitch vectoring authority are rectangular in shape and have one or more flaps oriented parallel to the pitch-yaw plane of the aircraft. These nozzles are often called 2-D (i.e., two-dimensional) because they use planar plates to divert flow. These nozzles can accommodate thrust reversal requirements as well, either by splitting a single vane and hinging it about its trailing edge to block flow or by pinching off the flow using multiple vanes (Figure 5). Other pitch-vectoring nozzle designs include various gimballing nozzles and the single expansion ramp nozzle (SERN).

The British Aerospace/McDonnell Douglas AV-8B Harrier family of aircraft (and their predecessors, the P1127 and the XV-6A Kestrel, circa 1959 and later) uses a special kind of pitch vectoring nozzle found only on their Rolls Royce Pegasus engine (Figure 6). The nozzle is an elbow that rotates on a bearing fitted to the engine case. Two nozzles ahead of the aircraft center of gravity use fan air for thrust, while two nozzles aft of the aircraft center of gravity use jet exhaust for thrust. The nozzles can rotate about 100^o (from directly aft to slightly forward of down). The nozzles create lift for vertical takeoff and landing when pointed down or thrust for forward flight when pointed aft. If pointed all the way forward, braking force (and lift) is created. Note that the Pegasus engine only vectors thrust through the aircraft center of gravity; therefore, the engine is used to control lift and thrust, not attitude. The four nozzles (port front and rear, starboard front and rear) provide a stable lifting force for the aircraft, and the rotation capability allows transition from vertical to horizontal flight and vice versa.

Most research has neglected yaw-only vectoring, perhaps because pitch control adds little mechanical complexity once yaw is introduced (for some nozzle configurations) or perhaps because yaw-only has fewer benefits than other forms of thrust vectoring. Note that some yaw-vectoring flight experiments have been performed on the Grumman F-14 for one-engine-out control, and nozzles with yaw only (or yaw plus reverse) could be designed in the same fashion as 2-D pitch-only nozzles.

Several nozzle designs are suitable for multi-axis thrust vectoring (i.e., combinations of pitch plus yaw or pitch plus yaw plus reverse). One type uses multiple paddles to divert flow (Figure 7). The paddles are hinged at their base and can be activated singly or in concert with each other to provide the required thrust vector. This type of nozzle has been used on research aircraft to investigate the basics of thrust vectoring under flight conditions. It is inefficient both from the vectoring and nozzle efficiency points of view and the paddles are heavy, but paddle nozzles are cheap, easy to model, and can be retrofitted to existing airframes albeit with significant weight penalties (e.g., F-18 HARV, Figure 8). Another type of multi-axis vectoring nozzle is the axisymmetric (round) design. An axisymmetric nozzle looks like and is only slightly more mechanically complex than a supersonic convergent/divergent nozzle. Both use metal petals driven by hydraulic actuators to optimize the shape of the nozzle for various flight conditions; however, the multi-axis thrust vectoring (MATV, Figure 9) nozzle can make changes besides nozzle exit area. The nozzle vectors thrust by shortening the actuators on one portion of the nozzle and lengthening them on the diametrically opposite portion, driving the nozzle exit out of plane. Since the nozzle is round, the deflection can be in any direction; therefore, the effective vectoring volume is a cone. The extent of the cone is fixed by the amount of petal overlap required to create a functional nozzle and the travel of the actuators. Axisymmetric nozzles are attractive for retrofit to existing aircraft, but they are much more difficult to integrate into the airframe that 2-D nozzles and have higher signatures. Other more complex designs can be used for multiaxis thrust vectoring such as the clamshell nozzle [ref. 1].

Fluidic thrust vectoring (FTV) turns the exhaust of an engine using the influence of a secondary fluid stream. The concept is theoretically intriguing; however, creating an FTV system that can provide vectoring sufficient for control at an economical engine bleed rate is very challenging. The challenge becomes more severe as Mach number increases (i.e., for the same bleed rate, vectoring angle decreases with Mach number). For these reasons, FTV may be practically limited to use as an aircraft trim device. Several techniques can be used to effect FTV. Shock-vector control (see Figure 2) injects a sheet of secondary air into the primary exhaust stream from a slot in the divergent flap of a convergent-divergent nozzle. The secondary flow effectively creates an obstruction to the primary exhaust, resulting in an oblique shock across the primary flow. As the supersonic primary flow crosses the oblique shock, it is vectored away from the slotted divergent flap. Varying the mass flow rate of the injected sheet controls the vectoring angle, and thrust vectoring levels adequate for transitory control ($>15^{o}$) have been achieved in static tests of this technique. Since the vectoring is achieved by creating a shock across the primary flow, moderate thrust losses are incurred. Other fluidic concepts include passive cavity designs that turn the flow by influencing boundary layer separation characteristics, synthetic jets that turn the flow without any net injected mass flow, devices that use the Coanda effect to turn the flow as it leaves the nozzle, and counterflow thrust vectoring designs that inject flow upstream into the primary exhaust (again creating an oblique shock, but with less secondary mass flow). Fluidic methods can be used in similar ways to control nozzle throat area for engine throttling and flow expansion for off-design thrust performance gains.

Benefits/Liabilities. Thrust vectoring provides agility, controllability, performance, and survivability benefits. Agility and controllability are particularly enhanced at low airspeeds and/or high angles of attack where aerodynamic control surfaces are least effective, thereby expanding the flight envelope. Performance is improved by reducing the size of aerodynamic control surfaces (or eliminating some entirely), since drag and weight for these surfaces decrease with size. Thrust vectoring is most efficient at low vectoring angles; therefore, trim drag reductions are easily achieved. Control surfaces are programmed for minimum drag instead of aircraft trim, and thrust vectoring can provide the required trimming forces. Survivability is enhanced by increased low airspeed control, since recovery from (or avoidance of) departure from controlled flight is easier. In addition, reduced control surface size can result in reduced aircraft signature if desired.

Thrust vectoring also increases design freedom. Tailless aircraft (Figure 10), direct side force control designs, and vertical takeoff and landing aircraft, among other concepts, become practical. Even more mundane aircraft could benefit from the application of thrust vectoring. Personal (roadable) aircraft, conventional passenger and cargo transports, and unconventional transports like the Blended-Wing-Body could be improved by the addition of thrust vectoring.

The additional weight required for implementation and increased nozzle complexity are the major liabilities of mechanical thrust vectoring systems. Some nozzle designs are detrimental to aircraft signature (aural, infrared, and/or radar). If thrust vectoring replaces conventional aerodynamic controls, some of the high-speed operating envelope can be lost unless the engine is oversized. Overall aircraft system life cycle costs could also increase on thrust-vectored aircraft, depending on the aircraft platform. Detailed systems analyses must be performed to make that determination.

Specific benefits are listed below:

Agility and Controllability Benefits

Enhanced Low Airspeed Agility and Controllability

Expanded Envelope (Post-Stall Maneuvering Capability)

Higher Instantaneous Turn Rates

Improved Fuselage Aiming

Performance Benefits

Reduced Takeoff Roll

Reduced Trim Drag

Reduced Control Surface Size (Weight and Drag Reductions)

Design Optimization (e.g., Supersonic Wing Design, Tail Volume Coefficients)

Safety/Survivability Benefits

Recovery from Deep Stall or Departure

Aerodynamic Control Surface Backup

Reduced Control Surface Size (Signature Reduction)

In addition to the benefits noted above, fluidic thrust vectoring holds promise of further improvements. Nozzle weight could actually decrease with an FTV system. Actuators and their structural supports are not required, and nozzle cooling requirements are reduced. Survivability is further enhanced by FTV due to its inherent signature benefits. Moving nozzle geometry and the associated multitude of gaps and edges are eliminated, and the fixed geometry of an FTV nozzle allows nozzle shaping freedom. In addition, life cycle cost savings could be realized. Parts count is drastically reduced from the typical mechanical nozzle (vectoring or not), and the entire FTV system is inherently less complex, reducing acquisition and maintenance costs. If other mechanical nozzle functions (e.g., throat area control and expansion control) are incorporated into the FTV nozzle, the benefits are magnified. On the other hand, note that some FTV nozzles (e.g., shock-induced turning) may increase nozzle noise.

Present Utilization of Technology. Pitch, yaw, and multi-axis vectoring nozzles are not currently in service on any commercial aircraft, although most jet transports use thrust reverser systems. As previously noted, the Harrier series of aircraft and some Eastern Eurasian attack aircraft use vectored thrust for V/STOL. Tactical military aircraft fitted with pitch-vectoring nozzles will begin entering service around the turn of the century (e.g., Su-37, F-22A). Note that the first pre-production F-22A Raptor (using 2-D pitch vectoring) flew on September 7, 1997. The Joint Strike Fighter (JSF) may utilize pitch plus yaw or pitch plus yaw plus reverse nozzles, and the vertical/short takeoff versions of the JSF will require at least pitch vectoring nozzles. The only other aircraft using these types of nozzles today are research and prototype aircraft (e.g., F-18 HARV, X-31, F-15 ACTIVE, YF-22, Su-37 prototype). Substantial increases in engine thrust-to-weight ratios (T/W) due to research in the Integrated High Performance Turbine Engine Technology (IHPTET) initiative will eventually result in higher T/W vehicles, making thrust vectoring much more attractive.

Configuration Integration. Center of gravity (cg) location with respect to nozzle location is critical on a thrust-vectoring aircraft. For example, if the nozzle is used for control, there must be a sufficient moment arm between the nozzle and the cg to let the vectoring provide control forces without unduly over-sizing the engine(s). Load paths must exist around the nozzle to transfer the forces generated by vectoring to the remainder of the airframe. In addition, nearby structure must not intrude into the vectoring volume produced by the nozzle. In other words, booms, tails, etc. must not be in the exhaust at any possible deflection angle. Note that the Su-37 can only utilize pitch vectoring (as currently configured), because yaw vectoring could damage the rearward-facing radar between its nozzles. The purpose of thrust vectoring integration on any given airframe must also be considered. Using vectoring for trim imposes completely different requirements than using vectoring for post-stall control or vertical takeoff and landing.

References.

1. Berrier, B. L., and Re, R. J., A Review of Thrust-Vectoring Schemes for Fighter Aircraft, AIAA Paper 78-1023, July, 1978.

2. Wing, David J.: “Fluidic Nozzle Technology,” Presentation to the Langley Aeronautics Technical Committee, August 20, 1996.

3. Berrier, Bobby: “Propulsion Airframe Integration Technology, Reflections, Babbling, Introspection, Rambling, Thoughts, Musing, Meandering, Ruminations, and Other Possibly Related War-Stories,” Presentation to the Langley Aeronautics Technical Committee, August 12, 1996.

4. Minton, David H.: *Boeing 737*, Aero Series No. 37, Tab Books, Blue Ridge Summit, PA, 1990, p. 22.

5. United Technologies Corporation: “The Aircraft Gas Turbine Engine and Its Operation,” Pratt & Whitney Operating Instruction No. 200, 1988.

6. Mangold, P.; and Wedekind, G.: “Inflight Thrust Vectoring, a Further Degree of Freedom in the Aerodynamic/Flightmechanical Design of Modern Fighter Aircraft,” AGARD Conference Paper 90N28528, April, 1990.

7. Taylor, John W. R. (editor), *Jane's All the World's Aircraft, 1988-89*, Jane's Information Group Limited, Surrey, UK, 1988, p. 714.

8. Markman, Steve; and Holder, Bill: *One-of-a-Kind Research Aircraft*, Schiffer Publishing Ltd., Atglen, PA, 1995, p. 12.

Bibliography.

Snow, Barton H.: “Thrust Vectoring Control Concepts and Issues,” SAE Conference Paper 901848, 1990.

Herrick, Paul W.: “Relationships Between Thrust Vectoring/Reversing Fighter Effectiveness and Air-to-Air Missile Technology,” SAE Conference Paper 901845, 1990.

Yetter, Jeffrey A.; Asbury, Scott C.; Larkin, Michael J.; and Chilukuri, Krish: “Static Performance of Several Novel Thrust Reverser Concepts for Subsonic Transport Applications,” AIAA 96-2649, 1996.

Herbst, Dr. W.-B.: “Thrust Vectoring - Why and How?,” ISABE Paper 87-7061, 1987.

Geidel, H. A.: “Improved Agility for Modern Fighter Aircraft, Part II: Thrust Vectoring Engine Nozzles,” ISABE Paper 87-7062, 1987.

Asbury, Scott C.; and Capone, Francis J.: “Multiaxis Thrust-Vectoring Characteristics of a Model Representative of the F-18 High-Alpha Research Vehicle at Angles of Attack from 0^o to 70^o,” NASA TP-3531, December 1995.

Re, Richard J.; and Carson, George T., Jr.: “Static Internal Performance of Ventral and Rear Nozzle Concepts for Short Takeoff and Vertical-Landing Aircraft,” NASA TP-3103, September 1991.

Asbury, Scott C.; Gunther, Christopher L.; and Hunter, Craig A.: “A Passive Cavity Concept for Improving the Off-Design Performance of Fixed Geometry Exhaust Nozzles,” AIAA 96-2541, July 1996.

White, S.N.: “Feasibility Study for Integrating Thrust Vectoring as a Primary Flight Control System,” NASA CR-165758, Rockwell International Corporation, 1981.

Dorsett, Kenneth M.; and Mehl, David R. (LMTAS): “Innovative Control Effectors (ICE),” Final Report for September 1994 - January 1996, Wright Labs TR-96-3043, January 1996.

Roetman, E. L.; Northcraft, S. A.; and Dawdy, J. R. (BDSG): “Innovative Control Effectors (ICE),” Final Report for October 1994 - January 1996, Wright Labs TR-96-3074, March 1996.

Krase, W. H., “Thrust Deflection for Cruise,” *J. Aircraft*, Vol. 4, No. 2, March-April 1967, pp. 162-164.

Coe, Paul L., Jr.; McLemore, H. Clyde; and Shivers, James P.: “Effects of Upper-Surface Blowing and Thrust Vectoring on Low-Speed Aerodynamic Characteristics of a Large-Scale Supersonic Transport Model,” NASA TM X-72792, November 1975.

Tape, R. F.; Glidewell, R. J.; and Berndt, D. E.: “STOL Characteristics of a Tactical Aircraft with Thrust Vectoring Nozzles,” AIAA 87-1835, June 1987.

Petit, John E.; and Scholey, Michael B.: “Analysis, Design and Test of Thrust Reverser and Thrust Vectoring Systems for STOL Transport Aircraft,” AIAA 73-1218, November 1973.

Petit, John E.; et al.: “Thrust Reverser and Thrust Vectoring Literature Review,” AFAPL-TR-72-4, April 1972.

Archom, Tanda L.: “Performance Comparison of Dual and Single Flow Thrust Vector Nozzles,” California Polytechnic Institute Presentation, September 18, 1996.

Carpenter, Dr. Thomas W.: “Cal Poly Thrust Vectoring Research,” California Polytechnic Institute Presentation, September 18, 1996.

Stephenson, Frank: “Jet Set (Interview with Dr. Anjaneyulu Krothapalli),” Florida State University, retrieved on August 7, 1996.

From the Internet.

NASA Photos: http://nix.larc.nasa.gov

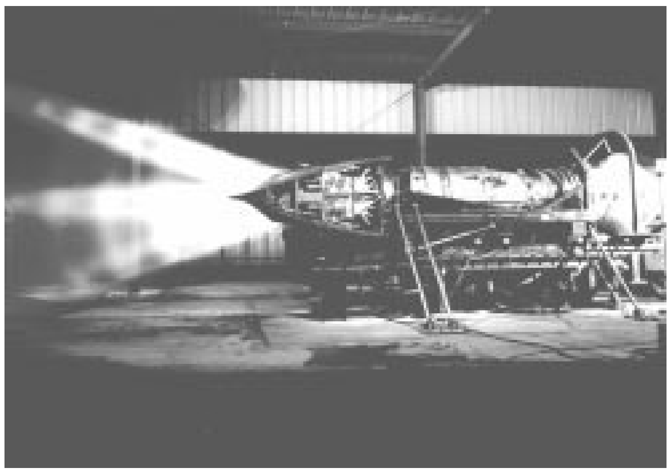

Figure 1. Time-lapse photo of Pratt & Whitney F119 in test stand showing pitch vectoring (P & W Photo).

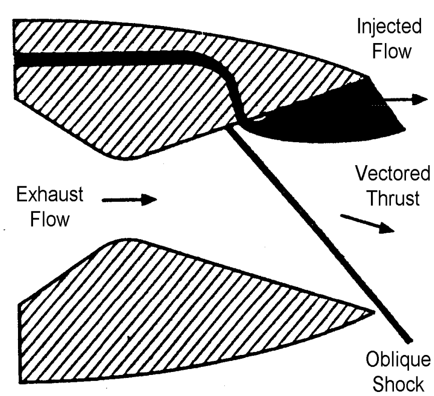

Figure 2. Shock vector control, a.k.a., shock-induced turning, from refs. 2 and 3.

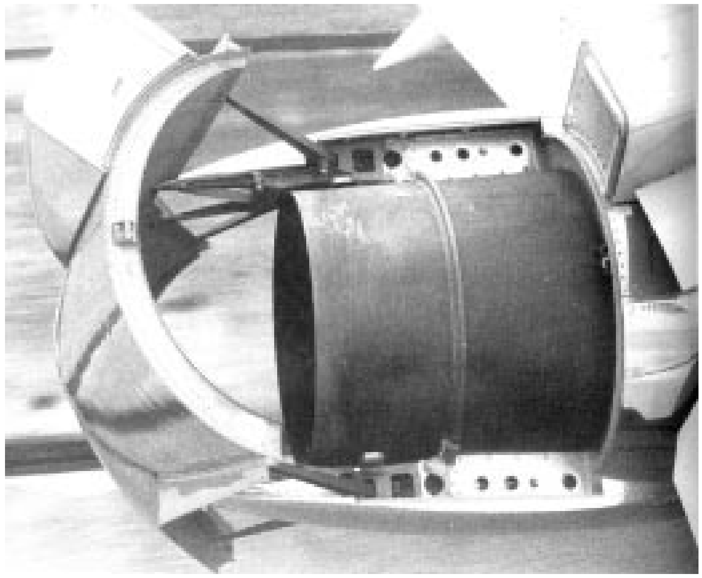

Figure 3. Clamshell thrust reverser on Boeing 737 (Boeing photo from ref. 4).

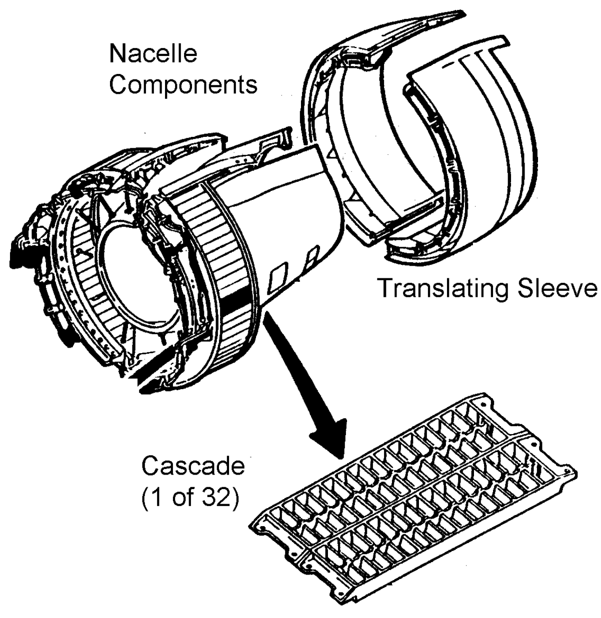

Figure 4. Cascade thrust reverser components, from ref. 5.

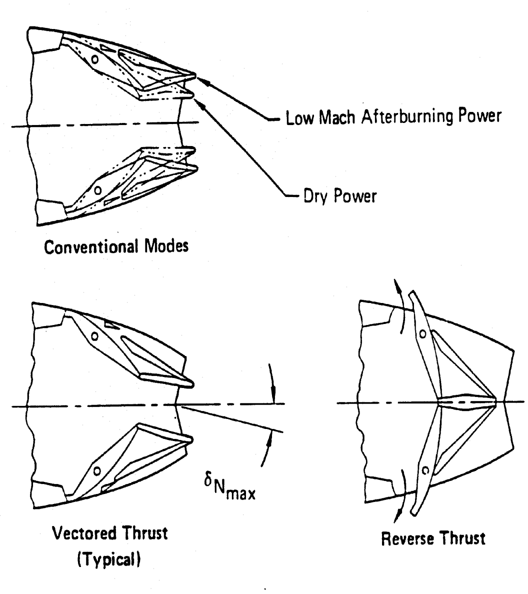

Figure 5. Pitch plus reverse thrust vectoring nozzle vane geometry, from ref. 6.

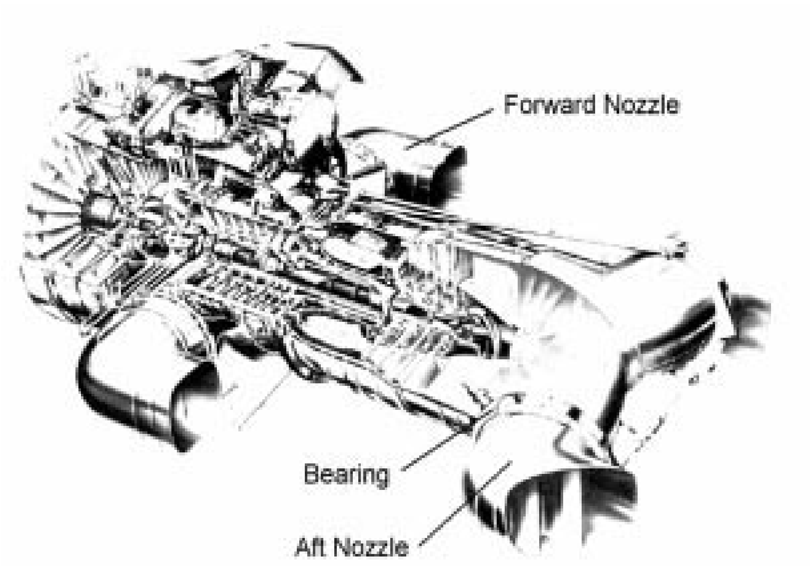

Figure 6: Rolls-Royce Pegasus 11-21 turbofan, from ref. 7.

Figure 7. Multi-paddle thrust vectoring nozzle on X-31 (NASA photo).

Figure 8. F-18 High-Alpha Research Vehicle (HARV) on test stand (NASA photo). (Note vectored thrust with respect to engine axis.)

Figure 9. F-16 Multi-Axis Thrust Vectoring (MATV) demonstrator with axisymmetric thrust vectoring nozzle. (USAF photo from ref. 8.)

Figure 10. Artist's concept of quasi-tailless X-31 (NASA photo).

Pneumatic Vortex Control

Background and Technical Description. Pneumatic vortex control is the technology of using high energy blowing air or suction to increase high-lift capability of aircraft and to also increase maneuver control of these aircraft. Several quite different concepts such as spanwise blowing for wing leading edges and control surfaces and fluid strake concepts have been developed to take advantage of this technique and are illustrated in figure 1 and described below in the following sections.

Leading Edge Spanwise Blowing: As the angle of attack of an aircraft wing or control surface such as a canard or horizontal tail is increased, several flow phenomena may occur [ref. 1]. A wing with a moderate leading-edge sweep of approximately 40 degrees will generally develop an attached leading edge flow that, as the angle of attack is increased, will accelerate to higher velocities and increase lift. At some angle of attack the upper surface high velocity (low pressures) cannot be sustained and the upper surface airflow separates and the wing begins to lose lift (stalls). For wings of higher leading-edge sweeps on the order of 60 degrees or greater, as the angle of attack is increased, a stable leading edge vortex begins to form on the wing upper surface behind the leading edge. This vortex consists of a tightly wound energetic tornado-like structure that effectively energizes the boundary layer and prevents the wing upper surface airflow from separating. At very high angles of attack the vortex will burst, beginning at the wing trailing edge and progressively moving forward towards the wing apex as angle of attack is increased. This will decrease lift and usually generates nose-up pitching moments.

Wing planforms designed with wing sweeps between 40 and 60 degrees lie in a region that generally realizes a leading edge vortex at lower angles of attack and a stall-like separation at higher angles of attack. It is in this region of sweep angles (40 to 60 degrees), particularly for fighter aircraft, that spanwise blowing (pneumatic) concepts have been devised to prolong the leading edge vortex and increase the usable angle of attack and controllable lift range of aircraft. Typically high energy air is directed transversely over the wing from a port located on the fuselage side slightly above the wing surface. The most common scheme positions the jet just aft and parallel to the wing leading edge as shown in figures 1a and b. A variation on this scheme distributes a portion of the air jets to outer wing panels so as to increase the wing span exposed to high energy air jets as shown in figure 1c [ref. 2]. Other variations on the theme have looked at pulsating jets as a means of reducing jet mass flow and increasing effectiveness.

Trailing Edge Spanwise Blowing: Spanwise blowing has also been studied to control the separation that can occur over trailing edge flaps at high lift conditions [refs. 3 and 4]. In this type of blowing scheme, a jet of high velocity air is directed transversely parallel to and behind the wing trailing edge flap hinge line (see fig. 1b). It has been shown that this air jet can substantially delay the onset of flow separation over the flap, thus increasing usable lift of the wing-flap system.

Fluid Strake: Another application of blowing has been developed that augments the lift of fighter type wings with a jet sheet formed by blowing from a series of small in-line holes located in the side of the fuselage ahead of the wing. The fluid strake is illustrated schematically in figure 1d and acts in a manner similar to a fixed physical strake to generate a stable vortex flow over the wing surface downstream of the blowing jets [ref. 5].

Forebody Yaw Control: Related to fluid strake is the forebody control concept (fig. 1e) that consists of round or slotted jet exits located near the aircraft nose and when used differentially provide useful yaw control at high angles of attack in the regime where vertical tails lose effectiveness [refs. 6-9]. Reference 8 reports on nose jet control experiments on a full scale F/A-18 in the NASA Ames Research Center National Full-Scale Aerodynamics Complex. Pneumatic nose jets for yaw control are similar in principal to the F-18 HARV articulated nose-strake experiments, in which small hinged nose strakes were asymmetrically deployed for yaw control at high angles of attack [ref. 10].

The foregoing discussions are vastly simplified since the mechanism of stall and vortex formation is a function of many factors including leading edge design (sharp leading edges at one extreme), leading and trailing edge control surfaces and boundary layer control devices such as vortex generators. Detailed information may be obtained from the extensive literature on the subject.

Benefits and Applications. Leading edge spanwise blowing has been investigated on wind tunnel models of various complexity and on a full scale F4C fighter aircraft. Wind tunnel models have represented F4, F-5F, YF-17, F/A-18, and generic models with wing sweeps up to 60 degrees. The full scale F4C experiments were conducted by McDonnell Douglas Corporation under contract to the U.S. Air Force. This aircraft was modified to incorporate a leading edge jet at the 13 percent chord location and a jet blowing over the trailing edge flap jet at the 88 percent chord location. A limited series of flight experiments ended in September 1979. Apparently results with the spanwise blowing system showed it was as effective as the standard boundary layer control system on the aircraft. NASA was interested in modifying this aircraft to determine if improvements could be made by placing additional spanwise blowing ports on the outboard panel of the wing. Although flight experiments were never carried out on a full-scale aircraft, a series of experimental wind tunnel tests investigated the effects of this distributed blowing system (fig. 1c). In general it was concluded the most favorable effects of spanwise blowing on the high-angle-of-attack dynamic lateral-directional stability and control characteristics were achieved with all blowing inboard [ref. 11]. All blowing outboard appeared to produce a maximum lift at a lower angle of attack than inboard blowing [ref. 12], and this can have a beneficial effect for Navy aircraft requiring good over the nose pilot view angles for carrier landings. Overall it did not appear from these tests on an F4C model that major improvements could be gained from the distributed blowing concept over and beyond the all inboard system.

Observations. Pneumatic blowing has received extensive attention from researchers; however, despite the large amount of research, these systems have not been incorporated on any operational aircraft up to this time. The most likely reason is that no clear cut advantages of pneumatic blowing has emerged to date when all the advantages (higher lift, greater control) are weighed against the disadvantages (loss of engine thrust due to compressor bleed, cost, complexity, and safety). Overall aircraft integration trades can be expected to lead designers towards less complex, lighter weight solutions for operational aircraft. The time may come however, when unique aircraft requirements, such as STOL, aggressive missile evasion maneuvers, signature issues, and size constraints may yet provide pneumatic vortex controls an opportunity to pay their way onto new aircraft designs.

References.

1. Campbell, James F.: “Augmentation of Vortex Lift by Spanwise Blowing,” *J. Aircraft*, Vol. 14. No. 9, September 1976, pp. 727-732.

2. Huffman, J. K.; Hahne, D. E.; and Johnson Jr., T.D.: “Experimental Investigation of the Aerodynamic Effects of Distributed Spanwise Blowing on a Fighter Configuration,” Presented at the AIAA 2nd Applied Aerodynamics Conference, August 21-23, 1984.

3. Dixon, C.J.: “Lift and Control Augmentation by Spanwise Blowing Over Trailing-Edge Flaps and Control Surfaces,” AIAA 72-781, August 1972.

4. Dixon, C. J.; Dansb, Ted; and Poisson-Quinton, Philippe: “Benefits of Spanwise Blowing at Transonic Speeds,” Presented at the XI ICAS Conference, Portugal, September 1978.

5. Zeigler, H.; Wooler, P. T.: “Aerodynamic Characteristics of a Jet Sheet Vortex Generator,” NASA Contractor Report 158904, June 1978.

6. Nugyen, L. T.; and Gilbert, W. P.: “Impact of Emerging Technologies on Future Combat Aircraft Agility,” AIAA 90-1304, May 1990.

7. Lamar, John E.: “High Angle of Attack Aerodynamics,” A Lecture in the AGARD Special Course Edition Entitled: Engineering Methods in Aerodynamic Analysis and Design of Aircraft, May 1991.

8. Lanser, Wendy R.; Meyn, Larry A.: “Forebody Flow Control on a Full Scale F/A-18 Aircraft,” *J. Aircraft*, Vol. 3, No. 6, November-December 1994, pp. 1365-1371.

9. Brandon, Jay M.; Simon, James S.; Owens, D Bruce; and Kiddy, Jason S.: “Free-Flight Investigation of Forebody Blowing for Stability and Control,” AIAA 96-3444, July 1996.

10. Murri, Daniel G.; Shah, Gautam H.; DiCarlo. Daniel J.; and Trilling, Todd W.: “Actuated Forebody Strake Controls for the F-18 High-Alpha Research Vehicle,” *J. Aircraft*, Vol. 32, No. 3, May-June 1995, pp. 555-562.

11. Hahne, David E,: “Free-Flight Wind-Tunnel Investigation of Effects of Spanwise Blowing on the Dynamic Lateral-Directional Stability and Control Characteristics of a 0.13-Scale Model of a Swept-Wing Fighter,” NASA TP 2492, Oct. 1985.

12. Huffman, J. K.; and Hahne, D. E.; and Johnson Jr., T. D.: “Experimental Investigation of the Aerodynamic Effects of Distributed Spanwise Blowing on a Fighter Configuration,” AIAA-84-2195, presented at the AIAA 2nd Applied Aerodynamics Conference, Aug. 21- 23, 1984, Seattle, WA.

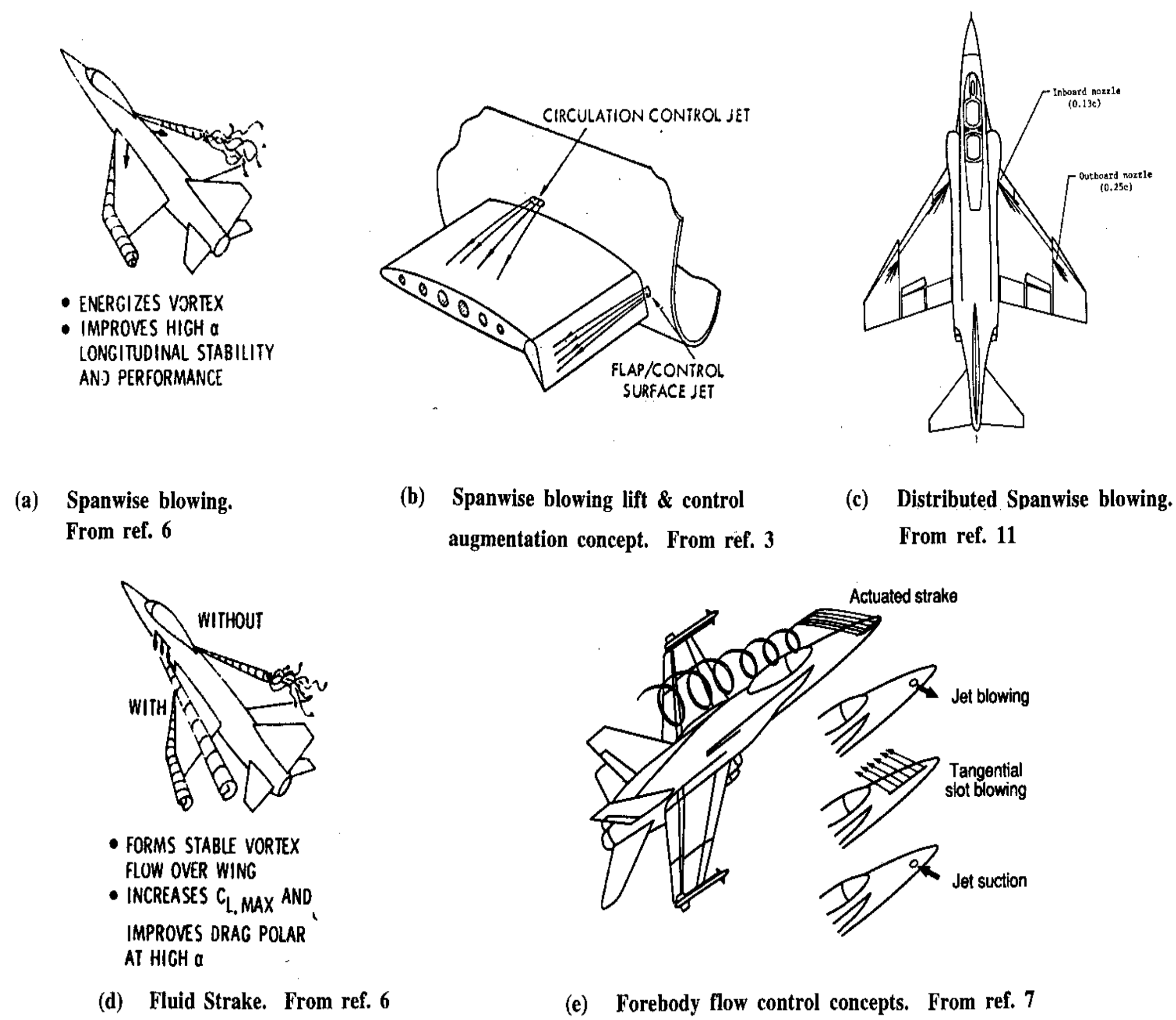

(a) Spanwise blowing. From ref. 6

(b) Spanwise blowing lift & control augmentation concept. From ref. 3

(c) Distributed Spanwise blowing. From ref. 11

(d) Fluid Strake. From ref. 6

(e) Forebody flow control concepts. From ref. 7

Figure 1. Pneumatic vortex control concepts.

Evolutionary Vehicle Concepts Utilizing SnAPII Technologies

Introduction

The technologies reviewed in Part I of this paper have all been tested and evaluated, at least to some extent, over the past eighty years. The historical data begs the question: based upon the possible performance increases these technologies offer, why haven't they been incorporated into modern aircraft designs? We suggest two reasons: perceived technical risk and, more importantly, the performance benefits of the individual technologies do not universally cover their life cycle costs.

Frequently, the design and life cycle costs of adding one technology are fundamentally similar to the cost of adding another different, yet potentially synergistic, technology. Therefore, the potential performance (and other) benefits of using several SnAPII technologies in synergy may outweigh the individual costs because the benefits are additive while the costs not not be. This section of the paper will illustrate the potential benefits of this design philosophy using both existing SnAPII technologies and existing aircraft design configurations.

The approach used was to conceptually retrofit an existing aircraft design (i.e., with a new wing, removal of the tails, change in engine integration, etc.) with alternate components incorporating SnAPII technologies. Two baseline aircraft types were selected: a current-technology, long-range conventional widebody aircraft (LRWB) and a current-technology, aluminum construction Blended Wing Body aircraft (BWB) [Ref. 1]. Conceptual models of these designs are shown in Figures 1 and 2 with design performance parameters shown in Table 1. Note that both designs have long range design missions, therefore their designs are dominated by requirements for efficient cruise flight.

Table 1: 1995 technology baseline aircraft performance parameters.

Parameter	LRWB	BWB
Design Takeoff Gross Weight (lb.)	590,000	1,345,200
Zero Fuel Weight (lb.)	368,245	734,500
Passengers	305	800
Design Range (n.m.)	6300	8500
Rate of Climb at Sea Level (fpm)	3030	2900
Takeoff Field Length (ft)	11,000	10,000
Landing Field Length (ft)	12,500	8500
Life Cycle Cost - Design Mission (cents/available-seat-mile)	3.7	2.7
Estimated Aircraft Price	$128M	$192M

Simple performance analysis equations for rate of climb, range, takeoff and landing distance (Figure 3) and a single-term, zeroth-order, weight-based empirical life cycle cost equation were calibrated to existing Flight Optimization System (FLOPS) [Ref. 2] and life cycle cost models of the baseline aircraft. A total of six conventional widebody and two Blended Wing Body designs were evolved and analyzed.

The context within which the analysis was conducted is purposely simplified through the use of the selected performance equations. The reason for this simplification is twofold: first, to allow the reader to reproduce the results in a similar fashion with his/her own assumptions and, second, to demonstrate the first-order effects of particular performance parameters on an overall aircraft design. Weight breakdown and mission performance data were used from the FLOPS analysis results to determine and calibrate inputs to the simple performance equations. Once completed, the results from the simple performance analysis of the baseline models were considered to be the baseline performance for comparison, not the actual FLOPS performance results. This is especially important in flight segment-critical analysis, i.e., rate of climb and range analyses where average flight values are quoted in the results. With the baseline simple performance "models" in-hand, the input parameters were adjusted in correlation to the new technologies implemented on each evolutionary concept (the assumptions for which are stated with the concept discussions). Note that the vehicles WERE NOT resized - they were retrofitted with new components resulting in identical planforms. Therefore, if a wing was replaced with a more efficient but equivalent weight design, the takeoff gross weight of the aircraft was reduced due to fuel savings. The structural weight, design wing loading, and engine size of the aircraft were not changed to take advantage of the reduced takeoff gross weight. Empty weight changes were only made when components were added, deleted, or modified from the baseline design. Therefore these designs are not optimized -- their structure and engine size could potentially be reduced to correspond to the fuel savings achieved through increased performance. Our approach is limited in scope but provides conservatives estimates with easily reproducible results. Additionally, note that the takeoff and landing distance equations do not account for FAR requirements in terms of balanced field length and missed approach and are therefore to be considered approximate at best.

Through performance parameters such as rate of climb, takeoff gross weight, fuel burn, takeoff and landing distances, approach speeds, and cost estimates are provided in the results. The reader can correlate these to higher-level system parameters inherent within the NASA Aeronautics and Space Transportation Technology Enterprise's Three Pillars for Success [Ref. 3]. First-order effects on the Pillar-One goals for increased safety, affordability, and national air transportation system capacity, as well as the goals for reduced emissions and aircraft noise, may be considered in the following relationships:

1) Safety increases are possible with decreased approach speeds.

2) Capacity can potentially increase when takeoff and landing distances decrease or when takeoff gross weight decreases. The first result can be attributed to the ability to build more, smaller runways. The second result can be achieved through decreased spacing made possible by vortex strength reduction at lower wing loading.

3) Affordability (from the standpoint of the consumer) may be proportional to the life cycle cost estimated savings stated in cents per available seat-mile.

4) Emissions reductions are largely proportional to fuel burn reductions without engine cycle improvements.

5) Noise reductions are perceived through increases in rate of climb or glideslope and elimination or reduction of noise sources. After takeoff, an increased rate of climb via enhanced high-lift performance without a change in jet velocity will decrease the noise "footprint" over an airport community through faster ground departure and reduced overflight distance. Similarly at landing, increased maximum lift capability without increases in airframe noise sources may be used to increase the glideslope and decrease the "footprint". An example might be the use of circulation control to eliminate the leading and trailing edge flaps. Note, however, that the acoustic effect of a technology such as circulation control on an integrated aircraft design in not known within the current body of literature.

Other non-performance-related effects of the SnAPII technologies are not explicitly discussed in this section but may be reviewed from the preceding section and implicitly deduced within the overall context of the Three Pillar goals.

Long Range Wide Body Evolutionary Concepts

LRWB Concept No. 1A

The first widebody evolutionary concept is shown in Figure 4. The concept employs the same two engines as the baseline, only mounted in Boundary Layer Ingestion (BLI) nacelles at the rear of the fuselage. This has several configurational effects, including the ability to shorten the landing gear, a requirement to move the wing rearward for both stability and control purposes and to move the landing gear closer to the now-displaced center of gravity. The BLI nacelles allow for a decrease in the parasite drag due to the fuselage at a cost of reduced engine efficiency. The positioning of the engines at the rear facilitates their use for thrust vectoring control. Though the method for vectoring high-bypass ratio turbofans is not definitively known, it may be possible through something as simple as nozzle-mounted turning vanes. The use of thrust vectoring conceivably allows the elimination of the empennage resulting in both drag reduction and structural weight savings but will require an increase in mounting hardware (and weight) relative to standard pylon-mounted nacelles. The shortened landing gear will result in a decrease in landing gear weight. A summation of the effects of these technologies on the input parameters of the simplified performance equations is given in Table 2. Note the assumption that the BLI penalty on engine performance is accounted for in the parasite drag input. The results from the analysis are recorded for comparison alongside the results from the other conventional evolutionary concepts in Table 8.

Table 2: Effect of SnAPII technology incorporation for LRWB 1A.

Parameter	Assumed Effect	Attributed to
$C_{D,o}$	-13%	Elimination of wing-pylon interference, removal of empennage, and implementation of BLI
C_D	-1%	$C_{D,trim}$ reduction due to implementation of thrust-vectoring control
$Weight_{empty}$	-3%	15% reduction in landing gear weight, elimination of empennage, doubling of nacelle weight to account for thrust vectoring

LRWB Concept No. 1B

Concept 1B (Figure 5) is identical to Concept 1A with exception of three additional SnAPII technologies. Wing-tip turbines are added for two purposes: to provide power for a suction pump powering a wing laminar flow control (LFC) system during cruise and to power a circulation control wing (CCW) during takeoff and landing. Additionally, it serves to break up the wing-tip vortex on approach for increased terminal area safety. LFC reduces the parasite drag attributable to the wing. The CCW provides increased high-lift capability for takeoff and landing. A summation of the effects of these technologies is given in Table 3. The results from the performance and cost analyses are, again, provided in Table 8.

Table 3: Effect of SnAPII technology incorporation for LRWB 1B.

Parameter	Assumed Effect	Attributed to
$C_{D,o}$	-25%	Elimination of wing-pylon interference, removal of empennage, and implementation of BLI and LFC
C_D	-1%	$C_{D,trim}$ reduction due to implementation of thrust-vectoring control
$Weight_{empty}$	-3%	15% reduction in landing gear weight, elimination of flaps and empennage, doubling of nacelle and air-conditioning weight to account for thrust vectoring and wing-tip turbines used for LFC/CCW, respectively
$C_{L,max}$	~+4%	Circulation control wing (CCW)
e (Oswald)	+5%	Load distribution tailoring with CCW and wing-tip turbine aspect ratio effect

LRWB Concept No. 2

Concept 2 (Figure 6) is very similar, in terms of technology content, to Concept 1B. Instead of using a wing-tip turbine to power the CCW, this concept uses engine bleed. This is facilitated by the use of a forward-swept wing (FSW) which reduces the amount of plumbing required to deliver engine bleed air to the powered lift system due to the proximity of the wing root to the tail-mounted engines. This configurational change eliminates the plausible use of wing-tip turbines and thus LFC is not implemented as in Concept 1B. It was assumed that the weight penalty (Table 4) for the FSW was not severe due to active control and composite construction. The results from the performance and cost analyses are provided for comparison to other LRWB concepts in Table 8.

Table 4: Effect of SnAPII technology incorporation for LRWB 2.

Parameter	Assumed Effect	Attributed to
$C_{D,o}$	-13%	Elimination of wing-pylon interference, removal of empennage, and implementation of BLI
C_D	-1%	$C_{D,trim}$ reduction due to implementation of thrust-vectoring control
$Weight_{empty}$	-1%	15% reduction in landing gear weight, elimination of flaps and empennage, doubling of nacelle weight to account for thrust vectoring and wing weight increase to account for forward swept wing penalty
$C_{L,max}$	~+4%	Circulation control wing (CCW)
e (Oswald)	+2%	Load distribution tailoring with CCW
$Thrust_{takeoff}$	-25%	Bleed compressor gases to blown flaps

LRWB Concept No. 3

Concept 3 (Figure 7) employs a variation of the Goldschmeid airfoil concept on the fuselage. The aircraft engines are again mounted aft on the fuselage in a manner similar to the previous three concepts. The Goldschmeid suction inlet is mounted forward of the engine inlet and the engine exhaust flow effects are assumed to parallel the Goldschmeid concept of trailing edge blowing. Again, wing-tip turbines are employed to provide power for a LFC system on the wing in cruise and to provide vortex reduction at landing. The empennage is eliminated due to thrust vectoring control and weight reductions similar to Concept 1A are assumed as indicated in Table 5. The results from the performance and cost analyses are provided for comparison to other LRWB concepts in Table 8.

Table 5: Effect of SnAPII technology incorporation for LRWB 3.

Parameter	Assumed Effect	Attributed to
$C_{D,o}$	-39%	Elimination of wing-pylon interference, removal of empennage, and implementation of LFC wing and Goldschmeid concept on fuselage
C_D	-1%	$C_{D,trim}$ reduction due to implementation of thrust-vectoring control
$Weight_{empty}$	-3%	15% reduction in landing gear weight, elimination of flaps and empennage, doubling of nacelle weight to account for thrust vectoring

LRWB Concept No. 4

This is almost a traditional wing tip-mounted engine aircraft concept (Figure 8). The engines employed are Advanced Ducted Propfans. Potentially, the large fan blades can be used to induce negative swirl in the tip vortex. This effect is assumed to dramatically reduce drag due to lift as indicated within the analysis input parameters shown in Table 6. The effects of spanload alleviation due to the tip mounted-engine on the wing weight and the increased size and weight of the vertical tail to account for engine-out conditions are assumed in the analysis inputs. The results from the performance and cost analyses are provided for comparison to other LRWB concepts in Table 8.

Table 6: Effect of SnAPII technology incorporation for LRWB 4.

Parameter	Assumed Effect	Attributed to
$C_{D,i}$	-20%	Wing-tip engine effect
$Weight_{empty}$	-1%	Wing weight reduction due to spanload alleviation and increase in vertical tail size and weight

LRWB Concept No. 5

The final conventional evolutionary concept is shown in Figure 9. This concept includes full span blown flaps and LFC powered by wing-tip turbines. The blown flaps system is assumed to result in a net weight reduction relative to the mechanical flap system. The blown flap system is assumed to be used to an extent during cruise flight in order to tailor the lift distribution. The wing-tip vortex strength on landing is reduced when the wing-tip turbines are locked in place. The analysis inputs for this concept are shown in Table 7. The results from the performance and cost analyses are provided for comparison to other LRWB concepts in Table 8.

Table 7: Effect of SnAPII technology incorporation for LRWB 5.

Parameter	Assumed Effect	Attributed to
$C_{D,o}$	-10%	LFC powered by wing-tip turbines
$Weight_{empty}$	-1%	Balance of elimination of at least one flap element and track mechanism with addition of blown-flap pneumatics
$C_{L,max}$	~+5%	Internally blown-flap system
e (Oswald)	+5%	Wing-tip turbine aspect ratio effect and load tailoring with blown-flap system
$Thrust_{takeoff}$	-25%	Bleed compressor gases to blown flaps

The five LRWB concepts presented here are meant only to represent possible implementation strategies, not the entire design space made possible through SnAPII design philosophy. Table 8 demonstrates that significant improvements over the baseline LRWB model are possible through the synergistic implementation of propulsion-airframe integration technologies. L/D improvements can be tremendous and may result in significant fuel savings. Technologies that allow for elimination of structure achieve additional economies. The life cycle cost reductions are not extreme though the reader should note that these are due only to fuel savings and will increase with both optimum vehicle sizing and manufacturing and operating cost advantages of several SnAPII technology implementations.

Table 8: Comparison of effects from baseline for all evolutionary LRWB concepts.

Parameter	1A	1B	2	3	4	5
Takeoff Weight	-12%	-15%	-10%	-17%	-9%	-10%
Rate-of-climb	+28%	+45%	+30%	+57%	+10%	+23%
L/D_{cruise}	+13%	+22%	+15%	+34%	+8%	+9%
$Weight_{fuel}$	-16%	-23%	-17%	-30%	-11%	-12%
Takeoff Distance	-25%	-70%	-38%	-36%	-22%	-40%
Rotation Speed	--	-50%	-50%	--	--	-50%
Landing Distance	-1%	-80%	-80%	--	--	-84%
Approach Speed	--	-50%	-36%	+2%	+9%	-50%
Life Cycle Cost	-6%	-7%	-4%	-8%	-4%	-5%

Blended Wing Body Evolutionary Concepts

BWB Concept No. 1

The first evolutionary BWB concept (Figure 10) utilizes a Goldschmeid airfoil concept for its centerbody section and LFC powered by winglet-mounted tip turbines to provide large decreases in parasite drag. Additionally, the concept employs thrust vectoring for control and trim drag reductions. The analysis inputs for this concept are given in Table 9 and the results for both BWB evolutionary concepts are provided for comparison in Table 11.

Table 9: Effect of SnAPII technology incorporation for BWB 1.

Parameter	Assumed Effect	Attributed to
$C_{D,o}$	-50%	Implementation of LFC wing and Goldschmeid concept on fuselage
C_D	-1%	$C_{D,trim}$ reduction due to implementation of thrust-vectoring control
$Weight_{empty}$	+2%	Weight increase equivalent to doubling of nacelle and air-conditioning weights to account for thrust vectoring and LFC implementation, respectively
$Mach_{cruise}$	-12%	Mach number reduction is required due to extremely thick centerbody, however this also allows a reduction in wing sweep

BWB Concept No. 2

The second BWB concept (Figure 11) again uses winglet-mounted tip turbines to power a LFC system for the wing but includes a blown flap system for increased takeoff and landing performance. Additionally, the concept employs thrust vectoring for control and trim drag reductions. Analysis inputs are provided in Table 10 and the results are shown in Table 11.

Table 10: Effect of SnAPII technology incorporation for BWB 2.

Parameter	Assumed Effect	Attributed to
$C_{D,o}$	-25%	Implementation of LFC wing
C_D	-1%	$C_{D,trim}$ reduction due to implementation of thrust-vectoring control
$Weight_{empty}$	+2%	Weight increase equivalent to doubling of nacelle and air conditioning weights to account for thrust vectoring and LFC implementation, respectively
$C_{L,max}$	~+5%	Internally blown flap system
$Thrust_{takeoff}$	-25%	Bleed compressor gases to blown flaps

It is important to note that the BWB already includes many SnAPII and other advanced technologies. The BWB is a highly integrated configuration which makes the addition of features (or technologies) more difficult to integrate and synergistically exploit. However, as the results in Table 11 demonstrate, there is considerable potential for the inclusion of SnAPII technologies within the palette of design alternatives to return impressive benefits relative to more traditional design approaches.

Table 11: Comparison of effects from baseline for all evolutionary BWB concepts.

Parameter	1	2
Takeoff Weight	-18%	-9%
Rate-of-climb	+38%	+20%
L/D_{cruise}	+60%	+26%
$Weight_{fuel}$	-44%	-23%
Takeoff Distance	-41%	-29%
Rotation Speed	--	-50%
Landing Distance	+30%	-68%
Approach Speed	--	-50%
Life Cycle Cost	-8%	-4%

Summary

The results of this simplified analysis indicate that considerable progress towards NASA's aeronautics goals in global civil aviation may be achieved through the use of SnAPII technologies. This observation is more true for conventional configurations due to their relatively low levels of configuration and technology integration than it is for BWB configurations due to their inherently high levels of integration and resulting technological synergy. Including SnAPII technologies in the set of design technologies traditionally pursued in NASA system studies will allow further leveraging of both technology sets. With the additional use of those advanced technologies currently available due to NASA research (such as composites, improved engines, and advanced operational procedures), the impact on the aeronautics goals could well be dramatic.

References

1. Liebeck, R. H.; Page, M. A.; and Rawdon, B. K.: “Evolution of the Revolutionary Blended Wing Body Subsonic Transport,” *Transportation Beyond 2000: Technologies Needed for Engineering Design*, NASA Conference Publication 10184, February 1996, pp. 431-460.

2. McCullers, L. A.: “Flight Optimization System Release 5.91 User's Guide”, http://avd00.larc.nasa.gov/flops/home.html, July 1996.

3. NASA Office of Aeronautics and Space Transportation Technology, *Three Pillars for Success*, March 1997.

Figure 1. Baseline current-technology, long-range conventional widebody aircraft.

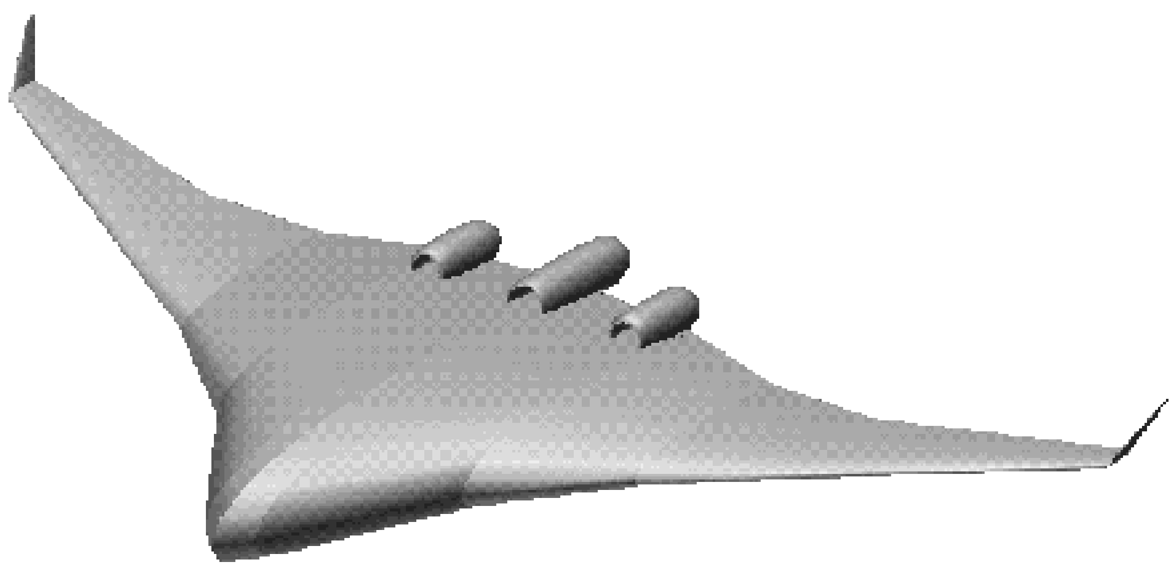

Figure 2. Baseline current-technology, aluminum construction Blended Wing Body aircraft.

$$R/C = \frac{(T - D)V_\infty}{W}$$

$$R = 2\sqrt{\frac{2}{\rho_\infty S}}\frac{1}{c_t}\frac{\sqrt{C_L}}{C_D}(\sqrt{W_0} - \sqrt{W_1})$$

$$s_{TO} = \frac{1.44W^2}{g\rho_\infty SC_{L,\,max}\{T - [D + \mu_r(W - L)]_{average}\}}$$

$$s_L = \frac{1.69W^2}{g\rho_\infty C_{L,\,max}[D + \mu_r(W - L)]_{0.7V_{TO}}}$$

where:	c_t	thrust specific fuel consumption (lb/lb/sec)
	C_L	lift coefficient
	$C_{L,max}$	miximum lift coefficient
	C_D	drag coefficient
	D	drag force (lb)
	g	acceleration due to gravity (ft/sec^2)
	L	lift force (lb)
	R/C	rate of climb (ft/sec)
	R	range (ft)
	s	field length (ft)
	S	reference wing area (ft^2)
	T	thrust (lb)
	V	velocity (ft/sec)
	W	aircraft gross weight (lb)
	μ_r	coefficient of rolling friction
	ρ	air density (slugs/ft^3)
with subscripts:	L	landing
	TO	takeoff
	0	start of cruise
	1	end of cruise
	∞	freestream conditions

Figure 3. Performance analysis equations used in this study.

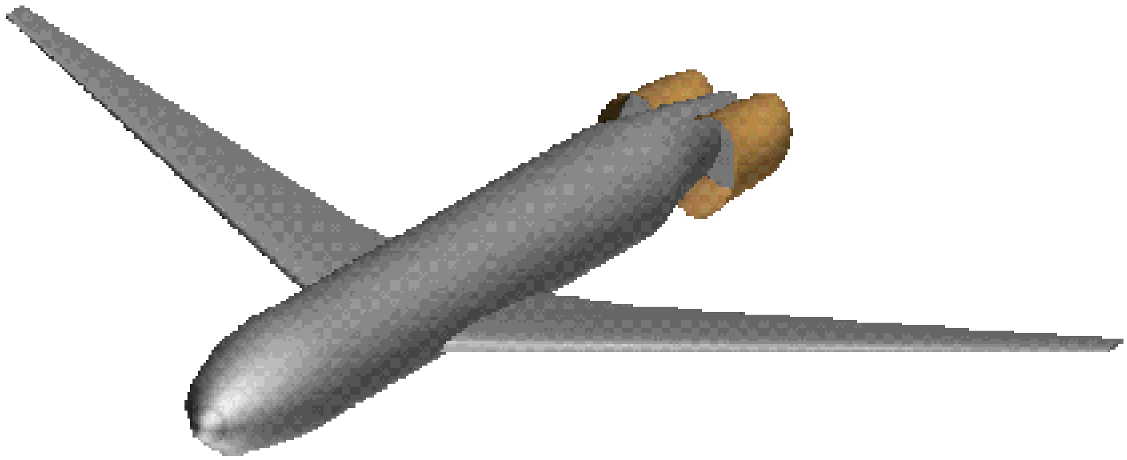

Figure 4. Long-range wide-body aircraft concept 1A.

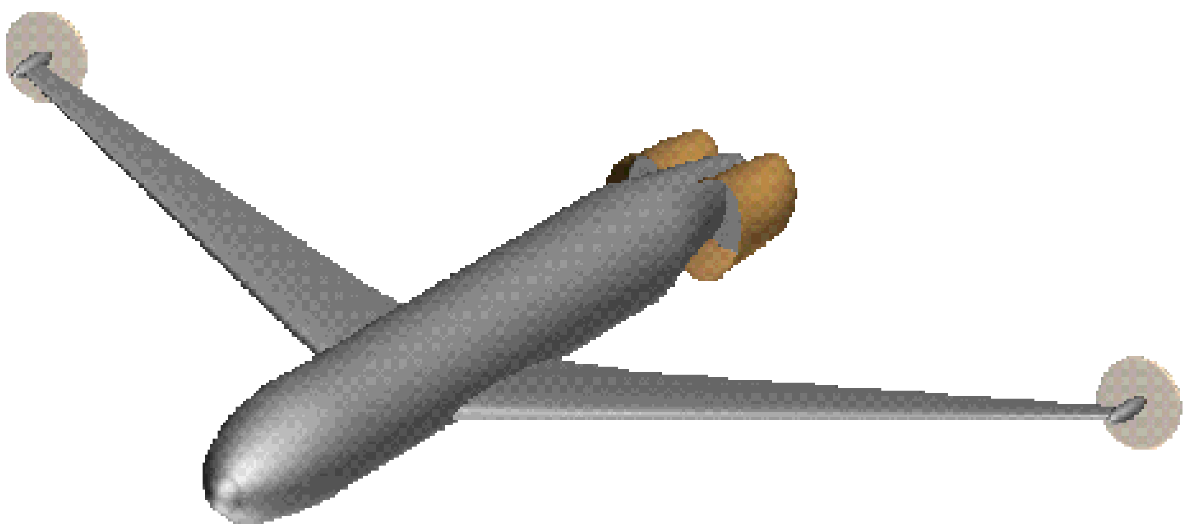

Figure 5. Long-range wide-body aircraft concept 1B.

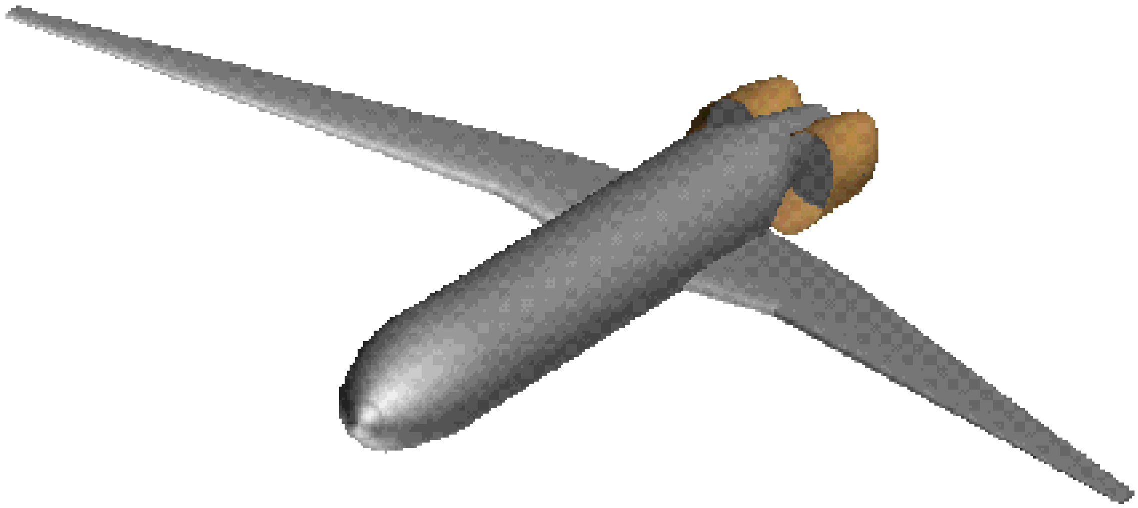

Figure 6. Long-range wide-body aircraft concept 2.

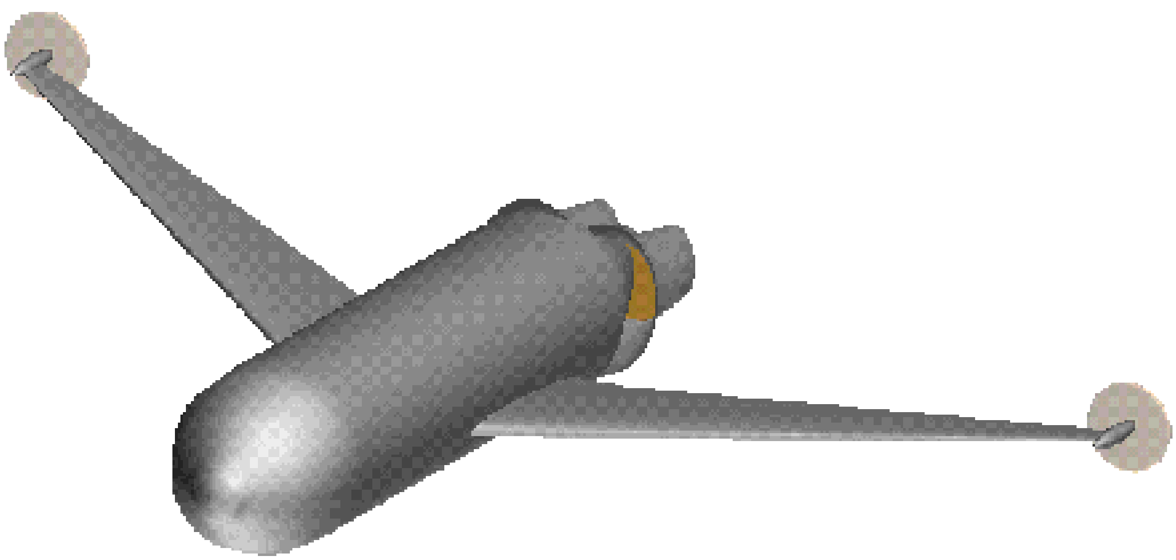

Figure 7. Long-range wide-body aircraft concept 3.

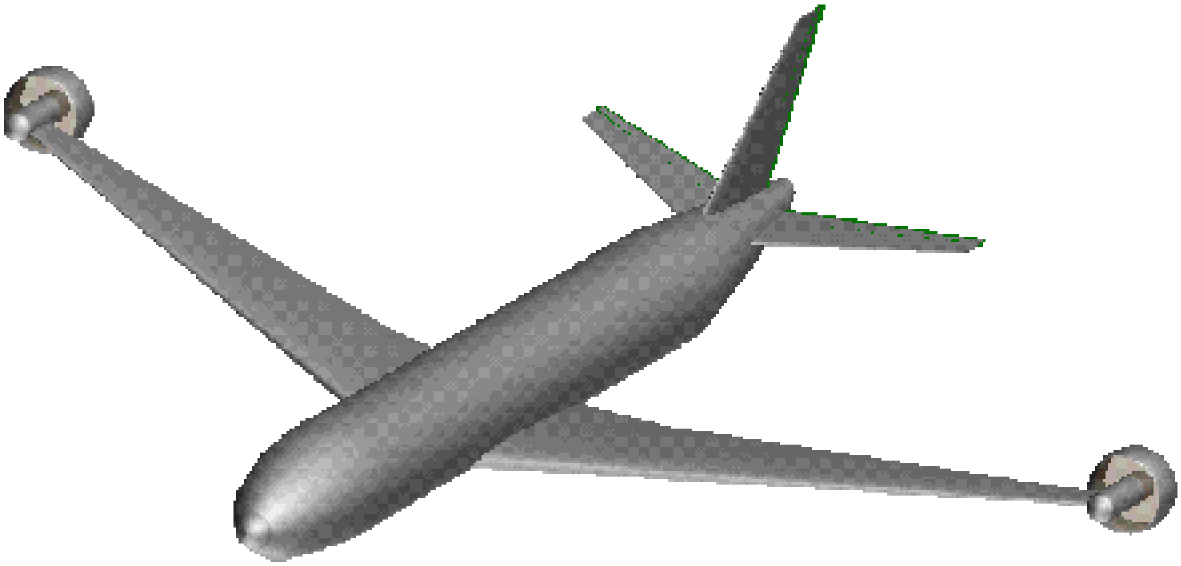
Figure 8. Long-range wide-body aircraft concept 4.

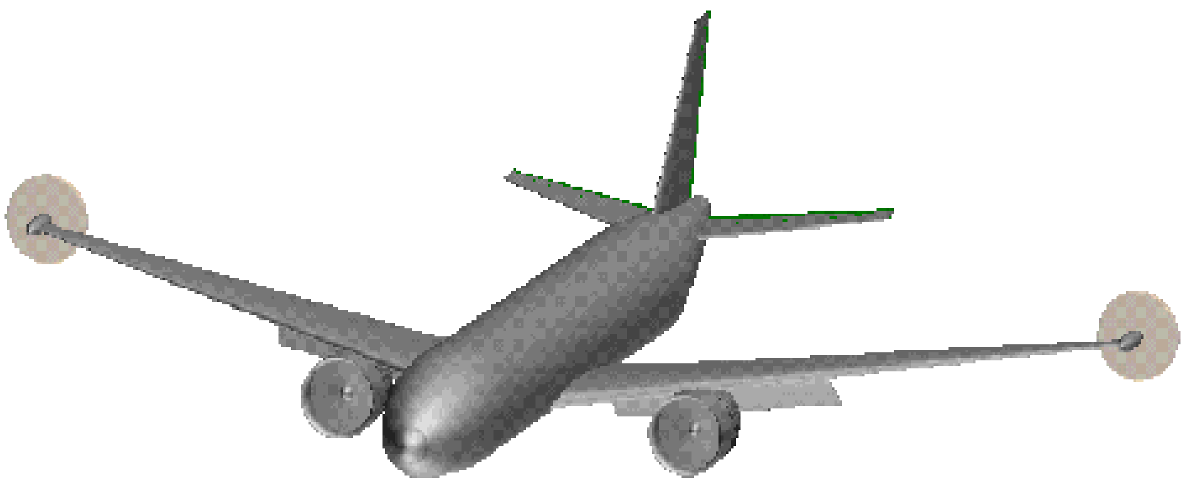
Figure 9. Long-range wide-body aircraft concept 5.

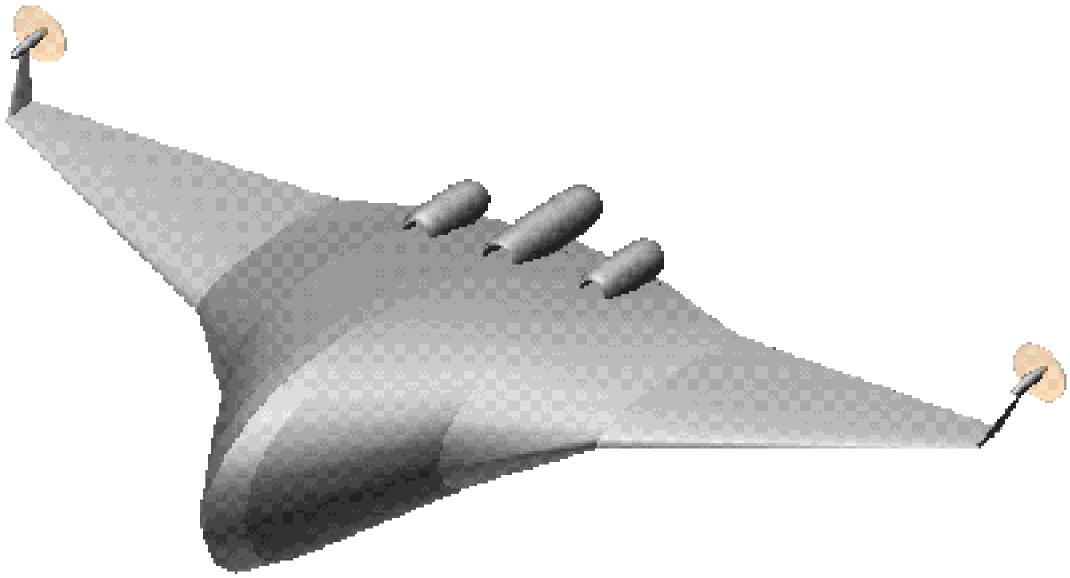

Figure 10. Blended wing-body concept No. 1.

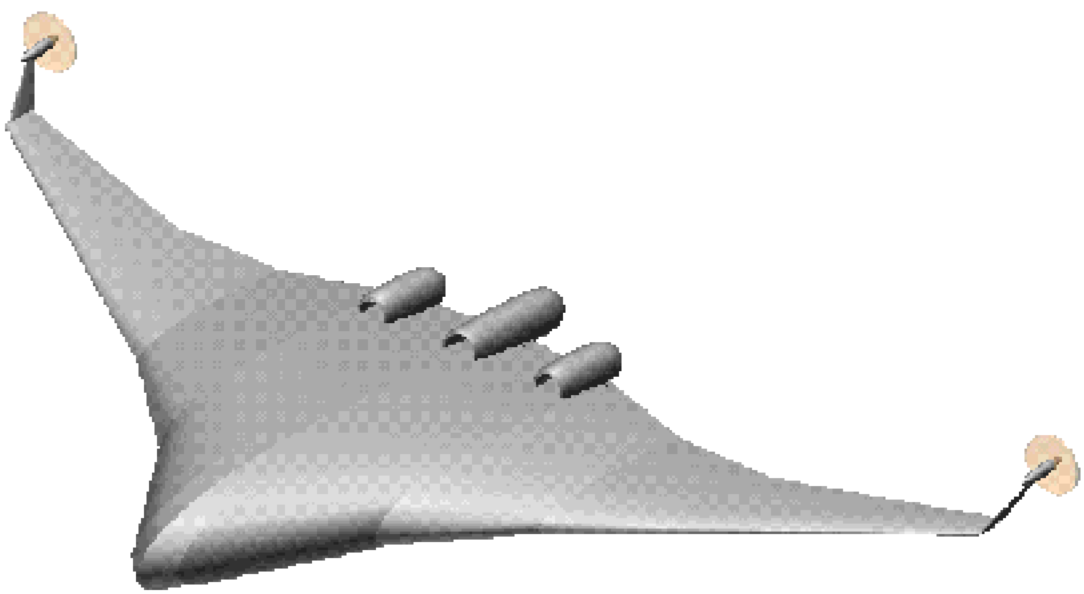

Figure 11. Blended wing-body concept No. 2.

Revolutionary Vehicle Concepts Utilizing SnAPII Technologies

The intent of this section is to exploit SnAPII technologies and other expected advances that may be available in approximately 20 years in order to develop ideas for future airplane concepts. There were no specific guidelines or constraints imposed on developing these concepts; members were free to think as far "out of the box" as they could. There is no detailed analyses of these concepts; the idea was to perform concept definitions using the knowledge presented in Technology Reviews and Evolutionary Vehicle Concepts sections of this document. Without question, these concepts require thorough systems analyses to determine their actual viability.

In order to facilitate a discussion of the relative benefits of each concept, a rating system was developed that attempts to relate its impact to the five goals described within Pillar One of the Aeronautics and Space Transportation Technology Three Pillars of Success. These five goals are to increase safety, reduce emissions, reduced noise, increase capacity, and improve affordability. For each of these goals, the following rating system was used:

+2 Concept has a **definite positive impact** on this goal

+1 Concept has a **perceived positive impact** on this goal

0 Concept has a **no impact** on this goal

-1 Concept has a **perceived negative impact** on this goal

-2 Concept has a **definite negative impact** on this goal

For each of the concepts, a basic description of the concept (mission, size, etc.,) will be presented. This will include the SnAPII technologies that will be employed, any other unique or significant features, and a ratings assessment based on the criteria established above.

Blended, Forward-Swept-Wing Body (BFSWB) Concept

The Blended, Forward-Swept-Wing Body (BFSWB) concept (figures 1 and 2) is a long-range transonic commercial passenger/cargo transport. As drawn, the concept is an 800-passenger, 7000 nautical mile range aircraft. Passengers are seated in a two-deck, three-class arrangement within the centerbody, cargo is outboard of the passengers, and fuel is in the wing.

Several SnAPII features are incorporated in this design. A circulation-controlled wing (CCW) powered by an auxiliary power unit is used to provide high C_L at takeoff and landing. The BWB in all of its permutations has low wing loading, so the CCW would enable very short takeoff runs and landing rollouts, relative to other very large subsonic transports. The three aft-mounted high-bypass ratio turbofan (or advanced ducted prop) engines incorporate boundary layer ingestion (trades increased specific fuel consumption, known as sfc, for reduced drag), thrust vectoring and reversing (allows simpler controls and less systems power consumption, plus reversing works synergistically with CCW for reduced field length requirements), and smart inlet and nozzle technology (reduced weight, noise and sfc). Laminar flow control, both natural and active, can be utilized on this configuration.

A summary of the ratings for this concept against the five aeronautical goals is provided below.

to Increase Safety	to Reduce Emissions	to Reduce Noise	to Increase Capacity	to Improve Affordability
+2	+1	+2	+2	+2
NOTE: Ratings range from +2 (definite positive impact) to -2 (definite negative impact).				

Safety. The BFSWB has some inherent safety features. Debris from an uncontained disk failure in the aft-mounted engines cannot penetrate the pressure vessel, the main wing structure, or the fuel tanks. In addition, staggering the engines helps guard against engine fratricide. Careful integration of the forward-swept design may yield a statically stable configuration with more center-of-gravity range than an aft-swept BWB. The thrust vectoring system provides an inherent propulsion-controlled aircraft (PCA), with normal control surfaces as backup. Note that although the escape paths are short, passenger egress may be a safety issue for some situations on all BWB configurations

Emissions. The clean design (tailless, minimal wetted area per passenger) requires fewer and smaller engines than equivalent technology conventional configurations. Performance improvements from the CCW, laminar flow, and smart inlets/nozzles will reduce emissions from first and second-order sizing effects.

Noise. The upper surface inlets on the BWB designs provide a large decrease in perceived forward-radiated noise, since the centerbody acts as a large shield. Smaller engines, fewer/smaller control surfaces, high takeoff/landing C_L, and smart inlet/nozzles will all reduce the community noise impact.

Capacity. The BFSWB, as previously noted, is an 800-passenger concept. It will require half as many airport operations as today's largest aircraft (747-400) to move the same number of passengers. The low wing loading of this design will also reduce the wingtip vortex strength, allowing less in-trail spacing between aircraft.

Affordability. Affordability correlates almost directly with weight. All of the SnAPII technologies work in harmony to improve performance (yielding a smaller, lighter aircraft for the same mission) and/or directly decrease weight. The large size of the BFSWB also helps with affordability, since more revenue passenger miles are generated per pound (both of fuel burned and aircraft purchased/maintained). The concept itself also yields affordability improvements through advanced manufacturing processes (e.g., unhanded parts, in-place assembly).

Distributed Engine Regional STOL (DERS) Concept

The Distributed Engine Regional Short-TakeOff and Landing (DERS) Concept (figures 3 and 4) is short-to medium range (500-1500 miles) transport capable of carrying 100-200 passengers. The DERS concept incorporates very revolutionary and interesting technologies. Passengers are seated in a two-class arrangements. The fuselage utilizes structurally integrated transparent composite fuselage panels for the viewing pleasure of the passengers. The first class cabin is a full-view section. The operator section with synthetic vision is located in the aft section of the aircraft. The airplane has no tails and employs an array of mini-engines integrated with the wing allowing tailoring of lift distribution, increased redundancy and providing low-speed lift augmentation for short takeoff and landing field performance. These low diameter engine components produced mostly high frequency noise that is actively controlled at the engines inlet and nozzle through the use of “smart materials”. These new-generation materials have shape changing capability and they will be used in the wing's leading and trailing edges to provide roll control and to tailor off-design performance to flight condition.

The DERS concept utilizes some SnAPII technologies. The tail engine uses the boundary layer ingestion inlet. In addition this tail engine is really another array of mini-engines integrated with the inlet/nozzle deflectors to produce a coanda effect for augmented thrust vectoring.

An assessment of the Distributed Engine Regional Short-TakeOff and Landing concept with respect to the five goals is contained in the following table.

to Increase Safety	to Reduce Emissions	to Reduce Noise	to Increase Capacity	to Improve Affordability
+2	-1	+1	+2	+2
NOTE: Ratings range from +2 (definite positive impact) to -2 (definite negative impact).				

Safety. The use of mini-engines distributed along the wing and in the tail engine section increase redundancy in case of engine failure. Load distribution tailoring, enabled by the use of a very high aspect ratio wing in conjunction with propulsion optimization with use of smart materials, produce alleviation of gust load/flutter problems to the structure of the wing.

Emissions. A mild negative impact to emission is assumed due to the reduced efficiency of the small scaled engines utilized in these concepts.

Noise. The elimination of flap/slats systems will greatly contribute to reduction in noise during landing and take-off operations. However, additional high frequency noise may be present, due to the additive nature of the noise from the individual jet engines.

Capacity. The efficient arrangement of passengers with the utilization of transparent composite fuselage panels contributes to an increased capacity. The full integration of the propulsive system for tailoring of off-design performance to flight condition contributes to more capacity because passenger revenue per mile will undoubtedly increase.

Affordability. The use of small interchangeable engines will reduce the operating cost and time delays due to mechanical problems at airports. Utilization of smart materials reduce weight because of the elimination of complex and heavy mechanical systems such as flaps/slats. In additions these material are light-weight so that overall empty weight of the aircraft will be reduced. Manufacturing savings will be realized because the outboard wing will be a constant symmetric section enabling extrusion manufacturing techniques.

Goldschmied Blended Joined Wing (GBJW) Concept

A blended-wing-body, joined with an aft-mounted forward-swept-wing, forms a blended-joined wing and is the basic concept for this large capacity, transonic transport. It will have winglets and three engines but no tail. Two engines are mounted aft and a third is associated with the Goldschmied suction blowing system. See figures 5 and 6 for a three view of the perspective and configuration, respectively.

SnAPII technologies and other features associated with this configuration are listed here. A Goldschmied suction-blowing system will be utilized for the promotion of laminar boundary layer over the thick part of the configuration. This will be needed over the top part of the wing. Circulation control over the slender portions of the wings, smart inlet/nozzle shaping for the engines, and propulsion control of the aircraft are also used.

The configuration should allow for easy egress, minimize tip vortices, and a minimization of unique wing parts through proper attention to the design and manufacturing process details.

An assessment of the Goldschmied Blended Joined Wing concept with respect to the five goals is contained in the following table.

to Increase Safety	to Reduce Emissions	to Reduce Noise	to Increase Capacity	to Improve Affordability
+2	+1	+2	+2	+2
NOTE: Ratings range from +2 (definite positive impact) to -2 (definite negative impact).				

The justifications of the ratings in the table are as follows:

Safety. Thrust vectoring, coupled with propulsion control of the aircraft, and easy egress from vehicle should enhance its safety of operation, even during times of an engine failure and crash landing. Moreover, with all engines located aft, the passengers should be better protected from engine blade failure.

Emissions. The reduction from four engines to two on the wing and one to provide for the suction/blowing system will lead to an aircraft with fewer emissions.

Noise. The reduction from four engines to two on the wing and one to provide for the suction/blowing system will lead to a quieter aircraft. Also, circulation control -- driven by the third engine -- will allow the aircraft to get higher faster during take-off and remain higher longer during landing, thereby reducing community noise. Moreover, the airframe noise should be reduced since most of it will have laminar flow.

Capacity. Due to the thrust vectoring, circulation control, along with reduced tip vortices, the aircraft should be able to get in and out of the airports more quickly. Moreover, during the take-off or landing portions the circulation control and thrust vectoring can be used to accommodate the trailing vortex systems from other aircraft.

Affordability. Reductions in the number of engines and the use of more common parts for the wings will lead to a reduction in cost of manufacture. Moreover, the use of laminar flow over most of the wings should reduce the direct operating costs.

Modified Chaplin V-Wing (MCVW) Concept

The basic concept is a modification to the Chaplin V-wing [ref. 1] and is envisioned as a replacement for the B-757/767 class of transonic transports. A conceptual three-view layout along with a perspective sketch are presented in figures 7 and 8. Note that the passengers sit in the wing, as shown in figure 9. As shown, the concept will have winglets and three engines but no horizontal tail. The engines are located in the root region. Pitch control is through thrust vectoring of these engines and directable, distributed trailing-edge blowing, also shown in figure 9. Lateral control is through the rudders on the winglets and differential vectoring/blowing.

SnAPII technologies and other features associated with this configuration are listed here. A Goldschmied suction-blowing system will be utilized for the promotion of a laminar boundary layer over the center part of the configuration coupled with boundary layer ingestion for the restarted boundary layer. Smart inlet/nozzle shaping for the engines, including thrust vectoring, and tip turbines are to be used. The latter are employed as an energy source for boundary-layer suction and promotion of significant laminar flow on the main wings. The flow removed will be used to provide positive static thrust along the wing trailing edge, a la Goldschmied.

The configuration should minimize tip vortices, as well as minimize unique wing parts through proper attention to the design and manufacturing process details. In particular, many wing sections may be similar provided the twist associated with the wing can be properly taken into account.

An assessment of the Modified Chaplin V-Wing concept with respect to the five goals is contained in the following table.

to Increase Safety	to Reduce Emissions	to Reduce Noise	to Increase Capacity	to Improve Affordability
0	+1	0	+1	+1
NOTE: Ratings range from +2 (definite positive impact) to -2 (definite negative impact).				

The justifications of the ratings in the table are as follows

Safety. Three engines instead of two should be a plus but this aircraft may have unusual flying characteristics; plus it has such a small rotation angle that thrust vectoring will be required for takeoff and landing.

Emissions. Reductions in drag due to improved boundary-layer flow will lead to a reduction in emissions. This is possible because during cruise the tip-turbine powered suction/blowing system will provide sufficient net static thrust so that the three main engines can be throttled back and yet have the aircraft maintain its design Mach number. Less required jet thrust means fewer produced emissions.

Noise. The sources of noise are the use of three engines instead of two, small rotation angle, and the tip turbines. Noise reduction comes from much laminar flow over the airframe and through the use of thrust vectoring. The net effect is for no change in noise level.

Capacity. Due to the thrust vectoring and minimizing trailing vortices, the aircraft should be able to get out of the airports more quickly once airborne. Landing could be accomplished by maintaining cruise altitude until just prior to the airport, then with thrust vectoring maintain attitude through a controlled stall ending at the beginning of runway in a low attitude flair; also know as ATOPS.

Affordability. The use of more common parts for the wings will lead to a reduction in cost of manufacture. Moreover, the use of laminar flow over most of the wings should reduce the direct operating costs.

Reference.

1. Chaplin, Harvey R.: "Application of Very Thick BLC Airfoils to a Flying Wing Type Transport Aircraft". SAE Tech. Pap. Ser. No. 901992, Oct. 1990.

SnAPII Civil Tilt-Rotor Concept at 2025 (SC2025)

The SnAPII Civil Tilt Rotor (SC2025) concept (figures 10 and 11) is a regional commercial transport concept that could be configured to seat from 30 to 60 passengers. As with current civil tilt rotor (CTR) concepts, the design is intended to increase passenger utility of air travel through increased access. This is accomplished by the ability to takeoff and land vertically and hover for extended periods of time, allowing the vehicle to access locations that are not equipped with runways. This capability enables point-to-point transportation, high-speed transportation to constrained locations such as downtown areas of major cities, off-loads capacity from major airports, and makes more efficient use of passenger time.

The key technology requirement for the SC2025 is the accelerated development of mini-turbine engine technology beyond the current cruise missile engines and Williams FJX turbofan. Engines that measure inches in fan diameter are envisioned that can be mass produced in large quantities and take advantage of advanced manufacturing technology and automation. The engines are conceptualized to be relatively standard such that thrust requirements can be met by adjusting the number of engines integrated with the configuration rather than developing new engines for varying thrust requirements. Due to high-rate mass production and standardization, the engines could potentially be very inexpensive ($100's) and therefore easily replaced, remanufactured, and recycled.

The mini-turbines are integrated with the SC2025 rotor blades to provide a powered-lift/augmented thrust blade capable of unprecedented disk loading and control. If engines are positioned across the rotor blades with inlets and nozzles that span the entire upper surface, they can be used to create a supercirculation effect at low-incident blade speeds. This effect is due to the acceleration of the flow over the blade upper surface into the engines and the ejection of engine exhaust at speeds that would normally be greater than blade trailing-edge flow speeds. The supercirculation effect will also “vector” the thrust flow with the streamlines creating additional lifting forces. For a range of blade speeds the blade may be inseparable, creating a situation allowing extremely high lift coefficients and very low blade rotation rates. This capability allows for smaller and lighter rotor blades for a given takeoff gross weight vehicle. The use of on-rotor engines eliminates the need for a rotor drive system and gearing because the engine thrust provides rotational energy. The use of multiple engines engenders redundancy and eliminates the nominal CTR requirement of cross-shafting mechanisms to account for engine-out performance. If active control of the engines is used, the blade lift distribution may be tailored for specific blade efficiencies. This capability may be traded-off against rotor noise reductions accomplished through the hyperacceleration of the tip vortex flows using the mini-turbine nearest the tip. Aircraft morphing technologies such as shape memory alloys may be used to selectively and “intelligently” shape blade leading and trailing edges as well as inlet and nozzles for on- and off-design conditions, enabling increased engine efficiency and blade aerodynamics as well as to allow simplifications in manufacturing design. The combined usage of morphing technologies and on-demand blade-lift distribution tailoring provides the opportunity for mechanism-less cyclic and collective control while in helicopter mode. The same effects used to provide powered lift from the rotor blades for helicopter mode are available to provide augmented thrust as the rotors tilt forward to airplane mode. Overall, these affects may significantly decrease the empty weight and both airframe and maintenance cost of the vehicle as well as increase the combined propulsive-aerodynamic efficiency to reduce fuel requirements.

Other SnAPII technologies used on the SC2025 concept are included in the aft-fuselage nacelle. This nacelle contains additional mini-turbines that ingest the fuselage boundary layer for drag reduction, utilize morphing nozzle features and tailored distribution of thrust to effectively provide “thrust vectoring” control and eliminate the requirement for a tail. This nacelle is extremely bluntly shaped, using morphing technologies such as synthetic jets and on-demand vortex generation to provide separation control both internally to reduce duct losses and externally to reduce profile drag. The use of these technologies has the potential to further increase the propulsive-aerodynamic efficiency of the airframe and lower both the empty weight and overall cost.

An alternative implementation of these technologies is depicted in figures 12 and 13. The integration is identical to the previously described concept except that, while in airplane mode, the rotor blades will rotate into the flow (feather), placing the rotor-mounted engines directly in the desired thrust line. This eliminates the need to use the rotors as propellers for airplane mode and instead relies on unaugmented engine thrust alone to power the vehicle.

A summary of the ratings, which are the same for this concept and the alternative concept, against the five aeronautics goals is shown below.

to Increase Safety	to Reduce Emissions	to Reduce Noise	to Increase Capacity	to Improve Affordability
+1	0	+1	0	+2
NOTE: Ratings range from +2 (definite positive impact) to -2 (definite negative impact).				

Safety. The SC2025 enjoys much higher propulsive redundancy than any state-of-the-art vehicle due to its multitude of mini-turbine engines. This provision eliminates requirements for cross-shafting or autorotation descent. Additionally, the thrust-vectoring control both in helicopter and airplane mode may provide a much greater degree of maneuverability than currently possible.

Emissions. The SC2025 will likely be more fuel efficient than both contemporary helicopters and CTRs through its superior performance. However, it is not evident that the mini-turbines can achieve a similar level of emissions reductions, on a per pound of thrust basis, as is forecast for larger high-bypass ratio turbofans. These effects may well cancel each other out.

Noise. Lower blade tip speeds during takeoff and landing operations combined with the possible dispersion of the tip vortex due to the hyperacceleration of the tip flow with a mini-turbine may possibly result in a significant noise reduction of the SC2025 compared to contemporary helicopters, regional airplanes, and the CTR. However, additional high frequency noise may be present, due to the additive nature of the noise from the individual jet engines.

Capacity. The SC2025 is not perceived to offer greater capacity increases than those forecast to be enabled by the (baseline scenario) introduction of the CTR during the next twenty years.

Affordability. It is perceived that engine life cycle costs may be significantly reduced using standardized, mass produced, and inexpensive mini-turbines. The removal of the power train, cross-shafting requirement, and empennage and the increased propulsive-aerodynamic efficiency should combine to achieve significant reductions in both airframe size/weight and fuel requirements resulting in considerable airframe-related life cycle cost reductions.

SnAPII Twin Fuselage (STF) Concept

The SnAPII Twin Fuselage (STF) concept is a transonic commercial passenger and/or cargo transport that could be used for regional hub, transcontinental, and trans-oceanic flights. This concept is shown in a perspective rendering (figure 14) and a three-view orthographic drawing (figure 15) The pilot would be located in the nose of one of the fuselages, and first-class seating would occupy the nose of the other.

This concept utilizes many SnAPII and aerodynamic features. The twin fuselages would be separated by a circulation-controlled wing (CCW). This CCW, powered by an auxiliary power unit, would provide high C_L at takeoff and landing when employed and would morph and/or actuate into a wing cross section that provides better performance at cruise conditions. A sketch of the CCW cross section showing areas that could be altered is presented in figure 16. The leading and trailing edges of the relatively blunt CCW wing would be conformed with a more efficient cruise shape, and the circulation control slot on the upper surface would be closed. The STF concept would include two tail-mounted engines, one at the end of each fuselage. These engines would take advantage of fuselage boundary-layer ingestion, smart inlet and nozzle technology, and thrust vectoring/reversing for both performance enhancement and configuration control. Finally, wing tip turbines would be mounted on the high aspect ratio outer wings to provide a vortex wake hazard reduction at takeoff and landing, as well as an energy generation device that would be used to power the suction boundary-layer laminar-flow control on the outer portions of the wing. Minimal flaps are incorporated and are utilized primarily for backup control following an engine out.

A summary of the ratings for this concept against the five aeronautics goals is provided below, followed by justification describing each rating for the STF concept.

to Increase Safety	to Reduce Emissions	to Reduce Noise	to Increase Capacity	to Improve Affordability
+2	+1	+2	+2	+2
NOTE: Ratings range from +2 (definite positive impact) to -2 (definite negative impact).				

Safety. The STF incorporates many features that increase safety, including wing-tip turbines that provide vortex wake hazard reduction during takeoff and landing, the main engines are located far away from passengers, the fuselages allow for plenty of egress routes in the event of an emergency.

Emissions. The STF concept may require smaller engines due to aerodynamic performance improvements (no vertical tails, deployable/morphing CCW, high AR wings with laminar flow) and the use of smart inlets and nozzles, thus possesses a perceived positive impact.

Noise. The noise generated by the STF concept would be less due to smaller engines (see above), shielded inlets, engine placement in the back, fewer and smaller flaps, and high C_L at takeoff and landing. The high C_L at low speeds will allow quicker climbout and descent in order to reduce community noise.

Capacity. The capacity of this concept would definitely be increased because of the use of twin fuselages, single- and/or dual-gate ingress and egress, and tip vortex hazard reduction that would increase airport throughput

Affordability. This concept improves affordability by utilizing existing technology enhancements, using the propulsion system to control the aircraft (thrust vectoring), and using extruded CCW parts to reduce manufacturing costs.

An alternative twin-fuselage concept called the Inboard Wing is shown in figures 17 and 18. This concept trades the aspect ratio provided by the outer wing panels for a reduction in induced drag. The fuselages act as endplates for the wide-chord wing between them (hence the name), and working in conjunction with the canted tails, greatly reduce the wing tip vortices. The tails are canted inboard and actually produce thrust due to their interaction with the weak wing vortex that does remain. Compared with the “standard” twin fuselage design, the Inboard Wing should have enhanced safety and capacity metrics due to negligible wing tip vortices and improved affordability due to reduced drag. Other twin fuselage concepts include replacing the outboard wing panels with a C-wing for increased span efficiency, or possibly an Inboard Wing biplane that uses a forward and an aft wing between the fuselages for increased lifting force and/or center-of-gravity margins. Ratings are the same as for the standard twin fuselage concept.

Trans-Oceanic Air-Train (TOAT)

The Trans-Oceanic Air Train (TOAT) is a vehicle system concept (figures 19 and 20) designed for long range transport of large quantities of cargo. The system design is optimized for low cost operational procedures, high volume, minimal infrastructure requirements, and easy on/off loading of standard 8x8x20 foot shipping containers. The vehicle system consists of two distinct vehicle designs which use advanced technology to make the in-flight, wing tip-to-wing tip connection which enables the system's superior long range performance.

The TOAT system concepts of two unique vehicle designs, the Lead and the Mule. Each Mule vehicle will rendezvous with the Lead vehicle and connect to either the Lead or another Mule to form the cruise configuration. The cruise configuration is a low transonic Mach number, high aspect ratio, span-loaded design intended for extremely fuel efficient flight and low structural running loads. The range of the cruise configuration is dictated by the both the fuel carrying capacity of the Lead vehicle and the number of Mule vehicles being ferried because the majority of the fuel volume is contained within the Lead vehicle. To adjust range, one simply adds or subtracts Mule vehicles as appropriate within the limits of the Lead vehicle's fuel capacity. Tanker versions of the Mule vehicles could be developed to enable extremely high-capacity, longer range versions of the system.

The Mule aircraft is a simple zero sweep, high thickness-to-chord ratio, unitary taper flying wing. It is intended to be uninhabited and capable of carrying significant numbers of the standardized 8x8x20 shipping containers currently used by the trucking/ocean-freight shipping industry. The zero sweep design allows for straight one-end loading and opposite-end unloading of cargo for excellent turn-around time operations. Due to its simple configuration, loading ramps and equipment could easily be integrated with the vehicle. The Mule would be powered by Advanced Ducted Propfans (ADPs) mounted on pylon structures incorporating shape change, “morphing” technology. The adjustability of these pylons will enable high side-to-side thrust “vectoring” with the ADPs during high sideslip in-flight connection procedures and precise maneuverability and trim control. In addition, the Mule design will incorporate morphing technology for leading edge and trailing edge shape adjustments for high-lift, trim control, roll maneuvering, and lift distribution tailoring.

The connection mechanisms may be made from “morphing” derived “inch worm” devices for high-speed, high-precision actuation and to provide aerodynamic seals at the connection point between Mules. The vehicles will also benefit from the use of engine-powered pneumatic control in the form of wing-tip blowing for precise maneuvers and suction for connection seals. Each Mule conceptually carries only enough fuel to provide takeoff, formation rendezvous, connection procedures, abort to alternate airstrip, and landing operations. The fuel for cruise flight, the crew, and the command, control and communications functions are all provided via the Lead vehicle. Each Mule will carry only enough onboard sensors to provide necessary operating data to the Lead for functional analysis and control and to allow autonomous flight following an aborted connection or in-flight failure.

A summary of the ratings for this concept against the five aeronautics goals is shown below.

to Increase Safety	to Reduce Emissions	to Reduce Noise	to Increase Capacity	to Improve Affordability
0	+2	0	+2	+2
NOTE: Ratings range from +2 (definite positive impact) to -2 (definite negative impact).				

Safety. There are obvious questions and concerns over the adequacy of actively controlled connection mechanism, close-in high-sideslip flight, fault tolerant structures, etc. It is perceived that advances in localized smart structures, parallel computational processing, sensor design, and artificial intelligence may be able to overcome these technical challenges. Finally, it is not apparent at this time whether politics would allow populated area overflight of these large RPVs unless military usage of RPVs and uninhabited aircraft proves successful.

Emissions. The TOAT system should enjoy outstanding aerodynamic performance due its span-loaded, high aspect ratio cruise configuration and moderate cruise Mach number. The use of ultra-high bypass ratio ADPs should generate very efficient levels of specific fuel consumption. Combined, these two effects should realize a dramatic reduction in aircraft emissions on a per pound of cargo per revenue mile basis.

Noise. The TOAT vehicles will require very high levels of takeoff thrust due to their equally high takeoff gross weights. The engines will likely be sized to this criterion (assuming typical field lengths) and will produce high levels of effective perceivable noise level (EPNL). For landing operations, the nominal wing loading will possibly produce reasonable performance though the number of landing gears may become significant noise sources. Overall, the noise performance for these vehicles is not likely to be superior to the current state-of-the-art primarily due to configurational effects.

Capacity. On a ton equivalent unit (TEU) basis per airport flight operation, the TOAT system is capable of carrying far more cargo than current freighters. The system is also capable of extremely rapid turn-around due to its load-on/load-off of standard containers and parallel processing of Mule vehicle capabilities.

Affordability. The general layout of the Mule vehicles is intended to promote exceptional affordability for manufacturing through constant-cross sections, straight lines, part commonality, and standard configuration regardless of payload and range capacity. The fuel efficiency of the cruise configuration should be considerably greater than current aircraft due in part to spanloader structural efficiency, high aspect ratio aerodynamics, tailless design, and the propulsive efficiency of the ADPs. Finally, life cycle cost would be impacted in a dramatic fashion due to very efficient operating procedures, minimal use of flight crew, and large cargo capacity.

Summary

The out-of-the-box, blue-skies brainstorming exercise to create potential concepts that would utilize SnAPII technology resulted in seven distinct concepts and at least two other alternatives. A ratings summary of all of the concepts follows. Remember that the ratings denote the committee's perception of the relative impact that the concept would make in the goals listed along the top of the column. While detailed aircraft systems analysis is required on every concept, it is important to note that the conclusion from this effort is that the potential truly exists for exploitation of synergistic interactions between the airframe and propulsion systems.

Concept	to Increase Safety	to Reduce Emissions	to Reduce Noise	to Increase Capacity	to Improve Affordability
BFSWB	+2	+1	+2	+2	+2
DERS	+2	-1	+1	+2	+2
GBJW	+2	+1	+2	+2	+2
Modified Chaplin V-wing	0	+1	0	+1	+1
SC2025	+1	0	+1	0	+2
SC2025, Version 2	+1	0	+1	0	+2
STF	+2	+1	+2	+2	+2
STF, Version 2	+2	+1	+2	+2	+2
TOAT	0	+2	0	+2	+2
NOTE: Ratings range from +2 (definite positive impact) to -2 (definite negative impact).					

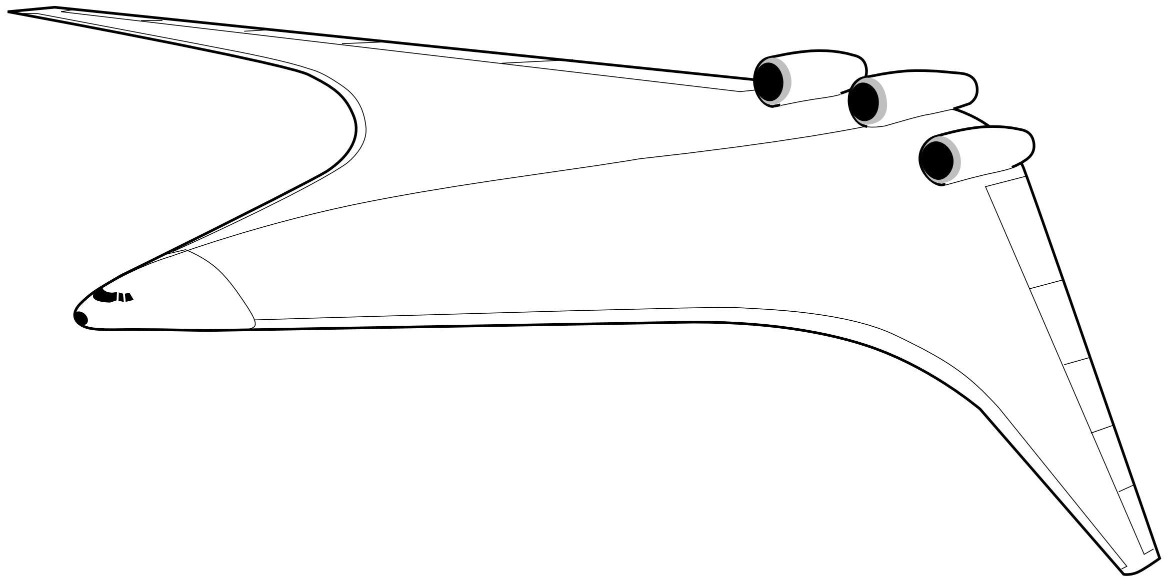

Figure 1. Blended, forward-swept-wing body concept perspective drawing.

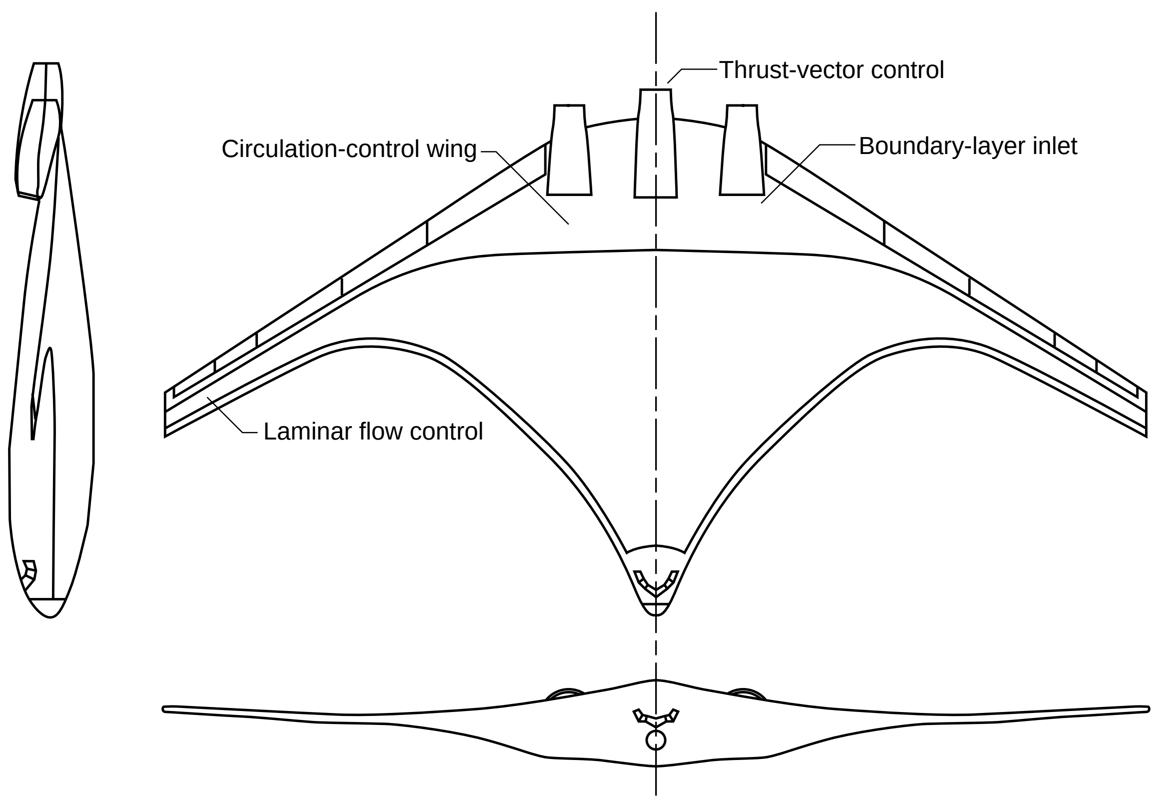

Figure 2. Blended, forward-swept-wing body concept orthographic three-view drawing.

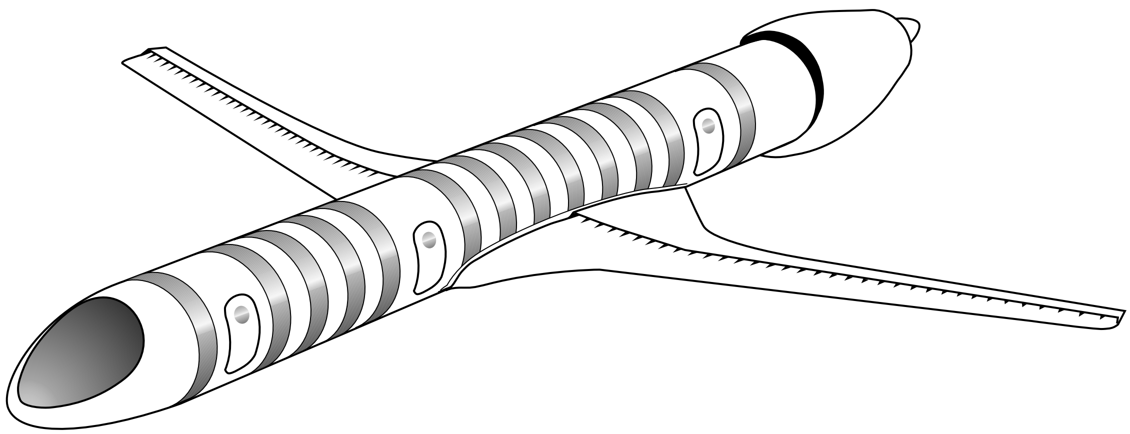

Figure 3. Distributed engine regional STOL concept perspective drawing.

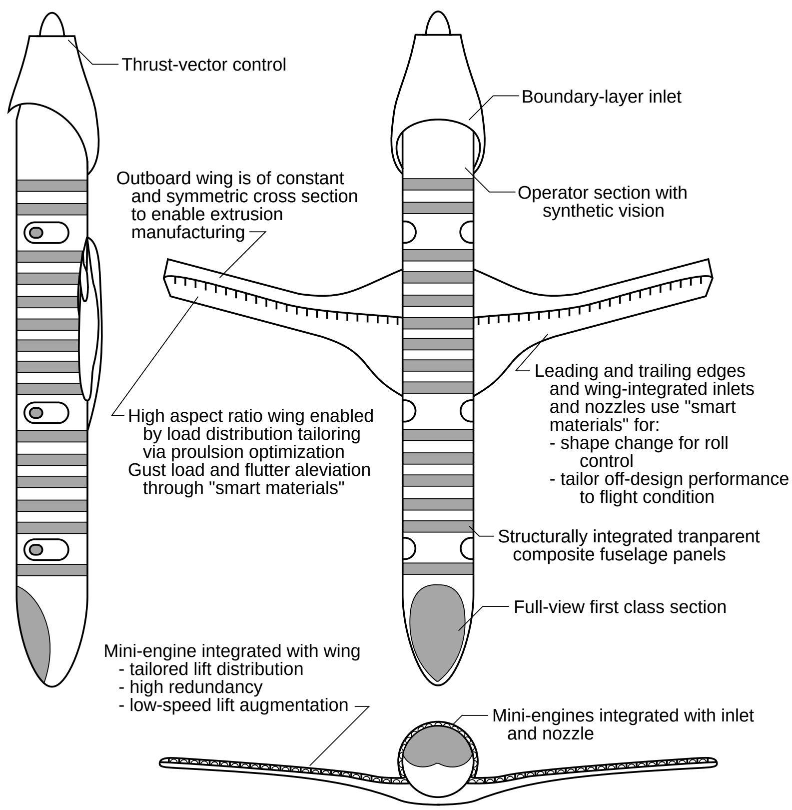

Figure 4. Distributed engine regional STOL concept three-view orthographic drawing.

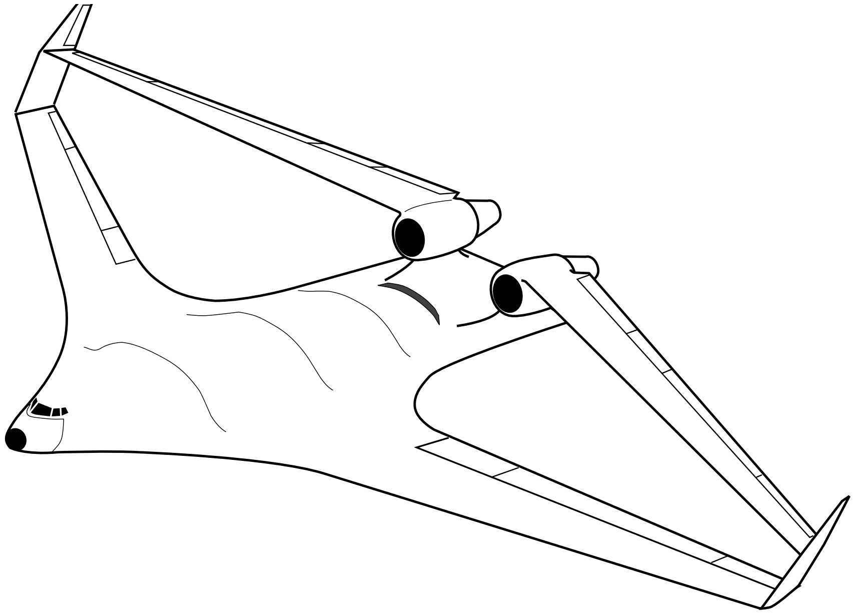

Figure 5. Goldschmied blended joined wing concept perspective drawing.

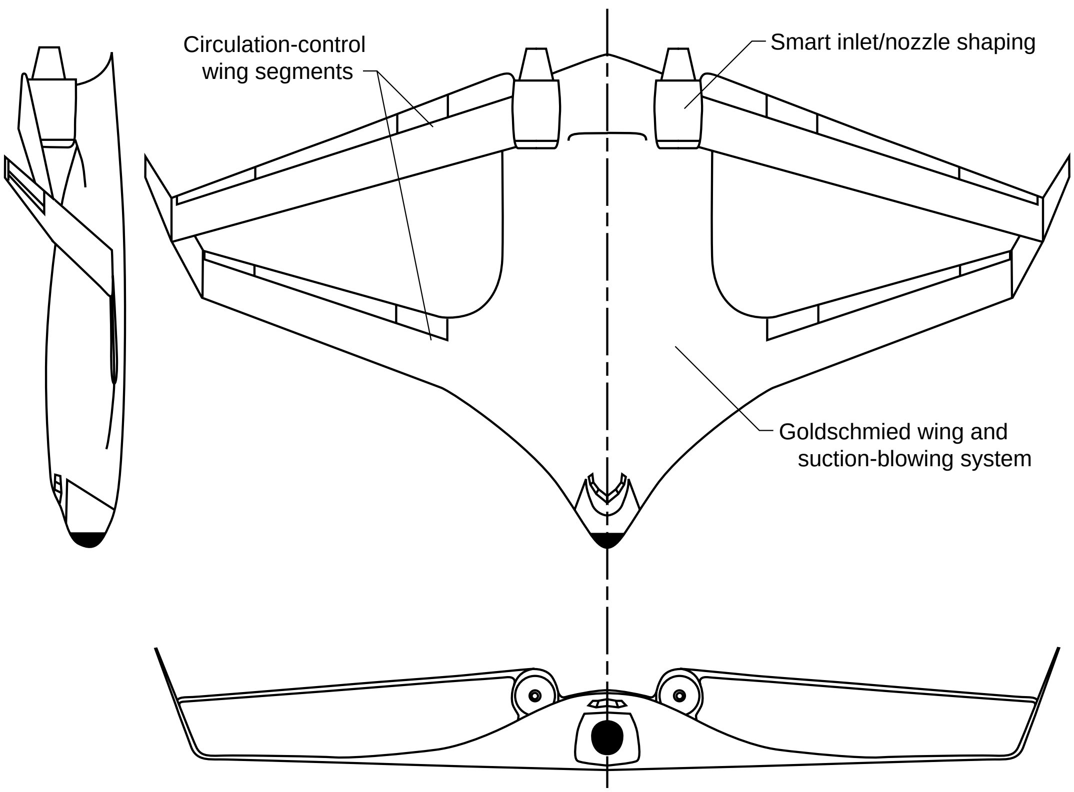

Figure 6. Goldschmied blended joined wing concept three-view orthographic drawing.

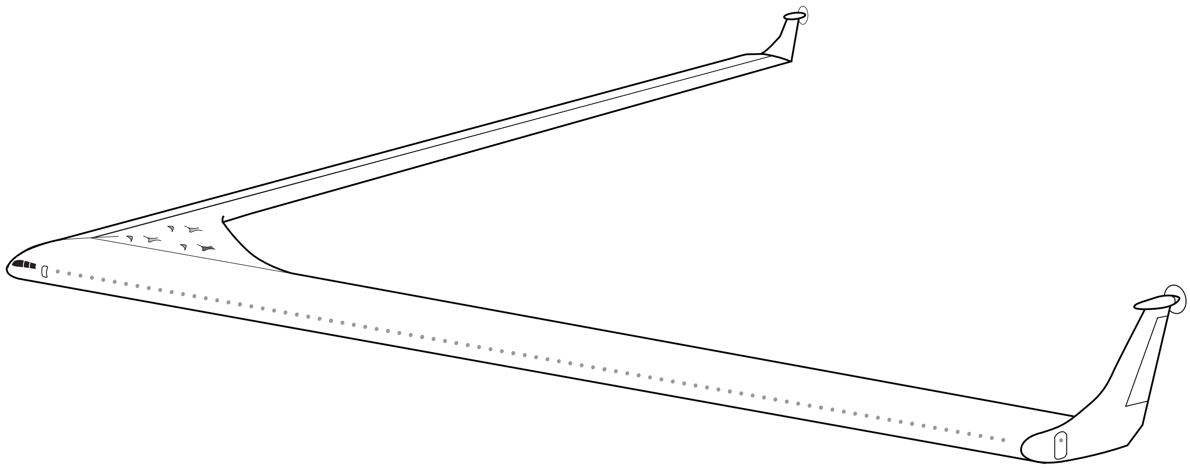

Figure 7. Modified Chaplin V-wing concept perspective drawing.

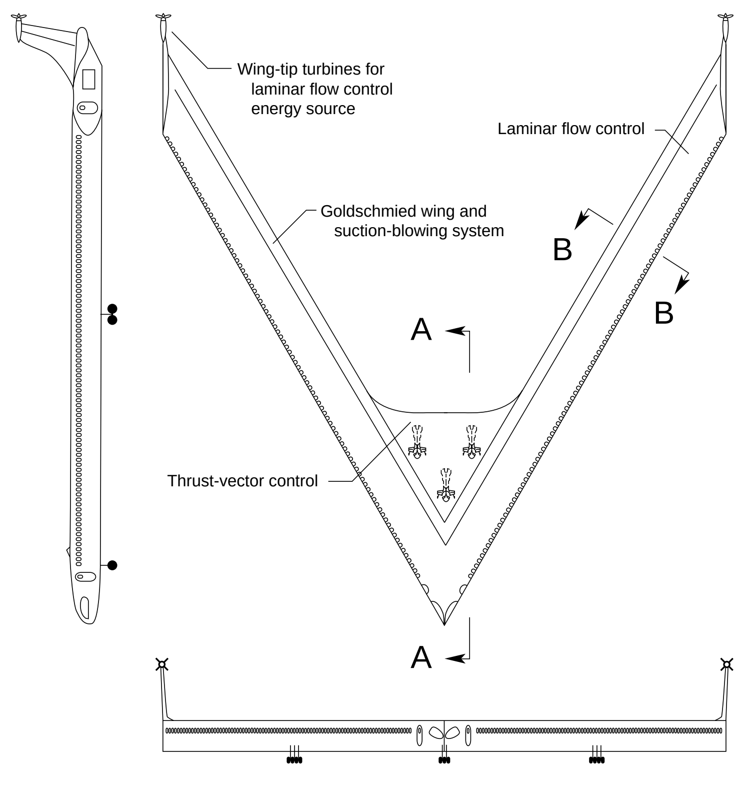

Figure 8. Modified Chaplin V-wing concept three-view orthographic drawing.

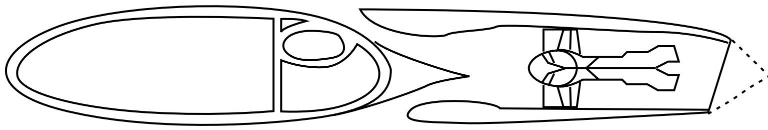

Section B-B

Streamwise cross section

F - Fuel

C - 4X4-ft. cargo tunnel

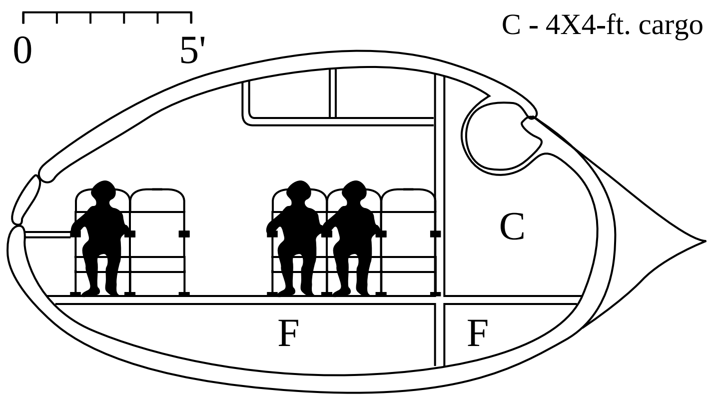

Section A-A

Crossflow section

Figure 9. Cross-section details of the Modified Chaplin V-wing concept. (See fig. 8 for section lines.)

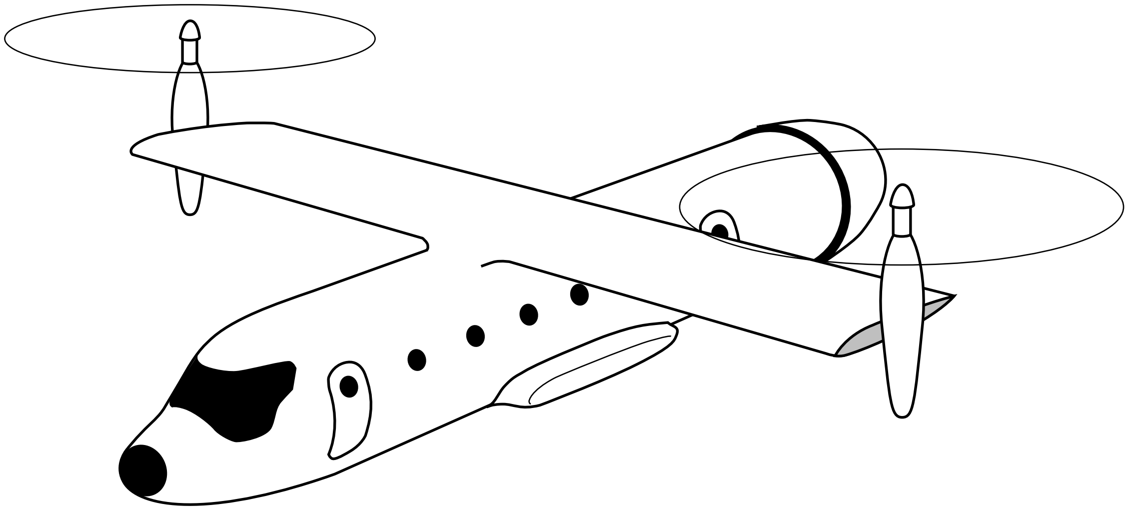

Figure 10. SnAPII civil tilt-rotor concept at 2025, version 1 perspective drawing.

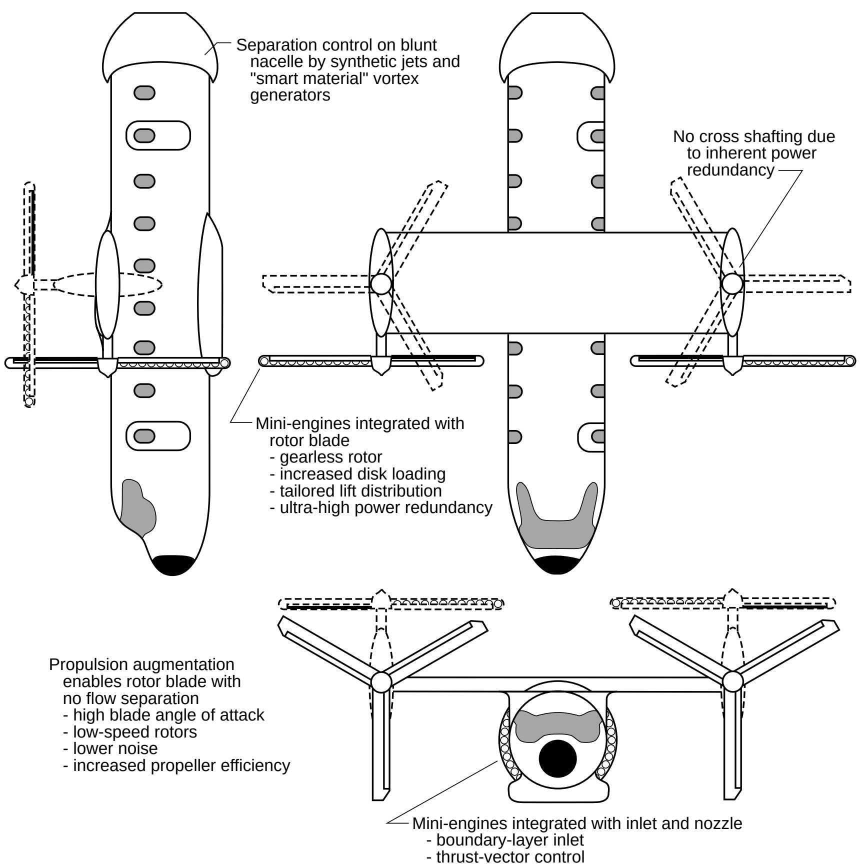

Figure 11. SnAPII civil tilt-rotor concept at 2025, version 1 three-view orthographic drawing.

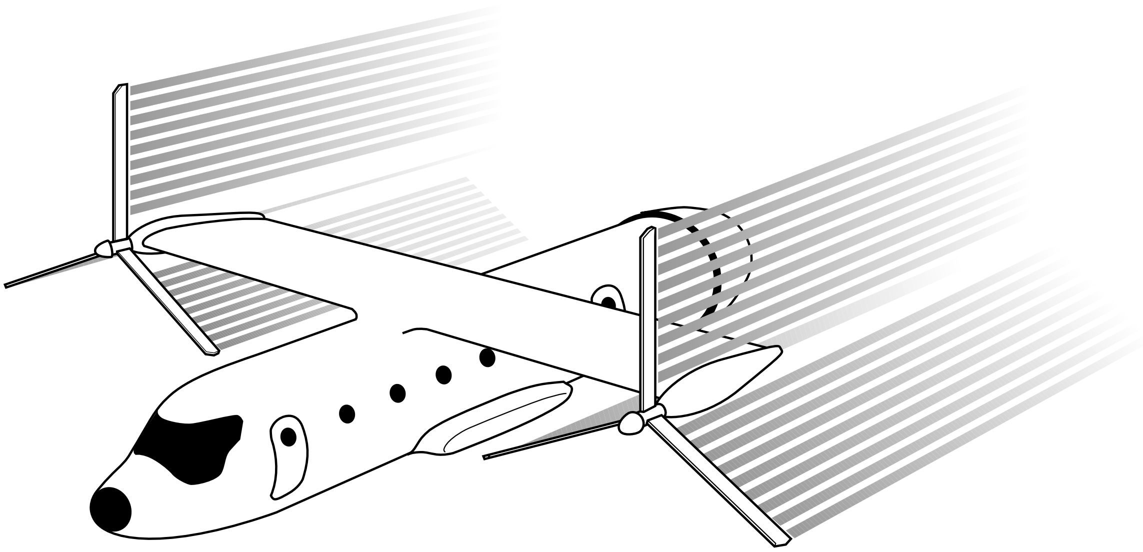

Figure 12. SnAPII civil tilt-rotor concept at 2025, version 2 perspective drawing.

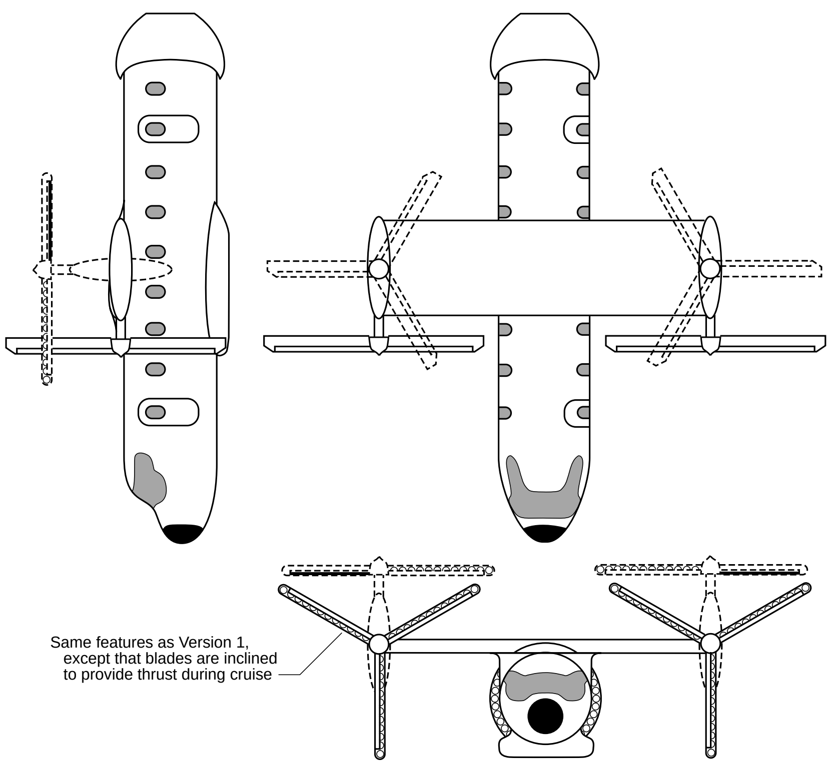

Figure 13. SnAPII civil tilt-rotor concept at 2025, version 2 three-view orthographic drawing.

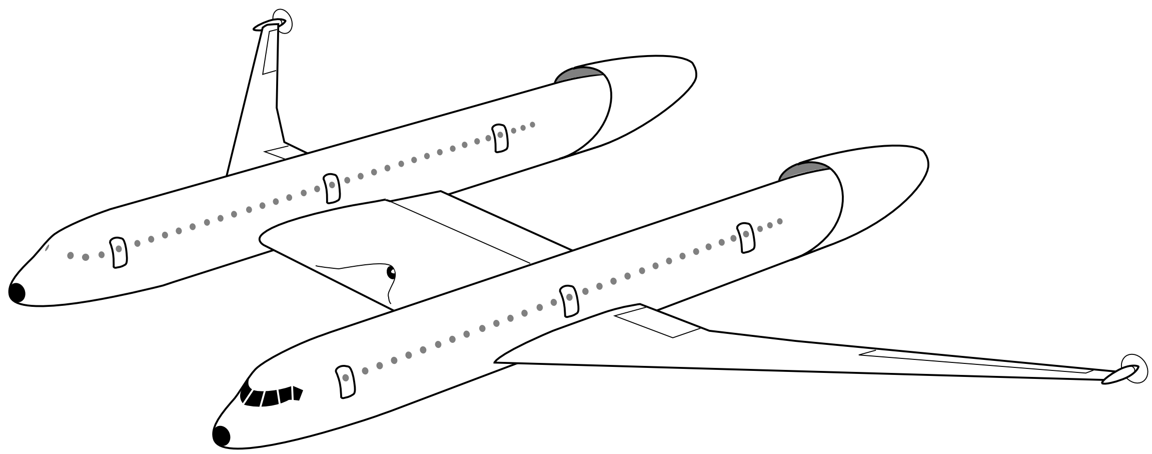

Figure 14. SnAPII twin fuselage concept, version 1 perspective drawing

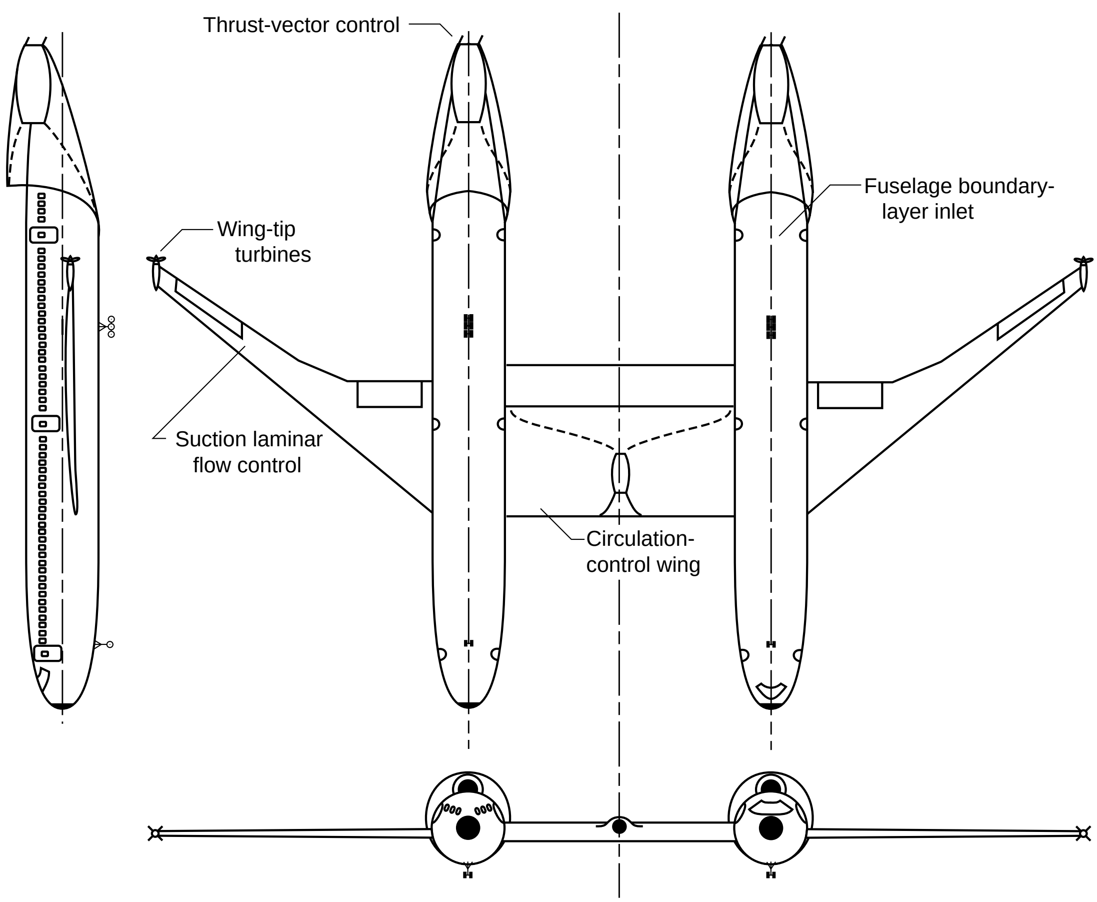

Figure 15. SnAPII twin fuselage concept, version 1 three-view orthographic drawing.

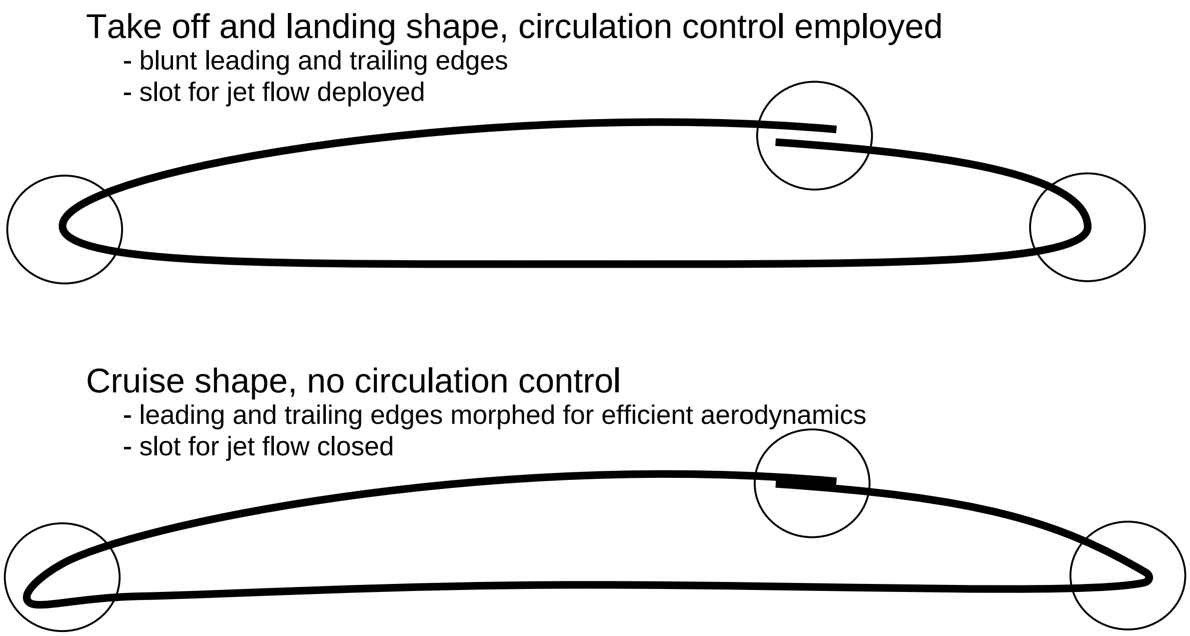

Figure 16. Circulation-control wing cross section showing areas that could be altered.

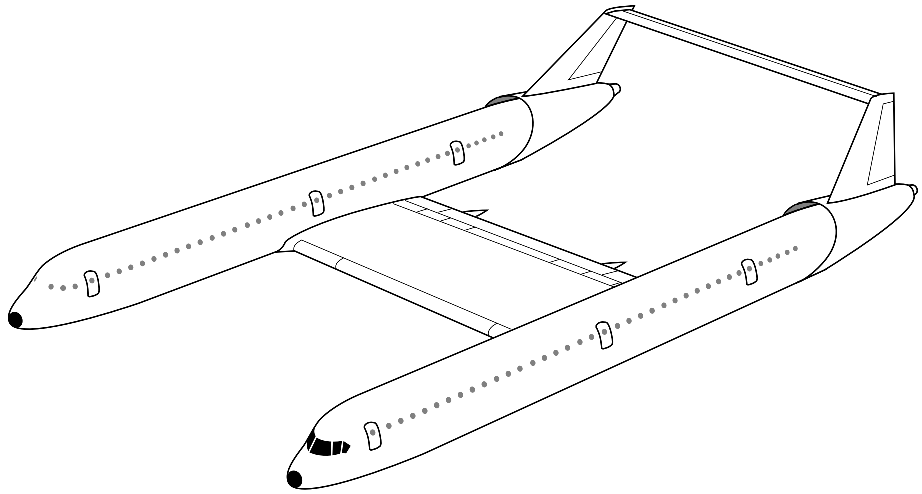

Figure 17. SnAPII twin fuselage concept, version 2 perspective drawing.

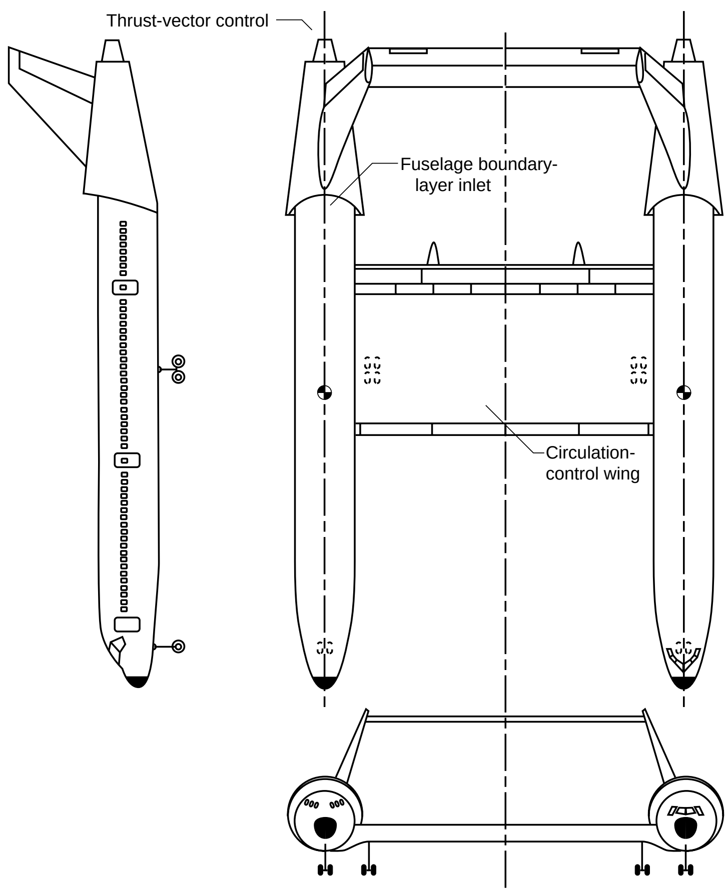

Figure 18. SnAPII twin fuselage concept, version 2 three-view orthographic drawing.

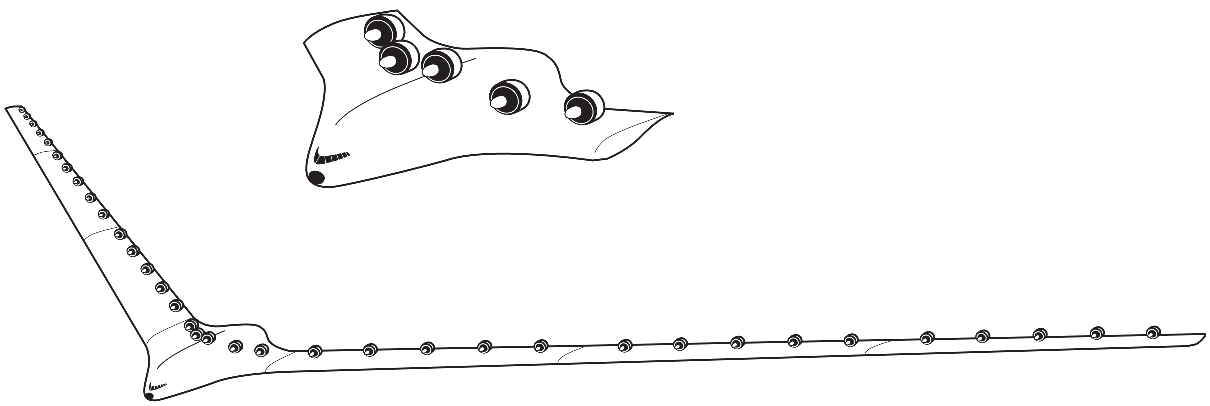

Figure 19. Trans-oceanic air-train concept perspective drawing.

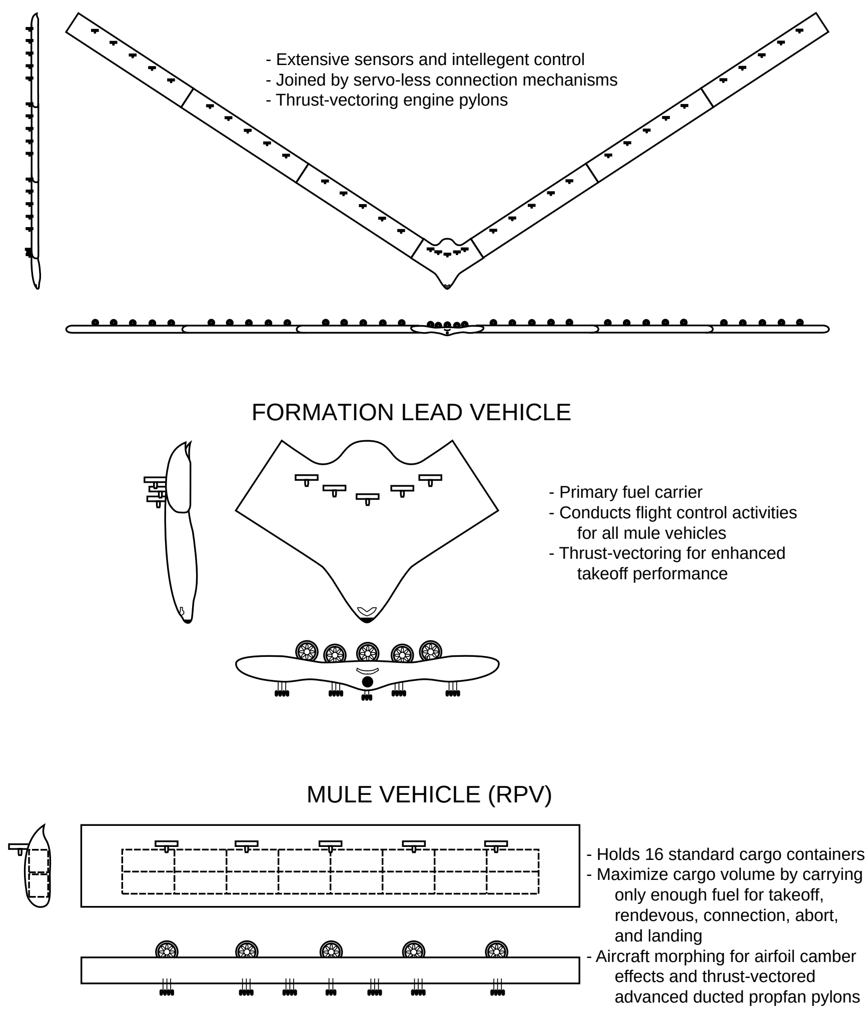

Figure 20. Trans-oceanic air-train concept three-view orthographic drawing.

Summary

This document has served to identify airframe/propulsion technologies and how beneficial interactions and integrations can result in synergistic effects. A host of technologies have been documented that use the additional energy added to the airplane system via the combustion of fuel (stored chemical energy) in the propulsion system and used in a way that provides for beneficial airframe-propulsion interactions. Other technologies that use more passive methods of extracting energy, such as wing-tip turbines, have also been documented. It is the intent of this paper to unbound the typical constraints imposed on basic performance metrics, such as high lift, cruise efficiency, and maneuver, by exploiting these technologies in a synergistic way. The documentation for each of these technologies includes a brief description of the concepts, current and/or past utilization, technology benefits, and issues for incorporating them into aircraft design.

Exploiting these propulsion/airframe integration technologies at lower speeds may lead to more efficient aircraft and/or entirely new vehicle concepts. The second part of the document addressed this in two ways. First, a synergistic application of these technologies was applied to existing aircraft concepts, one conventional (like the Boeing 777) and one unconventional (the Blended Wing-Body). Engineering estimates were then derived to provide some measure of the potential improvements by using these synergistic technologies.

Following this, an unconstrained design approach was applied using these technologies, resulting in a number of potential aircraft concepts. These concepts were weighed against the five goals of NASA's first pillar for aeronautics and space transportation success: "for U. S. leadership in the global aircraft market through safer, cleaner, quieter, and more affordable air travel." No detailed analyses were performed on these concepts; the intent was to create concepts definitions using the knowledge gained in the previous parts of the paper and the synergistic use of these technologies.

Recommendations

The following recommendations are made to continue the work initiated in this document:

(1) Based upon the evaluation presented herein of the potential benefits of applying SnAPII technologies in achieving the Agency's aeronautics goals, we recommend that system studies be initiated to independently assess our findings and perhaps provide the basis for future research in the SnAPII arena to be incorporated into new and existing programs. Those concepts that successfully pass the systems analyses could also be reasonable candidates for small-scale flight testing.

(2) Not withstanding recommendation number one, it is recommend that all future systems studies in aeronautics consider the application of SnAPII technologies (identified in the first part of this paper), in addition to the technologies currently funded in the aeronautics program for the evaluation of system benefits. This is an appropriate time to re-look at these with advancements in such areas as computational fluid dynamics, materials, manufacturing, as well as new methods to further optimize these technologies. Furthermore, many of these technologies have been adequately tested in wind tunnel settings, but lack flight test verification. Remotely-piloted small-scale flight testing could conceivably be utilized to provide data for these technologies in a flight airframe system to reduce risk and bring them to a higher level of application readiness.

(3) The idea of investigating a combined propulsion/airframe design using a minimum entropy production method may be a good analytical approach, complementing the systems analyses and experimental studies, to exploiting SnAPII technologies. Presently, this method has been applied to only aerodynamic drag-reduction problems, but extending this to SnAPII is a next logical step.

REPORT DOCUMENTATION PAGE			*Form Approved OMB No. 07704-0188*

1. AGENCY USE ONLY *(Leave blank)*

2. REPORT DATE
March 1998

3. REPORT TYPE AND DATES COVERED
Technical Memorandum

4. TITLE AND SUBTITLE
Synergistic Airframe-Propulsion Interactions and Integrations, A White Paper Prepared by the 1996-1997 Langley Aeronautics Technical Committee

5. FUNDING NUMBERS
282-10-01-01

6. AUTHOR(S)
Steven F. Yaros, Matthew G. Sexstone, Lawrence D. Huebner, John E. Lamar, Robert E. McKinley, Jr., Abel O. Torres, Casey L. Burley, Robert C. Scott, and William J. Small

7. PERFORMING ORGANIZATION NAME(S) AND ADDRESS(ES)
NASA Langley Research Center
Hampton, VA 23681-2199

8. PERFORMING ORGANIZATION REPORT NUMBER
L-17723

9. SPONSORING/MONITORING AGENCY NAME(S) AND ADDRESS(ES)
National Aeronautics and Space Administration
Washington, DC 20546-0001

10. SPONSORING/MONITORING AGENCY REPORT NUMBER
NASA/TM-1998-207644

11. SUPPLEMENTARY NOTES

12a. DISTRIBUTION/AVAILABILITY STATEMENT
Unclassified–Unlimited
Subject Category 01 Distribution: Standard
Availability: NASA CASI (301) 621-0390

12b. DISTRIBUTION CODE

13. ABSTRACT *(Maximum 200 words)*

This white paper addresses the subject of Synergistic Airframe-Propulsion interactions and integrations (SnAPII). The benefits of SnAPII have not been as extensively explored. This is due primarily to the separateness of design process for airframes and propulsion systems, with only unfavorable interactions addressed. The question ‘How to design these two systems in such a way that the airframe needs the propulsion and the propulsion needs the airframe?’ is the fundamental issue addressed in this paper. Successful solutions to this issue depend on appropriate technology ideas. This paper first details some ten technologies that have yet to make it to commercial products (with limited exceptions) and that could be utilized in a synergistic manner. Then these technologies, either alone or in combination, are applied to both a conventional twin-engine transonic transport and to an unconventional transport, the Blended Wing Body. Lastly, combinations of these technologies are applied to configuration concepts to assess the possibilities of success relative to five of the ten NASA aeronautics goals. These assessments are subjective, but they point the way in which the applied technologies could work together for some break-through benefits.

14. SUBJECT TERMS
Synergistic Airframe-Propulsion Interactions and Integrations (SnAPII), Propulsion-Airframe Integration (PAI), PAI Technologies, Advanced Concepts, Evolutionary and Revolutionary Vehicle Concepts

15. NUMBER OF PAGES
126

16. PRICE CODE
A07

17. SECURITY CLASSIFICATION OF REPORT	18. SECURITY CLASSIFICATION OF THIS PAGE	19. SECURITY CLASSIFICATION OF ABSTRACT	20. LIMITATION OF ABSTRACT
Unclassified	Unclassified	Unclassified	UL

End of Additional Reading